

**Assessing the mechanical state of sediment and rock  
during deformation: the example of the Bude  
Formation, South-west England**

Nicholas Philip John Harper

Submitted in accordance with the requirements for the degree of  
Doctor of Philosophy

The University of Leeds  
School of Earth and Environment  
May 2013

The candidate confirms that the work submitted is his own and that appropriate credit has been given where reference has been made to the work of others

This copy has been supplied on the understanding that it is copyright material and that no quotation from the thesis may be published without proper acknowledgement

Year of Submission for Examination: 2013

© 2013 The University of Leeds and Nicholas Philip John Harper

## Acknowledgements

There are many people I wish to thank for their support while I undertook this research. Firstly, I wish to thank my Supervisors, Geoff Lloyd and Richard Collier, and my Research Study Group Leader, Andrew McCaig. It is their belief in my ability, as well as their guidance and enthusiasm, both in the field and at the University of Leeds, that have been invaluable. I also wish to thank Ted Freshney and Richard Scrivener for their very useful discussions whilst in the field. Additional discussion was provided by past and present members of both the School of Earth and Environment: Simon Bottrell, Rob Butler, Quentin Fisher, Bill McCaffrey, Dan Morgan, Bill Murphy, Douglas Paton (Internal Examiner), Teresa Roncal-Herrero, Graham Stuart, Paul Wignall, Marjorie Wilson and Bruce Yardley.

As part of this work, I wish to thank Neil Cundall and Robert Marshall, who made the thin sections and polished blocks for me, respectively. To analyse the polished blocks, I used the Scanning Electron Microscope and Micro-probe. In this analysis, Eric Condliffe was invaluable in showing me how to operate the microscope and to interpret some of the observations and data. Also, although this was not used in the thesis, I am very grateful to Juan-Diego Rodriguez-Blanco, who undertook X-ray Powder Diffraction analysis on 10 shale samples to show the range of minerals present. Further, I greatly appreciated the help of Gary Keech and the other members of the Technical Staff who provided me with a microscope, stationery and cracking stories. Lastly, I must acknowledge Google Earth™ and the Ordnance Survey/EDINA for use of their publicly-available images during geological field mapping.

I cannot continue without thanking my friends and housemates, who provided assistance in many forms (as well as much needed distraction) during the course of my research. In particular thanks are due to my Postgraduate Student colleagues: Rachael Dale, Jon Poulter and Anja Schmidt in my 1<sup>st</sup> year, Rachael, Jon, and also Abi Clifton, Heather MacDonald, Jo Venus and Alan Wood in my 2<sup>nd</sup> year, and Stephen Amuda, Amy Atkins, Talal Al-Aulaqi, Pieter Bots, Andy Bray, Teddy Castalain, Santi Clerici and Cindy Lockwood during my 3<sup>rd</sup> and 4<sup>th</sup> years. I wish to further thank both my colleagues and Managers at Neflex Petroleum Consultants, who have encouraged and supported me during the time of my Thesis Referral.

However, my greatest thanks must go to my family, for their continuing love, support and encouragement throughout this endeavour. In particular, my parents for supported me throughout my research, in particular by providing health and safety cover (and also chauffeuring and meals) during my fieldwork in Bude, North Cornwall. Simply put, I couldn't have produced this thesis without them.

Lastly, this work would not have been possible without the financial support of the Natural Environmental Research Council, together with additional funding provided by the School of Earth and Environment, University of Leeds.

## Abstract

The general thesis aim was to establish geometric criteria to distinguish between folds formed in unlithified sediment and lithified rock using dip isogon analyses on folds in sediment, lithified rock, migmatites and model materials. The methods involved connecting points of equal dip and measuring layer thicknesses at these points to calculate fold classes and to understand class changes around the folded layer.

The criteria were applied to the Bude Formation folds and confirmed that the slump folds developed in sediment, but that also the Variscan tectonically-generated 'upright' chevron folds developed in sediment. 'Inclined-to-recumbent' chevron folds exhibit characteristics of folding in interbedded sediment and rock, suggesting that Variscan deformation affected the formation during lithification. The methods can be used to determine compressional structural evolutions with respect to lithification in other basins.

The specific thesis aim was to study the sedimentary and structural evolution of the Late Carboniferous Bude Formation, Culm Basin, SW England.

New sedimentary structures identified in the formation include: centimetric-scale mud-draped ripple laminations; decimetric-scale mud-draped and non mud-draped troughs; and metric-scale tabular cross-stratification. The sedimentary structures, plus analyses of palaeo-flow indicators, ichnofabrics and geochemistry, suggest that the formation records a mixed depositional environment, with fluctuating base levels and mainly fresh-to-brackish water conditions in a lacustrine or possibly marginal-marine setting.

The map work revealed decametric-scale local structures in the Black Rock foreshore that formed prior to chevron folding. The basin-scale Widemouth South Fault (WSF) juxtaposes the Bude and Crackington formations that are separated stratigraphically by 300 m. The movement along the WSF is considered using three structural models from the deformation accommodated to its north and its south. Although no model holds fully, the Freshney et al (1972) 'late' normal-faulted Widemouth South Fault model is the most plausible, suggesting that the Culm Basin accommodated progressive compressional deformation prior to extension.

### **Key words**

Chevron folds, Slump folds, Dip isogons, Bude Formation, Variscan deformation, Lithification, Mud-draped ripple laminations, Widemouth South Fault,

# Contents

Title page and submission of work	i
Acknowledgements	iii
Abstract	iv
Contents	v
Figure Contents	x
Abbreviations	xvi
<b>Chapter 1: Introduction</b>	<b>1</b>
1.1 Aims of the thesis	1
1.2 Definitions of sediment and rock	2
1.3 Thesis Description	3
<b>Chapter 2: Literature Review</b>	<b>4</b>
2.1 Types of remobilisation structure	4
2.1.1 Seismites	4
2.1.2 Gravity-driven phenomena	5
2.1.3 Deformation in slumps	7
2.1.4 Sub-surface sediment mobilisation	9
2.1.5 Effect of compression on the remobilisation of sediment	9
2.2 Compressional deformation in sediment and mechanical state determination	9
2.2.1 Review of soft sediment deformation theories	9
2.2.2 Structures generated in early post-depositional deformed strata	11
2.2.3 Effects of syn-depositional and tectonic deformation on deposition	11
2.2.4 Similarities and difference between slump and tectonically-generated folds	12
2.3 Structures, fabrics and compaction in deforming sediments and rocks	13
2.3.1 Sediment shear zones	13
2.3.2 Syn-depositional normal faulting	13
2.3.3 Slump fabrics	14
2.3.4 Axial-planar cleavage fabrics	14
2.3.5 Sediment compaction and cementation	16
2.4 Fold mechanics	18
2.4.1 Fold development stages	18
2.4.2 Pre-buckle shortening	18
2.4.3 Buckling	19
2.4.4 Forced folding	20
2.4.5 Chevron folding	21
2.5 Compressionaly-developed basins	23
2.5.1 Fold-and-thrust belts	23
2.5.2 Foreland basin	24

2.6 Variscan orogenesis and foreland basin processes	25
2.6.1 Regional compressional deformation in SW England	26
2.6.2 Deformation in the Culm Basin	28
2.6.3 Geometries of the fold structures in the Bude and Crackington formations	32
2.6.4 Structural geometries of beds in ‘upright’ chevron folds	34
2.6.5 Lloyd-Whalley shear modification model	35
2.6.6 Regional Metamorphism and geothermal gradients	37
2.6.7 Geochemistry of the Culm Foreland Basin deposits	39
2.7 Summary	39
<b>Chapter 3: Sedimentological interpretation of the Bude Formation</b>	40
3.1 Introduction	40
3.2 Methods	46
3.3 Facies within the Bude Formation	47
3.3.1 Siltstones and sandstones with ripple laminations (Facies 1a & b)	49
3.3.2 Trough cross-stratified sandstones (Facies 2)	52
3.3.3 Undulose and hummocky cross-stratified sandstones (Facies 3)	52
3.3.4 Tabular cross-bedded sandstone (Facies 4)	53
3.3.5 Planar laminated siltstones and sandstones (Facies 5a & b)	54
3.3.6 Amalgamated massive structure-less siltstones and sandstones (Facies 6 & 7)	55
3.3.7 Planar laminated shales (Facies 8)	56
3.3.8 Slump and internally-contorted beds (Facies 9a, b & c)	58
3.3.9 Channel fill facies (Facies 10)	59
3.4 Palaeo-flow directions	60
3.5 Ichnofabric analysis	61
3.6 Rock description analysis of Bude Formation samples	63
3.6.1 Siltstone and sandstone beds	63
3.6.2 Shale beds	65
3.6.3 Bedding-parallel pyrite minerals and ankerite veins within shale beds	65
3.7 Carbon-sulphur (C/S) geochemical analysis	67
3.8 Diagenetic mineral development in the Bude Formation	68
3.8.1 Diagenetic progression	69
3.9 Discussion	70
3.9.1 Description of the key features in the Bude Formation	71
3.9.2 Depositional environments represented in the Bude Formation deposits	71
3.9.3 Discussion of existing and new depositional models	77
3.9.4 Description of Bude Formation diagenesis using a paragenetic sequence	79
3.10 Conclusions	80

<b>Chapter 4: Geological mapping and evidence for progressive Variscan deformation in the Bude and Crackington formations</b>	82
4.1 Introduction	82
4.1.1 Description of the Black Rock and Wanson Mouth foreshore successions	82
4.1.2 Description of the King map	85
4.1.3 Description of the Sanderson (1979) and Lloyd and Whalley (1986) models	87
4.1.4 Models for the development of the Widemouth South Fault (WSF)	90
4.1.5 Discussion of the Widemouth South Fault (WSF) models	94
4.2 Methods	94
4.2.1 Foreshore mapping	94
4.2.2 Sedimentary logging	95
4.2.3 Structural data	95
4.3 Sedimentary evolution of the Black Rock-Wanson Mouth foreshores	98
4.3.1 Crackington Formation in the Wanson Mouth foreshore	102
4.4 Map description	102
4.4.1 Map description of the Black Rock foreshore	103
4.4.2 Map description of the Wanson Mouth foreshore	105
4.5 Structural evolution of the Black Rock foreshore	108
4.5.1 Black Rock Dip-section A-A'	109
4.5.2 Black Rock Dip-section B-B'	114
4.5.3 Black Rock Dip-section F-F'	116
4.5.4 Justification for construction of strike sections	119
4.5.5 Black Rock Strike-section C-C'	120
4.5.6 Black Rock Strike-section D-D'	123
4.5.7 Black Rock Strike-section E-E'	125
4.5.8 Black Rock Strike-section G-G'	129
4.5.9 Widemouth South Fault	132
4.5.10 Three-dimensional projection of the Black Rock foreshore succession	132
4.5.11 Summary of the geological evolution of the Black Rock foreshore	132
4.6 Structural evolution of the Wanson Mouth foreshore	133
4.6.1 Wanson Mouth Dip-section A-A'	135
4.6.2 Wanson Mouth Dip-section B-B'	138
4.6.3 Wanson Mouth Dip-section F-F'	140
4.6.4 Justification for construction of an oblique section	143
4.6.5 Wanson Mouth Oblique-section H-H'	143
4.6.6 Evolution of the Widemouth South Fault (WSF)	146
4.6.7 Summary of the geological evolution of the Wanson Mouth foreshore	147
4.7 Discussion	149

4.7.1 Comparison of the King (1967) map with that of the author	150
4.7.2 Geological evolution of the Black Rock-Wanson Mouth foreshores	152
4.7.3 Critical review of the structural evolution models	157
4.7.4 Consideration of other Culm Basin models	158
4.7.5 Strain accommodation in the two foreshore successions	160
4.8 Summary of findings from the Black Rock-Wanson Mouth foreshores	160
<b>Chapter 5: Analysis of slump and ‘early’ deformation structural geometries in the Bude Formation</b>	162
5.1 Introduction	162
5.1.1 ‘Early’, ‘pre-chevron’ and ‘pre-folding’ structures in the Bude Formation	162
5.1.2 Assessment of an ‘early’ deformation structure	164
5.2 Methods	166
5.3 Slump folds	169
5.3.1 Attached slump folds	169
5.3.2 Detached slump rafts within massive slump beds	173
5.3.3 Detached slump raft folds in the Black Rock Slump Bed at Lynstone	173
5.3.4 Detached slump raft folds in the Black Rock Slump Bed at Black Rock	178
5.4 Analysis of high angle, strata-bound normal faults	182
5.4.1 ‘Fanning’ array of high angle normal faults	182
5.4.2 Reversed high angle normal faults due to emergence on the palaeo-surface	184
5.4.3 Regional variations in ‘early’ high angle normal fault orientations	186
5.5 Analysis of low angle faults and associated folds	187
5.5.1 Recognition of ‘early’ contractional structures	187
5.5.2 Deformed strata below a normal-faulted sandstone bed	190
5.5.3 Regional variations in ‘early’ low angle thrust orientations	191
5.6 Discussion on Bude Formation slumps and ‘early’ structures	192
5.6.1 Discussion on the palaeo-slope direction assessment methodologies	194
5.7 Summary of slumping and ‘early’ deformation in the Bude Formation	195
<b>Chapter 6: Evidence for deformation in sediment from the Bude Formation</b>	196
6.1 Introduction	196
6.2 Bedding-parallel ankerite veins	196
6.3 Bulbous hinges in Bude Formation folded beds	198
6.3.1 Bulbous hinges in slump folded beds	199
6.3.2 Bulbous hinges in ‘upright’ chevron folded beds	200
6.3.3 Bulbous hinges in ‘inclined-to-recumbent’ chevron folded beds	200
6.4 Structural geometries of progressive Variscan deformation structures	201
6.4.1 Structural geometry of north-directed thrusts	201
6.4.2 Structural geometry of ‘upright’ chevron folds	202

6.4.3 Structural geometry of south-directed, ‘inclined-to-recumbent’ chevron folds	203
6.5 Mud injections cutting fold hinges	203
6.5.1 Mud injections cutting ‘upright’ chevron fold hinge zones	204
6.5.2 Mud injections cutting a south-verging chevron fold hinge zone	205
6.6 Discussion	206
6.7 Summary	207
<b>Chapter 7: Distinguishing folded structures in rock and sediment</b>	<b>208</b>
7.1 Introduction	208
7.2 Methods	208
7.3 Dip isogon analyses of rock, sediment, material and migmatite folds	211
7.3.1 Descriptions of folded rocks, sediments, model materials and migmatites	212
7.4 Dip isogon and quantitative layer thickness analyses	213
7.4.1 Folded rock in profile	213
7.4.2 Folded sediment	217
7.4.3 Folded model materials in profile	220
7.4.4 Folded migmatites in profile	220
7.5 Discussion	221
7.5.1 Initial application of methods to the Bude Formation	222
7.5.2 Dip isogon methods for oblique and plan-view sections through folded layers	225
7.5.3 Limits to the dip isogon and quantitative layer thickness methods	225
7.5.4 Proposed future work using the inverse thickness method	226
7.5.5 Potential other relationships to the fold geometric criteria	229
7.6 Summary of geometric criteria to distinguish folded rock and sediment in profile	230
<b>Chapter 8: Bude Formation lithification state during folding</b>	<b>231</b>
8.1 Introduction	231
8.2 Methodology	232
8.2.1 Description of the fold types recognised in the Bude Formation	233
8.3 Dip isogon and quantitative layer thickness analyses	234
8.3.1 Slump and ‘early’ folds in profile (Fold types: a, b & c)	236
8.3.2 ‘Upright’ chevron folds in profile (Fold type: d)	236
8.3.3 ‘Inclined-to-recumbent’ chevron folds in profile (Fold type: e)	241
8.4 Model for Bude Formation folds during deposition	241
8.4.1 ‘Early’ syn-depositional versus ‘early’ post-depositional dip isogon patterns	242
8.4.2 Model for ‘early’ syn and post-depositional fold dip isogon patterns	244
8.5 Geometries and lateral variation of structures in the Bude Formation	245
8.5.1 Review of the Sanderson (1979) and Lloyd and Whalley (1986; 1997) models	245
8.5.2 Chronology of the progressive Variscan deformation	247
8.5.3 Lithification states of the chevron folds during progressive deformation	248

8.5.4 Comparison of interlimb angle and shear strain (from Williams, 2005)	249
8.5.5 Variable shear strain model for Bude Formation folds (from Williams, 2005)	251
8.6 Inverse thickness method	252
8.6.1 Results	252
8.6.2 Interpretations and Evaluation	252
8.7 Application of results from the Widemouth South Fault (WSF)	254
8.7.1 Widemouth South 'late' normal fault model (Freshney et al, 1972)	254
8.7.2 Inverted Widemouth South Fault model	254
8.7.3 Application of the models to the Bude Formation coastal outcrops	256
8.8 Summary of the structural evolution for the Bude Formation	257
<b>Chapter 9: Discussion</b>	258
9.1 Introduction	258
9.2 Models for the Variscan orogenesis in SW Britain	258
9.2.1 The basement of sedimentary cover shortening model	258
9.2.2 'Thin-skinned' tectonics model	259
9.2.3 'Thick-skinned' tectonics model	260
9.3 Regional and basin-scale deposition and tectonics	261
9.3.1 Restoration of the progressive Variscan structures	264
9.3.2 Discussion of the Rusey Fault	265
9.3.3 Model for regional tectonics and Bude Formation deposition	265
9.4 Summary	266
<b>Chapter 10: Conclusions</b>	268
10.1 Re-interpretation of the Bude Formation depositional environment	268
10.2 Structural deformation in the Black Rock-Wanson Mouth foreshores	269
10.3 Deformation structures in the Bude Formation that occurred in sediment	269
10.4 Distinguishing folds developed in rock and sediment	270
10.5 Recommendations for further work	271
<b>References</b>	272

## Figures Contents

### Chapter 1: Introduction

Fig. 1.1: Location map for the Bude Formation in SW England	1
---	---

### Chapter 2: Literature Review

Fig. 2.1: Classification of structures formed by the effect of earthquakes on sediments	4
Fig. 2.2: Conceptual view of the range of sediment mobilisation processes	5
Fig. 2.3: Model of slump and turbidite generation on a slope in Western Ireland	6
Fig. 2.4: Schematic plan-views and cross-sections of deformation structures in a slump	7
Fig. 2.5: Schematic drawings and photographs of progressive structures in a slump sheet	8
Fig. 2.6: Seismic section of a mud volcano in the Barbados accretionary wedge	9
Fig. 2.7: Shear response to Newtonian, elastic and non-Newtonian, ductile fluids	10
Fig. 2.8: Schematic section of fold deformation and palaeo-slope variations in sediment	11
Fig. 2.9: Migrated seismic reflection profile through the northern Apennines, Italy	12
Fig. 2.10: The five patterns of disjunctive cleavage cutting beds	14
Fig. 2.11: Schematic cleavage development in shale under low-grade metamorphism	15
Fig. 2.12: Relationship between shale porosity and burial depth	17
Fig. 2.13: Simplified sketch of over-pressure conditions in an oil well	17
Fig. 2.14: Fold development stages through time	19
Fig. 2.15: Schematic sketches of a fault-bend, fault propagation and detachment fold	20
Fig. 2.16: Sketch of a flexural-slip chevron fold	22
Fig. 2.17: Schematic map, sketch and cross-section of a foreland basin	25
Fig. 2.18: Tectonic structural map of SW Britain and S Ireland	26
Fig. 2.19: Geological map of SW England with locations of Variscan foreland basins	26
Fig. 2.20: Schematic sections of progressive SW England passive margin inversion	26
Fig. 2.21: Map of the stratigraphy in Cornwall with major structural trends	27
Fig. 2.22: Variscan deformation structures and strata, restoration of structures and geographical positions of the main sections in relation to restored structures	29
Fig. 2.23: Distribution of Bude Formation chevron fold interlimb angles in N-S section, with graphs of interlimb angle versus axial plane dip angle	29
Fig. 2.24: N-S cross-sections of the Variscan deformation of SW Britain and S Ireland	29
Fig. 2.25: Schematic representations of progressive deformation in the Bude Formation	31
Fig. 2.26: Plot of fold amplitude against wavelength for folds in the Bude Formation	33
Fig. 2.27: Frequency plot of interlimb angles of folds in the Bude Formation	33
Fig. 2.28: Interlimb angle versus shortening versus bed thickness-to limb length ratio	34
Table 2.1: Data comparing theoretical and calculated inter-limb angles, shortening and bed thickness-to-limb length ( $t_0/L_0$ ) ratios in Bude and Crackington Formation folds	35
Fig. 2.29: Models for 'upright' chevron fold shear modification, with structural sections	36
Fig. 2.30: Illite crystallinity measurements and cross-section along North Cornwall coast	37

### **Chapter 3: Sedimentological interpretation of the Bude Formation**

Fig. 3.1a: Location map and BGS Bude Formation sedimentary log correlation panel	43
Fig. 3.1b: Low-detail sedimentary logs and their positions in the correlation panel	44
Fig. 3.1c: Collage of 18 sedimentary logs for the Bude and Crackington formations	45
Table 3.1: Characteristics to define oxygen-related depositional conditions and facies	47
Fig. 3.2: Combined sedimentary logs over a 25 m vertical section of the Bude Formation	48
Table 3.2: The sedimentary facies recognised in the Bude Formation outcrops	48
Fig. 3.3: Photographs and sketches of the Bude Formation sedimentary structures	51
Fig. 3.4: Sedimentary log through Tom's Cove Shale, north of Bude	57
Fig. 3.5: Sedimentary log through Tom's Cove Shale, south of Bude	58
Fig. 3.6 Comparison of palaeo-flow indicators from Bude Formation outcrops	61
Table 3.3: Sample numbers, locations and facies of 50 Bude Formation rocks	62
Fig. 3.7: Folk diagrams to classify the Bude Formation sandstones, siltstones and shales and to compare with deposits from other foreland basins	64
Table 3.6: Comparison of the relative proportions of quartz, feldspar and lithic fragments, grain size and matrix mud content of sandstone and siltstone samples	65
Fig. 3.8: SEM BSE-Z images showing bedding-parallel ankerite veins and comparing the amount of bedding-parallel pyrite minerals between different shales	66
Fig. 3.9: Total organic carbon versus sulphur for C/S analysis	68
Fig. 3.10: SEM BSE-Z image of mutually cross-cutting quartz and ankerite-siderite veins	69
Fig. 3.11: SEM BSE-Z image of an ankerite vein in shale with in-situ organic matter	69
Fig. 3.12: Microprobe spectrum comparing organic matter and polished block resin peaks	70
Fig. 3.13: Schematic sedimentary logs for a turbidite fan and shallow marine environment, with schematic diagram of sedimentary distribution in a deep lake	73
Fig. 3.14: Sketch of Bude Formation palaeo-geography and BGS sedimentary log panel	76
Fig. 3.15: Processes to generate mud-draped ripples from uni-directional currents	76
Fig. 3.16: Hypothetical paragenetic sequence for all lithologies in the Bude Formation	80

### **Chapter 4: Geological mapping and evidence for progressive Variscan deformation in the Bude and Crackington formations**

Fig. 4.1: Location map for the Bude Formation in SW England	83
Fig. 4.2: Comparative logs of the Bude Formation stratigraphy	84
Fig. 4.3: Geological map of the Black Rock-Wanson Mouth foreshores from King (1967)	86
Fig. 4.4: Model of chevron fold development by simple shear	88
Fig. 4.5: Regional interpretation from Saltstone Strand to south of Millook Haven	89
Fig. 4.6: Schematic sketches of the progressive deformation observed in the Culm Basin	91
Fig. 4.7: Diagrams from Enfield et al (1985) of the faults in the Wanson Mouth foreshore	92
Fig. 4.8: Geological evolution of the Widemouth South Fault in the eastern Culm Basin	92

Fig. 4.9: Sketch cliff profile above the two foreshores with sketch of overturned anticline and sketch diagram of the major 'late' Variscan faults in the Culm Basin	93
Fig. 4.10: Diagram showing original and final length measurements	97
Fig. 4.11: Diagrams of folded and restored local normal faults and thrusts, and criteria to define 'early' local structures in stacked beds	98
Fig. 4.12: Sedimentary log from the Black Rock foreshore of a channel structure	99
Fig. 4.13: Correlated sedimentary logs across local structures in the Black Rock foreshore	100
Fig. 4.14: Sedimentary log from Wanson Mouth in the upper Crackington Formation	101
Fig. 4.15: Map of areas in the two foreshores with sedimentary log and cross-section lines	103
Table 4.1 Table of 'upright' chevron fold geometries from the Black Rock foreshore	105
Fig. 4.16: Stereonets of three structures in Wanson Mouth foreshore	107
Fig. 4.17: Diagram of a fault-fold relationship in the Wanson Mouth foreshore	107
Fig. 4.18: Sections drawn across the Black Rock foreshore (Dip section A-A')	111
Fig. 4.19: Sections drawn across the Black Rock foreshore (Dip section B-B')	117
Fig. 4.20: Sections drawn across the Black Rock foreshore (Dip section F-F')	118
Fig. 4.21: Sections drawn across the Black Rock foreshore (Strike section C-C')	121
Fig. 4.22: Sections drawn across the Black Rock foreshore (Strike section D-D')	122
Fig. 4.23: Sections drawn across the Black Rock foreshore (Strike section E-E')	127
Fig. 4.24: Sections drawn across the Black Rock foreshore (Strike section G-G')	128
Fig. 4.25: 'Fence' diagram of the dip and strike sections across the Black Rock foreshore	131
Fig. 4.26: Diagrams for the restoration of deformation in the Black Rock foreshore	133
Fig. 4.27: Sections drawn across the Wanson Mouth foreshore (Dip section A-A')	137
Fig. 4.28: Sections drawn across the Wanson Mouth foreshore (Dip section B-B')	139
Fig. 4.29: Sections drawn across the Wanson Mouth foreshore (Dip section F-F')	142
Fig. 4.30: Sections drawn across the Wanson Mouth foreshore (Oblique section H-H')	144
Fig. 4.31: The folding in the two foreshores with the mean orientation of the fold envelope	147
Fig. 4.32: Diagrams for the two restoration models in the Wanson Mouth foreshore	148
Fig. 4.33: Dip-section F-F' across the two foreshores from this map work and the King map	151
Fig. 4.34: Three restoration models for the geological evolution of the two foreshores	155
Fig. 4.35: Sketches from Thompson and Cosgrove (1996) showing a plan view map of the deformation in the Rusey Cliff; and the cliff section with major faults at Rusey Cliff	159
<b>Chapter 5: Analysis of slump and 'early' deformation structural geometries in the Bude Formation</b>	
Fig. 5.1: Stratigraphic evidence for major thrust displacements	163
Fig. 5.2: Sketch of 'early' low-angle thrust stack at Lynstone and partial restoration	165
Table 5.1: Structural methods for studying palaeo-slope direction from analyses of slumps	167
Fig. 5.3: Criteria to define slump and 'early' structures in stacked beds	168
Fig. 5.4: Annotated photograph of channel incision and fill at Bude	169

Fig. 5.5: Photograph, sketch and stereonet of the Upton Slump Bed	170
Fig. 5.6: Geological map of the Black Rock Slump Bed (BRSB) at Lynstone	171
Fig. 5.7: Geological map of the BRSB with sedimentary logs at Black Rock	172
Fig. 5.8: Stereonet of restored slump raft folds in the BRSB at Lynstone	174
Table 5.2: Statistics of slump raft profile plane strike and hinge line elongation directions	174
Fig. 5.9: Fabric topology plots of profile plane strike versus axial plane strike, profile plane dip and interlimb angle for raft folds in the BRSB with a model for raft fold geometry	176
Fig. 5.10: Correlated sedimentary logs above the BRSB at Lynstone	176
Fig. 5.11: Stereonet of restored slump raft folds in the BRSB at Black Rock	179
Fig. 5.12: Fabric topology plots of profile plane strike versus axial plane strike, profile plane dip and interlimb angle for slump raft folds in the BRSB at Black Rock	180
Fig. 5.13: Photo-montage, sketch and stereonet of a strata-bound, high angle normal fault zone in a sandstone bed at Upton-Phillip's Point	183
Fig. 5.14: Photo-montage, sketch and sedimentary logs of high angle, reversed normal faults and syn- to early post-deformational strata at Upton	185
Fig. 5.15: Photograph of high angle, normal and reversed faults, Gulf of Corinth, Greece	185
Fig. 5.16: Stereonet of restored high angle, reversed normal faults at Upton	185
Fig. 5.17: Stereonet of restored mean high-angle normal faults with map of fault locations	186
Fig. 5.18: Photograph, sketch and stereonet of restored local structures at Northcott Mouth	188
Fig. 5.19: Photo-montage and sketch of deformed strata below a sandstone bed at Upton	190
Fig. 5.20: Restored sketches from Fig. 5.19 with a stereonet of the restored normal faults	191
Fig. 5.21: Stereonet of restored mean low angle faults with map of fault locations	192
Table 5.3: Table of comparison of different models for palaeo-slope analysis	194
<b>Chapter 6: Field evidence for deformation in sediment from the Bude Formation</b>	
Fig. 6.1: Photomicrograph and sketch of shale with bedding-parallel ankerite veins	197
Fig. 6.2: Sequentially-restored shale bed with deformed bedding-parallel ankerite veins	197
Fig. 6.3: Photograph and sketch of slump folded beds at Upton	199
Fig. 6.4: Photograph and sketch of an 'upright' chevron syncline at Upton-Phillips' Point	199
Fig. 6.5: Photograph and sketch of an 'inclined-to-recumbent anticline at Church Races	200
Fig. 6.6: Photograph and sketch of an 'inclined-to-recumbent' anticline at Phillip's Point	201
Fig. 6.7: Photograph and sketch of a thrust modified 'upright' chevron anticline	202
Fig. 6.8: Stereonet of mean 'upright' chevron fold and thrust data in the Bude Formation	202
Fig. 6.9: Stereonet of mean 'inclined-to-recumbent' fold data in the Bude Formation	203
Fig. 6.10: Photograph and sketch of a mud-injected, 'upright' chevron anticline	204
Fig. 6.11: Stereonet of mean data for mud injections cutting 'upright' chevron folds	204
Fig. 6.12: Photograph, sketch and stereonet of the North Widemouth 'inclined-to-recumbent' chevron anticline where a mud injection cuts the hinge and back-limb of the fold	206

**Chapter 7: Distinguishing folded structures in rock and sediment**

Table 7.1: Comparison of fold classes, dip isogon patterns and isogon relations to fold trace 209

Fig. 7.1: Idealised folds to calculate the layer thickness ratios 210

Fig. 7.2: Diagram plots for quantitative layer thickness analysis 210

Fig. 7.3: Dip isogon sketches of metamorphosed rock folds and slump folds 214

Fig. 7.4: Dip isogon sketches from slump folds and glacial till folds 215

Fig. 7.5: Dip isogon sketches of folds in model materials and migmatites 216

Fig. 7.6: Comparative dip isogon analyses of metamorphic rock folds with isogon logs 218

Fig. 7.7: Comparative dip isogon analysis of slump folds with isogon logs 218

Fig. 7.8: Comparative dip isogon analysis of glacial till and slump folds with isogon logs 219

Fig. 7.9: Comparative dip isogon analysis of migmatite and material folds with isogon logs 219

Fig. 7.10: Photo-montage and sketches of four Variscan progressive deformation fold events in the Bude Formation, including dip isogon analyses on all fold types and isogon logs 224

Fig. 7.11: Application of inverse thickness method for folded rock and folded sediment 228

**Chapter 8: Bude Formation lithification state during folding**

Table 8.1: Folds in the Bude and Crackington formations chosen for dip isogon analyses 232

Fig. 8.1: Map of Bude coastline showing the positions of numbered fold examples 233

Fig. 8.2: Photographs of the 5 Bude Formation fold types 235

Fig. 8.3 Dip isogon sketches of slump and ‘early’ folds (types: a-c) in the Bude Formation 237

Fig. 8.4: Dip isogon sketches of ‘upright’ chevron folds (type: d) in the Bude Formation 238

Fig. 8.5: Dip isogon sketches of 6 Bude Formation ‘inclined-to-recumbent’ and 2 Crackington Formation ‘recumbent’ chevron folds (type: e) 239

Fig. 8.6: Comparative dip isogon analyses of Bude Formation slump folds with isogon logs 240

Fig. 8.7: Comparative dip isogon analyses of chevron folds with isogon logs 240

Fig. 8.8: Syn-depositional and post-depositional dip isogon model 242

Fig. 8.9: Dip isogon analyses of Upton syn-depositional fold pair with isogon logs 243

Table 8.2: Table of lithification state for Bude Formation folded beds 248

Fig. 8.10: Interlimb angle versus axial plane angle in the Bude and Crackington formations 250

Fig. 8.11: Interlimb angle versus shear strain in the Bude and Crackington formations 250

Fig. 8.12: Diagram of mean south-directed shear strain in Bude Formation folds 251

Fig. 8.13: Application of inverse thickness method to Bude Formation chevron folds 253

Fig. 8.14: Two structural restoration models for application in the Bude Formation 255

**Chapter 9: Discussion**

Fig. 9.1: Sketches of the evolution of SW England prior to and during Variscan orogeny 259

Fig. 9.2: Simplified balanced cross-sections along the Pembrokeshire coast 260

Fig. 9.3: Sketch cross-sections of the Variscan deformation in SW England with Culm Basin cross-sections (from Shail & Leveridge, 2009), compared to sections from Warr (2002) 262

Fig. 9.4: Correlated Bude Formation sedimentary logs from Freshney et al (1972; 1979) 262

## Abbreviations

Fig. = Figure; circ. var. = Circular variance; st. dev. = Standard deviation;  
 $\mu\text{m}$  = micrometres; mm = millimetres; cm = centimetres; m = metres; dm = decimetres;  
 km = kilometres; e.g. = *exempli gratia* (for example); i.e. = *id est* (that is); et al = and others;  
 tan = Tangent; cos = Cosine; cot = Co-tangent;

## Acronyms

TM = Trade mark; RSG = Research study group; TSG = Tectonics Studies Group;  
 DDB = Dip domain boundary; IA = Interlimb angle; IC = illite crystallinity;  
 AMS = Anisotropy of magnetic susceptibility; SEM = Scattered electron microscope;  
 HREE = Heavy rare earth elements; LREE = Light rare earth elements;  
 FS = Fine grained sand; VFS = Very fine grained sand; BRSB = Black Rock Slump Bed;  
 LSB = Lynstone Slump Bed; SPS = Saturday's Pit Shale; TCS = Tom's Cove Shale;  
 EDINA = Edinburgh University Data Library; GEM = Google Earth<sup>TM</sup> montage;  
 DAM = Downslope (Average) Axis Method; GFPM = (Best-fit) Girdle to Fault Poles Method.

## Symbols

S = South; N = North; E = East; W = West; °C = degrees Celsius; h = Burial depth;  
 $\sigma_{\text{max}}$  or  $\sigma_1$  = Maximum principal stress;  $\sigma_{\text{min}}$  or  $\sigma_3$  = Minimum principal stress;  
 $\sigma_2$  = Intermediate principal stress;  $\sigma_M$  = Mean stress =  $P_C$  = confining (i.e. lithostatic) pressure;  
 $\sigma_{\text{eff}}$  = Effective stress;  $\sigma_{\text{BP}}$  = Bedding-parallel stress;  $\sigma_{\text{BN}}$  = Bedding-normal stress;  
 $\sigma_H$  = Horizontal stress;  $\sigma_V$  = Vertical stress;  $\sigma_N$  = Normal stress;  $\tau$  = Shear stress;  
 $P_f$  = Pore-fluid pressure;  $\lambda$  = Ratio of pore-fluid-to-lithostatic pressures (i.e. over-pressure);  
 $P_R$  = Rock lithostatic pressure;  $P_S$  = Sediment lithostatic pressure;  $P_W$  = Hydrostatic pressure;  
 $-e$  = Shortening degree;  $\gamma$  = Shear strain;  $l_0$  = Original bed length;  $l_1$  = Final bed length;  
 $t_0$  = Fold hinge thickness;  $t_\alpha$  = True layer thickness;  $n/t_\alpha$  = Inverse layer thickness;  
 $T_\alpha$  = Axial-parallel layer thickness;  $L_0$  = Original layer length between fold hinges;  
 $\alpha$  = Limb dip angle;  $\beta$  = Shear-modified limb dip angle;  $\omega$  = Fold axial plane dip angle;  
 $^\circ\Delta 2\theta$  = Angle between illite basal reflections;  $\pi$ -girdle = Fold profile plane great circle;  
 $d_{\text{max}}$  = (Normal) fault maximum displacement; L = (Normal) fault length;  $\beta$  = stretching factor;  
 $R_0$  = Vitrinite reflectance;  $S_N$  = Relative foliation age ( $S_0$  = bedding;  $S_1$  = first cleavage; etc.);  
 C = Carbon; S = Sulphur; O = Oxygen;  $\delta^{18}\text{O}$  = Ratio of isotopes: oxygen-18-to-oxygen-16;  
 $\delta^{13}\text{C}$  = Ratio of isotopes: carbon-13-to-carbon-12.

## Chapter 1: Introduction

### 1.1 Aims of the thesis and location of study

Fold deformation is common in sediment (e.g. slump folds) and in rock (e.g. tectonic fold belts). However, the geometric differences between folds in sediment and folds in rock are poorly understood. Thus, the general thesis aim was to study such folds in order to establish geometric methods to distinguish between folds in sediment and folds in rock.

The background to this study is that there is a need to understand how the mechanical state of deforming stacked layers (i.e. lithification state of beds) affects the resulting fold geometries (Waldron and Gagnon, 2011), with such folds being found in foreland basins and other fold-thrust belts. An improved understanding of the deformation conditions and processes in these regions is thus important for academic, as well as economic, reasons (e.g. hydrocarbon exploration). These active regions have been studied to understand their gravitational and tectonic structures (Jansma & Speed, 1993; Maltman, 1998; Nigro & Renda, 2004; Corredor et al, 2005), with a common structural feature being that syn-depositional deformation, especially folding, can occur in sediment (e.g. slump folds), penecontemporaneously with deformation at depth in more consolidated strata (e.g. fold belts) (Suppe, 1983; 1985; Hardy & Poblet, 1994).

The Late Carboniferous (Westphalian A-C) Bude Formation, Culm Basin, SW England (Reading, 1965; Freshney et al, 1972; 1979), was chosen as the study area due to the outcrop occurrence of both slump folds, clearly formed in sediment (Freshney et al, 1972), and the ‘archetype’ chevron folds of Ramsay (1974), assumed to have formed in rock. The study area comprises mainly, but not exclusively, an 8 km stretch of N-S trending, easily-accessible, well-exposed outcrops from Northcott Mouth (UK National Grid Reference: SS202087) to Wanson Mouth (SS195013) (Fig. 1.1) to test the general thesis aim. The rocks exposed here also provide an excellent analogue for both active and ancient foreland basins and fold-thrust belts.

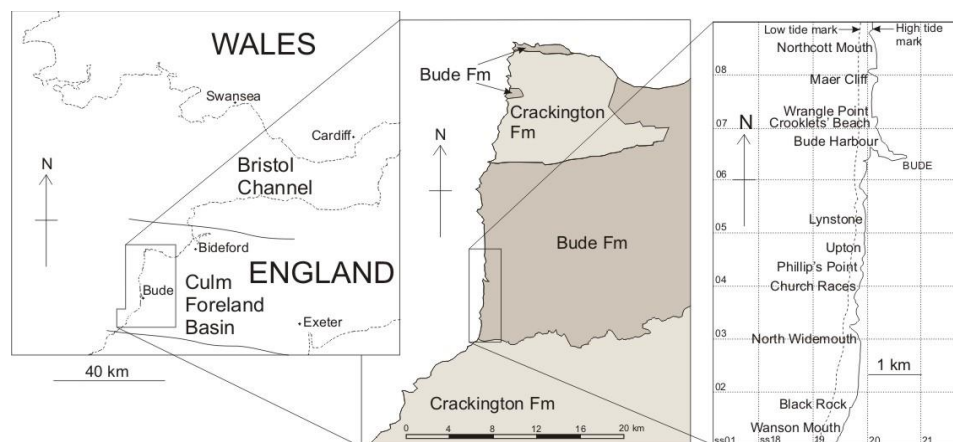


Fig. 1.1: Location map of SW England (left), a simple geological map of the Culm Basin (middle) and an inset map of the Bude coastal area (right) where fieldwork was undertaken (modified from Ordnance Survey<sup>TM</sup>/EDINA<sup>TM</sup> Digimap, 2010; Lloyd & Chinnery, 2002)

Thus, if it is possible to distinguish between folds in sediment and folds in rock, this would feed back into the Bude Formation lithification and deformation histories, and geological evolution, as the relative timings of lithification and deformation could be determined more precisely. To fulfil the general thesis aim, the burial and lithification states during Bude Formation folding were established using sedimentary-structural analyses (e.g. folded beds cut by mud injections or lying between ‘undeformed’ beds), and dip isogon and quantitative layer thickness analyses (Ramsay, 1967). However, an understanding of Bude Formation deposition relative to its deformation timing is required before undertaking the general thesis aim.

The sedimentary and structural evolution of the Bude Formation in the context of the Variscan deformation constitutes the specific thesis aim. At least six models for the Bude Formation depositional environment have been proposed by King (1971), Higgs (1984; 1986; 1991), Melvin (1986), Hartley (1991) and Burne (1995), whilst the structural evolution has been outlined previously by Ramsay (1974), Sanderson (1979) and also, Lloyd and Whalley (1986). Bude Formation deposition took place ahead of an evolving fold-thrust belt (Leveridge & Hartley, 2006; Shail & Leveridge, 2009). However, there are issues with the deformation timing with respect to both sedimentation and lithification. To fulfil the specific aim, an improved understanding was established of the Bude Formation depositional environment, from detailed sedimentary logging, as well as the timing and geometry of folds with respect to progressive Variscan deformation, using detailed structural mapping together with the Sanderson (1979) and Lloyd and Whalley (1986; 1997) chevron fold development methods.

In summary, the general aim was to investigate whether a geometric method is applicable to distinguishing the lithification state of folds during compressional deformation, including the chevron folds in the Bude Formation outcrops. The specific aim of this thesis was to investigate the sedimentary and structural evolution of the Bude Formation.

## 1.2 Definitions of sediment and rock

Underpinning this study of folding is the definition of the distinguishing characteristics of sediment and rock, including their mechanical state during folding, which is described here.

In sediment, individual grains are not “bound” together by cement, but can flow in a ductile manner. The grains act independently of, or lack “communication” with, each other, similar to how a bag of wet sand behaves (Borradaile, 1981). Thus, different parts of the same sediment unit may accommodate (e.g. compressional) stresses differently during folding. Also, sediment accommodates shear stresses poorly when fluid pressure is elevated (Hart et al, 2009).

In contrast, individual grains in rock are “bound” together (e.g. by cement), so that the grains only flow in a ductile manner at high temperatures (Weinburg & Mark, 2008). Thus, the grains exhibit dependence upon, or are in “communication” with, each other, so that rock units typically accommodate (e.g. compressional) stresses uniformly (e.g. during folding). Also, rock units can accommodate shear stresses relatively easily (Sanderson, 1979).

### 1.3 Thesis Description

Chapter 2 reviews the published literature on soft-sediment deformation structures and fabrics; fold mechanics observed in sediment and rock; and the history of Variscan orogenesis relevant to the Bude Formation.

Chapter 3 provides a re-assessment of the sedimentary facies, ichnofabrics, palaeo-flow indicators, petrography, mineralogy, carbon-sulphur geochemical analysis (Lloyd & Chinnery, 2002), diagenesis and stratigraphic evolution of the Bude Formation deposits between Northcott Mouth and Wanson Mouth (Fig. 1.1). From this re-assessment, models are discussed on the Bude Formation depositional environment.

Chapter 4 describes the detailed fieldwork undertaken on the faulted boundary (Widemouth South Fault) between the Bude and Crackington formations near Widemouth (SS195015) in the Black Rock and Wanson Mouth foreshore successions (Fig. 1.1). This fieldwork included mapping the two foreshore successions and also, studying and collecting data on the chevron folds in both foreshores, as well as the local structures that were previously not recognised within one of the foreshores. The apparently different deformation histories of these foreshores are explained using structural restorations.

Chapter 5 provides a review of the slumps and local structures that have been deformed by the chevron folds across 8 km of the Bude Formation outcrops between Northcott Mouth and Black Rock (SS202087-SS195015; see Fig. 1.1). From the relationships of the slumps and local structures, surrounding bedding and later overprinted folding, an improved explanation is proposed for the timing of slumping and local structural development with respect to both the Bude Formation deposition and compressional deformation history.

Chapter 6 presents additional field evidence for pre-lithification deformation from the slumps and local structures in the Bude Formation outcrops between Northcott Mouth and Black Rock (SS202087-SS195015; Fig. 1.1). This includes descriptions of ankerite veins, which are deformed by the local structures, and mud injections that cut the hinges of chevron folds.

Chapter 7 considers various geometrical methods from Ramsay (1967) that aid the interpretation of folded structures and fold deformation. In particular, specific fold profile geometric criteria are derived that distinguish between folds that developed in sediment and in sedimentary rock. These criteria provide a new approach to establishing the mechanical states of material during (fold) deformation.

Chapter 8 describes the application of the criteria derived in Chapter 7 to establish the mechanical state during (folding) deformation of the Bude Formation. The structures considered include the 'archetype' chevron folds of Ramsay (1974), from which a new understanding is gained of the relative timing of lithification during progressive Variscan tectonic deformation.

Chapter 9 assesses four models for the regional (SW England) Variscan deformation and places the Bude Formation deposits into the context of the Culm Basin structural evolution. This discussion leads onto the main conclusions that are provided in Chapter 10.

## Chapter 2: Literature review

Whilst fold deformation in lithified rocks has been studied extensively, there is a relative paucity of research into fold deformation in sediments. This is surprising given that delta toe fold-thrust belts, foreland basins and accretionary wedges contain large regions of folded sediment. As the general aim of this study is distinguishing between folding in sediment and in rock, this review concentrates upon deformation in clastic and inter-bedded clay-rich sediments, covering slump folds, the thixotropic nature of sediment and the styles of early post-depositional deformation. A review of compaction and cementation in clastic and clay-rich sediments follows, together with a comparison of the fabrics developed in deformed sediments with those in lithified rocks and models concerning formation of chevron folds. A review of fold-thrust belts and foreland basins introduces the brief overview of the Variscan deformation in SW England, which places the structures in the Culm Basin and particularly in the Bude Formation outcrops into a regional context, as set out in the specific aim of the thesis.

The Bude Formation coastal sections form the study area of this thesis and were chosen because of the opportunities to test whether different fold types developed during soft-sediment or post-lithification tectonic deformation. Due to its importance, the review of the literature on the depositional environment of the Bude Formation is deferred until Chapter 3.

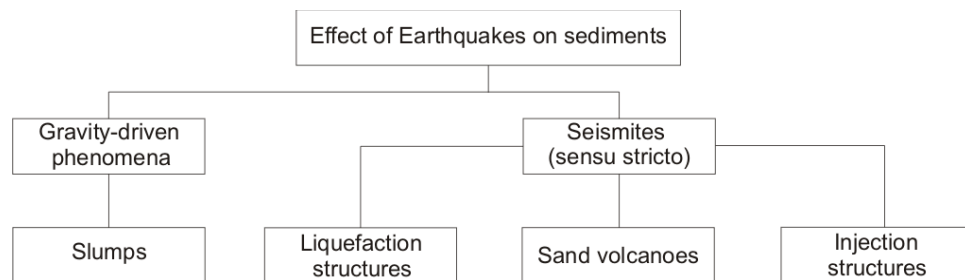


Fig. 2.1: Classification of structures formed by the effect of earthquakes on sediments (modified from Montenat et al, 2007)

### 2.1 Types of remobilisation structure

Remobilisation structures in sedimentary successions are important, not least as they may provide evidence for syn-depositional seismicity (Montenat et al, 2007) with two important types that form in sediment being recognised (after Montenat et al, 2007): (1) seismically-driven phenomena, or ‘seismites’ (summarised in Fig. 2.1); and (2) gravity-driven phenomena.

#### 2.1.1 Seismites

Seismically-driven phenomena and ‘seismites’ include: liquefaction structures; injection dykes; and sediment volcanoes (Montenat et al, 2007) and may be considered as types of soft-sediment deformation. Slumps are gravity-driven phenomena (Montenat et al, 2007) and may be produced by earthquakes (Owen, 1987) (see Fig. 2.1).

Both load compaction and seismic shocks can form liquefaction structures (Maltman & Bolton, 2003) in which sediment cohesion drops to zero (Maltman, 1998). Very fine to silt grained, water-saturated sediments are the most sensitive to liquefaction (Montenat et al, 2007), which may show flame and load structures, plus contorted internal stratification. Liquefaction in laminated sand can cause normal faulting and / or inclined folding, with large displacements accommodated where there is basal shearing (Owen, 1996).

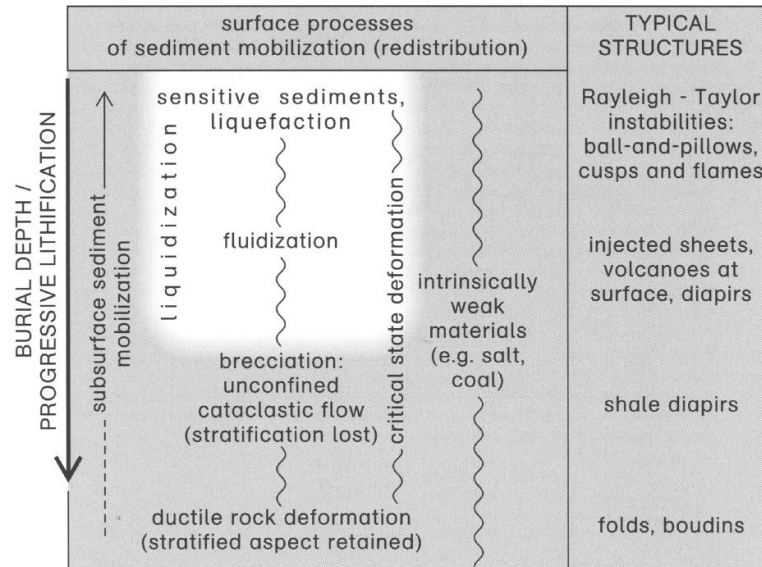


Fig. 2.2: Conceptual view of the range of sediment mobilisation processes. The untinted area indicates those processes, which are potentially most important in the generation of sediment mobilisation structures (from Maltman & Bolton, 2003)

Sediment volcanoes are centimetric to metric in scale and result from water-expulsion drawing up mud or sand through a fissure (Montenat et al, 2007). Mud volcanoes may occur either in tectonic regimes or from the “thermogenic cracking of organic-rich horizons” (Fig. 2.3; Deville et al, 2003; 2006). Sand volcanoes in sand-rich beds occur due to ‘independent’ particulate flow (Craig, 1997), with controls on their formation including: (1) rate of water expulsion; and (2) amount of sediment compaction (Burne, 1970).

Sediment injections occur due to fluidisation where rapid expulsion is focussed along pipe-like structures (Maltman & Bolton, 2003) (Fig. 2.2).

### 2.1.2 Gravity-driven phenomena

Gravity-driven phenomena include slumps, slides and truncation scars, with debris and grain flows plus turbidity currents also included by Montenat et al (2007). Thus, a variety of mechanisms cause sediment to move down a slope, which can be as shallow as  $0.14^\circ$  (e.g. Mississippi delta top; Prior & Coleman, 1978; Crans et al, 1980). On shallow slopes, sediment is often remobilised above over-pressured or under-compacted muds, especially in shallow and marginal marine settings (Elliott & Ladipo, 1981). These movements require that:

1. Remobilised sediment was at or within a few metres of the palaeo-surface;
2. Slopes are sufficiently steep for unstable sediment to be transported.

### Slump generation

Liquefied slump beds are common gravity-driven phenomena, with extension at the rear, compression at the front and shear structures throughout (McClay, 2004; Alsop & Marco, 2011). Slumps are a common fold deformation type in sediments where there is a slope. Their generation may coincide with fault movement and the transportation of both turbidites and debrites (Wignall & Best, 2000; Fig. 2.3). Likely triggers for slumps are: (1) a seismic event (Strachan & Alsop, 2006); (2) fluid over-pressure and liquefaction (Maltman & Bolton, 2003); and (3) sudden deposition over an unstable surface (Owen, 1987).

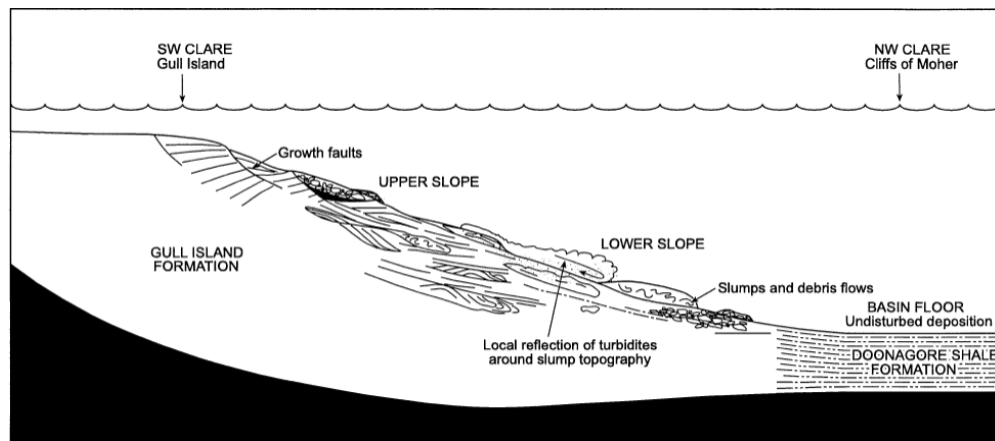


Fig. 2.3: Model of slump and turbidite generation in the Gull Island Formation, western Ireland, highlighting structures and depositional elements on the slope (from Wignall & Best, 2000).

### Palaeo-flow direction from slump folds

Palaeo-slope direction is the main control on the slump fold vergence direction (Woodcock, 1976; 1979; Wignall & Best, 2000; Strachan & Alsop, 2006; Fig. 2.3). Further slump fold geometric features, such as hinge line elongation direction, may also be employed to describe the palaeo-slope direction. This is useful in areas such as the Early Palaeozoic Anglo-Brabant fold belt where slump folds have been tectonically-deformed (Debacker et al, 2006).

### Analogies with landslides, avalanches and glaciers

Woodcock (1976) described slump beds as deposits that “retain their original sedimentary structures” and where deformation has the strongest influence on structural style. In contrast, Middleton and Hampton (1973) described sediment ‘gravity flows’ as the disaggregation and redeposition of sediment and other materials (e.g. turbidites, landslides, avalanches, etc.). In water-saturated sediment, deformation takes place in a series of thin shear zones (Hart et al, 2009). Sub-glacial sediments show recumbent folds, boudinage and augen

(Hart, 1999), as well as rotated clasts (Jeffery, 1922). However, ice and sediment have different rheological properties, resulting in slightly different behaviours in the two layers (Hart, 1999).

### 2.1.3 Deformation in slumps

Gravity-induced, down-slope slump movement involves extension at its ‘head’; contraction at its ‘toe’; and strike-slip faulting at its sides (Fig. 2.4a). A useful conceptual model for slumping is as a deformation ‘cell’, in which movement occurs as a sheet along an underlying detachment (Farrell, 1984; Debacker et al, 2009; Alsop & Marco, 2011). During slump movement, extension propagates backwards and upslope, whilst contraction occurs in the opposite direction (Fig. 2.4a), thereby causing increased incision into the underlying strata. As the slump movement slows and dewatering occurs along normal faults, cessation takes place (Farrell, 1984). This causes extension to concentrate onto one fault, whilst contraction may propagate backwards and upslope in a ‘piggy-back’ manner (Fig. 2.4b; Alsop & Marco, 2011).

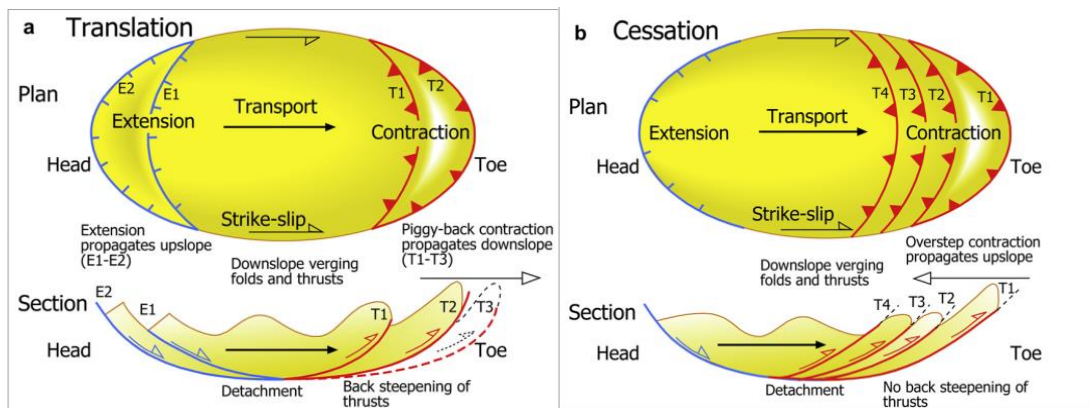


Fig. 2.4: Schematic plan-view (top) and cross-section (bottom) of contraction, extension and strike-slip structures generated in a slump during its translation (a), and subsequent cessation (b). The direction of transport associated with a ‘flow’ from left to right is shown by a black arrow, with sequential contractional thrusts (T1, T2, etc.) in red at the slump ‘toe’ and extensional faults (E1, E2) in blue at the ‘head’ (from Alsop & Marco, 2011)

### Model of structural evolution in slumps

The deformation ‘cell’ model provides a useful but simplified idea of the structural evolution that occurs during slumping. A more detailed model of this evolution is given by Alsop and Marco (2011) and is displayed in Fig. 2.5. This model is divided into five stages:

1. Initiation – density-driven fold initiation and / or horizontal shortening occurs, generating ‘upright’ buckle folds with a coaxial vertical movement or ‘flow’ of material into the hinges of the developing slump folds (Fig. 2.5a);
2. Translation – buckle folds increasingly verge down-slope until the lower limbs fail via thrusting. This results from non-coaxial down-slope, gravity-induced shear deformation and causes slump fold amplification (Fig. 2.5b-c);

3. Cessation – horizontal shortening continues and contraction-driven fold growth takes place above the slump thrusts, causing new buckles to develop before ‘lock-up’ of the slump folds (Fig. 2.5d; Alsop & Marco, 2011).
4. Relaxation – small-scale secondary slumping from slump anticlinal crests into synclinal troughs. This additional progressive remobilisation event, of Alsop and Marco (2011), is driven by non-coaxial horizontal movement of the slump folds (Fig. 2.5e).
5. Compaction – ‘flattening’ of the slump folds, leading to ‘mushroom’ or ‘box’ fold development. A further event, of Alsop and Marco (2011), that results from vertical shortening of the slump folds due to the overburden as sedimentation continues (Fig. 2.5f).

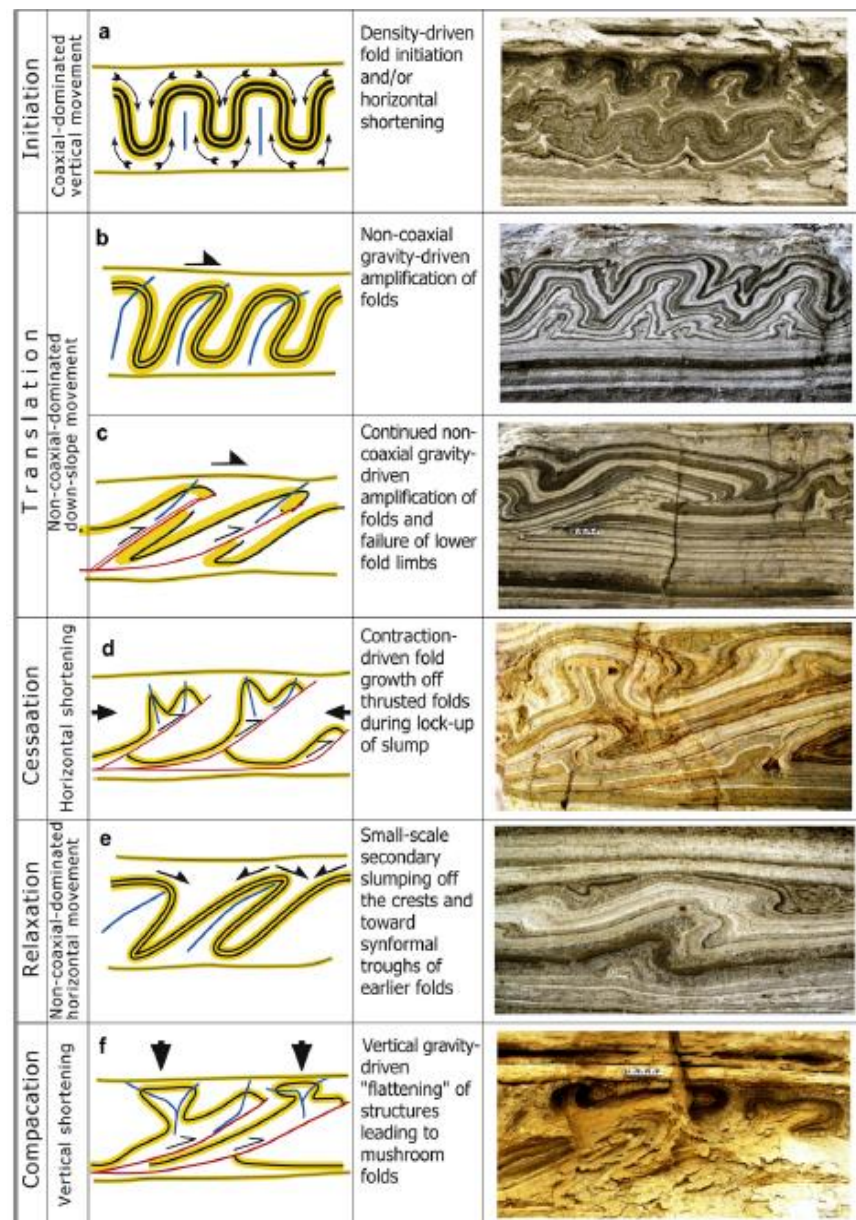


Fig. 2.5: Schematic drawings and photographs from the Dead Sea Basin, Israel, of structures generated during slump sheet initiation (a), translation (b & c), cessation (d), relaxation (e) and compaction (f). Folded beds are shown in yellow, while axial planes (blue) and thrusts (red) are also highlighted together with possible deformation styles (from Alsop & Marco, 2011)

### 2.1.4 Sub-surface sediment mobilisation

Another way to classify deformed sediments is via sub-surface sediment mobilisation (van Rensbergen et al, 2003), which include (Fig. 2.6): ‘flame’ and load structures (Owen, 2003), sand injections (Jolly & Lonergan, 2002) and mud volcanoes (Deville et al, 2003; 2006). The mobilisation is caused by pore-fluid over-pressures and elevated hydraulic gradients (Fig. 2.2; Maltman & Bolton, 2003), with the magnitude and duration of the force generating the structures, controlling the amount of deformation accommodated (Owen, 2003).

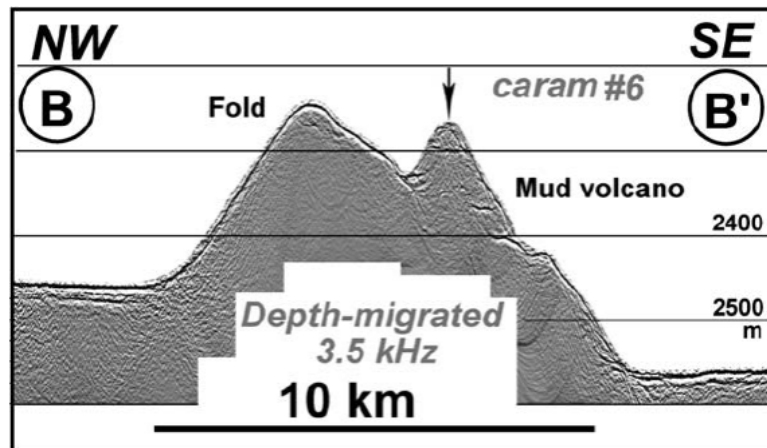


Fig. 2.6: Seismic section through a large fold in the Barbados accretionary wedge, showing a cross-cutting mud volcano (soft-sediment compressional deformation) (from Deville et al, 2006)

### 2.1.5 Effect of compression on the remobilisation of sediment

Liquefaction causing a temporary loss of sediment strength in slump folds can occur at very high shear stresses (Maltman, 1984), in which very high shear strains are accommodated in the slump folds. This causes the development of tight, ‘recumbent’ slump fold axial planes (Strachan & Alsop, 2006).

Another control on the intensity of remobilisation structures, is the proximity of the structure to either a local or a regional slope (Del Pino-Sanchez, 2006), where deposition of a thick bed, a storm event or earthquake can induce temporary liquefaction (Owen, 1987).

## 2.2 Deformation in sediment

As a general aim of the present research project is to establish the mechanical or lithification state of the Bude Formation deposits during fold deformation, published models for the mechanical behaviour of deforming sediments are highly relevant and are discussed below.

### 2.2.1 Review of soft sediment deformation theory

In water-saturated sediment, deforming material can be described as a non-Newtonian, pseudo-plastic or thixotropic fluid (Harris, 1977; Vigneresse, 2004). A shear stress ( $\tau$ ) imposed

upon a thixotropic fluid, causes a shear strain ( $\epsilon$ ), which is accommodated in the fluid (Fig. 2.7). Thixotropic fluids have no yield stress and decrease in viscosity ( $\eta$ ) with increasing shear stress ( $\tau$  - MPa) and strain rate ( $d\epsilon/dt$  – per second). This is illustrated in the rheogram (Fig. 2.7) of  $\tau$  vs.  $d\epsilon/dt$ , which has a flattening curve at high stresses for thixotropic fluids (Harris, 1977).

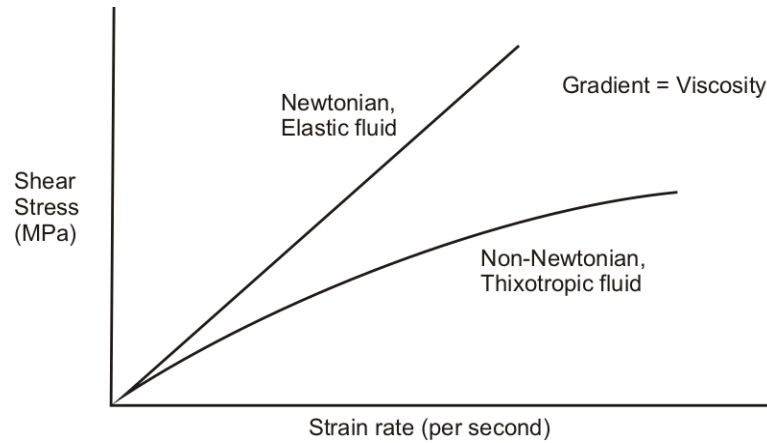


Fig. 2.7: Shear response to Newtonian (linear) and non-Newtonian (non-linear) fluids (modified from Price & Cosgrove, 1990), illustrating how non-Newtonian thixotropic fluid viscosity decreases with accommodation of increasing shear stress over time

In thixotropic fluids, internal deformation occurs “under an increasing duration of shearing stress”, causing separation of a “disperse phase in a multi-phase system” (Harris, 1977) within water-saturated sediment (Vignerresse, 2004). The grain movement may be described as ‘controlled’, with the partial cohesion between the grains being influenced by temperature and confining pressure (Craig, 1997). As the water-saturated sediment grains are sheared, they rotate either through the shearing direction (Glen et al, 1957) or into the shearing direction (Hooyer & Iverson, 2000). When the shear stress ( $\tau$ ) reduces, the structure of an ‘ideal’ thixotropic fluid will rebuild “at the same rate as the break-down process” (Harris, 1977). However, if structural recovery does not occur, the thixotropic fluid may accommodate the additional strain and / or expel fluids (after Waldron & Gagnon, 2011).

### **Plasticity of fine-grained sediment**

Fine-grained, clay-rich and water-saturated sediment has a plastic mechanical state, enabling it to undergo a permanent change in shape or size, without fracturing at stresses that exceed the elastic limit of the sediment (after Fossen, 2010). During deformation, plastic sediment may undergo strain-hardening and / or strain-softening (but not simultaneously) prior to a transition to stable sliding (Craig, 1997). Also, ‘plastic’ sediment does not have constant frictional properties (Lohrmann et al, 2003) but instead, the grains slide relative to each other whilst the layer maintains cohesion (Craig, 1997). Plastic behaviour occurred in the Neogene Chilean forearc syn-sedimentary deformation (Houston et al, 2008) and is linked to the

development of layer-bound, polygonal extensional faults, for example in the Palaeogene North Sea fine-grained deposits (Cartwright & Dewhurst, 1998).

### 2.2.2 Structures generated in early post-depositional deformed strata

Early post-depositional structures are described as having developed in sediment (Nigro & Renda, 2004; Lin et al, 2006). In the example from the Pliocene Mount Corvo beds, SW Sicily, Italy, by Nigro and Renda (2004), the deformed strata consist of stratigraphically-lower, pre-deformational beds that have a consistent palaeo-slope direction in which beds have similar thicknesses and slump folds verge in the same direction. However, the stratigraphically-higher, syn-deformational (growth) beds thicken onto the fold limbs and the slump folds verge away from the growing anticlinal hinge (Fig. 2.8). These criteria can be used to estimate the relative timing of deformation with respect to deposition. Also, the fold growth geometry depends on the sediment cohesion and angle of internal friction (Nigro & Renda, 2004).

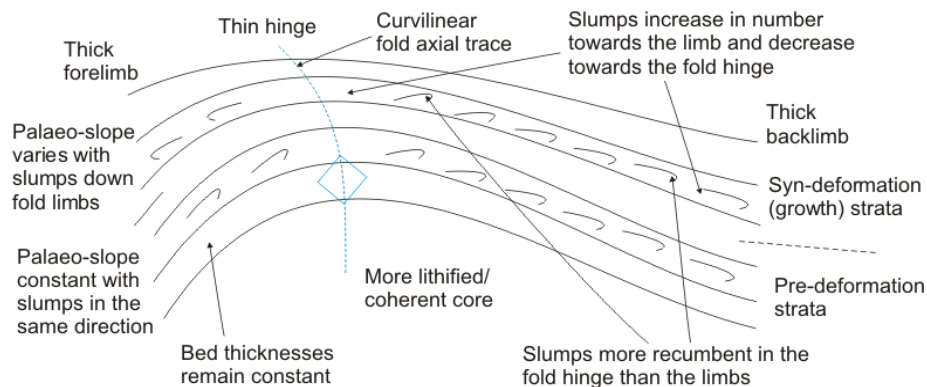


Fig. 2.8: Schematic section comparing fold deformation and palaeo-slope directions from a growing fold in sediment during deposition (modified from Nigro & Renda, 2004)

### 2.2.3 Effects of syn-depositional and tectonic deformation on deposition

In syn-depositional compressional settings, depositional patterns are affected by the growing structures (Burbank & Anderson, 2001). For example, growth geometries in fault-related folds may exhibit “fanning of limb dips, similar to those of growth strata” (Connors & Shaw, 1999). This apparent ‘fanning’ may be caused by local onlapping and toplapping unconformities, coupled with both compaction and diagenetic processes in the growth strata (Connors & Shaw, 1999). These onlapping unconformities may be related to periods of folding (after Shaw et al, 2004) and / or thrust deformation (Zoetemeijer et al, 1992; Fig. 2.9).

As fold limbs or thrust planes rotate during deformation, the position of each onlap truncation is highly variable (Shaw et al, 2004). As a fold grows and / or a thrust propagates during deposition, a thinned hinge succession or unconformity forms above the anticlinal crest. If thrust activity continues, this may lead to hinterland migration of the basin depo-centre (Zoetemeijer et al, 1992; Mouthereau et al, 2007; Mosar et al, 2010; Fig. 2.9).

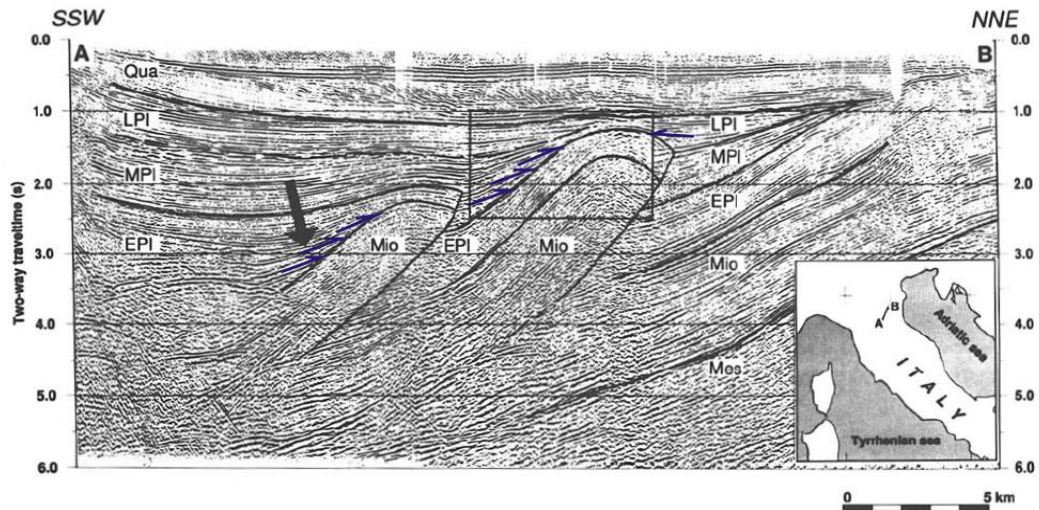


Fig. 2.9: Migrated seismic reflection profile through the Ferrara-Romagna thrust arc (northern Apennines, Italy) along profile A-B in inset map. (Mes = Mesozoic; Mio = Miocene; EPI = Early Pliocene; MPI = Middle Pliocene; LPI = Late Pliocene; Qua = Quaternary). Angular unconformities in Pliocene to Quaternary sediments formed by tectonic movement (purple arrows added as onlap reflectors). The black arrow shows a reflection truncation due to new thrust activation, which is also highlighted in the box (modified from Zoetemeijer et al, 1992)

#### 2.2.4 Similarities and differences between slump and tectonically-generated folds

Tectonically-generated folds have been compared to slump folds by many authors (Wilhelm & Ewing, 1972; Piper et al, 1973; McClay, 2004; Waldron & Gagnon, 2011) in order to define criteria that distinguish them in the field and in seismic sections, such as for the slumps in the Late Silurian Montgomery Trough, Wales (Woodcock, 1976). These slumps have both geometric similarities and differences to tectonically-generated folds, as described below.

##### Similarities

The two types of fold structure are initiated by a buckling process and generate similar structural styles, with the hinge line length, wavelength and amplitude all related to each other (Woodcock, 1976). Their hinge line length-to-wavelength ratios are described by a lognormal distribution (Hudleston, 1973), which suggests that these fold structures grow via a strain interaction process of periclinal linkage (Dubey & Cobbold, 1977). Also, common axial micro-fold lineations and axial planar spaced cleavage are observed in both cases (Tobisch, 1984; Engelder & Marshak, 1985; Jansma & Speed, 1993).

##### Differences

The differences between the two types of fold structure are as follows:

1. Gravity-induced folds appear in isolation, being underlain and overlain by 'undeformed' sediment, whilst 'tectonic' folds affect all the deposited beds (McClay, 2004);

2. Most slump folded layers have class 1C dip isogons (Woodcock, 1976), whilst folded layers in rock have class 1B (more coherent layer) and class 3 (less coherent layer) dip isogons (Ramsay & Huber, 1987);
3. Slump folds have much tighter interlimb angles (mean = 20°; Woodcock, 1976) than ‘tectonic’ folds (mean = 60°; Price & Cosgrove, 1990);
4. Syn-depositional (growth) folds are found within compressionally-deformed sediment (Zoetemeijer et al, 1992; Shaw et al, 2004; Corredor et al, 2005).

### 2.3 Structures, fabrics and compaction in deforming sediments and rocks

Distinct structures and fabrics develop when sediments are deformed. These features are observed in accretionary wedges (Maltman, 1987) and include:

1. Planar deformation bands, which are oblique to the bedding and with minor displacement accommodated;
2. Faults and shear breccia, which have large displacements and may form conjugate fault sets;
3. Scaly fabric or preferred orientation foliation of clay minerals, which is analogous to closely-spaced cleavage planes;
4. Web structures that are a ‘honey-comb’ of shear zones developed on sandy bedding planes;
5. Compression-like shear structures via mineral dissolution, veins and shear strain localisation, especially in finer-grained sediments (Shin et al, 2008).

#### 2.3.1 Sediment shear and fault zones

Sediment grain alignments occur where water contents are greater than 25% (Arch et al, 1988), via rotation and translation, either through the shear plane (Jeffery, 1922) or into and remaining within the shear plane (Hooyer & Iverson, 2000). Each sediment type accommodates shear strain rates differently (Maltman, 1987), with the level of shear stress having “little influence on the geometry of the shear zones” (Arch et al, 1988).

In addition, sediment cohesion decreases with increased water content (Maltman, 1987) so that at water contents above 45%, clay weakens and ‘flows’ pervasively, creating short narrow displacement ‘zone’ arrays (Maltman, 1987; Roberts & Hart, 2005). Shear zones only occur in sediments that display strain softening after the ‘peak’ strength is reached and where “particle volume reduction causes a decrease in horizontal stress”, which is a process that leads to “internal shear failure conditions and potential shear strain localisation” (Shin et al, 2008). Also, in sand, fault propagation and early back-thrusting occur at higher Young’s Modulus values (**E**), with wider fault zones occurring at higher dilation angles ( $\phi$ ) (Lin et al, 2006).

#### 2.3.2 Syn-depositional normal faulting

Syn-depositional normal fault planes contain features such as clay-smearing, grain mixing, a ‘damage zone’ containing deformation bands and also, precipitation of iron oxide or

carbonate (Bense et al, 2003; Caine & Minor, 2009). In examples from the Netherlands (Bense et al, 2003) and New Mexico, USA (Caine & Minor, 2009), it was found that:

1. Particulate flow is the main deformation mechanism during fault development;
2. Large fluctuations in hydraulic conductivity occur across the fault ‘damage zone’;
3. Early clay smearing results in the ‘damming’ of groundwater flow across the faults, promoting a flux of over-saturated fluids through fault-entrained sand-rich sediments.

### 2.3.3 Slump fabrics

In slump folding, deformation occurs whilst the material is still sediment. This can include foliation, with preferred grain alignment and silt-sand domains, which is sub-parallel the axial plane (Tobisch, 1984). These features are generated by a modified version of slump-induced grain rotation (after Jeffery, 1922), which occurs during water expulsion. This causes the slump fold hinge zones to compact (Tobisch, 1984) but without veins exploiting the fractures, so long as the slump does not undergo any later tectonic deformation (McClay, 2004). Folds within slump beds may also include: localised deformation on syn-sedimentary normal faults; convolute laminations; ‘ball-and-pillow’ structures; dewatering structures; sediment volcanoes; truncation by over-lying beds; occasional burrowing by organisms; undeformed clasts or fossils; and over-printing by pore-filling cement.

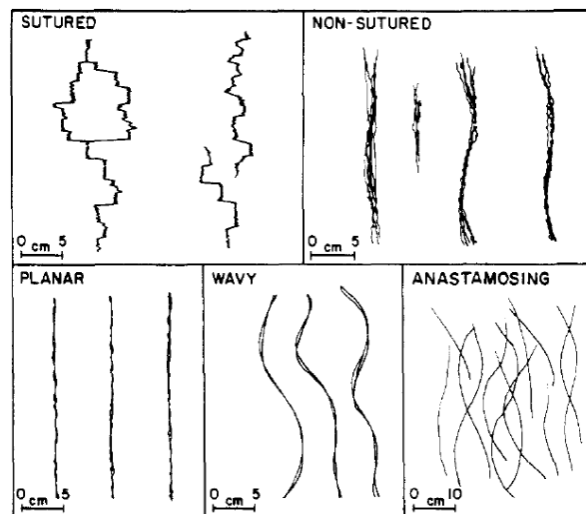


Fig. 2.10: Five patterns of disjunctive cleavage cutting beds (from Engelder & Marshak, 1985)

### 2.3.4 Axial-planar cleavage fabrics in phyllosilicates

There are numerous types of cleavage and schistosity, whose development is related to temperature (i.e. crustal depth) and lithology (i.e. phyllosilicates). In this thesis, only the development of cleavage is considered because schistosity, which is formed at about 350-375°C during high-grade metamorphism, does not occur in deformed sediment (Fossen, 2010). Cleavage forms via grain rotation, preferred orientation in the growth of minerals and pressure solution of solvent minerals. Where cleavage forms at shallow depths, ‘cohesive material-water

interaction' can form spaced cleavage planes in four ways (Price & Cosgrove, 1990): (1) pressure solution; (2) free-face dissolution; (3) fluid film diffusion; and (4) fluid advection via circulation. From this, five disjunctive cleavage types may be formed: (a) sutured; (b) non-sutured; (c) planar; (d) wavy; and (e) anastomosing (Fig. 2.10; Engelder & Marshak, 1985).

Non-tectonic compaction cleavage (Fig. 2.11a) forms in shale via reorientation of mineral grains and pore-space reduction. The primary foliation ( $S_0$ ; i.e. bedding) is reworked and dissolution may occur (Fossen, 2010). Grain dissolution causes a (pressure) solution cleavage to develop as first recognised by Sorby (1853). A tectonic-related disjunctive cleavage develops in shales that experience horizontal shortening due to horizontal maximum compressional stress ( $\sigma_{\max}$ ). Pressure solution in shales is important where grain dissolution causes clay minerals to concentrate, re-orientate and fracture along foliation planes, forming pencil cleavage (i.e.  $S_1$  foliation; Fig. 2.11b). Pencil cleavage also develops where there are local or regional changes in the stress field (Fossen, 2010).

Slaty cleavage develops where tectonic deformation continues to take place (Fosson, 2010; Fig. 2.11c). This cleavage type has closely-spaced domains, consisting of axial planar bands of less well-cleaved quartz-rich (Q) and more well-cleaved phyllite-rich or clay-rich (P) material (Borradaile et al, 1982). This low-grade metamorphic cleavage involves pressure solution, which may form fans where the planes converge towards the inner arc in less coherent pelites and slates, with the reverse in more coherent psammities and quartzites (Price, 1966). The cleavage plane spacing is defined using observations of the fabric and how this corresponds to illite crystallinity measurements (i.e. the difference between first (and second) order illite basal reflections ( $^{\circ}\Delta 2\theta$ ); Arkai et al, 2003). The spacing defined by Price and Cosgrove (1990) is:

1. Scaly, where domains can be observed in hand specimen or outcrop, which correspond to illite crystallinity (IC) values of  $> 10^{\circ} \Delta 2\theta$  (i.e.  $< 5\text{km}$  burial);
2. Slaty, where domains can only be observed using in thin section, which corresponds to IC-values of  $< 10^{\circ} \Delta 2\theta$  (i.e.  $> 5\text{ km}$  burial).

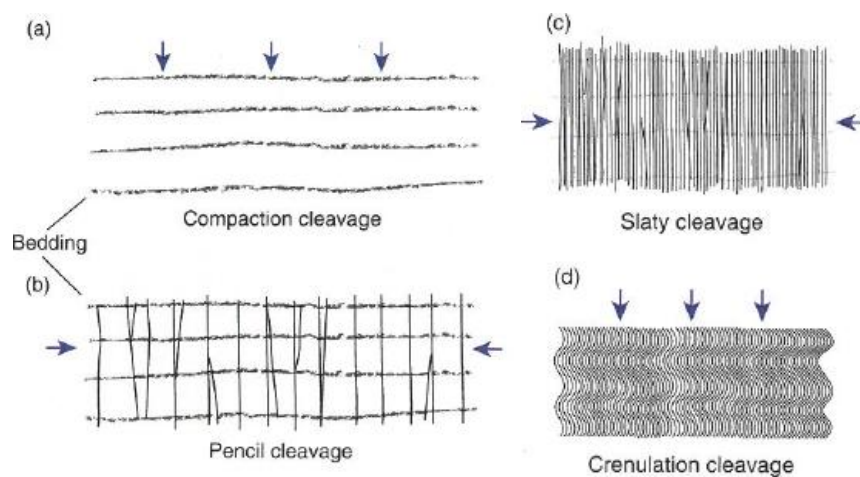


Fig. 2.11: Cleavage development in shale under non-metamorphic and low-grade metamorphic deformation. Maximum stress directions ( $\sigma_{\max}$ ) are indicated by the arrows (from Fossen, 2010)

Where the tectonic cleavage is affected by a change in the local or regional stress direction, a later cleavage may develop (i.e.  $S_2$  foliation or higher) as a crenulation cleavage, usually as a refolding of earlier phyllosilicate-developed cleavage (Fossen, 2010; Fig. 2.11d). This is described as “a set of closely-spaced, secondary, planar domains that create mechanical anisotropy in a cohesive material without any loss of cohesion” (Bayly et al, 1977).

### **Cleavage development in sediment and diagenetically-altered rock**

Where fold deformation occurs in slumps (Tobisch, 1984), water-saturated sediment (Maltman, 1998) or diagenetically-altered rock, a cleavage fabric develops in ‘preferred orientation’ zones (Engelder & Marshak, 1985). The zones result from the exploitation of fluid-escape pathways, either by mechanical grain rotation (Beutner, 1980; Engelder & Marshak, 1985) or by ‘independent’ particulate flow in which grains slide past each other (Borradaile, 1981; Craig, 1997). These grain movements are aided by:

1. “High fluid pressures, which may decrease the effective stress across grain boundaries” (Engelder & Marshak, 1985), leading to a scaly cleavage (Jansma & Speed, 1993);
2. Poor grain cohesion with high viscosity or ductility of clay grains (e.g. kaolinite; illite; etc.).

### **2.3.5 Sediment compaction, cementation and over-pressure**

Folding in sediment takes place at much shallower depths and nearer the surface than in lithified rock, making the roles of compaction and cementation important during deformation.

In shales, where there are no over-pressure effects during burial, there is a consistent relationship between porosity (in percentage) and vertical effective stress (in MPa) (i.e. burial depth – in km; Zoback, 2008; Fig. 2.12). Weller (1959) envisaged four stages of compaction: (1) Initial dewatering; (2) Closer grain packing, which increases sediment cohesion; (3) Pore space infill by clay minerals, which increases sediment cohesion; and (4) Deformation of clay minerals by mechanical compaction until all porosity is removed.

Where sands are uncemented, diagenetic change is limited under shallow burial. However as burial increases, porosity decreases and grain contacts increase in number and complexity (Palmer & Barton, 1987), forming a pressure solution of detrital quartz and consequently increasing amounts of cementation. However, where there is a high percentage of clay in the matrix, this retards pressure solution cementation (Molenaar, 1986).

In cemented material, there are strong bonds between grains. The binding cement may be either quartz, which precipitates at temperatures greater than 80°C (Walderhaug, 1994; Lander et al, 2008), or carbonate, which precipitates at surface temperatures (McKay et al, 1995; Caine & Minor, 2009). Where the sediment undergoes deformation, it becomes increasingly strain-hardened as the amount of cement in the pore spaces increases (Lambe & Whitman, 1969; Schofield & Wroth, 1978). However, if the normal stress ( $\sigma_N$ ) is sufficiently high to cause the cement to yield, the viscosity of the cemented sandstone reduces with

increasing stress (Fig. 2.7). This in turn, reduces the stress-dependence of the sediment stiffness, causing strain-softening and the material to return to being low-coherence sediment (Schofield & Wroth, 1978).

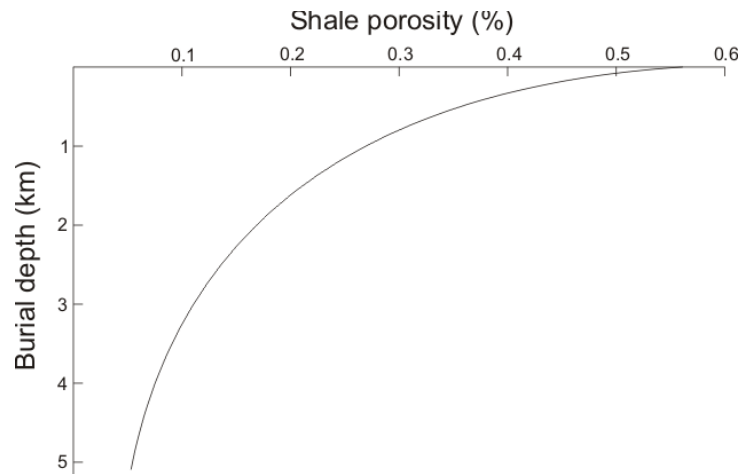


Fig. 2.12: Diagram exhibiting the ideal relationship between shale porosity and burial depth without over-pressure effects (modified from Zoback, 2008)

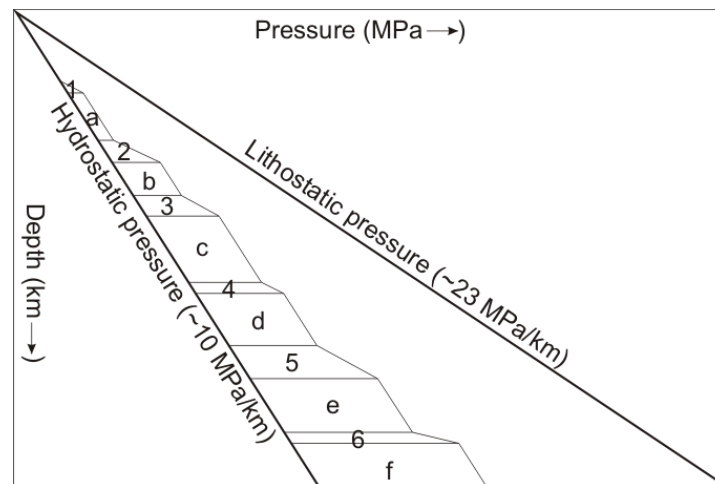


Fig. 2.13: Simplified sketch of over-pressure conditions in an oil well, showing six isolated stratigraphic compartments (a-f), which maintain hydrostatic pressure internally but which are each separated by a laterally-continuous seal (1-6) that increases pore pressure towards lithostatic pressure (after Zoback, 2008)

Pore-fluid pressure is important in both cemented and unbound sediment. Hydrostatic pressure ( $P_W$ ) occurs in sediment and rock where the pore and fracture networks are open to the surface and inter-connected, usually increasing with depth at a rate of 10 MPa/km (Zoback, 2008). However, if there are stratigraphic ‘compartments’ with poorly-connected pore and fracture networks, hydrostatic pressure can increase towards the lithostatic pressure of the sediment ( $P_S$ ) or rock ( $P_R$ ). This can occur in shale beds that are inter-bedded with more permeable sands and sandstones, generating over-pressure conditions, which move the stress

system towards failure (Zoback, 2008). This is illustrated in a simplified sketch example from an oil well (Fig. 2.13; after Zoback, 2008) where hydrostatic pressure ( $P_w$ ) is maintained internally in each of the six sandstone ‘compartments’, which are separated by laterally-continuous shale seals that increase the overall pore pressure towards lithostatic pressure ( $P_c$ ).

Bedding-parallel ‘beef’ veins form in sediment during over-pressure conditions. Usually, the veins grow from the centre to the edge, giving them an antitaxial texture (Rodrigues et al, 2009). Such veins occur often in shales and may be formed from quartz, calcite or even ankerite. Over-pressures that generate ‘beef’ veins may be due to either seismicity (Brothers et al, 1996), hydrocarbon generation in organic-rich muds (Rodrigues et al, 2009), or dilation during pre-buckle shortening (Price & Cosgrove, 1990).

## 2.4 Fold mechanics

Many authors have described chevron fold development in multi-layered sequences where the layers have contrasting competence (Ramsay, 1974; Tanner, 1989; Yang & Gray, 1994; Bazalgette & Petit, 2007; Bastida et al, 2007). This section contains an overview of the mechanics of fold initiation and buckling, including ‘forced’ folding, in multi-layered inter-bedded successions from both sediment and rock. It provides the background for a detailed review of chevron fold development.

### 2.4.1 Fold development stages

Based upon both theoretical and physical modelling (Ramsay, 1974; Price & Cosgrove, 1990), the development stages of buckle folds are (Fig. 2.14):

1. Pre-buckle shortening resulting from layer-parallel compression, inducing homogeneous layer thickening;
2. Buckling occurring at (relative) layer irregularities;
3. Buckling creating unstable contraction (i.e. deformation resistance decreases due to strain-softening, whilst the deformation rate increases);
4. Fold amplification until geometric or mechanical constraints cause strain hardening;
5. Fold deformation ‘locks-up’ at interlimb angles of about 60°.

### 2.4.2 Pre-buckle shortening

Parallel or sub-parallel compression of layers produces a period of homogeneous shortening before the initiation of buckle folding. The rate at which pre-buckle shortening occurs depends upon the stratigraphic stacking pattern, the confining pressure ( $P_c$ ) and the compressive strain-rate ( $de/dt$ ) (Price & Cosgrove, 1990).

The pre-buckle strain can be estimated by measuring the period during which a slow strain-rate operated (Price & Cosgrove, 1990). Accommodation of this strain can lead to the formation of either a pressure solution cleavage under metamorphic conditions or mechanically-

rotated alignment cleavage in sediments and diagenetically-altered rock (Engelder & Marshak, 1985). The transition to multi-layer buckling occurs via deformation in relatively thin coherent beds. This may generate small folds on larger-scale folds limbs (Price & Cosgrove, 1990).

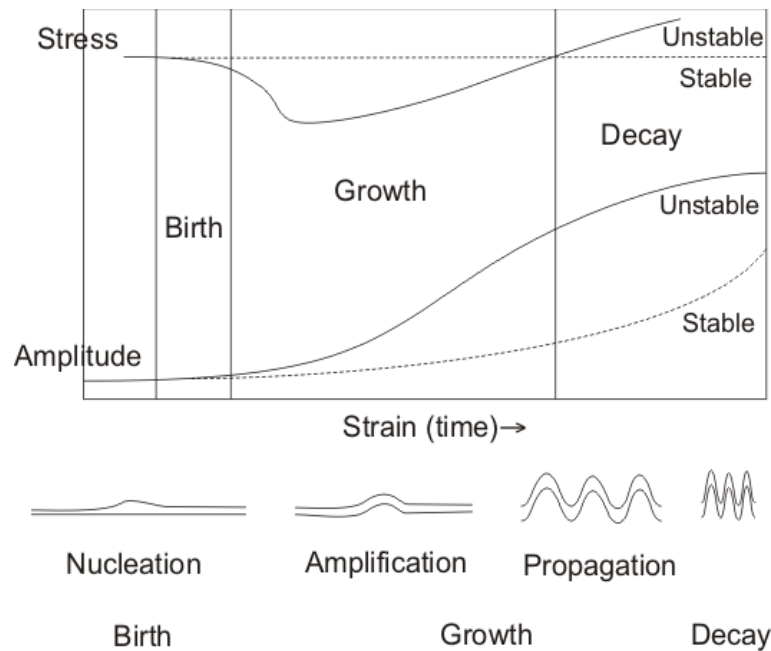


Fig. 2.14: Comparison of stress and amplitude variations in the development of experimentally-derived folds from initiation to 'lock-up' (modified from Price & Cosgrove, 1990)

Pre-buckle shortening can compact sediment and expel fluids from beds, causing the bedding plane fluid pressure to become sufficiently high to overcome its cohesive strength and the overburden weight (Price & Cosgrove, 1990). At sites of low cohesion, where the maximum ( $\sigma_{\max}$ ) and minimum ( $\sigma_{\min}$ ) principal stresses are parallel and normal to the bedding respectively, hydraulic fracturing and folds may be initiated (Price & Cosgrove, 1990). This allows fluids to move through and out of low permeable sediments (Cosgrove, 2001).

### 2.4.3 Buckling

Compressional stresses cause beds to flex where deposits form laterally-continuous sheets, creating broad buckle folds (Price & Cosgrove, 1990). Buckling develops due to either large compressive stresses parallel to high coherence contrast stacked layers (Fig. 2.14) and / or from additional torque causing layer instability (Twiss & Moores, 1992). The stresses generate high amplification rates, forming small tight folds. This leads to either layer-parallel flexural-slip, with no stretching or shortening in the outer or inner arcs (Tanner, 1989), or alternatively, to orthogonal flexure in which a line perpendicular to a layer remains unchanged after folding, with the outer arc stretching and the inner arc shortening (Price & Cosgrove, 1990).

For buckling to occur, a critical stress must be reached in order to overcome the folding resistance or critical strength of the material. Sedimentary rocks with relatively low critical

strengths include shales and siltstones; whereas limestones and sandstones have relatively high critical strengths (Nemcok et al, 2005).

#### 2.4.4 Forced Folding

Forced folding is another mechanism by which compressional deformation is accommodated. In contrast to buckle folding, forced folds are characterised by a geometry that is imposed upon the folded layers by the orientation and nature of an underlying thrust (Suppe, 1983; 1985). In this case, the beds are neither “free” to fold, nor to transmit any layer-parallel stresses. Instead, they are carried by the underlying thrust, which causes stretching or bending as folding progresses (Price & Cosgrove, 1990). This can create three forms of fold (Fig. 2.15):

1. Fault-bend folds, where deformation occurs when beds are displaced by large magnitudes along ‘ramp-flat’ thrusts, thereby creating ‘staircase’ geometries (Suppe, 1983);
2. Fault-propagation folds, where deformation occurs in a ‘process zone’ at an advancing thrust tip with asymmetric folds being overturned in the transport direction (Suppe, 1985);
3. Detachment folds, where deformation occurs via buckling above a bedding-parallel thrust in a weak detachment horizon, so that the fold grows above the maximum displacement point without any ramp thrust movement (Hardy & Poblet, 1994; Poblet et al, 1998).

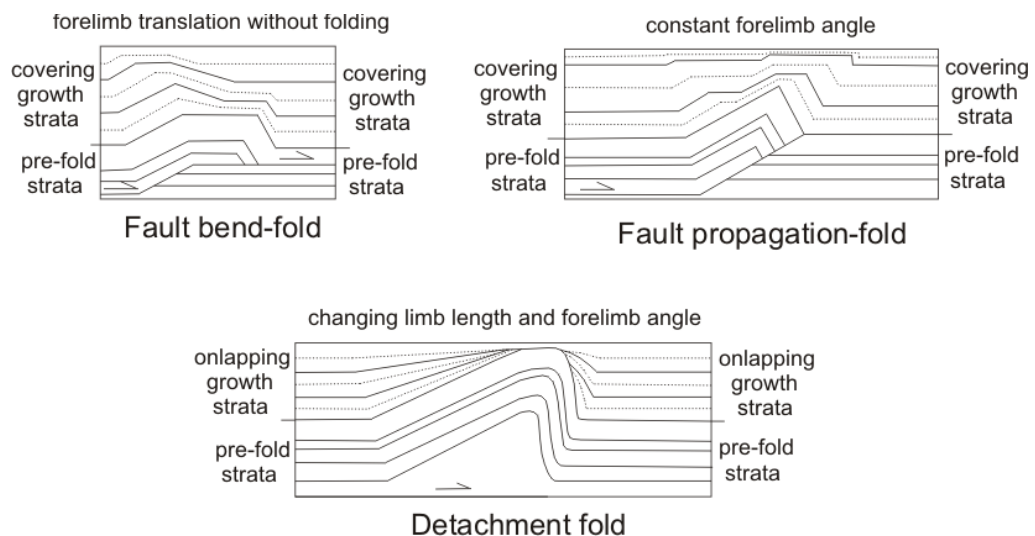


Fig. 2.15: Schematic sketches of a fault-bend, fault propagation and detachment folds where the depositional rate of the growth strata is slower than the uplift rate on the anticlinal crest (modified from Burbank & Anderson, 2001)

These types of fold are observed in numerous compressional settings, such as in foreland basins and accretionary wedges (Suppe, 1983; 1985; Maltman, 1998), in gravitationally-induced delta toe fold-thrust belts (Zoetemeijer et al, 1992; Corredor et al, 2005); and in sub-glacial environments (Phillips et al, 2008; Denis et al, 2009). Also in sub-glacial environments, folding occurs when glacial till sediment is in an over-pressured hydro-plastic state (Denis et al, 2009). Similar scenarios have been proposed for other folds in sediment. For

example, over-pressures resulting from hydrocarbon generation are a possible cause for the development of the Niger Delta toe fold-thrust belt (Corredor et al, 2005).

#### **2.4.5 Chevron folding**

The chevron folds in the coastal outcrops of the Bude Formation, SW England, are archetypal (Ramsay, 1974; Sanderson, 1974; Lloyd & Whalley, 1986; 1997; Tanner, 1989). In the original description of the folds by Ramsay (1974), it was suggested that the less competent layers in a sequence of more competent layers, ‘flowed’ into the fold hinge zones. This resulted in beds with bulbous hinges (i.e. thicker hinges than limbs) occurring in the less competent beds, alternating with uniform thickness hinges in the more competent beds. The beds have limb-dip variations due to varying bed thickness-limb length ratios (Ramsay, 1974; Sanderson, 1974). However, since this initial research into chevron folding, advances in the mechanics behind this type of deformation have led to at least five different models.

##### **High ductility contrast model (Ramsay, 1974)**

Ramsay (1974) introduced this model for bedded stacks of alternating competent and incompetent rock of high ductility contrast and largely uniform thickness. In the model, chevron folding occurs under constant stress and load when compressional deformation acts parallel to the layering, so that the incompetent bed “exerts no influence on fold stability”. Where there are small thickness variations between individual competent beds, deformation is accommodated by the limb faults, bulbous hinge zones or layer boudinage. In contrast, if there are large thickness variations between competent beds, “the fold limbs become curved”. Hinge zone dilation causes the hinges of competent beds to collapse into the incompetent beds with saddle reef formation between these beds involving “competent layer flow into the hinge”. During fold development, initiation is slow, but amplification is rapid. During the later stages, there is a progressive decrease in the shortening rate and fold growth, thereby causing either fold ‘lock-up’ at interlimb angles of about 60°, or limb thinning and hinge thickening at interlimb angles of less than 60°. Although the “strains in the hinge zone are related to the rates of shear” between beds on the limbs, the model is “not completely stable” throughout fold development.

##### **Flexural flow-flexural slip model (Tanner, 1989)**

Tanner (1989) suggested that chevron folds in rock develop by flexural flow between high coherence and low coherence beds during the initial stages of folding when bedding-parallel shear is uniformly distributed across a low coherence folding bed. In contrast, in more coherent beds, flexural slip occurs along some bedding planes, progressively amplifying the buckle folds. Where high coherence beds are more widely spaced, bedding-parallel shear is concentrated along the bedding, creating a flexural slip fold that develops striations in the slip direction on the limb bedding planes, towards the anticlinal hinge (Fig. 2.16). As the fold hinges

tighten, the limb bedding aligns increasingly orthogonal to the maximum compressional stress direction and so, accommodates both the compressional and shear stresses more easily.

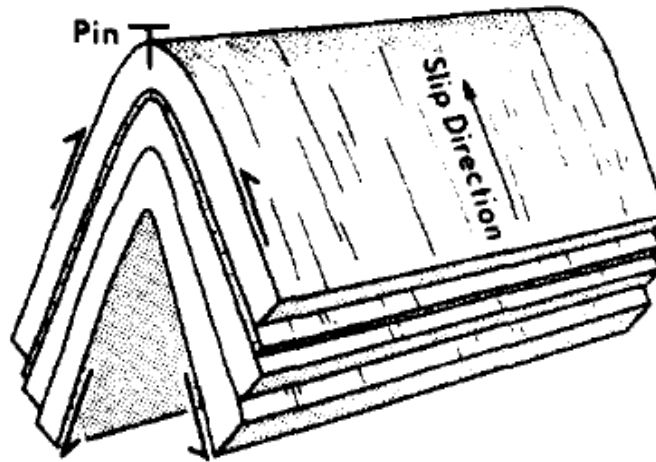


Fig. 2.16: Sketched flexural-slip chevron fold, showing displaced beds on the limbs. Striations suggest that the slip direction is towards the anticlinal hinge (from Tanner, 1989)

#### **Homogeneous shortening model (Yang and Gray, 1994)**

Yang and Gray (1994) suggest that chevron folds form by homogeneous shortening and pressure solution in rock under greenschist facies conditions, resulting in:

1. Layer-parallel shortening;
2. Tangential longitudinal strain due to buckling;
3. Fold tightening by inner arc collapse;
4. Spaced cleavage, which may develop at fold limb-dips as low as  $15^\circ$ ;
5. Minor fold flattening at metamorphic peak, demonstrated by 'mica-beard' growth.

#### **Localised dip-domain boundary model (Bazalgette & Petit, 2007)**

Experiments into fracture localisation in brittle paraffin wax multi-layers by Bazalgette and Petit (2007) suggested that during loading, axial-kink boundaries (i.e. dip-domain boundaries or DDBs) play a major role in the development of curvature in fractured buckle folds. Under low inter-layer friction conditions, DDBs remain relatively localised during shortening, leading to chevron folding via flexural slip (Fig. 2.16). Under high interlayer friction conditions, DDBs multiply laterally from an initial chevron fold via orthogonal flexure. However, a more discontinuous curvature is produced than is observed in outcrop examples.

#### **Homogeneous layer shortening model (Bastida et al, 2007)**

Bastida et al (2007) used finite element modelling to explore chevron fold development and suggested that homogeneous layer shortening, constrained by high layer coherence contrast, occurs during initial chevron fold growth. This type of shortening requires equiareal tangential longitudinal strain, which results from either parallel tangential longitudinal strain or flexural

flow. Also, their fold amplitude decay models agree with Ramsay's model (1974) with "high values of slip between layers, coupled with changes produced in the later stages of chevron folding", which can "bring an end to buckling, probably at interlimb angle values of 60-70°, inducing the onset of homogeneous strain". However, homogeneous strain is usually not coaxial and results in shearing of the chevron folds.

### **Summary of the models**

The chevron fold models of Ramsay (1974), Tanner (1989), Yang and Gray (1994), Bazalgette and Petit (2007) and Bastida et al (2007) agree regarding the layer properties (i.e. high relative layer competence contrast), kinematics (i.e. flexural slip; Fig. 2.16) and accommodation of deformation (i.e. homogeneous shortening). It is note-worthy that although chevron folds develop in rock, Bazalgette and Petit (2007) experimented using flexible paraffin wax multi-layers. As wax is not a rock, this raises the possibility that chevron folds may develop in other materials. This is investigated in this thesis.

## **2.5 Compressively-developed basins**

The literature review has concentrated so far on fold deformation, which occurs in many settings, such as fold-thrust belts and foreland basins. These settings are described below.

### **2.5.1 Fold-thrust belts**

Fold-thrust belts result from accommodating compressional deformation (Poblet & Lisle, 2011) that can occur during plate (e.g. Alps and Himalayas) and intra-plate collision (e.g. Yinshan belt, China; Davis et al, 1998). Special types of fold-thrust belts include deformed sediments in accretionary prisms, above subduction zones (e.g. Nankai Prism; Maltman, 1998), passive margins (e.g. Orange Basin, Namibia; De Vera et al, 2010); and delta toes (e.g. Po Delta; Zoetemeijer et al, 1992). Compressional deformation is tectonically-driven in both continental and intra-continental prisms; gravity-driven on continental margins and delta toes; and both tectonically-driven and gravity-driven in accretionary prisms (Poblet & Lisle, 2011).

The characteristics of individual fold-thrust belts can vary because the belts are affected by different factors, including (Poblet & Lisle, 2011):

1. Plate tectonic setting;
2. Whether just the sedimentary cover, or the cover and basement are involved in deformation;
3. Mechanical stratigraphy and lithification state (see chapters 6, 7 & 8);
4. Presence, distribution and thickness of a salt or shale décollement;
5. Occurrence of syn-deformation erosion and deposition;
6. Depth to décollement and effective elastic thickness of the lithosphere;
7. Occurrence of pre-existing basement structures (e.g. on an ancient passive margin);
8. Timing and rates of deformation.

### 2.5.2 Foreland basins

Foreland basins are a well-known type of fold-thrust belt that is generated by loading the autochthonous continental crust (i.e. foreland) with an allochthonous over-thrusting unit or hinterland (DeCelles & Giles, 1996; Nemcok et al, 2005; Shail & Leverage, 2009). They are often structurally-above an originally weak, thinned section of passive margin that developed following a previous rifting event, such as in the Mesopotamian Basin, northern Iraq (Pitman et al, 2004). The overlying deposits exerts a significant loading effect and the weakness of the thinned, over-ridden passive margin causes it to subside significantly (DeCelles & Giles, 1996). ‘Imbricate’ thrusts branch-off from a décollement and cut through the foreland basin deposits, generating fault-bend or fault-propagation folds (Nemcok et al, 2005). Examples are found in:

1. Miocene-Present Adriatic Foreland Basin (Zoetemeijer et al, 1992; Tavani et al, 2006);
2. Early Carboniferous Antler Foreland Basin, Nevada, USA (Jansma & Speed, 1993);
3. Tertiary West Alpine Foreland Basin, SE France (Sinclair, 1997; McCaffrey et al, 2002).

Three criteria have been suggested for recognising foreland basins, particularly where a basin has undergone uplift, exposure and erosion (Fig. 2.17); namely the presence of:

1. An elongate wedge of potential sediment accumulation (DeCelles & Giles, 1996);
2. A down-warping depression, whose subsidence rate increases with time (Kneller, 1991);
3. A depo-centre consisting of four parts (DeCelles & Giles, 1996):
  - a. A wedge-top or ‘piggy-back’ (minor) basin;
  - b. A fore-deep (major) basin;
  - c. A fore-bulge ‘positive’ (basement) structure;
  - d. A back-bulge (minor) basin.

The foreland basin model has been employed to describe the Culm Basin structure of SW England by Hartley and Warr (1990) and Warr and Hecht (1993) where it agrees with criterion 1 above. However, the basin-scale biostratigraphy (Freshney et al, 1972; 1979) is not of sufficient quality or continuity to demonstrate that criterion 2 is fulfilled, whilst the restricted extent of both the field and subsurface data do not allow the full demonstration of a four-part basin architecture. Alternatively, the Culm Basin has been described as a thrust-top (Shail & Leverage, 2009) or a ‘piggy-back’ basin (Coward & Smallwood, 1984; Warr, 2002).

A discussion of the Culm Basin and Variscan orogenesis is provided below in order to establish whether the deformation observed in the Bude Formation outcrops may reasonably be described as having occurred within a foreland basin. Further discussion of Variscan orogenesis across SW England and in the Culm Basin is provided in Chapter 9.

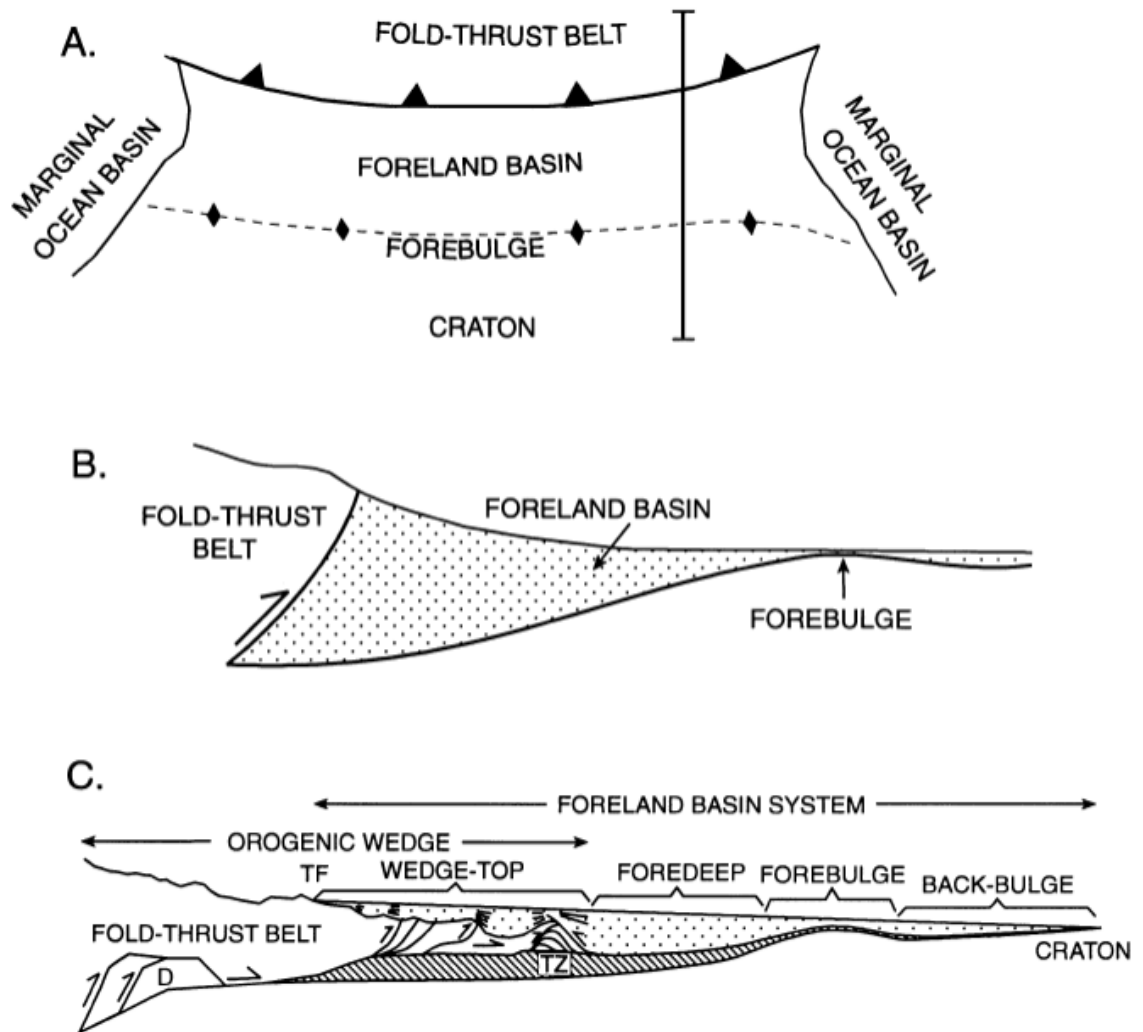


Fig. 2.17: Schematic diagrams (from DeCelles & Giles, 1996) of: (A) map view of a ‘typical’ foreland basin either side of marginal ocean basins; (B) foreland-basin geometry in transverse cross-section, following the line-of-section through A (10x vertical exaggeration); (C) cross-section depicting a simplified foreland basin (wedge-top, fore-deep, fore-bulge and back-bulge depo-zones; approximately true scale). Topographic front (TF), a schematic duplex (D) in the orogenic hinterland and a frontal triangle zone (TZ) are depicted. Progressive deformation (short fanning lines associated with thrust tips) in the wedge-top depo-zone is shown. The substantial overlap between the orogenic front and the foreland basin system is noteworthy

## 2.6 Variscan orogenesis and Culm Basin processes

The Variscan orogeny occurred during Rheic Ocean closure and creation of Pangaea through the Late Devonian to Early Permian (Shail & Leveridge, 2009). The deformation across SW Britain was part of the northern orogenic ‘front’ (Fig. 2.18) that stretched from Germany to southern Ireland (Shackleton, 1984; Coward & Smallwood, 1984) and possibly also, to Portugal (Warr, 2002; Fig. 2.19). This review concentrates on the deformation in SW England (Sanderson, 1979; Coward & Smallwood, 1984; Shail & Leveridge, 2009) and the Culm Basin in particular (Ramsay, 1974; Sanderson, 1974; Lloyd & Whalley, 1986; Tanner, 1989).

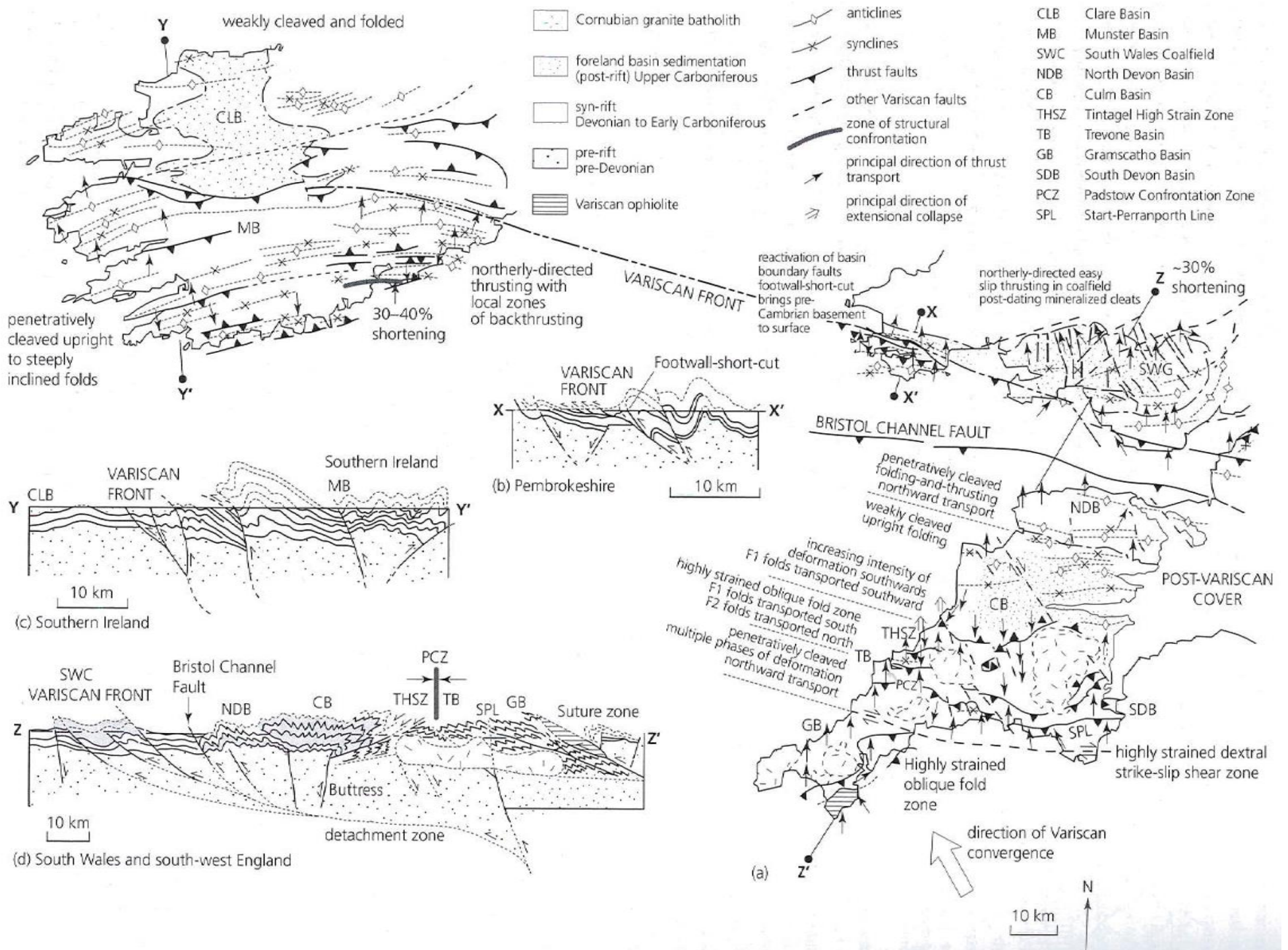


Fig. 2.18: Variscan deformation across the south of the British Isles (from Warr, 2002) showing: (a) A structural map of south-west Britain and southern Ireland; (b) A cross-section through Pembrokeshire, SW Wales; (c) A cross-section through southern Ireland; and (d) A cross-section through south Wales and SW England

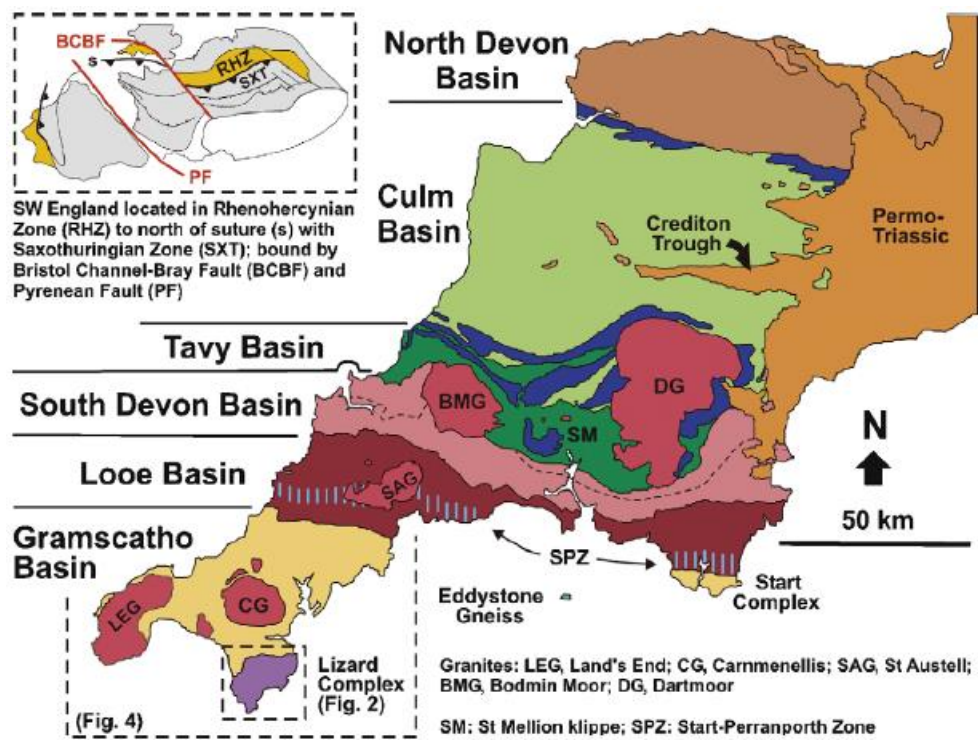


Fig. 2.19: Variscan foreland basins in SW England showing the Culm Basin as the structurally-highest and youngest Variscan basin, which lies between the inverted North Basin (north) and Tavy Basin (south) (from Shail & Leveridge, 2009)

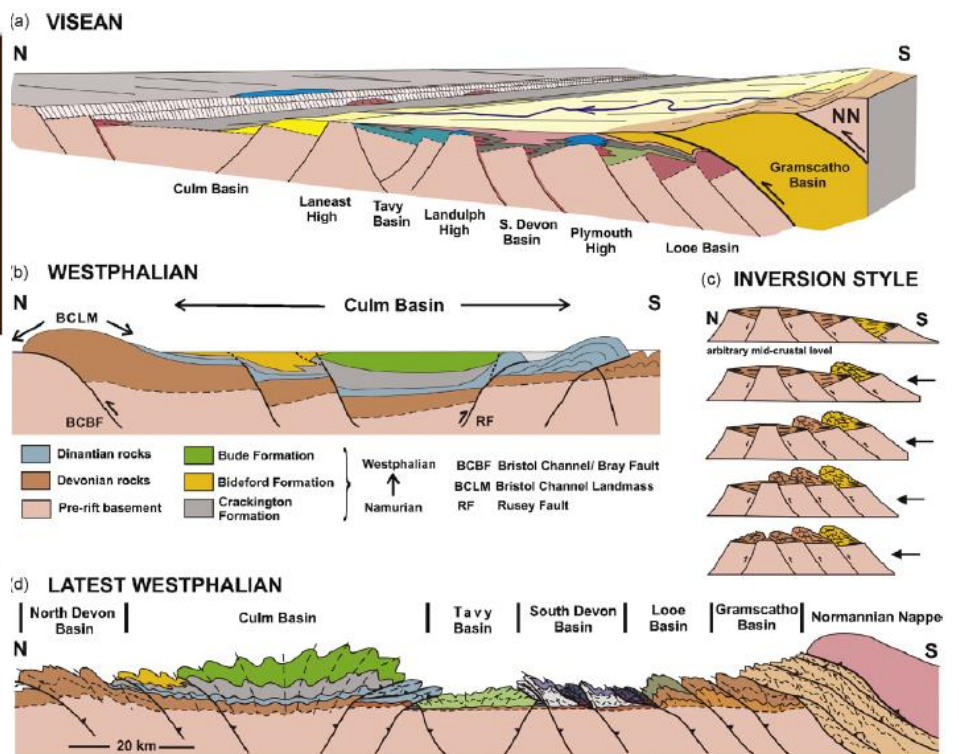


Fig. 2.20: Schematic N-S cross-sections of progressive SW England passive margin inversion: (a) Early stages (Visean); (b) Culm Basin detail (Westphalian) (c) Cartoon of rift basin geometry control on inversion; and (d) End-Westphalian (convergence ceased) (from Shail & Leveridge, 2009)

The Variscan fold-thrust belt of SW England is an amalgamation of small, ‘external’ foreland basins that grew during the Late Carboniferous (Warr, 2002). North-directed thrusting in the Culm Basin began in the late Visean, before the Variscan ‘Front’ moved to the north. This caused the North Devon Basin to uplift, supplying sediments into the Culm Basin during deformation (Warr, 2002). This ‘front’ does not represent the deformation limit, as far field deformation having been observed across northern England (Leeder, 1987). Instead, the Variscan deformation in SW Britain is progressive, with several over-printing relationships (Whalley & Lloyd, 1986; 1997; Shail & Leveridge, 2009).

### 2.6.1 Regional compressional deformation in SW England

North-west-directed Variscan orogenic oblique convergence (Gayer & Nemcok, 1994) began during the Middle Devonian (Shail & Leveridge, 2009; Figs. 2.19-2.20). The deformation was partially-controlled by east-west-striking dextral transform faults in south Devon and south Cornwall (Holdsworth, 1989; Warr, 2002; Fig. 2.18; SPZ in Fig. 2.19), involving passive margin inversion (Hartley & Warr, 1990). It has been proposed that the first stage of progressive Variscan deformation during Visean times was the Normannian Nappe emplacement onto the Gramscatho Basin (Shail & Leveridge, 2009). This resulted in northwards thrusting and associated folding (Coward & McClay, 1983) above a ‘thick-skinned’ mid-crustal décollement, which continued through to Westphalian times (Shail & Leveridge, 2009; Fig. 2.20). Alternative regional Variscan tectonic models in SW England are discussed in Chapter 9.

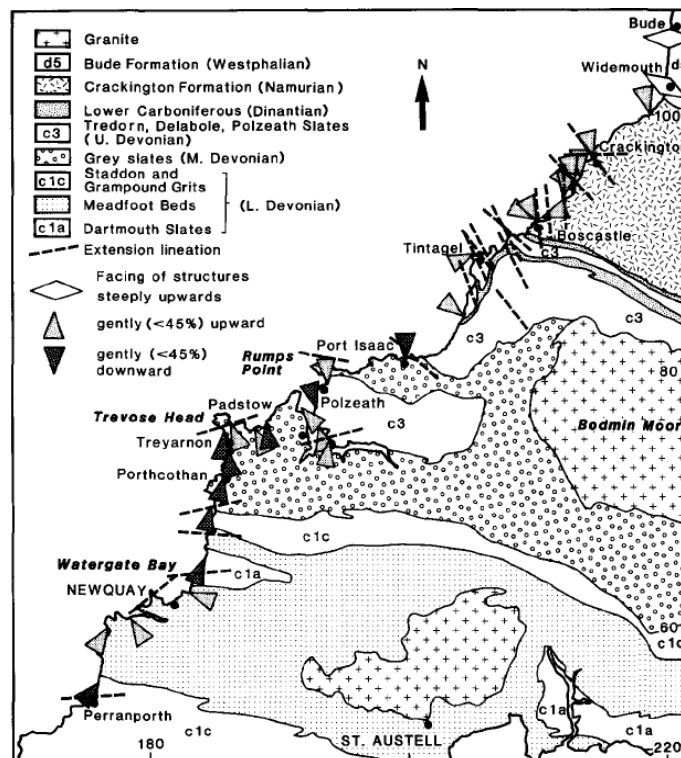


Fig. 2.21: Geological map of north Cornwall, with the main cleavage facing directions and finite extension lineations on the NW coast of Cornwall (from Shackleton et al, 1982)

The tectonic inversion across SW England resulted in the northwards progression of the Variscan foreland basin development, with each basin becoming infilled and then becoming deformed and undergoing metamorphism (Dodson & Rex, 1970; Coward & Smallwood, 1984). This has caused Carboniferous stratigraphy to young broadly towards the north, across SW England. The associated cleavage in these metamorphosed rocks strikes E-W, with extensional lineations oriented NNW-SSE (Fig. 2.21).

Shortening across SW England is estimated at approximately 150 km (Shackleton et al, 1982) and occurred at a displacement rate of between 0.25 cm/yr and 0.4 cm/yr (Coward & Smallwood, 1984). During the Late Carboniferous, there was a 'sticking point' as the northward propagation rate slowed to less than the slip rate and was replaced by south-directed back-thrust movement (Coward & Smallwood, 1984). Sanderson (1979) modelled the associated shear deformation as causing increased south-directed strain and tighter folds towards the south in the Culm Basin (Figs. 2.22-2.23). This model is described in more detail in chapters 4 and 8.

In contrast to the most widespread view, Selwood and Thomas (1986b) suggest that tectonic movement was directed southwards. In this model, the Boscastle Formation under-thrusts the Culm Basin along the Rusey Fault (Warr, 2002), with the 'Padstow Confrontation' to the south as a modified structure within a south-verging fold train (Selwood & Thomas, 1986a).

This overview of the regional context and geometry of the Culm Basin shows that the following features are consistent with it having developed in a foreland basin:

1. It fulfils criterion 1 of DeCelles and Giles (1996) in being part of a basin that is broadly strike-parallel to the deformation 'front' into which deformation propagates through time (Zoetemeijer et al, 1992; Mouthereau et al, 2007; Mosar et al, 2010);
2. The Devonian to Carboniferous strata are upwards coarsening and upwards shallowing, which is consistent with a relatively distal to relatively proximal position through time with respect to the Variscan deformation 'Front' (Freshney et al, 1972; 1979).

On the basis of the above discussion, it is considered appropriate to refer to the Culm Basin as a foreland basin (*sensu lato*). Even so, the general aim of this thesis is to investigate the mechanical state of folds, which are known to develop in a variety of contractional settings and thus, is not dependant upon the Culm Basin being a foreland basin.

### **2.6.2 Deformation in the Culm Basin**

The Culm Basin is the structurally-highest basin developed during the Variscan deformation (Ramsay, 1974; Sanderson, 1979; Whalley & Lloyd, 1986; Lloyd & Whalley, 1986). Before deformation and prior to a half-graben opening in the Early Carboniferous (Shail & Leveridge, 2009), the Culm area consisted of thin Middle Devonian to Early Carboniferous deposits south of thicker syn-rift deposits in the North Devon Basin (Shail & Leveridge, 2009).

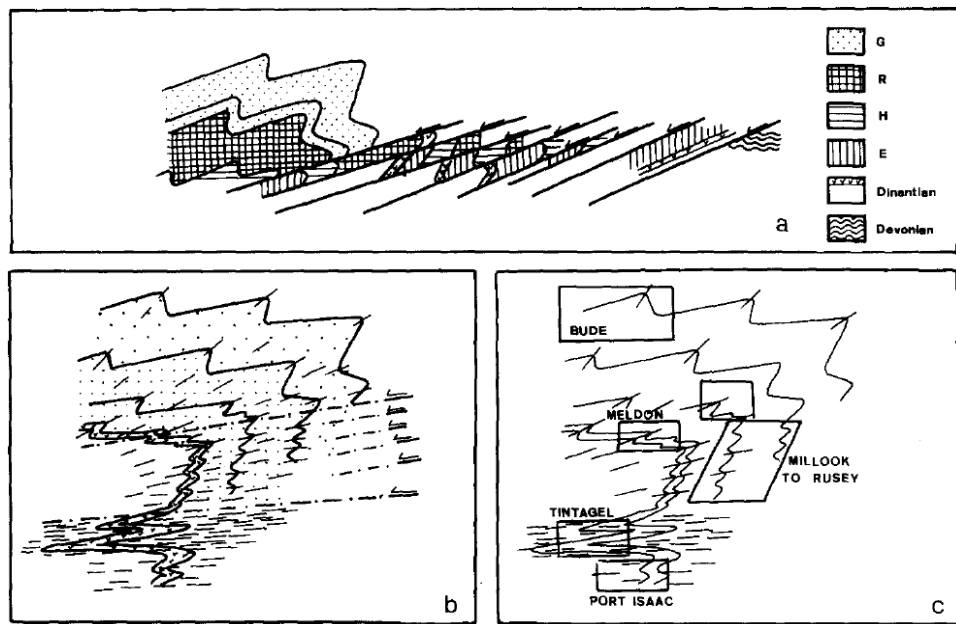


Fig. 2.22: Variscan deformation reconstructions: (a) Major, low-angle faults ( $D_2$  of Sanderson, 1979) and Carboniferous stratigraphy displayed from Widemouth to Boscastle, Cornwall; (b) Reconstruction of  $D_1$  structures of Sanderson (1979) from matching strata across the low-angle faults; and (c) Positions of the main sections in relation to reconstructed  $D_1$  structures (from Sanderson, 1979)

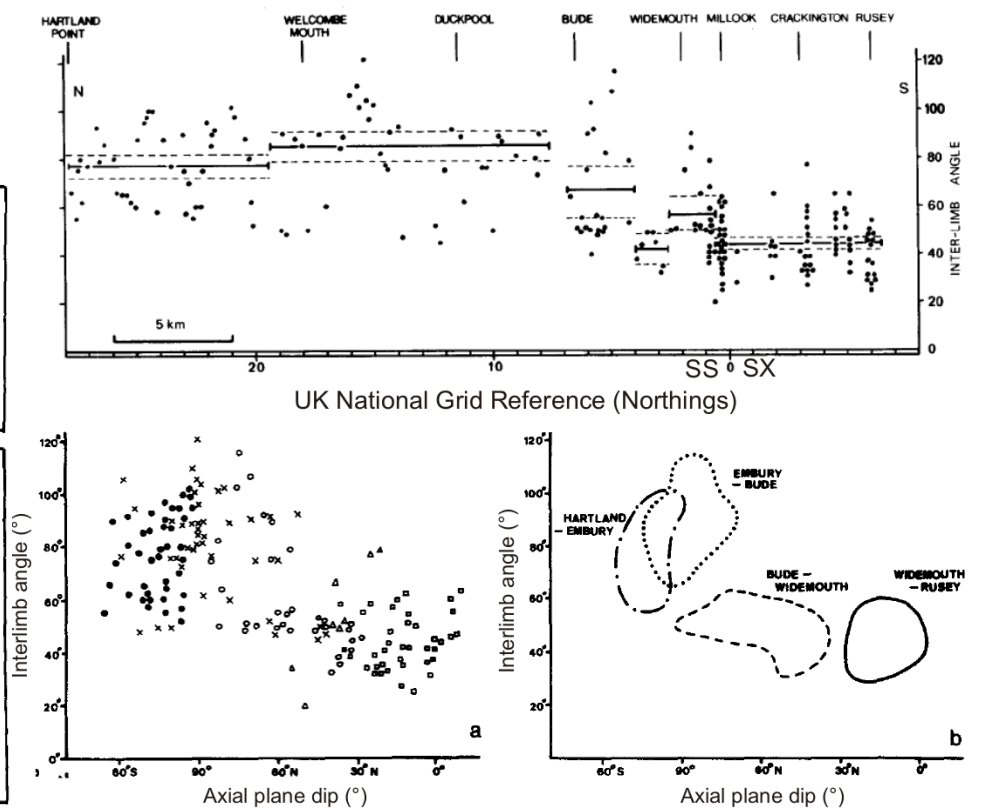


Fig. 2.23: Bude Formation chevron fold statistical analyses (from Sanderson, 1979): Fold interlimb angle distribution from Hartland to Rusey (top); and Graphs of inter-limb angle vs. axial plane dip along the Bude Formation coastal outcrops: scattergram (bottom left); and 67% bounds (bottom right)

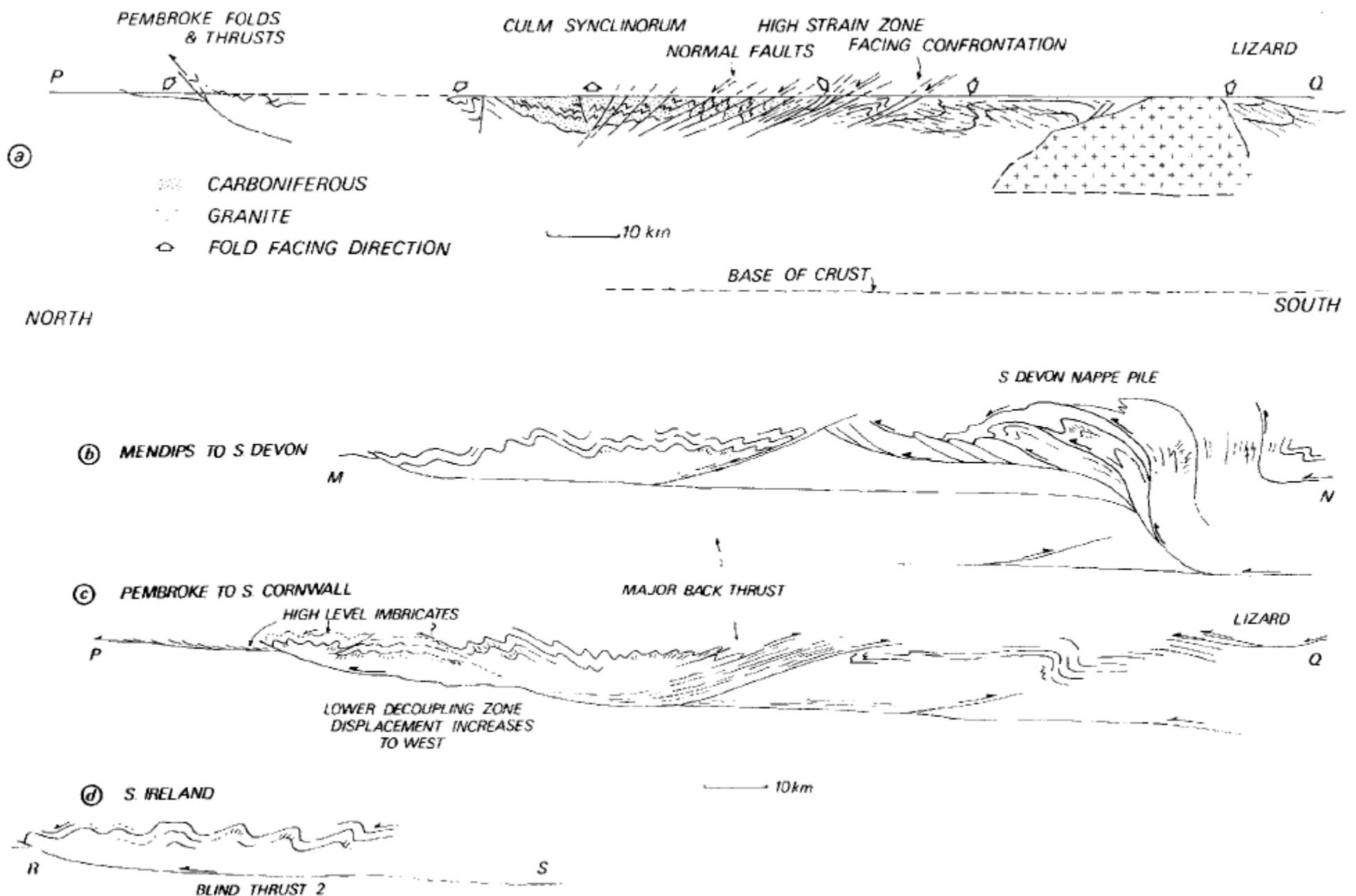


Fig. 2.24: Simplified regional structural cross-sections through the Variscan deformation (from Coward & Smallwood, 1984): (a) Cross-section through the Variscan deformation of SW Britain (the Lizard to Pembrokeshire). Also, suggested cross-sections through thrust and fold structures of: (b) South Devon to the Mendips; and (c) South Cornwall to Pembrokeshire; (d) Schematic section through southern Ireland to correlate with structures in south Wales. Notice in cross-section (c) the lower decoupling zone below the high level imbricates

During Variscan compression, both the northward-propagating deformation front and the inversion of the North Devon Basin caused the Culm Basin to subside (Selwood & Thomas, 1986b; Hartley & Warr, 1990; Warr, 2002). From a seismic survey across the Culm Basin, a south-dipping décollement was interpreted at 15-12 km in Cornwall and south Devon and also, at 13-10 km in north Devon (Brooks et al, 1984). This is the basis for the Shail and Leveridge (2009) ‘thick-skinned’ tectonic model where deformation propagated northward along a mid-crustal décollement and into the sedimentary cover. In this model, the décollement underlies the Culm Basin, as shown in the Coward and Smallwood (1984) cross-section (c) (Fig. 2.24). A comparison with their other cross-sections shows:

1. North-dipping normal faults in SW England (Freshney et al, 1972; Sanderson, 1979; Coward & Smallwood, 1984; see cross-section (a) in Fig. 2.24);
2. A nappe pile in S Devon and fold train in the Mendips (see cross-section (b) in Fig. 2.24);
3. Both folding and thrusting in south Wales (see cross-section (c) in Fig. 2.24);
4. A fold train in southern Ireland (see cross-section (d) in Fig. 2.24).

During the progressive Variscan deformation in the Bude Formation, decametric-scale ‘early’ (Enfield et al, 1985), metric-scale ‘pre-folding’ (Mapeo & Andrews, 1991) and kilometric-scale ‘pre-chevron’ (Lloyd & Chinnery, 2002) have been described. These are alternate names for the same deformation structures. Mapeo and Andrews (1991) described the ‘later’ ‘pre-folding’ bedding-parallel thrusts as over-printing the ‘earlier’ normal faulting.

‘Upright’ chevron folding dominates many of the outcrops to the north of Bude (UK Grid Reference: SS200067; Ramsay, 1974; Freshney et al, 1979; Sanderson, 1974; 1979; Lloyd & Whalley, 1986; 1997; Tanner, 1989). Whalley and Lloyd (1986) suggest that these chevron folds are associated with north-directed thrusts that cut the Bude Formation beds and have interpreted them as having exploited the slump beds. This suggests that contemporaneous deformation and sedimentation occurred in the Culm Basin (Leveridge & Hartley, 2006).

To the south of Bude, increasingly south-directed ‘inclined-to-recumbent’ chevron folds have been observed (Freshney et al, 1979; Sanderson, 1979). The south-directed folds formed by accommodating increasing amounts of south-directed shear strain to the south (Sanderson, 1979) and caused the ‘upright’ chevron folds to modify their geometries (Lloyd & Whalley, 1986; 1997). This shear deformation may have been the result of under-thrusting along the Rusey Fault at the south of the Culm Basin (Sanderson, 1972; Warr, 2002). In contrast, Warr (2002) suggested that this under-thrusting caused the ‘upright’ chevron folds to develop either at the same time as, or even after, the south-directed ‘inclined-to-recumbent’ chevron folds.

In the Lloyd and Whalley (1986; 1997) model, shear modification resulted in steepening of the south-dipping limbs of the original ‘upright’ chevron fold, with ‘inclined-to-recumbent’ chevron fold development on these limbs, as described in the experimental models of Ghosh (1966). However, shear modification has not been accommodated to the same degree

across the whole basin and has resulted in south-directed chevron folds with variable axial plane dip angles (Lloyd & Whalley, 1986). Alternatively, the folds may have been generated by back-thrusting (Warr, 2002; Shail & Leveridge, 2009), as observed in the Millook Nappe (Rathey & Sanderson, 1982). Similar folds occur in ‘triangle zones’ ahead of ‘blind’ thrusts (Jones, 1982).

A consequence of the progressive Variscan deformation in the Bude Formation is that a new but typically local cleavage set over-printed the previous set. All three sets are observed in Crackington Formation shale beds at Millook (Fig. 2.25i; Lloyd & Chinnery, 2002), enabling the Variscan structural evolution to be determined. The cleavage development at Millook includes fabrics related to north-directed thrust deformation ( $S_1$ ) in initially horizontal beds ( $S_0$ ); followed by ‘upright’ chevron folding ( $S_2$ ); and by south-directed shearing of the ‘upright’ chevron folds ( $S_3$ ) (Fig. 2.25i; Lloyd & Whalley, 1986; Lloyd & Chinnery, 2002). Although the structures are distinguished, it is emphasised that deformation was progressive, with different structures generated contemporaneously both laterally and with depth (Enfield et al, 1985).

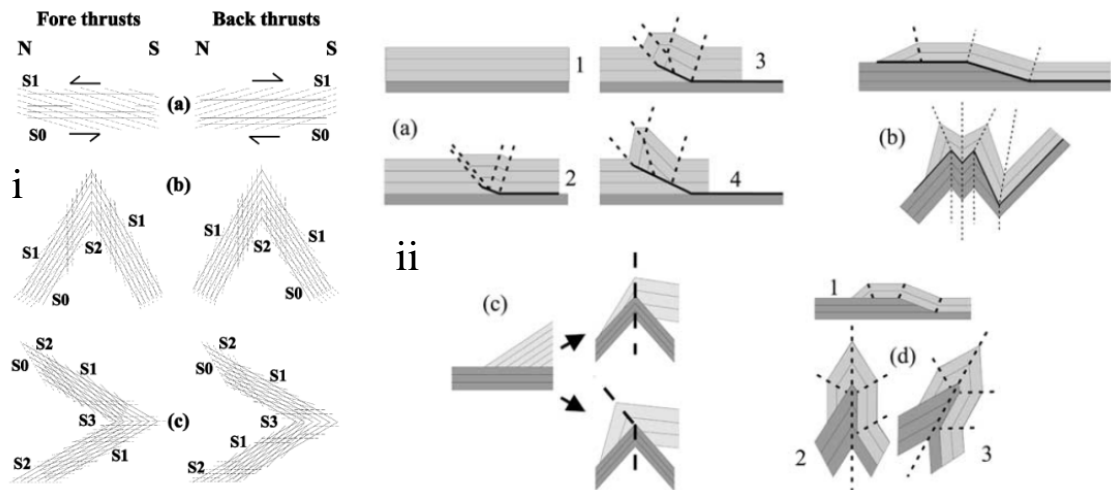


Fig. 2.25: Schematic diagrams of three progressive deformation ‘phases’ in the Bude and Crackington formations from: (i) over-printing cleavage patterns ( $S_N$  denotes relative foliation age); (ii) low-angle thrusts and chevron folding of the thrusts (from Lloyd & Chinnery, 2002)

The north-directed thrusts include hanging wall folds that have been affected by progressive Variscan folding (Lloyd & Chinnery, 2002; Fig. 2.25ii (a)). During ‘upright’ chevron folding, both ‘undeformed’ beds and beds involved in north-directed thrusting became steeply dipping (i.e.  $60^\circ$ ) (Fig. 2.25ii (b-c)). During south-directed ‘inclined-to-recumbent’ chevron folding, the originally north-dipping limbs may have become less steep and formed north-directed folds where thrusts and hangingwall folds were emplaced (Lloyd & Whalley, 1986; Fig. 2.25ii (d)). Alternatively, the north-directed folds may have been generated where north-directed thrusts exploited the slump beds (Enfield et al, 1985; Whalley & Lloyd, 1986).

The Variscan fold deformation throughout SW England was NW-directed (Gayer & Nemcok, 1994), so accommodating a transpressional component. This transpression caused

kilometric-scale regional NW-SE-striking dextral faults (e.g. Sticklepath Fault) to cut across earlier faults (Andrews, 1992; Peacock et al, 1998). This is associated with a variation in deformation directions along the strike of the Variscan 'Front' (Coward & Smallwood, 1984). Displacements on the cross-cutting faults range from millimetre to kilometres, with the smallest scale faults accommodating up to 38° of clockwise rotation (Peacock et al, 1998).

In the Bude and Crackington formations, steeply north-dipping normal faults cut the chevron folds (Freshney et al, 1972; Sanderson, 1979) and may represent post-Variscan extensional structures (Coward & Smallwood, 1984). The extensional reactivation of the faulted contact between the Bude and Crackington formations led to the development of the Permian Crediton Trough (Durrance, 1985). The extension may have been assisted by sinistral transtensional movement during orogenic collapse (Gayer & Cornford, 1992). This extension is associated with Cornubian granite batholith intrusions, and in turn with regional uplift, crustal thinning and exhumation (Coward & Smallwood, 1984; Warr, 2002). Also, during the Tertiary, both dextral and sinistral wrench movement was accommodated on some faults (e.g. Sticklepath Fault) (Williams et al, 1970; Freshney et al, 1972; Peacock et al, 1998) and has been associated with the development of the Bovey-Tracey Basin, central Devon, along the Sticklepath fault (Holloway & Chadwick, 1986).

In addition, soft-sediment structures have been described (Burne, 1970; Enfield et al, 1985; Hartley, 1991; Hecht, 1992) and syn-depositional tectonic deformation inferred in the Bude Formation (Hartley & Warr, 1990; Shail & Leveridge, 2009). It is these features, together with the geometries of the related fold structures, which form a general aim in this thesis.

### 2.6.3 Geometries of the fold structures in the Bude and Crackington formations

Fold deformation structures in the Bude and Crackington formations have been analysed by Davison et al (2004) based on remote sensing data collected using a photo-montage between Hartland Quay and Speke's Mill Mouth (SS222257-SS225247). This included an analysis of the chevron fold wavelengths, amplitudes and inter-limb angles from 62 folds (Figs. 2.26-2.27), yielding the following statistics:

1. Mean fold wavelength ( $\lambda$ ) of 146 m (st. dev.  $\pm$  108 m), mean fold amplitude ( $\mathbf{a}$ ) of 29 m (st. dev.  $\pm$  25 m) and a possible linear correlation of:  $\mathbf{a} = 0.19*\lambda$  ( $R^2 = 0.79$ ; Fig. 2.26);
2. Mean fold interlimb angle of 67° (st. dev.  $\pm$  20°), with bimodal peaks at interlimb angles of: 44°-55° (tighter folds) and 77°-99° (more open folds) (Fig. 2.27).

The Davison et al (2004) mean fold wavelength ( $\lambda$ ) and mean fold amplitude ( $\mathbf{a}$ ) suggest that the data scatter is sufficiently small that a linear correlation is applicable. However, some caution should be applied to the data, as this correlation appears to be applicable only for 'small' folds (i.e.  $\lambda < 200$  m;  $\mathbf{a} < 40$  m) (Fig. 2.26). At wavelength and amplitude values above these, the scatter in the data is too great to provide any meaningful correlation (Fig. 2.26).

Further data collection from chevron folds along the north Devon-north Cornwall coastline is required to provide a more robust analysis and statistically significant result.

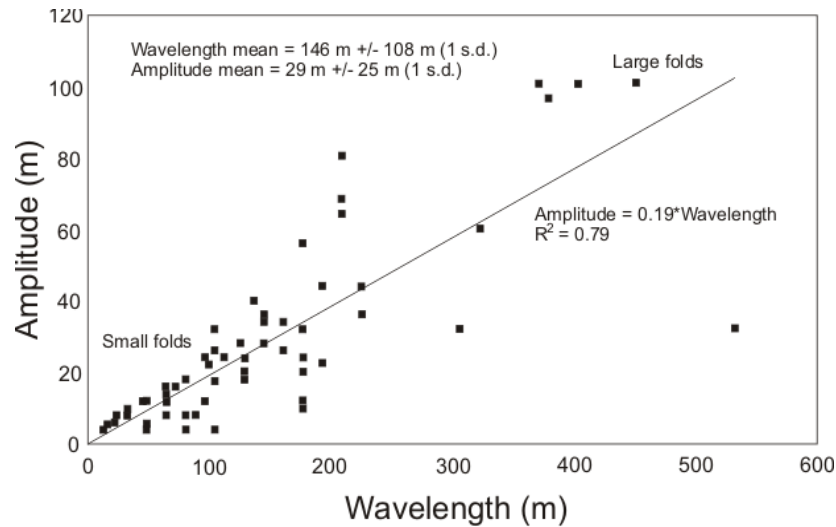


Fig. 2.26: Amplitude vs. Wavelength plot for chevron folds between Hartland Point and Speak Mill's Mouth (SS230278-SS225237;  $n = 62$ ), showing that the correlation of fold amplitude and wavelength is best for small folds (modified from Davison et al, 2004)

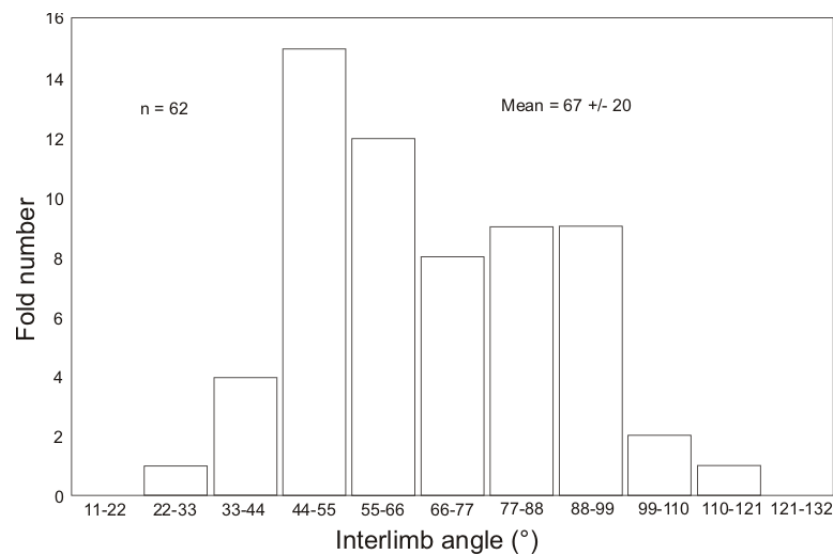


Fig. 2.27: Frequency plot of chevron fold interlimb angles between Hartland Point and Speak Mill's Mouth (SS230278-SS225237;  $n = 62$ ), showing a bimodal distribution for the fold interlimb angle data (modified from Davison et al, 2004)

Also, from Davison et al (2004), the results from the frequency plot of fold interlimb angles (Fig. 2.27) suggest that although a bimodal distribution may be interpreted. However, there is a large range of fold interlimb angles, of between  $22^\circ$  and  $121^\circ$  (Fig. 2.27), which may indicate that compressional strain was accommodated unevenly by the folded beds during Variscan deformation. However, as with the fold wavelength-fold amplitude data, insufficient folds may have been measured to provide a statistically significant result.

### 2.6.4 Structural geometries of beds in ‘upright’ chevron folds

The bulbous-hinged sandstone, siltstone and shale beds in Bude Formation ‘upright’ chevron folds have interlimb angles of less than  $70^\circ$ . Additional folding is accommodated in the beds via hinge expansion, in a direction sub-parallel to the minimum principal stress direction ( $\sigma_{\min}$ ). They are associated with saddle reefs where beds have separated at the fold hinge (Ramsay, 1974). In contrast, the only bulbous-hinged beds observed in the Crackington Formation are shale beds in the ‘inclined-to-recumbent’ chevron folds (Sanderson, 1974).

In the Bude and Crackington formations, estimates have been made of the amount of dimensionless shortening accommodated ( $-e$ ), of the dimensionless bed thickness-to-limb length ratio ( $t_0/L_0$ ) and of the interlimb angle (IA) of the folded beds (Sanderson, 1974; Fig. 2.28). The extension vector direction opposes that of shortening, so that extension is a positive direction ( $e$ ) and shortening is negative ( $-e$ ). The limb length ( $L_0$ ) (in metres) is measured between interlimb positions around each folded bed, whilst the bed thickness ( $t_0$ ) (in metres) is that measured at the hinge (Ramsay, 1967). Table 2.1 contains the calculated  $t_0/L_0$  ratios and the shortening ( $-e$ ) for the formations, together with the theoretical IA angle (Sanderson, 1974), which shows that:

1. IA angle is greater than the calculated angle for the Bude Formation folds;
2. IA angle is less than the calculated angle for the Crackington Formation folds.

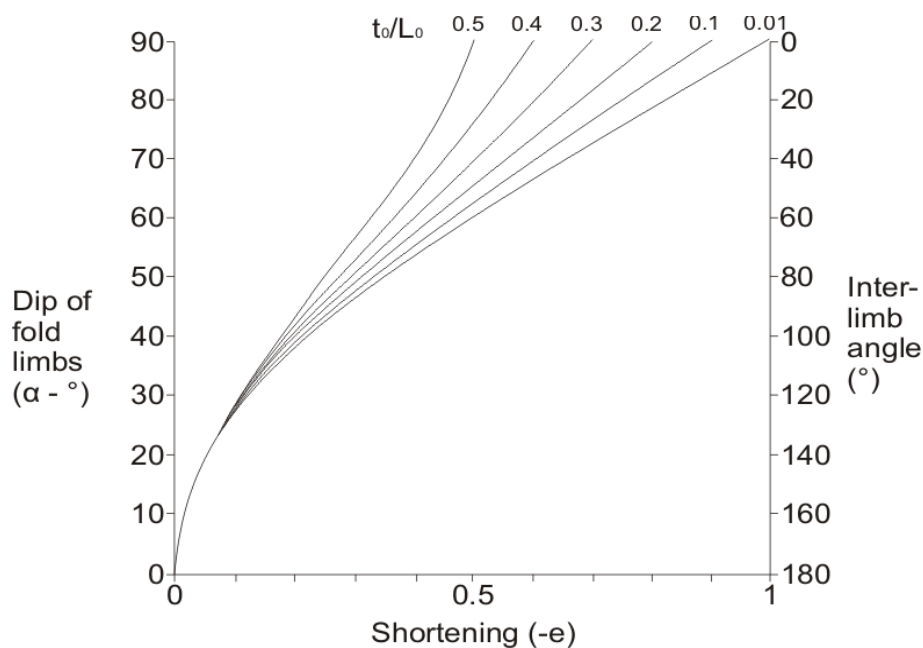


Fig. 2.28: Graph of interlimb angle (IA) versus shortening ( $-e$ ) for different bed thickness-to-limb length ( $t_0/L_0$ ) ratios in the Bude and Crackington formations’ folds (from Ramsay, 1967)

The discrepancy between the theoretical and calculated interlimb angles (IA) suggests that the folds in the Crackington Formation are too tight to be consistent with the model (Sanderson, 1974). The geometries of these chevron folds are investigated using the dip isogon and quantitative layer thickness methods of Ramsay (1967) in Chapters 7 and 8.

Formation	-e (shortening)	t <sub>0</sub> /L <sub>0</sub> ratio	Theoretical IA (°)	Calculated IA (°)
Crackington	0.38 (62%)	0.03	79	42 +- 15
Bude	0.55 (45%)	0.1	53	62 +- 15

Table 2.1: Tabulated data from Sanderson (1974) showing how theoretical inter-limb angles (IA) relate to shortening accommodated (-e) and bed thickness-to-limb length ( $t_0/L_0$ ) ratios; and compare to the calculated IA angles, for Bude and Crackington formations' folds

### 2.6.5 Lloyd-Whalley shear modification model

'Upright' chevron folds often have interlimb angles (IA) of 60°, which is their 'lock-up' angle (Ramsay, 1974), causing the limbs to dip at about 60° N or S. If a horizontal deformation with dimensionless shear strain ( $\gamma$ ) is applied to the folds, it causes the limbs to rotate from their initial angles ( $\alpha = 60^\circ$  or  $120^\circ$ ) to new angles ( $\beta$ ) that Ramsay (1967) described by:

$$\cot(\beta) = \cos(\alpha) + \gamma \quad (2.1)$$

Limbs rotate at different rates for the same shear strain, depending upon their initial and progressive orientations, thereby modifying the initial 'upright' chevron fold style. This modification is accommodated geometrically in three models for folds over a range of simple shear strains of:  $0 < \gamma < 1$ , as described by Lloyd and Whalley (1986) (see Fig. 2.29).

*Model 1* – The interlimb angle (IA) remains constant and geometric accommodation involves passive rotation of rock slices between rotating slip (i.e. fault) planes on either the 60° (Fig. 2.29i (d)) or 120° (Fig. 2.29i (e)) limbs, thereby conserving the modified fold area in the profile plane. In order to prevent over-riding or separation of rock slices on either side of the fault, three variations to the model are proposed; namely that both limbs rotate and faulting occurs on one of the following parts of the fold: (a) 'extending' (i.e. 60°) limb (Fig. 2.29i (a)); (b) 'contracting' (i.e. 120°) limb (Fig. 2.29i (b)); and (c) axial surface (Fig. 2.29i (c));

*Model 2* – IA varies with simple shear strain accommodation and limb-fault modifications, reducing the fault angle on the 60° (Fig. 2.29ii (a)) and 120° (Fig. 2.29ii (b)) limb;

*Model 3* – IA varies with simple shear strain accommodation but via fold modification only. The 120° limb can be modified and the 60° limb rotates passively, causing broadening of the original synform (Fig. 2.29iii (a)) or antiform (Fig. 2.29iii (b)).

These models have been applied by Lloyd and Whalley (1986) to the Bude Formation chevron folds between Bude and Widemouth Bay (Grid northings: 065-030; Fig. 2.29iv):

1. Faults and fault 'slices' at: 061, 039, 035 and 030, fit model 1;
2. Faults and fault 'slices' at: 063, 062, 059, 056, 054-052, and 034-032, fit model 2;
3. Folds at: 061, 057, 052, 040, 038, 036-035 and 031, fit model 3.

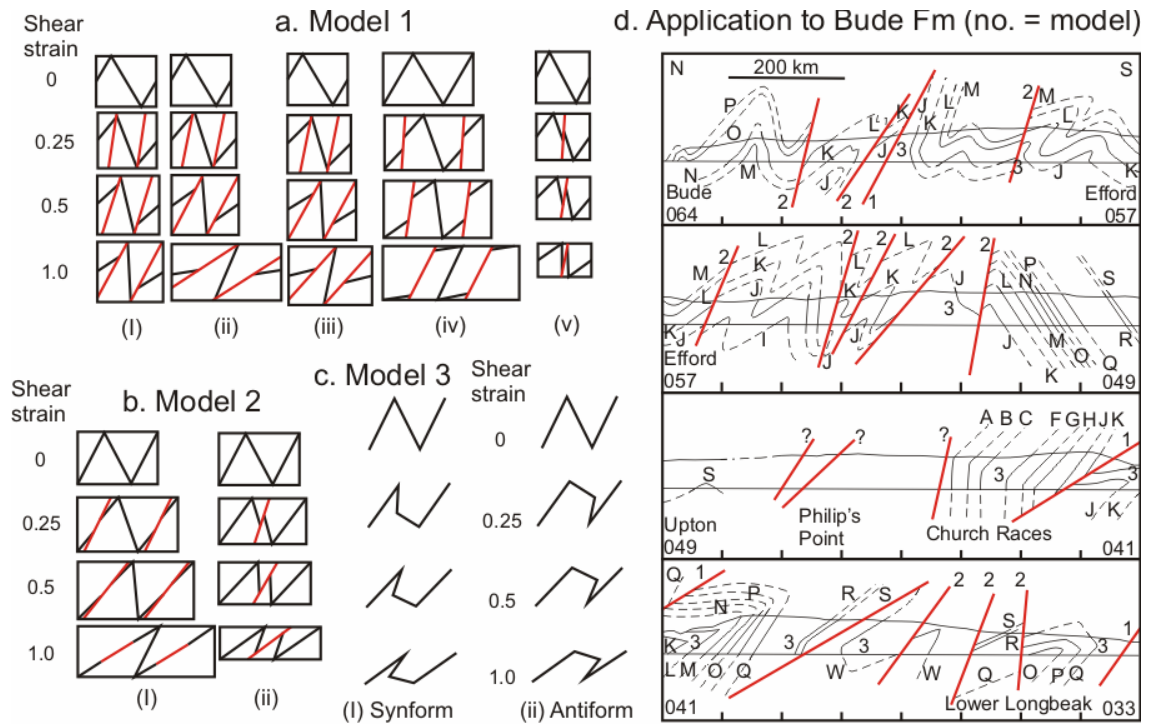


Fig. 2.29: Models for shear modification of 'upright' chevron folds (modified from Lloyd & Whalley, 1986): (i) Model 1: (a) axial plane fault, and  $60^\circ$  limb controls deformation; (b) axial plane fault, and  $120^\circ$  limb controls deformation; (c) axial plane fault, which itself controls deformation; (d) faulting on  $60^\circ$  limb, and  $120^\circ$  limb controls rotation; and (e) faulting on  $120^\circ$  limb, and  $60^\circ$  limb controls rotation; (ii) Model 2: (a) faulting on  $60^\circ$  limb, and  $120^\circ$  limb controls rotation; and (b) faulting on  $120^\circ$  limb, and  $60^\circ$  limb controls rotation; (iii) Model 3: (a) modification of a synform; and (b) modification of an antiform; and (iv) Schematic structural sections of the Bude to Widemouth coastline (amended from King, 1967; Freshney et al, 1972). Numbers 1, 2 and 3 relate to the model interpreted for the modified fold type. Letters A, B, C, etc. from King (1967) stratigraphy. UK national grid northings given at the ends of each section

The manner in which the shear deformation is accommodated by the original chevron folds varies from fold-to-fold. Furthermore, the amount of shear deformation accommodated by the Bude Formation strata varies irregularly, particularly in the coastal sections between Bude and Widemouth (SS202065-SS200029). However, where south-directed 'inclined-to-recumbent' chevron folds occur, there is a general decrease in fold axial plane angle from north to south, as suggested in the earlier model of Sanderson (1979). The Lloyd and Whalley (1986; 1997) back-shear model recognises this general decrease and develops on from the Sanderson (1979) model. Further comparisons of the two models are provided in chapters 4 and 8.

### 2.6.6 Regional metamorphism and geothermal gradients

Very low-grade metamorphism has affected the Palaeozoic deposits of the Culm Basin and SW England. From illite crystallinity (IC) results in the Crackington Formation shales, the degree of metamorphism increases south of Wanson Mouth (SS195015; Dodson & Rex, 1970;

Bishop, 1990; Warr & Hecht, 1993). The highest metamorphic grade reached is mid to upper greenschist facies (i.e.  $450^{\circ}\text{C} \pm 50^{\circ}\text{C}$ ) around Tintagel (SX0589; Primer, 1985b). This occurred before the Bodmin Granite intruded (Andrews et al, 1988), which is dated as  $287 \pm 2$  Ma (Darbyshire & Shephard, 1985). However, there is a sudden northwards decrease in IC-values across the Rusey Fault Zone (SX1497) from the Boscastle Formation epizonal-grade slates ( $> 300^{\circ}\text{C}$ ) to the Crackington Formation anchizonal-grade shales ( $150\text{-}300^{\circ}\text{C}$ ; Grainger & Witte, 1981; Bishop, 1990) (Fig. 2.30). This occurred despite palaeontological evidence to suggest that both formations were deposited in the same Namurian basin (Selwood et al, 1985).

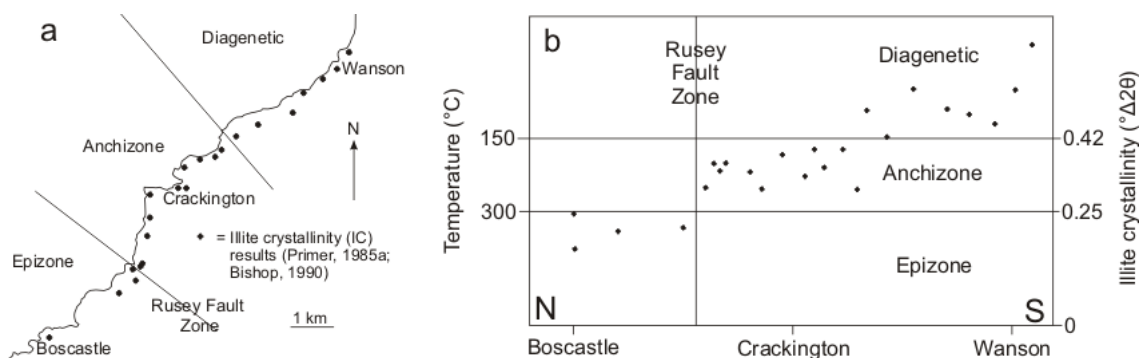


Fig. 2.30: Diagrams of illite crystallinity measurements (modified from Bishop, 1990): (a) Locations of illite crystallinity measurements along the north Cornwall coast; and (b) section along the north Cornwall coast giving the illite crystallinity (IC) and corresponding temperature values for different 'metamorphic' grades (after Kübler, 1967; Primer, 1985a; Bishop, 1990)

The Rusey Fault (SX127940) was interpreted as a thrust by Zwart (1964) and Thompson and Cosgrove (1996). It dips to the NE at more than  $30^{\circ}$  and moved in a top-to-NW direction, emplacing the higher-grade Boscastle Formation over the Crackington Formation at approximately 300 Ma (Warr et al, 1991). This explains the change in IC-values and temperature values recorded across the thrust (Grainger & Witte, 1981; Bishop, 1990) (Fig. 2.30). Following the thrust movement, the Rusey Fault has been deformed by south-directed shearing to obtain its present orientation (Sanderson, 1979; Lloyd and Whalley, 1986).

The metamorphic grade decreases gradually from anchizone to digenetic ( $300\text{-}150^{\circ}\text{C}$ ; Kübler, 1967) to the north of the Rusey Fault (Primer, 1985b; Kelm & Robinson, 1989; Warr & Hecht, 1993) (Fig. 2.30). The decrease in grade may have been sufficient to prevent the sealing of feldspars for metamorphic age dating, in which case the  $^{40}\text{K}\text{-}^{40}\text{Ar}$  age of 329 Ma for the timing of Crackington Formation metamorphism at Crackington (SX1497; Dodson & Rex, 1970) would reflect the age of metamorphism in an adjacent foreland basin, with the sampled grains used by Dodson and Rex (1970) having been eroded and re-deposited in the Crackington Formation. An alternative estimate for the timing of the thermal maximum in the Culm Basin comes from  $^{40}\text{K}\text{-}^{40}\text{Ar}$  whole rock ages for the North Devon Basin, which is dated as approximately 305 Ma (Dodson & Rex, 1970; Warr, 2002). The IC results of Primer (1985b)

and Bishop (1990) suggest that the temperature difference (approximately 75°C) across the Rusey Fault (SX127940) occurred as a result of heating on the Culm basin contact, following Rusey thrust sheet emplacement during northward thrusting (Primer, 1985a).

In order to explain the temperature difference, a geothermal gradient has been calculated by Cornford et al (1987) using an estimate of 7.0-5.8 km for the total pre-erosional sediment thickness of the Bude and Crackington Formations. This estimate was based on the depth to the Culm basin décollement from the seismic survey of Brooks et al (1984). However, in order to account for the temperature difference across the Rusey Fault Zone, these overlying deposits were possibly short-lived (approximately 5 Ma) (Cornford et al, 1987). Warr (1989) suggests that in order to attain this geothermal gradient, greenschist-grade metamorphic rocks had been thrust under the northern Culm basin. The total thickness of the Bude and Crackington formations may have been as much as 1600 m (Freshney et al, 1979) but probably less due to structural repetition (Lloyd & Chinnery, 2002). Thus, even with sediment compaction and major erosion during Variscan orogenesis, the 5.8-7 km burial range of Cornford et al (1987) appears to be too large. Two possible models are proposed to explain the temperature difference.

**Extremely high geothermal gradient/thin succession** – In this model, the present 3.0-3.5 km thickness of the Bude and Crackington formations reflects the maximum burial of the Crackington Formation shales (Cornford et al, 1987). For the shales to have reached a temperature of 250°C, a 70-80°C/km geothermal gradient was required, as has been suggested for the coeval Ruhr and Upper Rhine Basins (Cornford et al, 1987). This extremely high geothermal gradient would have required that simultaneous igneous activity took place, with accompanying metamorphism. Although peak temperatures occurred in the Culm Basin at approximately 305 Ma (Dodson & Rex, 1970) the Bodmin Granite emplacement is dated at 287 Ma ± 2 Ma (Darbyshire & Shephard, 1985), which casts doubt on this explanation.

**Elevated geothermal gradient/thick succession** – In this model, regional tectonic heating raised the geothermal gradient to 40°C/km (Warr, 2002), whilst up to 2 km of now eroded sediment was deposited above the topmost Bude Formation, as envisaged by Cornford et al (1987). If deposition continued, the later sediments may have been either locally deposited or of variable thickness in the basin. Also, as deposition was syn-tectonic (Warr, 2002; Shail & Leveridge, 2009), substantial thickness variations may have occurred. Nevertheless, it remains uncertain whether sediment thicknesses could have reached 7.0-5.8 km in the basin.

### **2.6.7 Geochemistry of the Culm Basin deposits**

Two geochemical studies have been undertaken in the Culm Basin. The first study is an analysis of rare crustal elements from the Bude and Crackington formations outcrops near Exeter, Devon (Haslam & Scrivener, 1991). From these results, it is suggested that: (1) the

provenance for both the Bude and Crackington formations is similar; (2) the beds are quartz-rich, and thus, resistant to weathering; and (3) the deposits are texturally mature.

The second study is the analyses of Light Rare Earth Elements (LREE) and Heavy Rare Earth Elements (HREE) (Diskin, 2008). From these results, it is suggested that the Bude Formation is depleted in LREEs and enriched in HREEs. This contrasts with the Bideford Formation in the northern Culm Basin and suggests that the two formations had different provenances. These findings agree with sedimentological studies on the Bude and Bideford formations by Higgs (1991) and Burne (1995), and are discussed further in Chapter 3.

## 2.7 Summary

This literature review of the geology of the Culm Basin focuses particularly upon the deformation structures formed in sediment and upon chevron fold mechanics, because of their relevance to the general aim of the thesis; namely, to establish the different characteristics of folds in sediment and folds in rock.

The review shows that deformation structures in the study areas encompass features formed by soft-sediment deformation and, in the case of slump folds, when the sediment was liquefied. Slump fold geometries have both similarities and differences when compared with tectonically-generated folds.

The review of fold geometries led onto a more specific discussion of chevron fold development. This included a brief overview of five chevron fold models that described layer properties, kinematics and strain accommodation during fold development.

Particular attention is given to the Variscan orogenesis, basin processes and chevron folds observed in the Late Carboniferous Bude Formation (Culm Basin, SW England), which is part of the specific aim of the thesis. This includes a critical analysis of whether it is appropriate to refer to the Culm Basin as a foreland basin. By reference to the criteria derived from studies of other foreland basins in the geological record, it is considered that the Culm Basin can be referred to as a foreland basin, *sensu lato*.

Lastly, this literature review introduces the key research issues that are explored and investigated in the following chapters. The first of these chapters describes the observations, data collected and analyses undertaken of the sedimentary facies observed in the Bude Formation outcrops, as part of the specific aim of the thesis. From the sedimentary data and observations, new insights are provided into the Bude Formation depositional environment and placed into the context of previously published models, as described in Chapter 3.

## Chapter 3: Sedimentological interpretation of the Bude Formation

### 3.1 Introduction

The Bude Formation is located in the Culm Basin, north Cornwall-north Devon, SW England, with some of its most accessible exposures found along the coast around Bude, north Cornwall. This sedimentary study of the Bude Formation deposits is part of the specific aim of the thesis, with the focus upon its coastal outcrops between Northcott Mouth (National Grid Reference: SS202087) and Black Rock (SS195015; Fig. 3.1a), which form a well-exposed sedimentary succession (see Chapter 1). A detailed facies analysis is supported by petrography, ichnological observations and published palaeo-flow indicators (Freshney et al, 1979; Higgs, 1991; Burne, 1995) as well as carbon-sulphur (C/S) data (Lloyd & Chinnery, 2002) in an attempt to develop an improved environmental interpretation.

Culm Basin deposition occurred during the Pennsylvanian (Bashkirian-Moscovian), equivalent to the Late Carboniferous (Westphalian A-C) (Reading, 1965; King, 1966; Freshney et al, 1972; 1979; Gradstein et al, 2004; Walker & Geissman, 2009). Basin subsidence has been interpreted to be driven by foreland flexural down-warping ahead of the Variscan mountain belt to the south together with uplift of the Bristol Channel Fault Zone to the north (Shackleton et al, 1982; Coward & Smallwood, 1984; Warr, 2002; Shail & Leveridge, 2009; see Chapter 2).

Stratigraphically, the Bude Formation lies above the turbiditic Crackington Formation deposits in the central and southern Culm Basin (Freshney et al, 1979; Melvin, 1986; Warr, 2002). The generally coarsening-up and cyclic deltaic Bideford Formation lies in the northern Culm Basin and includes black shale beds with *listeri* and *amaliae* goniatites that correlate with the middle-to-top Crackington Formation and base Bude Formation (de Raaf et al, 1965; Li, 1990; Higgs, 2004). In the study area, the laterally-continuous Tom's Cove and Saturday's Pit shales were correlated by King (1971) based on the presence of brackish-water tolerant fish and lateral stratigraphic thickness changes measured (Freshney et al, 1972; 1979), the thicknesses being about 70 m at Northcott Mouth, 25 m at Bude and 105 m at Upton (Figs. 3.1a & b).

Many of the sedimentary structures in the Bude Formation outcrops have been well documented. Many beds are observed to be sharp-topped and sharp-based with flutes on the bed bases, which are indicative of turbidite beds (Higgs, 1991; Burne, 1995). However, there is a continuing debate about the Bude Formation depositional environment, which has given rise to at least six contrasting depositional models, these being:

**Model 1: Fining-up delta (King, 1971):** This model discusses the small (no scale), cyclic, fining-up packages of fine-grained sandstones to siltstones to carbonaceous shales, the latter having been deposited in a variably saline environment. Each package was interpreted as representing a change from fluvial conditions, with rapid fine sand sedimentation during a period of oscillatory flow, to slow deposition (suspension fall-out) under relatively deepwater

conditions. Specific black shales contain lacustrine palaeoniscoid fish *Cornuboniscus budensis* and brackish-water tolerant coelacanthid *Rhabdoderma elegans* (Forey, 1981). A limited and variable trace fossil assemblage has been used to infer variable salinities. From the cyclical stratigraphic architecture of the Bude Formation, a correlation was proposed with nine localised deltaic cycles as in the Bideford Formation (de Raaf et al, 1965).

**Model 2: Wave and storm influenced shallow water environment (Higgs, 1984):** Rippled bedding surfaces and ripple cross-lamination in Bude Formation siltstones to very fine sandstones, with only slightly asymmetric ripple crests, have been interpreted as oscillatory ripples. The slight ripple asymmetry was interpreted as either: (a) shoaling, where oscillatory motions became asymmetric; or (b) combined flows, where oscillatory wave motion occurred in tandem with a uni-directional current. Also, hummocky cross-stratification was described and interpreted as the product of storm-wave oscillations, whilst sharp-based, normal-graded, very fine sandstones were considered typical of waning-energy event beds. The sedimentary structures are interpreted to represent wave-influenced deposition in the lower to mid-shoreface, coupled with periodic marine inundation of an otherwise fresh to brackish water lake setting, was also suggested on the basis of the palaeontological evidence from Freshney et al (1979).

**Model 3: Prograding turbidite fan (Melvin, 1986):** This model invokes deposition of the Crackington and Bude formations within a delta-fed subsea fan. The thick Bude Formation sandstones are interpreted as the deposits from turbidity currents in a relatively shallow basin. A key observation by Melvin (1986) is that upwards-thickening and upwards-thinning packages are no more common than symmetric packages, but that all of these occur much less frequently in the Bude Formation than do disorganised packages. He suggested that siltstone and sandstone deposits within both formations are interbedded with laterally-continuous “key” shales that resulted from delta-lobe abandonment. Whilst Melvin (1986) recognizes the importance of external variables, such as active seismicity and downslope resedimentation, his model emphasizes autocyclic lobe switching as the major control on facies architectures.

**Model 4: Shallow marine ramp (Hartley, 1991):** In this model, a predominantly turbiditic sequence was deposited on a shallow sub-aqueous fan (Melvin, 1986) or a brackish-water, low-angle, shallow-marine ramp that lacked a single significant feeder channel system. The slumps and ‘debrites’ are recognised as key deposits, with ‘debris flows’ generated from slope failure on the fan or ramp system. Palaeo-current directions suggest that there was a south-dipping palaeo-slope, with failure on an unstable northern margin from the Bideford Formation delta.

**Model 5: Freshwater lake (Higgs, 1986; 1991):** Higgs developed his 1984 interpretations further, with a model that considers the early Westphalian ‘Lake Bude’ to have been an

equatorial freshwater lake in which there were characteristic alternating periods of sand-poor and sand-rich sedimentation. An idealised cycle was described as comprising in ascending order: dark grey laminated mudstones with sparse (centimetric scale) event beds; light grey silty mudstones with one or two event beds (up to 30 cm thick); a thick (decimetric to metric scale) sandstone; silty mudstone facies association; and laminated mudstones facies association. The key sedimentary structure that Higgs (1986; 1991) recognised was the centimetric-scale, asymmetric, sinuous-crested combined-flow ripples, which was interpreted as being deposited from waning storm-generated turbidity currents in a lake shoreface environment that was affected by wave processes. Higgs (1991) also recognised seismites, which occur due to syn-depositional earthquake activity (see Chapter 2), and 0.2 m deep scours.

Integrating this sedimentology with palaeontological signatures and C/S ratios from five silty mudstones, it was suggested that in a lower to mid-shoreface environment, each idealised cycle coincided with a trend from brackish water to freshwater and back to brackish water conditions. Three of the mudstones were recognised as fully marine, based upon the presence of goniatites and pelagic bivalves described by Freshney et al (1979). Except when over-topped during sea-level highstands, the model invoked a sill that blocked the pre-Bude Formation E-W seaway from open marine conditions, so that brackish (and rarely marine) salinities developed and thick black shales were deposited. Higgs (1986; 1991) interpreted the sandstones as event beds fed by river-derived underflows and reworked by wave-oscillations above the storm wave base. The absence of cycles containing nearshore or emergent facies occurred as a result of:

1. A regional sill that separating the depositional environment from a full marine connection, which was sufficiently high that only during eustatic maximum flooding was it over-topped;
2. Monsoonal conditions that generated an annual flood;
3. Relatively distal deposition beyond shoreline progradation.

**Model 6: Variably-oxygenated inactive fan (Burne, 1995):** In this model, the Bude Formation is proposed to be very similar to the underlying Crackington Formation, with the exception of thick sandstone units being present. Also, depositional continuity with the Bideford Formation deltaic deposits in the northern-most Culm Basin is questioned. The Bude Formation facies are interpreted as 10-60 m thick “non-random alternations” between: (1) black shale facies, from fine-grained turbidites in a generally anoxic basin; (2) muddy siltstone facies, from current-influenced, oxygenated environments (possible fan levees); (3) inter-bedded sandstone-shale facies, from either levee, lobe or inter-channel turbidite environments; and (4) sandstone-dominated facies from channel-fill and fan valley environments.

A shallow shelf depositional environment is not invoked for the Bude Formation deposits as in Higgs (1991). Instead, hummocky cross-stratification resulted from anti-dunes and rippled bed tops resulting from reworking by the tail of a waning turbidity current. Thus, the



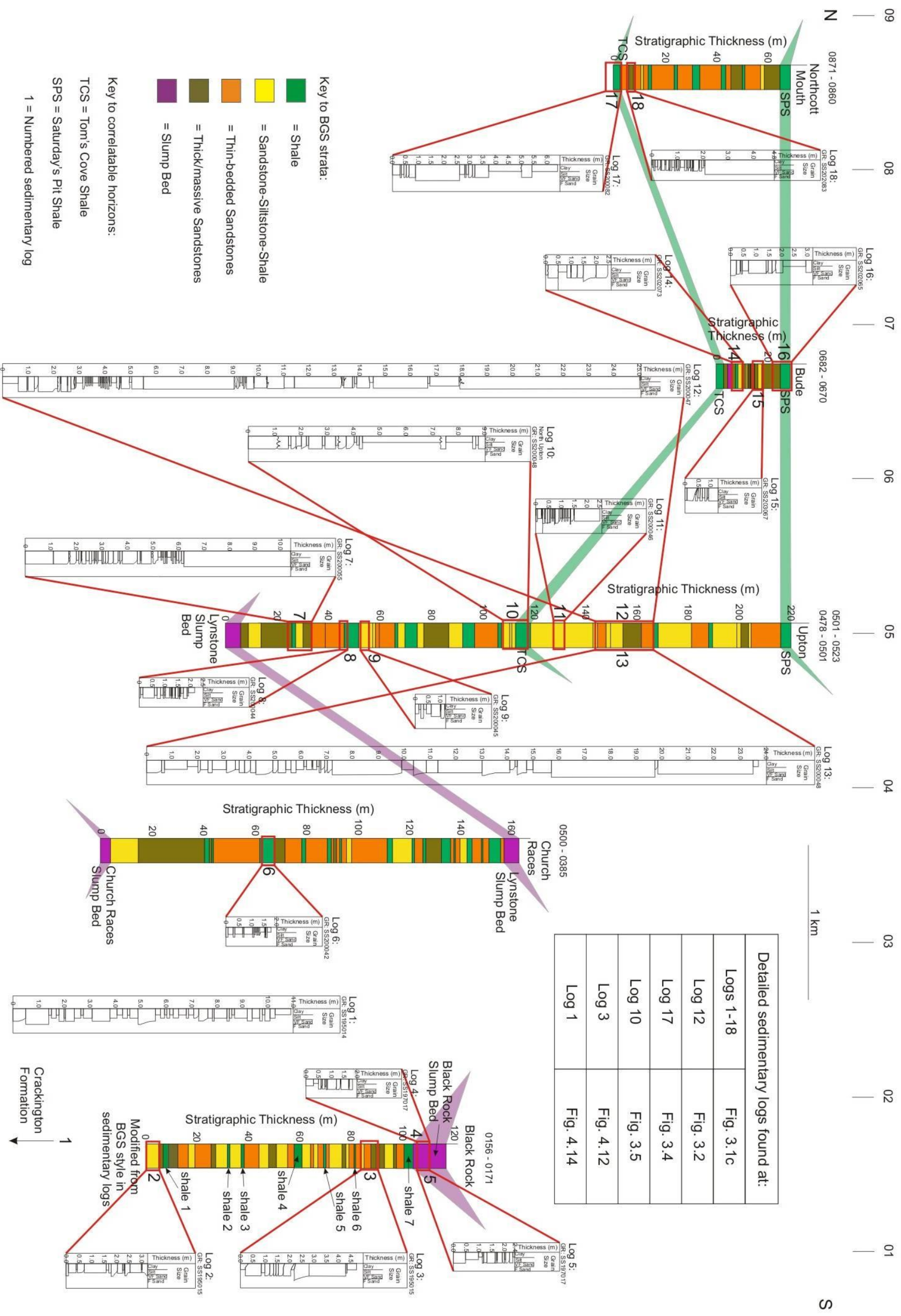
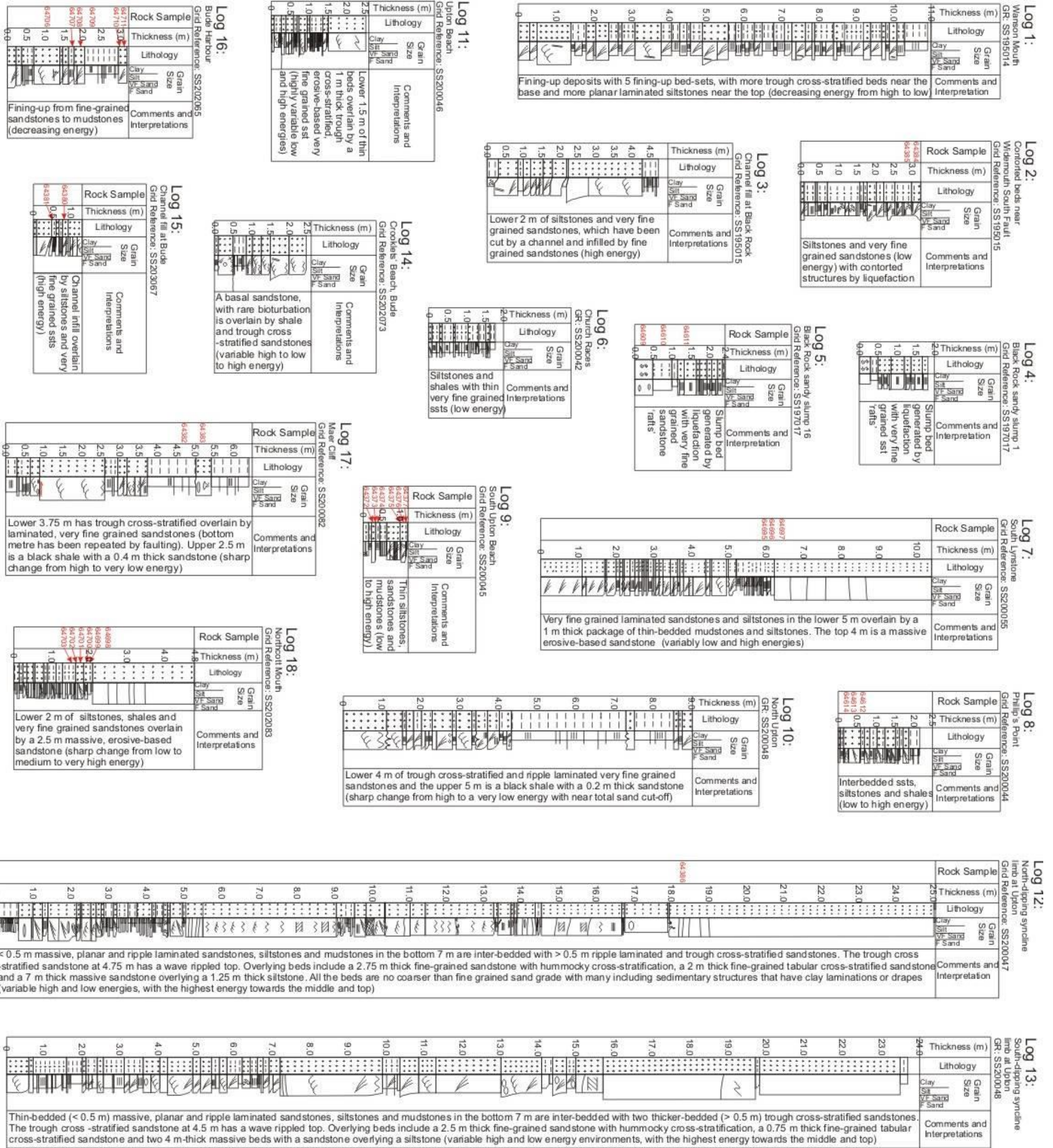


Fig. 3.1b: Correlation panel of BGS coloured logs shown in Fig. 3.1a with the 17 correlated Bude Formation sedimentary logs from Northcott Mouth to Black Rock (SS202083-SS195015) and one log from the Crackington Formation at Wanson Mouth (SS195014). Each sedimentary log displays bed thickness and grain size. The full log suite is shown in Fig. 3.1c. The coloured logs are correlated using two laterally-continuous black shales, the Tom's Cove Shale (TCS) in logs 10 and 17, and the Saturday's Pit Shale (SPS) in log 16. Shales 1-7, which are highlighted in the Black Rock coloured log, are described and discussed in Chapter 4



**Fig. 3.1c: Collage of the detailed sedimentary logs for the Bude Formation (2-18) and Crackington Formation (1), showing bed thickness, grain size, sedimentary structures, lithology, rock sample numbers and a brief set of comments and interpretation for each log. A less detailed version of the logs are correlated with coloured logs gathered and modified from BGS sedimentary descriptions in Fig. 3.1b**

- Key for all sedimentary logs:**
- Lithology:**
- = Shale
  - = Siltstone
  - ... = Sandstone
  - ⊖ = Massive slump bed
- Sedimentary Structures:**
- ≡ = Planar laminations
  - ∩ = Ripple coset laminations
  - ∩ = Trough cross-stratification
  - ∩ = Undulose cross-stratification
  - ∩ = Hummocky cross-stratification
- Syn-depositional Structures:**
- ∩ = Soft-sediment deformation
  - ∩ = 'Flame' and load structures
  - ∩ = Syn-depositional normal faults
- Other Features:**
- ∩ = Bioturbation
  - ∩ = Rip-up mud clasts
  - ∩ = Siderite diagenetic nodule
  - ∩ = Low-angle detachments
  - ∩ = Fold hinge thrust
- 64377 = Rock sample number

The lack of agreement on the depositional environment has necessitated a reassessment of the sedimentary structures. An analysis of sedimentary data has led to a new facies scheme and a comparison between the facies recognised in this work and those by other authors. From this, a re-interpretation of the Bude Formation depositional environments is proposed.

### 3.2 Methods

As part of reassessing the depositional environments, 17 detailed sedimentary logs of the Bude Formation outcrops were taken between Northcott Mouth and Black Rock (SS201087-SS198016), plus another log in the Crackington Formation at Wanson Mouth (SS195014), with a photographic record of each logged section and sample numbers provided (Fig. 3.1c). The full logs describe bed thickness and colour, lithology, sedimentary structures, grain size, diagenetic features, syn-depositional structures and ichnofabrics. From the detailed logs, a facies scheme with ichnofabric descriptions was developed, with North Upton log 12 (SS200047) considered representative of the deposits (Fig. 3.2) because it includes almost all the observed facies types.

The ichnofabric analysis compared the logged associations to those associations described by Higgs (1991) and Burne (1995). Likewise, the palaeo-flow indicators from 7 examples of trough cross-stratification structures and 22 examples of tool marks and ripple laminations have been measured across the field study area between Northcott Mouth and Black Rock (SS202087-SS195015). These data have been compared with the results of Freshney et al (1979), Higgs (1991) and Burne (1995). The palaeocurrent data from flutes, grooves and tool marks collected by Melvin (1986) was outside the study area to the north of Northcott Mouth and so has not been compared with these results.

In order to provide a context for the Bude Formation deposits, stratigraphic correlation of the continuous black shales was undertaken using sedimentary descriptions and logs from the BGS Memoirs (Freshney et al, 1972; 1979). The 17 detailed sedimentary logs taken between Northcott Mouth and Black Rock (SS201087-SS195015) were placed into their relative lateral and stratigraphic positions using the BGS correlated logs, providing further details on the vertical stacking patterns for palaeo-environmental reconstruction (Figs. 3.1a & b), despite the lateral stacking patterns being restricted by the width of outcrop on the coastal foreshore.

Rock samples, tied to the logs (Fig. 3.1c), were collected across the study area in order to test for differences in the mineral proportions related to the deposition of the facies. Folk diagrams show the estimated proportions of quartz, feldspar, lithic fragments and mud in different sandstone, siltstone and slump beds; along with the proportions of clay, organic matter and carbonates in shale beds, obtained from microscopic petrographic analysis of 50 thin sections. The composition of the samples was compared with results from two studies by Freshney et al (1979) and six from other foreland basin deposits (Schwab, 1986).

Eight of the samples (six shales and two sandstones) were turned into polished blocks in order to study the micro-structures of the slump and chevron folded beds at Upton (SS200046)

and Bude (SS201065), using a scanning electron microscope (SEM) in the backscattered electron (BSE) atomic number (Z) contrast mode, combined with an energy dispersive X-ray microanalysis. As with thin section analysis, the SEM was used to identify minerals, including diagenetic phases, as well as cross-cutting and over-printing relations in the different lithologies. This enabled a diagenetic sequence for the Bude Formation to be proposed. For example, pyrite framboid populations and their sedimentary fabrics provided a proxy for depositional oxygenation conditions (Table 3.1; Bond et al, 2004).

Oxygenation conditions	Framboidal populations	Sedimentary fabric
Euxinic (Anaerobic)	Small (< 5 $\mu\text{m}$ ); abundant with narrow size range	Finely laminated
Lower dysoxic (Lower dysaerobic)	Small (< 5 $\mu\text{m}$ ); abundant but with rare, large framboids	Finely laminated
Upper dysoxic (Upper dysaerobic)	Moderately common to rare; broad size range with only small proportions < 5 $\mu\text{m}$ diameter	Some micro-burrowing; bioturbation partly obscures fine laminations
Oxic (Aerobic)	No framboids, very rare pyrites	Burrowed-to-massive; no fine laminations

Table 3.1: Summary of characteristics to define oxygen-related depositional conditions and facies in shale beds (from Bond et al, 2004)

The previously published results of carbon-sulphur (C/S) geochemical analyses in the Bude Formation (Lloyd & Chinnery, 2002) have been incorporated into this study because it provides a measurable proxy for syn-depositional water salinities, following the methods of Berner and Raiswell (1984) with a chemical proxy used (ratio of sulphur (S) to organic carbon (C)). In freshwater samples, the amount of sulphur can be either zero or very low compared to the amount of carbon (i.e.  $S < 0.8\%$ ) and vice versa in marine samples (i.e.  $S > 1.5\%$ ).

Brackish-water samples contain intermediate amounts of sulphur (i.e.  $0.8\% < S < 1.5\%$ ). From calculations of the total amounts of organic carbon (C) and sulphur (S), an S:C ratio is defined, providing a salinity proxy during deposition (from the methods of Berner & Raiswell, 1984):

1. Relatively low S:C ratio values ( $< 0.06$ ) indicating a freshwater depositional environment;
2. Relatively high S:C ratio values ( $> 0.25$ ) indicating a marine depositional environment;
3. Values in the range of 0.06 to 0.25, indicating a brackish-water depositional environment.

### 3.3 Facies within the Bude Formation

The Bude Formation beds contain a range of sedimentary structures (Table 3.2), with the most abundant being planar laminations and two types of ripple coset laminations within siltstones and very fine-grained sandstones. Previously unrecognised trough cross-stratified beds and rare tabular cross-stratified beds were identified by the author (Figs. 3.1c & 3.2). The trough structures occasionally display mud draped bases, whilst reactivation surfaces are occasionally observed in trough cross-stratified beds.

Key for sedimentary log 12:

- Lithology:**  
 --- = Shale  
 --- = Siltstone  
 ... = Sandstone
- Sedimentary Structures:**  
 ≡ = Planar laminations  
 ↗ = Ripple coset laminations  
 ↘ = Trough cross-stratification  
 ~ = Hummocky cross-stratification  
 ≡≡ = Tabular cross-beds
- Syn-depositional Structures:**  
 ~ = Soft-sediment deformation  
 λ = 'Flame' and load structures
- Other Features:**  
 ~~~ = Bioturbation  
 ○ = Rip-up mud clasts  
 ○ = Siderite diagenetic nodule  
 — = Low-angle detachments

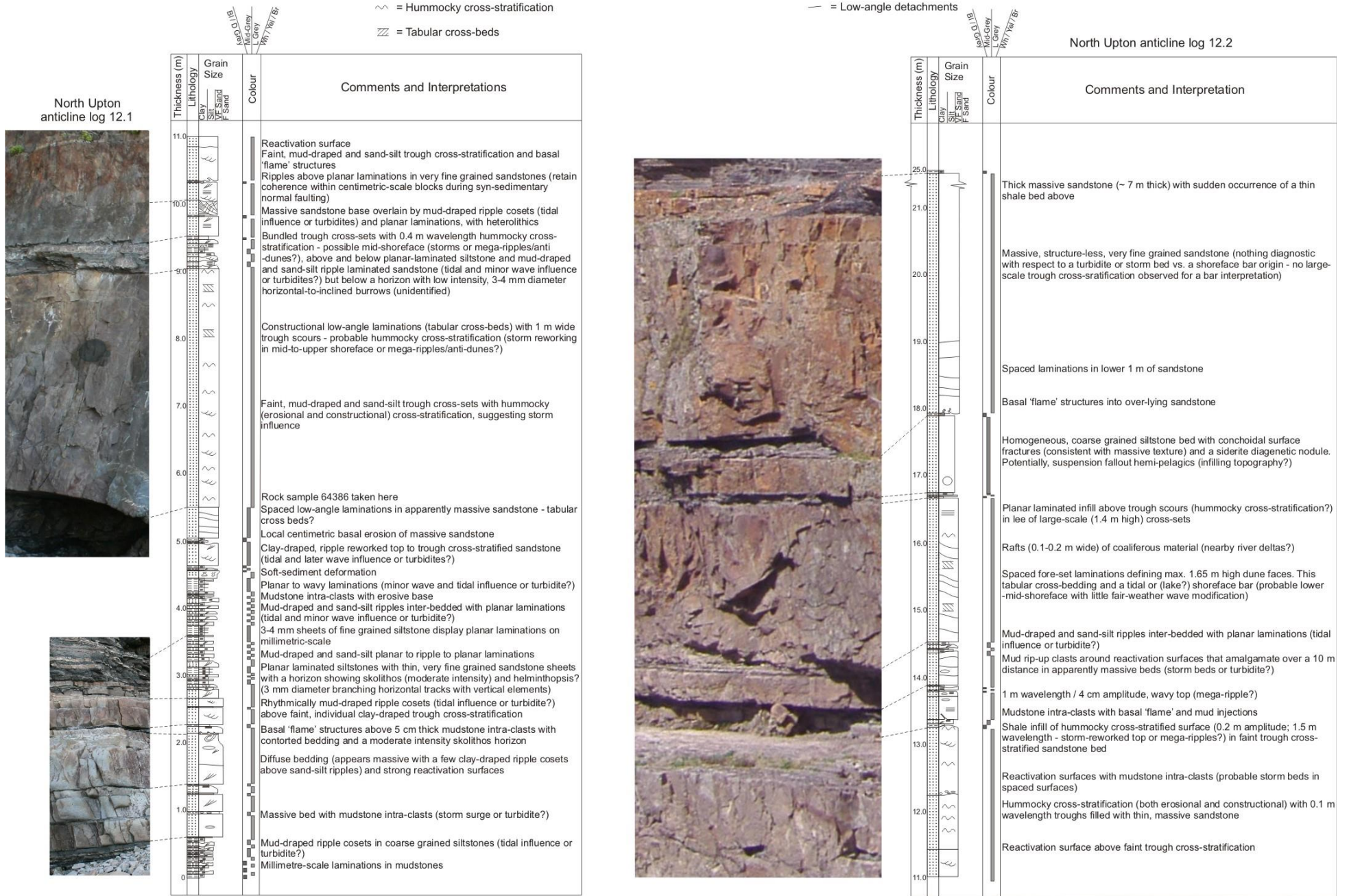


Fig. 3.2: Combined sedimentary logs over a 25 m vertical section in the cliffs from North Upton anticline (SS200047) showing most of the sedimentary facies types described in this chapter

| Parameter                                                | Thickness of bed (m)            | Grain size range    | Sedimentary structure dimensions (m)                                        | Sedimentary structure description                                                                                                       | Other features                                                                                                                                    | Facies (Higgs, 1984) | Facies (Higgs, 1986)                | Facies (Melvin, 1986) | Facies (Higgs, 1991)              | Facies (Hartley, 1991) | Facies (Burne, 1995)              |
|----------------------------------------------------------|---------------------------------|---------------------|-----------------------------------------------------------------------------|-----------------------------------------------------------------------------------------------------------------------------------------|---------------------------------------------------------------------------------------------------------------------------------------------------|----------------------|-------------------------------------|-----------------------|-----------------------------------|------------------------|-----------------------------------|
| 1a: Ripple laminated sandstones and siltstones           | < 0.5                           | Silt-Very fine sand | Stoss: 3.0-7.5 cm; Lee: 0.5-2.5 cm; Amplitude: 0.5-1.25 cm                  | Common rhythmic silt-sand laminations in asymmetric, sinuous-crested ripples with some ripples cross-cutting                            | Rare rip-up mud clasts. Sedimentary structures observed within sharp topped-sharp based beds. Mid to dark grey                                    | Yes                  |                                     | Yes                   | Yes                               |                        | Yes                               |
| 1b: Mud-draped ripple laminated sandstone and siltstones | < 0.5                           | Clay-Very fine sand | Stoss: 3.0-7.5 cm; Lee: 0.5-2.5 cm; Amplitude: 0.5-1.25 cm                  | Rare rhythmic clay-silt laminations in mud-draped, asymmetric, ripple cosets with some cosets cross-cutting                             | Rare rip-up mud clasts. Sedimentary structures observed to rework sharp topped-sharp based beds. Mid to dark grey                                 |                      |                                     |                       |                                   |                        |                                   |
| 2a: Trough cross-stratified sandstone                    | 0.2 - 5.0                       | Very fine sand      | Width: 5-15 cm; Depth: 2-5 cm                                               | Bundled and individual troughs incise lower structures. Infilling sediment overlies margins                                             | Common rip-up mud clasts; rare load-'flame' structures on bed base. Light to mid grey                                                             |                      |                                     |                       |                                   |                        |                                   |
| 2b: Mud-draped trough cross-stratified sandstone         | 0.2 - 1.0                       | Clay-Very fine sand | Width: 5-15 cm; Depth: 2-5 cm                                               | Rare mud-draped bases to bundled and individual troughs that incise lower structures. Infilling sediment overlies margins               | Same as above                                                                                                                                     |                      |                                     |                       |                                   |                        |                                   |
| 3a: Undulose cross-stratified sandstone                  | Effects beds on decimetre scale | Very fine sand      | Undulations: wavelengths 10-15 cm; amplitude ~ 1 cm                         | Rare undulations have sandy horizon (1-2 cm thick) with mud rip-up clasts above an erosion surface in trough cross-stratified sst       | Basal mud drapes or ripple coset laminations, followed by trough cross-stratification structures above undulations. Light to dark grey            | Yes                  | Yes                                 |                       | Yes                               |                        | Anti-dunes                        |
| 3b: Hummocky cross-stratified sandstone                  | Effects beds on metre scale     | Very fine sand      | Hummocks: wavelengths 1-2 m; amplitude 10-15 cm                             | Erosional scours alternate with low-angle cross-stratification. Aggradational with convex-up surfaces                                   | Light to mid grey                                                                                                                                 | Yes                  | Yes                                 |                       | Yes                               |                        |                                   |
| 4: Tabular cross-bedded sandstone                        | > 1.4                           | Fine sand           | Large-scale (amplitude up to 1.4 m) cross-beds                              | Large-scale, sharp-based, tabular cross-sets                                                                                            | Same as above                                                                                                                                     |                      |                                     |                       |                                   | Mention                |                                   |
| 5a: Planar laminated beds                                | < 0.2                           | Silt-Very fine sand | Silt lam.: 0.1-0.25 mm; Sand lam.: 0.25-0.5 mm                              | Thin silt-sand laminations                                                                                                              | No mud rip-up clasts. Mid grey                                                                                                                    |                      | Yes                                 | Yes                   | Yes                               |                        | Yes                               |
| 5b: Mud-draped planar laminated beds                     | < 0.2                           | Clay-Very fine sand | Mud lam.: < 0.1 mm; Silt/Sand lam.: 0.1-0.5 mm                              | Rare thin, bundled, mud-silt/sand, 'tramine' laminations. Silt/sand interspersed with minor mudier laminations and vice versa           | No mud rip-up clasts. Muddier laminations may include bedding-parallel carbonate veins (0.1-2.0 mm thick). Mid to dark grey                       |                      |                                     |                       |                                   |                        |                                   |
| 6: Amalgamated, massive siltstone                        | 0.1 - 4.0                       | Silt                | No structures; bioturbation occasionally; Burrows: < 1 cm wide; < 5 cm long | Massive, amalgamated bedding. Rare burrows cause sediment mixing. Some bed bases include flutes, indicative of turbidites               | Conchoidal fractures; some basal loads-'flames'; few low density/diversity ichnofabrics: Skolithos; Mid to dark grey (light in burrows)           |                      | Yes                                 | Yes                   | Yes                               |                        | Yes                               |
| 7: Amalgamated massive sandstone                         | 0.1 - 8.0                       | Very fine sand      | No structures; bioturbation occasionally; Burrows: < 1 cm wide; < 5 cm long | Same as above                                                                                                                           | Same as above but with Skolithos & Helminthopsis ichnofabrics observed                                                                            |                      | Yes                                 | Yes                   | Yes                               |                        | Yes                               |
| 8: Planar laminated shale                                | 0.02 - 6.0                      | Clay                | Laminations: < 0.1 mm                                                       | Thin clay laminations with silt-very fine sand grained, bedding-parallel stringers. Bedding-parallel carbonate veins (0.1-2.0 mm thick) | Some contorted bedding and veins. Local structures may affect bed thicknesses. Dark grey to black                                                 |                      | Dark mudstone and interbedded shale | Yes                   | Black shale and interbedded shale | Yes                    | Black shale and interbedded shale |
| 9a: Internally-contorted bed                             | Within beds on decimetre scale  | Clay-very fine sand | Stringers: 1-5 cm thick; Contortions/slumps: 3-5 cm thick                   | Mud-draped slump structures and contortions within each affected bed                                                                    | Poorly-developed E-W-striking joints within slump and other liquefaction structures. Bedding-parallel contorted carbonate veins. Mid to dark grey |                      |                                     |                       | Seismites                         |                        | Slurrites                         |
| 9b: Attached slump bed                                   | Thin beds on metre scale        | Clay-very fine sand | As planar laminated and ripple coset laminated structural dimensions        | Individual beds remain in stratigraphic order and retain original sedimentary structures (planar or ripple coset laminated)             | Slump structure formed after E-W-striking joints and bedding-parallel carbonate veins in shales. Mid to dark grey in cohesive beds                |                      |                                     |                       |                                   |                        |                                   |
| 9c: Disaggregated massive slump bed                      | Unit on tens of metre scale     | Clay-very fine sand | Massively bedded with sand rafts: < 1 m thick;                              | Massively bedded, disaggregated matrix includes detached folded sand rafts and normal-faulted blocks in slump head                      | No E-W-striking, bedding sub-perpendicular joints as in other beds. Rare siderite nodules. Slump associated with black shales. Mid to dark grey   |                      | Yes                                 | Yes                   | Yes                               | Debrites               | 'Slumped' beds                    |
| 10: Channel fill facies (various lithologies)            | Stacked beds up to 2 m          | Clay-fine sand      | Channel: > 2 m deep; > 20 m wide; Metric-scale cross-beds may fill channel  | Stacked beds infill channel structure; Basal thin shale horizon; Stacked either with sst-silt-shale beds or cross-bedded sst            | Two channels observed at Bude and Black Rock; N-S channel axes; channels truncate earlier beds; Stacked beds: light to dark grey                  |                      |                                     |                       | Scours                            |                        | Yes                               |

Table 3.2: Table of the different sedimentary facies recognised in the Bude Formation outcrops together with a table of comparison for the different recognised facies by the author with that of Higgs (1984; 1986; 1991), Melvin (1986), Hartley (1991) and Burne (1995)

These deposits are variously inter-bedded with very fine to fine sand-grade, metric to decametric scale massive beds; internally-contorted sandstones and siltstones; planar laminated shales; and rare massive slump beds. The massive to amalgamated beds, many with flutes on bed bases, include occasional low density and diversity bioturbated tops with *Skolithos* and *Helminthopsis* ichnofabrics. Two erosive-based channels with mud-covered bases and infilled by massive and trough cross-stratified sandstones were observed in outcrop (see Fig. 3.1c). The following adds detail and interpretations to the sedimentary facies outlined in Table 3.2.

### **3.3.1 Siltstones and sandstones with ripple laminations (Facies 1a and b)**

Facies 1a siltstones and sandstones with ripple laminations equate to the common ripple laminations of Burne (1995), which are also described as combined-flow or sinuous-crested, quasi-symmetrical ripples as observed at North Upton (SS200047) by Higgs (1986; 1991). Facies 1b consists of mud-draped ripple cosets that alternate between sand or silt laminations and mud laminations (Figs. 3.1c, 3.2 & 3.3b, d & g). Some mud-draped structures are deposited in a near-rhythmic pattern, with cycles of sandier / siltier ripple laminae giving way to thinner, millimetric laminae that alternate with clay partings (Fig. 3.3g). Silty and sandy laminae then increase in grain size and thickness, with a progressive loss of muds, before the cycle (3-8 cm long) is repeated. The mud-draped ripples of facies 1b may be interbedded with facies 1a ripples, but the former are usually found at the tops of beds otherwise dominated by facies 1a siltstone and sandstone ripple laminations. The mud-draped ripples and ripple cosets of facies 1a and 1b have not been differentiated in previous studies.

In the siltstone beds, the dimensions of both types of ripple laminations are: 3.0-5.0 cm wide stoss sides; 0.5-1.5 cm wide lee sides; and 0.5-0.75 cm amplitudes. In the sandstone beds, the ripple dimensions are: 5.0-7.5 cm wide stoss sides; 1.5-2.5 cm wide lee sides; and 0.75-1.25 cm amplitudes (Fig. 3.3e). From these data, the ripple index range has been estimated as 6.5-8.5, whilst ripple symmetry index ranges from 2.5-3 (Reading, 1996; Collinson et al, 2006). From these estimates, the similar sized facies 1a ripples and facies 1b mud-draped ripple laminations are generally interpreted as representing unidirectional current action. However, some ripples, in particular bed-top ripple forms, include more symmetric geometries that overlap between current and wave ripple forms (Collinson et al, 2006), as also interpreted by Higgs (1991).

#### **Facies interpretation**

One possible mechanism to generate mud-draped ripples (facies 1b) is fluctuating current activity due to semi-diurnal or diurnal, astronomical tidal cyclicity (Visser, 1980). Mud drapes would represent deposition during slack tidal phases, whilst silty/sandy ripples or ripple cosets would represent active tidal sediment transport and deposition. No herringbone cross-bedding was observed in the Bude Formation, but this could be explained by the occurrence of a dominant tidal current that was sufficiently energetic to transport sediment, compared to a

subordinate tidal current that was not (after Visser, 1980). Centimetric-scale mud-draped ripples are described from modern sub-tidal channel-fill deposits in the SW Netherlands. They occur in ebb-dominated 0.2-2.5 m high tidal dunes that exhibit demonstrably semi-diurnal mud couplets in their bottomsets, separated by a thin layer of sandy ripple laminations of opposing current direction, produced by the subordinate flow (Visser, 1980; de Boer et al, 1989).

If the dominant currents had a lower velocity in the case of the facies 1b setting, then it is feasible that ripple coset laminations might represent only the dominant flow, with the mud-drapes being the slack water and subordinate flow phases (Reading, 1996). The modern Oosterschelde example of Visser (1980) shows successive tidal bundles (foreset laminae separated by slack water mud drapes) thickening and thinning with a sinusoidal cyclicity due to the spring-neap-spring cycles, with evidence of slack water mud drapes and subordinate flow current reversals. Fig. 3.3g illustrates the near-rhythmic changes in the ratio of silty / sandy laminae to mud drapes in the Bude Formation ripple cosets at North Upton (SS200047). These mud-draped cosets hint at a tidal cyclicity. However, in the absence of observed current reversals, which could be considered diagnostic of tidal influence when taken together with the near-rhythmic structures, alternative causes for these small-scale structures are considered also.

Ainsworth et al (2012) describe sediments from coastal deposits of the modern Lake Eyre in Australia. Facies include mud-draped tabular cross-beds and trough cross-bedding up to 0.25 m in thickness. Paired mud drapes (mud couplets defining bundles) are described as common. Mud-draped, small-scale (5-8 cm wavelength) symmetric ripple forms are also present (wavy bedding in the terms of Ainsworth et al, 2012). Lake Eyre is non-marine, being located in an intracratonic playa lake setting. Ainsworth et al (2012) ascribe the observed sedimentary structures to meteorological “tides”, related to cyclical daily changes in wind direction and velocity, in combination with weekly or monthly variations in fluvial discharge. This raises an alternative set of mechanisms for generating Bude Formation facies 1b mud-draped ripples and ripple cosets that would otherwise require a nearshore, shallow water depositional environment.

Mud drapes have also been generated in experimental conditions that are centimetric-scale dune forms deposited from muddy-sandy turbidity current underflows (Baas et al, 2011). In both facies 1b mud-draped ripples and these small-scale dunes, finer-grained elements would have formed during locally and episodically waning flow conditions. Longer term waning flow conditions may result in mud-draped tops to beds and structures (Kneller & Branney, 1995).

Ripple-laminated siltstones and sandstones can have a turbiditic origin, but are not themselves diagnostic of this. For example, flute-marks on these bed bases (as observed in the Bude Formation) or on the bed bases of massive or fining-up sandstones, would provide stronger evidence. Also, turbidity currents generated from storm or slump-generated suspended sediment, or direct fluvial discharge, may occur in both lacustrine and marine environments at various water depths (Reading, 1996). Thus, other palaeoenvironmental evidence is needed in order to establish the cause of the observed ripple laminations, which is discussed in section 3.9.

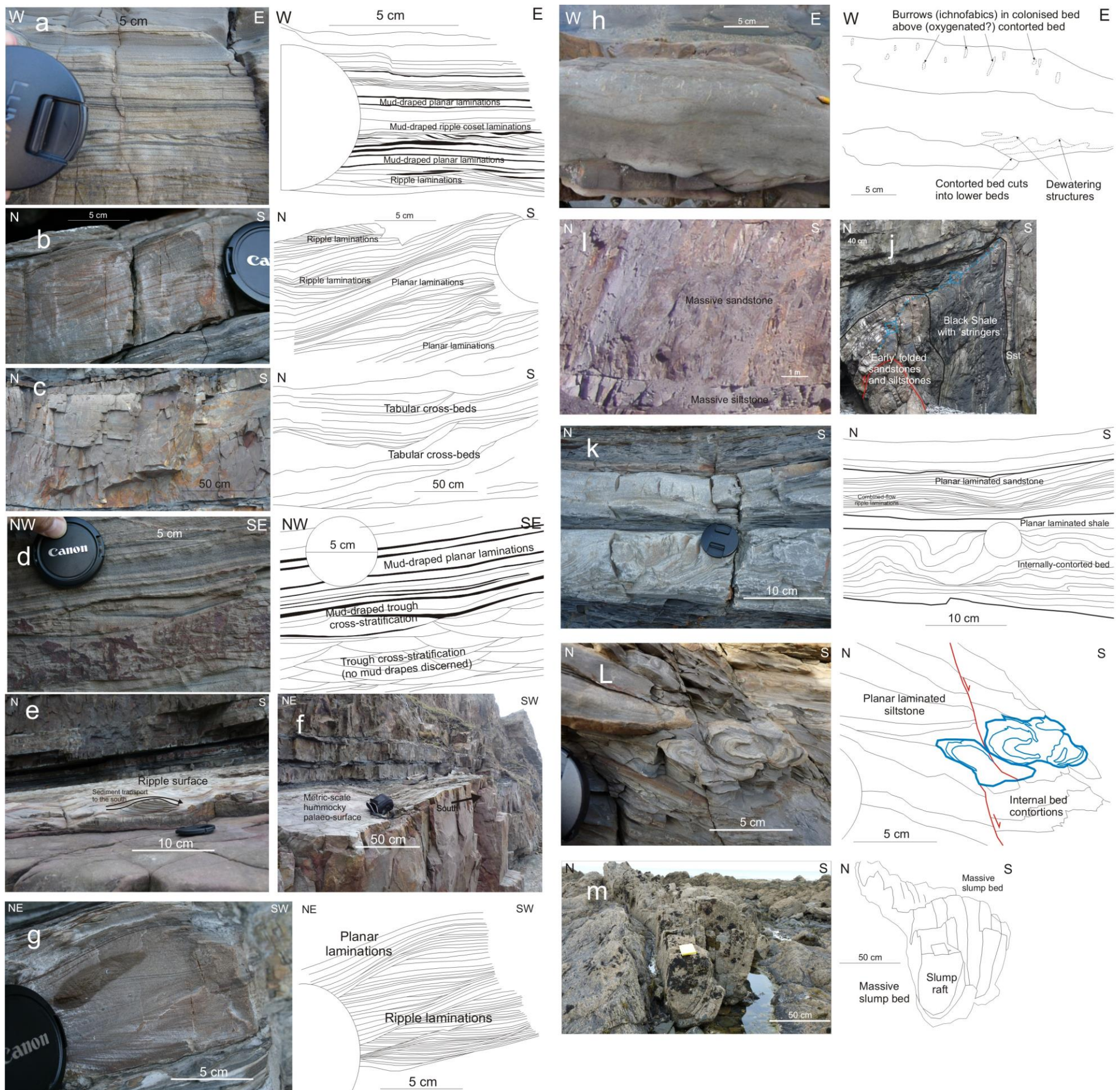


Fig. 3.3: Photographs and sketches of the facies observed in the Bude Formation: (a) mud-draped ripple coset (facies 1b) and planar laminations (facies 5b) above ripple laminations with no mud-draped structures (facies 1a) near Bude (ss200063); (b) sharp-top sharp-base bed with ripple laminations (facies 1a) inter-bedded with planar laminations (facies 5a) at Upton (ss200047); (c) 1.4 m thick tabular cross-beds (facies 4) at Upton (ss200047); (d) mud-draped trough cross-stratification (facies 2b) and infilling mud-draped planar laminations (facies 5b) above trough cross-stratification structures with no mud drapes (facies 2a) at Upton (ss200047); (e) ripple laminated surface with a general southwards palaeoflow direction on top of a thick sandstone bed and ripples that have indices of between 2 and 3 at Upton (ss200047); (f) thick sandstone bed with metric-scale wavelength hummocky cross-stratification (facies 3b) at Upton (ss200047); (g) sharp-top sharp-base bed with ripple laminations (facies 1a) overlain by planar laminations (facies 5a) at Upton (ss200047); (h) bioturbation (*Skolithos*) at the top in an otherwise structure-less bed (facies 7) and with liquefaction structures (facies 9a) at the base in the Black Rock foreshore (ss196015); (i) stacked, amalgamated, massive (8 m thick) sandstone (facies 7) and (5 m thick) siltstone beds (facies 6) at Upton (ss200047); (j) variably-thick black shale bed (facies 8) with sandstone and siltstone 'stringers' above 'early' folded sandstone and siltstone beds near Lynstone (ss200052); (k) two sharp top-sharp base beds (inter-bedded with planar laminated shale (facies 8)), with basal bed displaying internal contortions (facies 9a) and the top bed having ripple (facies 1a) and planar laminations (facies 5a) with no mud drapes at Maer Cliff (ss200075); (l) planar laminated siltstone bed (facies 5a) with two small slumps (facies 9a) with small syn-depositional faults exploiting the liquefied structures at Wrangle Point (ss200072); and (m) massive disaggregated slump bed with detached slump sandstone raft folds (facies 9c) in the Black Rock foreshore (ss195017).

### **3.3.2 Trough cross-stratified sandstones (Facies 2a and b)**

There are two types of trough cross-stratified sandstones that include centimetric to decimetric scale bundled (stacked) or individual trough sedimentary structures. One facies includes rare mud draped trough bases (facies 2b), whilst the other is more common and has no mud draped bases (facies 2a; Figs. 3.1c, 3.2 & 3.3d). This facies is not described by previous authors. The troughs incise lower structures, whilst infilling sediment pinches onto and onlaps the trough margins. The sedimentary structures are 5-15 cm wide and 2-5 cm deep, and the fine grained trough cross-stratified sandstones are between 0.2 and 5.0 m thick. The sandstones include common rip-up mud clasts and rare load-‘flame’ structures on bed bases (Table 3.2). Occasional low-angle reactivation surfaces are observed, especially in thicker beds.

#### **Facies interpretation**

Troughs form as a result of high energy current flows that occur commonly in fine-grained sandstones, at mean flow velocities of more than 50 cm/s (Collinson et al, 2006). Such conditions occur in shallow lacustrine or shallow marine settings around the mid-shoreface, above the storm-weather and below the fair-weather wave base. The required velocities may be generated by either tidal current flows or storm events (Reading, 1996). In the case of mud-draped troughs (facies 2b), there must be an interval to develop a period of slack water between the development of each trough and its subsequent infilling onlapping deposit (Fig. 3.3d).

The presence of laterally extensive reactivation structures can be caused by changes in base level (Collinson et al, 2006) but are more commonly formed by storm reworking. Mud-draped bases on both trough structures and reactivation surfaces within the bed forms could indicate fluctuating current velocities, resulting from astronomical tidal processes within a marine setting (Ainsworth et al, 2012). However, the mud drapes alone demonstrate that there was a lower energy environment following the erosive trough generation, with perhaps some clastic bypass (B. Gréselle, 2012, pers. comm.). Where troughs are formed by storm currents, subsequent fairweather conditions must have a lower energy.

### **3.3.3 Undulose and hummocky cross-stratified sandstones (Facies 3a and b)**

Undulose and hummocky structures in the Bude Formation are found within trough cross-laminated sandstone beds, some of which also include low-angle erosive reactivation surfaces (Figs. 3.1c, 3.2 & 3.3f). The undulations (facies 3a) have wavelengths of 10-15 cm and amplitudes of approximately 1 cm. Other authors have not described this facies clearly, although it is included as a smaller scale hummocky cross-stratified structure by Higgs (1991). The undulations incise the underlying trough cross-laminated sandstones (facies 2) and are overlain by further trough cross-stratified sandstones. Each undulation has a basal mud layer and contains a 1-2 cm thick fine grained massive or ripple laminated sandy horizon with rip-up clasts (Table 3.2). They are associated with the hummocks, as is observed at North Upton

(SS200047). The hummocky structures (facies 3b) show concave-up (hummock) and convex-up (swale) surfaces, bound packages of low-angle cross-bedding, which sometimes include reactivation surfaces, and often have an aggradational character. They are overlain by variably thick shale beds (see facies 8 below) that infill the palaeo-bathymetry. The symmetrical hummocks and occasional swales were described by Higgs (1984; 1986; 1991) and have wavelengths of 1-2 m and amplitudes of 10-15 cm, making them an order of magnitude larger than the undulations (Table 3.2).

### **Facies interpretation**

The undulations (facies 3a) may represent destruction-construction ‘events’ by storm water flowing down gutters where gradients are high (Collinson et al, 2006). The erosional surface marks sediment bypass and is infilled by later lower-energy sandy deposits. The hummocky (facies 3b) structures (Fig. 3.3f) may result from ‘events’ such as combined storm wave oscillations and strong unidirectional currents (Reading, 1996) in the lower-to-mid-shoreface, below the zone of reworking by fairweather wave action (Higgs, 1986; 1991). The fetch needs to be tens of kilometres in order to generate sufficient storm waves (Reading, 1991). Also, undulose and hummocky structures may form in lacustrine or marine settings (Reading, 1996). Where storm waves generate hummocky cross-stratification in a marine environment, the hummocks may be associated with infaunal suspension feeders (Burne, 1995; Reading, 1996), but this was not observed in the Bude Formation. In the Higgs (1991) model, the storm waves have reworked such significant amounts of sediment downslope that the Bude Formation deposits never moved into the fairweather upper shoreface environment. This aspect of the model is problematic, especially in a lacustrine environment as envisaged by Higgs (1986; 1991), as base levels were probably highly variable (Reading, 1996; Nichols, 1999). Burne (1995) suggested that the hummocks formed as anti-dunes, mega-ripples or via fluidisation processes. However, the symmetry of the observed hummocks and the lack of internal dewatering features make these explanations difficult to support.

### **3.3.4 Tabular cross-bedded sandstone (Facies 4)**

At North Upton (SS200047), there is an example of this distinctive, metric-scale, tabular, sharp-based cross bedding (Figs. 3.1c, 3.2 & 3.3c). This facies is not described clearly by other authors and only mentioned briefly by Higgs (1991). Tabular cross-beds, found only in fine-grained sandstones, appear to have neither mud-draped bases to structures, nor conclusive evidence for reactivation surfaces. The planar foreset structures are up to 1.4 m high (Table 3.2).

### **Facies interpretation**

The rare structures are likely to have developed in high energy depositional environments such as in a migrating dune or sand wave, with a non-erosive base, where flow

velocities exceeded 50 cm/s (Collinson et al, 2006). Such conditions occur in both lacustrine and marine settings. Such a dune crest is inferred to have been straight on the basis of consistent foreset geometry (Fig. 3.3c). There is no evidence seen of reactivation surfaces that would have indicated emergence and / or fair-weather wave-reworking of the dune. The absence of such structures may suggest that depth fluctuations were not large when the tabular cross-beds formed (Collinson et al, 2006). Although mud drape couplets have not been seen in the exposed example, the presence of a sub-aqueous sand wave or bar form could be explained by significant tidal ebb or flow current activity (Reading, 1996). However, given the absence of specific tidal features, it is more likely to have been generated by storm wave activity in a lower shoreface depositional environment, with the lack of erosion into underlying strata and the presence of tabular cross-beds precluding a turbidity current origin (Reading, 1996; Collinson et al, 2006).

### **3.3.5 Planar laminated siltstones and sandstones (Facies 5a and b)**

There are two types of planar laminated siltstones and sandstones observed in the Bude Formation outcrops. The planar laminated facies 5a is common and includes stacked silt and/or sand laminations, whilst the mud-draped planar laminated facies 5b is rare and includes rhythmic mud and silt-to-sand laminations. These laminations are laterally-continuous stacks of parallel, very fine sand or silt alternating with mud laminations (Figs. 3.1c, 3.2 & 3.3a & d). They have been observed by Higgs (1986; 1991), Melvin (1986) and Burne (1995); but the mud draped planar laminated facies 5b is not described by other authors. The beds that contain both types of planar laminations are less than 0.2 m thick and mud rip-up clasts are absent. The planar laminated structures are occasionally observed to be associated with ripple laminated deposits (facies 1a and 1b) and trough cross-stratified sandstones (facies 2a and 2b) (Fig. 3.3a, b, d, k & l). The lamination thicknesses are less than 0.1 mm for mud laminations; 0.1-0.25 mm for silt laminations; and 0.25-0.5 mm for sand laminations. The mud draped planar laminations have a rhythmic ‘tramline’ pattern that consists of stacks of sandier and siltier laminations, but with few mud laminations, alternating with stacks where the reverse is observed (Fig. 3.3a). Furthermore, some of the mud laminations may be expanded by bedding-parallel carbonate veins that are 0.1-2.0 mm thick. Planar laminations may also be observed in association with both trough cross-stratification and ripple lamination facies (Table 3.2).

### **Facies interpretation**

Various alternative explanations for planar laminated facies 5a have been proposed with either: low-energy hemi-pelagic settling of sediment (Collinson et al, 2006); high-energy flows from unidirectional flows close to the bed (Baas et al, 2011); or high density turbidity currents with sediment concentrations up to 0.36 (Leclair & Arnott, 2005). It has also been proposed that such flows, where linked with ripple laminations, may be from turbidity currents on either a lacustrine ramp (Higgs, 1991) or in a deep marine environment (Burne, 1995). The mud-draped

planar laminated facies 5b represent hemipelagic fallout during episodes of minimum current activity (Reading, 1996). Where quasi-rhythmic stacking is observed, this could conceivably relate to astronomical or meteorological “tides” (Ainsworth et al, 2012), thereby controlling the balance between local current activity and terrigenous input. Independent palaeoenvironmental indicators, such as C/S and ichnofabric analyses, would be needed to assess these possibilities.

### 3.3.6 Amalgamated massive structureless siltstones and sandstones (Facies 6 and 7)

Bed thicknesses in the massive or amalgamated structureless sandstone and siltstone beds (facies 6 and 7) (Figs. 3.1c, 3.2 & 3.3i) vary greatly, but are up to 8.0 m thick for facies 7 sandstone beds and 4.0 m for facies 6 siltstone beds (Table 3.2). The sandstone beds are very fine to fine sand grade and have conchoidal fractures, rare reduction spots and basal load-‘flame’ structures. Some massive sandstones show flute casts on basal surfaces. In a very few massive sandstone and siltstone beds (around a dozen beds), which have no flute casts, bioturbation may also be observed. Ichnofabrics are of low abundance, diversity and density and are centimetric-scale structures within the top 0.1 m of these few beds. Where ichnofabrics are observed, the beds are dominated by vertical *Skolithos* burrows (Figs. 3.2 & 3.3g) up to 10 mm wide and 50 mm long. In a few siltstone beds, *Helminthopsis* is observed (Fig. 3.3h) but there are no stenohaline fauna (i.e. echinoderms, bivalves) from a marine setting (Nichols, 1999).

#### Facies interpretation

The deposition of these beds may have occurred in one of three ways: by rapid dumping from either collapsing surge-like high-density turbidity currents (Reading, 1996); deposition from sustained high-density turbidity currents in a subaqueous fan (Kneller & Branney, 1995); or rapid suspension fallout from storm-generated clouds of sediment in the water column, which is the preferred interpretation of Higgs (1991). In the Kneller and Branney (1995) model, thick massive sands are laid down from a gradual aggradation beneath a sustained turbidity underflow, where the lower part of the flow becomes hyper-concentrated and settling is hindered. Traction structures are retarded, as there is little rheological difference at the boundary between the lower flow and the newly laid-down, dewatering deposit (Kneller & Branney, 1995). Such massive sand deposits occur at concentrations above 0.36 (Leclair & Arnott, 2005).

Rapid suspension fallout may occur in a marine setting, but is more likely in a stratified lacustrine setting from sediment-laden river discharges. In the latter case, the input waters are denser than the surface lake waters (i.e. epilimnion) but could be less dense than the cold bottom waters (i.e. hypolimnion) (Nichols, 1999). This causes sediment-laden flows along the thermocline between the top and bottom waters and a rain of very fine grained sediment onto the lake floor (Reading, 1996). However, the absence of distinguishing features may cause some beds to lose any pre-existing sedimentary structures through internal liquefaction and / or disruption (see Chapter 2). The limited range of ichnofabrics and the lack of stenohaline fauna

associated with this facies, and others in the Bude Formation, suggests a fresh to brackish water depositional environment, perhaps with some anoxia (Nichols, 1999). If the oxygen content and / or water salinity increased due to ephemeral storm activity, liquefaction and / or marine incursion, this could have resulted in higher levels of colonisation (Reading, 1996). Descriptions of the ichnofabrics observed in this study and by other authors are provided in Section 3.5.

### 3.3.7 Planar laminated shales (Facies 8)

Planar laminated shale beds (facies 8) vary in thickness between 0.02 m (thin shales) and 6.0 m (laterally-continuous black shales). Laminations are on a millimetric scale. Some thin shale beds and all the black shale beds include planar laminated siltstones (facies 5a) and very fine sandstones (facies 5b), in the form of 0.01-0.05 m thick ‘stringers’ (Figs. 3.1c, 3.3j & 3.4-3.6), as described by King (1971), Higgs (1986; 1991), Melvin (1986), Hartley (1991) and Burne (1995). The sandstone beds within facies 8 contain numerous burrows with *Diplocratorion* being most common and *Arenicolites*, *Phycodes*, *Skolithos* and *Teichichnus* much rarer (Higgs, 1991). Occasionally, the shale beds are also inter-bedded with thin (0.05-0.1 m thick) and internally-contorted beds (Fig. 3.4; Table 3.2). In the black shale beds, *Planolites* ichnofabrics have been observed between sandstone ‘stringer’ inter-beds, with body fossils of fish, goniatites and pelagic bivalves in distinct pyritised shale layers (King, 1967; Freshney et al, 1972; 1979; Higgs, 1991). Abundant bedding-parallel ankerite veins also occur within these beds.

There are two thick black shale beds, correlated by Freshney et al (1972; 1979) from King (1967) between Northcott Mouth and Black Rock (SS202087-SS195015) that provide good marker horizons. In stratigraphic-order, the Bude Formation black shale beds are:

1. Tom’s Cove Shale, with a prominent (0.2-0.4 m) massive sandstone (Figs. 3.1a & b, 3.4 & 3.5) and associated with the fish *R. elegans* (Freshney et al, 1972; 1979);
2. Saturday’s Pit Shale, with numerous sandstone ‘stringers’ (Figs. 3.1a & b, 3.3j & 3.6) and associated with the fish *C. budensis* (Freshney et al, 1972; 1979).

### Facies interpretation

The shale beds are interpreted as reflecting a restricted or marginal sub-aqueous setting with low-energy, hemi-pelagic fall-out of clays (Figs. 3.3j-k & 3.4-3.6), with the silty and sandy stringers could due to fall-out from suspended sediment in the water column, perhaps distal to a storm event or as distal turbidites, with the latter being the more likely in discontinuous beds (Reading, 1996). The amount of clastic input may have varied due to environmental changes, with increased input producing the thin (1.0-5.0 cm) planar laminated siltstone and sandstone ‘stringers’ and laid down either in pulses or possibly seasonal changes from material suspended in distant river output (Burne, 1995). In contrast, Higgs (1991) suggested that the mudstone was deposited in a low-velocity current, such as a river-fed surface plume entering more saline

waters. The mudstone and inter-bedded 'stringers' are interpreted by Higgs (1991) to be couplets or seasonal varves deposited during an annual wet (i.e. monsoon) and dry season cycle.

The preservation of the fish fossils in the Tom's Cove and Saturday's Pit shales suggest that the depositional environments were largely brackish water and dysoxic. The oxygen depletion may have resulted from increased organic activity (i.e. eutrophication) when clastic supplies increased (Burne, 1995). Such low levels of oxygen could be tolerated by the *Planolites* burrowers (Gringras et al, 2009). However, the presence of *R. elegans* (King, 1971) indicates that salinity conditions may have varied (Forey, 1981). The black shales therefore corresponded with intervals of increased salinity, which may have occurred as a result of either a marine transgression that brought more marine conditions (Freshney et al, 1972; 1979), or increased subsurface seepage, as has been invoked in the Early Cretaceous South Atlantic 'Pre-Salt' lacustrine environments (Harris et al, 2004).

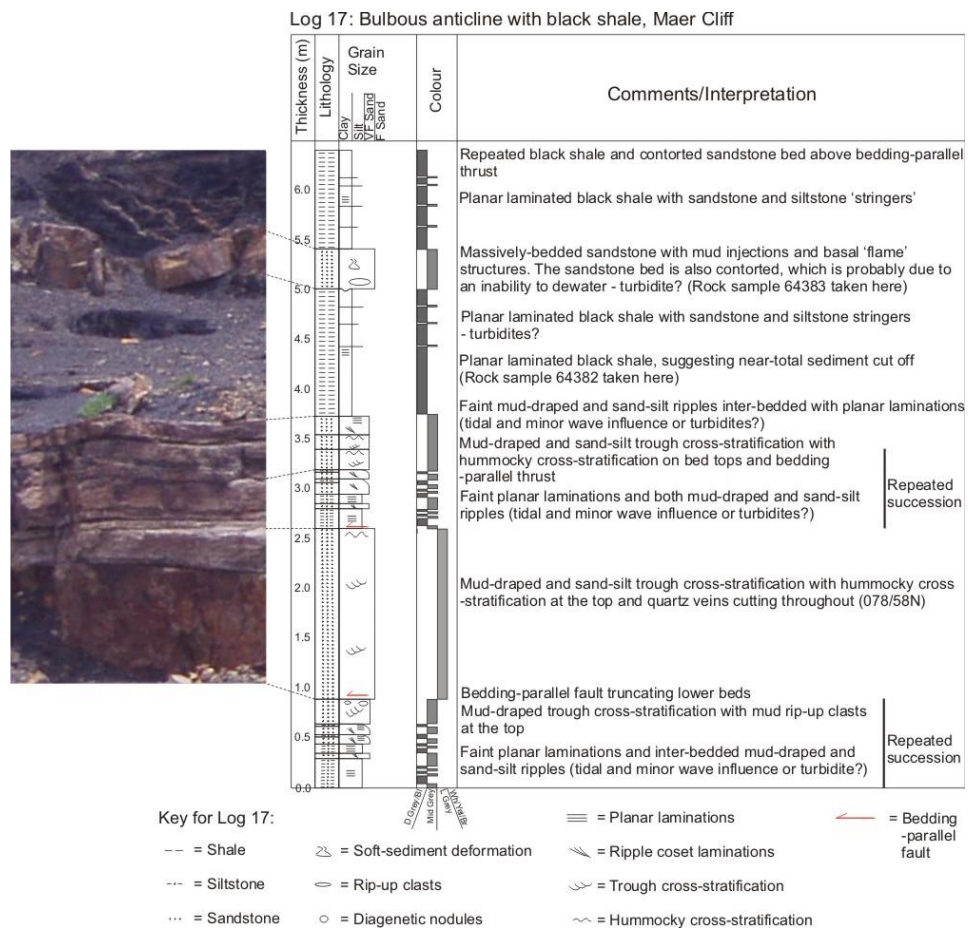


Fig. 3.4: Sedimentary log 17 at Maer Cliff (SS200082), showing repeated successions bound by bedding-parallel faults below the laterally-continuous Tom's Cove Shale (see Figs. 3.1a, b & c)

Such marine transgressions could be due to continued subsidence during prolonged intervals of reduced sediment input; but is perhaps more likely to be due to a 4<sup>th</sup>-order glacio-eustatic sea level rise, given the presence of globally widespread transgressive marine bands during the Westphalian (Freshney et al., 1979; Rippon, 1996; Higgs, 2004). Alternatively, sub-

surface seepage (Harris et al, 2004) may suggest that large volumes of more saline fluids leaked into the Culm Basin during Bude Formation deposition; but this has not been demonstrated. Thus, the thick continuous black shale beds are interpreted as representing deposition either during significant increases in base level when the area became distal, or alternatively, when near-clastic sediment cut-off occurred due to possible avulsion elsewhere (Nichols, 1999).

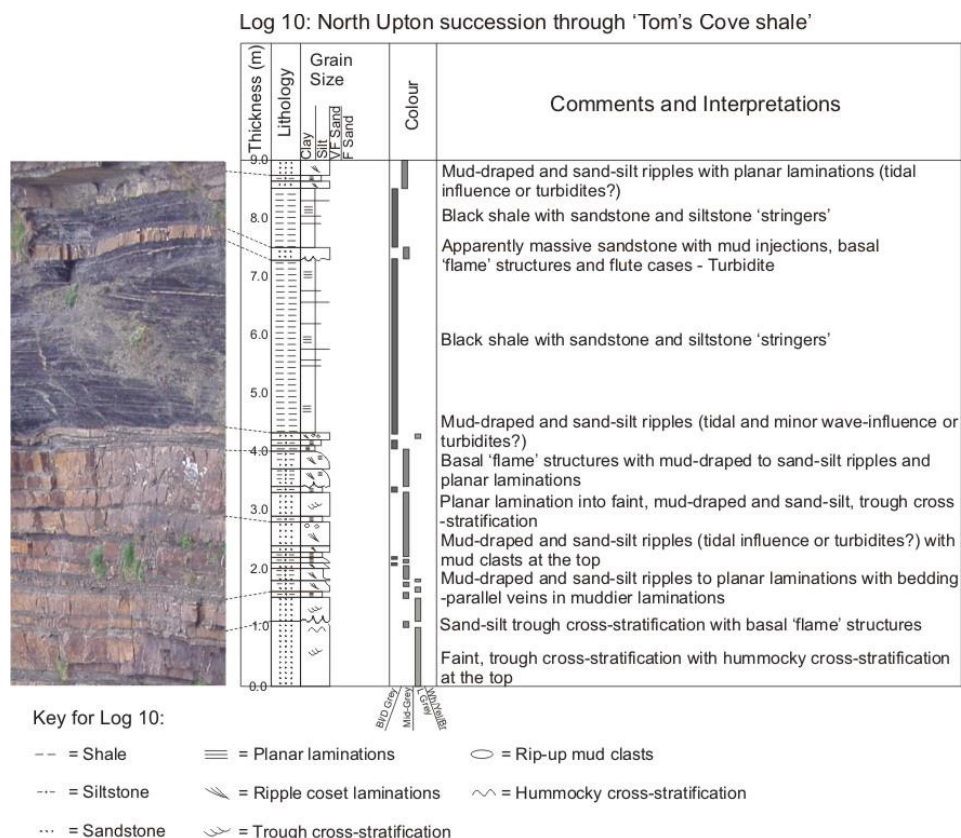


Fig. 3.5: Sedimentary log 10 at North Upton (SS200049) for comparison with the Maer Cliff section (see Fig. 3.4), with the laterally-continuous Tom's Cove shale (see Figs. 3.1a, b & c)

### 3.3.8 Slump and internally-contorted beds (Facies 9a, b and c)

Slump and internally-contorted beds occur at centimetric (facies 9a; internal bed contortions) to decametric-scales (facies 9c; massive slumps), with grain sizes between clay and very fine sand grade, as recognised by Higgs (1991). The internal contortions were described by Higgs (1991) as 'seismites' (see Chapter 2) and by Burne (1995) as 'slurrites'. The internally-contorted beds (facies 9a) (Figs. 3.1c, 3.3k, l & m & 3.4; Table 3.2) are laterally persistent over a few kilometres only (Hartley, 1991), forming mud-draped, convolute, inclined fold or load structures. The bed tops may be load deformed or have sand volcanoes (Burne, 1970). There are also attached slump beds (facies 9b) comprised of thin (centimetric-scale) inter-bedded shales, siltstones and sandstones that retain their original sedimentary structures in isoclinal, recumbent, fold structures. Massive, disaggregated, mud-rich slump beds (facies 9c) (Fig. 3.3m) are associated with shale deposition and include metric-scale, isoclinally-folded, sandstone 'rafts'.

All of the slump and internally-contorted beds represent varieties of sedimentary remobilisation at or near the palaeo-surface (van Rensbergen et al, 2003). Potential triggers include storm waves (Owen & Moretti, 2008), seismic activity or over-steepened slopes (Del Pino-Sanchez, 2006). A key requirement is that the slumping involves a deforming force that exceeds the sediment strength (Owen, 1987; see Chapter 2).

### **Facies interpretation**

The massive slump beds (facies 9c; Fig. 3.3m) have well-defined bed tops and bases, suggesting that their external surface was cohesive, whilst their disaggregated nature suggests that their beds underwent gravitationally-induced shear deformation and liquefaction (Owen & Moretti, 2008). The shear deformation caused any coherent sedimentary layers within the disaggregated matrix, to form 'recumbent' sheath-like folds (Strachan & Alsop, 2006). They are interpreted by Hartley (1991) as being the product of a debris flow. It is likely that their deposition would have modified the palaeo-surface topography. This is considered in Chapter 5 for the Black Rock Slump Bed at Black Rock (SS197017) and at South Lynstone (SS200051).

In contrast, internal cohesion is retained in the attached slump folded beds of facies 9b (after Owen, 1987), as observed at North Upton (SS200047) and Phillip's Point (SS200044). The attached slump beds and recumbent fold axial planes are consistent with multi-bed liquefaction on a slope, with gravitationally-induced shear stress over the bed top (Woodcock, 1979; Strachan & Alsop, 2006; Debacker et al, 2009).

### **3.3.9 Channel fill facies (Facies 10)**

Individual channel structures with stacked sedimentary bed fill occur rarely, with only two examples recognised within the Bude Formation outcrops: in the south-facing cliff at Summerleaze Beach, Bude (SS200067); and in the Black Rock foreshore (SS196016) (Fig. 3.1c). Both have a north-south oriented channel axis, which is sub-parallel to the coastline. The Summerleaze channel is up to 1 m deep and over 20 m wide; whilst in the Black Rock channel is 1 m deep and 10 m wide. Although similar structures are recognised by Burne (1995) elsewhere along the outcrops, only 0.2 m thick scour infills are recognised by Higgs (1991).

The channels formed by erosion of earlier beds. The channel bases are overlain by a thin mudstone bed above, with a stack of more confined sandstone and siltstone beds filling the channels. Once filled, deposition returns to less confined bedding stacking patterns (Table 3.2).

### **Facies interpretation**

These rare examples of channels may be indicative of changing base levels, due either to a fall in sea or lake level (Reading, 1996; Nichols, 1999) or tectonic-related uplift and palaeo-slope steepening (McCaffrey et al, 2002). In the absence of emergence indicators, the channels may represent subaqueous feeder channels of a turbidite form (Reading, 1996). According to

Burne (1995), the generation of the channels may result from levee, lobe or inter-channel systems. If the channels developed in a shelf slope with turbidites, they are more likely to be stacked and avulsing, rather than individual channels (Reading, 1996; McCaffrey et al, 2002). It is possible that other similar individual channels have not been recognised or are located inland.

### 3.4 Palaeo-flow directions

The sole marks on the bases of Bude Formation facies 1, 6 and 7 turbidite beds provide palaeo-flow direction indicators that are linked to palaeo-slopes. Sole marks have been measured: stratigraphically between the Tom's Cove and Saturday's Pit Shales from Bude to Widemouth by Burne (1995) and Higgs (1991) and are plotted in rose diagrams; between the Hartland Quay (base Bude Formation) and Saturday's Pit shales north of Bude by Freshney et al (1979) and are plotted in a circular diagram; and between Northcott Mouth and Black Rock in this work and are plotted in two circular diagrams for erosional and depositional indicators.

From the grooves and bounce marks (sample size,  $n = 115$ ), plus flutes, prod marks and longitudinal scours ( $n = 51$ ) measured by Higgs (1991), the palaeo-flow directions ranged between SE and SW, with directions being highly variable from bed-to-bed (Fig. 3.6a). From the tool marks ( $n = 31$ ), current scours ( $n = 74$ ) and cross-laminations ( $n = 250$ ) measured by Burne (1995), the dominant palaeo-flow directions were towards the S and SW, although eastward flow directions were found in some beds (Fig. 3.6b). From the flutes ( $n = 24$ ) and prod casts and grooves ( $n = 14$ ) measured by Freshney et al (1979), flows occurred in all directions, with a north-south channel axis found north of Bude (Fig. 3.6c).

From the orientations of trough cross-stratification ( $n = 7$ ), tool marks ( $n = 20$ ) and ripples ( $n = 2$ ) measured during this work, a highly variable range of palaeo-flow directions are suggested for both north and south of Bude (Fig. 3.6d), being: to the north at Northcott Mouth (A), Bude (B) and Black Rock ; to the west at North Lynstone (D), Upton-Phillip's Point (F) and Church Races (G); to the east at Maer Cliff (B); and to the south at North Upton (E).

These directions are corrected for tectonic tilt and show separately the erosional (trough) and depositional (tool marks and ripples) palaeo-flow indicators (Fig. 3.6d). The depositional features were generated during waning flows that may be related strongly to palaeo-slope direction. In contrast, the erosional features were generated during high energy incising flows and thus may be unrelated to palaeo-slope direction (Collinson et al, 2006).

Higgs (1991) and Burne (1995) suggested that there was a regional south-dipping palaeo-slope to the south of Bude, with possibly some bathymetry. In contrast, to the north of Bude (Freshney et al, 1979), the large variations in palaeo-flow directions suggest an undulating and changing palaeo-surface. Possible reasons for the range of palaeo-flow directions include:

1. Basin margin slope direction variations;
2. Avulsion of turbidite sheets across the basin floor;
3. Local bathymetry on the palaeo-surface.

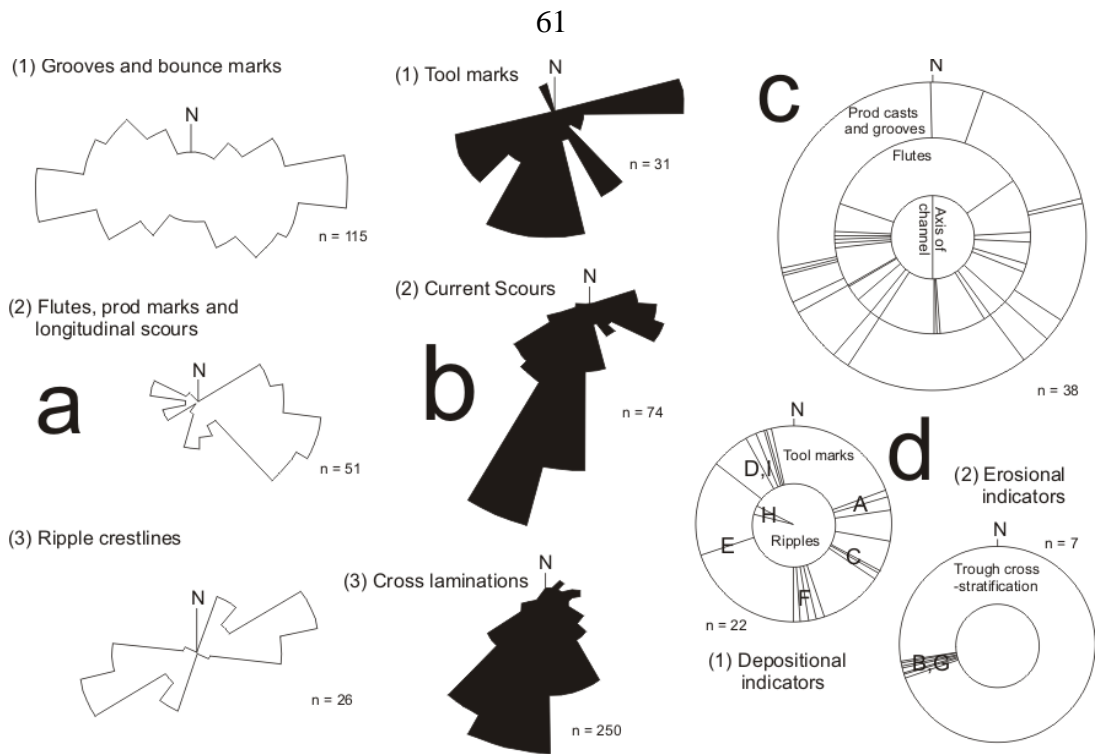


Fig. 3.6: Comparison of palaeo-flow indicators from Bude Formation outcrops. Measurements taken from Bude to Widemouth by: (a) Higgs (1991); and (b) Burne (1995); (c) north of Bude by Freshney et al (1979); and from Northcott Mouth to Black Rock in this work, with depositional and erosional indicators at: A. Northcott Mouth; B. N Maer Cliff; C. S Maer Cliff; D. Bude; E. Lynstone; F. Upton; G. Upton-Phillip's Point; H. Church Races; and I. Widemouth

### 3.5 Ichnofabric analysis

Ichnofabric analysis was undertaken in order to provide another control on the palaeo-environmental conditions. Only a few ichnofabrics have been observed in the Bude Formation beds, with a low density of *Skolithos* and *Helminthopsis* burrows in the metric-scale massive sandstones and siltstones (facies 6 & 7). In the sandstones and siltstones within thick black shale intervals (facies 8), Higgs (1991) found *Diplocraterion* were common, but *Arenicolites*, *Phycodes*, *Skolithos* and *Teichichnus* more rarely. *Planolites* ichnofabrics were found within the black shale laminations by Higgs (1991) and Burne (1995). In the interbedded nodules within the black shale beds, King (1967) found *Planolites* and *Cochlichnus* ichnofabrics, as well as palaeoniscid fish *Cornuboniscus budensis* and *Elonichthys aitkeni*, an acanodian fish *Acanthodes wardi* and a crustacean *Crangopsis huxleyi*.

These results suggest that the black shale beds (facies 8) were deposited in a shelf or ramp setting, probably below the storm wave base (Higgs, 1991). The ichnofabric community, which is best developed in the upper part of facies 6 and 7 beds, may have resulted from recolonisation during a period of reduced sediment input, following event bed deposition (Reading, 1996). Where *Skolithos* ichnofabrics are observed (e.g. Fig. 3.3h), it suggests that the sandstones and siltstones of facies 6 and 7 were deposited on a shallow oxygenated shelf or ramp in the lower to middle shoreface and is consistent with the facies described in section 3.3.

Apart from some apparent horseshoe crab traces (Xiphosurid *Kouphichnium*) and fish trails (*Undichna*) (King, 1971), the low density and diversity of ichnofabrics in other facies may be due to variations in non-marine salinities, temperature and sedimentation rates (Bjerstedt, 1987), plus oxygen content and substrate consistency (Martin, 2004). The lack of ichnofabrics suggests that deposition occurred mainly under unfavourable conditions for burrowers.

From the sedimentary logs in Freshney et al (1972; 1979) (Fig. 3.1) and reproduced by Lloyd and Chinnery (2002), the Bude Formation sediment pile may be up to 1300 m thick and deposited over a one million year period. In which case, the mean sedimentation rate was about 1.3 mm/yr, potentially providing enough new nutrients for the burrowing organisms. Their absence implies the presence of stressed palaeoenvironments. The implications of salinity (i.e. water chemistry) and oxygen content on ichnofabrics are discussed later in sections 3.7 and 3.8.

| <b>Sample no.</b> | <b>Location</b> | <b>Facies</b> | <b>Sample no.</b> | <b>Location</b> | <b>Facies</b> |
|-------------------|-----------------|---------------|-------------------|-----------------|---------------|
| 64367*            | SS200046        | <b>9b</b>     | 64607             | SS200044        | <b>8</b>      |
| 64368             | SS200046        | <b>9b</b>     | 64608             | SS200044        | <b>9a</b>     |
| 64369             | SS200046        | <b>5a</b>     | 64609             | SS197017        | <b>9c</b>     |
| 64370*            | SS200046        | <b>8</b>      | 64610             | SS197017        | <b>9c</b>     |
| 64371             | SS200046        | <b>2b</b>     | 64611             | SS197017        | <b>9a</b>     |
| 64372             | SS200045        | <b>7</b>      | 64612             | SS200044        | <b>5a</b>     |
| 64373             | SS200045        | <b>5a</b>     | 64613             | SS200044        | <b>2a</b>     |
| 64374*            | SS200045        | <b>8</b>      | 64614             | SS200044        | <b>1a</b>     |
| 64375*            | SS200045        | <b>8</b>      | 64695             | SS200055        | <b>5a</b>     |
| 64376             | SS200045        | <b>1a</b>     | 64696             | SS200055        | <b>1b</b>     |
| 64377*            | SS200045        | <b>8</b>      | 64697             | SS200055        | <b>7</b>      |
| 64378             | SS200045        | <b>5b</b>     | 64698             | SS202083        | <b>7</b>      |
| 64379             | SS200046        | <b>9a</b>     | 64699             | SS202083        | <b>5b</b>     |
| 64380             | SS203067        | <b>10</b>     | 64700             | SS202083        | <b>5a</b>     |
| 64381             | SS203067        | <b>10</b>     | 64701             | SS202083        | <b>1a</b>     |
| 64382*            | SS200083        | <b>8</b>      | 64702             | SS202083        | <b>5b</b>     |
| 64383*            | SS200083        | <b>9a</b>     | 64703             | SS202083        | <b>1b</b>     |
| 64384             | SS195015        | <b>5b</b>     | 64704             | SS202083        | <b>5b</b>     |
| 64385*            | SS195015        | <b>9a</b>     | 64705             | SS202083        | <b>2a</b>     |
| 64386             | SS200047        | <b>7</b>      | 64706             | SS202065        | <b>2b</b>     |
| 64602             | SS200044        | <b>1b</b>     | 64707             | SS202065        | <b>5a</b>     |
| 64603             | SS200044        | <b>8</b>      | 64708             | SS202065        | <b>1a</b>     |
| 64604             | SS200044        | <b>5b</b>     | 64709             | SS202065        | <b>8</b>      |
| 64605             | SS200044        | <b>8</b>      | 64710             | SS202065        | <b>7</b>      |
| 64606             | SS200044        | <b>1a</b>     | 64711             | SS202065        | <b>1a</b>     |

Table 3.3: Sample numbers, locations and facies of the 50 Bude Formation rocks collected for thin section analysis (see Fig. 3.1c). An asterisk marks the 8 samples for SEM BSE-Z analyses

### 3.6 Petrographic description of Bude Formation rock samples

Thin section analyses of 50 rock samples (24 sandstones, 9 siltstones, 7 shales and 8 slump or contorted beds) provided a petrographic description of each facies type found in the outcrops between Northcott Mouth and Black Rock (SS202087-SS195015). This enabled the mineralogical differences between facies to be identified. As described in Section 3.2 (Methods), the sample locations were tied to the sedimentary logs where possible (Fig. 3.1c) and are given in Table 3.3. The results are described below.

#### 3.6.1 Siltstone and sandstone beds (of facies 1, 2, 5, 6, 7 and 9)

The relative proportions of quartz, feldspar and lithic fragments, as well as the amount of matrix mud and the maximum grain size have been established from thin section analysis of each of the 9 siltstone and 24 sandstone samples. The mean and standard deviation of all the samples are displayed in a Folk diagram (Fig. 3.7a) and have been compared with two similar studies by Freshney et al (1979), where similar results were found for each parameter tested (Table 3.4). These results contrast with those of Burne (1995), who suggests that the Bude Formation sandstones and siltstones have higher feldspar and lower rock fragment contents. The results from this work show that there is:

1. High proportions of quartz (79 %  $\pm$  standard deviation 9 %);
2. Very low proportions of feldspar (3 %  $\pm$  1 %);
3. Relatively high proportions of lithic fragments (18 %  $\pm$  5 %),
4. High matrix mud contents (25 %  $\pm$  6 %) with a minimum of 15% mud;
5. Very fine to fine grained sand grades (0.187 mm  $\pm$  0.065 mm) as the maximum grain size.

The general consistency in the mineralogy between facies suggests that the clastic material came from the same provenance. However, there is a variation in the amount of matrix mud content between the massive slump beds (facies 9c) with at least 50 % matrix mud, and the lower matrix mud contents for the other facies. This high mud content may have helped to retain the elevated fluid pressures in the massive slump beds (facies 9c) during and shortly after slump deposition (Maltman & Bolton, 2003; see Chapter 2).

The results from each sample were plotted onto a Folk diagram in order to link the quantitative rock descriptions with Folk's terminology. In Folk's classification, the sandstone and siltstone samples are found to be either quartz arenite or predominantly sub-lithic arenite. From Fig. 3.7a, all the facies contain high proportions of quartz (65-95 %); reasonably high proportions of lithic fragments (5-30 %); and low proportions of feldspar (0-5 %). This suggests that, in general, the Bude Formation sandstones and siltstones are texturally mature, as previously suggested by Melvin (1986), Higgs (1991) and Burne (1995). The planar and ripple coset laminated siltstones and sandstones (of facies 1 and 5) have slightly higher quartz but slightly lower feldspar and lithic fragment content than in the trough cross-stratified, massive

and internally-contorted / slumped siltstones and sandstones (of facies 2, 6, 7 and 9). However, these facies groups cannot be distinguished clearly from each other due to the overlaps in measured grain proportions (Fig. 3.7a). It is noted that the average relative grain components for the Bude Formation deposits are similar to those for deposits from other foreland basins (after Schwab, 1986; Fig. 3.7b), which suggests that all these basins have similar textural maturity.

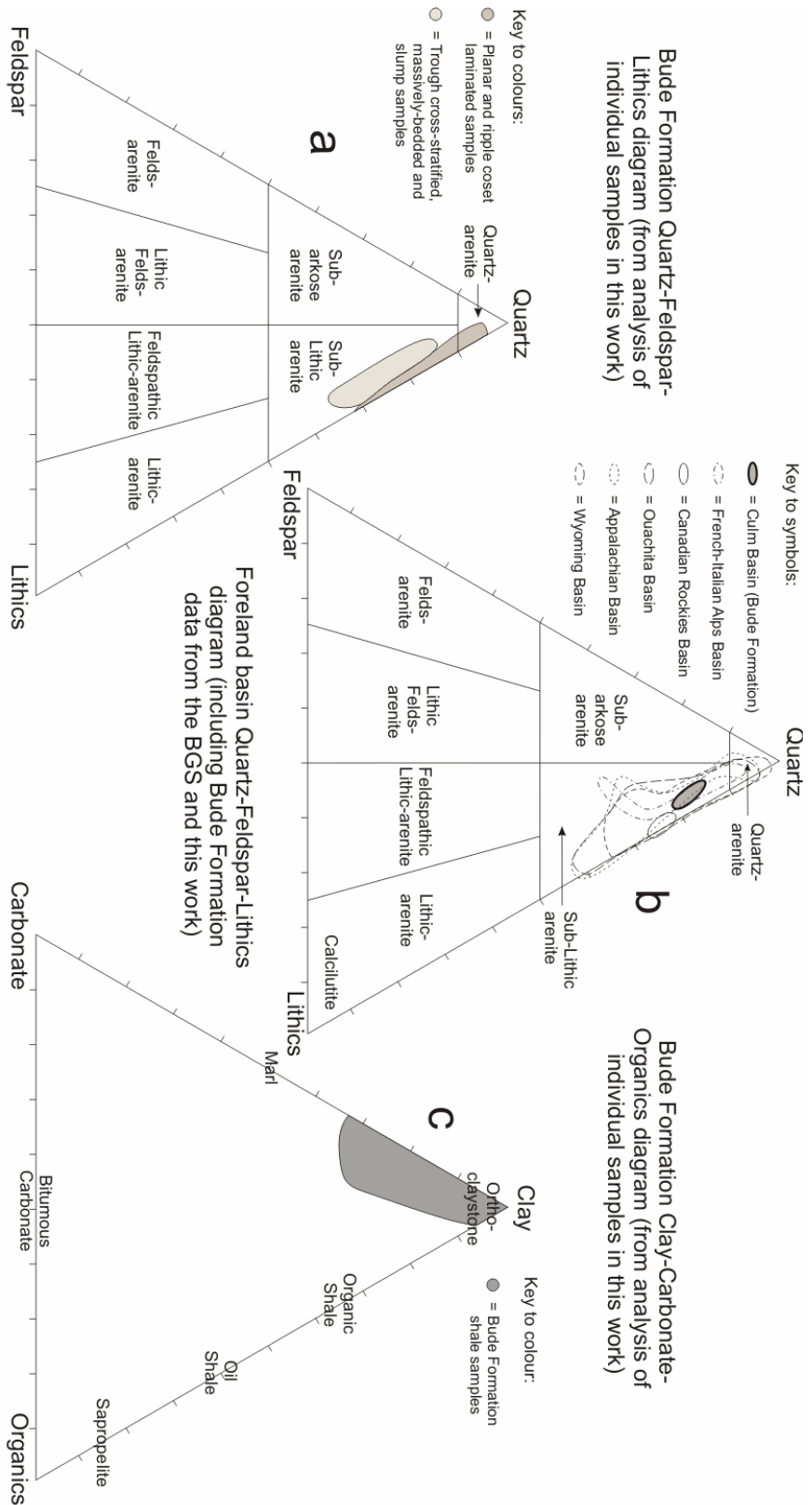


Fig. 3.7: Folk diagrams to: (a) classify the Bude Formation sandstones and siltstones (Q = quartz; F = feldspar; L = lithic fragments). The sandstones and siltstones all contain 15% or more matrix mud. Notice the close association between the brown-grey zone that denotes ripple sandstones and planar laminated sandstones and siltstones (Facies 1 & 5) and the grey zone, with trough cross-stratified, massive and contorted / slumped sandstones and siltstones (Facies 2, 6, 7 & 9); (b) compare the percentage of quartz (Q), feldspar (F) and lithic fragments (L) in the Bude Formation sandstones and siltstones (filled shapes) with those in deposits from other foreland basins (various outlined open shapes; Schwab, 1986); and (c) classify the Bude Formation shales (Clay-Carbonate-Organics), as shown within the dark grey zone. The shales are dominated by clay with < 5% quartz. However, the samples contain variable amounts of diagenetic carbonate in either bedding-parallel veins or in the matrix

| Parameters           | Study 1: Mean (+- st. dev.) - Freshney et al (1979) | Study 2: Mean (+- st. dev.) - Freshney et al (1979) | Study 3: Mean (+- st. dev.) - This work |
|----------------------|-----------------------------------------------------|-----------------------------------------------------|-----------------------------------------|
| Quartz (%)           | 82 (9) - calculated                                 | 84 (10) - calculated                                | 79 (9)                                  |
| Feldspar (%)         | 4 (1) - calculated                                  | 4 (2) - calculated                                  | 3 (1)                                   |
| Lithic Fragments (%) | 14 (3) - calculated                                 | 12 (2) - calculated                                 | 18 (5)                                  |
| Matrix mud (%)       | 26 (6)                                              | 31 (4)                                              | 25 (6)                                  |
| Max. grain size (mm) | 0.25 (0.065)                                        | 0.187 (0.1)                                         | 0.187 (0.065)                           |

Table 3.4: Comparison of the relative proportions of quartz, feldspar and lithic fragments, grain size and matrix mud content of sandstone and siltstone samples from two studies by Freshney et al (1979), and samples in this work

### 3.6.2 Shale beds (of facies 8)

A similar petrographic comparative analysis has been carried out for the thin sections from the seven Bude Formation shale samples. The relative percentages of clay, carbonate and organic minerals are shown in a Folk triangular diagram (Fig. 3.7c). There are minor amounts of organic matter and a large range in the amounts of carbonate (ankerite-siderite) minerals. All the shale samples contain less than 5 % quartz. Thus, the shales are described as either orthoclaystones or marly-orthoclaystones (Fig. 3.7c).

### 3.6.3 Bedding-parallel pyrite minerals and ankerite veins in shale beds (facies 8)

Bedding-parallel pyrite minerals and ankerite veins are observed from the scanning electron microscope (SEM) analyses of Bude Formation shale bed samples. These diagenetic features were studied in order to assess their timing in relation to the deposition and burial processes and also, to establish the environmental conditions during the shale bed deposition.

#### Bedding-parallel pyrite minerals

SEM analyses were undertaken on eight Bude Formation samples, of which six are from shale beds (facies 8). Four samples were from thin, discontinuous shale beds in Bude Formation slump and chevron folded beds (Fig. 3.8a) and two samples from continuous ‘marine-band’ (Freshney et al, 1979) chevron folded shale beds (Fig. 3.8b). Petrographic analyses showed that bedding-parallel pyrite framboids occur in one thin, discontinuous shale sample. The results from the two contrasting shale beds are summarised in Fig. 3.8.

Block 64375 of facies 8 (Fig. 3.8a) from an ‘upright’ chevron syncline at Upton (SS200045) has: (1) finely-laminated, kaolinite-rich matrix; (2) large concentrations of < 5 µm-diameter framboids; and (3) ‘zones’ between pyrite concentrations with rare, variably-sized framboids. In contrast, Block 64382 of facies 8 (Fig. 3.8b) from the Tom’s Cove Shale in an ‘upright’ chevron anticline at Maer Cliff (SS200079) has no finely-laminated, kaolinite-rich matrix and no framboidal pyrite minerals.

According to Bond et al (2004), the presence of bedding-parallel pyrites suggests that there was anoxia at the water-sediment interface during deposition (Table 3.1). In the Bude Formation, bedding-parallel pyrite framboids are present in only one of six sampled thin discontinuous shales and are absent in the sampled continuous black shales. Using the criteria of Bond et al (2004) in Table 3.1, this suggests that the depositional oxygenation conditions in the thin discontinuous shale (facies 8) within block 64375 (Fig. 3.8a), fluctuated between euxinic-lower dysoxic and upper dysoxic. In contrast, in the continuous black shale (facies 8), within block 64682 (Fig. 3.8b), the depositional environment remained consistently oxygenated. The lack of pyrite in the other discontinuous shale beds may suggest that there was insufficient sulphur to form pyrite; most likely due to salinities being too low during deposition (Berner & Raiswell, 1984). As a result, the oxygenation degree cannot be estimated for these beds.

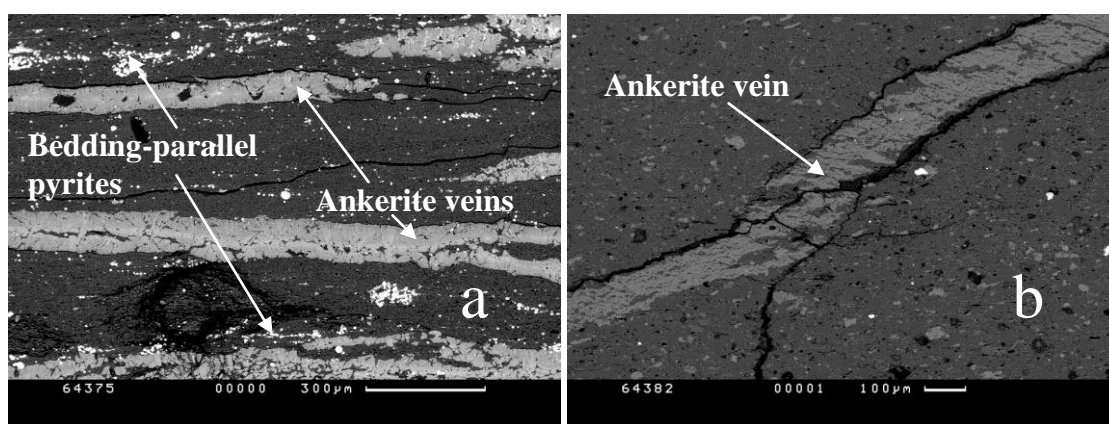


Fig. 3.8: SEM BSE-Z images of: (a) block 64375 of facies 8, with large variations in bedding-parallel framboidal pyrite mineral populations ( $< 5 \mu\text{m}$  diameter). The pyrites are inter-bedded with bedding-parallel ankerite veins; and (b) block 64382 of facies 8, where there are no framboidal pyrites but an ankerite vein has been precipitated

### Bedding-parallel ankerite veins

Bedding-parallel carbonate veins are a diagenetic feature, observed both in outcrop and from petrographic analyses (thin section and SEM analyses). From the results of the analyses, the veins are composed of ankerite (Iron (II) calcium carbonate). This result contradicts Burne (1995), who stated that the veins are composed of siderite. The ankerite veins were observed in a large number of shale beds, as well as in all the shale samples used in petrographic analysis.

The best observations of the bedding-parallel ankerite veins are from block 64375 of facies 8 (Figs. 3.8a). The petrographic analysis of this discontinuous shale bed sample identified variations in the mineralogical phases of the ankerite veins, including a phase transition between dark grey, Mg-poor ankerite found towards the vein edge, and mid-grey, Mg-rich ankerite found towards the vein centre. These mineralogical phases were not present in the thick, 'marine-band' (Freshney et al, 1979) continuous shale sample block 64382 of facies 8 (Fig. 3.8b).

Instead, the ankerite vein appears as a smaller number of less well-formed, bedding-parallel veins, which cut from top centre to bottom left in the SEM image (Fig. 3.8b).

Ankerite is an iron (II) calcium carbonate ( $\text{FeCa}(\text{CO}_3)_2$ ) that lies on a spectrum between siderite (iron (II) carbonate ( $\text{FeCO}_3$ )) and calcite (calcium carbonate ( $\text{CaCO}_3$ )) and is indicative of fresh-to-brackish water conditions (McKay et al, 1995). The Bude Formation ankerite veins are observed in shale beds and, occasionally, in clay laminations. In numerous outcrop examples, the ankerite veins were found to have been folded or kinked by local structures, which are described in Chapter 6.

### **Carbonate veins elsewhere in the Culm Basin**

Similar bedding-parallel siderite veins have been described in shale beds from both the Bude and Crackington formations (De Wall & Warr, 2004). They reported that these veins have rhombohedral crystals, with c-axes oriented in a north-south direction and plunging at  $45^\circ\text{N}$  (i.e. face north). De Wall and Warr (2004) suggest that the siderite precipitated during deposition from a constant hydrothermal fluid flowing south-to-north through the Culm Basin. In contrast, quartz-ankerite veins have been described between Crackington and Millook (Mackintosh, 1967) and quartz-siderite veins at Hartland and Millook (Beach, 1977). In both cases, Mackintosh (1967) and Beach (1977) suggested that the veins precipitated from within the host rocks and the fluids migrated into the surrounding shales.

## **3.7 Carbon-sulphur (C/S) geochemical analysis**

A carbon-sulphur (C/S) geochemical study has been undertaken on several Bude Formation shale beds by Lloyd and Chinnery (2002; Fig. 3.9). However, the locations of the samples are not provided. The results from the C/S analysis are used as a salinity proxy, where a higher S:C ratio indicates that the formation was deposited under more saline conditions (Berner & Raiswell, 1984). The Lloyd and Chinnery (2002) study results (Fig. 3.9) indicate that the Bude Formation commonly has a low S:C ratio. This is consistent with the results from C/S analysis undertaken by Higgs (1991) and suggests that the deposits were laid down in fresh-to-brackish water conditions (Lloyd & Chinnery, 2002). Slight salinity increases may have resulted from temporary structural-breaching of a lake sill, or alternatively, from sub-surface seepage, as has been modelled for the Early Cretaceous South Atlantic Pre-Salt lakes (Harris et al, 2004). Alternatively, variable river discharges and lake base levels may affect salinity (i.e. water chemistry; Reading, 1996).

In either case, the environment would have been a hostile, resulting in few burrowing organisms, as was observed in the study area. The exception to the low S:C ratios are in two Bude Formation laterally-continuous shale beds. Lloyd and Chinnery (2002) do not identify the beds but they are possibly the Sandy Mouth and Warren Gutter Shales, making them consistent with four out of the five samples taken by Higgs (1991). The two higher S:C ratios obtained by

Lloyd and Chinnery (2002) are similar to those from their Crackington Formation shale samples, which suggest that more normal saline marine conditions occurred at these times. It is possible in these cases that salinity increases occurred as a result of either eustatic transgression events (Higgs, 1991) or significant structural-breaching of the lake sill.

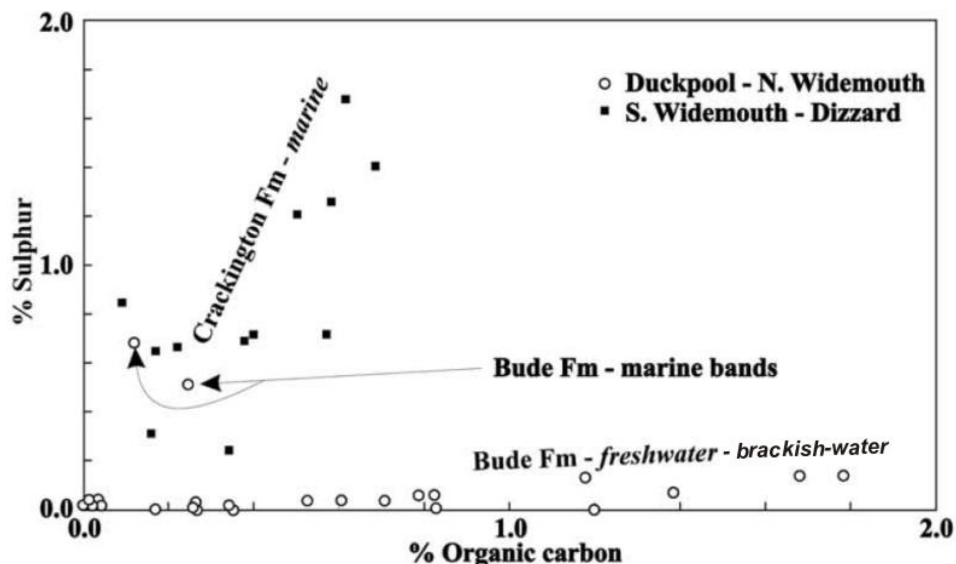


Fig. 3.9: Comparison of total organic carbon and sulphur for C/S analysis (salinity proxy from the methods of Berner & Raiswell, 1984) with data from Lloyd and Chinnery (2002) for shale and black shale beds in the Bude Formation and shale beds in the Crackington Formation

### 3.8 Diagenetic mineral development in the Bude Formation

An important aspect of basin evolution is that deposits undergo diagenesis as they are buried. In the case of the Bude Formation, the diagenesis occurred (Warr et al, 1991; Warr & Hecht, 1993) in a dominantly turbiditic depositional environment (Higgs, 1991; Burne, 1995) with S:C ratios that indicate generally low salinities (Lloyd & Chinnery, 2002; Fig. 3.9). Except for two laterally-continuous black shales, the low S:C ratios found, as well as the presence of bedding-parallel ankerite veins in many shale beds, suggest that the geochemical signature of the Bude Formation deposits is different to that of normal marine deposits (Higgs, 1991; Burne, 1995). The Bude Formation geochemistry and diagenesis is not fully established, but a complete geochemical study is beyond the scope of this research. However, preliminary petrographic analyses of Bude Formation rock samples have provided insights into the diagenetic, geochemical and temperature evolution of these deposits.

#### 3.8.1 Diagenetic progression

Petrographic analyses of Bude Formation rock samples (Figs. 3.10-3.12) found that a series of over-printing reaction products formed during diagenesis. These are as follows.

A quartz vein set in Block 64367B from facies 9b at Upton (SS200046) variably exploits fracture sets, some of which appear to be bedding-parallel (Fig. 3.10). The quartz veins

precipitated either from a super-saturated fluid or from local pressure solution, possibly during Variscan deformation. If the quartz vein precipitated from local pressure solution, this may have occurred at any time during Variscan deformation. However, if the quartz vein precipitated from a super-saturated fluid, it is not known if the fluids were hotter than or similar in temperature to the Bude Formation at the time of precipitation. From geochemical experiments undertaken by Walderhaug (1994) and Lander et al (2008), quartz may precipitate at temperatures as low as 80°C (see Chapter 2), providing a minimum temperature for their generation. In contrast, Davison et al (2004) suggests that quartz precipitation in the Bude Formation occurred at temperatures between 190°C and 280°C, providing a maximum temperature for their generation. However, these latter temperatures are too high as very low grade metamorphic minerals have not been observed.

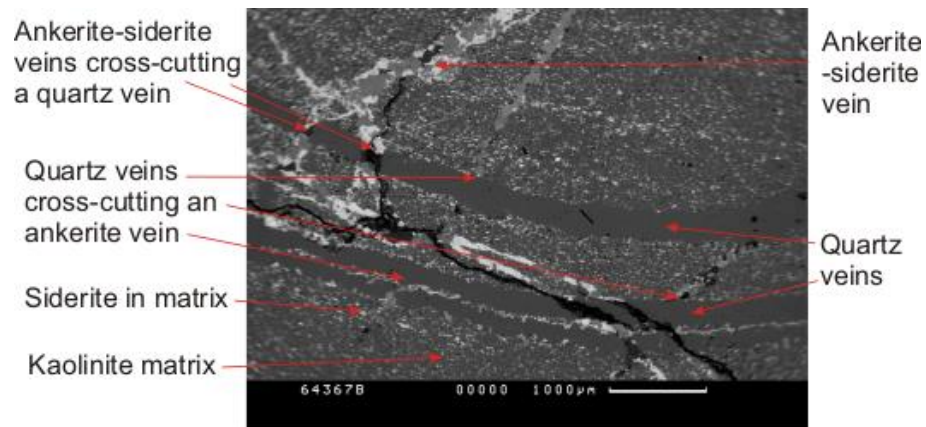


Fig. 3.10: SEM BSE-Z image showing mutually-cross-cutting quartz (mid-dark grey) and ankerite-siderite (dark grey to light grey) veins within a kaolinite-rich shale bed from block 64367B of facies 9b (SS200046)

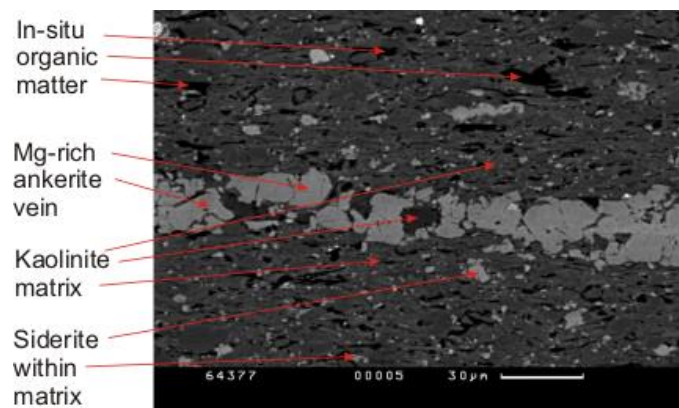


Fig. 3.11: SEM BSE-Z image showing an ankerite bedding-parallel vein within a kaolinite-rich shale bed from block 64377 of facies 8 (SS200045)

There is an ankerite-siderite vein generation that obliquely cross-cuts the quartz veins from Block 64377 of facies 8 at Upton (SS200045) (Fig. 3.11). Beach (1977) also observed

similar quartz-siderite vein sets in the Bude Formation, demonstrated that the two vein sets displayed preferred orientations and suggested that the veins developed within the sandstone beds. However, the timing of the quartz and ankerite-siderite precipitation in the Bude Formation with respect to the Variscan deformation is not established.

In the underlying Crackington Formation, the same vein sets have been described as quartz-ankerite by Mackintosh (1967) and quartz-siderite by Beach (1977). However, De Wall and Warr (2004) also observed these siderite veins and suggested that the veins precipitated from a hot fluid interaction with the sandstones and shales at temperatures over 150°C.

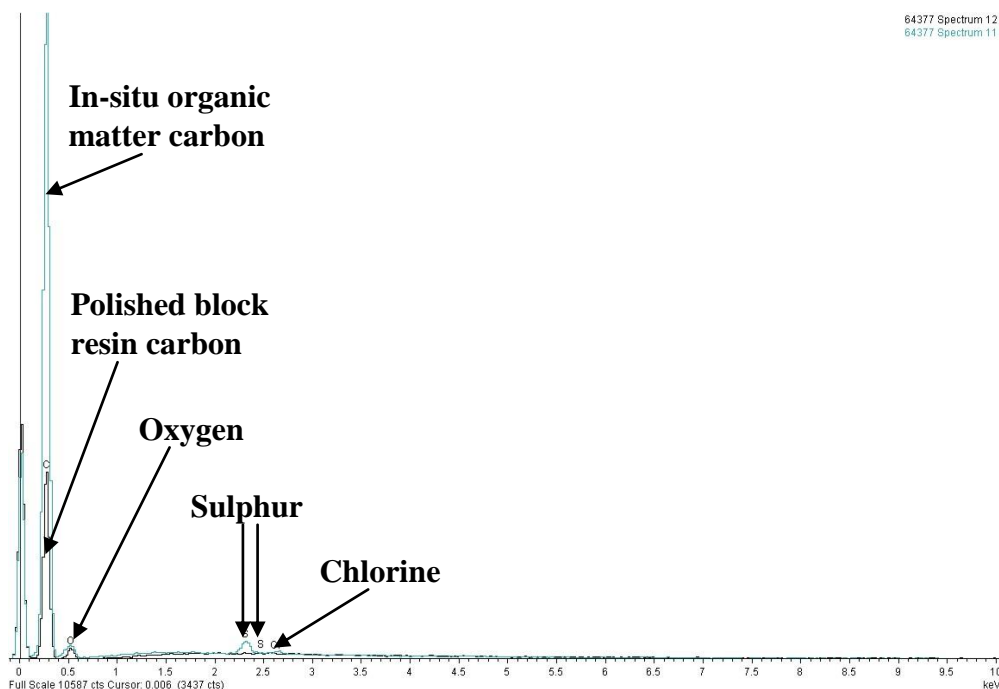


Fig. 3.12: Comparative microprobe spectra in block 64377 (facies 8) of peaks for carbon from in-situ organic matter (spectrum 11 – turquoise) and polished block resin (spectrum 12 – black)

Minor amounts of organic matter or hydrocarbons were detected from SEM-EDX analysis of shale block 64377 of facies 8 at Upton (SS200045). This was established by recognising that the carbon peak from the sample was much higher than that obtained from the carbon-coated resin block surrounding the sample (Fig. 3.12).

### 3.9 Discussion

This discussion provides an overview of the key sedimentary features and observations, the different published Bude Formation depositional models and also, the stratigraphy, sedimentary facies, palaeo-flow indicators, ichnofabrics, petrography and geochemistry of the beds between Northcott Mouth and Black Rock (SS202087-SS195015). Then following on from the petrographic insights into the diagenetic minerals in Bude Formation rock samples, there is a brief discussion on some aspects of the paragenetic sequence for the Bude Formation.

### 3.9.1 Summary of the key features in the Bude Formation

The key features observed in the Bude Formation beds are:

1. Sharp top-sharp base beds with sole marks on some bed bases (Higgs, 1991; Burne, 1995; and this study);
2. Two types of ripple laminated structures newly distinguished in this study (Figs. 3.1c, 3.2 & 3.3a-b) (i.e. facies 1a, equivalent to quasi-symmetrical ripples of Higgs (1991) or the ripple laminations of Burne (1995); and facies 1b, mud-draped ripple cosets);
3. Newly described occasional trough (facies 3) cross-stratification as well as tabular cross-stratification (facies 5) with reactivation surfaces (Figs. 3.1c, 3.2 & 3.3c-d);
4. Occasional 1-2 metre wavelength erosional structures associated with low-angle cross-stratification, interpreted as either hummocky cross-stratification (facies 4 of this study) (Higgs, 1991) or anti-dune structures (Burne, 1995) (Figs. 3.1c, 3.2 & 3.3f);
5. Slump and contorted beds (facies 9) (this study; Higgs, 1991; Figs. 3.1c & 3.3k, l & m);
6. Palaeo-flow directions measured from turbidite sole marks suggesting SW to SE palaeo-slope directions between Bude and Widemouth, but with a large spread across all directions north of Bude (Freshney et al, 1979; Higgs, 1991; Burne, 1995; this study; Fig. 3.6);
7. Apparently rare channels (facies 10) within the generally sheet-like bedding (Burne, 1995), indicating occasional sediment bypass and avulsion (Fig. 3.1c);
8. Low diversity and density ichnofabrics, except in the black shale beds (facies 8) (Higgs, 1991; Burne, 1995; this study; Fig. 3.1c);
9. Local structures that effect surrounding depositional thicknesses;
10. A lack of stenohaline ichnospecies (i.e. echinoderms, bivalves), which suggests that the depositional environment was non-marine;
11. Generally relatively low sulphur-carbon ratios (Lloyd & Chinnery, 2002; Fig. 3.9);
12. Occasional bedding-parallel pyrite framboids in shale beds (Fig. 3.8a).

### 3.9.2 Interpretation of depositional environments for the Bude Formation

The Bude Formation beds have a varied set of sedimentary facies, together with a wide range of palaeoflow directions, low diversity and density ichnofabrics and non-marine salinity proxy results from carbon-sulphur analysis. The facies include associated sandstones and siltstones with ripple (facies 1a; Fig. 3.3b) and planar laminations (facies 5a; Fig. 3.3h) as well as massive structureless beds (facies 6 and 7; Fig. 3.3i) with sharp-tops and sharp-bases. Some of these beds have basal flute, tool and prod marks (Freshney et al, 1979; Higgs, 1991; Burne, 1995) and are indicative of turbidites (Reading, 1996; Collinson et al, 2006) that may stack as a fan (Burne (1995; Fig. 3.13a). The basal marks provide generally southwards palaeoflow indicators between Bude and Widemouth (SS200065-SS199027) (Higgs, 1991; Burne, 1995).

The newly-described facies include mud-draped ripple (facies 1b) and planar (facies 5b) laminations (Fig. 3.3a & e) and trough cross-stratification (facies 2a and 2b; Fig. 3.3d), with

occasionally associated reactivation structures, as well as a non-mud-draped tabular cross-bed (facies 4; Fig. 3.3c). The facies are usually typical of astronomical tidal bedforms in a shoreface environment (Collinson et al, 2006; Ainsworth et al, 2012; Fig. 3.13b) and are often associated with hummocky cross-stratification (facies 3b; Fig. 3.3f) from storm-wave activity (Fig. 3.13b). These facies are interbedded on a decametric-scale with turbidite beds in the log from North Upton (SS200047; Fig. 3.2), suggesting that palaeo-slopes were present during deposition.

Marine-influenced Late Carboniferous shale (facies 8) “marine bands” (Freshney et al, 1972; 1979) are recognised as having been deposited during 4<sup>th</sup>-order ( $10^5$  yr) cycles of sea level change (Rippon, 1996). However, the decametric alternations of Bude Formation beds with turbiditic (facies 1a, 5a, 6 and 7) and mud-draped facies (facies 1b and 2b) are more frequent than black shale repetitions and thus occurred more frequently than 4<sup>th</sup>-order cycles.

The ichnofabrics associated with these beds are generally of low diversity and density. Where ichnofabrics have been observed, they are dominated by vertical *Skolithos* burrows. The burrowers are found in a shoreface depositional environment, which in the Bude Formation was only occasionally sufficiently oxygenated for them. A higher diversity of ichnofabrics is found in the thick, continuous black shale beds (facies 8). The ichnofabrics include common *Diplocraterion*, and rare *Arenicolites*, *Phycodes*, *Skolithos* and *Teichichnus* from sandstones and siltstones within thick black shale intervals, together with both *Planolites* and *Cochlichnus* ichnofabrics in the black shale laminations (King, 1967; Higgs, 1991; Burne, 1995).

Other structural, sedimentary and geochemical features are present in the Bude Formation outcrops, including local deformation structures that effect on metric to decimetric scales, local depositional thicknesses (Fig. 3.6), internal-contorted beds (facies 9a) and slump beds (facies 9b and 9c). The slumps of facies 9 formed when wet sediment became unstable and moved down a palaeo-slope during deposition, possibly as a result of rapid burial, storm waves or earthquakes (Owen, 1987; Owen & Moretti, 2008; see Chapter 2). In the case of the decametric-scale massive slump beds (facies 9c) the most likely trigger appears to be an earthquake (Del Pino-Sanchez, 2006) because of the very large forces required to generate the volumes of liquefied sediment in such beds (Owen, 1987).

A key geochemical feature of the Bude Formation is the variable carbon-sulphur (C/S) ratios from both the thin, discontinuous and thick, continuous shale beds (Lloyd & Chinnery, 2002) and the bedding-parallel pyrite framboids from thin, discontinuous shale beds (facies 8). In the thin, discontinuous shales, the C/S ratios are generally very low, which suggests a fresh to brackish water environment; whilst in two of the thick, continuous shale beds (Sandy Mouth and Warren Gutter Shales) C/S ratios are higher and indicate more marine salinities (Higgs, 1991). The bedding-parallel pyrite framboids form near the sediment-water interface under, anoxic conditions where reduced sulphur is present (Bond et al, 2004). This may suggest that these conditions occurred in a generally poorly-oxygenated lacustrine environment, which was affected by temporary marginal marine incursions that caused the reduced sulphur levels (after

Bond et al, 2004). Potentially, there was a sill tens to hundreds of metres high that cut the basin off from fully marine conditions (Higgs, 1991). This sill may have been occasionally overtopped (Higgs, 1991) or breached by active structures.

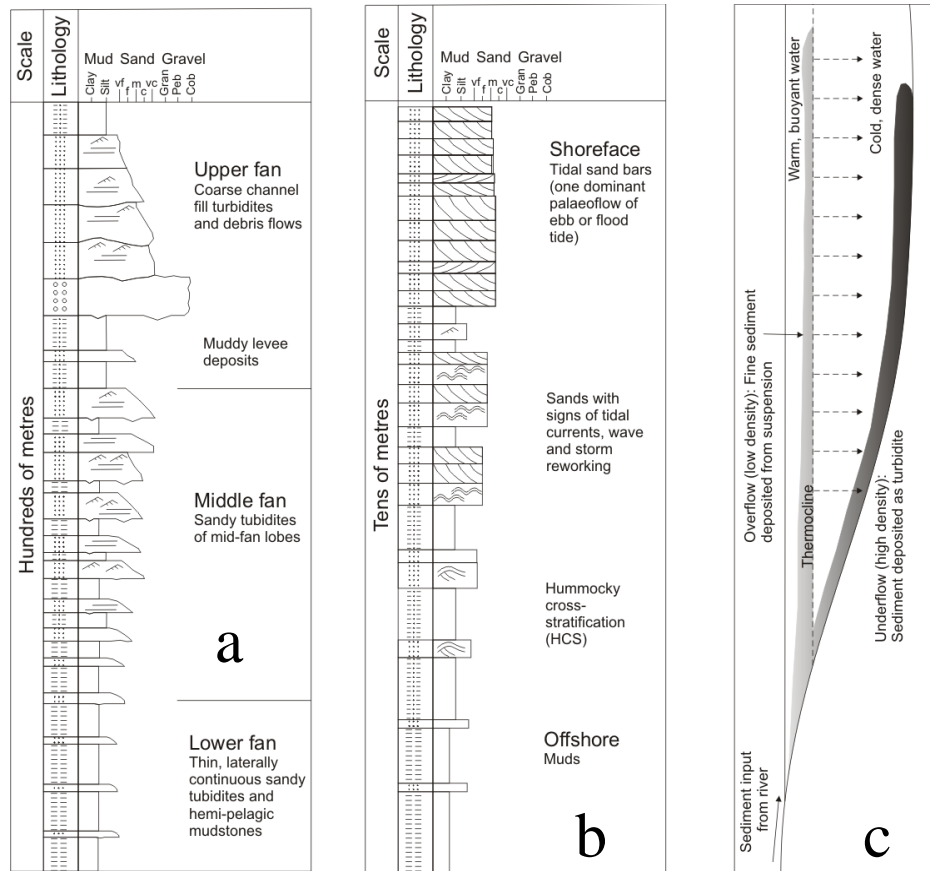


Fig. 3.13: Schematic sedimentary log stacking patterns and clastic sediment distribution (modified from Nichols, 1999). The logs display an idealised: (a) deep water turbidite fan at various levels and distances from source; (b) shallow marine environment dominated by tidal and storm processes. The logs are placed with: (c) a schematic diagram of sediment distribution in a deep lake in which turbidity flows occur

The Bude Formation may have experienced fluctuating depositional environments as evidenced by the alternations of demonstrably turbidite beds and possible tidal bedforms, with low diversity and density ichnofabrics and variable salinity proxy results. A deep lacustrine depositional environment, possibly up to hundreds of metres deep, may at times be inferred by the turbidites laid down on the slope (Higgs, 1991) or basin floor (Burne, 1995). However, base level changes are likely to have occurred, bringing parts of the basin into a shoreface setting either due to variable water levels (Reading, 1996; Nichols, 1999) and / or uplift and subsidence in a tectonically-active basin (Warr, 2002; Leveridge & Hartley, 2006). The depositional environment may have varied both laterally and temporally (i.e. vertically or stratigraphically) due to possible growing structures, causing variable bathymetry (Leveridge & Hartley, 2006) and which may be associated with lateral stratigraphic thickness variations (Freshney et al,

1972; 1979; Figs. 3.1 & 3.14). The lateral variations in the depositional environment during Westphalian B are suggested to be kilometric-scale (Fig. 3.14) from the relative stratigraphic locations deduced from the sedimentary logs taken during this work (Figs. 3.1b & c). Variable basin bathymetry during deposition may have caused turbidity current deflections, accounting for the variable palaeo-flow directions observed by Freshney et al (1979); Higgs (1991), Burne (1995) and in this work (see Fig. 3.6). Further discussion of basin-scale structures during Bude Formation deposition and its palaeo-environmental significance is provided in Chapter 9.

The facies recorded in the Bude Formation outcrops include mud-draped structures that may indicate deposition from an astronomical tidal regime (Collinson et al, 2006; Ainsworth et al, 2012). If the facies were associated with a phase when the basin was connected to open marine conditions, then the lack of marine fauna would imply that whilst well oxygenated, local salinities were low (Fig. 3.9). This could have inhibited the presence of a diverse fauna and stenohaline ichnospecies, implying that the Bude Formation was deposited at the “fresh” end of an estuarine system (Reading, 1996), with significant run-off being received from the Variscan mountain belt. However, a major problem with this interpretation is the lack of evidence for a saline wedge having (repeatedly) travelled into such an estuary, as might be expected from the inference of current velocity fluctuations (Reading, 1996).

Alternatively, the lack of faunal diversity is also consistent with lacustrine deposition (Reading, 1996). However, lacustrine environments are not generally known to be affected by tides. Thus, a discussion is provided below of alternative models that explain the presence of mud-draped ripple laminated structures based upon Baas et al (2011) and apparent meteorological “tidal” bedforms described by Ainsworth et al (2012).

### **Generation of mud-draped ripple and planar laminations**

Centimetric-scale mud-draped ripple and planar laminations have been identified in the Bude Formation outcrops (Figs. 3.3a-b). Mud drapes are usually associated with astronomical tidal regimes over single tidal and spring-neap tidal cycles (Fig. 3.15a; Collinson et al, 2006) that occur in marine lower to middle shoreface settings. An alternative explanation for the generation of mud drapes on ripple laminations is provided by the experimental work on fine-grained muddy sand turbidity flows by Baas et al (2011), in which mud-draped ripple and planar laminations developed during several runs within centimetric-scale dune structures (Fig. 3.15b).

The experiments with suspended sediment of different clay contents measured turbulent flows over run times of up to two hours under waning flow conditions. As clay concentration increased, five flow types were generated over a smooth, fixed surface. Centimetric-scale ripple laminations were generated under turbulent flows, turbulence-enhanced transitional flows and lower transitional plug flows; whilst millimetric-scale planar laminations were generated under upper transitional plug flows and quasi-laminar plug flows. Under the three ripple lamination-forming flows, as clay concentration increased, ripple amplitude and wavelength increased too.

The nature of the laminated structures formed varied with flow duration (Fig. 3.15b). Under ripple lamination-forming flows at clay concentrations of 6.9%, a migrating decimetric-scale ripple or dune developed after 1 hour of flow where the lee slope was eroded and sediment was redeposited on the stoss slope. This created a series of rhythmic silt / mud and sand laminations ( $t_3$ ; Fig. 3.15b), similar to the Bude Formation mud-draped ripples (facies 1b). As the flow continued, separate laminations became composed of inter-mixed sand, silt and mud ( $t_4$ ; Fig. 3.15b), similar to the Bude Formation ripples (facies 1a), although without any of the apparent cyclicity in bundle spacing shown in Fig. 3.15a. During the runs by Baas et al (2011), the ripple indices became increasingly symmetric, with indices of 2-3 ('overlap range' between current and wave ripples; Collinson et al, 2006), as also observed in the Bude Formation.

These experimental results by Baas et al (2011) for mud-drape generation on sedimentary structures, suggest that a turbidite association can be ascribed clearly only where it can be demonstrated that mud-draped ripple laminations sit within sharp-top, sharp-base beds with basal flute marks. Unfortunately, there have been no observational results published yet confirming these experimental results. However, if they are not confirmed, it does not necessarily demonstrate that the mud-draped ripple laminations (facies 1b) and associated mud-draped facies resulted from astronomical tides. Instead, a discussion of how such apparent tidal bedforms could be generated in a lacustrine environment is provided below.

### **Generation of apparent tidal bedforms**

Decimetric-scale mud-draped trough and metric-scale tabular cross-stratification, as well as reactivation surfaces are occasionally observed in the Bude Formation outcrops (Fig. 3.3c-d). Generally, these structures have been used to indicate astronomical tidal influence upon sedimentation (Collinson et al, 2006; Ainsworth et al, 2012). The mud-draped trough cross-stratification structures may have been developed from high energy erosive tidal flows, perhaps with some storm influence, in a mid-shoreface setting (Reading, 1996). The tabular cross-stratification structures may have been developed from high energy tidal flows that formed a metric-scale dune, sand wave or bar in a mid-to-lower shoreface setting (Collinson et al, 2006). The reactivation surfaces may have been developed from depth fluctuations resulting from base level changes during tidal ebb and flow or from superimposed storm events (Collinson et al, 2006). These apparent tidal bedforms are also inter-bedded with metric-scale hummocky cross-stratified structures, indicating probable storm reworking in the lower shoreface.

However, the Bude Formation lacks stenohaline (i.e. echinoderm, bivalve) ichnospecies and most shale beds recorded non-marine signatures from C/S analysis, apart from two of the continuous shale beds found higher in the stratigraphic column (Lloyd & Chinnery, 2002; Fig. 3.9). The lack of stenohaline ichnospecies and the wide occurrence of non-marine salinity proxies, together suggest that an astronomical tidal regime may not have affected the Bude Formation depositional environment.

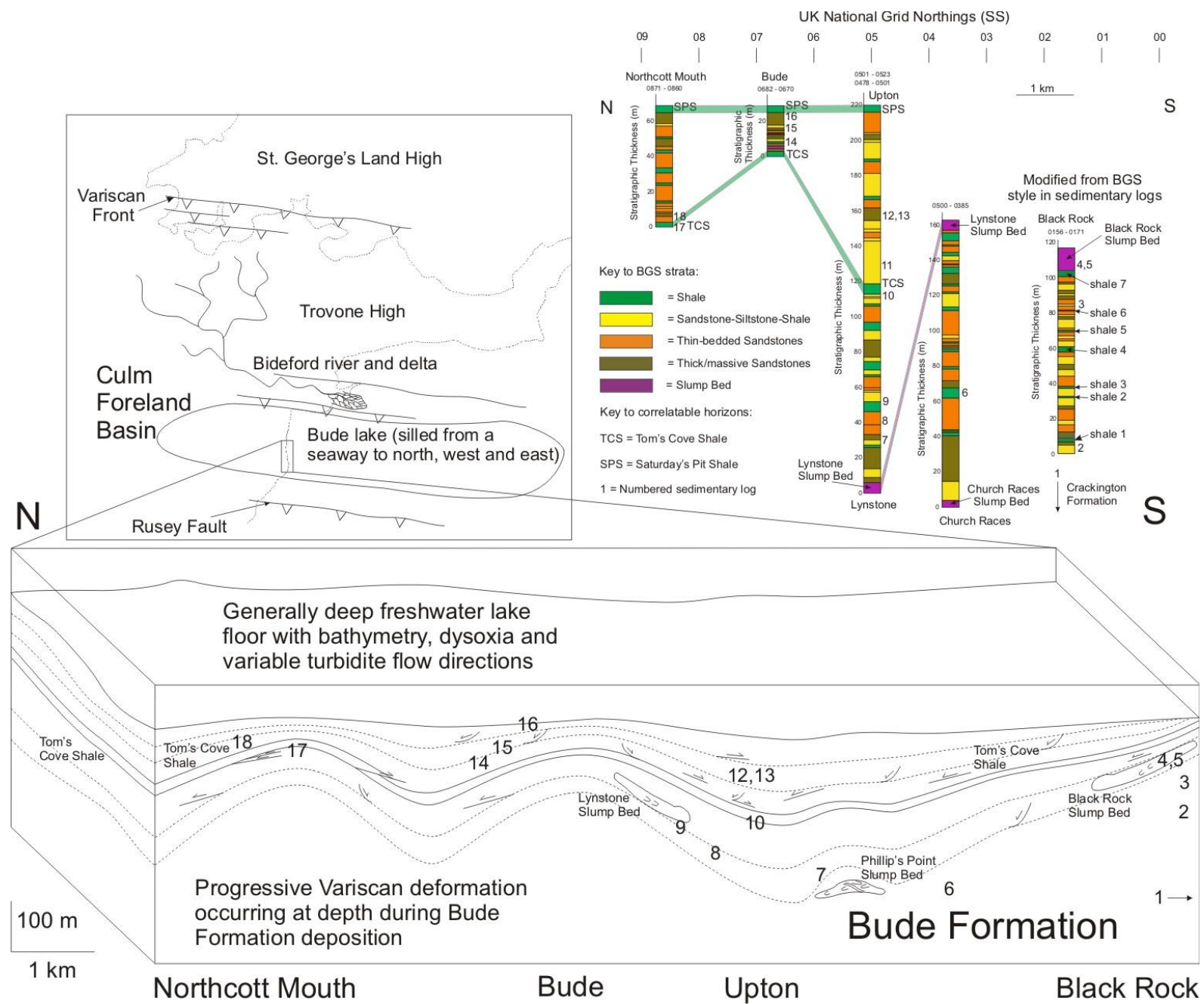


Fig. 3.14: Vertically-exaggerated, simplified schematic 3-D sketch of Bude Formation palaeo-geography between Northcott Mouth and Black Rock (bottom) and where it is located in the Culm Basin (top left). Positions of sedimentary logs 1-18 (see Fig. 3.1c) taken in the field study area are shown both in the 3-D sketch and in the correlation panel of Bude Formation summary sedimentary logs (top right) from Figs. 3.1a & b (modified from Freshney et al, 1972; 1979)

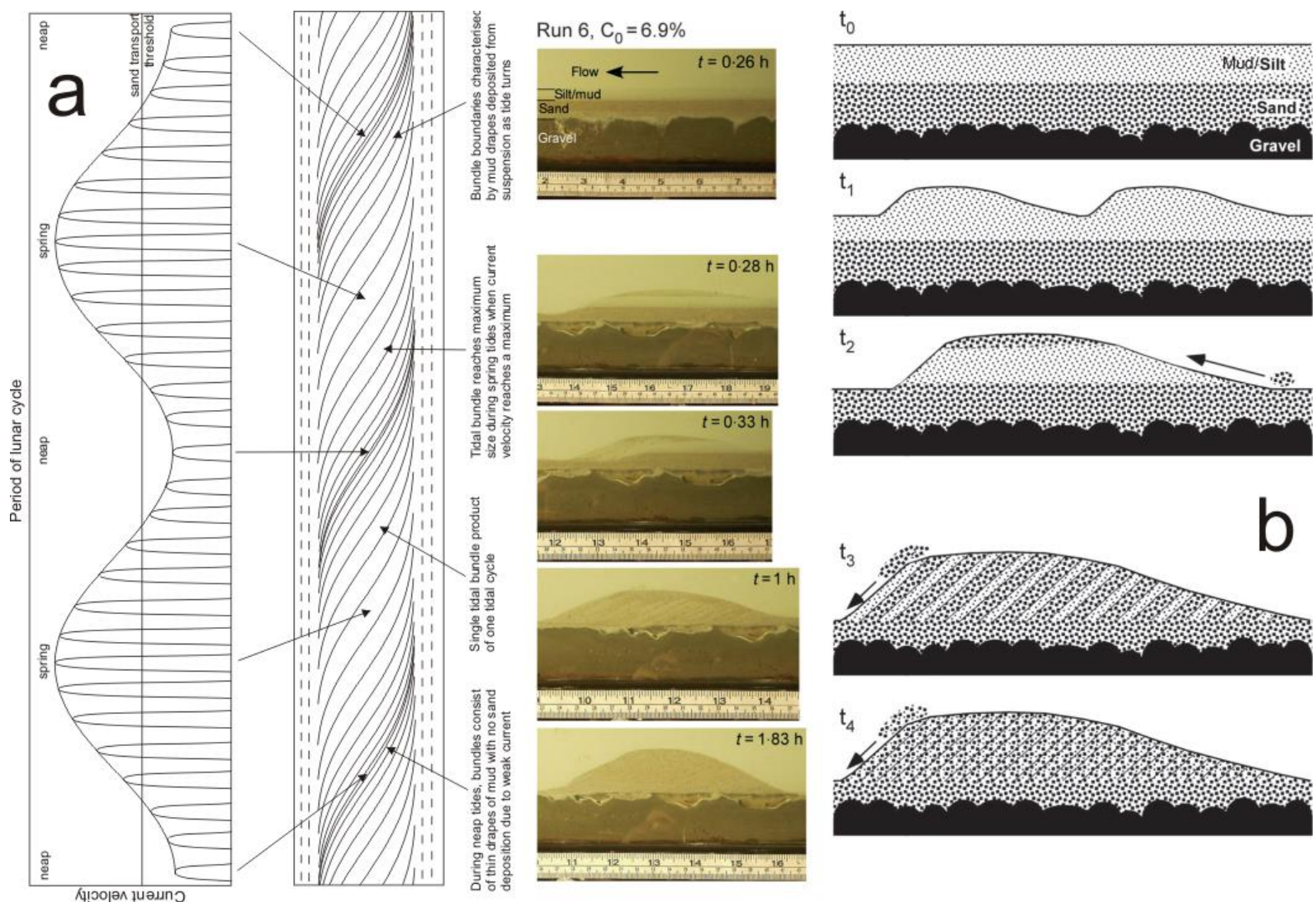


Fig. 3.15: Comparison of processes to generate mud-draped ripple structures from strongly uni-directional flows within: (a) tidal beds (modified from Collinson et al, 2006); and (b) in muddy-sandy turbidites (from the experimental runs of Baas et al, 2011)

An alternative model for generating tidal bedforms within a lacustrine or marginal marine environment has been demonstrated by Ainsworth et al (2012) in the shoreline deposits of the modern Lake Eyre, Australia. These authors have described sediments with facies that include mud-draped tabular cross-beds and trough cross-bedding up to 0.25 m in thickness, as described in Section 3.3.1 on siltstones and sandstones with ripple laminations (Facies 1a and b). Lake Eyre is non-marine and is located in an intracratonic playa lake setting. In comparison, the Bude Formation was situated within a Late Carboniferous *sensu lato* foreland basin setting (see Chapter 2). Ainsworth et al (2012) ascribed the observed sedimentary structures in Lake Eyre to meteorological “tides”, which are related to cyclical daily changes in wind direction and velocity, in combination with weekly or monthly variations in fluvial discharge. This raises an alternative set of mechanisms for generating Bude Formation mud-draped ripple laminations (facies 1b) within a shoreface depositional setting, without requiring a full marine connection.

### 3.9.3 Discussion of existing and new depositional models

In this chapter, descriptions were provided of six existing depositional models for the Bude Formation, which are:

1. Fining-up delta (King, 1971);
2. Wave and storm influenced shallow water environment (Higgs, 1984);
3. Prograding turbidite fan (Melvin, 1986);
4. Shallow marine ramp (Hartley, 1991);
5. Freshwater lacustrine environment (Higgs, 1986; 1991);
6. Variably-oxygenated inactive fan (Burne, 1995).

In most of the models, a single non-marine depositional environment has been invoked for the Bude Formation. The exception is the prograding turbidite fan model of Melvin (1986). From the results of C/S analysis (Lloyd & Chinnery, 2002), fresh to brackish water conditions dominated, except during the deposition of the Sandy Mouth and Warren Gutter shales (facies 8; Higgs, 1991; Burne, 1995). There is no evidence for fluvial deposition from the King (1971) model (Burne, 1995), as in the coeval Bideford Formation delta (de Raaf et al, 1969; Li, 1990). Instead, a turbidite-dominated depositional environment has been suggested (Melvin, 1986; Hartley, 1991; Higgs, 1991; Burne, 1995). However, a connection between the Bideford and Bude formations inferred by Hartley (1991) has not been demonstrated (Burne, 1995).

A significant debate has been generated on the Bude Formation depositional environment by Higgs (1991) and Burne (1995). The key facies for these two authors is the centimetric-scale ripple laminations (facies 1a; Figs. 3.3a-b) that may represent either waning flow structures from turbidity (and storm-generated) flows with minor wave influence (Higgs, 1991) or reworking of turbidite bed tops by the tail of the same turbidity current (Burne, 1995). The presence of a minor wave influence would suggest that the turbidites were deposited in a

shoreface environment from sediment-laden river flows, which were denser than the fresh to brackish waters (Higgs, 1991). In contrast, Burne (1995) suggested that the turbidites were transported along channels to the basin floor or deep shelf. The present study recognises the presence of sharp-topped, sharp-based turbidite beds with flute-marks locally evident on their bases. The isolated nature of some of these beds may be consistent with being a down-dip product of storm reworking events in the upper shoreface (Reading, 1996). Systematic stacking architectures that would necessitate the presence of a subaqueous fan system (Melvin, 1986; Burne, 1995; Fig. 3.13a) have not been recognised in the present study, although this does not preclude the presence of shoreline-derived turbulent underflows (Fig. 3.13c; Reading, 1996).

Higgs (1991) recognised metric-scale undulations at North Upton (SS200047) and interpreted them as lower shoreface hummocky cross-stratification (facies 3b; Fig. 3.3f). The Burne (1995) alternative model for the hummocks is that they are deep water anti-dunes. However, from the present study, the symmetry of observed hummocks, the lack of internal dewatering, the rarity of the associated *Skolithos* ichnofabrics, and the low angle reactivation structures in underlying beds (Fig. 3.2), make the Burne (1995) explanations difficult to support.

During the brief intervals when salinities increased (Fig. 3.9), water densities may have increased sufficiently for sediment-laden river waters to have been less dense than the lake waters (Nichols, 1999). This may have generated river-fed surface plumes (Higgs, 1991), high concentration sediment clouds (Burne, 1995) or near-clastic sediment cut-off (Higgs, 1991; Burne, 1995), causing shale deposition (facies 8).

Alternatively, if marine black shales (facies 8) equate to eustatic highstands (Higgs, 1991) then clastic sedimentation may have shifted in a landward direction, such that these shale beds represent more distal sedimentation. Also, this muddy environment in the black shales (facies 8; Figs. 3.3i, 3.4 & 3.5) was probably more oxygenated, with increased ichnofabric diversities in some interbedded sandstones (Freshney et al, 1979; Higgs, 1991; Burne, 1995). On rare occasions, the brackish water environments became either dysoxic, with restricted *Planolites* assemblages (Higgs, 1991; Burne, 1995), or anoxic, with bedding-parallel pyrite framboids precipitated (after Bond et al, 2004; Fig. 3.8a). Generally however, the Bude Formation beds show either low density and diversity ichnofabrics or a complete absence (Fig. 3.3h), as observed by both Higgs (1991) and Burne (1995).

Furthermore, a number of new facies have been either recognised or described more fully during this work:

1. Facies 1b of centimetric-scale mud-draped ripple laminations (Figs. 3.1c, 3.2 & 3.3a);
2. Facies 2a of trough cross-stratification and facies 2b of mud-draped trough cross-stratification (decimetric-scale) (Figs. 3.1c, 3.2 & 3.3d);
3. Facies 4 of a metric-scale tabular cross-bed (Figs. 3.1c, 3.2 & 3.3c);
4. Facies 5b of millimetric-scale mud-draped planar laminations (Figs. 3.1c, 3.2 & 3.3a & d).

The mud-draped facies may suggest that tidal bedforms were generated (Collinson et al, 2006) in the Bude Formation, albeit from possible meteorological “tides” related to wind direction and fluvial discharge variations into a lake or fresh to brackish water body (after Ainsworth et al, 2012). On a decametric-scale, these facies are interbedded with turbidite beds, as described by Higgs (1991) and Burne (1995). On the kilometric-scale, between the Tom’s Cove and Saturday’s Pit shales, lateral stratigraphic thicknesses vary between about 70 m at Northcott Mouth, about 25 m at Bude and about 105 m at Upton (Fig. 3.1a & b; Freshney et al, 1972; 1979). This suggests that the Bude Formation deposits were affected by Variscan deformation during deposition (Leveridge & Hartley, 2006).

### **Mixed depositional environment**

The occasional presence of apparent “tidal” bedforms in amongst turbidite deposits may suggest that a variable depositional environment existed within the Culm Basin during Bude Formation deposition. This mixed depositional environment may have continually evolved both laterally (i.e. coeval turbidite and potential meteorological “tidal” deposition) and / or vertically (i.e. stratigraphically or temporally). For example, there were two marine transgressions where clastic sediment supply was greatly reduced, as shown by the metric-scale, laterally-continuous ‘marine band’ black shales (facies 8; Freshney et al, 1979; Higgs, 1991; Burne, 1995).

### **3.9.4 Description of Bude Formation diagenesis using a paragenetic sequence**

Following deposition, the Bude Formation beds underwent compaction and burial diagenesis (Warr et al, 1991; Warr & Hecht, 1993). From petrographic analyses of the Bude Formation rock samples a hypothetical paragenetic sequence has been constructed (Fig. 3.16) of the diagenetic mineral development and precipitation:

1. Framboidal pyrites (5  $\mu\text{m}^+$ ) precipitated just below the sediment-water interface;
2. Bedding-parallel ankerite veins precipitated in mud beds near the palaeo-surface;
3. Quartz veins that infill fractures and cross-cut bedding-parallel ankerite veins;
4. Siderite-ankerite veins that cross-cut both the quartz and bedding-parallel ankerite veins.

The diagenetic alternations found in all the lithologies indicate that varying degrees of dilation and contraction occurred during mineral transformations and compaction (Fig. 3.16). Where dilation occurred in the Bude Formation either fluid over-pressure conditions increased or mineral growths expanded into pore spaces.

Also, the preliminary petrographic analyses of the Bude Formation rock samples suggest that there is a significant area of low-temperature geochemical research that could be undertaken on the diagenesis of the deposits, which were laid down in fresh to brackish water (Fig. 3.9) that included a possible anoxic environment (Fig. 3.8). Although some research has been undertaken into deposits from such environments, such as in the Late Cretaceous

Marshybank Formation, Alberta and British Columbia, Canada (McKay et al, 1995), the Bude Formation may provide an informative area for such as investigation of geochemical models and diagenetic alterations.

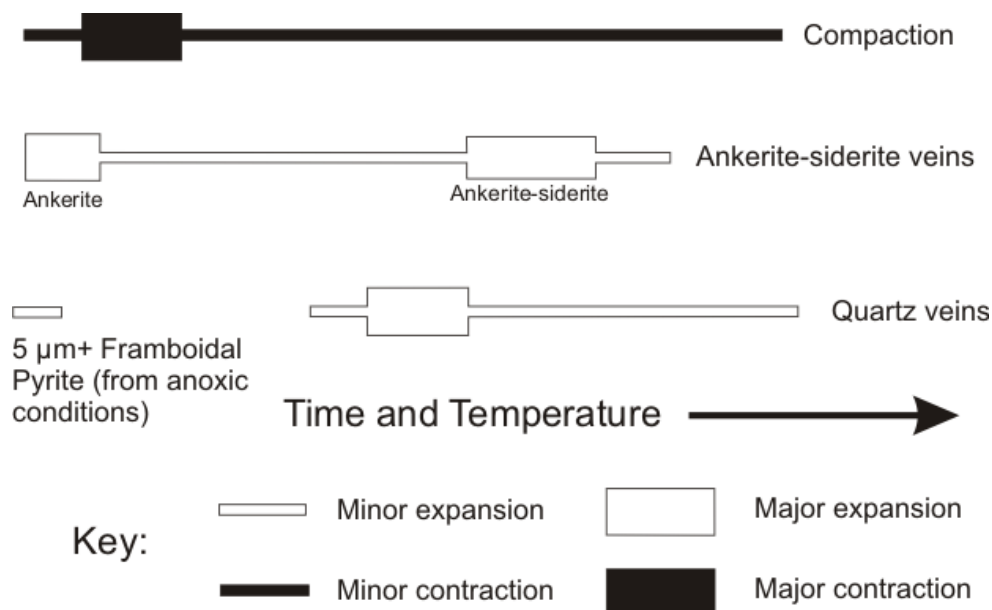


Fig. 3.16: Hypothetical paragenetic sequence for all lithologies in the Bude Formation showing increasing diagenetic alteration with time and temperature to the right. The relative amount of expansion and contraction due to the mineral development or precipitation is also noted

### 3.10 Conclusions

The Bude Formation contains a number of key sedimentary and geochemical features that have been studied in this chapter by the author for the specific thesis aims and include:

1. Previously unidentified centimetric-scale mud-draped ripple laminations (facies 1b) that could have been generated by uni-directional meteorological “tidal” currents or short duration muddy sandy turbidity flows;
2. Centimetric-scale non mud-draped ripple (facies 1a) and millimetric-scale planar laminated beds (facies 5a), as well as metric scale massive structureless beds (facies 6 and 7) with both sharp tops and sharp bases, plus basal sole marks, which are likely to have been generated from turbidity flows (slope-derived or down-dip of shoreface storm reworking events);
3. Previously unidentified decimetric-scale mud-draped troughs (facies 2b) that may be interpreted as meteorological “tidal” bedforms;
4. More fully described metric-scale tabular cross-stratification (facies 4) and reactivation surfaces that may relate to storm activity in the lower shoreface;
5. Rare metric-scale symmetrical undulations from oscillatory flows that could have been driven by storm waves, generating hummocky cross-stratification (facies 3b);
6. Metric to decametric scale slumps and contorted beds (facies 9), resulting from earthquakes, sediment loading or storm wave activity, showing fold deformation in sediment;

7. Occasional low diversity and density *Skolithos* ichnofabrics, with a slightly more diverse suite of ichnofabrics found in some clastic beds within black shale beds (facies 8);
8. Absence of stenohaline ichnospecies, suggesting non-marine environments;
9. Results from carbon-sulphur (C/S) analysis that suggest that in all but two of the Bude Formation continuous black shale beds (Sandy Mouth and Warren Gutter shales), fresh to brackish water proxy salinities occurred during deposition.

Together, these features suggest that the Bude Formation was deposited in a fluctuating, mainly fresh to brackish water environment, with low diversity and density of ichnofabrics. These features may suggest that the Bude Formation beds were laid down in a lacustrine or possibly marginal marine environment, possibly situated behind a sill in a tectonically active basin. Salinity changes may have resulted from variations in either river discharge, or lake base levels, or through influxes of saline water. Fourth-order marine transgressions may explain the presence of the thicker, continuous black shales of marine character. These characteristics of the Bude Formation suggest that it developed in a complex, variable and mixed depositional environment and that simple models are probably inadequate.

One possibility is that the Bude Formation beds are stacked turbidites and meteorological “tidal” bedforms, generated by variations in wind direction, storm activity and fluvial discharge within a lake that experienced significant changes in base level. The frequency of the decametric turbidite to shoreface dominated alternations is much greater than the fourth-order eustatic-driven marine black shales. The high frequency of these alternating palaeoenvironments may suggest that there was a (possibly fifth-order) climatic control on the sediment flux and / or base level superimposed upon the longer term progressive Variscan tectonic deformation.

Following this review of the depositional environment for the Bude Formation, Chapter 4 will look at the geological mapping of the Black Rock and Wanson Mouth foreshores on the faulted boundary of the Bude and Crackington formations. This was undertaken to describe the juxtaposed fold structures in the two foreshore successions across the Widemouth South Fault (WSF) and how the deformation observed in this small area is important for understanding the structures across the Culm Basin. This contributes to the general aim of the thesis, to describe whether folds in sediment and sedimentary rock may be distinguished based on their geometries, and also the specific aim of the thesis, to understand the geological evolution of the Culm Basin.

## Chapter 4: Geological mapping and evidence for progressive Variscan deformation in the Bude and Crackington formations

### 4.1 Introduction

This chapter is concerned with establishing the deformation history of the Black Rock foreshore in the Bude Formation and the Wanson Mouth foreshore in the Crackington Formation. The two foreshore successions have been affected strongly by Variscan deformation and are juxtaposed by the Widemouth South Fault (King, 1967; Freshney et al, 1972; Enfield et al, 1985; Anderson & Morris, 2004). Study of the deformation history in the two successions provides an understanding of the chevron fold geometries that are typical in the Culm Basin (Freshney et al, 1972; 1979; Ramsay, 1974; Sanderson, 1974; 1979; Lloyd & Whalley, 1986; 1997; Davison et al, 2004). This is of direct relevance to the specific thesis aim, to understand the geological evolution of the Culm Basin, and also provides some contribution to the general aim, namely to establish criteria for distinguishing between folds in rock and sediment.

In this chapter, a review is provided of the current literature on the stratigraphy of the Bude and Crackington formations from Freshney et al (1979) and where the Black Rock and Wanson Mouth foreshores sit relatively within this stratigraphy. This follows on from Chapter 3, which looked at the different depositional models for the Bude Formation. The review also assesses: (1) the map work of King (1967) and the structural features described in this map; (2) models for the progressive deformation of the chevron folds in the Culm Basin, with a critical review of the Sanderson (1979) and Lloyd and Whalley (1986; 1997) models; and (3) the Widemouth South Fault, with descriptions of four models for its development. Following this, descriptions are provided of the sedimentary data that were collected in the form of logs and correlated in the Black Rock foreshore where laterally-continuous beds were recognised.

Structural data were collected from every fold and fault in both foreshores and are described on a geological map that shows the key sedimentary and structural features. Cross-sections have been drawn with three dip sections across both foreshores that cut the Widemouth South Fault (WSF), four strike sections within the Black Rock foreshore only and one oblique section within the Wanson Mouth foreshore only. In the Black Rock foreshore, laterally-continuous beds allowed a 3D structural overview. These cross-sections have also been restored in order to understand the deformation that affected each foreshore. From the restorations, models are discussed for the progressive deformation of both successions.

#### **4.1.1 Description of the Black Rock and Wanson Mouth foreshore successions**

The Bude Formation sits in the Culm Basin, SW England (Fig. 4.1), stratigraphically above the Crackington Formation (King, 1967; Freshney et al, 1972; 1979; Higgs, 1984; 1986; 1991; Melvin, 1986; Burne, 1995). Both formations experienced Late Carboniferous Variscan

deformation, producing the classic trains of ‘Ramsay-type’ chevron folds, with ‘upright’ and south-directed ‘inclined-to-recumbent’ fold styles, with anticlinal hinges in the same direction as shear strain, across 28 km of well-exposed coast (Freshney et al, 1972; 1979; Ramsay, 1974; Sanderson, 1974; 1979; Lloyd & Whalley, 1986; 1997; Davison et al, 2004; see Chapter 2).

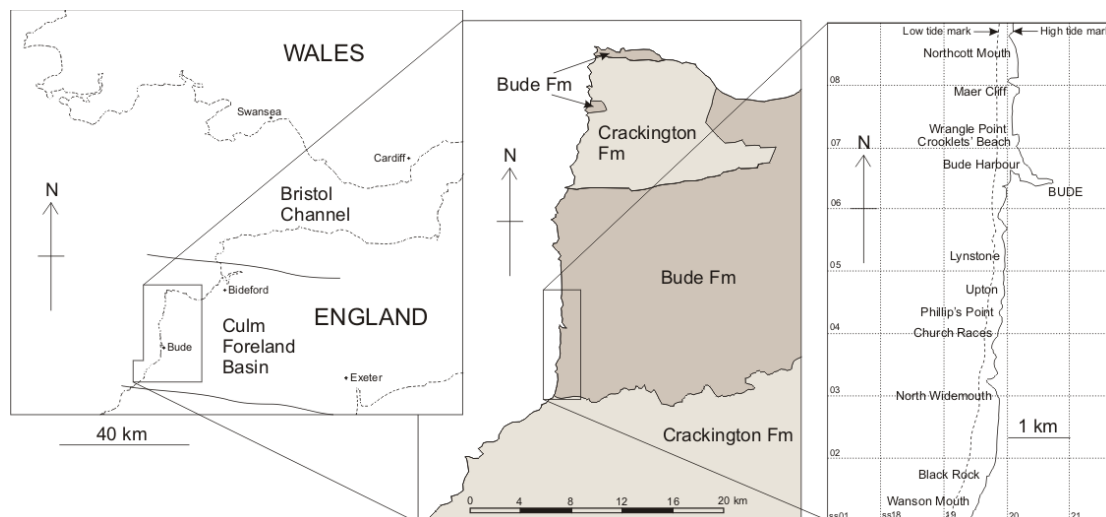


Fig. 4.1: Location map of SW England (left), a simple geological map of the Culm Basin (middle) and an inset map of the Bude coastal area (right) where fieldwork was undertaken (modified from Ordnance Survey<sup>TM</sup>/EDINA<sup>TM</sup> Digimap, 2010; Lloyd & Chinnery, 2002)

Faults observed along the coastal outcrops cut the chevron folds and are related to movements during the latter ‘stages’ of and after the Variscan deformation (Freshney et al, 1972; Enfield et al, 1985; Durrance, 1985; Peacock et al, 1998) and are termed ‘late’. Local extensional and contractional structures developed before chevron folding being termed ‘early’ (Whalley & Lloyd, 1986), ‘pre-chevron’ (Lloyd & Chinnery, 2002) or ‘pre-folding’, as observed by Mapeo and Andrews (1991) at Menachurch Point (SS202093), Sandy Mouth (SS201101) and Northcott Mouth (SS201085). Tests are conducted in this work to assess whether they occurred prior to chevron folding and if so are termed ‘early’.

All of these deformation styles are rarely observed together, complicating their study and comparison. One area that includes all these Variscan deformation structures is in the Black Rock and Wanson Mouth foreshores (SS197017-SS195013), thereby providing a microcosm of the depositional and structural elements in the 28 km of deformed and repeated outcrops. The purpose of the geological mapping is to use this microcosm to consider the geological evolution of the Culm Basin, particularly the deformation in the Bude Formation and its relationship with that in the Crackington Formation. This includes testing whether ‘early’ structures exist in both foreshores and whether there are any depositional thickness variations around the structures. Thus, the foreshores are remapped to provide more structural details on the original mapping area of King (1967) shown in Fig. 4.3, and which was used in Freshney et al (1972). A description of the King (1967) map (Fig. 4.3) is provided in Section 4.1.2.

Despite their proximity, the stratigraphy of the two foreshore successions differs greatly, as shown in the Culm Basin stratigraphic columns (Fig. 4.2) produced by the British Geological Survey (Freshney et al, 1972; 1979; modified by Lloyd & Chinnery, 2002), where:

1. The Black Rock foreshore succession from the Black Rock Slump Bed includes up to 120 m of stratigraphy in the Bude Formation;
2. The Wanson Mouth foreshore succession is directly above the Embury black shale (*G. listeri*; early Westphalian) in the Crackington Formation, suggesting that the WSF has cut out approximately 300 m of stratigraphy, including the boundary between the Crackington and Bude formations at the Hartland Quay Shale (Fig. 4.2; Freshney et al, 1979).

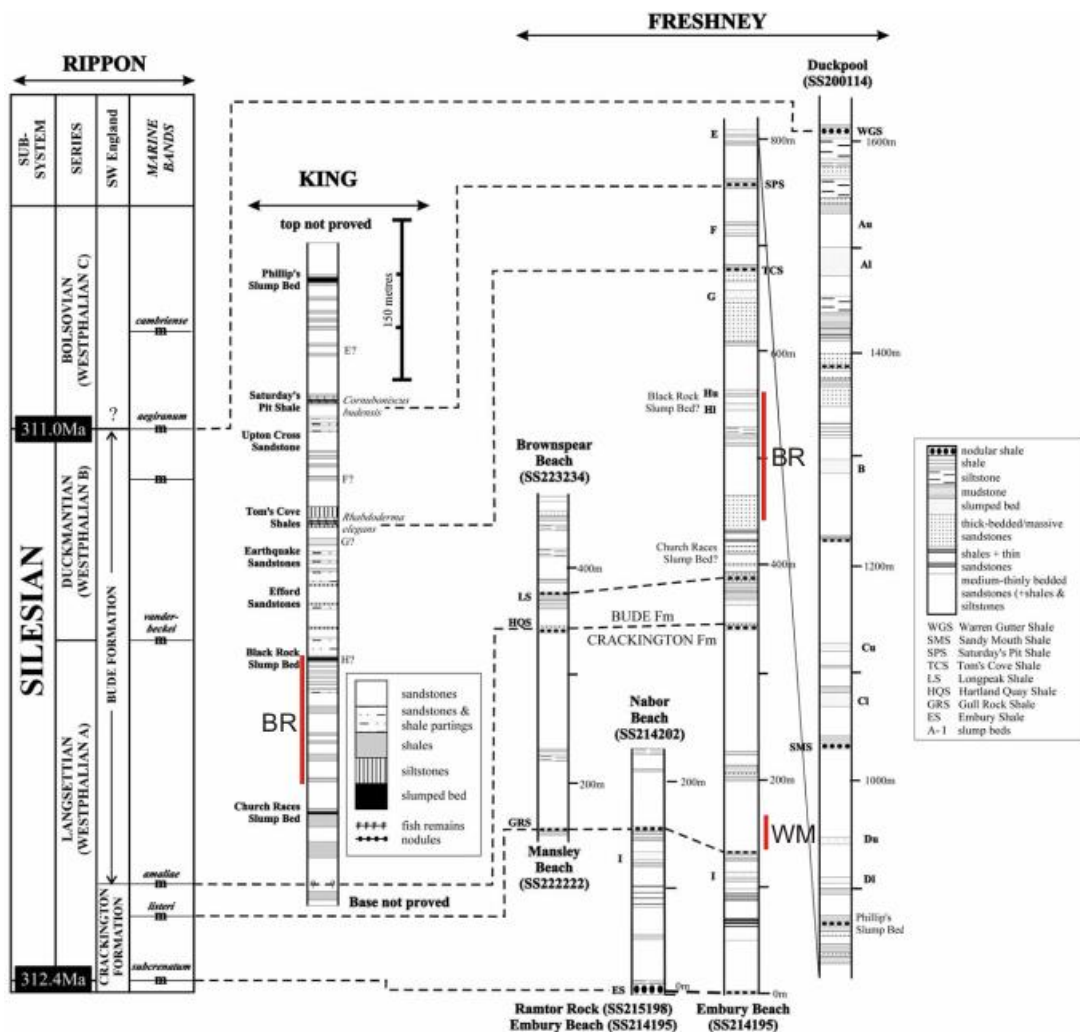


Fig. 4.2: Bude Formation stratigraphy (from Lloyd & Chinnery, 2002). Left: generalised UK Late Carboniferous stratigraphy (after Rippon, 1996); Centre: ‘restricted’ composite succession between Bude and Wanson Mouth (King, 1967); Right: ‘complete’ succession (Freshney et al, 1979). Black Rock (BR) and Wanson Mouth (WM) stratigraphic sections (solid red lines) are projected onto the Freshney et al (1979) column to show their stratigraphic separation (~ 300 m)

Freshney et al (1972) suggested that the structural positions of the foreshores are within the “upper limb of a major fold (anticline)” that extends to Bude and the strata are “overturned

to the south” (see Fig. 2.22, taken from Fig. 2 of Sanderson (1979)). The foreshores are cut by the Widemouth South Fault (WSF; Williams et al, 1970; Freshney et al, 1972; Enfield et al, 1985). The Wanson Mouth foreshore lies south of the WSF within a fault zone in the Crackington Formation that has been deformed by south-directed ‘inclined’ chevron folds (Sanderson, 1979; Enfield et al, 1985). The Black Rock foreshore lies north of the WSF in the Bude Formation and contains an ‘upright’ chevron fold train (Freshney et al, 1972; Sanderson, 1979). These contrasting structural styles on either side of the WSF provide a context for testing models to explain the progressive development of Variscan structures.

#### **4.1.2 Description of the King map**

The King (1967) map (Fig. 4.3) shows the contrasting deformation structures of the Black Rock foreshore (Bude Formation) and Wanson Mouth foreshore (Crackington Formation), which lie either side of the Widemouth South Fault (WSF; SS19620144-SS19400166). The WSF truncates all structures adjoining it in either foreshore, and thus, must at least for the later part of its activity, post-date the deformation in both foreshores.

The King (1967) map is mostly very detailed, but contains areas termed as ‘geologically complex’; for example (see Fig. 4.3) in area ‘A4’ SW of the WSF and area ‘A5’ in the strongly-faulted southern Wanson Mouth foreshore (SS19550134-SS19330146). The areas were largely ignored in the geological interpretations presented by King (1967) and subsequently by Freshney et al (1972). However, they are shown here to be critical to the understanding of the deformation history of not only this small section but also the whole 28 km of coastal section.

In order to introduce greater locational precision, reference is made to the area sub-divisions produced in the geological mapping undertaken in this study. These sub-divisions are wholly independent of the King (1967) map (Fig. 4.3), being based purely upon interpreting the data collected in this study. However, the three sub-divisions of the Bude formation (areas A1 to A3) and the three of the Crackington formation (areas A4 to A6) correspond sufficiently closely to the descriptions of King (1967) to be useful here as cross-references.

#### **Black Rock foreshore**

To describe the King (1967) map, three areas were defined in the Black Rock foreshore by the author as having different types and degrees of ‘geological complexity’ (areas A1 to A3).

In the northern part of the foreshore (area A1; Fig. 4.3), there is a steeply north-dipping set of stacked beds including a decametric-scale chevron fold pair with E-W-oriented axes (SS19610167-SS19450167). Freshney et al (1972) described the folds as parasitic en echelon periclinal on the “broken northern limb of the northern anticline”. An important marker bed in area A1 (Fig. 4.3) is the 12 m thick Black Rock Slump Bed, which lies within a shale bed. North of the slump bed, there are two further laterally-continuous stratigraphically higher shale beds.

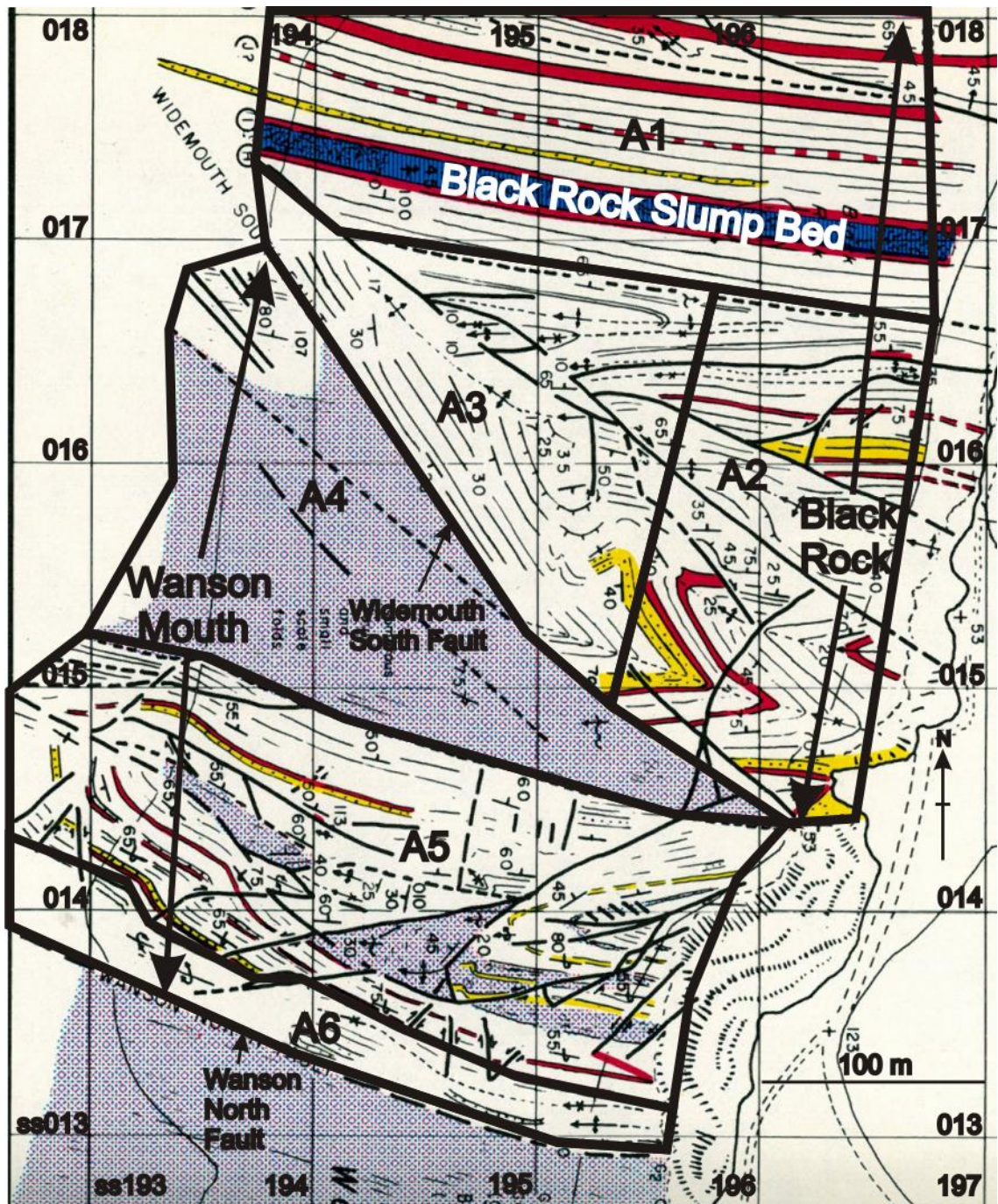


Fig. 4.3: Geological map of the Black Rock-Wanson Mouth foreshores from King (1967) and reprinted in Freshney et al (1972), including the locations of areas (A1-A6) described in this text. The foreshores have been remapped at a higher resolution during this work (see gusset)

In the south-eastern foreshore (area A2; Fig. 4.3), King (1967) observed a hundreds of metres scale train of five chevron folds (three anticlines and two synclines) with E-W-oriented axes plunging towards the WNW. In the King map, several faults cause a few metres of offset in area A2 (Fig. 4.3), including one that strikes NW-SE across the foreshore (SS19670152-SS19370173) and cuts through the hinge of a chevron syncline at SS19650154.

In the central and western foreshore (area A3; Fig. 4.3), a complex set of structures was observed, including a set of local, decametric-scale faults together with folds that have N-S-

oriented axes between SS19510162 and SS19530155. The structures sit on the southern limb of a chevron anticline with a NW-SE-oriented axis (SS19530163-SS19430167). The chevron fold train in area A2 (Fig. 4.3) dies out around these local structures.

### **Wanson Mouth foreshore**

The Wanson Mouth foreshore lies to the south of the WSF and has generally steeply north-dipping beds that are truncated against sinistral and dextral faults in a strongly faulted and folded area. Again, reference is made to the areas defined by the author (i.e. areas A4 to A6) in order to aid describing the King (1967) map. In area A4 (Fig. 4.3), King (1967) was unable to correlate beds across the foreshore due to the ‘geological complexity’. In contrast, in area A6 (Fig. 4.3), the beds lie to the north of the Wanson North Fault and appear to be relatively undeformed by the sinistral and dextral faults. In between these areas, in area A5 (Fig. 4.3), structures are shown in the King (1967) map and include:

1. A significant sinistral NNE-SSW-striking fault (SS19590145-SS19350138);
2. A chevron anticline with the hinge zone cut by faults (SS19550140-SS19470138);
3. Two complex arrays of NW-SE-striking, E-W-striking, and NE-SW-striking faults.

### **4.1.3 Description of the Sanderson (1979) and Lloyd and Whalley (1986) models**

The Black Rock and Wanson Mouth foreshore successions include alternately ‘upright’ and ‘inclined-to-recumbent’ chevron folds (King, 1967; Freshney et al, 1972; Sanderson, 1979; Anderson & Morris, 2004). Sanderson (1979) and Lloyd and Whalley (1986; 1997) have described the generation of both of these chevron fold types in the Culm Basin and developed geometric models, which are useful for understanding the folds observed in the two foreshore successions. These two models are described and critically assessed here.

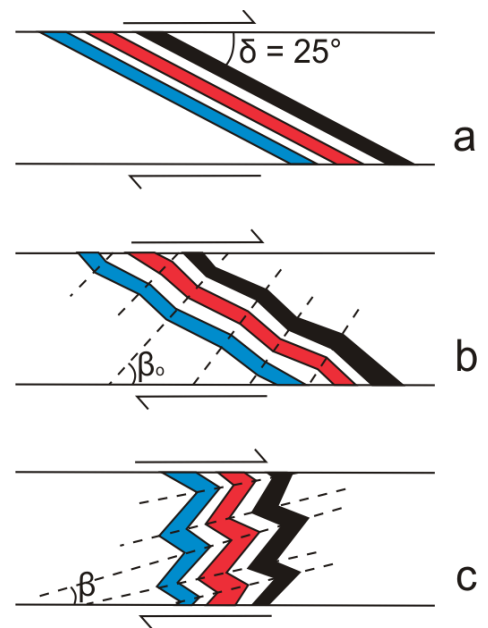
#### **Sanderson (1979) model of chevron fold development**

In order to explain the occurrence of ‘inclined-to-recumbent’ chevron folds, Sanderson (1979) used the Ghosh (1966) experimental models in which shear deformation affected beds that dipped in the same direction as the shear deformation (Fig. 4.4a). In the Sanderson (1979) model, this equates to the originally south-dipping beds of ‘upright’ (chevron) folds. Using the Ghosh (1966) model, the south-dipping beds (dip angle  $\delta$ ) rotated to steeper south-dipping angles and developed ‘inclined-to-recumbent’ chevron folds with north-dipping axial planes ( $\beta_0$ ) (Fig. 4.4b). The interlimb angles (ILAs) of the resulting ‘inclined-to-recumbent’ chevron folds are tighter (30°-40°) than the original ‘upright’ folds (60°-70°). The ‘upright’ chevron folds developed by flexural-slip along bedding planes (Tanner, 1989) until they reached an ILA of approximately 60° (Ramsay, 1974). Accommodation of south-directed shear strain developed the ‘inclined-to-recumbent’ chevron folds (Sanderson, 1979) that tightened the folds via passive

flattening (Ramsay, 1974). The tightening continued until the folded beds ‘locked-up’ (Ramsay, 1967) and formed cleavage parallel to the fold axial planes at dip angle  $\beta$  (Fig. 4.4c).

Sanderson (1979) used the Ghosh (1966) model also for the regional development of the south-directed, ‘inclined-to-recumbent’ chevron folds (Fig. 4.4), predicting and demonstrating that throughout the Culm Basin the south-directed shear deformation caused a regional decrease in both fold interlimb angle (ILA) and axial plane dip (APD) towards the south. However, whilst a regional decrease in ILA and APD is observed from north-to-south across the Culm Basin, the two parameters are too large to fit the Sanderson model between Widemouth and Saltstone Strand (including the Wanson Mouth foreshore) and too low between Higher Longbeak and Widemouth (including the Black Rock foreshore).

Fig. 4.4: Model of chevron fold development by simple shear, based on experiments by Ghosh (1966): (a) Initial geometry with folded beds dipping at  $\delta$ ; (b) Fold initiation with axial planes at  $\beta_0$  to shear zone; and (c) Folds at maximum shortening with axial planes at  $\beta$  to shear zone



In order to explain this anomaly, Sanderson (1979) suggested that “there is both a regional and local correlation between ILA and APD”, whereby the Higher Longbeak to Widemouth section “may represent a zone of low shear strain”, whilst the Widemouth to Saltstone Strand section showed low but increasing shear strain accommodation before “the transition to recumbent folds south of Saltstone Strand”. Sanderson (1979) observed that south of Saltstone Strand ‘inclined-to-recumbent’ chevron folds had lower ILA and APD values and suggested that this occurred because the folds were situated on the steep south-dipping limb of a regional anticlinorium, whilst the ‘upright’ chevron folds are on the shallow north-dipping limb of this structure (see Fig. 2.22).

#### **Lloyd and Whalley (1986) model of chevron fold development**

The Lloyd and Whalley (1986) model is an extension to the Sanderson (1979) model that is designed to explain the effect that south-directed shearing had on the geometries of ‘upright’ chevron folds (see Chapter 2) as well as the occurrence of ‘recumbent’ chevron folds.

In their model, the south-dipping ‘upright’ chevron fold limbs were subject to a compressional regime during south-directed shearing, causing south-directed ‘inclined-to-recumbent’ folds to develop. In contrast, the north-dipping limbs were subject to an extensional regime. The resulting normal faults either exploited the ‘upright’ chevron fold axial surfaces (Model 1; Church Races, SS200043) or the north-dipping limb (Model 2; Lynstone, SS200052; and Saltstone-Millook, SS184002; Fig. 4.5). Where no normal faulting occurred, the original fold hinge is modelled to have either opened (increased ILA; Model 3; Lower Longbeak, SS199034) or tightened (decreased ILA; Model 3; between Bude and Efford, SS200060) (see Chapter 2). Lloyd and Whalley (1986) suggest that during fold tightening, cleavage develops in the shales.

Comparing the two models, the Lloyd and Whalley (1986) model is consistent with the results from the shearing experimental models on already dipping beds by Ghosh (1966) (Fig. 4.4), which was also the basis for the Sanderson (1979) model. Thus, the Lloyd and Whalley (1986) model is in agreement with the Sanderson (1979) model in this regard. This was noted by Anderson and Morris (2004), who recognised that localised south-directed shear deformation caused modification of the initial ‘upright’ chevron geometry, as described by both Sanderson (1979) and Lloyd and Whalley (1986; 1997). Anderson and Morris (2004) also suggested that the primary differences between the models are that:

1. The Sanderson model considered how the initial ‘upright’ fold axial planes and interlimb angles evolved with increasing shear strain to produce ‘inclined-to-recumbent’ folds
2. The Lloyd-Whalley model considered the limbs of initial ‘upright’ chevron folds as movement planes, so producing the different ‘inclined-to-recumbent’ chevron fold types.

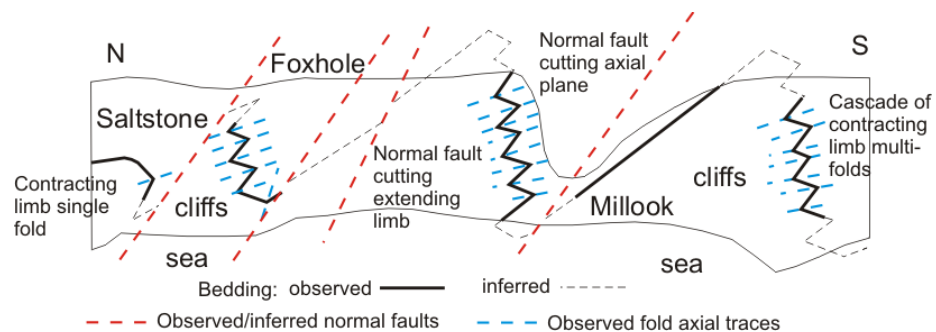


Fig. 4.5: Schematic regional interpretation from Saltstone Strand to south of Millook Haven (SS184002), showing a ‘cascade’ of chevron folds (modified from Lloyd & Whalley, 1997)

The progressive deformation suggested by the models for south-directed shear, has generated at least three over-printing cleavage sets, although these are rarely observed together. One location where this occurs is at Millook (SS185002; Fig. 4.5), but only in tightly-folded shale beds (Lloyd & Chinnery, 2002; see Chapter 2). The three over-printing cleavage sets are:

1. Close to bedding-parallel, related to north-directed thrusting ( $S_1$ );
2. Parallel to ‘upright’ chevron fold axial planes after being restored ( $S_2$ );
3. Parallel to south-directed ‘inclined-to-recumbent’ chevron fold axial planes ( $S_3$ ).

#### 4.1.4 Models for the development of the Widemouth South Fault (WSF)

The Widemouth South Fault (WSF) is a regional structural feature in the Culm Basin where ‘upright’ and south-directed ‘inclined’ chevron folds are juxtaposed (Freshney et al, 1972; Sanderson, 1979). The ‘inclined’ chevron folds are equivalent to the ‘inclined-to-recumbent’ chevron folds of Sanderson (1979). The movement on the WSF caused 300 m of stratigraphy to be missing across it (Freshney et al, 1979; pers. comm., 2010; Fig. 4.2). Structural interpretation of the foreshore successions relies on understanding the deformation accommodated on the WSF, which has been described alternatively as:

1. A ‘late’ Variscan normal fault (Freshney et al, 1972; pers. comm., 2010; Fig. 4.6);
2. An inverted north-directed Variscan thrust (Enfield et al, 1985; Fig. 4.7);
3. A north-directed thrust that was extensionally reactivated as a listric normal fault, which further east led to the development of the Crediton Trough (Durrance, 1985; Fig. 4.8);
4. A Tertiary dextral wrench fault (Williams et al, 1970; Durrance, 1985; Fig. 4.9).

##### **Model 1: ‘Late’ extensional fault model (Freshney et al, 1972; pers. comm., 2010)**

This is the simplest model explaining the WSF (Fig. 4.6) in which the Variscan deformation occurred at different stratigraphic levels. Both the Bude and Crackington formations accommodated progressive ‘upright’ chevron fold deformation and then, south-directed shear deformation. This led to the development of south-directed ‘inclined’ chevron folds on the south-dipping limbs of originally ‘upright’ chevron folds (Ghosh, 1966; Sanderson, 1979; Lloyd & Whalley, 1986; 1997; Fig. 4.4). Following fold development at different stratigraphic and structural levels, the two domains were juxtaposed against each other by ‘late’ normal fault movement along a north-dipping WSF (Fig. 4.6; Freshney et al, 1972).

‘Late’ extensional movement along the WSF is suggested from work on Anisotropy of Magnetic Susceptibility (AMS) by Anderson and Morris (2004). AMS analyses of the folded beds in the ‘upright’ chevron fold adjacent to the WSF (SS19630146) (i.e. ‘upright’ chevron anticline E; see gusset) suggest that a late-stage stretching occurred along the fault. However, Anderson and Morris (2004) could not determine whether the stretching fabrics resulted from normal faulting in the ‘upright’ chevron anticline hinge during south-directed shear deformation (Lloyd & Whalley, 1986), or from ‘late’ post-Variscan extension.

The Freshney et al (1972) model describes normal faults from Wanson Mouth southwards to the Rusey Fault, which trend 245°-280° and dip at 45°-80° to the north. Although the total regional throw of all the normal faults between the WSF and the Rusey Fault is considered to be approximately 300 m, the individual fault throws are less than 3 m. This suggests that the ‘late’ normal faults are small scale and thus, could not produce the 300 m stratigraphic separation between the Bude and Crackington formations across the WSF as shown in the logs by Freshney et al, 1979 (Fig. 4.2).

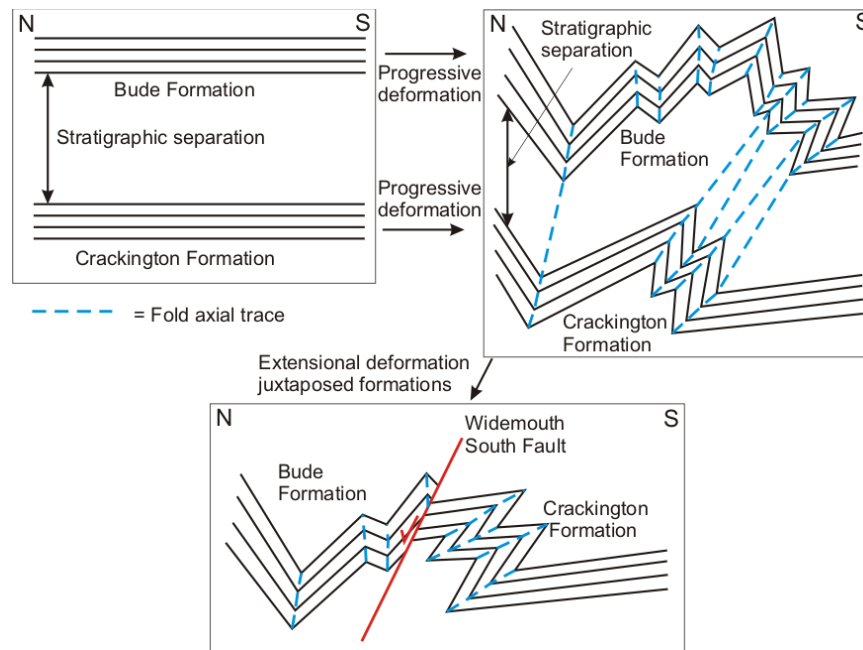


Fig. 4.6: Schematic sketches of the progressive deformation in the Crackington and Bude formations prior to being placed together by the ‘late’ extensional WSF movement

#### **Model 2: Inverted thrust model (Enfield et al, 1985)**

In this model, the Crackington Formation was emplaced onto the Bude Formation along the Wanson Mouth thrust duplex (Fig. 4.7), prior to chevron folding and cutting out at least 300 m of stratigraphy (Fig. 4.2). If a 30°S thrust dip angle is assumed, this suggests that the Wanson Mouth beds have been transported at least 500 m to the north during emplacement. In detail, the thrusts include the Wanson North Fault (WNF), which is viewed as the roof thrust whilst the sub-parallel fault to the north is an ‘imbricate’ (floor) thrust to the WNF (Fig. 4.7). The Wanson Mouth beds have a downward-facing, southwards younging direction and truncate against the thrusts (Fig. 4.7). This suggests that the beds and faults may have been inverted by rotation to steeply north-dipping attitudes. Between the two faults, there appears to be a lateral ‘ramp’ structure. The thrusting may have caused up to 300% of local thickening in the foreshore.

Following emplacement, the formations either side of the WSF experienced the same deformation history. In the model, the thrusting created a “northward verging thrust zone”, which generated ‘upright’ chevron folds. According to the Coward and Smallwood (1984) model, as described by Enfield et al (1985) (see Chapter 2), these ‘upright’ chevron folds were modified by a single rotational deformation from north-directed to being south-directed. The change in tectonic movement direction occurred as the northward propagation rate reduced to less than the slip rate, thereby causing the tectonic movement to switch directions. This change is inferred to have generated the south-directed ‘inclined’ chevron folds, following the Sanderson (1979) model of southward increase in intensity of south-directed shear deformation. The thrusts were folded and attained their steeply north-dipping attitudes on the overturned limbs of these folds, on the scale of the foreshore (Fig. 4.7; Enfield et al, 1985).

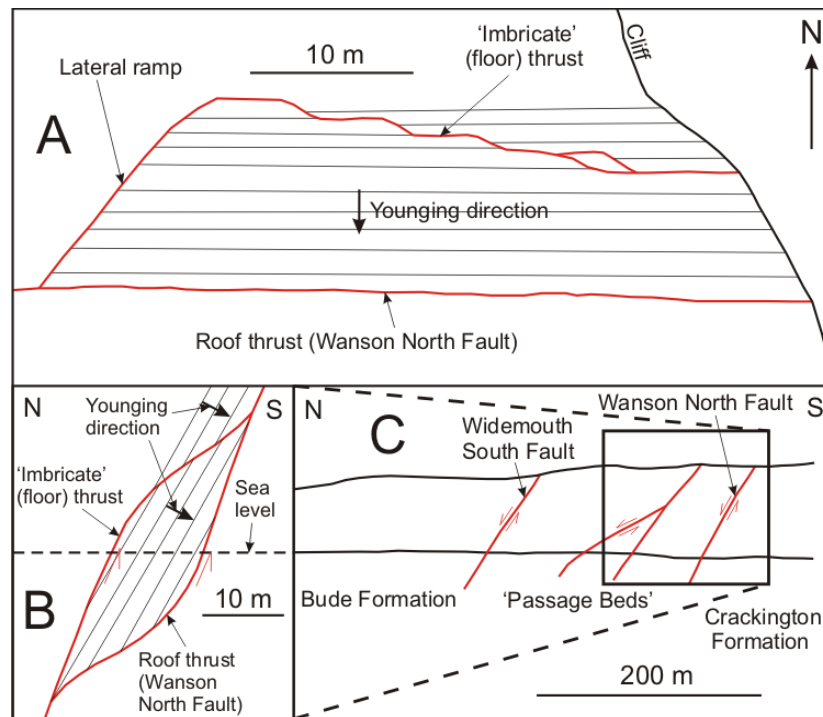


Fig. 4.7: Sketch diagrams from Enfield et al (1985) showing all major faults in the Wanson Mouth foreshore: (a) simplified map of the foreshore showing the Wanson North Fault (roof thrust) and an 'imbricate' thrust in the Wanson Mouth duplex; (b) simplified cross-section of the duplex shown in (a); and (c) cliff section of the Wanson Mouth-Black Rock foreshores

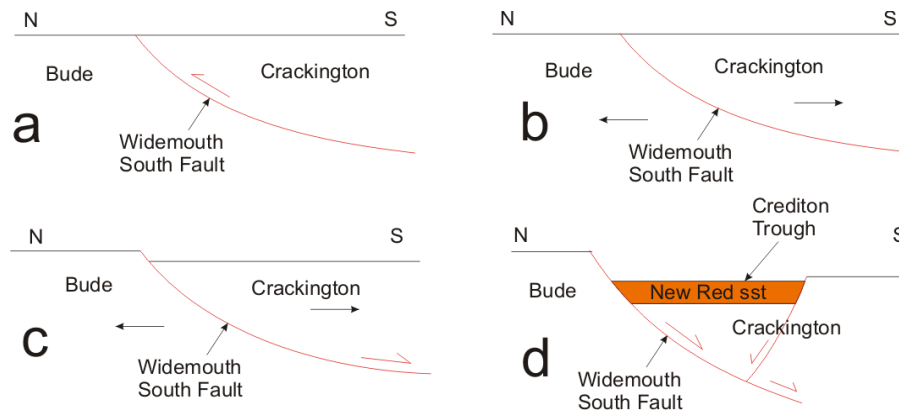


Fig. 4.8: Geological evolution of the Widemouth South Fault in the eastern Culm Basin (modified from Durrance, 1985): (a) initial north-directed thrust, emplacing the Crackington Formation onto the Bude Formation; (b) extensional stresses affect the fault; (c) extensional movement on the reactivated fault; and (d) development of the extensional Crediton Trough

### Model 3: Extensionally reactivated thrust model (Durrance, 1985)

The WSF is a basin-scale fault and can be traced to the east towards the Crediton Trough. In the model, strong seismic reflectors below the Crediton Trough have been interpreted as a south-dipping listric normal fault (Fig. 4.8d) that reactivated along the line of a buried north-directed Variscan thrust (Figs. 4.8b & c). This thrust has been interpreted to have emplaced the Crackington Formation onto the Bude Formation (i.e. an earlier form of the WSF)

(Fig. 4.8a). Durrance (1985) did not consider whether fold deformation had occurred prior to or following the thrust movement, and so the relative timing of thrusting is not known. The normal fault movement occurred during the Permian forming the extensional Crediton Trough (Fig. 4.8d). However, Durrance (1985) does not suggest Variscan chevron folding deformed the thrust. The model was produced to explain the formation of the Crediton Trough as an extensional basin and its New Red sandstone deposition (Fig. 4.8d). The NE-dipping WSF is oriented 127/68NE and juxtaposes the Black Rock and Wanson Mouth foreshore successions, which casts some doubt on the whether the model can be applied in the mapping area.

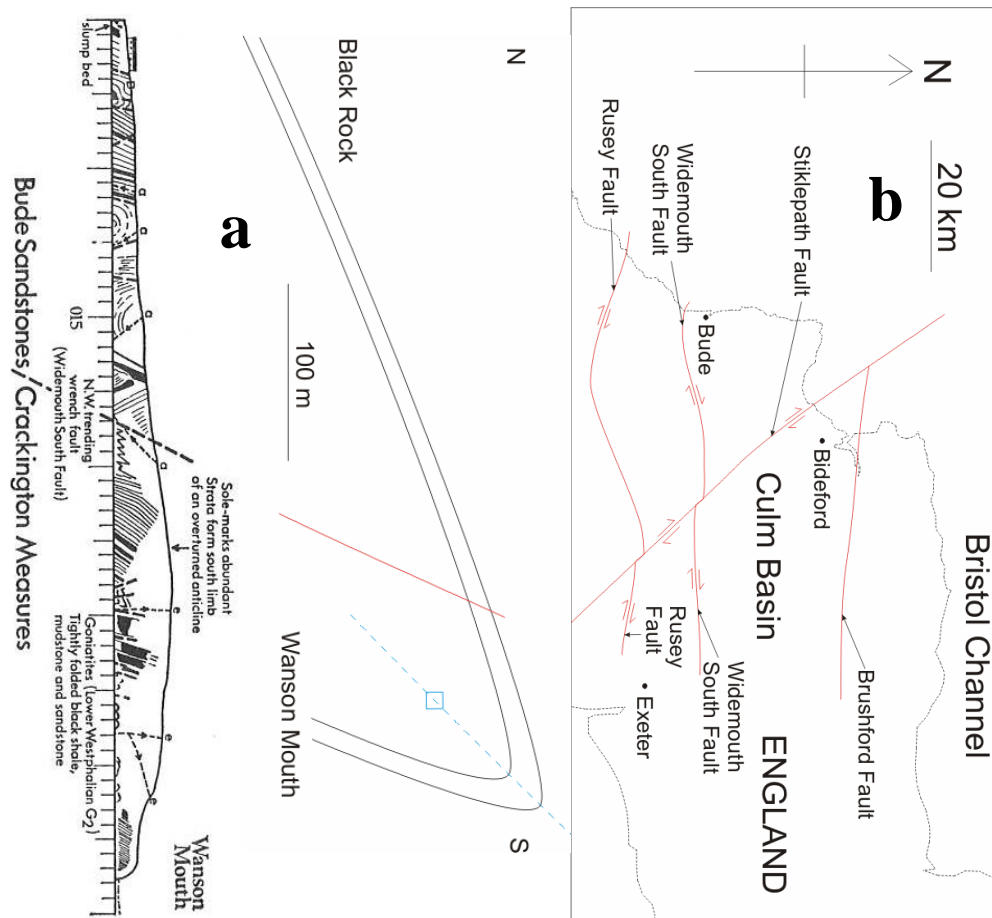


Fig. 4.9: (a) Sketch structural cliff profile above the Black Rock-Wanson Mouth foreshores with schematic fold sketch to show overturned anticline. The WSF is described as a wrench fault but the annotations **a** and **e** are not described by Williams et al (1970) and (b) Sketch diagram of the major 'late' Variscan fault movements in the Culm Basin with the dextral WSF of Freshney et al (1972) as a possible Reidel shear to the dextral Sticklepath Fault of Peacock et al (1998)

#### **Model 4: Dextral wrench fault model (Williams et al, 1970)**

Williams et al (1970) observed that in the immediate area around the WSF there are several "subsidiary fractures and joint patterns in the foreshore", although they do not show the structures in any figure. Whilst the structures were not observed during this mapping project (see gusset) they may exist in the areas of 'geological complexity' on the King (1967) map (Fig.

4.3). However, this model is considered unlikely because strike-slip movement along the WSF could not produce the 300 m of stratigraphic separation between the two foreshore successions. Williams et al (1970) described the WSF as a Tertiary dextral wrench fault (Fig. 4.9a) whilst Durrance (1985) noted that the WSF at the coast may be part of a tear fault system (Fig. 4.9b).

#### **4.1.5 Discussion of the Widemouth South Fault (WSF) models**

The four models outlined above attempted to explain how the juxtaposition of ‘upright’ and ‘inclined’ chevron folded strata across the WSF occurred. Model 4, the purely wrench fault model of Williams et al (1970), appears to be unlikely because it could not produce the 300 m of stratigraphic separation between the two foreshore successions (Freshney et al, 1979; Fig. 4.2). Also, the fractures and joints in the foreshores that would suggest that minor dextral strike-slip reactivation of the WSF occurred (Williams et al, 1970) have not been found. In contrast, the models of Freshney et al (1972), Enfield et al (1985) and Durrance (1985) explain the stratigraphic separation between the foreshore successions. Model 1, the normal fault model of Freshney et al (1972), is also consistent with the ‘late’ extension inferred from the AMS analysis of Anderson and Morris (2004). These models will be considered further in this chapter

## **4.2 Methods**

Sedimentary and structural geology data were gathered during this mapping in order to study the chevron folds, the local faults and folds on the limbs and across the hinges of ‘upright’ chevron folds and the tectonic significance of the Widemouth South Fault (WSF) that separates the Black Rock and Wanson Mouth foreshores.

### **4.2.1 Foreshore mapping**

As part of the mapping work, montages of relatively high-resolution aerial imagery were used from the publicly-available Google Earth™ resource. It is noted that the use of the Google Earth™ resource is now becoming more common in geological mapping (Blenkinsop, 2012). These images are used solely as the base map slips for the detailed map, in order to locate accurately the beds and structures in the foreshores. The geological map (see gusset) is divided between the Black Rock foreshore (SS196017-SS195015), NE of the WSF, and the Wanson Mouth foreshore (SS195015-SS195013), SW of the WSF. Also, the mapping data has been overlain onto a conventional OS map for comparison, whilst the GEM images have been removed in another example of the map in order to provide clarity on the data (see gusset).

Although dipping beds and structural trends can be interpreted directly from the Google Earth™ images, there are limitations to this resource; in particular, it is difficult to discern beds that are sub-horizontal to shallow dipping (i.e. sub-parallel to the plane of view) and in some locations, beds and structures are obscured by sand, boulders and seaweed.

### 4.2.2 Sedimentary logging

Sedimentary logging was undertaken to describe the different facies in each foreshore (see Chapter 3 for methods and data collected), to interpret the depositional environments of both successions and to describe the younging using an inverted 'Y' symbol pointing in the younging direction. The data have also been used to test whether there are strong lateral thickness changes across the foreshores associated with any of the structures. In the Black Rock foreshore, laterally-continuous shale beds, numbered 1-7, were mapped to divide the strata into packages. The data collected in these less detailed sedimentary logs are lithology, bed thickness and grain size. However, as there is a lack of fossils, only lithostratigraphic correlations of shale beds were possible. Where fault deformation had caused the repetition of beds, the duplicated strata have been removed to give the original stratigraphic thickness.

### 4.2.3 Structural data

The field structural data collection consisted of measuring the strike and dip of bedding, cleavage and both normal and thrust fault planes, together with the plunge and azimuth of fold hinge lines and fault plane striations (see gusset). These data sets were plotted onto stereonet in order to analyse the geometries of each deformation structure. To analyse the folds, the fold profile plane is found from the  $\pi$ -girdle line plotted through poles to bedding planes, using the methods of Davis and Reynolds (1996) and Lisle (2004). As cleavage was only observed rarely in tightly folded shale beds, as mentioned by Freshney et al (1979), the fold axial plane orientations have been plotted perpendicular to the profile plane, using fold axis plunge data from well-exposed bedding surfaces. Where angular data (in degrees) are expressed as a mean, this is provided with a calculated circular variance value.

In order to provide a structural overview of both foreshores and estimate the amount of shortening accommodated in the two successions, eight cross-sections have been drawn:

1. Three dip-sections (bearing 010°-190°), cutting across both foreshores sub-parallel to the dip directions of the chevron folded beds (A-A', B-B' & F-F'; see gusset);
2. Four strike-sections (bearing 100°-280°) in the Black Rock foreshore sub-perpendicular to the dip directions of the chevron folded beds (C-C', D-D', E-E' & G-G');
3. One oblique section (bearing 135°-315°) in the Wanson Mouth foreshore sub-perpendicular to two faults that are oriented obliquely to other structures (H-H').

Following the methods of Davis and Reynolds (1996), each cross-section line has been placed where there is good foreshore exposure and surface geological control. The dip section line orientations were chosen to be parallel to the tectonic transport direction (Fossen, 2010). As the foreshores are at sea level, the structural mapping data was transferred onto the cross-sections, with corrections made for apparent dip and then the beds projected without vertical exaggeration above and below the horizontal surface. The laterally-continuous black shale beds

provided key stratigraphic markers in the Black Rock foreshore and allowed the sections to be balanced, as undertaken for example by McQuarrie (2004) in the Zagros Mountains, Iran. This allows a fence diagram to be drawn, showing the 3D structure of the Black Rock foreshore. Unfortunately, no marker beds were found in the Wanson Mouth foreshore (see gusset).

### **Structural restoration**

Balanced restorations assume that cross-sectional area, and where possible line lengths, are preserved, whilst restored sections can have gaps and overlaps due to fault movement (Fossen, 2010). The flexural slip mechanism (see Chapter 2) assumes that line length and bed thickness are conserved. It was applied to the Bude Formation by Ramsay (1974) and Tanner (1989) to model chevron folding along bedding planes. The flexural slip mechanism allows more coherent beds to move past each other along ‘weak’ bedding planes and assumes that there is no compaction or movement out-of-section during restoration (Fossen, 2010). Two examples of cross-sections that have been balanced by preserving line length are in the Rocky Mountains, Alberta, Canada (Dahlstrom, 1969) and the Zagros fold-thrust belt, Iran (McQuarrie, 2004).

To test if the cross-sections balance (see Davis & Reynolds, 1996), the restorations were undertaken separately for each foreshore, to allow for the different structural styles either side of the WSF (Freshney et al, 1972). All the sections, apart from Black Rock strike-section G-G’, were pinned to this fault. In the latter case, the cross-section does not reach the WSF, so was pinned to local thrust stack 6. The restorations are undertaken in steps for practicality and to make the structural relationships clear. Structural restoration also allows the current models of Freshney et al (1972) and Enfield et al (1985) to be tested and to develop new models.

The restoration of each cross-section involves a pragmatic approach in which balancing is undertaken individually for each bed, which can move relative to other beds via the flexural slip mechanism (Ramsay, 1967; Tanner, 1989). The ‘pin points’ are individual to each bed and are placed where a bed is truncated by the WSF or otherwise at the full extent of the outcrop. Thus, balancing was undertaken for each bed and by comparison to the other adjacent restored beds so that bed thicknesses are consistent, as required in the flexural slip model (Tanner, 1989). However, balancing may not be achieved fully where the beds have been folded, or cut by a fault with movement out-of-plane of section (Fossen, 2010). In these cases, ‘space problems’ may occur, with gaps ‘appearing’ through the removal of thrusts and overlaps from normal faults, but do not appear to be significant with respect to the overall structural interpretation.

### **Shortening estimates**

Using the methods of Ramsay (1974), shortening estimates in the Black Rock foreshore were made using line (bed) lengths along laterally-continuous beds. Two methods were used to obtain the original ( $I_0$ ) and final ( $I_1$ ) bed lengths (in metres) in each Black Rock cross-section, both using string laid along the laterally-continuous beds, with the string lengths measured

using a ruler with millimetre spacing (Fossen, 2010). The generally applicable method for estimating a shortening value for each cross-section involves measuring laterally-continuous beds across the whole length of each section (Fig. 4.10b), as undertaken by McQuarrie (2004). Where possible in order to account for ‘out-of-plane’ movement, a minimum shortening value was estimated between ‘pin positions’, again along laterally-continuous shale beds (Fig. 4.10a), also as undertaken by McQuarrie (2004). In the Black Rock foreshore case, the ‘pin positions’ are between pairs of anticlinal hinges from trains of:

1. ‘Upright’ chevron folds trending sub-parallel to Black Rock dip section A-A’;
2. Local structures trending sub-parallel to Black Rock strike-sections C-C’, D-D’ and E-E’.

The mean percentage shortening ( $e$ ) estimated using the original ( $l_0$ ) and final ( $l_1$ ) bed lengths (in metres) is found from the formula (Davis & Reynolds, 1996; Fossen, 2010):

$$e = -100(l_1 - l_0) / l_0 \quad (4.2)$$

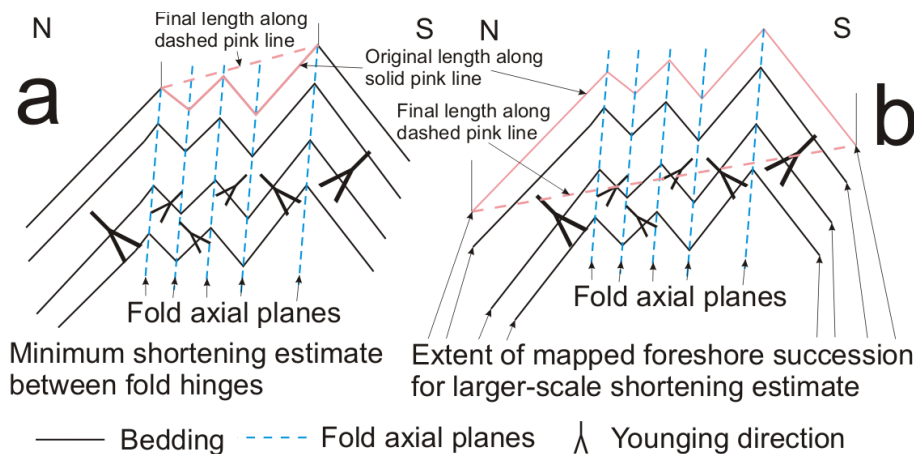


Fig. 4.10: Diagram showing original and final length measurements along pink lines taken for: (a) a minimum shortening estimate between fold hinges; and (b) a larger-scale shortening estimate across the mapped foreshore extent

The shortening accommodated in the Wanson Mouth succession cannot be estimated as accurately as for the Black Rock succession because no marker beds could be correlated across the faults. Instead, for each laterally continuous bed, line lengths have been measured between faults using the string method, in order to provide a range of shortening estimates for each cross-section (Fig. 4.10b). The shortening estimates ( $e$ ) for each cross-section in both foreshores are given as both a range and as a mean, together with the standard deviation.

#### Determination of ‘early’ structures

The timing of the local decametric scale structures in the Black Rock foreshore is assessed to establish whether they occurred prior to chevron folding and also whether this was at or near the palaeo-surface. Using the Mapeo and Andrews (1991) methods developed in the

Bude Formation, local structures are considered as ‘early’ structures where they have been deformed by ‘upright’ chevron folding (i.e. a refolded structure).

Some local structures are tilted and lie on the ‘upright’ chevron fold limbs. The criteria to demonstrate whether these are ‘early’ structures are developed from the seismic section interpretations in the Po Delta, Italy, by Zoetemeijer et al (1992) and Niger Delta, Nigeria, by Corredor et al (2005) and also outcrop studies in the Pliocene Mount Corvo beds, SW Sicily, Italy, by Nigro and Renda (2004) (see Chapter 2). The criteria are as follows (Fig. 4.11):

1. ‘Undeformed’ beds both overlying and underlying the locally deformed strata;
2. *Toplap truncations* of local structures and deformed beds by either overlying ‘undeformed’ beds or deformed beds in another local stacked structure;
3. Variable thicknesses of ‘undeformed’ beds overlying the local structures (i.e. *growth strata*)

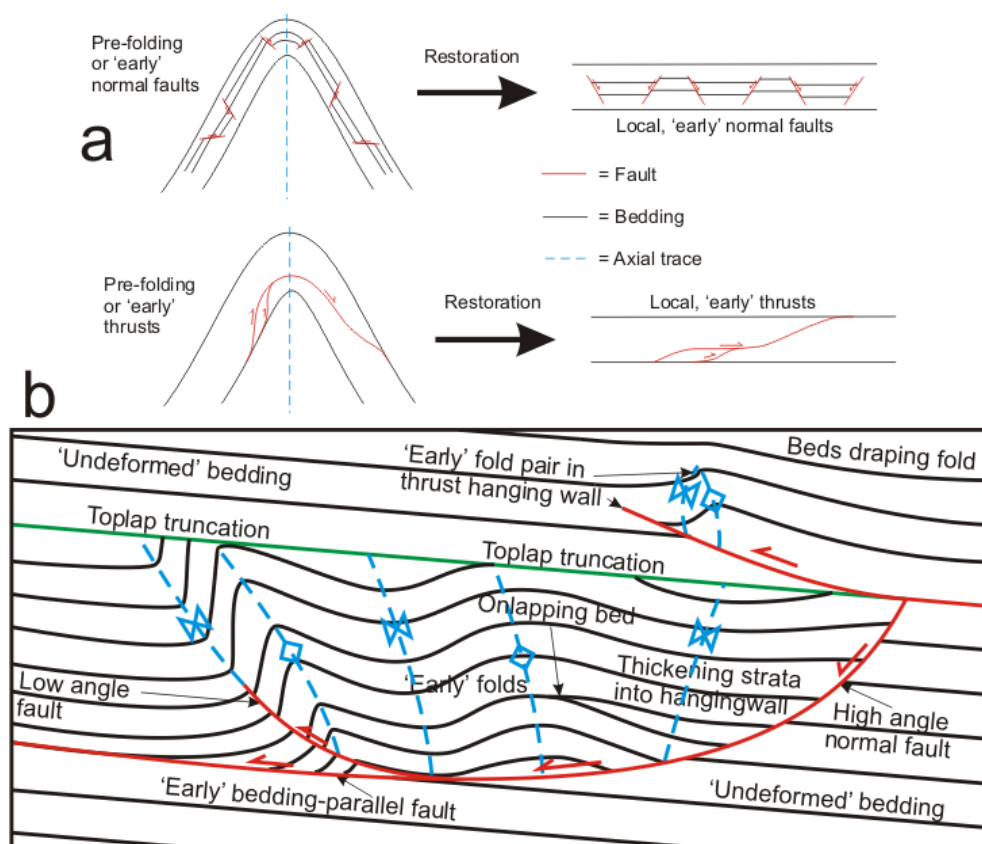


Fig. 4.11: Schematic diagrams of: (a) folded and restored local normal faults and thrusts, which are used to define a local structure as ‘early’ (modified from Mapeo & Andrews, 1991); and (b) criteria to define ‘early’ local structures with associated growth strata, with structures incising ‘undeformed’ underlying beds and being tolap truncated by overlying ‘undeformed’ beds (Zoetemeijer et al, 1992; Nigro & Renda, 2004; Corredor et al, 2005)

### 4.3 Sedimentary evolution of the Black Rock-Wanson Mouth foreshores

The sedimentary structures and ichnofabrics observed in the Black Rock foreshore succession and elsewhere in the Bude Formation are described in Chapter 3. The lower Bude

Formation beds in the Black Rock foreshore include a succession of variably-continuous sandstone, siltstone and shale beds all with grain sizes no coarser than fine-grained sand grade (Fig. 4.12; see Fig. 3.1c). Some sandstone and siltstone beds pinch-out over distances of tens to hundreds of metres, whilst the shale beds (numbered 1-7b) are mainly continuous. In addition, one channel structure has been observed (SS19580153), which has a shale bed basal drape, a massively-bedded sandstone infill and an overlying clay-draped, trough cross-stratified bed (Fig. 4.12; see Chapter 3). The sedimentary structures and ichnofabrics observed in the Black Rock foreshore and elsewhere in the Bude Formation are described in Chapter 3.

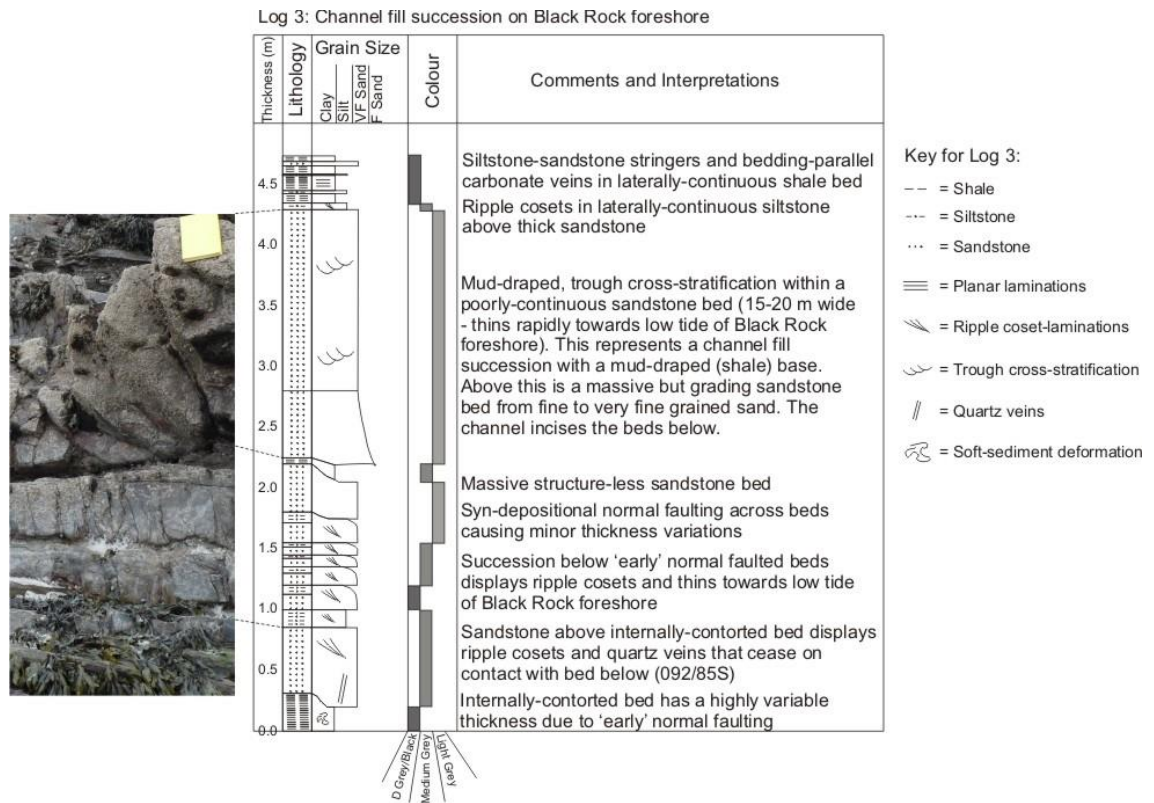


Fig. 4.12: A sedimentary log taken in the Black Rock foreshore (SS19580153), which represents an apparently uncommon channel structure within the Bude Formation outcrops

The initial aim of the sedimentary analysis and detailed mapping in the Black Rock foreshore was to assess the stratigraphic thickness of the succession compared to the whole Bude Formation (Freshney et al, 1979) and whether there are thickness changes in the foreshore. To undertake this assessment, five sedimentary logs have been taken with bed thickness and lithology measurements collected (Fig. 4.13). The sedimentary record of log E shows that at least 120 m of Bude Formation strata are exposed in the foreshore, which according to Freshney et al (1979), is about a tenth of the Bude Formation stratigraphic thickness (Fig. 4.2).

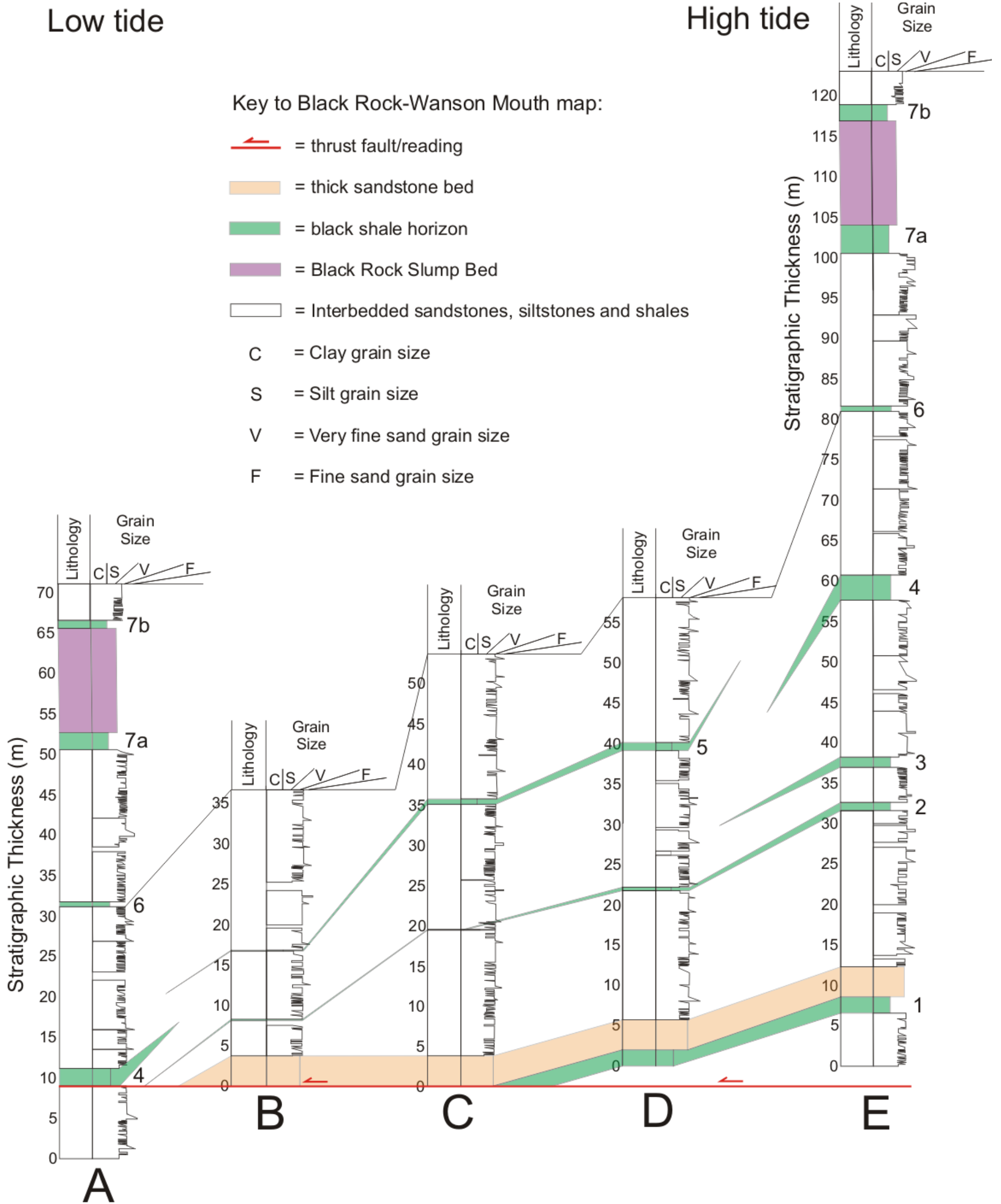


Fig. 4.13: Correlated simplified sedimentary logs across local structures in the Black Rock foreshore. The correlated logs show the variation in deposition thicknesses between the thick sandstone bed and laterally-continuous shale bed 6, which are up to 36 m different between logs B and E. Sedimentary log location lines are drawn on the map in yellow (see gusset & Fig. 4.15)

In order to test for lateral thickness changes, the five sedimentary logs were correlated using strongly-continuous shale beds (Fig. 4.13). Comparison of logs B and E (Figs. 4.13b & e) shows that there is a 36 m maximum stratigraphic thickness difference between shale beds 1 and 6. In the 36 m of additional strata, shale beds 2-5 either onlap onto, or have been truncated by, other beds (Fig. 4.13; see gusset). It is possible that there is further local fault repetition of the beds, although these faults may be bedding-parallel and thus difficult to locate. Unfortunately, without biostratigraphic control, lithostratigraphic correlation of the shale beds has been used.

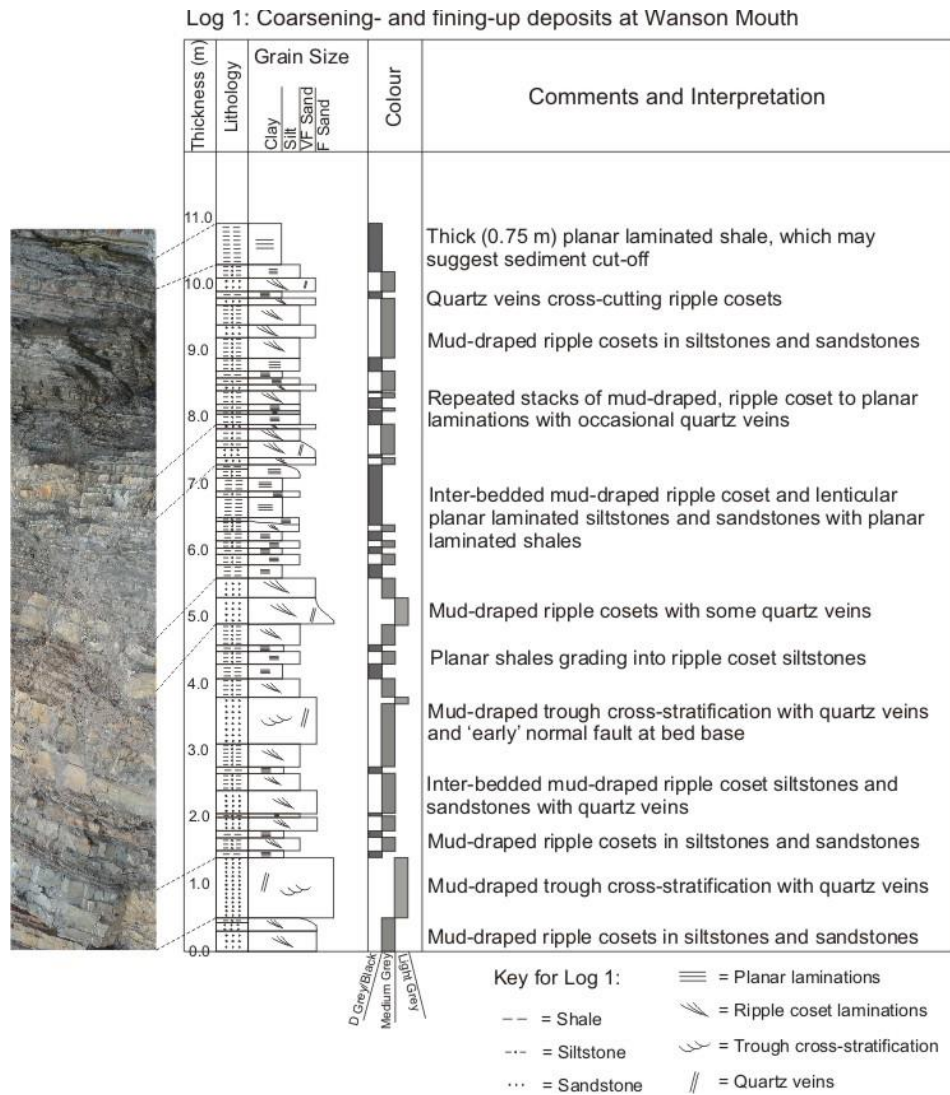


Fig. 4.14: Sedimentary log from the cliffs at Wanson Mouth in the upper Crackington Formation (SS19550136), showing thin beds with similar facies to parts of the Bude Formation

The stratigraphic thickness variations occur around local structures, which lie between shale beds 1 and 6 and have been logged on the limbs and up to the hinges of the 'upright' chevron folds in the Black Rock foreshore (Fig. 4.13 & see gusset). The additional strata are especially noticeable between logs D and E where shale beds 3-5 pinch-out (Figs. 4.13d & e). During this local structural development, it is suggested that accommodation space was created on the limb of fold pair 6 and the 'growth' or additional strata accumulated here. In contrast, in

the stratigraphically-higher sedimentary stack between shale beds 6 and 7a, there is neither fault repetition nor local structures. The bedding stack has the same stratigraphic thickness across the foreshore as shown in logs A and E (Figs. 4.13a & e). The 12 m thick Black Rock Slump Bed was laid down after deposition of shale bed 7a and prior to shale bed 7b. The slump bed is described in greater detail in Chapter 5.

### 4.3.1 Crackington Formation in the Wanson Mouth foreshore

The upper Crackington Formation beds in the Wanson Mouth foreshore are stratigraphically-below the Bude Formation in the Black Rock foreshore and consist of a sub-vertical to overturned succession of folded sandstone, siltstone and shale beds, some of which may pinch-out over distances of tens to hundreds of metres (Freshney, pers. comm., 2010). They have been interpreted as turbidite deposits within a deep marine fan (Melvin, 1986).

As with the Bude Formation beds, grain sizes are no coarser than fine-grained sand and there are abundant sole marks on bed bases (Williams et al, 1970; Melvin, 1986; see Chapter 3). In order to interpret the stacking patterns and facies present in the Wanson Mouth foreshore, 11 m of section was logged (SS19550136; Fig. 4.14; see Fig. 3.1c), which consisted of mud-draped ripple coset laminated sandstones and siltstones. Occasional trough cross-laminated sandstones were found in the bottom 5.5 m of the logged section, whilst in the top 5.5 m, there are no trough cross-laminated sandstones and few ripple laminated sandstones and siltstones (Fig. 4.14; see Chapter 3). Instead, the stack is dominated by planar laminated siltstones with some shales, which is indicative of lower energy depositional environments (Collinson et al, 2006).

## 4.4 Map description

As discussed previously, the lower Bude Formation of the Black Rock foreshore and the upper Crackington Formation of the Wanson Mouth foreshore are separated by the Widemouth South Fault (WSF; oriented: 127/68NE; 132/65NE; 134/67NE), which truncates all structures and beds in both foreshores (King, 1967; Freshney et al, 1972; pers. comm., 2010; Fig. 4.3; see gusset). The stratigraphic separation between the two foreshore successions is 300 m (Fig. 4.2; Freshney et al, 1979). This is likely to be the vertical displacement accommodated by this fault and would explain the juxtaposition of apparently different structural sections. The WSF may have been part of a 'late' normal fault that cuts all the structures (Freshney et al., 1972; Fig. 4.6); or an inverted thrust duplex (Enfield et al, 1985; Fig. 4.7); or a north-directed thrust that has been reactivated by 'late' Variscan extension (Durrance, 1985; Fig. 4.8).

Approximately 125000 m<sup>2</sup> of the two foreshores were mapped and divided into six areas (Fig. 4.15; see gusset); three each for the Black Rock foreshore (areas A1 to A3) and Wanson Mouth foreshore (areas A4 to A6) that match the areas described in the King (1967) map (Fig. 4.3). Structural measurements were taken of the beds, folds and faults. To understand the geological evolution of the two foreshores, five sedimentary logs were taken (yellow lines

on map in gusset) and eight cross-sections were drawn (orange lines on map in gusset). The cross-sections are described in Sections 4.5 and 4.6 after the map description of each foreshore.

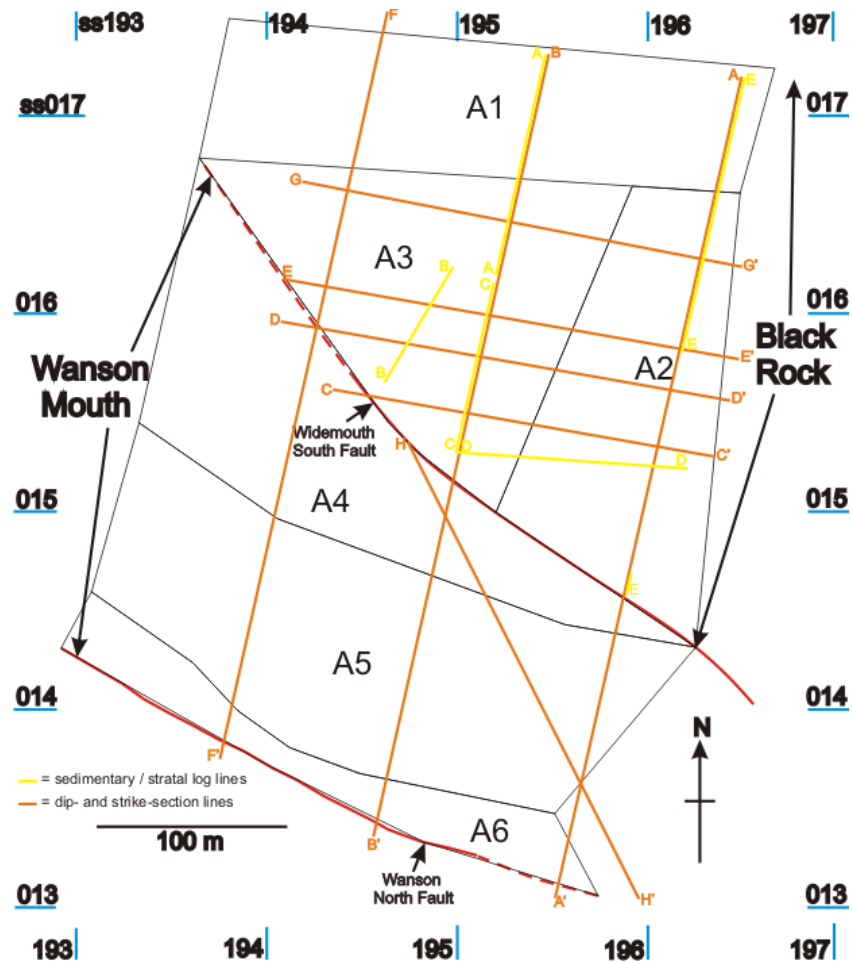


Fig. 4.15: Simplified map of the locations of areas (A1-A6) in the Black Rock-Wanson Mouth foreshores as well as sedimentary log (yellow) and cross-section (orange) lines (also see gusset)

#### 4.4.1 Map description of the Black Rock foreshore

The Black Rock foreshore lies in the southern-most outcrops of the Bude Formation (see gusset) with the mapped part of the foreshore covering an area of approximately 50400 m<sup>2</sup>. Shale beds numbered 1 to 7b have been mapped across this foreshore. Other important beds include a thick basal sandstone bed immediately above shale bed 1 and the Black Rock Slump Bed that was deposited after shale bed 7a and prior to shale bed 7b. All these beds provide constraints on the thicknesses of the stratigraphic packages and the structural geometries.

The foreshore was divided into three areas (areas A1 to A3) distinguished by their differing type and degree of structural complexity. In the northern part of the foreshore in area A1 (Fig. 4.15; see gusset), there are steeply north-dipping beds with two laterally-continuous shales beds (6 & 7a). This includes periclinal fold pair 7 highlighted by the folding of shale bed 5 with E-W-oriented axes that are refolded by ‘upright’ chevron anticline A (SS19610166-SS19440165). In the south-eastern foreshore in area A2 (Fig. 4.15; see gusset), a train of five

‘upright’ chevron folds (three anticlines and two synclines) occurs, which have E-W-oriented axes that plunge to the NNW (see gusset).

In the central and western foreshore, in area A3 (Fig. 4.15; see gusset), a complex set of local fault and fold structures occur with generally N-S-oriented axes. These local structures lie between shale beds 1 and 6 (see gusset). They consist of a similar set of local faults and folds lying on the southern limb of ‘upright’ chevron anticline A around SS195015, together with thrust stacked beds on its northern limb around SS195016. Other structures include a set of NNE-SSW-striking and NW-SE-striking faults (SS19570158-SS19510164) that cut the thick basal sandstone bed across the ‘upright’ chevron anticline A axis. There is also no ‘upright’ chevron fold train in area A3 (Fig. 4.15; see gusset), but the WNW-ESE-trending ‘upright’ chevron anticline A occurs across the foreshore (SS19650156-SS19390172; see gusset).

### **Local structures**

The local decametric-scale folds and faults observed in area A3 (Fig. 4.15; see gusset) have not been described previously in the literature for the Black Rock foreshore. However, they are significant features of the Variscan geological evolution in the Culm Basin (Enfield et al, 1985; Mapeo & Andrews, 1991). Some local structures in the foreshore are categorised as ‘early’ because they have been deformed across the hinge zone of ‘upright’ chevron anticline A, in areas A2 and A3 (Fig. 4.15; see gusset), following Mapeo and Andrews (1991).

Other local structures can be categorised as ‘early’ following the convention of Zoetemeijer et al (1992), Nigro and Renda (2004) and Corredor et al (2005). This includes ‘undeformed’ beds overlying the local structures, deformed beds in the local structures being top-lap truncated by ‘undeformed’ or locally-deformed beds and variable stratal thicknesses between laterally-continuous shale beds in the five correlated sedimentary logs (Fig. 4.13).

The five sedimentary logs across the foreshore show that there is 36 m of additional strata between shale beds 2 and 5 in log E (Fig. 4.13e) compared to log B (Fig. 4.13). Log E also shows that shale beds 3 and 4 pinch out on the north-dipping limb of ‘upright’ chevron anticline A. Shale bed 2 is repeated across areas A2 and A3 (Fig. 4.15; see gusset) and thus, it is possible that further ‘early’ fault repetition of beds may have occurred but cannot be proven.

### **Fold pair 7 on the broken limb of the northern anticline (Freshney et al, 1972)**

There is the periclinal fold pair 7 (SS19610166-SS19440165) that is a significant structure in the Black Rock succession and which has been described as parasitic en-echelon periclinal folds on the “broken limb of the northern anticline” by Freshney et al (1972). In this work, fold pair 7 was remapped to determine whether it is related to the chevron folding or has been refolded by the ‘upright’ chevron folds. From the mapping, it was found that the fold pair has been refolded by ‘upright’ chevron anticline A at SS19450167 (see gusset). The fold axes merge on the north-dipping limb of ‘upright’ chevron anticline A between dip-sections A-A’ and B-B’

at SS19610166 and also, on its south-dipping limb at SS19440165. Following the convention of Mapeo and Andrews (1991), this suggests that fold pair 7 is an ‘early’ structure that formed in the Black Rock foreshore succession prior to ‘upright’ chevron folding, which contradicts the Freshney et al (1972) model. This may also suggest that there is an unrecognised bedding-parallel thrust that underlies fold pair 7, which causes repetition of the Black Rock beds.

#### ‘Upright’ chevron fold deformation

The ‘upright’ chevron fold train in the eastern Black Rock foreshore in area A2 (Fig. 4.15; see gusset) contains three anticlines and two synclines. The axial plane of ‘upright’ chevron anticline E has been cut by the WSF at SS19590146 (see gusset). The structural data for the ‘upright’ chevron folds are given in Table 4.1. There are strong similarities in the geometries of the folds, with their profile planes having a generally north-south axis, sub-vertical axial planes and tight interlimb angles between 50°-60°.

| Fold name                     | Profile plane | Axial plane | Northern limb bedding | Southern limb bedding | Interlimb angle (°) |
|-------------------------------|---------------|-------------|-----------------------|-----------------------|---------------------|
| ‘Upright’ chevron anticline A | 002/85W       | 093/89S     | 103/76N               | 104/51S               | 53                  |
| ‘Upright’ chevron syncline B  | 013/87E       | 102/83S     | 104/51S               | 100/72N               | 57                  |
| ‘Upright’ chevron anticline C | 005/85W       | 092/70N     | 100/72N               | 125/37SW              | 71                  |
| ‘Upright’ chevron syncline D  | 178/65E       | 103/71N     | 125/37SW              | 084/72N               | 71                  |
| ‘Upright’ chevron anticline E | 001/85E       | 088/84N     | 084/72N               | 094/57S               | 51                  |

Table 4.1: Table of ‘upright’ chevron fold geometries from the Black Rock foreshore

#### ‘Late’ sub-vertical faults

In the central Black Rock foreshore (SS19550160) in area A3 (Fig. 4.15; see gusset), there is a set of local, sub-vertical, dextral faults that cross-cut the ‘upright’ chevron anticline A. The first fault to form, termed ‘late’ fault  $\beta$ , is NNE-SSW-striking (SS19550159) and was cut subsequently by a NW-SE-striking fault  $\alpha$  (SS19530160). Offsets on the basal sandstone bed suggest that fault  $\alpha$  has accommodated up to 20 m of horizontal displacement and where it cuts fault  $\beta$ , 5 m of horizontal displacement is accommodated (see gusset). As there are no overlying undeformed deposits, it is difficult to establish the age of the faulting. Also, the fault planes have been strongly eroded, so no structural measurements could be taken. Similar faulting has been observed across the Culm Basin, which may have resulted from Variscan dextral faulting (Peacock et al, 1998) and / or Tertiary dextral wrench faulting (Williams et al, 1970; Fig. 4.9).

#### 4.4.2 Map description of the Wanson Mouth foreshore

The Wanson Mouth foreshore lies within the faulted boundary between the Crackington and Bude formations, south of the WSF (Freshney et al, 1972; Enfield et al, 1985; see gusset), with the mapped part covering an area of approximately 74200 m<sup>2</sup>. The deposits are generally

steeply north-dipping and have been deformed by both high-angle north-dipping faults and south-directed ‘inclined’ chevron folds (Freshney et al, 1972; Enfield et al, 1985). Although a shale bed contains early Westphalian goniatites (Williams et al, 1970), it has proved difficult to correlate beds within this foreshore.

There are three areas within the foreshore that have different types and degrees of structural complexity. In the northern part of the foreshore, there is a steeply north-dipping set of stacked beds to the north of an E-W-striking fault, in area A4 (Fig. 4.15). In the central foreshore, in area A5 (Fig. 4.15), there is a complex set of fault and fold structures. The structures include a south-directed ‘inclined’ chevron fold pair and a steeply NNW-dipping fault that ramps through the strata. The ‘inclined’ chevron fold pair is equivalent to the ‘inclined-to-recumbent’ chevron folds of Sanderson (1979). In addition, near the cliffs, there is a 50 m long NE-SW-striking fault zone with significant fault damage in its centre (see gusset). In the southern foreshore in area A6 (Fig. 4.15), between the Wanson North Fault (WNF) and the E-W-striking fault A immediately north the WNF, the beds are steeply north-dipping and truncate against the faults, as described by Enfield et al (1985) (see Fig. 4.7).

### **South-directed, ‘inclined’ chevron fold deformation**

The Wanson Mouth foreshore contains a south-directed, ‘inclined’ chevron fold pair in area A5 (Fig. 4.15; see gusset), with overturned steep north-dipping beds on the long limbs of the folds (Enfield et al, 1985) and which have been interpreted to result from south-directed shear strain accommodation (Sanderson, 1979). Alternatively, the ‘inclined’ chevron fold pair may be ‘z-folds’ on the limb of a larger-scale fold. A stereonet shows the orientations of the ‘inclined’ chevron anticline profile plane as 017/74E, its fold axial plane as 085/40N (Fig. 4.16a) and its interlimb angle as 46° (Fig. 4.16a).

### **Oblique faults**

Cross-cutting the Wanson Mouth foreshore, in area A5 (Fig. 4.15), is a steeply NNW-dipping fault (oriented: 071/74N; 065/75NW; SS19590145-SS19400140; Fig. 4.16b) that strikes sub-parallel to the ‘inclined’ chevron fold pair axes (Enfield et al, 1985; see gusset). The oblique fault dips steeply to the NW and cut through the overturned steeply north-dipping strata, causing bed truncation. Where the oblique fault changed its strike orientation, decametric-scale splay faults have cross-cut and deformed the beds, causing periclinal fold pairs to develop (Fig. 4.17). This suggests that the oblique fault occurred after ‘inclined’ chevron folding and is a high-angle thrust or reverse fault that developed fault-propagation folds (see Fossen, 2010). Enfield et al (1985) describes the oblique fault as a thrust with a “southerly sense of over-thrusting” that produces “folds with a southerly vergence” (i.e. the periclinal fold pair in Fig. 4.17). Although these folds are described in the Wanson Mouth foreshore, further investigation is required to assess whether similar folds occur elsewhere in the Culm Basin.

A stereonet is provided showing the orientations of the decametric-scale synform in one of the fault-propagation fold pairs at SS19400142, with a profile plane oriented 013/68E and axial plane oriented 105/88S (Fig. 4.16c). The diagram shows the fault-fold relationship (Fig. 4.17) with the oblique fault and a splay fault together with the synform described in the stereonet in Fig. 4.16c in area A5 (Fig. 4.15; see gusset).

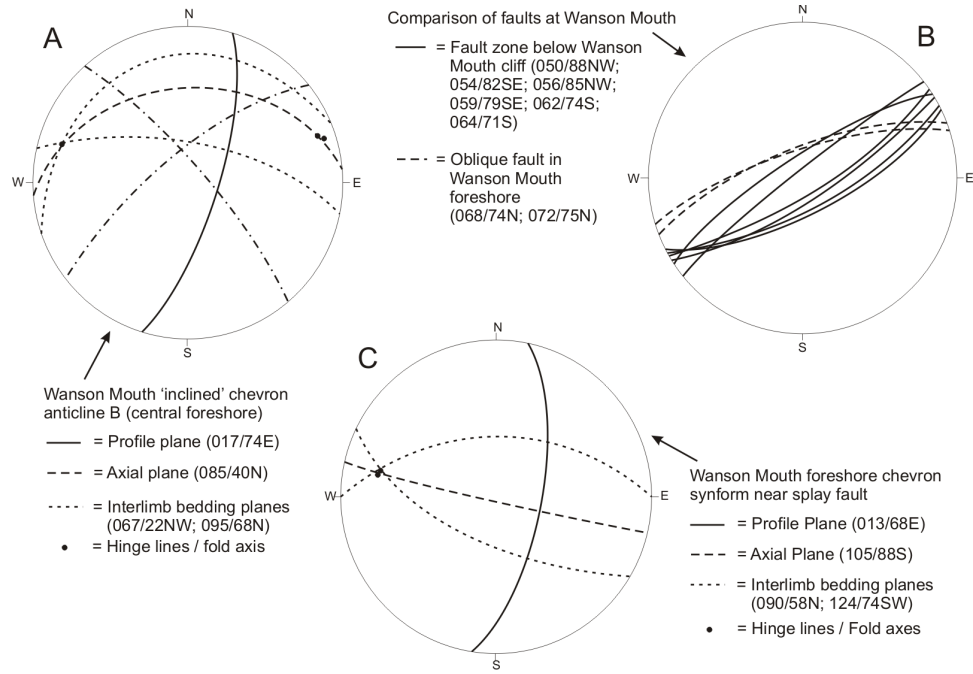


Fig. 4.16: Stereonets with a southern hemisphere projection for the Wanson Mouth foreshore, with data from the: (a) 'Inclined' chevron anticline in the central foreshore (SS19440138); (b) Steep north-dipping faults cutting the foreshore; and (c) Periclinal synform associated with a splay fault emerging from the oblique fault (SS19400142) (see Fig. 4.17)

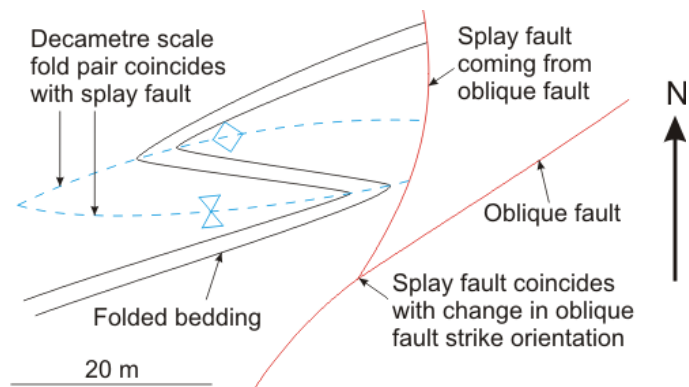


Fig. 4.17: Schematic map showing the relationship between the oblique fault, a splay fault and a minor fold pair from an example in the Wanson Mouth foreshore at SS19420141

In area A5 (Fig. 4.15), an oblique fault zone occurs below the cliff (SS19570141-SS19540138; see gusset) and is oriented: 050/88NW; 054/82SE; 056/85NW; 059/79SE; 062/74SE; 064/71SE (Fig. 4.16b). The fault zone length is unknown, as its NE extension is

obscured by boulders. Also, the amount of horizontal offset accommodated by the fault zone cannot be estimated as bed correlation across it is impossible. On the King (1967) map (Fig. 4.3), the fault zone was interpreted as accommodating sinistral movement, which is consistent with anti-clockwise block rotations in the zone. Sinistral movement suggests that the fault zone developed at a different time to the steeply NNW-dipping fault. As there are no overlying 'undeformed' deposits, the timing is unknown but the movement may have resulted from either 'late' sinistral transtension (Freshney et al, 1972; Gayer & Cornford, 1992).

#### **'Late' cross-cutting faults**

The Wanson Mouth foreshore consists of folds in areas A4, A5 and A6 (Fig. 4.15; see gusset) that are cross-cut by generally E-W-striking, steeply north-dipping faults (Williams et al, 1970; Freshney et al, 1972). Four north-dipping faults have been identified in the foreshore with two of them, including the Wanson North Fault, offsetting all previous structures:

1. Wanson North Fault (WNF; SS19570131-SS19320142; oriented: 107/81N; 115/82N) is the bounding fault between the upper Crackington Formation at Wanson Mouth and middle Crackington Formation to the south (Freshney, pers. comm., 2010);
2. An E-W-striking fault, defined here as fault A, just to the north of the WNF (SS19550135-SS19340146; oriented: 095/56N; 108/63N), as described by Enfield et al (1985) and shown in Fig. 4.7, may have dextrally-offset the beds and structures by approximately 50 m;
3. An E-W-striking fault, here defined as fault B, offset by the steeply NNW-dipping oblique fault at SS19530143 (offset fault is oriented: 093/47N; 094/64N; 113/48N);
4. An E-W-striking fault, here defined as fault C, south of the WSF that is interpreted as being located present day in a sand-filled gully (SS19400150-SS19570145) to account for changes in bedding orientation, but as measurements could not be taken of this fault, it is not known if it is extensional, strike-slip or offset by the oblique fault.

Measurements taken of the E-W-striking faults indicate that most have only small lateral changes in orientation (see gusset). Fault A may have also accommodated 50 m of dextral offset across the 'inclined' chevron fold pair axes (SS19440137-SS19380141). This movement may have occurred during 'late' Variscan normal faulting (Freshney et al, 1972) and / or Tertiary wrench movement (Williams et al, 1970; Fig. 4.9), but is not proven.

#### **4.5 Structural evolution of the Black Rock foreshore**

The Black Rock foreshore lies within the Bude Formation immediately to the north of the Widemouth South Fault (WSF; oriented: 127/68NE; 132/65NE) and contains a series of over-printing faults and folds that are described in this section using three dip sections and four strike sections. In each cross-section, the beds have been projected up to 60 m above and below the foreshore outcrop, which sits at sea level. From the sedimentary logs taken across the Black

Rock foreshore, all beds are the right-way up (Figs. 4.12 & 4.13). To compare the dip and strike sections, individual descriptions are provided of the location, dominant structural features, local structures, determination of whether the local structures are ‘early’ and a sequential set of structural restorations. The restorations are undertaken in steps for practicality and to make the structural relationships clear. Also, in the cross-section descriptions, a letter, number or symbol is given to distinguish the structures and has no intended relationship to structural timing. This remains consistent across each cross-section and restored cross-section.

The three dip sections A-A’, B-B’ and F-F’ (oriented 010°-190°; see gusset & Fig. 4.15 for locations) are sub-perpendicular to the ‘upright’ chevron fold profile planes and are bounded to the south by the Widemouth South Fault (WSF; oriented: 127/68NE; 132/65NE) and to the north by the beds that sit stratigraphically above the Black Rock Slump Bed. The four strike sections C-C’, D-D’, E-E’ and G-G’ (oriented 280°-100°; see gusset & Fig. 4.15 for locations) are sub-parallel to the ‘upright’ chevron fold profile planes and are bounded to the west by the Widemouth South Fault (WSF) and to the east by beach deposits. No strike-section continues across the WSF into the Crackington Formation beds to the west, which are largely below the low tide mark and hence not exposed.

As no beds and structures traverse the WSF, the continuation of each dip section to the south into the Crackington Formation (Wanson Mouth foreshore) is described separately (see Section 4.6), whilst discussion of the structural significance of the WSF is left until sections 4.6 and 4.7. Freshney et al (1972) suggested that the movement on the WSF related to ‘late’ normal faulting. Alternatively, Enfield et al (1985) suggested that the WSF is an inverted north-directed thrust that occurs on the overturned limb of an ‘inclined’ chevron fold syncline. One of the purposes of studying these two foreshores is to gain an improved understanding of the structural significance of the WSF in the Culm Basin and hence, which explanation is the more likely.

To establish the structural evolution of each foreshore, observations were made of the stacked and cross-cutting local faults and folds in the Black Rock foreshore. Some of the structures that are deformed around the ‘upright’ chevron fold hinges are truncated by overlying beds and other local cross-cutting structures and also, lie below the ‘undeformed’ beds. Where this is demonstrated, they can be termed “local ‘early’ structures”. Similar structures have been observed elsewhere in the Bude Formation by Mapeo and Andrews (1991), who described them as ‘syn-sedimentary’ and as refolded around ‘upright’ chevron fold hinges. Further criteria to demonstrate that some local structures are ‘early’ were developed from Zoetemeijer et al (1992), Nigro and Renda (2004) and Corredor et al (2005) (Fig. 4.11).

#### **4.5.1 Black Rock Dip-section A-A’**

The 250 m long Black Rock dip section A-A’ is oriented 010°-190° (SS19650173-SS19590146; Fig. 4.18; see gusset & Fig. 4.15 for location) and lies across this succession in areas A1 and A2 (Fig. 4.15). It includes a right way-up succession of Bude Formation beds up

to 120 m thick (see sedimentary log E; Fig. 4.13e), including eight recognisable shale beds, a 5 m thick sandstone bed above shale bed 1 and the 12 m thick Black Rock Slump Bed deposited between shale beds 7a and 7b (Fig. 4.18). The five shale beds sitting between the slump bed and the thick sandstone bed are of variable lateral-continuity. Shale beds 3 and 4 are only identified in the foreshore around the area of dip section A-A' and onlap the beds stratigraphically above shale bed 2. Shale beds 2 and 6 are laterally continuous across the foreshore, whilst shale bed 5 is in the projection above the foreshore, onlapping a bed above a folded fault (fault 2; Fig. 4.18); but is observed elsewhere in outcrop (see gusset) and in the sedimentary logs (Fig. 4.13).

### **'Upright' chevron folds**

The dominant structures shown in dip section A-A' are five folds (three anticlines and two synclines) in an 'upright' chevron fold train observed in profile (Fig. 4.18a). The younging directions suggest that the beds become younger towards the synclinal hinges and thus, were deformed from a right way-up sub-horizontal orientation. These chevron folds have mean wavelength of  $102 \pm$  standard deviation 29 m; mean amplitude of  $7.8 \pm 3.4$  m; mean interlimb angle of  $61 \pm$  circular variance  $1^\circ$ ; and mean axial plane angle of  $80 \pm 1^\circ$  S, which is in agreement with other workers (e.g. Freshney et al, 1972). The individual fold geometries are described previously in Section 4.4.1 (see Fig. 4.15; Table 4.1).

The minimum shortening accommodated by this fold train was estimated along shale beds 1, 2, 5 and 6, between the hinges of 'upright' chevron anticlines A and E, using the 'conservation of line length' method as 17-30 % (mean  $21.5 \pm 4.8$  %; Fig. 4.18a). A simple line length analysis across the dip section was also undertaken along six laterally continuous beds and the shortening was estimated as 27-42 % (mean  $33.8 \pm 5.6$  %; Fig. 4.18a). The greatest shortening estimate in both cases is from shale bed 1. Sanderson (1979) estimated that approximately 50 % shortening was accommodated between Widemouth and Saltstone, but this included measurements from the Wanson Mouth foreshore as well (see section 4.6). The smaller shortening values estimated here for the Black Rock foreshore may indicate that deformation was reduced immediately to the north of the WSF, which would represent the hanging wall to the 'late' normal fault of Freshney et al (1972) or the footwall to the thrust duplex of Enfield et al (1985). Thus, in order to maintain Sanderson's overall estimate, the shortening would need to concomitantly increase within the Wanson Mouth foreshore, to the south (see Section 4.6).

### **Widemouth South Fault**

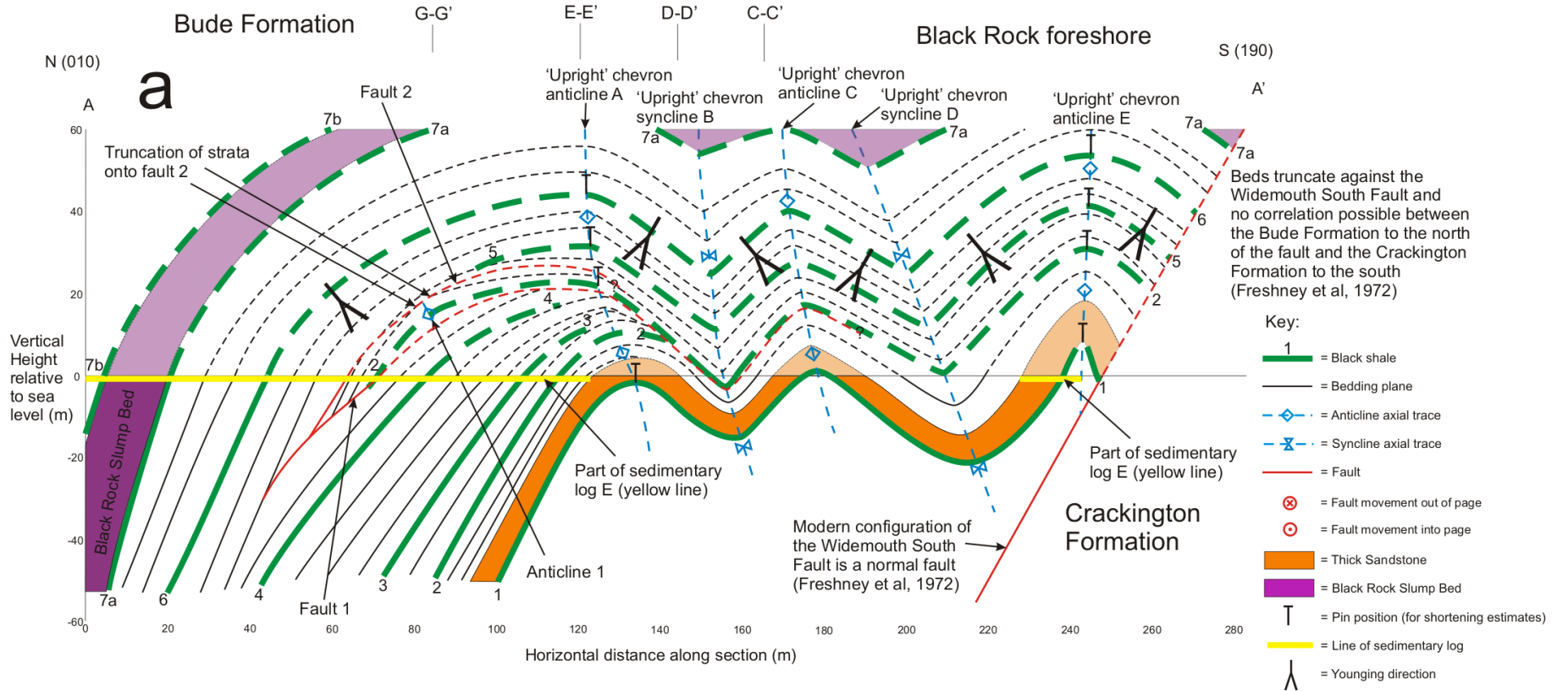
The WSF cuts the axial trace of 'upright' chevron anticline E (see gusset), truncating all the beds (Fig. 4.18a) and thus, is later than the all the deformation. In section 4.1.3, the WSF was alternatively described as a dextral wrench fault by Williams et al (1970), a normal fault by Freshney et al (1972) and an inverted north-directed thrust by Enfield et al (1985). The modern configuration of the WSF is as a normal fault, which is consistent with Freshney et al (1972).

**Black Rock dip-section A-A'**

Section observed today  
(Scale 667:1)

Shortening estimated between 'upright' chevron anticlinal hinges is between 17% and 30%

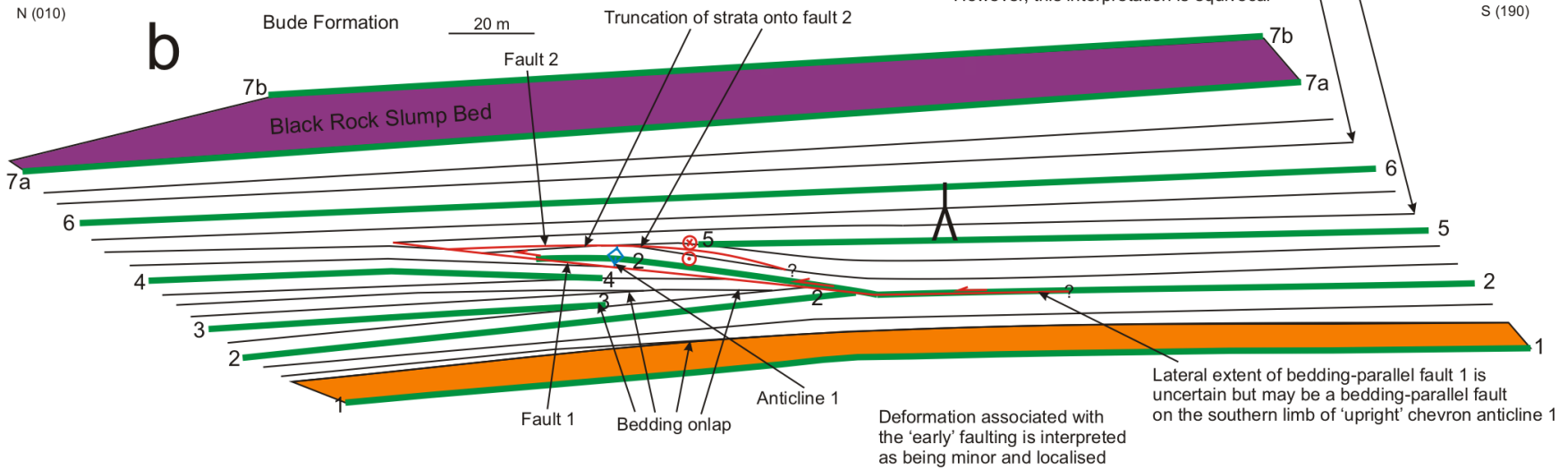
Shortening using line lengths is between 27% and 42%



**Black Rock restored dip section A-A' 1**

Removal of 'upright' chevron folding following the Ramsay and Tanner models  
(Scale 667:1)

Restored beds appear to be truncated along a moderately steep south-dipping line, which coincide the position of the Widemouth South Fault (WSF). If this is an earlier form of the WSF, then it had a reverse or thrust configuration. However, this interpretation is equivocal



**Black Rock restored dip section A-A' 2**

Removal of local deformation  
(Scale 667:1)

Beds cross the 'truncation' line from the previous restored dip section when local deformation has been removed

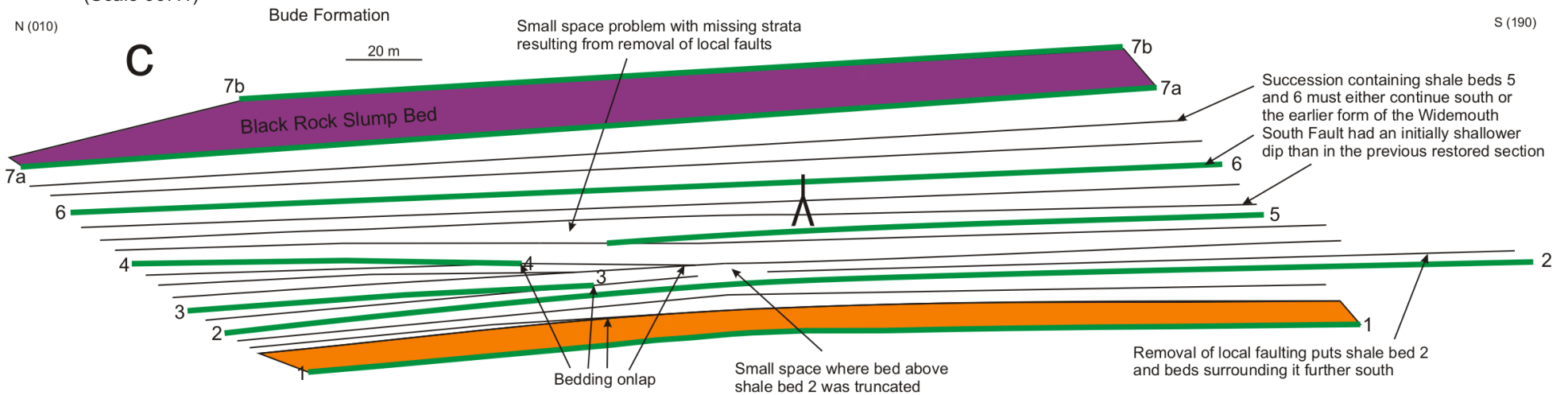


Fig. 4.18: Sections drawn across the Black Rock foreshore (SS19650173-SS19590146; see Fig 4.15 & gusset), showing the evolution of Variscan structures in: (a) Dip-section A-A'; (b) Restored dip-section A-A' 1 (removal of 'upright' chevron folding); and (c) Restored dip-section A-A' 2 (removal of local structures). Fault 1 'ramped' through the strata and its hanging wall folded beds were truncated by fault 2. Both faults are described as 'early' structures and were folded by 'upright' chevron anticline A

### **Stacked and cross-cutting local deformation structures**

The northern limb of ‘upright’ chevron anticline A includes the steeply north-dipping Black Rock Slump Bed and a thickened package of onlapping beds, as shown in log E (Figs. 4.13e). This limb has two stacked, local, north-dipping tens of metres long faults that are deformed by the ‘upright’ chevron folds (Figs. 4.18a-b).

The structurally lower fault 1 has a metric-scale anticline in its hanging wall at SS19630165 (see gusset). Fault 1 cuts the thickened package of Bude Formation beds that includes shale bed 2. This shale bed is found also in the hanging wall of fault 1, where it moved to the north and has been folded into a fault-related anticline 1 (Figs. 4.18a-b). Fault 1 does not appear to cut the strata on the southern limb of ‘upright’ chevron anticline A and, thus, is likely to be bedding-parallel on this limb. The lateral extent of this bedding-parallel fault is uncertain because it is difficult to observe in outcrop.

The structurally higher fault 2 and its associated deformation are only observed on the northern limb of ‘upright’ chevron anticline A. Fault 2 truncates some of the beds and emplaces other locally-deformed beds stratigraphically-above shale bed 2 (Figs. 4.18a-b). This suggests that fault 1 and its associated deformation developed first and fault 2 cut through the deformed beds before both faults were deformed. To the south, fault 2 has not been observed and may be either a bedding-parallel fault or be local to the northern limb of ‘upright’ chevron anticline A. Fault 2 is west-trending and outcrops in the foreshore 50 m south of the Black Rock Slump Bed. Also, ‘undeformed’ beds have been observed overlying fault 2 between shale beds 6 and 7a.

The two faults have slightly different dip angles in outcrop and may coalesce below the foreshore. Above the local faults is a bedding stack, including shale bed 6, that is not deformed by the faults, suggesting that the local structures have died out in this stack (Figs. 4.18a-b).

### **Determination of ‘early’ deformation**

Faults 1 and 2 are stacked structures that have been deformed by the ‘upright’ chevron folds in dip section A-A’ (Fig. 4.18a) and are considered therefore to be ‘early’ structures following the Mapeo and Andrews (1991) refolded structure criterion (Fig. 4.11a). The faults and anticline 1 are considered to be ‘early’ structures from the ‘undeformed’ beds and toplap truncation criteria following the Zoetemeijer et al (1992), Nigro and Renda (2004) and Corredor et al (2005) convention (Fig. 4.11b).

There is a 36 m stratigraphic thickness difference between shale beds 1 and 6 when comparing sedimentary logs B and E (Figs. 4.13b & e). This coincides with the stacked ‘early’ structures on the limb between ‘upright’ anticline A and syncline D and may represent either ‘growth’ strata around the local structures at or near the palaeo-surface, bed repetition from unrecognised local bedding-parallel structural stacking or the ‘damage zone’ around a thrust fault. This area showing the thickness difference is approximately 100 m across and a ‘damage zone’ with bed repetition around a major thrust is likely to be much more extensive than this.

Also, no beds show clear thickening and thinning trends around the local structures that would result from deposition in bathymetric lows around local structures at the palaeo-surface. This may suggest that at least a component of the 36 m thickness difference between sedimentary logs B and E (Figs. 4.13b & e) results from bed repetition from further but as yet unrecognised local structures.

The local structures may result also from the accommodation of minor Variscan compressional deformation (Mapeo & Andrews, 1991) in sediment that is likely to have been unconsolidated. North-directed thrusts have previously been shown to have exploited Bude Formation slump beds when they were unconsolidated (Whalley & Lloyd, 1986).

Furthermore, the north-trending fault 1 and west-trending fault 2 moved in different directions, but not in the directions of the SE to SW palaeo-slopes inferred from the palaeo-flow indicators of Higgs (1991) and Burne (1995). The fault 1 movement is similar to the NNW palaeo-slope directions at Widemouth (SS199027) from the author (see Fig. 3.6). This suggests that either a palaeo-slope origin cannot be ascribed to the structures or palaeo-slopes were not consistently to the south. Further descriptions of the palaeo-slopes during Bude Formation deposition are provided from analysis of slump raft folds in massive slump beds in Chapter 5.

### **Restoration of the dip section**

In the first restoration ‘step’ of dip section A-A’ (Fig. 4.18b), the ‘upright’ chevron folded beds have been restored to be sub-horizontal with the ‘early’ structures remaining. It also removes the WSF, causing the beds at the southern end of the foreshore to now define a steeply south-dipping ‘line of truncation’ for which there are two possible explanations. Firstly, this may suggest that prior to chevron folding, a steep thrust or reverse fault (presumably an earlier form of the Widemouth South Fault) truncated the Black Rock foreshore succession. The second possible interpretation is that no fault was present to truncate the beds at this stage and the Black Rock succession of the Bude Formation continued to the south. These possible interpretations are considered further in sections 4.5.9 and 4.7.

In the second restoration ‘step’ of dip section of A-A’ (Fig. 4.18c), removal of fault 2 causes ‘space problems’, with some strata now possibly missing. Out-of-plane movement is the most likely explanation to account for the ‘space problems’ but they remain difficult to explain. Removal of fault 1 places the folded shale bed 2 into its original position, greatly increasing the original length of the shale bed to the south (Fig. 4.18c). This causes the beds at the southern end of the foreshore to cross the south-dipping ‘line of truncation’ unevenly (Fig. 4.18b). The two possible explanations for this truncation line lead to two alternatives; that the WSF had a shallower dip than in restored dip section A-A’ 1 (Figs. 4.18b-c), or that there was no fault present to truncate the beds and the Black Rock succession of the Bude Formation continued to the south. These possible interpretations are considered further in sections 4.5.9 and 4.7.

### 4.5.2 Black Rock Dip-section B-B'

The 190 m long Black Rock dip section B-B' is oriented 010°-190° (SS19550174-SS19510152; Fig. 4.19; see gusset & Fig. 4.15 for location) and lies across the foreshore in areas A1 and A3 (Fig. 4.15). It includes a right way-up succession of Bude Formation beds, which are up to 70 m thick on the steeply north-dipping limb of 'upright' chevron anticline A (see sedimentary log A; Fig. 4.13a) and are up to 55 m thick on its south-dipping limb (see log C; Fig. 4.13c). The succession includes five recognisable black shale beds, the 5 m thick sandstone bed as well as the 12 m thick Black Rock Slump Bed. The three shale beds (2, 5 & 6) between the thick sandstone bed and slump bed are laterally continuous across much of the foreshore. Shale beds 5 and 6 are projected above the foreshore as they are observed elsewhere in outcrop (see gusset), in the sedimentary logs (Fig. 4.13) and in dip section A-A' (Fig. 4.18).

#### Widemouth South Fault and 'late' cross-cutting faults

In dip section B-B' (Fig. 4.19a), the WSF cuts the southern limb and the axial trace of 'upright' chevron syncline D (see gusset), truncating all the beds (Fig. 4.19a) and thus, is later than the 'upright' chevron folding. In addition, the 'upright' chevron anticlinal hinge has been offset by a local, sub-vertical, dextral, decametric scale 'late' fault  $\alpha$ , that accommodated 2-3 m of extensional movement (SS19530163). 'Late' fault  $\alpha$  is described in the Section 4.4 (also see gusset) and may have resulted from 'late' normal faulting (Freshney et al, 1972). It cuts the hinge zone of 'upright' chevron anticline A, does not extend to the WSF (Fig. 4.19a; see gusset) so that its timing with respect to the WSF is unknown. As the 'late' faulting is localised around dip section B-B' (Fig. 4.19a), the presence of these local faults is consistent with the structures observed in dip section A-A' (Fig. 4.18a; see gusset).

#### 'Upright' chevron folds

The dominant structure in dip section B-B' (Figs. 4.19a-b) is 'upright' chevron anticline A observed in profile across the foreshore (SS19530163; see dip section A-A'; Fig. 4.18a) and 'upright' chevron syncline D just north of the WSF (Figs. 4.19a-b; SS19510153). It appears therefore that the other folds ('upright' chevron syncline B and anticline C) in the chevron fold train have died out westwards across the foreshore along their axes in the 100 m from dip section A-A' to dip section B-B' (see gusset). This may suggest that some of the latter 'upright' chevron folds developed as periclinal (e.g. 'Whale's Back' chevron anticline at Bude; SS200065; Dubey & Cobbold (1977)). Also, the younging directions are towards the synclinal hinges and thus, the beds were deformed from a right way-up sub-horizontal orientation.

It was not possible to estimate the minimum shortening accommodated by the 'upright' chevron folding. Instead, a simple line length analysis across the dip section was undertaken along seven laterally continuous beds with shortening estimated at 20-39 % (mean  $30.5 \pm 5.0$  %; Fig. 4.19a) and the greatest shortening along shale bed 5. As with dip section A-A' (Fig. 4.18a),

maintaining Sanderson's overall estimate of 50 % shortening between Widemouth and Saltstone would require that the shortening increased concomitantly within the Wanson Mouth foreshore, to the south (see Section 4.6).

### **Local structures on the south-dipping limb between the 'upright' chevron folds**

On the south-dipping limb, there are three stacked and cross-cutting local decametric-scale faults with folds in the surrounding beds (Figs. 4.19a-c). A structurally-lower decametric-scale fault 3 cuts to the NE through the strata and has fold pair 3 in its hanging wall that deformed beds up to and including shale bed 5 (Figs. 4.19a-c; see gusset).

The anticline in fold pair 3 (SS19520155) and deformed beds were truncated by decametric-scale fault 4 that emplaced other locally-deformed beds at SS19520155 (see gusset). Beds correlated across fault 4 suggest that that the fault 'ramped' for tens of metres to the east through the strata, where it either died out or went into another 'flat' and thus, it is considered to be a thrust (Figs. 4.19a-c; see gusset). In the hanging wall to fault 4, the decametric scale fold pair 4 affected beds up to and including shale bed 6 (Figs. 4.19a-c; see gusset) but not above, just north of the WSF at SS19510152 (see gusset). Fault 4 also cut the high-angle bedding-parallel fault 5, which itself cut towards the east and exploited shale bed 5. Fault 5 cut down through the strata and truncated underlying beds and the syncline in fold pair 3 (Figs. 4.19a-c; see gusset). The beds between faults 4 and 5 were folded into the decametric scale syncline 5.

### **Local structures in the hinge zone of 'upright' chevron anticline A**

Folded across the hinge zone of 'upright' chevron anticline A, there is the stacked and cross-cutting, local, tens of metres long fault 6 that has 'ramped' through the basal sandstone bed. It has repeated beds, suggesting that it is a thrust. Fault 6 is connected to decametric-scale thrust stack 6 that trends to the west (Figs. 4.19a-c; see gusset). Thrust stack 6 has uplifted shale bed 2, which is truncated by fault 2 at SS19530165 (see gusset; Figs. 4.19a-b).

The decametric-scale periclinal fold pair 7 has been described as parasitic en-echelon periclinal folds on the "broken limb of the northern anticline" by Freshney et al (1972). However, in section 4.4.1, fold pair 7 was shown to be refolded by 'upright' chevron anticline A at SS19450167 and have axes that merge on the north-dipping limb of the 'upright' anticline between dip-sections A-A' and B-B' at SS19610166 and also, on its south-dipping limb at SS19440165 (see gusset). Therefore, following the convention of Mapeo and Andrews (1991), this suggests that fold pair 7 is an 'early' structure that formed in the Black Rock foreshore succession prior to 'upright' chevron folding, which contradicts Freshney et al (1972).

### **Determination of 'early' deformation**

Fault 6 is folded around the hinge zone of 'upright' chevron anticline A in dip section B-B' (Fig. 4.19a) and from the refolded structure criterion (Fig. 4.11a) is considered to be an

‘early’ structure. The ‘undeformed’ beds criterion can be applied also to fold pairs 4 and 7, with the truncated structure criterion applied to syncline 5, fold pair 3 and to the beds above thrust stack 6. Thus, these are also considered to be ‘early’ structures (Fig. 4.11b).

As described with respect to dip section A-A’ (Fig. 4.18), there is a 36 m stratigraphic thickness difference when comparing sedimentary logs B and E (Figs. 4.13b & e; see gusset) that may be in part due to bed repetition from further but as yet unrecognised local structures. This is likely to have occurred in sediment that was unconsolidated and had accommodated minor Variscan compressional deformation, consistent with Mapeo and Andrews (1991).

Also, the E-W-trending ‘early’ structures moved obliquely to the SE to SW palaeo-slope directions of Higgs (1991) and Burne (1995), and the NNW palaeo-slope directions at Widemouth (SS199027) from the author (see Fig. 3.6). This suggests that either a palaeo-slope origin cannot be ascribed to the structures or palaeo-slopes were not consistently to the south.

### **Restoration of the dip section**

In the first restoration ‘step’ of dip section B-B’ (Fig. 4.19b), the local, sub-vertical, ‘late’ dextral fault  $\alpha$  was removed. Following this minor restoration, the sequence remains truncated along the line of the present Widemouth South Fault (Fig. 4.19b). This first restoration ‘step’ for dip section B-B’ brings the deformed beds in the Black Rock foreshore to the same deformation ‘stage’ (i.e. ‘upright’ chevron folding) as observed in dip section A-A’ (Fig. 4.18a) and the following set of restorations is consistent with that of dip section A-A’ (Figs. 4.18a-c).

In the second restoration ‘step’ of dip section B-B’ (Figs. 4.19c), the ‘upright’ chevron folded beds are unfolded to the sub-horizontal and is consistent with restored dip section A-A’ 1 (Fig. 4.18b). In the third restoration ‘step’ of dip section B-B’ (Fig. 4.19d), the ‘early’ stacked and cross-cutting local structures have been removed, causing beds at the southern end of the foreshore to cross the south-dipping ‘line of truncation’ irregularly (Fig. 4.19d). Removal of the ‘early’ faults also introduces ‘space problems’ and possibly missing strata, which is most likely explained by out-of-plane movement. This is consistent with restored dip section A-A’ 2 (Fig. 4.18c) and will be discussed further in sections 4.5.9 and 4.7.

### **4.5.3 Black Rock Dip-section F-F’**

The 150 m long Black Rock dip section F-F’ is oriented 010°-190° (SS19480176-SS19440158; Fig. 4.20; see gusset & Fig. 4.15 for location) and lies across the foreshore in areas A1 and A3 (Fig. 4.15). It includes a right way-up succession of Bude Formation beds, which is up to 100 m thick, including four recognisable shale beds 2, 5, 6 and 7a as well as the 12 m thick Black Rock Slump Bed (Fig. 4.20a). The shales sit stratigraphically below the slump bed and are laterally continuous across much of the foreshore (see gusset). Shale beds 5 and 6 are projected above the foreshore because they are observed elsewhere in outcrop (see gusset), in the sedimentary logs (Fig. 4.13) and in the other two dip sections (Figs. 4.18a & 4.19a).

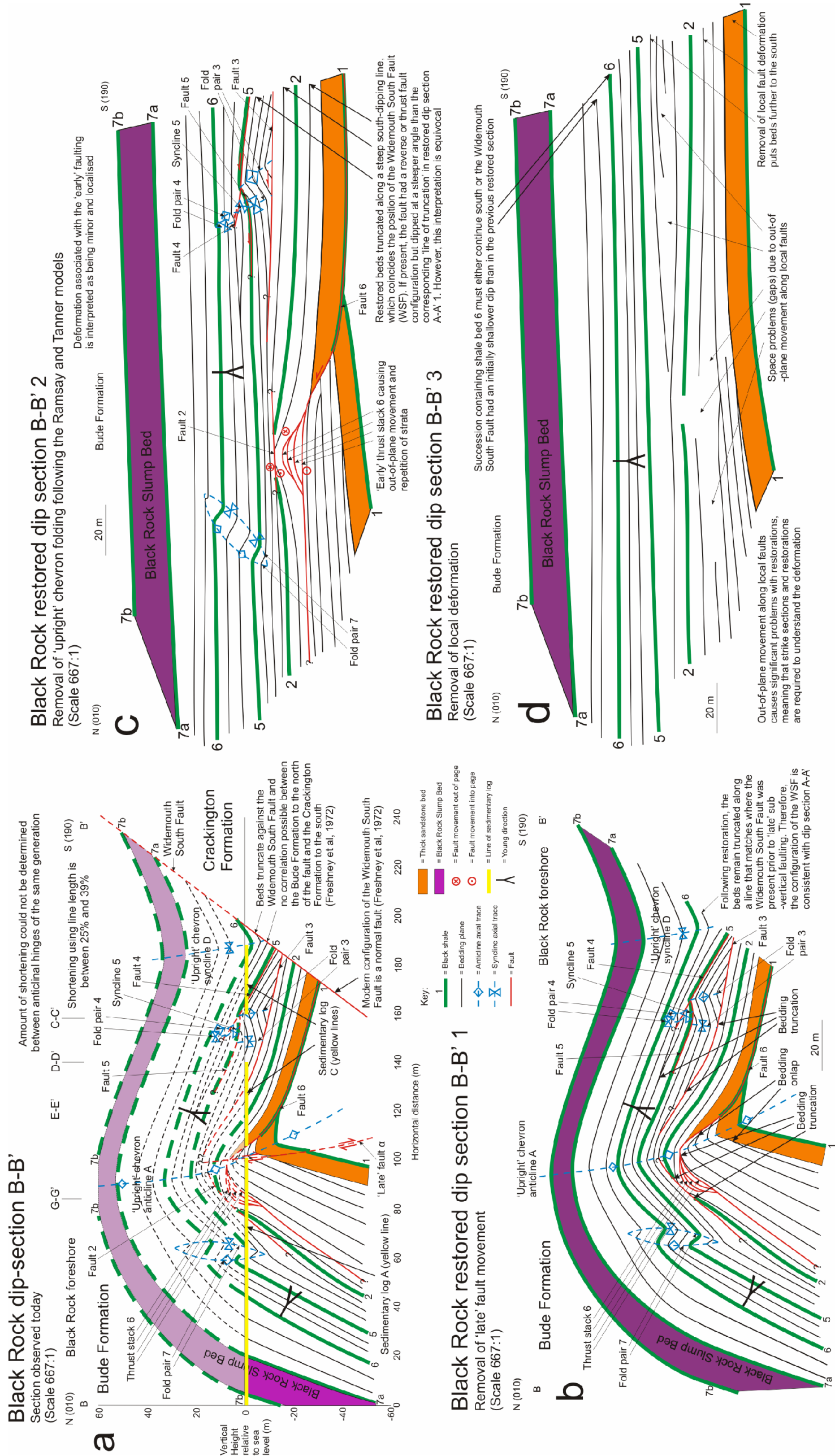


Fig. 4.19: Sections drawn across the Black Rock foreshore (SS19550173-SS19510152; see Fig 4.15 & gusset) showing the evolution of Variscan structures in: (a) Dip-section B-B'; (b) Restored dip-section B-B' 1 (removal of 'late' faulting); (c) Restored dip-section B-B' 2 (removal of 'upright' chevron folding); and (d) Restored dip-section B-B' 3 (removal of local structures). Local deformation is described as being 'early' structures and was found between shales 1 and 6

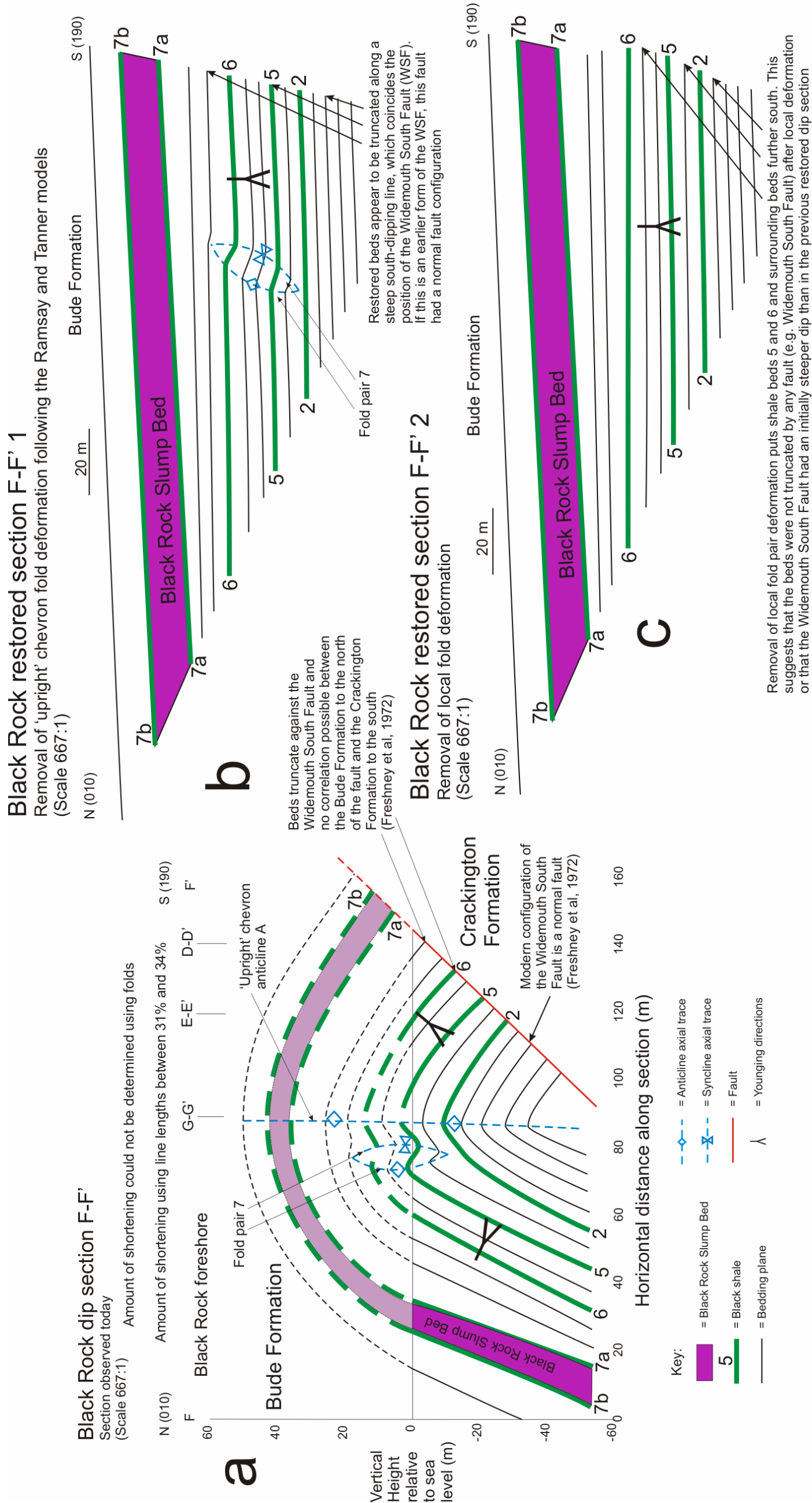


Fig. 4.20: Sections across the Black Rock foreshore (SS19480175-SS19440158; see Fig 4.15 & gusset) showing the evolution of Variscan structures in: (a) Dip-section F-F'; (b) Restored dip-section F-F' 1 (removal of 'upright' chevron folding); and (c) Restored dip-section F-F' 2 (removal of local structures). Fold pair 7 only affects the beds around shales 5 and 6 and does not deform the Black Rock Slump Bed, so is described as an 'early' structure

### **‘Upright’ chevron folds and Widemouth South Fault**

The dominant structure in dip section F-F’ is the ‘upright’ chevron anticline A in profile (Fig. 4.20a; SS19460166), which is also displayed along its axis in dip sections A-A’ and B-B’ (Figs. 4.18a & 4.19a). No other ‘upright’ chevron folds occur in this dip section because they have either died out along their axes (i.e. ‘upright’ chevron syncline B and anticline C) or have been cut by the WSF (i.e. ‘upright’ chevron syncline D and anticline E). The younging directions suggest that the beds become younger towards the synclinal hinges and thus, were deformed from a right way-up sub-horizontal orientation. In dip section F-F’ (Figs. 4.20a), the WSF cuts the southern limb of ‘upright’ chevron anticline A truncating all the beds and thus, is later than the ‘upright’ chevron folding.

It was not possible to estimate the minimum shortening accommodated by the ‘upright’ chevron folding. Instead, a simple line length analysis across the dip section taken along six laterally continuous beds has shortening estimated at 28-34 % (mean  $31.6 \pm 1.8$  %; Fig. 4.20a). As with the other dip sections (Figs. 4.18a & 4.19a), maintaining Sanderson’s overall estimate of 50 % shortening between Widemouth and Saltstone would require that shortening concomitantly increased to the south in the Wanson Mouth foreshore (see Section 4.6).

### **Local deformation structures**

The northern limb of ‘upright’ chevron anticline A includes the local fold pair 7 (Figs. 4.20a-c) folded by this ‘upright’ chevron fold west of dip section F-F’ at SS19450167 (see gusset) and described with dip section B-B’ (see Section 4.5.2; Figs. 4.19a-c).

### **Determination of ‘early’ structures**

Fold pair 7 is not shown to be deformed around the hinge zone of ‘upright’ chevron anticline A in dip section F-F’ (Fig. 4.20a) but as refolded on the map at SS19450167 (see gusset), so can be considered as an ‘early’ structure following the refolded structure criterion (Fig. 4.11a; see Section 4.4.1). Fold pair 7 is also considered to be an ‘early’ structure from the ‘undeformed’ beds criterion (Fig. 4.11b). Two of the four criteria are met to describe these local structures as being ‘early’ (see Fig. 4.11b).

### **Restoration of the dip section**

The restorations of dip section F-F’ (Figs. 4.20b & d) are the same as dip section A-A’ (Figs. 4.18b & c). The restoration interpretations are considered in sections 4.5.9 and 4.7.

#### **4.5.4 Justification for construction of strike sections**

The dip sections in the Black Rock foreshore reveal that a number of structures, such as the ‘upright’ chevron fold deformation and some of the local ‘early’ structures (Figs. 4.18-4.20) have moved sub-parallel to the dip section orientation. Also, there are a number of structures

that have moved obliquely or sub-perpendicular to the dip section orientation, such as the ‘late’ sub-vertical faulting and some of the local ‘early’ structures. The out-of-section movement causes ‘space problems’, especially in the final restored dip section ‘stages’ (Figs. 4.18c, 4.19d & 4.20c) and so the sections do not balance properly. In order to evaluate the out-of section movement, four strike sections have been drawn perpendicular to the dip sections (oriented 100°-280°; see gusset & Fig. 4.15 for locations), as described in section 4.2.3.

#### **4.5.5 Black Rock Strike-section C-C’**

The 170 m long Black Rock strike section C-C’ is oriented 280°-100° (SS19440156-SS19640154; Fig. 4.21; see gusset & Fig. 4.15 for location) and lies across the Black Rock foreshore in areas A2 and A3 (Fig. 4.15). Strike section C-C’ is perpendicular to the dip-sections, sub-parallel to the line of sedimentary log D (Fig. 4.13d) and of which 4.5 m is shown in a sedimentary log from the foreshore in Fig. 4.12 (see Section 4.3). It includes a right way-up succession of Bude Formation beds that are up to 80 m thick, including five recognisable shale beds (1, 2, 5, 6 and 7a) and the 5 m thick basal sandstone bed (Fig. 4.21a; see gusset). Shale beds 5 and 6 are projected above the foreshore as they are observed elsewhere in outcrop (see gusset), in the sedimentary logs (Fig. 4.13) and in the dip sections (Figs. 4.18-4.20). Whilst the Black Rock Slump Bed is absent in this part of the foreshore, it is projected onto the strike section in order to show the fold geometries.

#### **‘Upright’ chevron folds and Widemouth South Fault**

The ‘upright’ chevron anticline C and the WSF are shown in strike section C-C’ (Fig. 4.21a). The section line cuts across this ‘upright’ chevron fold at an acute angle to its axis, resulting in its axial trace having a shallow apparent dip. ‘Upright’ chevron anticline C does not continue across the strike section (Fig. 4.21a) because the fold dies out between dip sections A-A’ and B-B’ (Figs. 4.18a & 4.19a; see gusset). The WSF cuts the beds and ‘early’ structures in the western foreshore (see gusset) but does not cut any of the ‘upright’ chevron folds in the strike section (Fig. 4.21a).

#### **Stacked and cross-cutting local deformation structures**

Four decametric-scale faults and four sets of decametric-scale folds occur in strike section C-C’ (Figs. 4.21a-b), and are stacked structures in close proximity to each other, constrained between the stratigraphic limits of shale beds 2 and 6. In the western foreshore, the stacked and cross-cutting local faults 3, 4 and 5, together with fold pairs 3 and 4 and syncline 5 are shown in strike section C-C’ (Figs. 4.21a-b) and also dip section B-B’ (Fig. 4.19a-c; see Section 4.5.2). Also, fault 3 is folded around the hinges of ‘upright’ chevron anticline C, whilst decametric-scale fold pair 6 at SS19490155 (see gusset) is truncated by the WSF. Fold pair 6 affects beds up to and including shale bed 6, just north of the WSF at SS19490154 (see gusset).

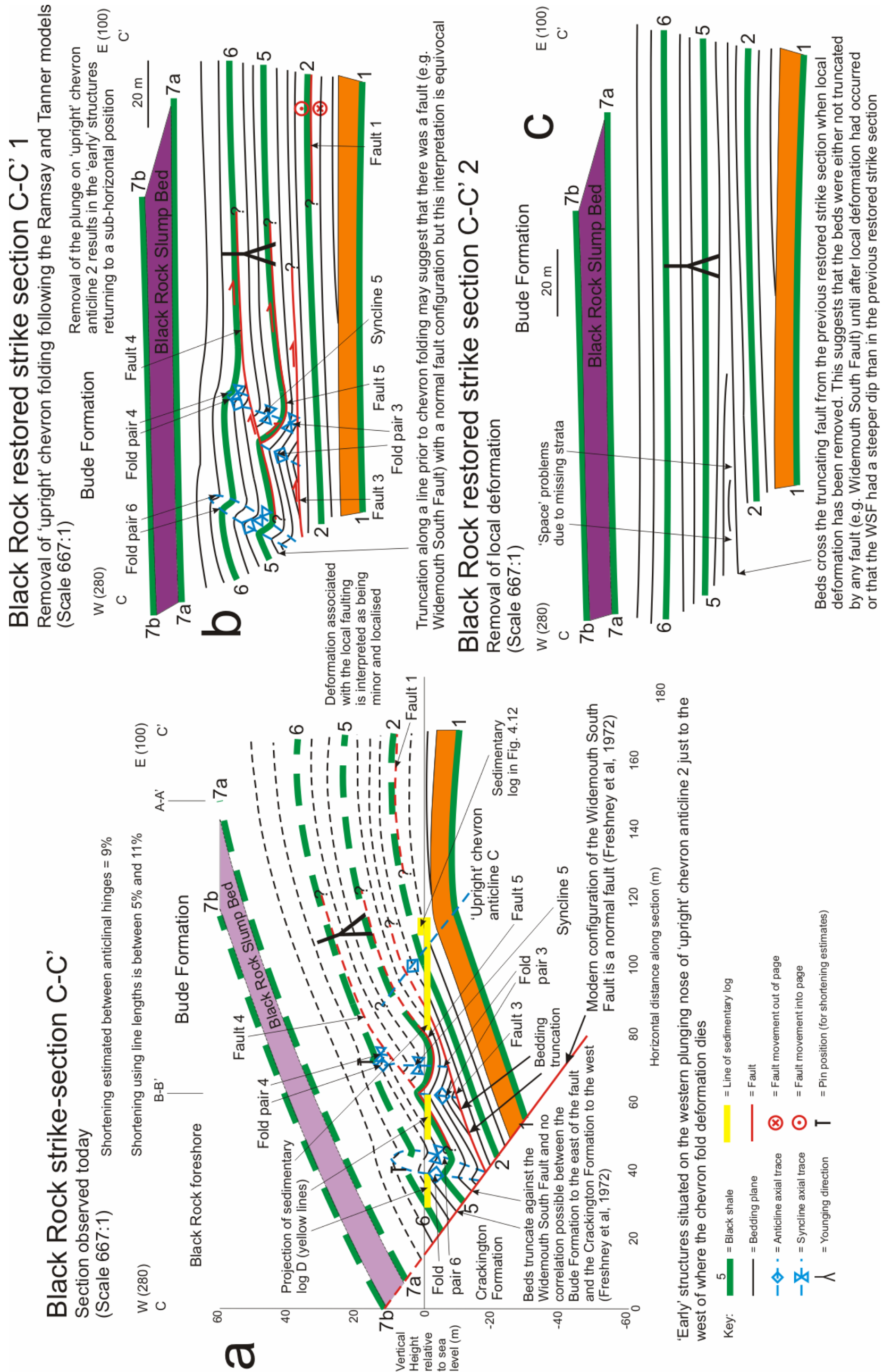


Fig. 4.21: Sections drawn across the Black Rock foreshore (SS19450156-SS19640154; see Fig 4.15 & gusset) showing the evolution of Variscan structures in: (a) Strike-section C-C'; (b) Restored strike-section C-C' 1 (removal of 'upright' chevron folding); and (c) Restored strike-section C-C' 2 (removal of local structures). Local deformation is described as 'early' structures and was found between shales 2 and 6

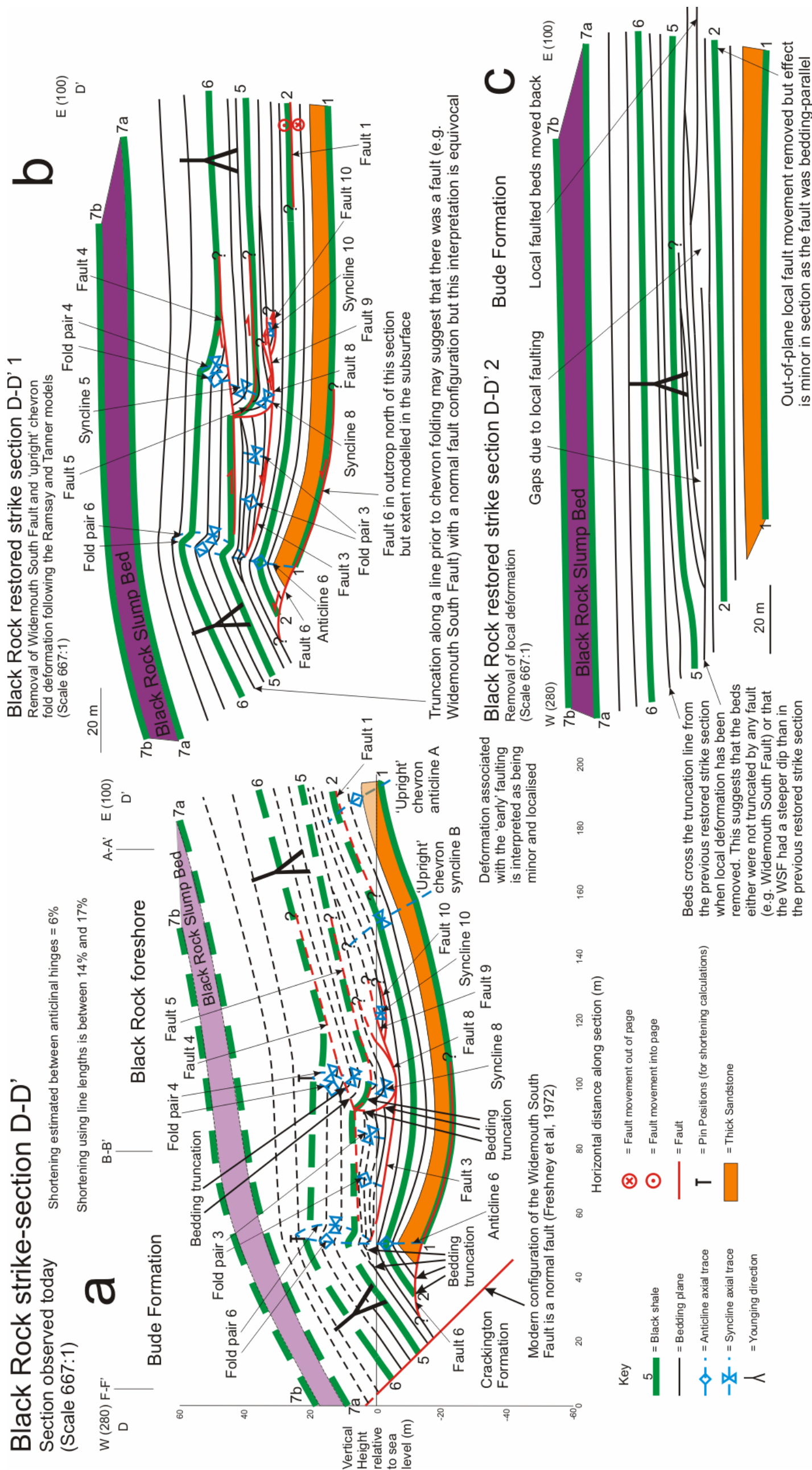


Fig. 4.22: Sections drawn across the Black Rock foreshore (SS19440159-SS19640156; see Fig 4.15 & gusset) showing the evolution of Variscan structures in: (a) Strike-section D-D'; (b) Restored strike-section D-D' 1 (removal of 'upright' chevron folding); and (c) Restored strike-section D-D' 2 (removal of local structures). Local deformation is described as 'early' structures and was found between shales 2 and 6

In the eastern foreshore, there is bedding-parallel fault 1 within shale bed 2. This fault moved to the north (see dip section A-A'; Figs. 4.18a-b) but its lateral extent cannot be determined because it is bedding-parallel and is only projected in the area of dip-section A-A'.

#### **Determination of 'early' deformation**

Fault 3 is folded around the hinge of 'upright' chevron anticline C (Fig. 4.21a), and from the refolded structure criterion (Fig. 4.11a) is considered to be an 'early' structure. The 'undeformed' beds criterion can be applied to fold pairs 4 and 6, with the truncated structure criterion applied to syncline 5 and fold pair 3, so these structures are considered as 'early' structures also (Fig. 4.11b), as is described for dip section B-B' (Fig. 4.19a; see Section 4.5.2). As described for dip section A-A' (Fig. 4.18), there is a 36 m stratigraphic thickness difference when comparing sedimentary logs B and E (Figs. 4.13b & e; see gusset) that may be due to bed repetition from further but as yet unrecognised local structures. This is likely to have occurred in sediment that was unconsolidated and had accommodated minor Variscan compressional deformation (Mapeo & Andrews, 1991).

#### **Shortening of the local structures**

The shortening accommodated by the local folds along shale bed 6 between the anticlinal hinges of fold pairs 4 and 6 (Fig. 4.21a) was estimated at 9 %. All the strike sections are perpendicular to the chevron fold tectonic movement direction, so the minimum shortening estimates have the least effect from this folding and most from the local folding. A simple line length analysis across strike section C-C' along 11 laterally continuous beds gave an estimated shortening of 5-11 % (mean  $8.3 \pm 1.8$  %; Fig. 4.21a), with the greatest shortening along shale bed 5. This shows that some local deformation occurred out-of-plane of the dip sections.

#### **Restoration of the strike section**

The restorations of strike section C-C' (Figs. 4.21b & c) are the same as dip section A-A' (Figs. 4.18b & c). The restoration interpretations are considered in sections 4.5.9 and 4.7.

#### **4.5.6 Black Rock Strike-section D-D'**

The 190 m long Black Rock strike section D-D' is oriented 280°-100° (SS19430159-SS19640156; Fig. 4.22; see gusset & Fig. 4.15 for location), is perpendicular to the dip sections and lies across the Black Rock foreshore in areas A2 and A3 (Fig. 4.15). It projects a right way-up succession of Bude Formation beds that are up to 80 m thick, including five recognisable shale beds and the 5 m thick basal sandstone bed (Fig. 4.22a; see gusset). The five shale beds (1, 2, 5, 6 and 7a) were correlated across much of the foreshore, with shale beds 5 and 6 projected above the foreshore because they are observed elsewhere in outcrop (see gusset), in the sedimentary logs (Fig. 4.13) and in the other dip and strike sections (Figs. 4.18-4.20 & 4.21).

Whilst the Black Rock Slump Bed is absent in this part of the foreshore, it is projected onto the strike section in order to show the fold geometries.

### **‘Upright’ chevron folds and Widemouth South Fault**

The ‘upright’ chevron anticline A and syncline B are shown in strike section D-D’ (Fig. 4.22a). The section line cuts across ‘upright’ chevron syncline B at an acute angle to its axis, resulting in its axial trace having a shallow apparent dip. The deformation associated with the chevron syncline does not continue across the strike section (Fig. 4.22a) as the fold dies out between dip sections A-A’ and B-B’ (Figs. 4.18a & 4.19a). In contrast, the ‘upright’ chevron anticline A axis crosses the foreshore and is shown in all three dip sections (Figs. 4.18a, 4.19a & 4.20a). In this strike section, the WSF cuts the beds and ‘early’ structures in the western foreshore, but none of the ‘upright’ chevron folds (see gusset).

### **Stacked and cross-cutting local deformation structures**

Strike section D-D’ (Figs. 4.22a-b) contains several stacked and cross-cutting local structures, some of which appear in strike section C-C’ (Figs. 4.21a-c), and are in close proximity to each other, constrained between the stratigraphic limits of shale beds 2 and 6. The structures are eight decametric-scale faults with a set of associated folds in surrounding beds.

### **Western foreshore**

In the western foreshore, there is fault 6 that moved the thick basal sandstone bed to the west at SS19520163 (see gusset) and is interpreted as a thrust (see dip section B-B’; Fig. 4.19a-c). With no exposure of the thrust to the west of SS19490164, it may not have cut through all the beds in the sub-surface, (see gusset) and so, is shown to cut the beds only to a point between shale beds 2 and 5 (Figs. 4.22a-c). Also, the thrust was folded by ‘upright’ chevron anticline A at SS19490164 (see gusset). In the hanging wall to fault 6, fold pair 6 was observed around shale beds 5 and 6. The axial traces of the fold pair connect to the axial trace of anticline 6, that deforms the same stack of beds around shale bed 2 (Figs. 4.22a-c; see gusset).

### **Central foreshore**

In the central foreshore, to the east of fold pair 6 and between shale beds 2 and 6, there are five faults and associated folds, including faults 3, 4 and 5, together with fold pairs 3 and 4 and also syncline 5, as shown in dip section B-B’ (Fig. 4.19a-c) and strike section C-C’ (Figs. 4.21a-b). Also, fault 4 thrusts over bedding-parallel fault 5, as described in dip section B-B’ (Figs. 4.19a-c), as well as another bedding-parallel fault 8 at SS19520155 (see gusset). Fault 8 moved to the east and connects to fault 5 between shale beds 2 and 5, which have been folded to form syncline 8 at SS19550158 (Figs. 4.22a-b; see gusset). Faults 5 and 8 cut down through the strata and truncated both the underlying beds and syncline 5 (Figs. 4.22a-b; see gusset).

### **Eastern foreshore**

In the eastern foreshore, fault 9 connected to fault 8 and cut down through the strata to the east for tens of metres. Between faults 8 and 9, the beds are folded into syncline 9 at SS19560156, but as the fold axis is parallel to the line of strike-section D-D', it is displayed only on the map (see gusset). Fault 9 connected to fault 10 that cut down through the strata to the east in beds overlying shale bed 2 at SS19570156 (Figs. 4.22a-b; see gusset). As with faults 8 and 9, the beds between faults 9 and 10 are folded into syncline 10 at SS19580156. Faults 9 and 10 cut down through the strata to the east and have truncated both the underlying beds and syncline 10 (Figs. 4.22a-b; see gusset). The faults (5, 8, 9 & 10) and fault-related synclines (5, 8 & 10) here connect to each other and thus, it is likely that their deformation is related.

Also, there is the bedding-parallel fault 1 in shale bed 2, which is deformed by 'upright' chevron anticline A and moved to the north as shown in dip section A-A' (Figs. 4.18a-b).

### **Determination of 'early' deformation**

Fault 1 is folded around the hinge of 'upright' chevron anticline A, and following the refolded structure criterion (Fig. 4.11a) is considered to be an 'early' structure. The 'undeformed' beds criterion can be applied to fold pairs 4 and 6, with the truncated structure criterion applied to synclines 5, 8 and 10, as well as to fold pair 3. Therefore, these are considered to be 'early' structures also (Fig. 4.11b). There is a 6 m stratigraphic thickness difference between shale beds 2 and 5 when comparing sedimentary logs B and C (Figs. 4.13b-c) that may be due to bed repetition from further but as yet unrecognised local structures. This is likely to have occurred in sediment that was unconsolidated and had accommodated minor Variscan compressional deformation (Mapeo & Andrews, 1991).

### **Shortening by the local structures**

The minimum shortening accommodated by the local folds along shale bed 6 between the anticlinal hinges of fold pairs 1 and 3 is estimated to be 6 % in strike section D-D' (Fig. 4.22a). A simple line length analysis along six laterally continuous beds across the strike section produced a shortening estimate of 14-17 % (mean  $15.4 \pm 0.9$  %; Fig. 4.22a) with the greatest shortening along shale bed 2.

### **Restoration of the strike sections**

The restorations of strike section D-D' (Figs. 4.22b & c) are the same as for dip section A-A' (Figs. 4.18b & c). The restoration interpretations are considered in sections 4.5.9 and 4.7.

#### **4.5.7 Black Rock Strike-section E-E'**

The 190 m long Black Rock strike section E-E' is oriented  $280^\circ$ - $100^\circ$  (SS19430162-SS19640158; Fig. 4.23; see gusset & Fig. 4.15 for locations), is perpendicular to the dip

sections and lies across the Black Rock foreshore in areas A2 and A3 (Fig. 4.15). It projects a right way-up succession of Bude Formation beds that is up to 75 m thick, including six recognisable shale beds (1, 2, 3, 5, 6 and 7a) and the 5 m thick basal sandstone bed (Fig. 4.23a; see gusset). Shale beds 1, 2, 5 and 6 were correlated across much of the foreshore, but shale bed 3 onlaps beds in the area of dip section A-A' (Fig. 4.18a). Shale beds 5 and 6 are projected above the foreshore because they are observed elsewhere in outcrop (see gusset), in the sedimentary logs (Fig. 4.13) and in the other dip and strike sections (Figs. 4.18-4.20 & 4.21-4.22). Whilst the Black Rock Slump Bed is absent in this part of the foreshore, it is projected onto the strike section in order to show the fold geometries.

### **'Late' cross-cutting faults**

In strike section E-E' (Fig. 4.23a), there is a set of local, metric-scale, sub-vertical faults that cut the basal sandstone bed in outcrop (SS19540161-SS19560159; see gusset) and the shale beds 2 and 5 in the projection above the foreshore (Fig. 4.23a). In dip section B-B' (Fig. 4.19a) and on the map (see gusset), the faults cut the 'upright' chevron anticline A axis, suggesting that they are 'late' faults. There are two NNE-SSW-striking faults, here 'late' faults  $\beta$  and  $\gamma$ , which accommodated extension with up to 3 m of vertical displacement, whilst the NW-SE-striking 'late' fault  $\alpha$  cross-cuts the 'late' faults  $\beta$  and  $\gamma$  and accommodated compression with up to 4 m of vertical displacement (Fig. 4.23a).

In contrast to that observed in the foreshore (see gusset) and shown in dip section B-B' (Fig. 4.19a) the 'late' faulting does not cut the 'upright' chevron anticline A in this section. Also, the 'late' faults have not been cross-cut by the WSF and therefore, their timing relative to the WSF is unknown. The minor 'late' faulting is localised around dip section B-B' (Fig. 4.19a) and strike section E-E' (Fig. 4.23a), so their presence is consistent with the structures shown in the other dip and strike sections (Figs. 4.18a, 4.20a, 4.21a & 4.22a; see gusset).

### **'Upright' chevron folds and Widemouth South Fault**

Strike section E-E' (Figs. 4.23a-b) cross-cuts the 'upright' chevron anticline A axis at an acute angle, resulting in the apparent dip of its axial trace being shallow. The axis of 'upright' chevron anticline A crosses the foreshore and is shown in all three dip sections (Figs. 4.18a, 4.19a & 4.20a). The WSF cuts the beds and the 'early' structures in the western foreshore (see gusset), but not any of the 'upright' chevron folds in the strike section (Fig. 4.23a).

### **Stacked and cross-cutting local deformation structures**

In the western and central foreshore, between shale beds 1 and 6, there are five stacked and cross-cutting local decametric-scale faults and folds, including faults 3, 4, 5, 6 and 8, together with fold pairs 3 and 4 as well as synclines 5 and 8 that are shown in strike section D-D' (Figs. 4.21a-b; see Section 4.5.6).

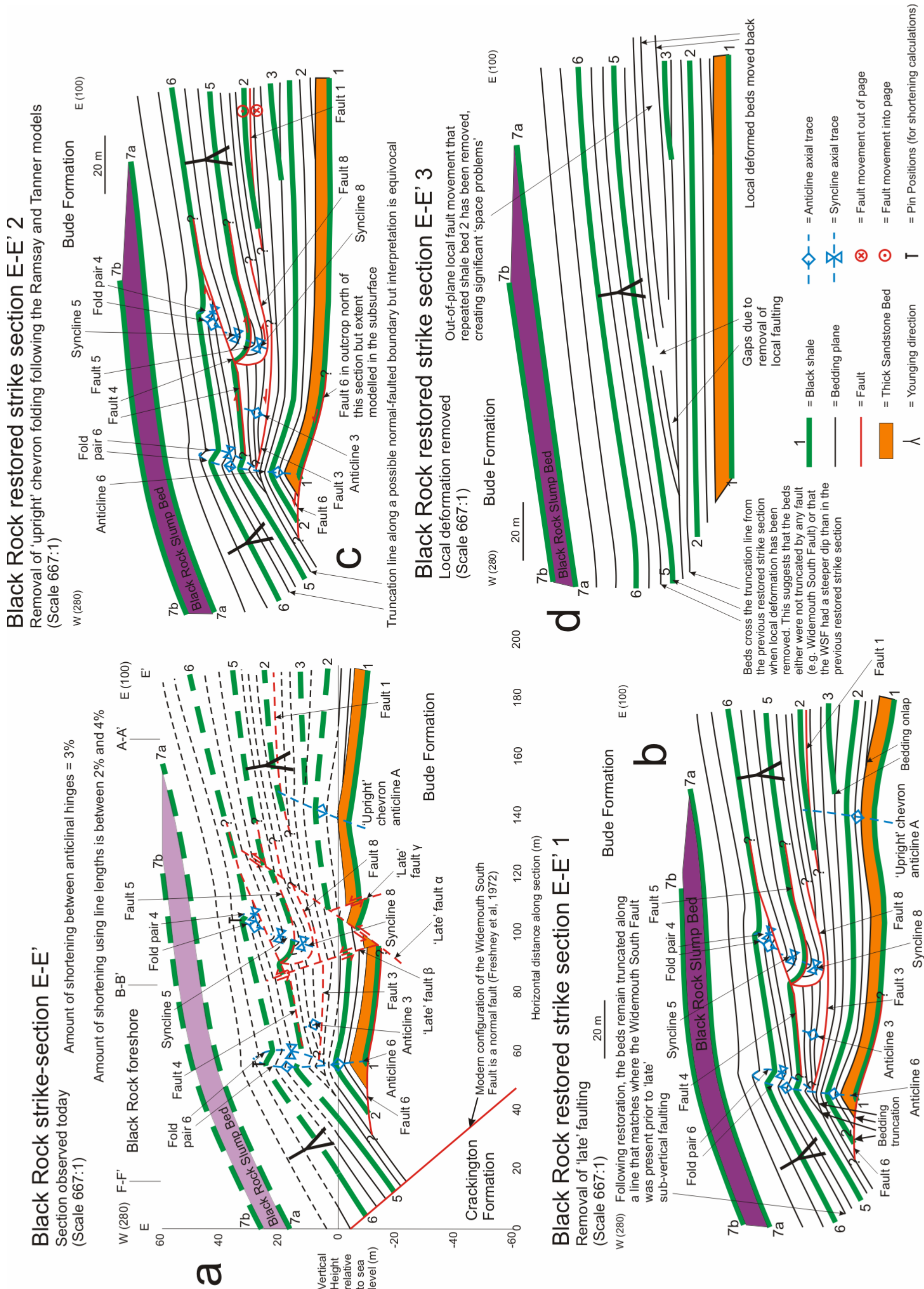


Fig. 4.23: Sections drawn across the Black Rock foreshore (SS19430162-SS19640158; see Fig 4.15 & gusset) showing the evolution of Variscan structures in: (a) Strike-section E-E'; (b) Restored strike-section E-E' (removal of 'late' faulting); (c) Restored strike-section E-E' 2 (removal of 'upright' chevron folding); and (d) Restored strike-section E-E' 3 (removal of local structures). Local deformation is described as 'early' structures and was found between shales 1 and 6

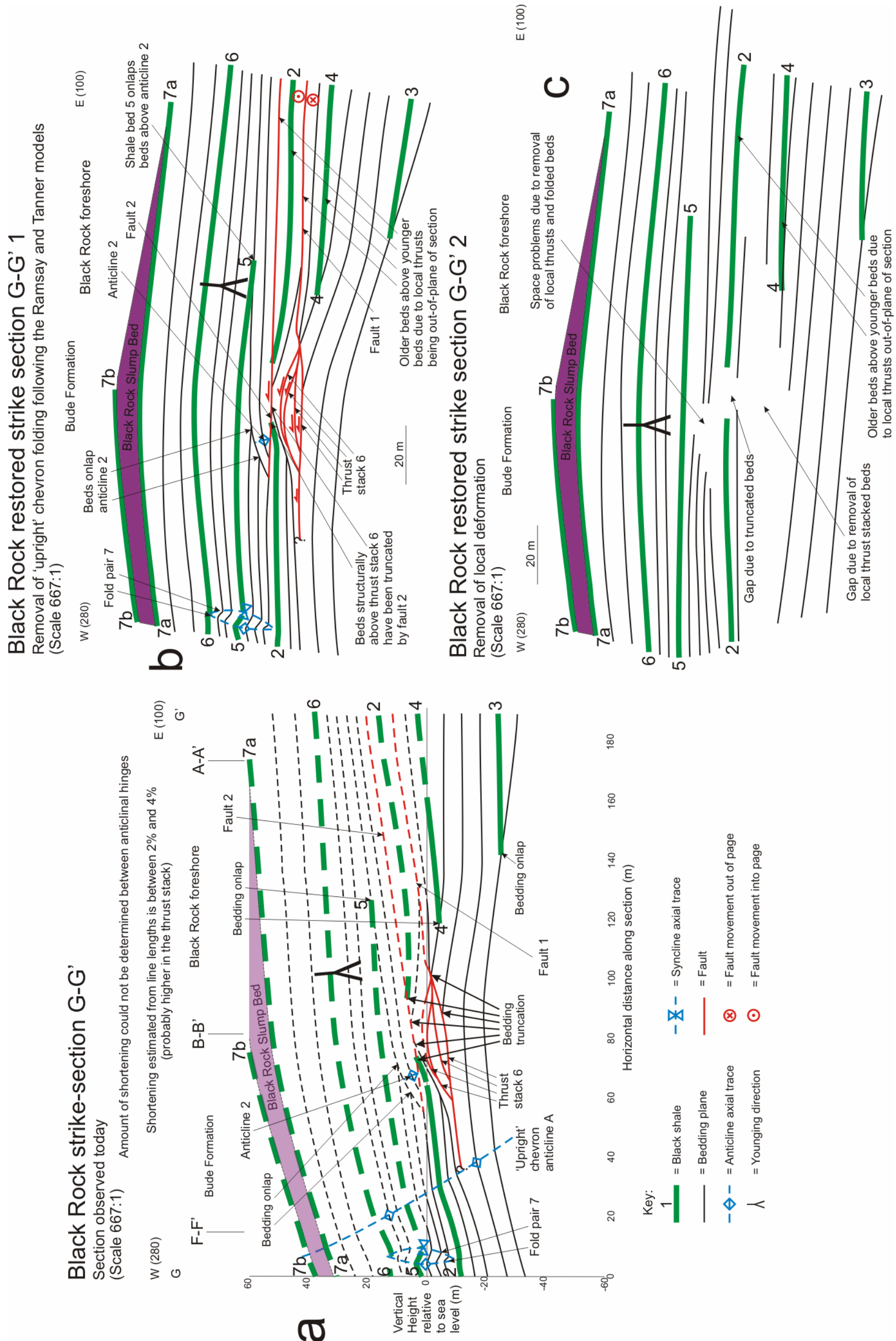


Fig. 4.24: Sections drawn across the Black Rock foreshore (SS19440166-SS19640163; see Fig 4.15 & gusset) showing the evolution of Variscan structures in: (a) Strike-section G-G'; (b) Restored strike-section G-G' 1 (removal of 'upright' chevron folding); and (c) Restored strike-section G-G' 2 (removal of local structures). Local deformation is described as 'early' structures and was found between shales 2 and 5

In the eastern foreshore, there is the bedding-parallel fault 1 within shale bed 2, which moved to the north and was deformed by ‘upright’ chevron anticline A. The lateral extent of fault 1 is not known because it is bedding-parallel, but is projected where the line of dip-section A-A’ crosses this section, as described in strike section C-C’ (Fig. 4.22a-b).

#### **Determination of ‘early’ structures**

Fault 1 is folded around the hinge of ‘upright’ chevron anticline A (Figs. 4.23a-b) and following the refolded structure criterion (Fig. 4.11a) is considered to be an ‘early’ structure. The ‘undeformed’ beds criterion can be applied to fold pairs 4 and 6, with the truncated structure criterion being applied to anticline 3 as well as synclines 5 and 8. Thus, all these structures are considered as ‘early’ (Fig. 4.11b). As described for dip section A-A’ (Fig. 4.18), there is a 36 m stratigraphic thickness difference when comparing sedimentary logs B and E (Figs. 4.13b & e) that may be in part due to bed repetition from further but unrecognised local structures. This is likely to have occurred in unconsolidated sediment and had accommodated minor Variscan compressional deformation (Mapeo & Andrews, 1991).

#### **Shortening by the local structures**

In strike section E-E’, the estimated shortening accommodated by the local folds along shale bed 6 between the anticlinal hinges of fold pairs 4 and 6 is 3% (Fig. 4.23a). A simple line length analysis along six laterally continuous beds across the strike section gave a shortening estimate of 2-4 % (mean  $3.2 \pm 0.3$  %; Fig. 4.23a), with the greatest shortening along shale bed 5.

#### **Restoration of the structures**

The restorations of strike section E-E’ (Figs. 4.23b-d) are the same as dip section B-B’ (Figs. 4.19b-d). The restoration interpretations are considered in sections 4.5.9 and 4.7.

#### **4.5.8 Black Rock Strike-section G-G’**

The 190 m long Black Rock strike section G-G’ is oriented  $280^{\circ}$ - $100^{\circ}$  (SS19440166-SS19640163; Fig. 4.24; see gusset & Fig. 4.15 for location), is perpendicular to the dip sections and lies across the Black Rock foreshore in areas A2 and A3 (Fig. 4.15). It projects a right way-up succession of Bude Formation beds that are up to 80 m thick, including six recognisable shale beds (2-7a) (Fig. 4.22a; see gusset). Shale beds 2 and 6 in this strike section are laterally continuous across much of the foreshore (see gusset), whilst shale beds 3, 4 and 5 onlap beds between the lines of dip sections A-A’ and B-B’ (see gusset). Shale beds 5 and 6 are projected above the foreshore as they are observed elsewhere in outcrop (see gusset), as well as in the sedimentary logs (Fig. 4.13) and other cross-sections (Figs. 4.18-4.20 & 4.21-4.23). Whilst the Black Rock Slump Bed is absent in this part of the foreshore, it is projected onto the strike section in order to show the fold geometries.

### **‘Upright’ chevron folds**

Strike-section G-G’ (Fig. 4.24a-b) cross-cuts the ‘upright’ chevron anticline A fold axis at an acute angle, resulting in the apparent dip of the chevron fold axial trace being shallow. The axis of ‘upright’ chevron anticline A crosses the foreshore and is shown in all three dip sections (Figs. 4.18a, 4.19a & 4.20a). It should be noted that the WSF is buried beneath sand towards the low tide mark and therefore, has not been projected onto this strike section (Fig. 4.24a).

### **Stacked and cross-cutting local deformation structures**

In strike section G-G’ (Figs. 4.24a-b), the stacked and cross-cutting local structures include the thrust stack 6 that has uplifted shale bed 2. This caused shale bed 2 to be truncated by fault 2 at SS19530165, emplacing other locally-deformed beds (see gusset), as described in dip section B-B’ (Figs. 4.19a-c; see Section 4.5.2). The beds folded by anticline 2, which include shale bed 5, that lie in the hanging wall to fault 2, onlap and drape the fold structure. The beds above shale 5 up to the Black Rock Slump Bed have a layer-cake stacking pattern that is ‘undeformed’ by the local structures.

In the eastern foreshore, underlying fault 2, there is bedding-parallel fault 1 that moved to the north and caused shale bed 2 to be emplaced over shale bed 4, as described in dip section A-A’ (Figs. 4.18a-b; see Section 4.5.1). Also, fold pair 7 is observed in this section, as also described in dip sections B-B’ (Figs. 4.19a-c) and F-F’ (Figs. 4.20a-b; see Section 4.5.3).

### **Determination of ‘early’ structures**

No structures have been folded around the hinge zone of ‘upright’ chevron anticline A in strike section G-G’ (Fig. 4.24a) and therefore, cannot be considered as ‘early’ structures following the Mapeo and Andrews (1991) convention (Fig. 4.11a). The ‘undeformed’ beds criterion can be applied to fold pair 7 and anticline 2, with the truncated structure criterion applied to the beds above thrust stack 6 (Fig. 4.11b). As two of the four criteria are met, the local structures are interpreted as being ‘early’ *sensu lato* (Fig. 4.11).

### **Shortening by the local structures**

There is no fold train in strike section G-G’ (Fig. 4.24a), and so a minimum shortening estimate cannot be made. Instead, a simple line length analysis along laterally continuous beds across the strike section produced a shortening estimate of 2-4 % (mean  $2.9 \pm 0.4$  %) with the greatest shortening around shale bed 5 (Fig. 4.24a).

### **Restoration of the strike section**

The restorations of strike section G-G’ (Figs. 4.24b & c) are the same as dip section A-A’ (Figs. 4.18b & c). The restoration interpretations are considered in sections 4.5.9 and 4.7.

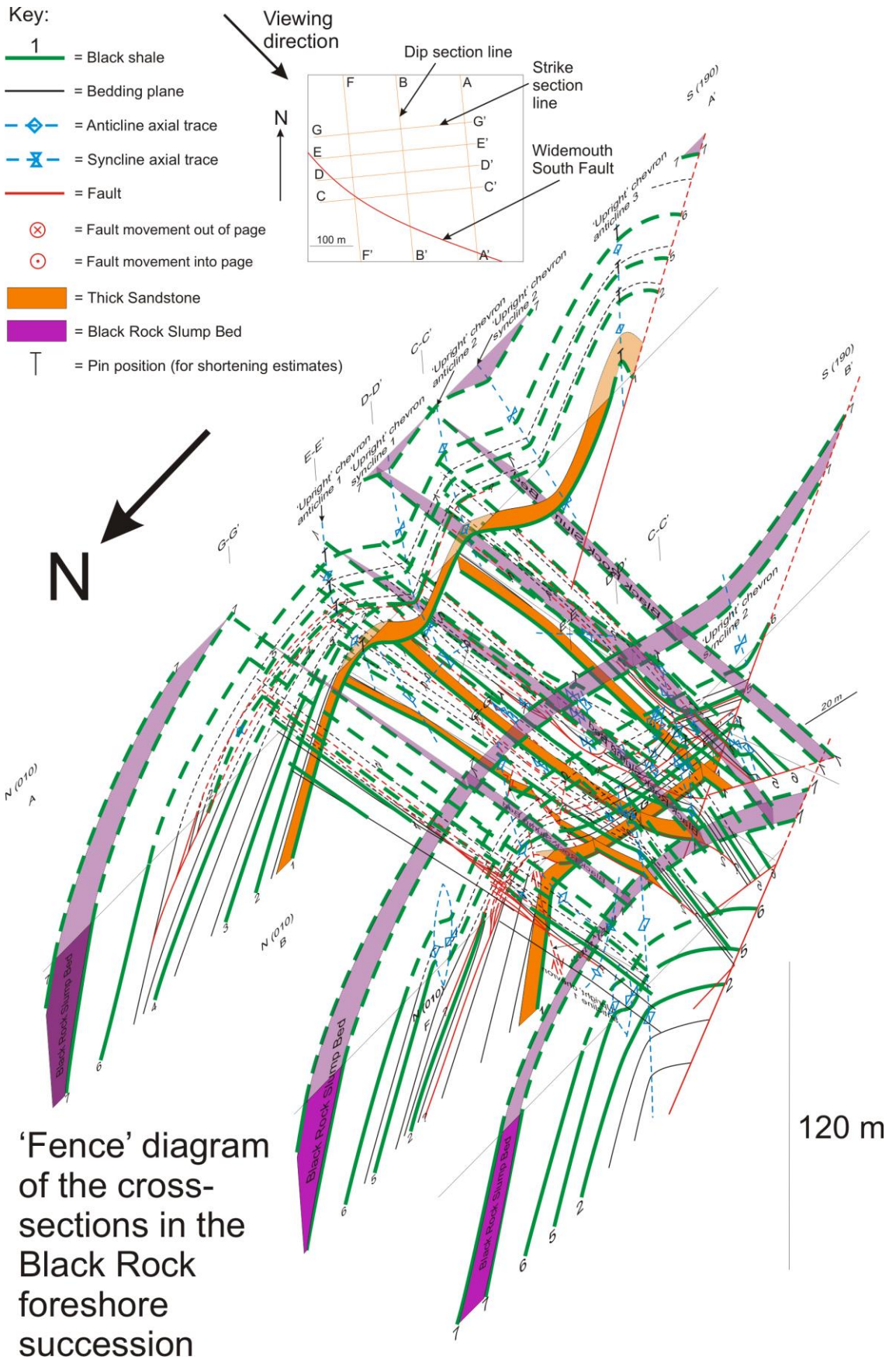


Fig. 4.25: 'Fence' diagram of the dip and strike sections across the Black Rock foreshore succession, correlating laterally-continuous beds and highlighting the geometric variations in the 'upright' chevron folds from east-to-west

#### **4.5.9 Widemouth South Fault**

No structures or beds traverse the steep NE-dipping Widemouth South Fault (WSF) in the southern Black Rock foreshore. This suggests that the WSF is a fault that moved after chevron folding and that this movement is extensional, consistent with Anderson and Morris (2004). As the restorations of the Black Rock structures are treated separately to those in the Wanson Mouth succession (see Section 4.6), ‘lines of truncation’ appeared in the restored section ‘stages’ where the WSF occurs. These ‘lines of truncation’ were recognised and / or inferred to represent potentially early forms of the WSF. However, if no ‘line of truncation’ was defined after a restoration ‘step’, it was interpreted to indicate that no earlier form of the WSF existed at this ‘stage’. Restoration of each structure suggested that any earlier form of the WSF changed its configuration from restored section to restored section (e.g. compare dip section A-A’ and restored dip section A-A’ (Figs. 4.18a-b).

It was recognised also that the configuration of the WSF did not remain consistent across the same ‘stage’ of restoration of the sections (e.g. compare restored dip section A-A’ 1 (Fig. 4.18b) and restored dip section F-F’ 1 (Fig. 4.20b). The inconsistency in its configuration between restored sections that are only a few hundreds of metres apart may suggest that the WSF is a ‘late’ fault (Freshney et al, 1972) and that there was no earlier form of the WSF during restoration. Further discussion of the WSF is provided in sections 4.6 and 4.7.

#### **4.5.10 Three-dimensional projection of the Black Rock foreshore succession**

The Black Rock dip and strike sections provide stratigraphic constraint on the structures described in the corresponding restored sections, using eight shale beds, the Black Rock Slump Bed and the thick sandstone bed. The constraint on the structures allows a 3D ‘fence’ diagram to be constructed with the strike sections cross-cutting the dip sections (Fig. 4.25).

The variation in structural geometries across the foreshore succession is highlighted best in the ‘fence’ diagram (Fig. 4.25) by the change from a train of ‘upright’ chevron folds in dip section A-A’ (Fig. 4.18a), to an ‘upright’ chevron fold pair in dip section B-B’ (Fig. 4.19a) and then to a single ‘upright’ chevron anticline in dip section F-F’ (Fig. 4.20a). This suggests that significant geometric changes occur along the E-W axial extents of the chevron folds over tens to hundreds of metres distance in the Bude Formation succession, as described for the ‘Whale’s Back’ periclinal chevron anticline at Bude (SS200065) by Dubey and Cobbold (1977).

#### **4.5.11 Summary of the geological evolution of the Black Rock foreshore**

The restoration of the deformation in the Black Rock foreshore has revealed several ‘stages’ of geological evolution (Figs. 4.26a-c). Although structures are distinguished, Variscan deformation is viewed as being progressive, as described by Freshney et al (1972). Deformation includes stacked and cross-cutting local ‘early’ structures constrained both laterally, as shown on the map (see gusset) and cross-sections and also, stratigraphically by the laterally-continuous

shales they lie between or deform, which are used as correlatable horizons (Figs. 4.21b, 4.22b, 4.23c, 4.24b & 4.26c). The ‘upright’ chevron folds have refolded or tilted the ‘early’ structures (Figs. 4.18a, 4.19b, 4.20a & 4.26b; see gusset). Cross-cutting the ‘upright’ chevron folds, there are local, minor, sub-vertical, dextral faults (Figs. 4.19a, 4.23a & 4.26a; see gusset).

The ‘early’ structures were defined as occurring prior to chevron folding using the Mapeo and Andrews (1991) convention and as structures that occurred at or near the palaeo-surface using the criteria following Zoetemeijer et al (1992), Nigro and Renda (2004) and Corredor et al (2005) (see Fig. 4.11). This is likely to have occurred in unconsolidated sediment that had accommodated minor Variscan deformation (Mapeo & Andrews, 1991). The ‘early’ structures moved commonly in different directions to the SE to SW palaeo-slope directions of Higgs (1991) and Burne (1995) (see Chapter 3), so either a palaeo-slope origin cannot be ascribed to the structures, or this implies that palaeo-slopes were not consistently to the south.

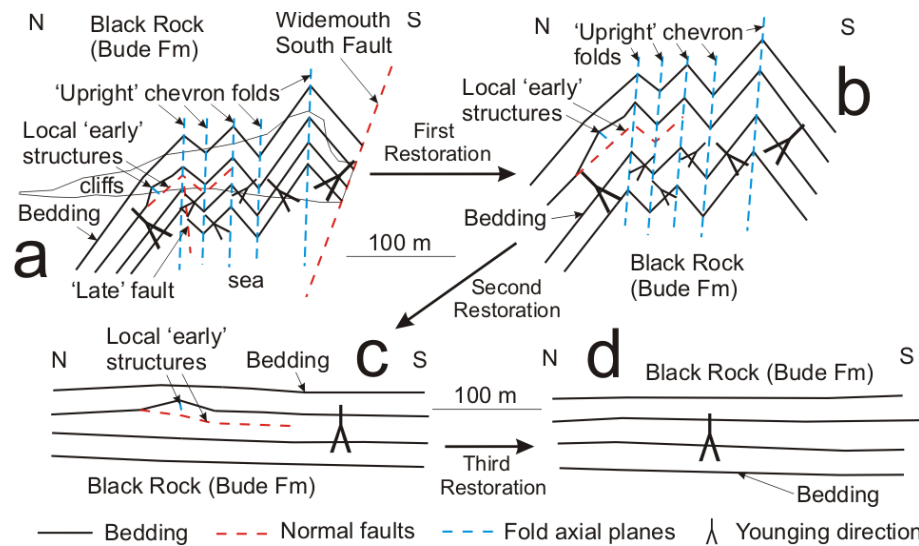


Fig. 4.26: Schematic section diagrams for the restoration of deformation in the Black Rock foreshore. Restorations: (a) Present situation; (b) ‘Late’ faulting removed; (c) Removal of ‘upright’ chevron folds; and (d) Removal of local ‘early’ structures

#### 4.6 Structural evolution of the Wanson Mouth foreshore

The Wanson Mouth foreshore lies within the Crackington Formation immediately to the south of the Widemouth South Fault (WSF; oriented: 127/68NE; 132/65NE) and north of the Wanson North Fault (WNF; oriented: 115/83N) (see gusset). The WSF is a significant tectonic feature as it juxtaposes the Bude and Crackington formations in the Culm Basin (Williams et al, 1970; Freshney et al, 1972; Sanderson, 1979; Durrance, 1985; Enfield et al, 1985) and its structural significance and possible geological evolution are described in this section. Across the WSF, there is a 300 m stratigraphic difference between the two successions (Freshney et al, 1979; see Fig. 4.2) and no structures or beds traverse the fault. Accordingly, the Wanson Mouth dip sections are described separately from the Black Rock dip sections (see Section 4.5).

The Wanson Mouth foreshore has a series of faults and folds that are described using three dip sections and one oblique section. The dip-sections A-A', B-B' and F-F' are oriented 010°-190° (see gusset & Fig. 4.15 for locations), which are sub-parallel to the profile planes of the 'inclined' chevron folds. The 'inclined' chevron folds are equivalent to the 'inclined-to-recumbent' chevron folds of Sanderson (1979). The oblique section H-H' has been drawn at an angle to the dip sections, is oriented 315°-135° (see gusset & Fig. 4.15 for location) and is sub-perpendicular to the strike of the oblique faults. In the sections, the beds have been projected up to 60 m above and below the foreshore outcrop. In the cross-section descriptions, a letter or number is given to distinguish the structures and has no intended relationship to structural timing. This remains consistent across each cross-section and restored cross-section.

A minimum shortening could not be estimated in the Wanson Mouth beds because there are no multiple folds or fold trains. Instead, shortening estimates were made using a simple line length analysis on all the beds projected in the dip-sections and compared to the Sanderson (1979) estimate that approximately 50 % shortening was accommodated between Widemouth and Saltstone. The Wanson Mouth shortening estimates were also compared with those obtained from the Black Rock dip sections (Figs. 4.18-4.20).

### **Restoration of the structures**

The Crackington Formation beds in the Wanson Mouth foreshore proved difficult to correlate across the faults, as found by previous authors (e.g. King, 1967; Williams et al, 1970; Freshney et al, 1972; Enfield et al, 1985), preventing the estimation of the displacement accommodated along the faults. Freshney et al (1972) suggested that extensional movement was tens of metres on each fault between Wanson and Rusey, but with little detailed justification.

Consequently, the two models from Freshney et al (1972) and Enfield et al (1985) that have been developed to explain the occurrence of the structures in the foreshore succession are used to guide two separate restorations of the dip and oblique sections (Figs. 4.27-4.30). The restorations are undertaken in steps for practicality and to make the structural relationships clear.

In the first set of restorations, it is assumed that the Wanson Mouth faults are 'late' normal fault structures, which occurred after 'inclined' chevron folding, as described by Freshney et al (1972). In the second set of restorations, the assumption is that the Wanson Mouth faults preceded the 'inclined' chevron folding, as described by Enfield et al (1985). These two sets of restoration provide a basis for comparing the models discussed in section 4.7.

For the restoration of the 'inclined' chevron folds in both models, application of the Ghosh (1966), Sanderson (1979) and Lloyd and Whalley (1986; 1997) models would cause the beds to be on the south-dipping limb of a larger-scale 'upright' chevron fold (see Section 4.1.3). However, it was not demonstrated that there was an 'upright' chevron fold on a larger-scale than the Wanson Mouth foreshore. Thus, geometric restorations of the 'inclined' chevron folds were undertaken in which the beds retain their present overturned steep northwards dip.

The first 'late' fault model (Freshney et al, 1972) restoration 'step' removes the Wanson Mouth faults, which are modelled to cross-cut all previous structures. The removal of the faults places the beds into positions where they may have been on the overturned limbs of the hundreds of metres long 'inclined' chevron fold pair. The second 'late' fault model restoration 'step' removes the 'inclined' chevron fold deformation in which the beds retain their present overturned steep northwards dip. The third 'late' fault model restoration 'step' returns the beds to a right way-up, sub-horizontal bedding pattern following Crackington Formation deposition.

The first pre-folding fault model (Enfield et al, 1985) restoration 'step' removes the 'inclined' chevron folding, which is assumed to have deformed the faults in the Wanson Mouth foreshore. In this restoration, the beds and faults retain their present overturned steep northwards dip. The second pre-folding fault restoration 'step' returns the beds and faults to a pre-folding state in which the beds are the right way-up. The third pre-folding fault restoration 'step' removes the stacked faults in order to return them to a right way-up, sub-horizontal bedding pattern following Crackington Formation deposition and in which they may have been prior to deformation.

#### **4.6.1 Wanson Mouth Dip-section A-A'**

The 140 m long Wanson Mouth dip section A-A' (Fig. 4.27a) is oriented 010°-190° (SS19590146-SS19560131; see gusset & Fig. 4.15 for location) and lies across the Wanson Mouth foreshore in areas A4, A5 and A6 (Fig. 4.15). This dip section includes a generally steep north-dipping, overturned succession of Crackington Formation beds, of which 11 m is shown in a sedimentary log from the cliff section in Fig. 4.14 (see Section 4.3). This log was taken to establish both the younging direction and the deep-water depositional environment of these Crackington Formation turbidite beds, as described by Melvin (1986).

In contrast to the Black Rock foreshore, this succession does not include any recognisable shale beds, making bed correlation difficult (Fig. 4.27a; see gusset). However, as the beds are generally laterally-continuous turbidite sheet sands (Melvin, 1986) the beds measured in the foreshore outcrop can be projected confidently both above and below the line of the dip-section (Fig. 4.27a).

#### **'Inclined' chevron folds**

The dominant structure shown in dip section A-A' is an 'inclined' chevron fold pair in profile (Fig. 4.27a) that deformed the beds in the foreshore succession, causing the long limbs to be overturned and dip steeply to the north. In contrast, the tens of metres long short limb between the anticline and syncline has a shallow northwards dip. The fold amplitude is  $17.5 \pm$  st. dev. 6.5 m, but the wavelength cannot be measured as there are no other 'inclined' chevron folds in the foreshore. Although the beds on the long fold limbs are overturned, the beds on the short limbs remain the right way-up albeit with a shallow ( $\sim 30^\circ$ N) northwards dip. This

suggests that the ‘inclined’ chevron folds developed as an anticline-syncline pair (i.e. from beds folded when right-way up) and that the beds became overturned due to the accommodation of south-direction shear deformation (Sanderson, 1979; Lloyd & Whalley, 1986; 1997).

### **Shortening estimates**

It was not possible to estimate the minimum shortening accommodated by the ‘inclined’ chevron folds as there is no fold train. Instead, a simple line length analysis was undertaken in each fault block with shortening estimated from 15 laterally-continuous beds as 42-82 % (mean  $65.7 \pm 15.4$  %; Fig. 4.27a). These values are somewhat inconsistent with the Sanderson (1979) 50 % shortening estimate between Widemouth and Saltstone, which includes the Wanson Mouth foreshore. The shortening estimates are much higher than those estimated using the same method from six beds in Black Rock dip section A-A’ with 27-42 % (mean  $33.8 \pm 5.6$  %; Fig. 4.18a; see Section 4.5.1). This suggests that the shortening was enhanced immediately south of the WSF and consequently, that local shortening variations are large. Thus, Sanderson’s 50 % shortening value should be treated with caution.

### **Important faults**

The important faults observed in dip section A-A’ (Fig. 4.27a; see gusset) include:

1. The Wanson North Fault (WNF; SS19580131-SS19320142);
2. The Widemouth South Fault (WSF; SS19630143-SS19430159);
3. A fault that cuts obliquely across the foreshore, here termed the oblique fault, which is truncated just south of the WSF (SS19590145-SS19400139; oriented: 068/74NW);
4. A fault, here termed fault A (SS19550135-SS19340146; oriented: 108/63N), which is 30 m north of the WNF.

The four faults truncate the steeply north-dipping beds (Fig. 4.27a) and two major fault blocks are recognised in the foreshore outcrop (see gusset). In the southern fault block between the WNF and fault A, only steeply north-dipping beds were observed. Fault A truncated the steeply north-dipping beds on the limb of the ‘inclined’ chevron anticline.

The ‘inclined’ chevron fold pair and oblique fault are in the northern fault block between fault A and the WSF (Fig. 4.27a). The oblique fault has a general strike trend of 070°-250° (see gusset), dips steeply to the NW, cuts through the overturned steeply north-dipping stratigraphy and causes bed truncation. This suggests that the oblique fault occurred after ‘inclined’ chevron folding. However, as it was difficult to correlate the strata across the faults, the oblique fault may be either a normal fault or high-angle reverse fault. Enfield et al (1985) described this fault as a thrust, which had a “southerly sense of over-thrusting” that produced “folds with a southerly vergence” (i.e. the periclinal fold pair in section 4.4.2; see Fig. 4.17).



## **Restoration of the structures**

To describe the progression of deformation in the Wanson Mouth foreshores, two models have been developed. One model follows a restoration sequence where the faults in the foreshore are ‘late’ (i.e. after ‘inclined’ chevron folding; after Freshney et al, 1972; Figs. 4.27a-d), whilst the other model has a restoration sequence where the faults occur prior to folding (after Enfield et al, 1985; Figs. 4.27d & 4.27e-f). The two restoration sequence models are described in Section 4.6 and are applied to the structural restoration ‘steps’ of this dip section.

### **4.6.2 Wanson Mouth Dip-section B-B’**

The 160 m long Wanson Mouth dip section B-B’ (Fig. 4.28a) is oriented 010°-190° (SS19510152-SS19450134; see gusset & Fig. 4.15 for location) and lies across the Wanson Mouth foreshore in areas A4, A5 and A6 (Fig. 4.15). The dip section includes a generally steep north-dipping overturned succession of Crackington Formation turbidite beds (Fig. 4.28a; see gusset), as described by Melvin (1986).

#### **‘Inclined’ chevron folds**

The dominant structure shown in dip section B-B’ is an ‘inclined’ chevron fold pair in profile (Fig. 4.28a) that deformed the beds in the foreshore succession, causing the beds on the long limbs to be overturned and dip steeply to the north. In contrast, the beds on the short limbs remain the right way-up albeit with a shallow northwards dip (~ 30°N). This suggests that the ‘inclined’ chevron folds developed as an anticline-syncline pair (i.e. from beds folded when right-way up) and that the beds became overturned due to the accommodation of south-direction shear deformation (Sanderson, 1979; Lloyd & Whalley, 1986; 1997).

#### **Shortening estimates**

It was not possible to estimate the minimum shortening accommodated by the ‘inclined’ chevron folding as there is no fold train. Instead, a simple line length analysis was undertaken in each fault block with shortening estimated from 18 laterally-continuous beds as 38-64 % (mean  $49.8 \pm 10.7$  %; Fig. 4.28a). These values are consistent with the Sanderson (1979) 50 % shortening estimate between Widemouth and Saltstone, which includes the Wanson Mouth foreshore. However, the shortening estimates are much higher than those estimated using the same method from seven beds in Black Rock dip section B-B’ of 20-39 % (mean  $30.5 \pm 5.0$  %; Fig. 4.19a; see Section 4.5.2), but slightly lower than those for the Wanson Mouth dip section A-A’ (Fig. 4.27a; see Section 4.6.1). This suggests that the shortening was enhanced immediately south of the WSF and consequently, that local shortening variations are large. Thus, Sanderson’s 50 % shortening value should be treated with caution.

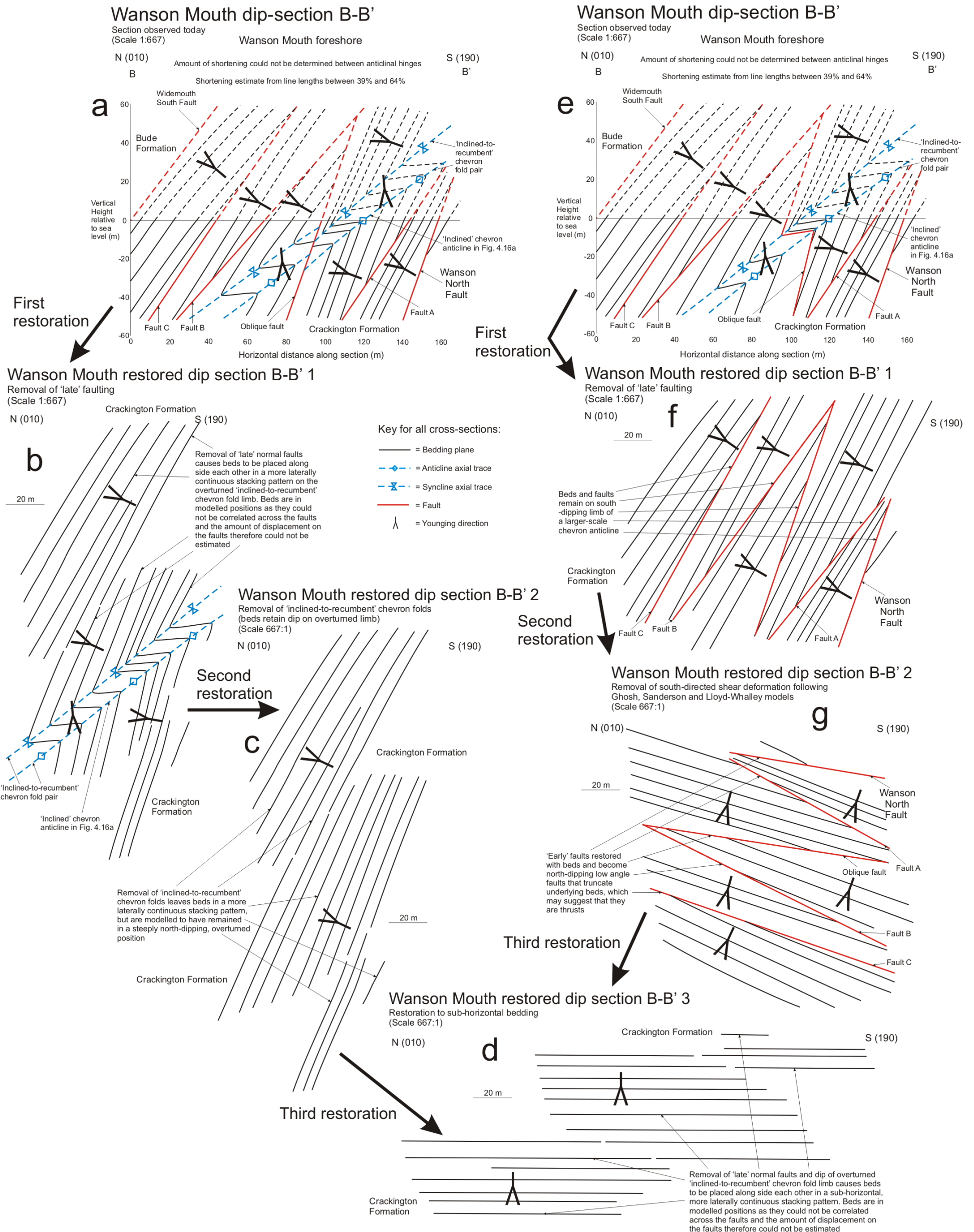


Fig. 4.28: Sections drawn across the Wanson Mouth foreshore (SS19510152-SS19450134; see gusset), showing the evolution of Variscan structures. In the 'late' fault model, the restoration sequence is: (a) Dip-section B-B'; (b) Restored dip-section B-B' 1 (removal of 'late' faulting); (c) Restored dip-section B-B' 2 (removal of 'inclined' chevron folding); and (d) Restored dip-section B-B' 3 (removal of overturned northwards-dipping beds). In the pre-folding fault model, the restoration sequence is: (e) Dip-section B-B'; (f) Restored dip-section B-B' 1 (removal of 'inclined' chevron folding); (g) Restored dip-section B-B' 2 (removal of overturned northwards-dipping beds); and (d) Restored dip-section B-B' 3 (removal of faulting)

### **Important faults**

The important faults observed in dip section B-B' (Fig. 4.28a; see gusset) are:

1. The WNF (SS19580131-SS19320142), as described in dip-section A-A' (Fig. 4.27a);
2. The WSF (SS19630143-SS19430159), as described in dip-section A-A' (Fig. 4.27a);
3. The oblique fault (SS19590145-SS19400139; oriented: 068/74NW), as described in dip-section A-A' (Fig. 4.27a), but which is in the central foreshore in this dip section;
4. Fault A (SS19550135-SS19340146; oriented: 108/63N), which is 20 m north of the WNF and is described in dip-section A-A' (Fig. 4.27a);
5. A fault, here termed fault B (SS19520144-SS19380147; oriented: 093/47N), which is 30 m to the north of the oblique fault;
6. Another fault, here termed fault C (SS19550146-SS19380151), which is inferred from differently oriented beds either side of a sand-filled gully, which is 40 m south of the WSF.

The six faults truncate the steep north-dipping beds (Fig. 4.28a), forming five fault blocks in this part of the foreshore (see gusset). The 'inclined' chevron fold pair was cut by the oblique fault between faults A and B (Fig. 4.28a). In the other four fault blocks, only steeply north-dipping beds are observed. The apparent dip of the steep north-dipping beds and that of the WSF in dip-section B-B' (Fig. 4.28a) cause them to appear sub-parallel to each other.

### **Restoration of the structures**

To describe the progression of deformation in the Wanson Mouth foreshores, two models have been developed. One model follows a restoration sequence where the faults in the foreshore are 'late' (i.e. after 'inclined' chevron folding; after Freshney et al, 1972; Figs. 4.28a-d), whilst the other model has a restoration sequence where the faults occur prior to folding (after Enfield et al, 1985; Figs. 4.28d & 4.28e-g). The two restoration sequence models are described in Section 4.6 and are applied to the structural restoration 'steps' of this dip section.

#### **4.6.3 Wanson Mouth Dip-section F-F'**

The 220 m long Wanson Mouth dip-section F-F' (Fig. 4.29a) is oriented 010°-190° (SS19440158-SS19390136; see gusset & Fig. 4.15 for location) and lies across the Wanson Mouth foreshore in areas A4, A5 and A6 (Fig. 4.15). The dip section includes a generally steep north-dipping overturned succession of Crackington Formation turbidite beds (Fig. 4.29a; see gusset), as described by Melvin (1986).

### **Fold deformation**

The dominant feature shown in dip section F-F' is the steeply north-dipping beds (Fig. 4.29a) on the overturned limb of the 'inclined' chevron syncline. The oblique fault is not present in the foreshore along the dip section F-F' line (Fig. 4.29a), but is found cutting the beds to the

west of the dip section (see gusset). Decametre-long splay faults and periclinal fold pairs occur where changes occur in the oblique fault orientation as shown in dip section F-F'. A schematic map in Fig. 4.17 shows the fault-fold relationship with the oblique fault in this example at SS19400142 in area A5 (Fig. 4.15; see gusset; see Section 4.4.2). The synform in this example is described in a stereonet (Fig. 4.16c) from Section 4.4.2, with the profile plane oriented 013/68E; and axial plane oriented 105/88S (Fig. 4.16c). This periclinal fold pair developed on the overturned long limbs of the 'inclined' chevron folds and have overturned-to-upside down younging directions, suggesting that the folds developed as an antiform-synform pair (i.e. from beds folded when overturned). This is consistent with the observations of "folds with a southerly vergence" (i.e. the periclinal fold pair in Fig. 4.17) by Enfield et al (1985).

### **Shortening estimates**

It was not possible to estimate the minimum shortening accommodated by the 'inclined' chevron folding as there is no fold train. Instead, a simple line length analysis was undertaken in each fault block with shortening estimated from 15 laterally-continuous beds as 31-76 % (mean  $49.2 \pm 17.7$  %; Fig. 4.29a). These values are consistent with the Sanderson (1979) 50 % shortening estimate between Widemouth and Saltstone, which include the Wanson Mouth foreshore. Also, the shortening estimates are much higher than those estimated using the same methods from six beds in Black Rock dip section F-F' with 28-34 % (mean  $31.6 \pm 1.8$  %; Fig. 4.20a; see Section 4.5.3). Furthermore, the estimates are similar to those for Wanson Mouth dip section B-B' (Fig. 4.28a; see Section 4.6.2), but slightly lower than those for the Wanson Mouth dip section A-A' (Fig. 4.27a; see Section 4.6.1). This suggests that the shortening was enhanced immediately south of the WSF and consequently, that local shortening variations are large. Thus, Sanderson's 50 % shortening value should be treated with caution.

### **Important faults**

The important faults observed in dip section F-F' (Fig. 4.27a; see gusset) are described in section B-B' (Fig. 4.28a) and are: (1) the WNF (SS19580131-SS19320142); (2) the WSF (SS19630143-SS19430159); (3) the oblique fault (SS19590145-SS19400139), which is above the foreshore in this section; (4) fault A (SS19550135-SS19340146), which is 30 m north of the WNF; (5) fault B (SS19520144-SS19380147); and (6) fault C (SS19550146-SS19380151).

The faults, including the WSF, truncate the steeply north-dipping beds (Fig. 4.29a), forming five fault blocks in this part of the foreshore outcrop (see gusset). There is a minor decametre-long fold pair causing local perturbation of the generally steeply north-dipping beds within the fault block between fault A and fault B (Fig. 4.29a; see gusset). In the other four fault blocks, only steeply north-dipping beds were observed (Fig. 4.29a).

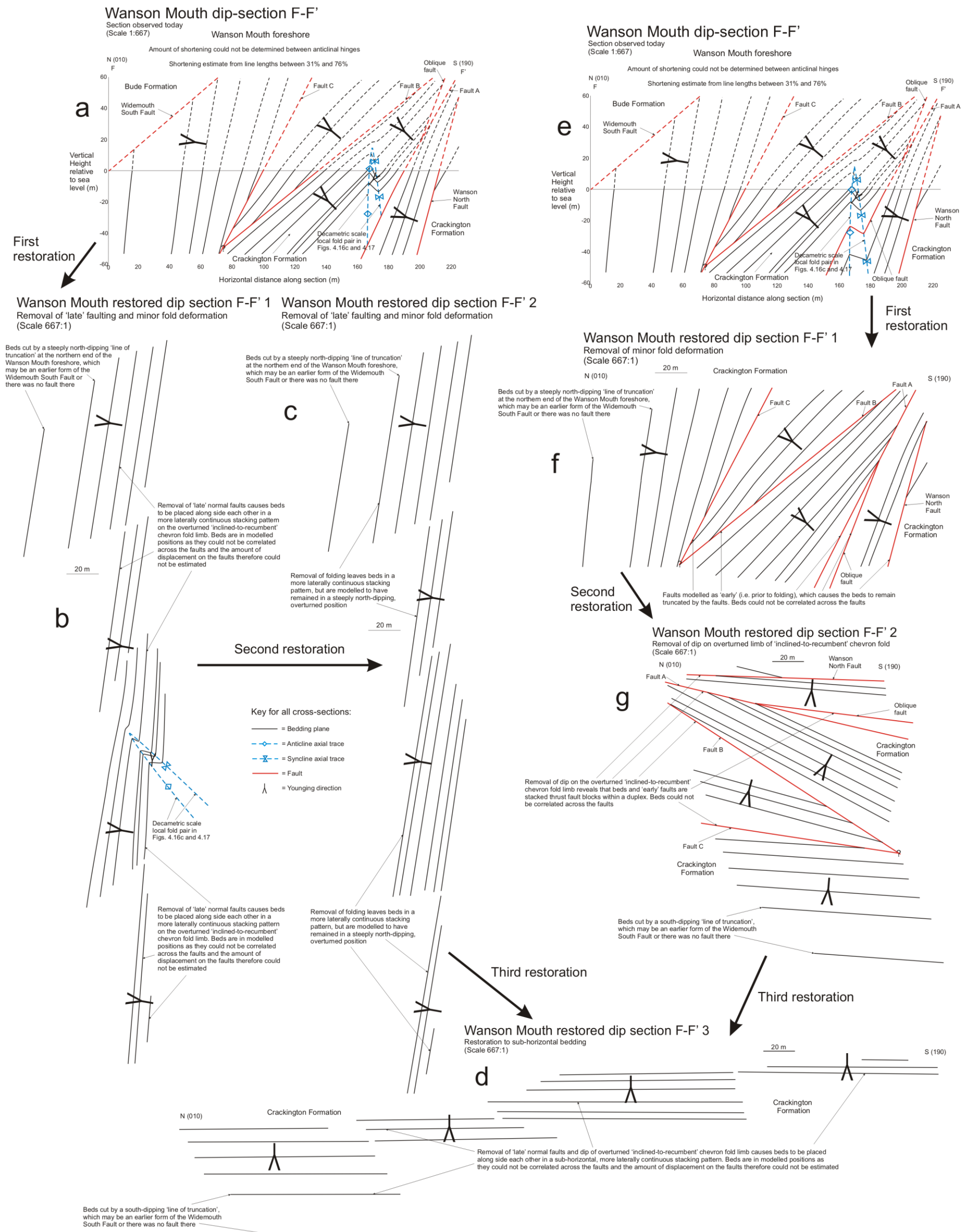


Fig. 4.29: Sections drawn across the Wanson Mouth foreshore (SS19440158-SS19390136; see gusset), showing the evolution of Variscan structures. In the 'late' fault model, the restoration sequence is: (a) Dip-section F-F'; (b) Restored dip-section F-F' 1 (removal of 'late' faulting); (c) Restored dip-section F-F' 2 (removal of folding); and (d) Restored dip-section F-F' 3 (removal of overturned northwards-dipping beds). In the pre-folding fault model, the restoration sequence is: (e) Dip-section F-F'; (f) Restored dip-section F-F' 1 (removal of folding); (g) Restored dip-section F-F' 2 (removal of overturned northwards-dipping beds); and (d) Restored dip-section F-F' 3 (removal of faulting)

## **Restoration of the structures**

To describe the progression of deformation in the Wanson Mouth foreshores, two models have been developed. One model follows a restoration sequence where the faults in the foreshore are ‘late’ (i.e. after ‘inclined’ chevron folding; after Freshney et al, 1972; Figs. 4.29a-d), whilst the other model has a restoration sequence where the faults occur prior to folding (after Enfield et al, 1985; Figs. 4.28d & 4.28e-g). The two restoration sequence models are described in Section 4.6 and can be applied to the structural restoration ‘steps’ of this dip section. In the restorations of dip section F-F’, the decametric-scale periclinal fold pair (see Fig. 4.17) is removed in the same restorations as the ‘inclined’ chevron folding (Figs. 4.29c & g).

### **4.6.4 Justification for construction of an oblique section**

The dip and restored dip sections (Figs. 4.27-4.29) in the Wanson Mouth foreshore show that the oblique fault moved at an angle to the dip section orientation and thus, accommodated at least some out-of-section movement. In order to describe this movement, an oblique section H-H’ (Fig. 4.30) has been drawn at an angle to the dip sections and sub-perpendicular to the strike of the oblique faults. This oblique section does not continue to the NW over the WSF into the Bude Formation beds because the section has been drawn to study the deformation in the Wanson Mouth foreshore and also the Black Rock outcrops are below the low tide mark and therefore inaccessible to study.

### **4.6.5 Wanson Mouth Oblique section H-H’**

The 250 m long Wanson Mouth oblique section H-H’ (Fig. 4.30a) is oriented 135°-315° (SS19480154-SS19580130; see gusset & Fig. 4.15 for location) and lies across the Wanson Mouth foreshore in areas A4, A5 and A6 (Fig. 4.15). The oblique section is at an angle of 35° anti-clockwise to the Wanson Mouth dip sections and thus, many of the dips are apparent (i.e. less than true dip). Oblique section H-H’ is bounded to the NW by the Widemouth South Fault (WSF) and to the SE by the Wanson North Fault (WNF) in the cliff in the southern Wanson Mouth foreshore (see gusset). It includes a succession of Crackington Formation turbidite beds (Fig. 4.30a; see gusset), as described by Melvin (1986).

### **‘Inclined’ chevron folds**

The dominant structure shown in oblique section H-H’ is an ‘inclined’ chevron fold pair in profile (Fig. 4.30a) as described in the dip sections (Figs. 4.27a, 4.28a & 4.29a), causing the beds on its long fold limbs to be overturned and dip steeply to the north. In contrast, the beds on the short fold limbs remain the right way-up albeit with a shallow (~ 30°N) northwards dip. This suggests that the ‘inclined’ chevron folds developed as an anticline-syncline pair (i.e. from beds folded when right-way up) and that the beds became overturned due to the accommodation of south-directed shear deformation (Sanderson, 1979; Lloyd & Whalley, 1986; 1997).

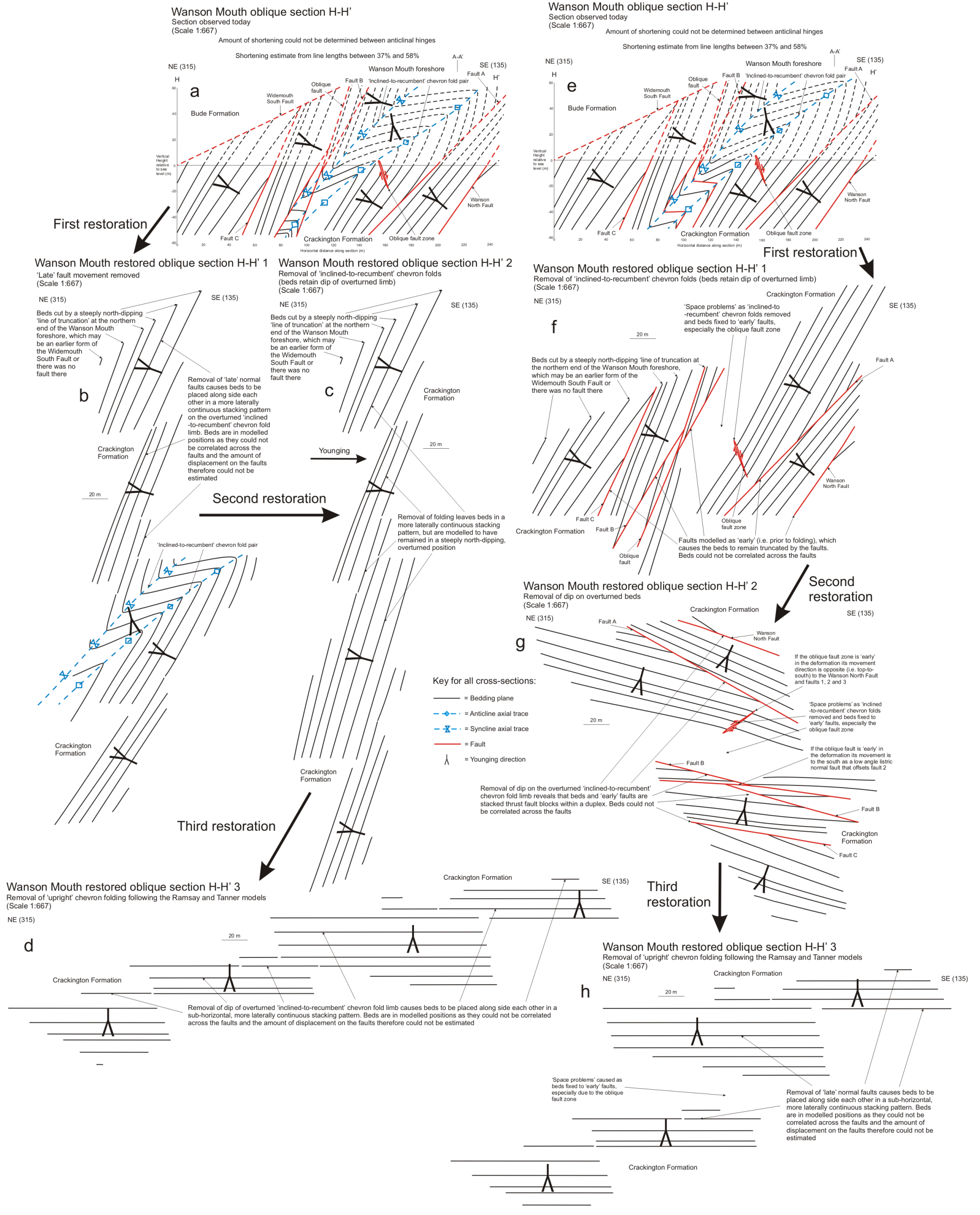


Fig. 4.30: Sections drawn across the Wanson Mouth foreshore (SS19480154-SS19580130; see gusset), showing the evolution of Variscan structures. In the 'late' fault model, the restoration sequence is: (a) Oblique-section H-H'; (b) Restored oblique-section H-H' 1 (removal of 'late' faulting); (c) Restored oblique-section H-H' 2 (removal of 'inclined' chevron folding); and (d) Restored oblique-section H-H' 3 (removal of overturned northwards-dipping beds). In the pre-folding fault model, the restoration sequence is: (e) Oblique-section H-H'; (f) Restored oblique-section H-H' 1 (removal of 'inclined' chevron folding); (g) Restored oblique-section H-H' 2 (removal of overturned northwards-dipping beds); and (h) Restored oblique-section H-H' 3 (removal of faulting)

### **Shortening estimates**

It was not possible to estimate a minimum shortening accommodated by the ‘inclined’ chevron fold deformation as there is no fold train. Also, as the section is oblique to the main north-south tectonic direction (i.e. of the dip sections and Sanderson (1979)), a simple line length analysis would provide an underestimated shortening value for the foreshore succession. Therefore, a direct comparison cannot be made with the results from either the dip sections or Sanderson (1979), and so the shortening estimates for the oblique section are not provided.

### **Important faults**

There are six faults in oblique section H-H’ (Fig. 4.30a; see gusset), all of which are described in dip section B-B’ (Fig. 4.28a) and are: (1) the WNF (SS19580131-SS19320142); (2) the WSF (SS19630143-SS19430159); (3) the oblique fault (SS19590145-SS19400139); (4) fault A (SS19550135-SS19340146), which is 40 m north of the WNF; (5) fault B (SS19520144-SS19380147); and (6) fault C (SS19550146-SS19380151).

A minor oblique fault zone has also been observed in the foreshore (SS19540138-SS19570141), which is 50 m long, strikes ENE-WSW and has accommodated sinistral transtensional movement (King, 1967). The fault zone cuts the ‘inclined’ chevron folded beds in the foreshore outcrop across the oblique section (Fig. 4.30a) and has possibly accommodated extensional movement. The oblique fault zone orientation in the foreshore varies along its strike, with the SW tip oriented 064/71S; and the NE tip oriented 056/85NW, as shown in a stereonet from Fig. 4.16a (see Section 4.4.2; see gusset).

The six faults and oblique fault zone truncate the steeply north-dipping beds (Fig. 4.30a), forming five fault blocks in the foreshore (see gusset). The ‘inclined’ chevron fold pair has been cut by the oblique fault between fault B and fault C and also, by the oblique fault zone between fault A and fault B (Fig. 4.30a). In the other fault blocks, only steeply north-dipping beds were observed.

### **Restoration of the structures**

To describe the progression of deformation in the Wanson Mouth foreshores, two models have been developed. One model follows a restoration sequence where the faults in the foreshore are ‘late’ (i.e. after ‘inclined’ chevron folding; after Freshney et al, 1972; Figs. 4.28a-d), whilst the other model has a restoration sequence where the faults occur prior to folding (after Enfield et al, 1985; Figs.4.28e-h). The two restoration sequence models are described in Section 4.6 and can be applied to the structural restoration ‘steps’ of this oblique section. However, it should be noted that many of the dips are apparent (i.e. less than true dip). Also, in the restorations of oblique section H-H’, the oblique fault zone is removed in the same restorations as the other faults (Figs. 4.28b & h), causing ‘space problems’ if the oblique fault zone was present prior to the chevron folding as the beds cannot be restored next to each other.

#### 4.6.6 Evolution of the Widemouth South Fault (WSF)

The Widemouth South Fault (WSF) has juxtaposed the Black Rock and Wanson Mouth foreshores and no structures or beds cross the fault. From analysis of the BGS sedimentary logs (Freshney et al, 1979; Fig. 4.2), the strata either side of the WSF are separated by about 300 m. The orientations of the WSF and possible earlier forms of this fault are described in the dip-section and oblique-section descriptions for both foreshores.

One possible model highlighted in the section descriptions assumes that the WSF was present prior to the chevron folding found in both foreshores. However, in this model, the 'line of truncation' changes its orientation from restoration-to-restoration. Furthermore, there are often differences in the orientations of possible earlier forms of the WSF when the truncation lines are compared for each of the restored matching pairs of dip sections from the two foreshores. Good examples of these differences are:

1. The steep southwards dip of the 'line of truncation' in the Black Rock restored dip section B-B' 3 (Fig. 4.19d; see Section 4.5.2) compared to it being sub-horizontal in the Wanson Mouth restored dip section B-B' 3 (Fig. 4.28d; see Section 4.6.2);
2. The steep northwards dip of the 'line of truncation' in the Black Rock restored dip section F-F' 2 (Fig. 4.20c; see Section 4.5.3) compared to it having a steep southwards dip in the Wanson Mouth restored dip section F-F' 3 (Fig. 4.29d; see Section 4.6.3).

The other possible model for the WSF is that the fault is a 'late' structure that truncated the beds after chevron fold deformation (Freshney et al, 1972) and that no fault existed prior to this 'late' movement, allowing the beds in each foreshore succession to be laterally-continuous at their respective stratigraphic levels. As no beds or structures cross the WSF, the amount of vertical displacement accommodated on the WSF during this deformation must have been greater than the wavelength of the folds in both foreshore successions. The stratigraphic displacement on the WSF is 300 m (Freshney et al, 1979; Fig. 4.2). This is much greater than the tens of metres of extensional movement interpreted across individual 'late' normal faults in all the coastal outcrops between Widemouth and Rusey by Freshney et al (1972).

#### Comparison of the shortening estimates and fold envelopes across the WSF

There are significant differences in the degrees of shortening accommodated either side of the WSF in each foreshore section. In the Black Rock foreshore, the mean percentage shortening estimate is consistently around 33 %, whilst in the Wanson Mouth foreshore, although less accurate, the estimates are approximately between 50 % and 65 %. Thus, the mean percentage shortening accommodated to the south of the WSF is 1.67 to twice that to north of the WSF. This work has also shown that across the foreshores local variations in shortening are large. Sanderson's 50 % shortening estimate between Widemouth and Saltstone does not take into account these local variations and so should be treated with caution.

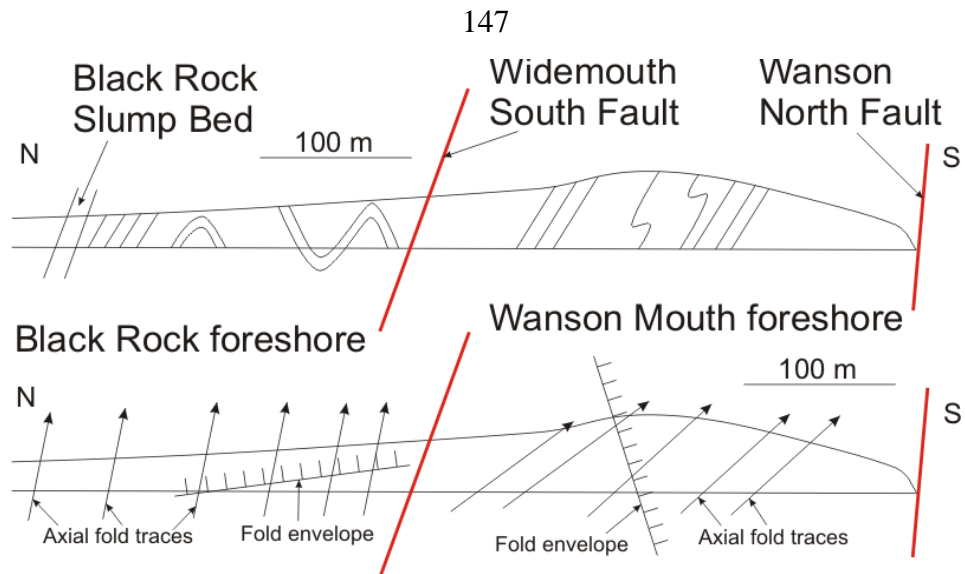


Fig. 4.31: The Black Rock and Wanson Mouth foreshore sections with a representation of the folding in the cliffs in the upper profile and the mean orientation of the fold envelope (stippled line) in the lower profile (modified from Sanderson, 1979)

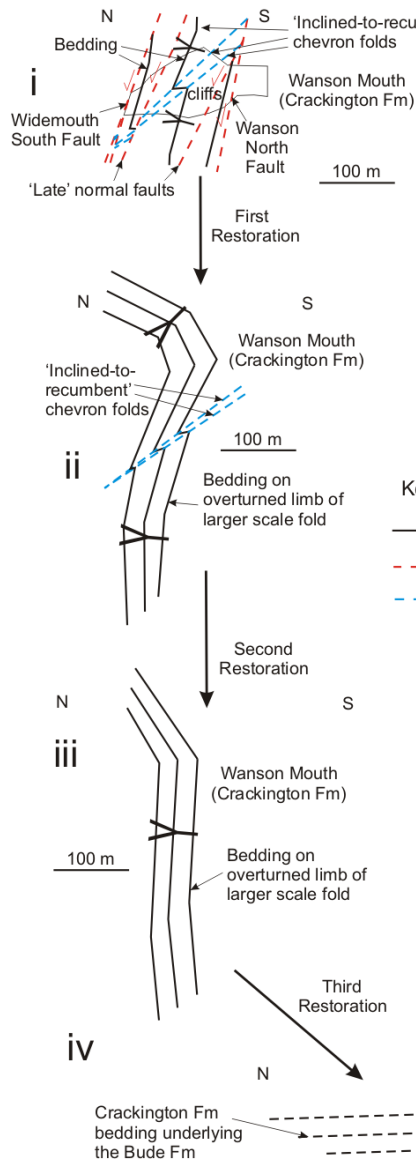
Another aspect of the deformation across the WSF concerns the different orientations of the fold envelopes for the chevron folds in the foreshore successions (Fig. 4.31). The ‘upright’ chevron folds in the Black Rock foreshore have a sub-horizontal fold envelope, whilst the ‘inclined’ chevron folds in the Wanson Mouth foreshore have a steep southwards dipping fold envelope. The orientations of the envelopes given here are consistent with those determined by Sanderson (1979) for the two foreshore successions (Fig. 4.31).

One possible explanation for the large difference in the shortening estimates and fold envelope orientations across the WSF is that the two successions were folded at different structural ‘levels’ and then, juxtaposed after the chevron folding that caused the shortening, as described in the Freshney et al (1972) model. Alternatively, the beds may have been deformed in the same location but with increased shortening in the Wanson Mouth succession due to the accommodation of a greater component of shear deformation, causing tighter folds and less steep axial planes, as described by Sanderson (1979). This issue will be discussed in section 4.7.

#### 4.6.7 Summary of the geological evolution of the Wanson Mouth foreshore

The restoration of the deformation in the Wanson Mouth foreshore reveals that several progressive ‘stages’ of geological evolution took place (Figs. 4.32a-b). Although structures are distinguished, the Variscan deformation is viewed as being progressive (Freshney et al, 1972; Enfield et al, 1985). Importantly, it does not appear that any ‘early’ structures occurred that meet the criteria of Mapeo and Andrews (1991), Zoetemeijer et al (1992), Nigro and Renda (2004) and Corredor et al (2005) (see Section 4.5 & Fig. 4.11). Due to the difficulty of correlating the beds across the faults in the Wanson Mouth foreshore, two alternate models for its structural restoration have been developed by Freshney et al (1972) and Enfield et al (1985). Both of these models are discussed further in section 4.7, where both foreshores are considered.

### A - Freshney et al (1972) Widemouth South normal fault model



### B - Enfield et al (1985) thrust duplex model

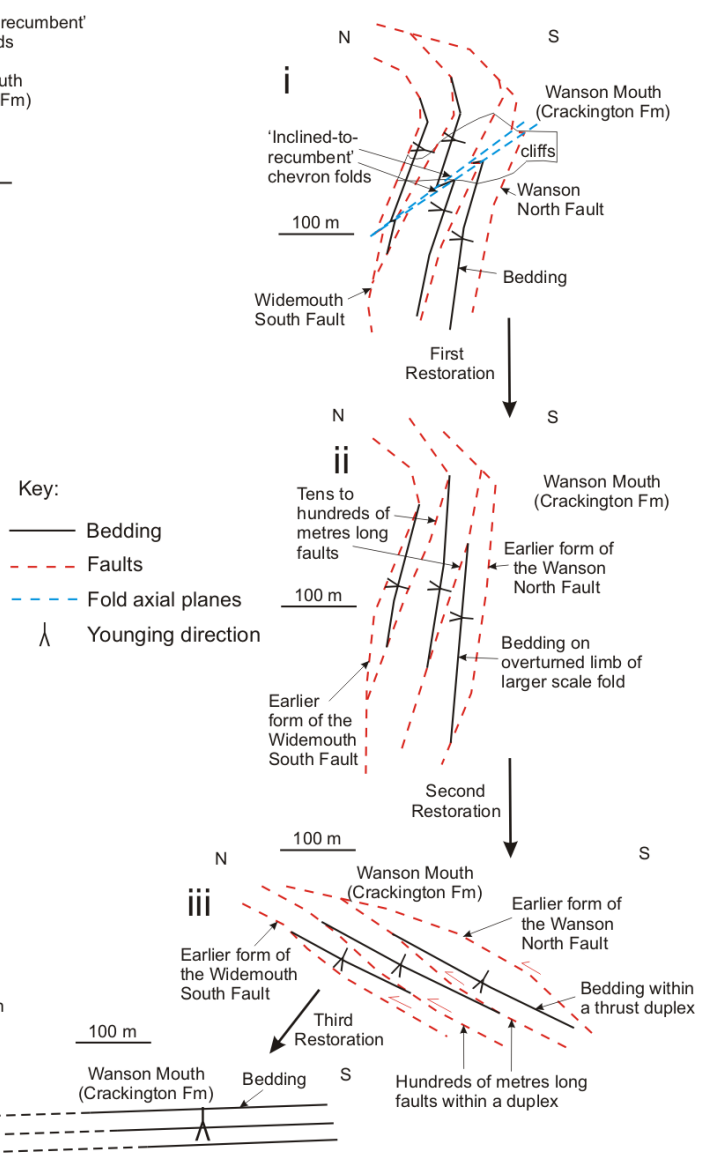


Fig. 4.32: Schematic section diagrams showing progressive deformation restoration in the Wanson Mouth foreshore succession: (a) Restorations following the Freshney et al (1972) 'late' normal fault model: (i) Present situation; (ii) 'Late' faulting removed; (iii) 'Unfolding' chevron folds to overturned steep north-dipping beds; and (iv) Beds restored to right-way up, sub-horizontal; and (b) Restorations following the Enfield et al (1985) inverted thrust duplex model: (i) Present situation; (ii) 'Unfolding' chevron folds to overturned steep north-dipping beds and faults; (iii) Restoration of beds and faults to a north-directed thrust duplex; and (iv) Removal of faults with beds restored to right-way up, sub-horizontal

The 'late' normal fault model (Freshney et al, 1972) proposed that the steep north-dipping faults cut the 'inclined' chevron fold pair (Figs. 4.27a-b, 4.28a-b, 4.29a-b, 4.30a-b & 4.32a (i-ii)). In the first restoration 'step', the 'late' faults are removed to leave the steep north-

dipping beds on the limbs of the ‘inclined’ chevron fold pair. In the second restoration ‘step’, the ‘inclined’ chevron folds are removed and the beds retain their overturned steep northwards dip (Figs. 4.27c, 4.28c, 4.29c, 4.30c & 4.32a (iii)). This did not involve the Ghosh (1966), Sanderson (1979) and Lloyd and Whalley (1986; 1997) models (see Section 4.1.3), where removing the ‘inclined’ chevron folds would cause the deformed beds to be placed onto the south-dipping limb of a larger-scale ‘upright’ chevron fold. This omission is because it has yet to be demonstrated conclusively that an ‘upright’ chevron fold occurred on a larger-scale than the Wanson Mouth foreshore despite large-scale folds appearing in other Culm Basin cross-sections. The third restoration ‘step’ removes the overturned steep northwards bedding dip to a right way-up, sub-horizontal bedding pattern after Crackington Formation deposition (Figs. 4.27d, 4.28d, 4.29d, 4.30d & 4.32a (iv)).

The inverted thrust duplex model (Enfield et al, 1985) proposed that the steep north-dipping faults in the foreshore sit either on the overturned limbs of an ‘inclined’ chevron fold pair (Fig. 4.27a, 4.28e, 4.30e & 4.32b (i)) or have been deformed by a local fold pair (see Fig. 4.29e). The first restoration ‘step’ removes the ‘inclined’ chevron fold pair (Fig. 4.27e, 4.28f, 4.30f & 4.32b (ii)) and the local fold pair (see Fig. 4.29f), whilst the beds retain their overturned steep northwards dip. This restoration does not involve the Ghosh (1966), Sanderson (1979) and Lloyd and Whalley (1986; 1997) models for the same reason in the ‘late’ fault model (see Section 4.1.3). The second restoration ‘step’ returns the overturned steep northwards bedding dip to a right way-up bedding pattern, causing the faults to become shallow south-dipping (Figs. 4.27f, 4.28g, 4.29g, 4.30g & 4.32b (iii)), which can be interpreted as north-directed imbricate thrusts within a duplex. Enfield et al (1985) (Fig. 4.7) envisaged that this thrusting emplaced the Crackington Formation onto the Bude Formation. The third restoration ‘step’ (Figs. 4.27d, 4.28d, 4.29d, 4.30d & h and 4.32b (iv)) removes the north-directed faults and places the beds into a right way-up, sub-horizontal bedding pattern after Crackington Formation deposition.

## 4.7 Discussion

This chapter has reviewed the current literature on the stratigraphy of the Bude and Crackington formations from Freshney et al (1979) and where the Black Rock and Wanson Mouth foreshores sit relatively within this stratigraphy. Further reviews related to:

1. The map work of King (1967) and the structural features described in his map;
2. Models for the progressive deformation of the chevron folds in the Culm Basin, with a critical review of the Sanderson (1979) and Lloyd and Whalley (1986; 1997) models;
3. How the different structures have become juxtaposed across the Widemouth South Fault, (WSF) with descriptions of four models for its development (Williams et al, 1970; Freshney et al, 1972; Durrance, 1985; Enfield et al, 1985; Figs. 4.6-4.9), in order to clarify aspects of the geological evolution in both foreshores.

There followed an analysis of the sedimentary data collected in both foreshore successions and the correlation of the laterally-continuous beds in the Black Rock foreshore in order to aid the geological mapping. This led to an examination of the structures from both foreshore successions as presented in the map and then in dip, strike and oblique sections.

In this discussion, the map work and structural data from King (1967) (Fig. 4.3) are compared with that produced in this study using dip-section F-F' across both successions (Fig. 4.32). Using the results of this comparison, the models from Section 4.1.4 are combined with the mapping and structural data from this work in order to:

1. Compare models for the progressive Variscan deformation of the two foreshores based upon the models of Freshney et al (1972) and Enfield et al (1985);
2. Propose a new model for the Black Rock-Wanson Mouth foreshore structures that can be applied to the Bude Formation and beyond, throughout the Culm Basin.

This is followed by a comparison of three models for the evolution of the Widemouth South Fault (WSF) using restored sections developed from those in Sections 4.5 and 4.6:

1. Widemouth South 'late' normal fault model (Freshney et al, 1972);
2. Inverted thrust duplex model (Enfield et al, 1985);
3. Hypothetical inverted Widemouth South Fault model, from this work.

The discussion continues by considering the relevance of the Durrance (1985) model for the WSF beneath the Crediton Trough and the Thompson and Cosgrove (1996) model for the Rusey Fault to explain the evolution of the WSF. Lastly in this discussion, there is a consideration of the strain accommodated in both foreshore successions.

#### **4.7.1 Comparison of the King (1967) map with that of the author**

King (1967) undertook geological mapping in the Black Rock and Wanson Mouth foreshores as part of a wider project to correlate the coastal outcrops of the Bude Formation. At the time, the chevron-folded Bude Formation was thought to be structurally continuous and relatively simple. However, from the King (1967) mapping (Fig. 4.3), which is shown in Freshney et al (1972), it was recognised that the outcrops were geologically complex.

The geological mapping of the Black Rock-Wanson Mouth successions in this study (see gusset) covers the southern-most part of the King (1967) map (Fig. 4.3) and included collecting additional structural and sedimentary data to augment that of King (1967). A comparison of the two maps shows consistency in the measurements and the positions of the major features (e.g. the Black Rock Slump Bed and WSF). However, due to 'geological complexity', large areas have been left 'blank' on the King (1967) map (Fig. 4.3), but which the present mapping and structural analysis has revealed contain structural features that are important to interpreting the geological evolution of the Black Rock-Wanson Mouth foreshores.



(Fig. 4.33) to be interpreted. An important feature is the WSF that separates the two foreshores. Unfortunately, King (1967) did not provide structural data for any faults mapped in Fig. 4.3 and consequently these faults are modelled on the King dip section as being vertical (Fig. 4.33b).

In the Black Rock foreshore (left hand side of Figs. 4.33a & b), the structures include ‘upright’ chevron anticline 1 with the Black Rock Slump Bed on the north-dipping limb and the WSF cross-cutting the south-dipping limb (see gusset). The anticline is projected above the foreshore using the shale beds to constrain the fold geometry. In the King (1967) map (Fig. 4.3), three shale beds are recognised stratigraphically above the Black Rock Slump Bed and the present work also recognises six shale beds stratigraphically below the slump bed (see sections 4.3 to 4.6). Using the two maps (Fig. 4.3; see gusset) and dip sections (Fig. 4.33), a better constraint can be placed upon structures in the Black Rock foreshore.

An important contradiction between the two maps (see gusset; Fig. 4.3) involves two faults in the King (1967) dip-section (Fig. 4.33b) that are shown to cut periclinal fold pair 7 on the north-dipping limb of ‘upright’ chevron anticline A (boundary of areas A1 & A3; Figs. 4.3 & 4.15; see gusset). In this present study, no faults were observed to cut fold pair 7, which was refolded by ‘upright’ chevron anticline A at SS19450167 (see sections 4.4.1 & 4.5.2; Fig. 4.19).

In the Wanson Mouth foreshore (right hand sides of Figs. 4.33a-b), the steeply north-dipping Crackington Formation beds are truncated against steeply north-dipping faults. In the King (1967) dip section (Fig. 4.33b), the northern part of the Wanson Mouth foreshore has been left as an area of ‘structural complexity’ (area A4 on the King map; Fig. 4.3) with no data presented. In this work, the dip-section (Fig. 4.33a) contains steeply north-dipping beds in area A4 (Fig. 4.15; see gusset) that are truncated against the steeply north-dipping faults.

In the central and southern Wanson Mouth foreshore (area A5 on the King map; Fig. 4.3), the King (1967) dip section (Fig. 4.33b) includes steeply north-dipping beds that, again, are truncated against the faults but interspersed with areas of ‘geological complexity’. In this map work, the beds in the dip section (Fig. 4.33a) also dip steeply to the north in area A5 (Fig. 4.15; see gusset), but a fold pair is shown that is related to splay faults that coincide with the steeply NNW-dipping oblique fault (see Fig. 4.17). Although there are areas of ‘geological complexity’ marked in the King (1967) map (Fig. 4.3) and the resulting dip-section (Fig. 4.33b), the significant tectonic structures in both foreshores have been described. Significantly more structural data were added in this map work (see gusset), which allows the relative timings of the structures and their geometries in the foreshore successions to be understood better. One such set of deformation structures are the local ‘early’ structures in the Black Rock foreshore.

#### **4.7.2 Geological evolution of the Black Rock-Wanson Mouth foreshores**

To explain the presence of the structures observed in both the Black Rock and Wanson Mouth foreshores, three models have been considered. A discussion of the models is presented using the restorations for both foreshore successions (see sections 4.5 & 4.6; Fig. 4.34). In each

cross-section (Figs. 4.34a (i), b (i) & c (i)), the Black Rock foreshore has an ‘upright’ chevron fold train (Fig. 4.18a), whilst the Wanson Mouth foreshore has an ‘inclined’ chevron fold pair (Figs. 4.27a, 4.28a & 4.29a). The ‘inclined’ chevron fold pair has overturned steep north-dipping beds on the long limbs (Enfield et al, 1985), resulting from south-directed shear accommodation (Sanderson, 1979). Alternatively, this chevron fold pair may be ‘z-folds’ on the limb of a larger-scale fold. Also, from the sedimentary logs of Freshney et al (1979) (Fig. 4.2), there is a 300 m stratigraphic separation between the two foreshore successions across the WSF.

The series of restorations of the dip sections were described separately across both the Black Rock (Figs. 4.18-4.20) and Wanson Mouth foreshores (Figs. 4.27-4.29). The structural details vary between the restorations, but the final restoration in each case shows sub-horizontal beds with a stratigraphic separation of 300 m between the two formations across the Widemouth South Fault (WSF; Figs. 4.34a (iv), b (v) & c (v)). Also, the timing of chevron folding in each foreshore is not known relative to the other foreshore and so is treated separately in the model restorations. This was undertaken for practical reasons as the only demonstratable limit is that the Bude Formation deformation cannot be earlier than that in the Crackington Formation. Each model is reviewed using the dip sections and their restorations (see sections 4.5 & 4.6) with the restorations undertaken in steps for practicality and to make the structural relationships clear.

#### **Widemouth South ‘late’ normal fault model (Freshney et al, 1972)**

In the Freshney et al (1972) normal fault model (see Fig. 4.6), the WSF has been modelled as a ‘late’ normal fault that juxtaposed the Black Rock and Wanson Mouth foreshore successions after Variscan deformation (Fig. 4.34a (i)). This model appears to be plausible because the WSF truncates all structures on both sides with no correlation between the fold sets. Thus, the last displacement on the fault must have been greater than the wavelength of the folds.

The first restoration ‘step’ (Fig. 4.34a (ii)) removes the 300 m stratigraphic separation between the two foreshores (see Fig. 4.2), which occurred along the normal faults, including the WSF. The beds are restored to their pre-‘late’ normal fault positions without ‘space problems’ occurring. In the dip sections across both foreshores (Figs. 4.18-4.20 & 4.27-4.29), a ‘line of truncation’ appears along the course of the ‘late’ WSF and it is noted whether the restoration causes the beds to cross this line. Under the Freshney et al (1972) model, removing the faults and the stratigraphic separation would not generate a ‘line of truncation’. Consequently, the beds are modelled as being continuous in each foreshore (Fig. 4.34a (ii)). In this restoration ‘step’, the Black Rock foreshore succession has a separate ‘upright’ chevron fold train on the shallow north-dipping limb of a larger-scale fold, whilst the Wanson Mouth foreshore has a separate ‘inclined’ chevron fold pair on the southern limb of another larger-scale fold.

The second restoration ‘step’ (Fig. 4.34a (iii)) removes the ‘inclined’ chevron folding with the beds retaining their present overturned steep northwards dip across the Wanson Mouth foreshore (Fig. 4.34a (iii)). In the now separate Black Rock foreshore succession, the ‘upright’

chevron fold train is interpreted as being on the north-dipping limb of a larger scale ‘upright’ chevron anticline. Under the Freshney et al (1972) model, the foreshore successions have a stratigraphic separation of 300 m (Fig. 4.2), with their deformed beds continuing to be laterally continuous (Fig. 4.34a (iii)).

In the third restoration ‘step’ (Fig. 4.34a (iv)), the overturned, steep northwards dip of the beds return to right way-up, sub-horizontal orientations. The beds in each foreshore are shown as two layer-cake successions, separated by a stratigraphic distance of 300 m (Freshney et al, 1979; Fig. 4.2), and also, continue to be laterally continuous (Fig. 4.34a (iv)).

### **Inverted thrust duplex model (Enfield et al, 1985)**

In the Enfield et al (1985) thrust duplex model, the WSF and other faults in the Wanson Mouth foreshore have been viewed as an inverted thrust duplex that emplaced the Crackington Formation (Wanson Mouth) onto the Bude Formation (Black Rock) (Fig. 4.7). In this model, the vertical displacement on this duplex must have been 300 m or the stratigraphic separation between the successions from Freshney et al (1979) (Fig. 4.2), with the WSF and WNF (Wanson North Fault) forming the ‘sole’ and ‘roof’ thrusts to the duplex (Figs. 4.7 & 4.34b (i)).

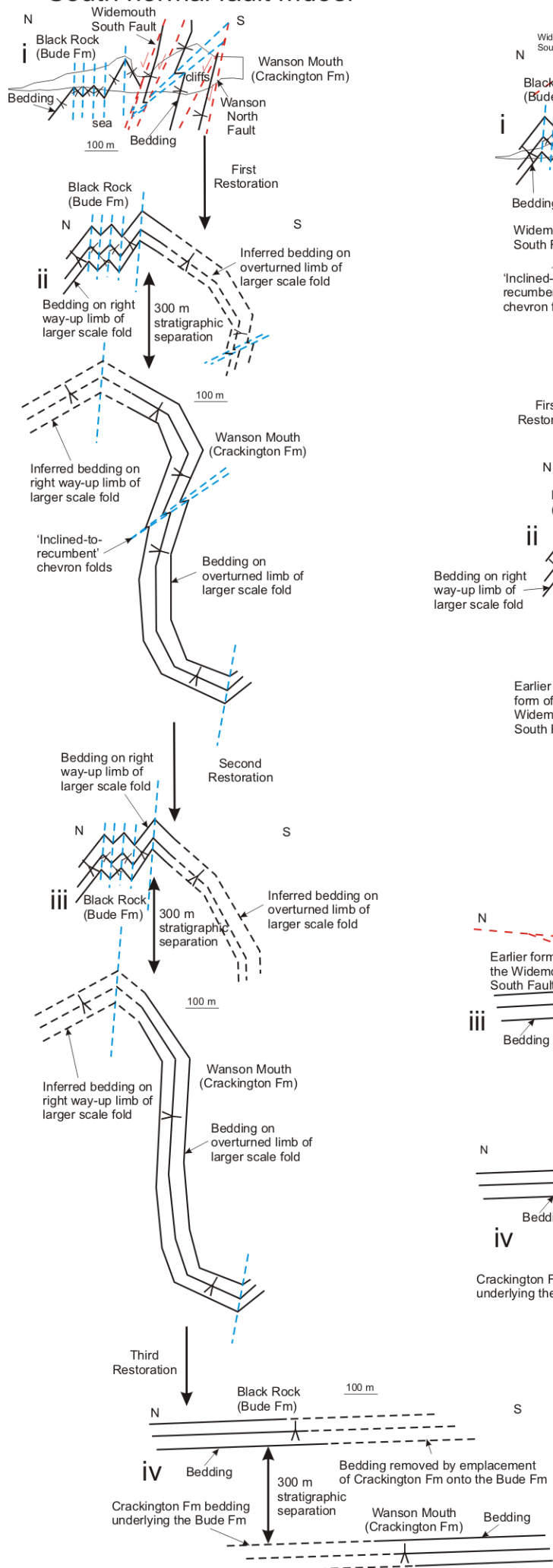
Enfield et al (1985) proposed that the other inverted thrusts caused bed truncations in the foreshore (see Fig. 4.7), rather than being due to ‘late’ normal fault movement as in the Freshney et al (1972) ‘late’ normal fault model. It was further proposed by Enfield et al (1985) that the thrust duplex is on the steep north-dipping limbs of the ‘inclined’ chevron fold pair in the foreshore. Also, the thrust duplex may have been folded above the beds in the Black Rock foreshore, raising the possibility that the WSF may be in outcrop under Widemouth Sands north of the Black Rock foreshore (Fig. 4.34b (i)).

The first restoration ‘step’ (Fig. 4.34b (ii)) removes the ‘inclined’ chevron fold pair. The beds and faults retain their present overturned steep northwards dip across the Wanson Mouth foreshore (Fig. 4.34b (ii)). In the Black Rock foreshore, the ‘upright’ chevron fold train lay on the north-dipping limb of a larger-scale ‘upright’ chevron anticline. The deformed beds in both foreshores remain juxtaposed along the WSF as the duplex inverted floor thrust (Fig. 4.34b (ii)).

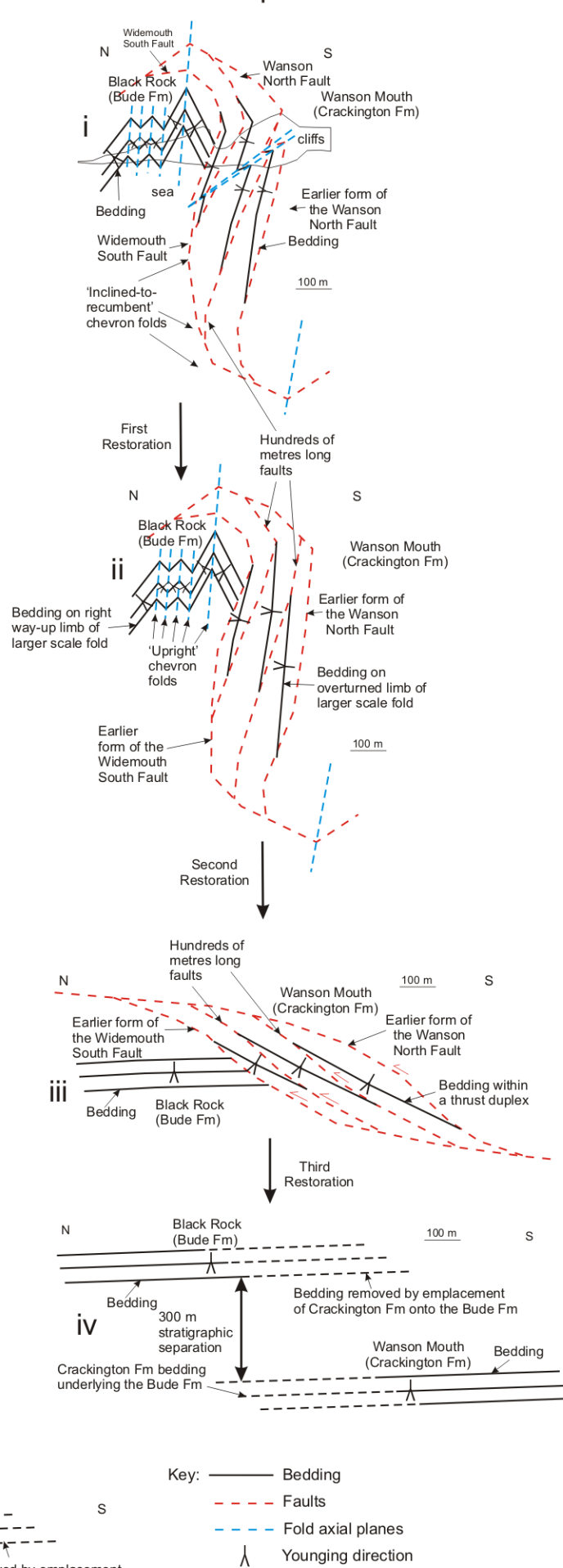
In the second restoration ‘step’ (Fig. 4.34b (iii)), the overturned steep northwards dip of the beds and faults are removed and the beds in the Black Rock foreshore succession are restored to right way-up, sub-horizontal orientations. The beds and faults in the Wanson Mouth foreshore succession are in this model part of a thrust duplex that has emplaced the Crackington Formation onto the Bude Formation (Figs. 4.7 & 4.34b (iii)).

In the third restoration ‘step’ (Fig. 4.34b (iv)), the faults, including the WSF and WNF, that form the thrust duplex (Fig. 4.7) are removed and the beds returned to right way-up, sub-horizontal orientations. The beds in each foreshore are shown as two laterally continuous layer-cake successions separated by a stratigraphic distance of 300 m (Freshney et al, 1979; Fig. 4.2) that have crossed the line marking the position of the WSF (Fig. 4.34b (iv)).

### A - Freshney et al (1972) Widemouth South normal fault model



### B - Enfield et al (1985) thrust duplex model



### C - Inverted Widemouth South Fault model

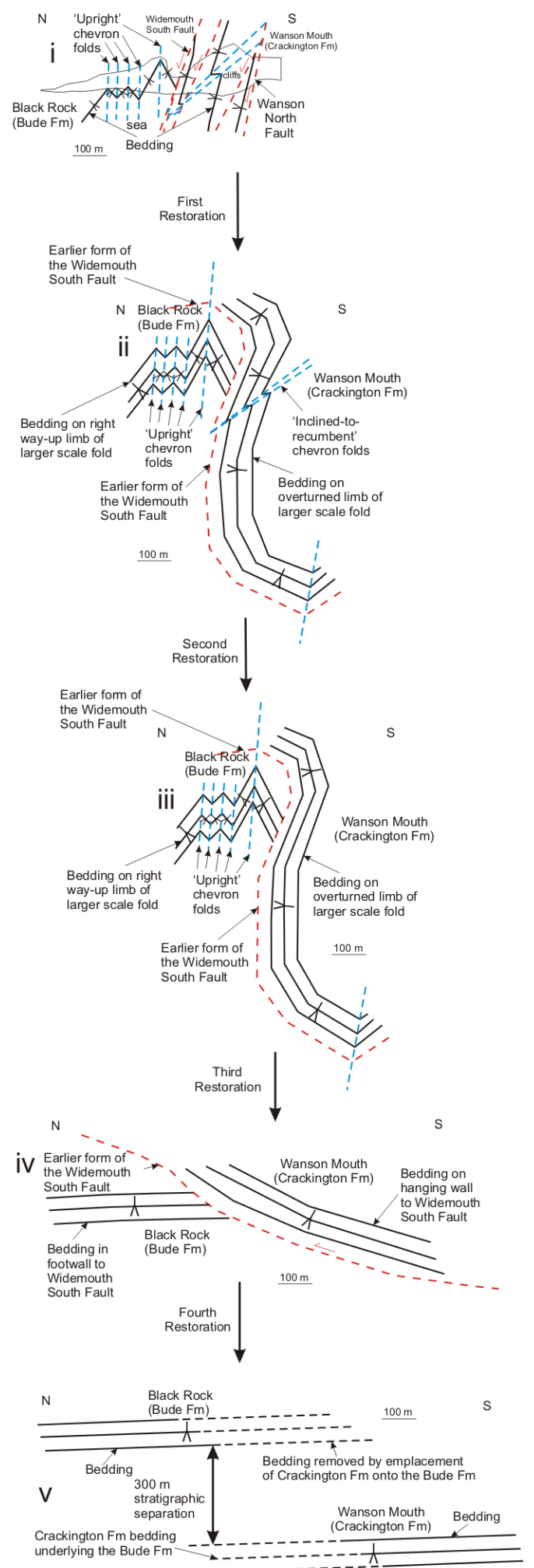


Fig. 4.34: Three schematic structural restoration models to explain the geological evolution of the Black Rock and Wansong Mouth foreshores. The models are: (a) the Freshney et al (1972) 'late' normal fault model, where 300 m of normal vertical movement was accommodated along the Widemouth South Fault (WSF) following Variscan fold deformation in each foreshore; (b) the Enfield et al (1985) thrust duplex model, where 300 m of compressional vertical movement was accommodated prior to Variscan folding along the WSF and other faults observed in the Wansong Mouth foreshore; and (c) the inverted Widemouth South Fault model, which does not include additional thrust faults proposed by Enfield et al (1985) but which has been reactivated as a 'late' normal fault

### **Hypothetical inverted Widemouth South Fault model**

This hypothetical inverted Widemouth South Fault model is developed here as a tentative alternative to the Freshney et al (1972) and Enfield et al (1985) models and incorporates elements of both models. The development of this alternative model is motivated by the relatively recent findings of Anderson and Morris (2004), who suggested that the last movement on the WSF was extensional, and also, that the Enfield et al (1985) model does not describe any extensional deformation occurring in the Wanson Mouth foreshore.

In the hypothetical inverted Widemouth South Fault model proposed here, the faults in the Wanson Mouth foreshore succession are viewed as 'late' normal faults (Fig. 4.34c (i)) that cause only tens of metres of displacement, as described by Freshney et al (1972). However, after Freshney et al (1979), the beds in the two foreshore successions have a stratigraphic separation of 300 m across the WSF (Fig. 4.2). Thus, in order to explain the stratigraphic separation, the 'late' normal fault movement is modelled as the reactivation of the WSF, which is modelled as having had an earlier form.

The first restoration 'step' (Fig. 4.34c (ii)) removes the faults, except for the WSF, and the beds are restored to their pre-'late' normal fault positions, retaining their present overturned steep northwards dip across the entire Wanson Mouth foreshore. As the WSF is not removed, the beds and structures remain juxtaposed against this fault in both foreshores (Fig. 4.34c (ii)). In this restoration, the Black Rock foreshore succession has an 'upright' chevron fold train on the shallow north-dipping limb of a larger-scale chevron anticline; whilst the Wanson Mouth foreshore has the 'inclined' chevron fold pair on the overturned north-dipping limb of this larger-scale chevron anticline (see Section 4.6). Also, the earlier form of the WSF was deformed by 'inclined' chevron folds and had a steep northwards dip on their overturned limbs in the Wanson Mouth foreshore. Above the Black Rock foreshore succession, the WSF is shown to be deformed by the 'upright' chevron folding, as described in the Enfield et al (1985) model.

The second restoration 'step' (Fig. 4.34c (iii)) removes the 'inclined' chevron fold pair. The Wanson Mouth beds retain their present overturned steep northwards dip across the entire foreshore (Fig. 4.34c (iii)). In the Black Rock foreshore succession, the 'upright' chevron fold train is interpreted to be on the north-dipping limb of this larger scale chevron anticline (Fig. 4.34c (iii)). Also, the earlier form of the WSF is still present and cuts the overturned limb of the larger-scale chevron fold (Fig. 4.34c (iii)).

In the third restoration 'step' (Fig. 4.34c (iv)), the overturned, steep northwards dip of the beds has been removed in the Wanson Mouth foreshore, whilst the beds in the Black Rock foreshore have been restored to right way-up, sub-horizontal orientations. The beds and faults in the Wanson Mouth foreshore succession are shown on the hanging wall to the earlier form of the WSF, which has emplaced the Crackington Formation (Wanson Mouth foreshore) onto the Bude Formation (Black Rock foreshore) (Fig. 4.34c (iv)). Thus, this earlier form of the WSF is interpreted as a thrust that has accommodated a vertical displacement of 300 m.

In the fourth restoration ‘step’ (Fig. 4.34c (v)), the thrust emplacement along the earlier form of the WSF has been removed and all the beds have been returned to right way-up, sub-horizontal orientations. The beds in each foreshore are shown as two layer-cake successions separated by a stratigraphic distance of 300 m (Freshney et al, 1979; Fig. 4.2), that have crossed the line marking the position of the WSF (Fig. 4.34c (v)).

### 4.7.3 Critical review of the structural evolution models

All the models have been developed using the current understanding of the Variscan deformation in the Culm Basin to explain the juxtaposition of the Black Rock and Wanson Mouth foreshore successions and how the different structures may have developed and been brought together. However, the timing of chevron folding in each foreshore is not known relative to the other foreshore and so is treated separately in the model restorations. This was undertaken for practical reasons as the only demonstratable limit is that the Bude Formation deformation cannot be earlier than that in the Crackington Formation. In order to assess the three models, a critical review is provided here.

In the Freshney et al (1972) normal fault model (Fig. 4.34a), the Widemouth South Fault (WSF) has been modelled as a ‘late’ normal fault that accommodated the 300 m of vertical movement between the relative stratigraphic positions of the Black Rock beds in the Bude Formation and the Wanson Mouth beds in the Crackington Formation (Fig. 4.2). However, Freshney et al (1972) also suggested that the amount of normal movement on the individual faults between Widemouth and Rusey was only of the order of tens of metres. Indeed, the vertical movement accommodated along the ‘late’ faults in the Black Rock foreshore is only 2-3 m (Figs. 4.19a & 4.23a). This suggests that ‘late’ normal fault movement along the WSF was insufficient to cause the juxtaposition of the two successions, which is an important shortcoming in the Freshney et al (1972) model.

In the Enfield et al (1985) inverted thrust duplex model (Fig. 4.34b), the WSF and the other faults observed in the Wanson Mouth foreshore have been modelled as inverted north-directed thrusts (see Fig. 4.7). Enfield et al (1985) suggested that the truncated Wanson Mouth foreshore beds reflected the inverted faults in a thrust duplex that emplaced the Crackington Formation over the Bude Formation prior to chevron folding (Fig. 4.34b (iv)). However, it has been impossible to correlate the beds across the faults and no thrust cleavage associated with these faults has been observed previously, or in this study, in the Wanson Mouth foreshore. Thus, thrust truncation of the Wanson Mouth beds, including along an earlier form of WSF, has not been demonstrated as support for the thrust duplex model.

In the hypothetical inverted Widemouth South Fault model, only the WSF has been modelled as an inverted north-directed thrust in the Wanson Mouth foreshore, which has been reactivated as a ‘late’ normal fault. The other faults in the Wanson Mouth foreshore were modelled as ‘late’ normal faults.

A further issue in regards to the Enfield et al (1985) thrust duplex model (Fig. 4.34b) and also, the inverted Widemouth South Fault model from this work (Fig. 4.34c) is that if the faults, including the WSF, were inverted then the deformation observed in the Wanson Mouth foreshore succession (see gusset) would affect the beds in the Black Rock foreshore succession. In the case of the inverted Widemouth South Fault model (Fig. 4.34c), the 'inclined' chevron folds are offset between the foreshore successions by the 'late' extensional movement on the WSF. However, the WSF cut all previous structures (see gusset) and no structures from either foreshore succession have been observed in the other. This suggests therefore that neither inverted fault model is applicable.

However, the 300 m stratigraphic separation between the juxtaposed Black Rock and Wanson Mouth successions (Freshney et al, 1979; Fig. 4.2) requires that a significant amount of movement has occurred along the WSF. As stated previously, the WSF cut all previous structures (see gusset), suggesting that the last displacement on the fault must have been greater than the wavelength of any previous structure. From Anderson and Morris (2004), this movement was extensional. Consequently, the accommodation of only tens of metres of vertical displacement during 'late' normal faulting on any individual fault, as suggested by Freshney et al (1972), is far too little for the WSF, requiring that the vertical displacement accommodated by the 'late' extension on the WSF was of the order of 300 m. This is feasible but as yet has not been demonstrated. Thus, in all other regards, and in the absence of other plausible models, the Freshney et al (1972) 'late' normal fault model is preferred currently as an explanation for the deformation observed in both foreshore successions and along the Widemouth South Fault, but with a significantly greater displacement than those authors interpreted.

#### **4.7.4 Consideration of other Culm Basin fault models**

In the Culm Basin, there are two significant basin-scale faults, the Widemouth South Fault (WSF) and the Rusey Fault. The WSF is described by Durrance (1985) as continuing beneath the Crediton Trough in Section 4.1.4 (Fig. 4.8) and the Rusey Fault is described by Thompson and Cosgrove (1996) at Rusey Head to the south of Crackington (Fig. 4.35). In both models, the faults are modelled as north-directed thrusts that were reactivated as normal faults following Variscan deformation. Fault descriptions and how they relate to the deformation along the WSF in the Black Rock and Wanson Mouth foreshore successions is provided here.

#### **Comparison of the Widemouth South Fault with the Rusey Fault**

In an attempt to explain further the complex deformation in the Black Rock and Wanson Mouth successions, the WSF is compared to the regional-scale Rusey Fault on the southern boundary of the Culm Basin at Rusey Head (Fig. 4.35). Here, the Westphalian Crackington Formation fine-grained turbidite sands sit in the hanging wall to the north of the Rusey Fault and the Namurian Boscastle Formation silty turbidites in the footwall to the south

(Fig. 4.35a). Thompson and Cosgrove (1996) described the two formations as being part of the same sedimentary system with a turbidite fan prograding through the Culm Basin. However, as with the WSF, a significant portion of stratigraphy is missing across the Rusey Fault.

The Rusey Fault strikes between 120-170° (Fig. 4.35b), dips at angles greater than 30°NE and cuts a fault zone in between the two formations, with dissected folds that show a well-developed cleavage that is oriented 016/59E. Although no slickensides or thrust-related cleavage planes were observed on the faults by Thompson and Cosgrove (1996), they interpreted the Rusey Fault as a thrust with a top-to-NW movement, which cut the Variscan chevron fold hinges and limbs. This movement sense is consistent with that suggested by Zwart (1964). After the Variscan thrusting, the Rusey Fault also accommodated multi-phase deformation, including NE-SW-trending extension and dextral oblique to strike-slip movement following Variscan thrusting. Thus, the Rusey Fault may have accommodated ‘late’ extensional deformation, similar to that of the WSF (Freshney et al, 1972).

In addition to the Thompson and Cosgrove (1996) model, the Rusey Fault has been alternatively described by Warr (2002) as having developed from north-directed under-thrusting of the Culm Basin and by Shail and Leveridge (2009) as a ‘late’ south-directed thrust. A brief discussion of these three models for the Rusey Fault will be provided in Chapter 9.

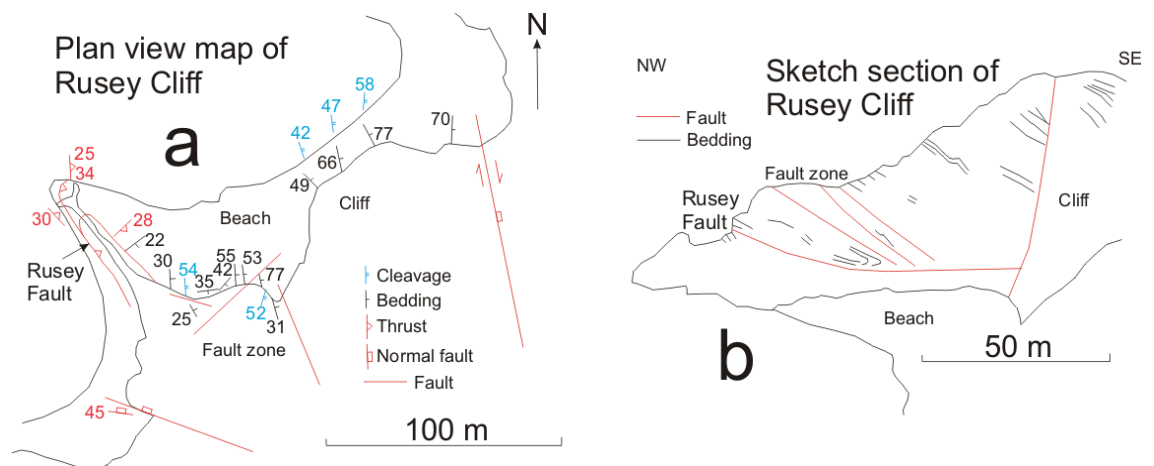


Fig. 4.35: Sketches taken from Thompson and Cosgrove (1996) showing: (a) a plan view map of the deformation in the Rusey Cliff; and (b) the cliff section with major faults at Rusey Cliff

### Applying the Durrance (1985) and Thompson and Cosgrove (1996) models to the WSF

The Thompson and Cosgrove (1996) model described the thrust movement along the Rusey Fault as occurring after chevron folding, whereas the timing of thrusting with respect to the folding is uncertain in the Durrance (1985) model. Using the two models, if an earlier form of the WSF had been a ‘late’ north-directed thrust, then a significant south-dipping, low angle fault would be expected to cut the folded beds in both the Black Rock and Wanson Mouth foreshore successions. However, this has not been observed. Furthermore, if the ‘late’ normal fault movement on the present WSF had been a few tens of metres (Freshney et al, 1972), the

'late' north-directed thrusts would have been offset by the WSF. However, no such thrust has been observed either. On this evidence, the Durrance (1985) and Thompson and Cosgrove (1996) models cannot be applied to the WSF in the Black Rock and Wanson Mouth foreshores.

#### **4.7.5 Strain accommodation in the two foreshore successions**

In the Freshney et al (1972) model, the large difference in the fold-related shortening estimates found across the WSF results from the two successions being folded at different structural 'levels' and being juxtaposed after the chevron folding. This suggests that the amount of fold-related shortening accommodated during Variscan deformation increased to the south and thus, the Crackington Formation has been shortened more than the Bude Formation. From Sanderson (1979), accommodation of south-directed shear deformation caused tighter folds, less steep axial planes and increased shortening south from Bude to Rusey Cliff (see Chapter 2). However, this pattern of a lateral southwards increase in the amount of fold-related shortening is locally punctuated across the 'late' normal faults, such as the Widemouth South Fault (WSF).

Another possibility to explain the difference in the amount of strain accommodated by the Bude and Crackington formations is due to the mechanical stratigraphy of the deposits. From Melvin (1986), the Crackington Formation is much more mud-rich with generally thinner and more laterally-continuous sandstone beds than in the Bude Formation. This suggests that if both formations were or became lithified during Variscan deformation, the Crackington Formation was generally less coherent, could accommodate more flexural slip movement along its bedding planes (Tanner, 1989) and thus, may have been able to accommodate more fold-related shortening (Sanderson, 1979) than the Bude Formation.

The Widemouth South Fault and other faults in the Wanson Mouth foreshore are significant in terms of their extensional strain accommodation. The WSF accommodated extension during its last movement (Anderson & Morris, 2004), but the amount of displacement can not be readily calculated. The same is the case for the other faults in the Wanson Mouth foreshore. Although Freshney et al (1972) proposed that normal movement on any individual fault between Wanson Mouth and Rusey was only tens of metres, precise estimates of the amount of movement are not available. In order to provide better estimates of both the displacement on the normal faults, including the WSF, and the amount of shortening accommodated by the chevron folds, a seismic survey could be undertaken to look at the top 5 km of sedimentary cover. Such a seismic survey would also test whether the two formations are cut by kilometric-scale north-directed thrusts as envisaged by Enfield et al (1985).

### **4.8 Summary of findings from the Black Rock-Wanson Mouth foreshores**

From the map work (see gusset) undertaken in the Black Rock and Wanson Mouth foreshores, an improved understanding has been gained of the geometries of the progressive Variscan deformation structures in both foreshores and the timing of movement along the

Widemouth South Fault (WSF) that juxtaposes the two foreshore successions. The juxtaposition of very different deformation styles across the WSF and the 300 m stratigraphic gap between the foreshore successions is an important and only partially explained feature of the geology. Three models have been considered for explaining the structural evolution of the WSF and the deformation accommodated in the two foreshore successions. Although no model can be demonstrated to hold fully, it is concluded that the Freshney et al (1972) model of a 'late' normal-faulted Widemouth South Fault is the most plausible, although with some modification.

The Black Rock and Wanson Mouth foreshores contain all of the progressive Variscan and 'late' Variscan deformation structures (Williams et al, 1970; Freshney et al, 1972; 1979; Ramsay, 1974; Sanderson, 1979; Durrance, 1985; Enfield et al, 1985; Whalley & Lloyd, 1986; Lloyd & Whalley, 1986; 1997) and many of the depositional elements (Melvin, 1986; Higgs, 1991; Burne, 1995; see Chapter 3) observed in the Culm Basin. Thus, the area represents a microcosm of the geologic evolution of the basin. This is of direct relevance to the specific aim of the study, to understand the geological evolution of the Culm Basin, and also provides some contribution to the general aim, namely to establish criteria for distinguishing between folds in rock and sediment.

Lastly, the foreshores have provided an appropriate locality for evaluating structural models devised to explain the progressive Variscan structural development, particularly as very different structural styles are visible across the Widemouth South Fault. This includes a series of stacked and cross-cutting local structures in the Bude Formation that are classed as 'early' and that have been deformed by 'upright' chevron folds in the Black Rock foreshore. In Chapter 5, examples of these structures from outcrops between Northcott Mouth and Black Rock (SS202087-SS195015) are described in more detail because of their importance to the general aim of the thesis to establish criteria for distinguishing between folds in rock and sediment.

## Chapter 5: Analysis of slump and ‘early’ deformation structural geometries in the Bude Formation

### 5.1 Introduction

This chapter is concerned with establishing the criteria for assessing whether slump folds and local structures occurred prior to chevron folding and whether they developed in sediment. This follows on from Chapter 4, in which such structures were recognised in the Black Rock foreshore. This is of direct relevance to the general aim of the study, namely to establish criteria for distinguishing between folds in rock and sediment.

In this chapter, a review of the current literature is provided for the previous work by Enfield et al (1985) on ‘early’ structures, Mapeo and Andrews (1991) on ‘pre-folding’ structures and Lloyd and Chinnery (2002) on ‘pre-chevron’ structures. Following this, the sedimentary and structural data collected from the Bude Formation slump folds are analysed. In particular, the massive Black Rock Slump Bed with detached slump raft folds is described and tests are undertaken on the orientations and geometries of these folds using fabric topology plots and statistical calculations. One test of the data is to ascertain whether the Black Rock Slump Bed (see Figs. 3.1a, b & c) described in the Black Rock (SS197017) and Lynstone foreshores (SS200053) are the same or different beds. The sedimentary logs of the bedding overlying the two massive slump beds are correlated across each slump bed to demonstrate whether thickness changes in the strata could be detected, thereby indicating syn-depositional slope failures.

Structural data were collected across the study area between Northcott Mouth and Wanson Mouth (SS202087-SS195013) from 29 high-angle, strata-bound normal faults, plus 35 bedding-parallel faults or low-angle thrusts together with their associated fold deformation. Tests as to whether the structures are ‘early’ (i.e. prior to chevron folding and at or near the palaeo-surface) use three diagnostic criteria developed from the structural analyses of Zoetemeijer et al (1992), Nigro and Renda (2004) and Corredor et al (2005).

Determination of the palaeo-slope directions for the slumps is made using criteria described for slump folds by Strachan and Alsop (2006) and slump faults by Debacker et al (2009). These methods cannot be applied to the ‘early’ structures as they are not slumps. Both sets of slump methods are also reviewed in order to ascertain whether there are further comparable criteria from either model that have yet to be demonstrated.

#### **5.1.1 ‘Early’, ‘pre-chevron’ and ‘pre-folding’ structures in the Bude Formation**

The Bude Formation outcrops from Northcott Mouth to Black Rock (SS202087-SS196015; see Chapter 4) contain several types of Variscan deformation structure, such as chevron folds and thrusts (Freshney et al, 1972; 1979; Ramsay, 1974; Sanderson, 1979; Whalley & Lloyd, 1986; Lloyd & Whalley, 1986; 1997) and structures that are deformed on

chevron fold limbs (Enfield et al, 1985; Mapeo & Andrews, 1991; Lloyd & Chinnery, 2002). These latter structures include: (1) bedding-parallel faults and low-angle thrusts, commonly associated with hanging wall fault-bend folds (see Chapter 4); (2) high-angle, normal and reversed faults; (3) disaggregated, massive slump beds (Hartley, 1991) containing detached slump raft folds (see Chapter 3); and (4) attached slump folds (see Chapter 3).

In Chapter 4, faults and folds that were deformed by the ‘upright’ chevron folds in the Black Rock foreshore (Bude Formation) were also shown to be ‘early’ structures that formed in unconsolidated sediment at or near the palaeo-surface during deposition. This chapter aims to assess whether these ‘early’ structures (i.e. ‘pre-folding’ or ‘pre-chevron’) are found across the Bude Formation outcrops between Northcott and Black Rock, how they relate to Variscan deformation and what their timing is with respect to deposition.

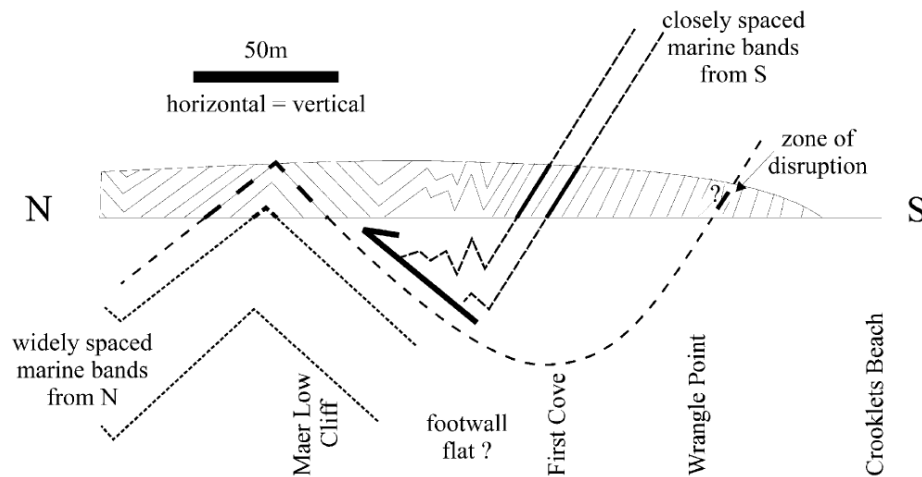


Fig. 5.1: Stratigraphic evidence for major thrust displacements (see Fig. 1.1 in Chapter 1 for location). Two narrowly-spaced ‘marine bands’ on the southern limb of a syncline between Wrangle Point and Maer Cliff (SS200074-SS200077) do not reappear on the northern limb but are replaced by two more widely-spaced ‘marine bands’ (from Lloyd & Chinnery, 2002)

Previous work suggests that some of the bedding-parallel faults and low-angle thrusts are associated with a general northward propagation of the Variscan deformation front (Enfield et al, 1985), and that some may exploit Bude Formation slumped beds (Whalley & Lloyd, 1986; Warr, 2002; Leveridge & Hartley, 2006). In the Bude (SS200067) to Duckpool (SS200115) coastal section, ‘pre-chevron’ thrust sheets are variably top-to-south and top-to-north (Lloyd & Chinnery, 2002). This change in thrust direction may reflect ‘space problems’ during northward propagation of the Variscan deformation front. According to Lloyd and Chinnery (2002), the ‘pre-chevron’ structures are part of “a 3D intra-formation stack, which is at any single locality an instantaneous representation of an orogenic front propagating into its own foreland basin”.

These faults may have been under-recognised as they are commonly bedding-parallel (see Chapter 4). Where ‘pre-chevron’ or ‘early’ low-angle thrusts ‘ramped’ through the beds, changes in the depositional stacking patterns have been observed. An example of this occurs

between Wrangle Point and Maer Cliff (SS200074-SS200077) where apparently laterally-continuous black shales or ‘marine bands’ show a narrow stratigraphic spacing and cut-offs on a ‘pre-chevron’ low-angle thrust hangingwall but a wider stratigraphic spacing immediately on the footwall (Fig. 8 of Lloyd & Chinnery, 2002; Fig. 5.1). Lloyd and Chinnery (2002) used sedimentary logs across this thrust to suggest that the two sedimentary stacks are not lateral equivalents. However, the ‘marine bands’ contain no fossils making biostratigraphic correlation impossible, so the Lloyd-Chinnery model of separate stacks is not proven.

As demonstrated in Chapter 4, ‘early’ (‘pre-folding’ or ‘pre-chevron’) structures in the Bude Formation may have generated depositional patterns that reflect active deformation whilst the beds were being laid down as sediment. This is the case for the massive slump beds where these gravity-driven liquefied deformation structures (Woodcock, 1979; Alsop & Holdsworth, 2002; Strachan & Alsop, 2006) were deposited on a slope (see Chapter 2) at the palaeo-surface (Enfield et al, 1985). In contrast, the ‘pre-folding’ structures between Sandy Mouth and Northcott Mouth (SS201098-SS202087) have been interpreted as ‘post-lithification’ by Mapeo and Andrews (1991) although the authors also describe these structures as “syn-sedimentary”.

The evidence for ‘post-lithification’ deformation comes from the presence of quartz veins on the fault planes. Also, hot quartz-rich fluids of up to 300°C are known to have flushed through the Culm Basin deposits throughout Variscan deformation (De Wall & Warr, 2004) and this suggests that the quartz veins of Mapeo and Andrews (1991) on the ‘pre-folding’ structures may have formed during continued Variscan deformation as flexural slip planes that were continually exploited as chevron folds developed (Tanner, 1989).

### **5.1.2 Assessment of an ‘early’ deformation structure**

In order to assess whether ‘early’ deformation occurred post-lithification, a partially-restored section was produced from an outcrop at Lynstone (SS200053) (Fig. 5 of Enfield et al, 1985; Fig. 5.2). The stratigraphy in the partially-restored section (Fig. 5.2b) has been divided into 10 stratigraphic units above the ‘Black Rock Slump Bed’ (BRSB). Towards the base of the section, a normal fault cross-cuts the lower 5 units and becomes a listric fault into the slump bed. On the hanging wall, there are units 1, 3, 4 and 5, whilst on the footwall, there are only units 2 and 5. Unit 6 displays a ramp-flat geometry over Unit 5, is apparently unaffected by the normal fault and fills the topography across the fault. Units 7-9 are stacked low-angle thrusts above Unit 6, whilst Unit 10 shows no deformation structures and drapes all the lower units that contain ‘early’ structures (Fig. 5.2b). This suggests that deposition of Unit 10 followed the ‘early’ deformation, and thus, these structures developed at or near the palaeo-surface prior to lithification (Enfield et al, 1985) from the ‘undeformed’ bed criterion of Zoemeijter et al (1992), Nigro and Renda (2004) and Corredor et al (2005) (see Chapter 4).

It is possible that the normal fault that cuts the slump bed represents volume loss from this bed by dewatering due to the weight of overlying or over-riding beds (see Chapter 2). Also,

if the ‘early’ normal fault moved soon after the slump bed was deposited, the fault movement may have controlled the accommodation space before Unit 5 was deposited (Fig. 5.2b). Consequently, the ‘early’ thrusts that cut and stack units 7-9 above units 5-6 may have occurred in beds prior to lithification at or near the palaeo-surface following the growth strata criterion of Zoemeijter et al (1992), Nigro and Renda (2004) and Corredor et al (2005) (see Chapter 4).

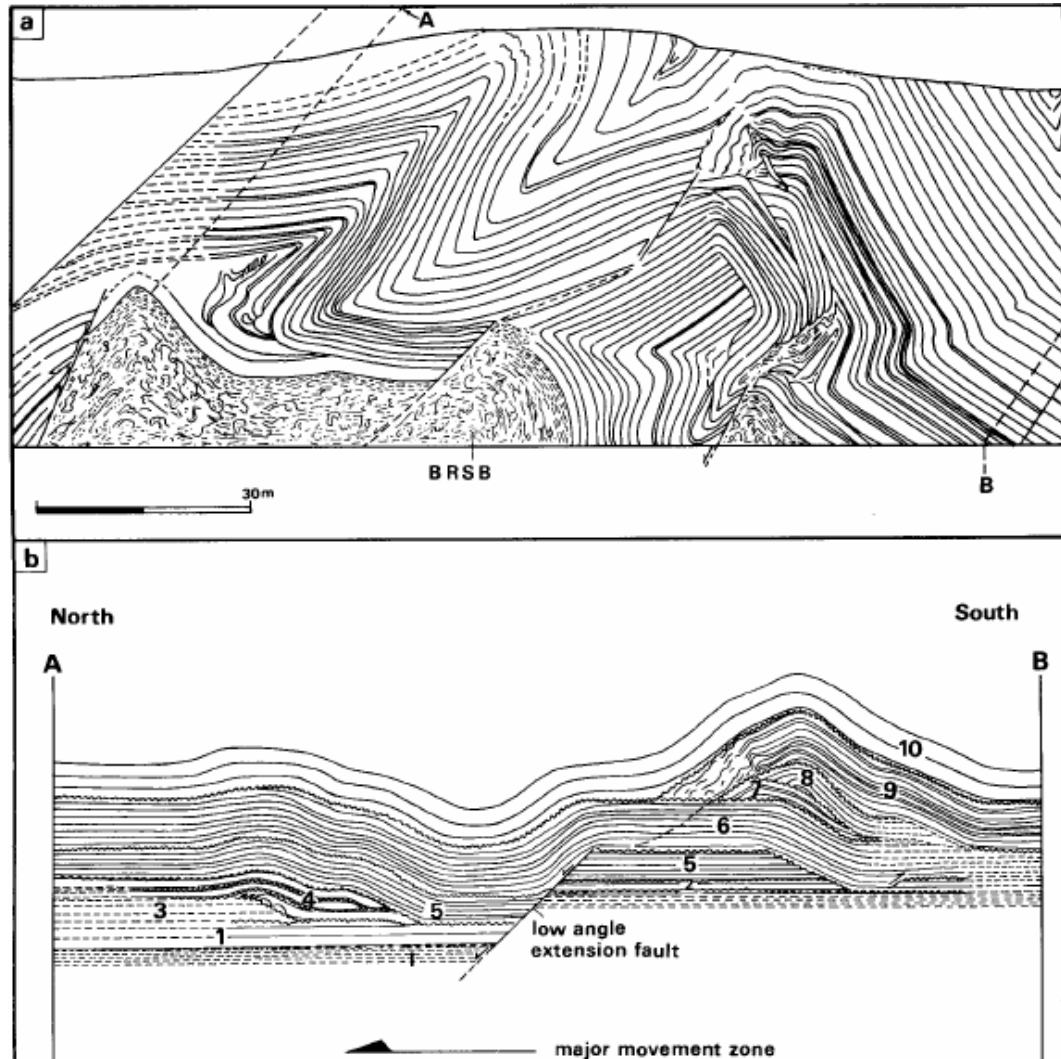


Fig. 5.2: Diagrams of: (a) antiformal ‘early’ low-angle thrust stack affecting beds immediately above the ‘Black Rock Slump Bed’ (BRSB – ornamented at the base of the sections) at Lynstone (SS200053); (b) partial restoration of deformation in (a), removing ‘late’ chevron folding effects. Enfield et al (1985) has not maintained the exact scale. Major movement direction relates to the ‘early’ north-directed thrusts (both diagrams from Enfield et al, 1985)

In order to generate the slump structures, fluid over-pressures were close or equal to lithostatic pressure (see Chapter 2). In this study of the slumps and local structures deformed by later chevron folds, the type locations employed in the Bude Formation are at: Lynstone (SS200053); Upton-Phillip’s Point (SS200044-SS200045); and Northcott Mouth (SS202082). Measurements from these structures allow a series of tests to be undertaken. For the massive

slump beds at Black Rock (see Fig. 3.1c) and Lynstone, a test has been undertaken to assess whether these beds can be correlated, as is proposed by Freshney et al (1972), or whether they are separate beds. A further test on the slump folds is to see if a statistical relationship exists between the slump fold elongation direction and the profile plane strike direction. From the methods of Alsop and Strachan (2006), the elongation direction is used to estimate the palaeo-slope direction (Table 5.1). In the case of the massive slump bed at Black Rock, the slump folds are oriented vertically into the ground, so the elongation direction cannot be measured.

However, at Lynstone, both parameters can be calculated.

The local structures have been assessed as to whether they formed at or near the palaeo-surface within sediment. A further test is to assess whether they relate to either movements down a palaeo-slope or to progressive Variscan deformation structures. In Chapter 3, palaeo-flow indicators from sole marks on turbidite bed bases were used as a proxy for the palaeo-slope directions identified by Freshney et al (1979), Higgs (1991), Burne (1995) and the author. The palaeo-flow results provide a control on palaeo-slope directions across the study area.

## 5.2 Methods

Data collection and analysis was undertaken on the slump and local structures deformed by chevron folds using circular statistics to calculate mean structural orientation values (Fig. 5.3). The data collected were structural measurements along bedding, fold axial and fault planes, for hinge lines and fault plane striations and hinge line elongation directions. Where angular data (in degrees) are expressed as a mean, this is given with a circular variance value.

In the Bude Formation outcrops between Northcott Mouth and Black Rock (SS202087-SS195015), there is a massive slump bed (i.e. Black Rock Slump Bed) containing sandy slump raft folds (Enfield et al, 1985; Hartley, 1991). Unrestored data from the raft folds in the slump bed have been plotted onto a Google Earth™ base slip together with fold axis plunge and profile plane data. Statistical analyses of the geometric data from the raft folds at Black Rock (SS197017) and Lynstone (SS200053) were undertaken to assess whether:

1. The two slump beds occurred during the same event;
2. The slump beds spread out or cut a ‘channel’ into the palaeo-surface;
3. The slump raft fold profile plane strike is parallel to the hinge line elongation direction.

As slumps indicate that near-surface deformation occurred on a palaeo-slope (Woodcock, 1979; Alsop & Holdsworth, 2002; see Chapter 2), a series of methods from Strachan and Alsop (2006) have been employed on the raft fold data to determine the palaeo-slope direction for each massive slump bed (Table 5.1). Although these methods are thorough, an additional method is proposed in this chapter, which is analogous to the “Best-fit Girdle to Fault Poles” (BGFP) slump fault method from Debacker et al (2009). In the “Best-fit Girdle to Bedding Poles” (BGBP) slump folds methods the fold profile plane of the  $\pi$ -girdle may be

aligned with the fold maximum elongation direction, and thus, to the down-slope direction as well (**bold** in Table 5.1). A test is undertaken involving structural and statistical analyses to assess whether the BGBP method is appropriate for the case of slump raft folds. The test statistics employ the calculation of the mean of two proportions using the Z-statistic, which is assumed under the Null hypothesis to have a Standard Normal distribution (mean 0; variance 1).

| <b>Slump folds (from Strachan &amp; Alsop, 2006)</b>                                           |
|------------------------------------------------------------------------------------------------|
| Little length change in direction parallel to strike of controlling palaeo-slope               |
| Folds have axes parallel to palaeo-slope strike and hence have undergone no hinge rotation     |
| Vergence or facing direction deemed as slip direction and assumed to be down-slope direction   |
| Folds generated by heterogeneous simple shear about the slip direction                         |
| In slumps, fold asymmetry senses oppose each other about down-slope average axis               |
| Maximum fold elongation direction is aligned down-slope                                        |
| <b>Fold profile plane is aligned with maximum fold elongation direction (i.e. down-slope)</b>  |
| Fold hinges will verge and face in a statistical arc about transport direction                 |
| With applied shear stress, folds tighten and hinges rotate into a transport-parallel direction |
| Slumping direction is parallel to mean axial-planar intersection of opposed vergence folds     |
| Hinges rotate at either end to form curvi-linear fold geometries                               |

Table 5.1: Summary table of structural methods applied to studying palaeo-slope direction from analyses of slumps (from Strachan & Alsop, 2006). The method in **bold** is a new method that is presented and tested in this chapter to enhance this palaeo-slope methodology

Three fabric topology plots are provided separately for the slump bed at Lynstone and Black Rock in order to assess the relationships between the slump fold profile plane strike direction and the axial plane strike direction, profile plane dip and fold interlimb angle (all in degrees). Regression analysis on each cross-plot assesses the degree of correlation (i.e. alignment) between the measurements using the  $R^2$  statistic. In this case, an  $R^2 = +1$  indicates either a perfect direct or reverse alignment, whilst an  $R^2 = 0$  indicates no alignment.

In this study, local structures have been observed in the Bude Formation outcrops that are tilted on the limbs of chevron folds, as described in Chapter 4. In order to establish whether the local structures occurred at or near the palaeo-surface (i.e. during deposition), and so, prior to chevron folding (i.e. ‘early’) criteria have been developed from seismic section interpretations in the Po Delta, Italy by Zoetemeijer et al (1992) and Niger Delta, Nigeria, by Corredor et al (2005), and also, outcrop studies in the Pliocene Mount Corvo beds, SW Sicily, Italy, by Nigro and Renda (2004) (see chapters 2 & 4). The criteria are (see Fig. 5.3):

1. *‘Undeformed’ beds* both overlying and underlying the locally deformed strata;
2. *Toplap truncations* of local structures and deformed beds by either overlying ‘undeformed’ beds or deformed beds in another local stacked structure;
3. Variable thicknesses of ‘undeformed’ beds overlying the local structures (i.e. *growth strata*)

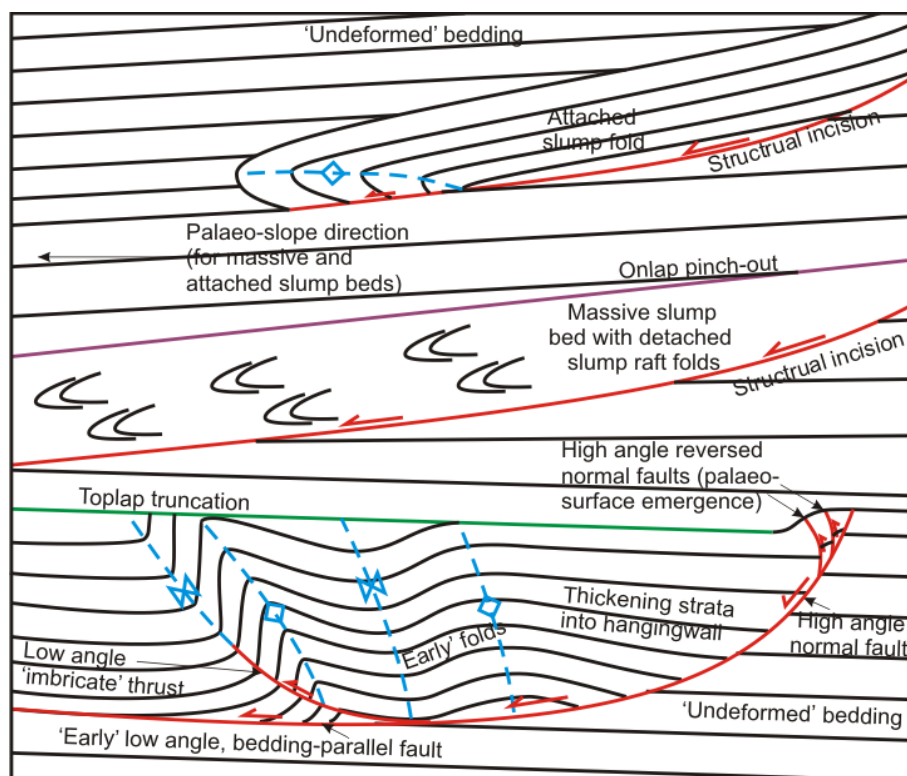


Fig. 5.3: Schematic diagram of criteria to define slump and 'early' structures in stacked beds, with the structures incising 'undeformed' under-lying beds and being overlain by 'undeformed' beds. The slump fold facing directions are preferentially aligned with the palaeo-slope direction (see Table 5.1; Strachan & Alsop, 2006).

Where local structures are tilted on chevron fold limbs, restorations using stereonet are used to re-orientate the structural data to sub-horizontal and the restored data plotted for each structure. The error attached to the restoration, using a  $2^\circ$  grid on a Lambert equal-area projection stereonet is ca.  $1^\circ$ , which is important as a small angular change may have significant effects on low-angle fault behaviour if elevated fluid pressures occurred (Zoback, 2008).

Striations on fault plane veins provide data on structural propagation directions. To test if the striations are quartz (Mapeo & Andrews, 1991), acid tests using a bottle of approximately 10% HCl and scratch tests using a steel pen knife have been undertaken.

In order to measure the thickness and depositional variations within growth strata above the candidate slumps and 'early' structures, sedimentary logs have been taken. Where more than one log was taken above a structure, correlation of stratigraphic horizons has been undertaken and the positions of onlapping and toplapping, and / or laterally-continuous beds, presented on sketches of the growth strata. From the log correlation and resultant reconstruction of stratal geometries, the timing of structural uplift or subsidence is established.

In addition to slump and local structures, incising channels and their sedimentary fill are observed in outcrop. Channels are observed at Summerleaze Beach, Bude (SS201067; Fig. 5.4) and Black Rock (SS196015) (see chapters 3 & 4), which indicate that there were palaeo-slopes within the Bude Formation. Tool marks on the basal channel infill sandstones provide only data

on the palaeo-flow axis of the channel rather than the palaeo-slope direction. Instead, palaeo-flow indication data from Freshney et al (1979), Higgs (1991), Burne (1995) and the author provide a control on palaeo-slope directions across the study area (see Chapter 3).

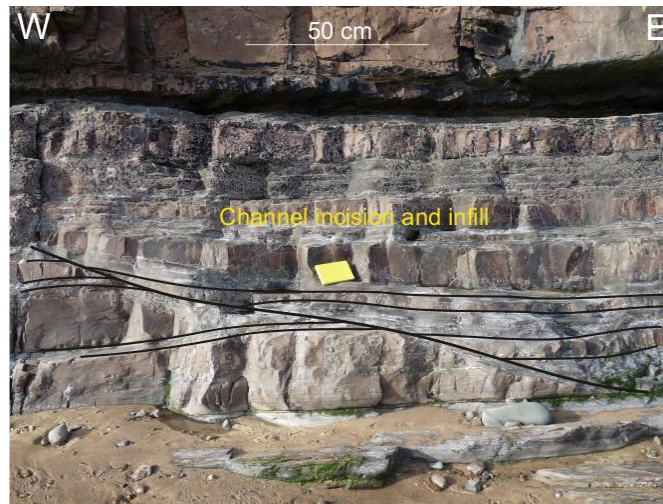


Fig. 5.4: Oriented, scaled and annotated photograph of a channel incision and fill succession in relatively sheet-like strata in the cliff at Summerleaze Beach, Bude (SS201067)

### 5.3 Slump folds

Within the Bude Formation, there are several beds and structures that have been described as slumps (Burne, 1970; Enfield et al, 1985; Hartley, 1991; see Chapter 3). In this chapter, soft-sediment deformation structures are reassessed to establish whether they are types of slump and, if so, whether they are attached slump folds or massive slump beds containing detached folds. In each case, it is established whether the slump beds:

1. Lie in between ‘undeformed’ deposits that have been truncated below the slump bed and younger deposits which infill topography above the slump bed;
2. Display dewatering structures (i.e. sand volcano, mud injection; Burne, 1970; Montenat et al, 2007; see Chapter 2) and slump scars;
3. Are indicative of the palaeo-slope direction (Strachan & Alsop, 2006).

#### 5.3.1 Attached slump folds

A low cliff section at Upton (SS200045) contains a ‘recumbent’ fold with discernable bedding attached (Fig. 5.5), which lies above ‘undeformed’ deposits and is truncated by a bed that overlies the fold. No striations were observed on this truncation surface. The ‘undeformed’ beds both drape above and infill the accommodation space ahead of the fold although no significant bed thickness changes were observed (implying sedimentation by suspension fall-out). The infilling beds are cut by a north-directed thrust and this fault ‘zone’ has been eroded (Fig. 5.5). No extensional slump scar typical of slump folds was observed within this outcrop but this may be either eroded or is not exposed in the cliff. Despite not meeting the growth strata

criterion, the fold is considered to have developed at or near the palaeo-surface from the 'undeformed' beds and bed truncation criteria following the Zoetemeijer et al (1992), Nigro and Renda (2004) and Corredor et al (2005) convention (Fig. 5.3) (also see Chapter 4).

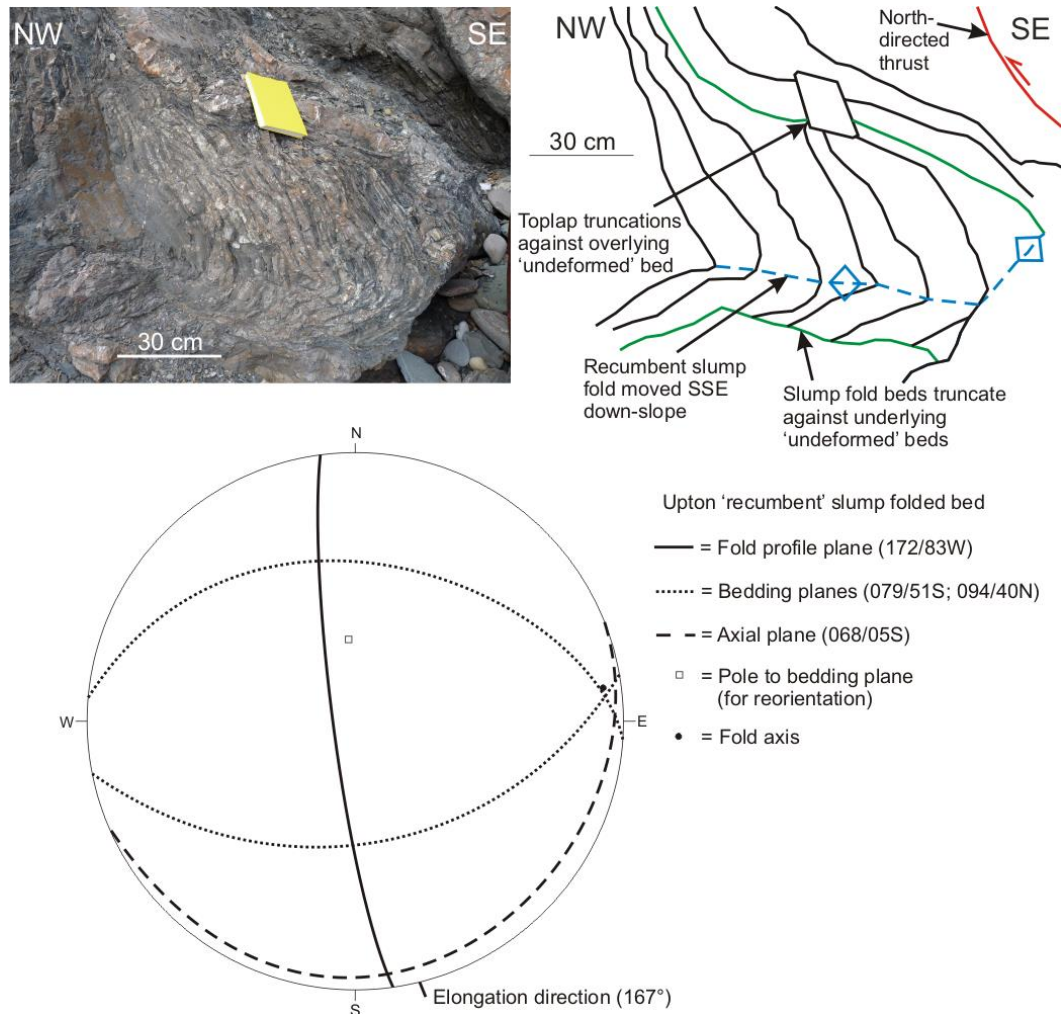


Fig. 5.5: Annotated photograph (top left) and sketch (top right) of the SSE-verging Upton attached slump fold (SS200045). A stereonet with a southern hemisphere projection shows the mean orientations of all measured beds in the Upton slump fold (bottom)

As the surrounding bedding dips at approximately 20°S, the fold structural data have been restored using stereonet analysis (Fig. 5.5). The folds face downwards towards the SSE on the overturned limb, which is sub-parallel to the profile plane strike direction (172°) and the hinge line elongation direction (167°). The fold has a tight interlimb angle of 41° (Fig. 5.5) and a curvi-linearity of 108° that has developed symmetrically about the hinge line elongation direction. The elongation direction is sub-parallel to the palaeo-flow indicators of Higgs (1991), Burne (1995) and from this work (see Chapter 3). From the methods of Strachan and Alsop (2006) and the criteria considering that it was at or near the palaeo-surface (Fig. 5.3), this suggests that the Upton 'recumbent' fold is an attached slump fold (*sensu lato*) that moved as one unit with its beds down a SSE-oriented palaeo-slope (Fig. 5.5).

W

### Foreshore

Key to logs and map:

Bedding plane reading

South-verging, 'inclined-recumbent' anticline axis

Lynstone Slump Bed outcrop

Lynstone Slump Bed subcrop

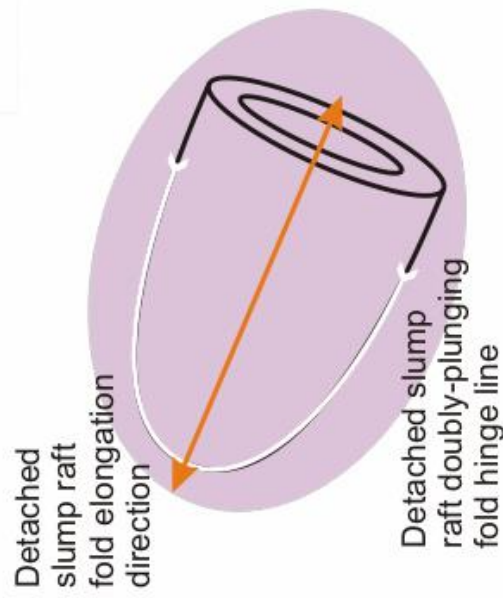
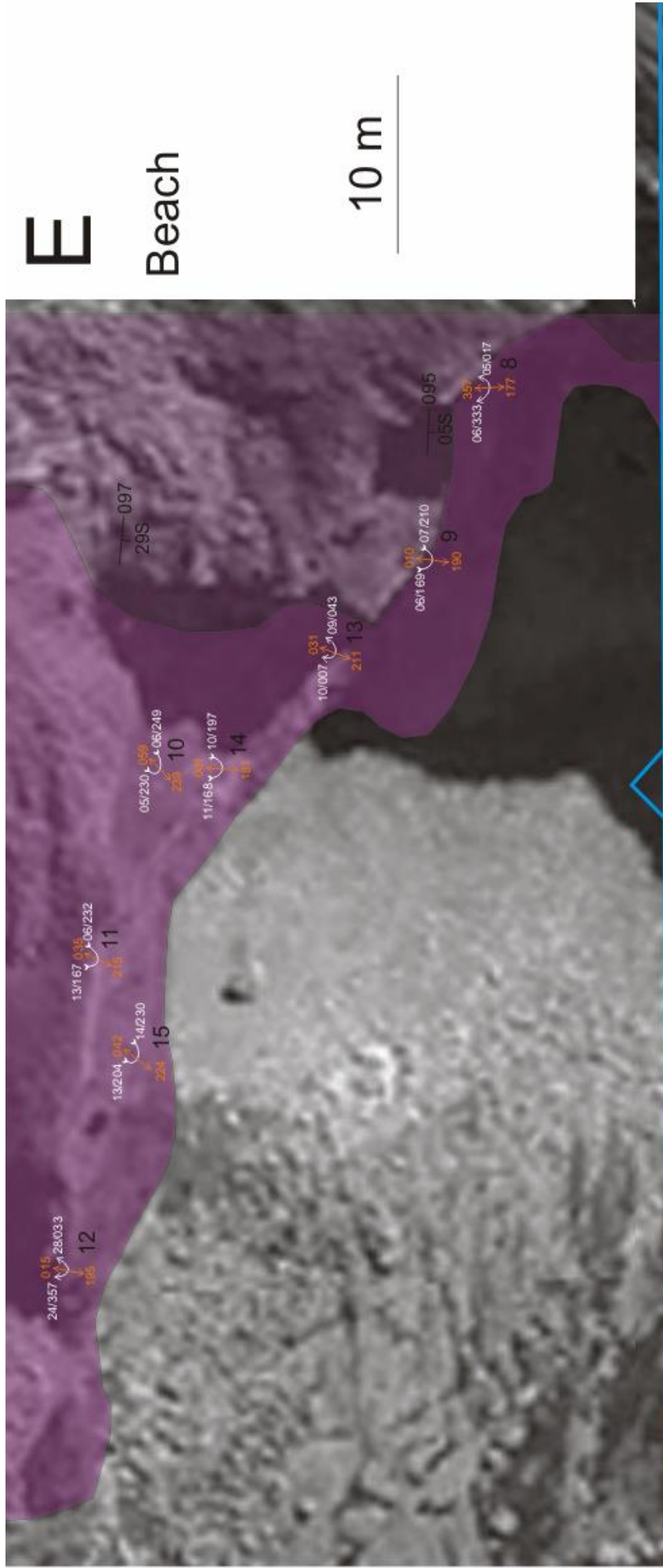
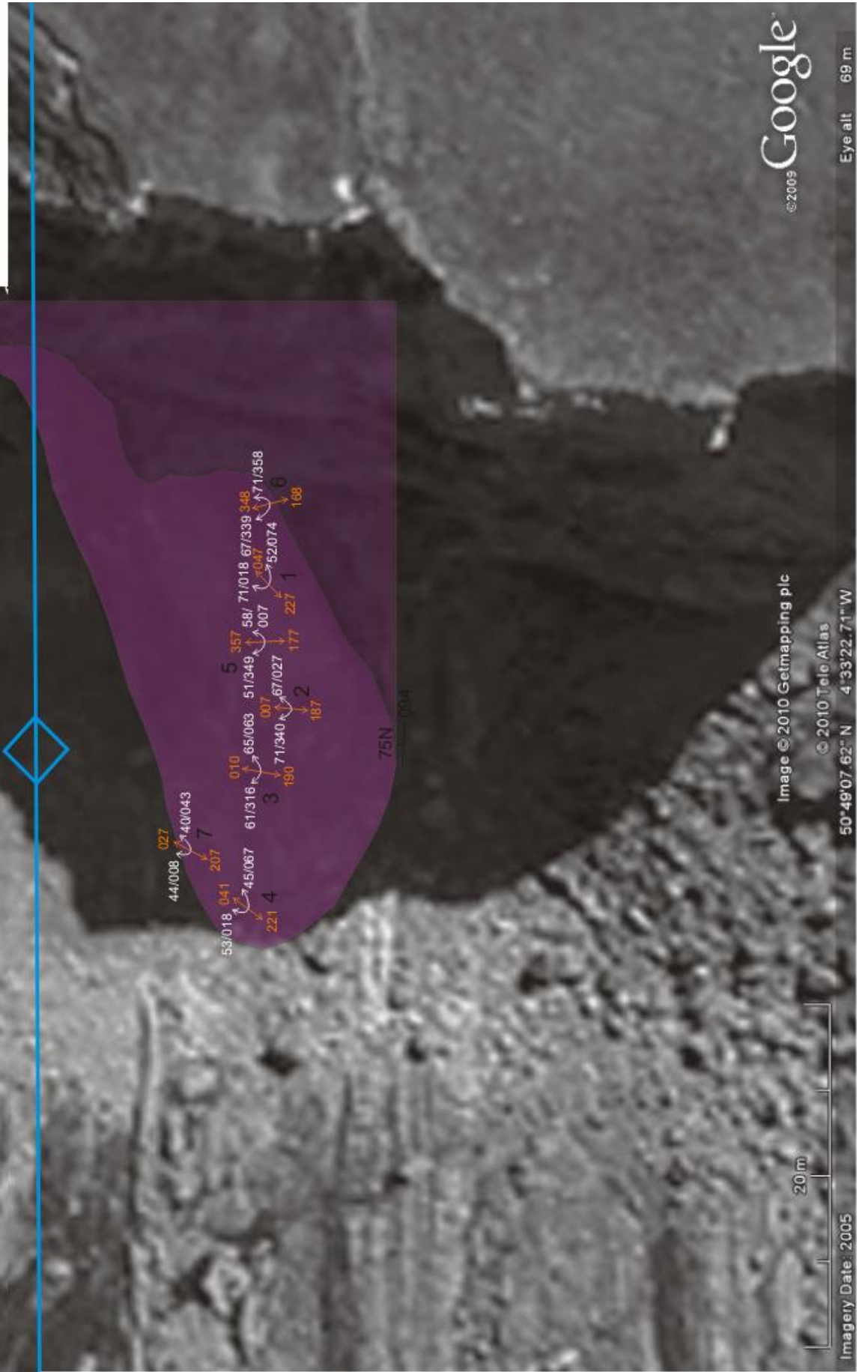
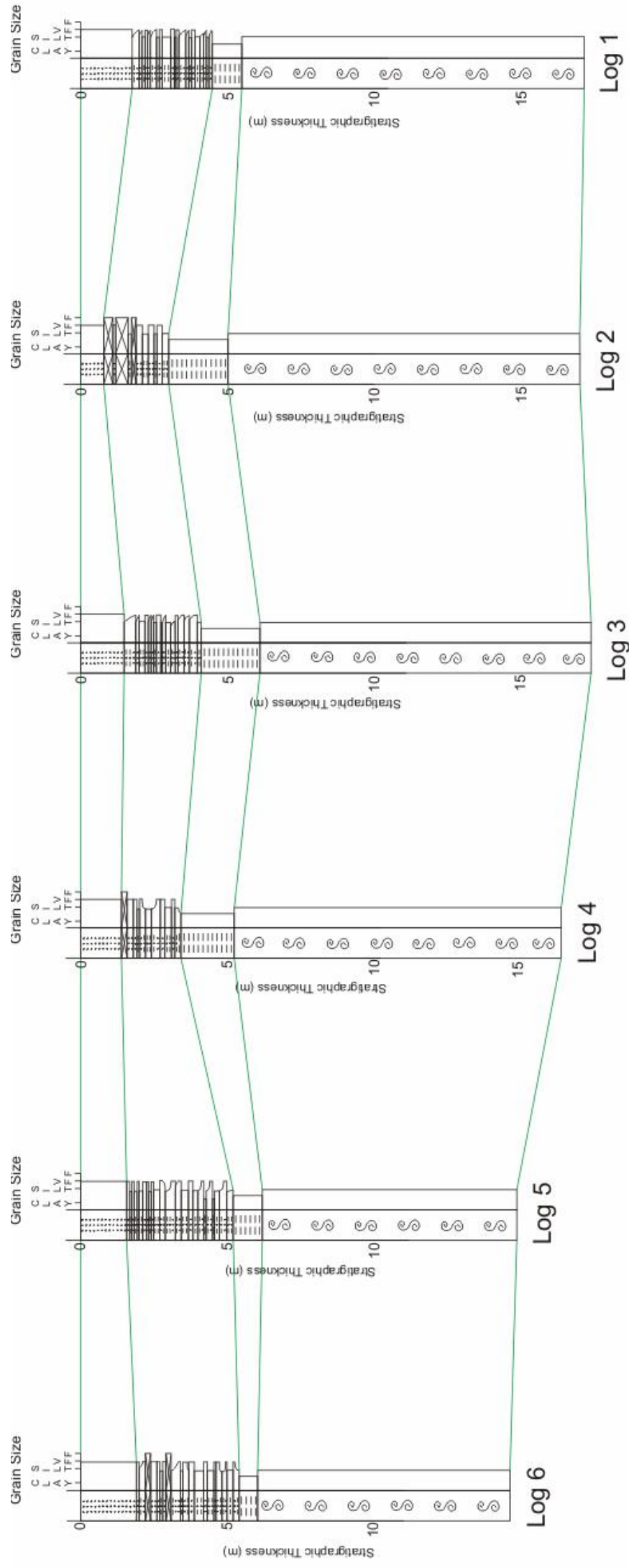


Fig. 5.6: Map of the detached sandstone slump 'raft' folds in the Black Rock Slump Bed at Lynstone (SS200053) showing locations of doubly-plunging 'raft' folds





W

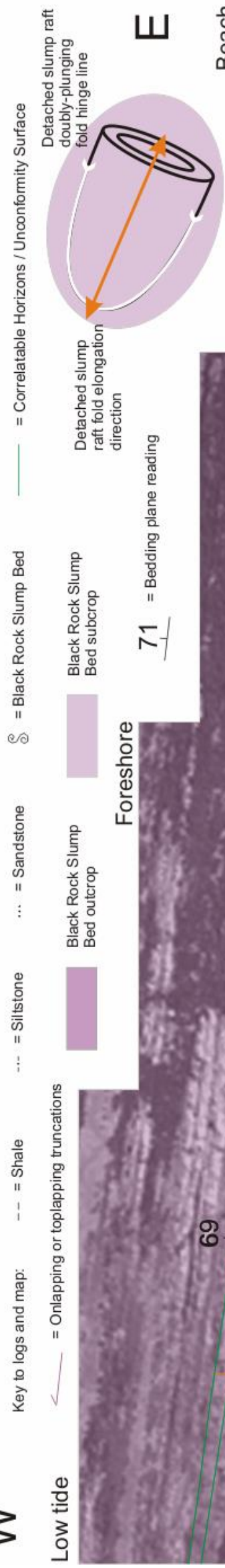


Fig. 5.7: Map of the detached sandstone slump 'raft' folds in the Black Rock Slump Bed at Black Rock (SS197017) showing the locations of the doubly-plunging 'raft' folds and correlated sedimentary logs describing the variation in slump bed and growth strata thicknesses

### 5.3.2 Detached slump rafts within massive slump beds

Massive, disaggregated Bude Formation beds (Enfield et al, 1985; Whalley & Lloyd, 1986; Figs. 5.6-5.7; see Chapter 3) are found in two examples from the study area between Northcott Mouth and Black Rock, which are jointly referred to as the Black Rock Slump Bed by Freshney et al (1972) and Enfield et al (1985) (see Figs. 3.1a, b & c). In both cases, they contain isolated fold raft structures that are not observed in the underlying and overlying ‘undeformed’ beds. The overlying beds have a variably-thick infill over the massive beds at both Black Rock (Fig. 5.7) and Lynstone (Figs. 5.2 & 5.6; Enfield et al, 1985). However, no observations have been made of an extensional slump scar. The massive bed is considered to have developed at or near the palaeo-surface consistent with all three criteria following the Zoetemeijer et al (1992), Nigro and Renda (2004) and Corredor et al (2005) convention (Fig. 5.3).

At Lynstone (SS200053), data were collected from 15 detached raft folds and at Black Rock (SS196017) 30 detached raft folds were measured. The structural analysis of these two sets of slump rafts is described in detail below and includes fabric topology plots comparing the slump fold profile planes with other slump raft structural geometries. Similar plots have been drawn by Strachan and Alsop (2006) and Strachan (2008) but they have concentrated on comparison of the slump raft structural geometries with the slump fold hinge lines, which are perpendicular to their profile planes. The descriptions of the Black Rock Slump Bed commence with those from Lynstone (Fig. 5.6) and are followed by those from Black Rock (Fig. 5.7).

### 5.3.3 Detached slump raft folds in the Black Rock Slump Bed at Lynstone

The structural data collected from 15 detached slump rafts in the ‘Black Rock Slump Bed’ at Lynstone were restored using stereonet (Fig. 5.8). As the slump bed at Lynstone is folded around a south-directed, ‘inclined-to-recumbent’ chevron anticline, each slump raft fold was restored individually to sub-horizontal based on the orientations of the surrounding beds.

The results from restoration using a stereonet (Fig. 5.8) gives the mean axial plane orientation for the slump rafts as 107/11S (strike circular variance  $\pm 8^\circ$ ;  $n = 15$ ), making them ‘reclined’ sheath fold structures. The raft folds face downwards towards the SSW on their overturned limbs, which is sub-parallel to the elongation direction. The rafts also have isoclinal-to-‘elastica’ (i.e.  $20^\circ$  to  $-20^\circ$ ) interlimb angles and doubly-plunging hinge lines with a large degree of curvi-linearity ( $154^\circ \pm 5^\circ$ ;  $n = 15$ ) about the elongation direction (Fig. 5.8). The mean slump raft hinge line elongation direction ( $201^\circ \pm 14^\circ$ ;  $n = 15$ ) is parallel to the mean profile plane strike direction ( $201^\circ \pm 12^\circ$ ;  $n = 15$ ; mean profile plane is 021/85W) and sub-parallel to the palaeo-flow indicators provided by Higgs (1991), Burne (1995) and this work (see Chapter 3). From the methods of Strachan and Alsop (2006) and the criteria considering that it was at or near the palaeo-surface (Fig. 5.3), this suggests that the ‘Black Rock Slump Bed’ at Lynstone is a massive slump bed that moved down a SSW-oriented palaeo-slope (Fig. 5.8).

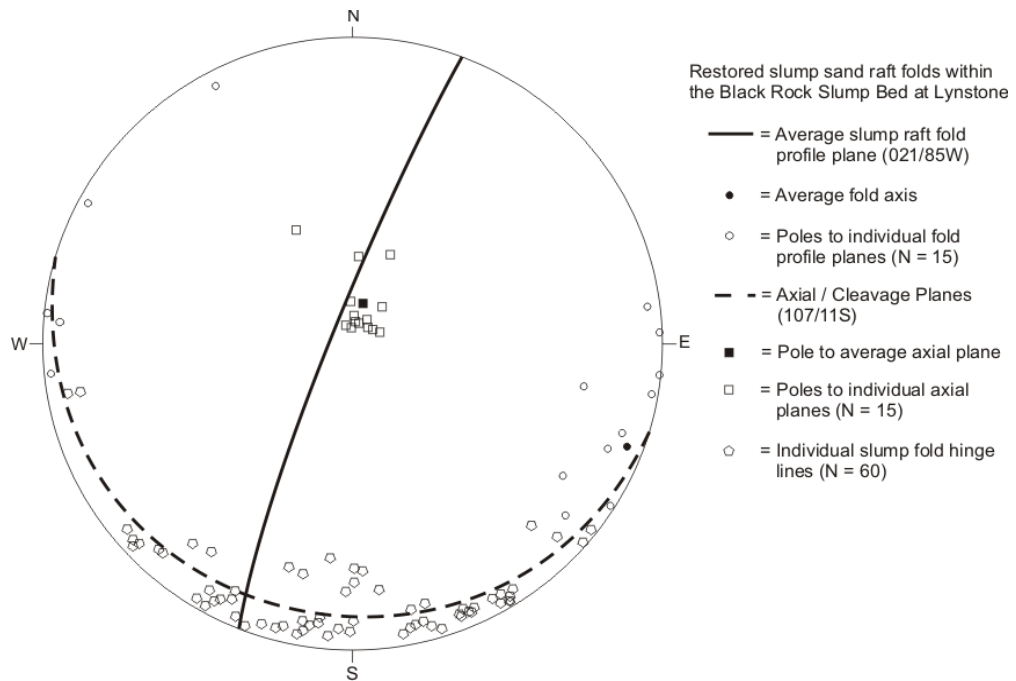


Fig. 5.8: Stereonet with a southern hemisphere projection showing restored mean orientations of all detached slump raft folds within the Black Rock Slump Bed at Lynstone (SS200053)

| <b>H<sub>0</sub></b> : Detached slump raft fold profile plane strike direction and hinge line elongation direction ARE parallel; <b>H<sub>1</sub></b> : The two directions are NOT parallel |             |
|---------------------------------------------------------------------------------------------------------------------------------------------------------------------------------------------|-------------|
| Mean profile plane strike direction (MP)                                                                                                                                                    | 201.27      |
| Mean elongation direction (ME)                                                                                                                                                              | 200.60      |
| Variance profile plane strike direction (VP)                                                                                                                                                | 13.97       |
| Variance elongation direction (VE)                                                                                                                                                          | 14.03       |
| N (profile plane strike direction) = NP                                                                                                                                                     | 15          |
| N (elongation direction) = NE                                                                                                                                                               | 15          |
| <b>Z = ((MP-ME)/√((VP/NP) + (VE/NE)))</b>                                                                                                                                                   | <b>0.39</b> |
| Sample size (K)                                                                                                                                                                             | 2           |
| <b>99% confidence limit on Z-statistic that H<sub>0</sub> is true</b>                                                                                                                       | <b>2.58</b> |

Table 5.2: Statistics used to determine that the detached slump raft profile plane strike and hinge line elongation directions are parallel (from the methods of Hayslett & Murphy, 1971)

As the mean profile plane strike direction is parallel to the hinge line elongation direction, the profile plane may be a proxy for the down-slope average axis (see Tables 5.1-5.2; from the methods of Strachan & Alsop, 2006). In order to justify this statistically, the profile plane strike and elongation direction data have been analysed.

In this statistical analysis, there are two hypotheses. The Null Hypothesis (**H<sub>0</sub>**) is “The detached slump raft fold profile plane strike direction and hinge line elongation direction are parallel”. The alternative hypothesis (**H<sub>1</sub>**) is “The detached slump raft fold profile plane strike direction and hinge line elongation direction are **not** parallel”. The results of statistical analysis on the profile plane strike and elongation direction data (Table 5.2; after Hayslett & Murphy,

1971) show that there is greater than a 99% confidence that the two directions are parallel. This suggests that both directions are oriented down-slope (from the methods of Strachan & Alsop, 2006), which is important as it may not be possible to measure the elongation direction at each outcrop. The profile plane data also provide a quality control on the elongation direction data.

Also, it is suggested that in lithified rock, sheath folds display asymmetric, curvi-linear hinge lines about their profile and axial planes (Alsop & Holdsworth, 2004). However, this has not been demonstrated in the detached slump raft folds that developed from liquefied sediment. One potential reason for this is that during deformation, the liquefied sediment grains in detached slump rafts undergo ‘independent’ flow (Craig, 1997) and the heterogeneous shear strain associated with the deformation is not accommodated (see Chapter 2).

### **Evidence for spreading of the ‘Black Rock Slump Bed’ at Lynstone**

In the ‘Black Rock Slump Bed’ at Lynstone no incision of the underlying beds by the slump bed was observed (Fig. 5.6; see gusset). The restored slump raft fold orientations show that the folds near the cliff trend southwards, and near the foreshore, south-westwards. This provides a test of whether the raft folds were spreading out during slump movement.

Fabric topology plots were constructed to describe whether the restored profile plane strike direction (aligned with the palaeo-slope direction) is related to either the slump raft axial plane orientation (Fig. 5.9a) or the profile plane dip angle (Fig. 5.9b), and so describe the 3D slump raft fold geometry. There is a strong positive relationship between the restored profile plane strike direction and the restored axial plane strike direction ( $R^2 = 0.9650$ ) (Fig. 5.9a), but no relationship between the restored profile plane strike direction and the restored profile plane dip angle ( $R^2 \approx 0$ ) (Fig. 5.9b). The results of the topology plot in Fig. 5.9a suggest that there is an orthogonal relationship between the restored profile plane strike direction and the restored axial plane strike direction and that the raft folds show large variations in movement direction.

Together with the sedimentary observations, this may suggest that the slump bed was deposited directly onto the palaeo-surface, and that it had lost sufficient energy (i.e. waning flow) to incise the underlying beds. A model is proposed showing the raft fold geometries as they spread out and is illustrated in Fig. 5.9c.

### **Development of detached slump raft isoclinal-‘elastica’ interlimb angles**

In the Black Rock Slump Bed at Lynstone, the slump raft folds have isoclinal to ‘elastica’ interlimb angles (i.e.  $20^\circ$  to  $-20^\circ$ ). According to Strachan and Alsop (2006), slump raft folds tighten when their orientations are increasingly sub-parallel to the main down-slope direction. To test if this relationship holds for the raft folds, a third fabric topology plot (Fig. 5.9d) compares for each slump raft fold compares the profile plane strike direction (aligned with palaeo-slope direction; see Table 5.2) and the fold tightness (i.e. interlimb angle), giving a strong correlation between the parameters ( $R^2 = 0.7507$ ).

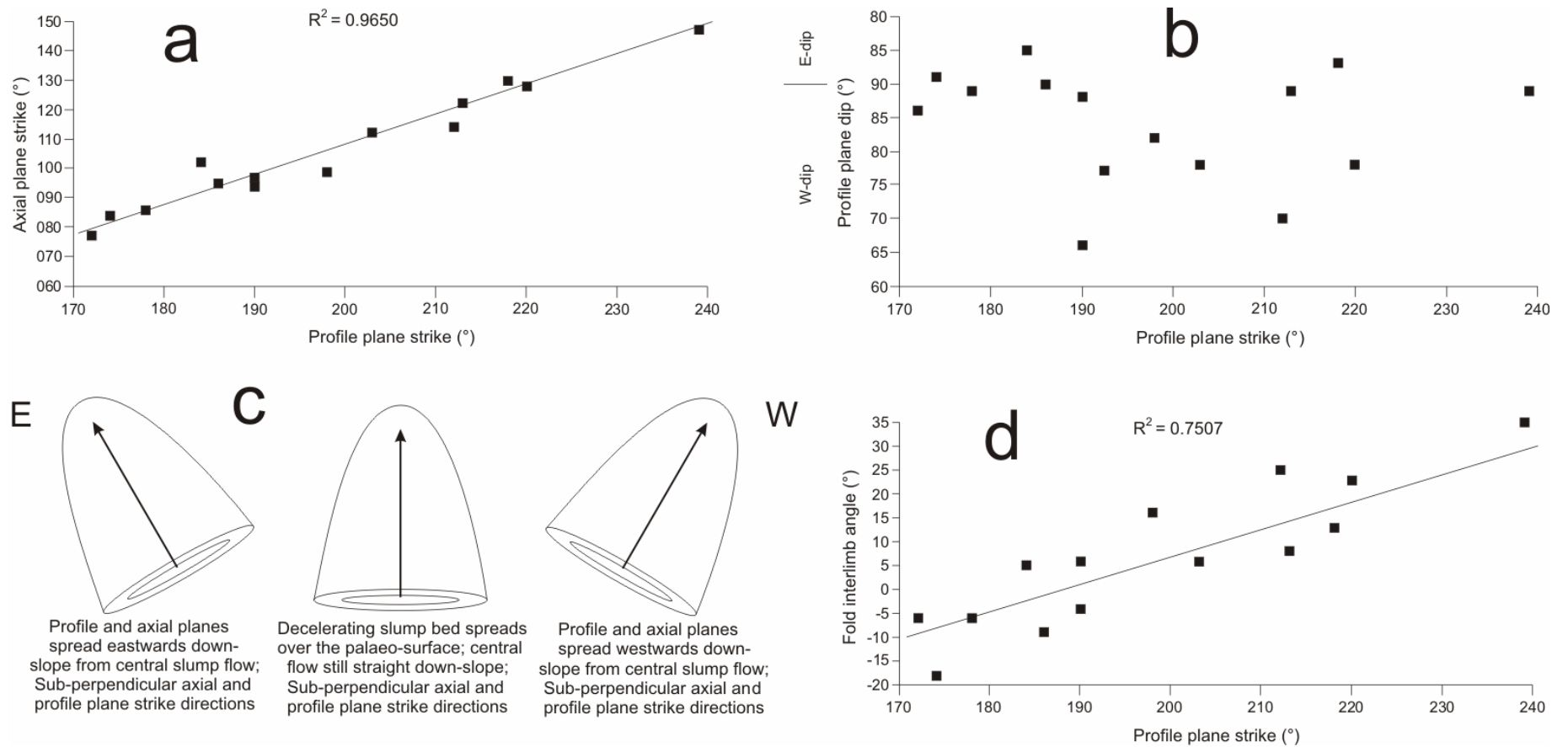


Fig. 5.9: Fabric topology plots and a plan-view idealised sketch representation of slump fold rafts in the Black Rock Slump Bed at Lynstone. The fabric topology plots describe the variation in profile plane strike orientation for the detached slump raft folds with: (a) axial plane strike orientation (good positive correlation;  $R^2 = 0.9650$ ); (b) profile plane dip (no correlation); and (d) fold tightness or interlimb angle (positive correlation;  $R^2 = 0.7507$ ). The plan-view idealised sketch representation of the slump fold rafts in the Black Rock Slump Bed at Lynstone (c) displays idealised raft geometries

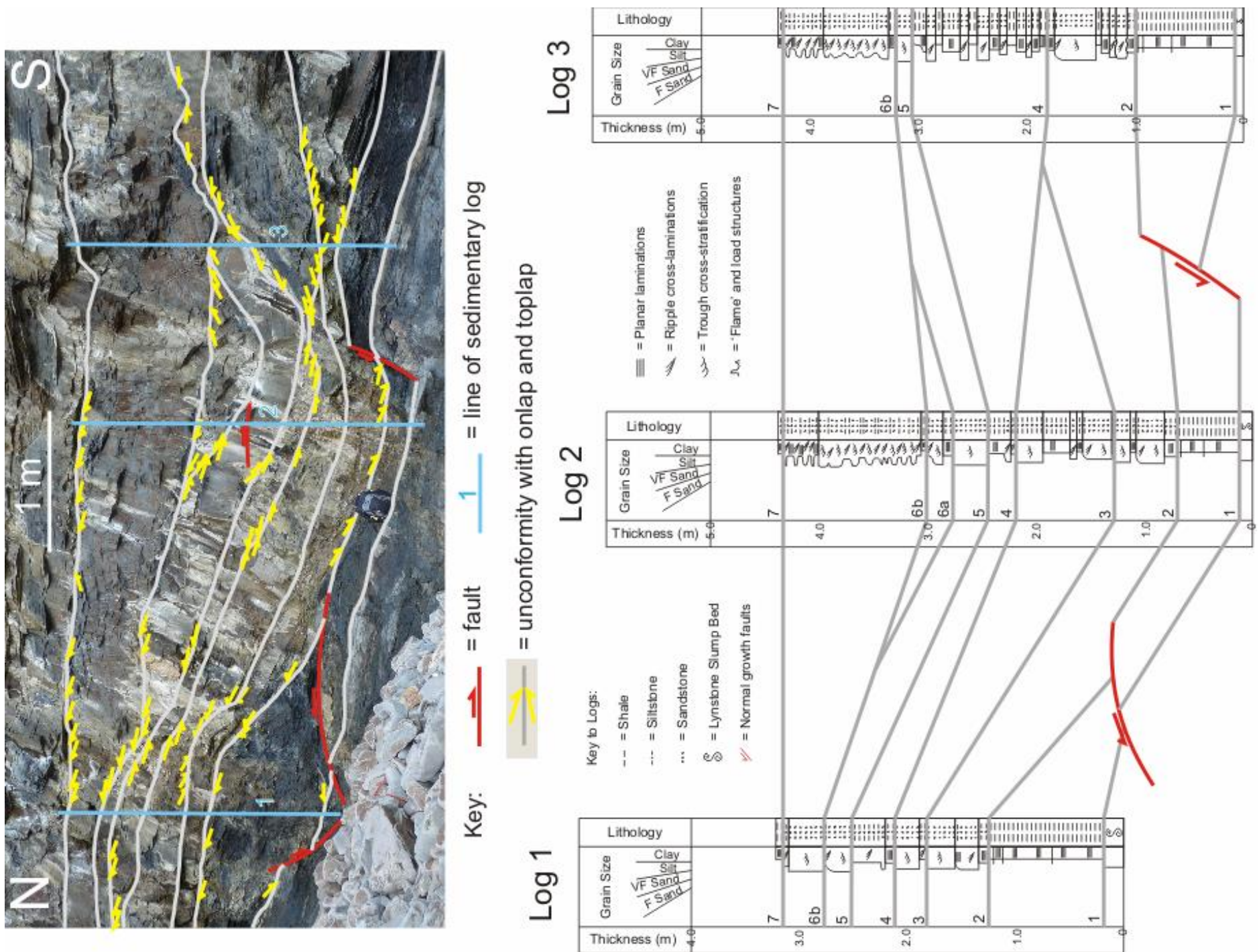


Fig. 5.10: Correlated sedimentary logs (bottom) across a syn-depositional high-angle normal fault and low-angle fault that control the variable subsidence and thickness of growth strata units (top) above the Black Rock Slump Bed at Lynstone (SS2000055). The annotations on the photograph (top) provide details on the variations in unit thickness and the stratigraphic cut-offs (i.e. onlapping and toplapping truncations)

This suggests that there is a strong relationship between palaeo-slope direction and raft fold interlimb angle. This is consistent with the Strachan-Alsop model in which the raft folds tighten due to gravitationally-induced shear strain accommodation during slump transportation.

### **Growth strata deposited above the ‘Black Rock Slump Bed’ at North Lynstone**

Above the ‘Black Rock Slump Bed’ at North Lynstone (SS200055), variable thicknesses of stacked beds, together with both onlap and toplap truncations of beds have been observed, as is also described by Enfield et al (1985) at Lynstone (SS200053) (Fig. 5.2). As with the Lynstone outcrop, normal faults are associated with variably thick stacked beds. Three correlated sedimentary logs have been taken across the faults over a distance of 10 m (Fig. 5.10) in order to establish whether the stratigraphic stacking pattern was affected over short lateral distances by the normal fault movement, following massive slump bed deposition. These logs show that there are seven identified stratigraphic units, plus an additional eighth local unit (number 6a) recorded in log 2 only. The thickness of the units in logs 2 and 3 is approximately 4 m, but is only approximately 3 m thick in log 1 (Fig. 5.10). The log details are:

*Unit 1* is thickest in log 3 (> 1 m) and sits in a roll-over anticline above one of the extensional faults and has toplap truncations beneath Unit 2;

*Unit 2* is approximately the same thickness across the logs (0.5 m) and generally onlaps onto Unit 1 except around the position of log 3;

*Unit 3* is thin (0.15 m) around log 3, thickens around log 2 (0.8 m) but has toplap truncations and so thins between log 2 and log 3;

*Unit 4* has toplap truncations beneath Unit 5, is thin around logs 1 and 2 (0.2 m), but thickens considerably around log 3 (> 1 m; Fig. 5.10);

*Unit 5* has toplap truncations beneath units 6a and 6b and also consistent thickness (0.2 m);

*Unit 6a* is observed only in log 2 (0.2 m thick), has toplap truncations under Unit 6b and sits above one of the normal faults (Fig. 5.10);

*Unit 6b* is thin around log 1 (0.3 m), onlaps onto Unit 5, thickens considerably between logs 2 and 3 (> 1 m) and has toplap truncations beneath Unit 7;

*Unit 7* does not display any thickness changes and has continuous beds across the logged area.

Three conclusions can be drawn from the thickness variations of the units in Fig. 5.10:

1. In the proximity to log 3, some accommodation space was generated on the low-angle listric normal fault hanging wall during the deposition of Unit 1, which caused a roll-over anticline to develop. The subsequent units are thin with numerous stratigraphic cut-offs, suggesting that limited accommodation space was generated above the roll-over anticline at this stage.
2. Close to log 2, some accommodation space was generated on the high-angle extensional fault hangingwall during deposition of Units 3, 6a and 6b, suggesting that the fault was reactivated in extension during deposition.

3. Close to log 1, some accommodation space was generated on the high-angle extensional fault footwall during deposition of Unit 4, but erosion occurred during or just after deposition of units 3 and 6a, so that both are missing on the footwall, suggesting that the footwall experienced repeated burial and non-deposition or erosion.

The development of variably thick beds (i.e. growth strata) and stratigraphic cut-offs above the Black Rock Slump Bed suggests that there is a link between the accommodation space generated above the faults and the depositional thicknesses (Fig. 5.10). Where such a link exists, massive slump bed deposition generates local accommodation space. However, as the slump beds are liquefied structures, variable dewatering may result in fault-controlled variable thicknesses of 'undeformed' growth strata above a massive slump bed as observed by Enfield et al (1985) in Fig. 5.2 and also in the correlated sedimentary logs from Figs. 5.7 and 5.10.

#### **5.3.4 Detached slump raft folds in the Black Rock Slump Bed at Black Rock**

Structural data were collected from 30 detached raft folds within the Black Rock Slump Bed at Black Rock (Fig. 5.7), which have the same geometries as the slump raft folds in the Black Rock Slump Bed at Lynstone (Fig. 5.6). The results of stereonet analysis on restored data (Fig. 5.8) show that all the unrestored rafts face vertically downwards or are steeply dipping to the north. The massive bed sits on the steeply north-dipping limb of 'upright' chevron anticline A and is between shale bed 7a and 7b (see Chapter 4), with the base of the massive bed truncating shale bed 7a (see gusset). The structural restoration of the Black Rock Slump Bed involves 'unfolding' the 'upright' chevron folds so that all the beds are sub-horizontal.

The restoration of the structures using a stereonet gives the mean axial plane orientation for the rafts as 098/17N (strike circ. var.  $\pm 3^\circ$ ;  $n = 30$ ), making them 'reclined' sheath folds (Fig. 5.11). The interlimb angles are isoclinal-to-'elastica' (i.e.  $20^\circ$  to  $-20^\circ$ ) and the doubly-plunging raft hinge lines have a large degree of curvi-linearity ( $122^\circ \pm 5^\circ$ ;  $n = 30$ ) (Fig. 5.11) about the mean profile plane strike direction. The folds face in the same direction as the mean profile plane strike direction. The raft hinge line elongation direction could not be measured as the raft fold hinges face into the ground to the north at Black Rock. Accordingly, the mean profile plane strike direction ( $013^\circ \pm 1^\circ$ ;  $n = 30$ ) was used as a proxy for the down-slope average axis (see Tables 5.1 & 5.2; from the methods of Strachan & Alsop, 2006). The statistical geometric significance of the association between the profile plane strike direction, fold hinge line elongation direction and palaeo-slope direction is described in section 5.3.3 (Table 5.2). The mean profile strike direction suggests that the Black Rock Slump Bed at Black Rock was transported down a north-dipping palaeo-slope during Bude Formation deposition. This palaeo-slope direction opposes the directions from the palaeo-flow indicators of Higgs (1991) and Burne (1995), but is sub-parallel to those from this work at Widemouth (see Chapter 3) and may imply that either there were variable palaeoslope directions within the basin during deposition.

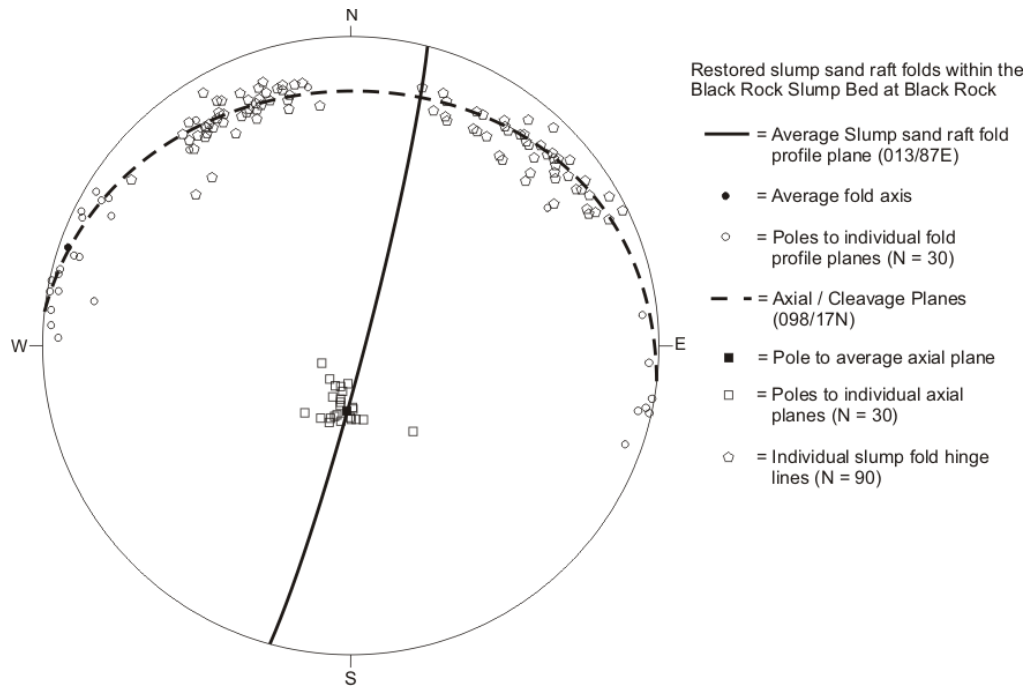


Fig. 5.11: Stereonet with a southern hemisphere projection showing restored mean orientations of all detached slump raft folds within the Black Rock Slump Bed at Black Rock (SS197017)

### Recognition of separate massive slump beds

In Freshney et al (1972), the Black Rock Slump Bed is apparently observed at both Black Rock (SS196017) and Lynstone (SS200053) and the outcrops were assumed to be from the same bed. Consequently, this bed has been used as a marker horizon to correlate the Bude Formation between the two locations from the work of King (1967). Correlated logs with the Black Rock (BRSB) and Lynstone slump bed (LSB) positions are provided in Figs. 3.1a & b.

The results from stereonet analysis on the axial plane orientations for the two slump raft sets (Figs. 5.8 & 5.11) established that the massive slump bed at Black Rock was transported to the north but to the south at Lynstone. Thus, the so-called Black Rock Slump Bed is, in fact, two slump beds, hereafter called the “Black Rock Slump Bed” and the “Lynstone Slump Bed” (see Figs. 3.1a & b). This suggests that the slump beds moved down different palaeo-slopes in separate Culm Basin ‘events’ during Bude Formation deposition and clearly invalidates treating these slump beds as laterally-continuous structures.

### A constrained environment for the Black Rock Slump Bed

The basal shale below the Black Rock Slump Bed has laminations defined by bedding-parallel ankerite veins that have been truncated against the base of the massive slump bed. The basal truncations may represent either truncation during slump movement or a ‘channel’ cut into the underlying shale bed. Under this ‘channel’ hypothesis, the slump raft fold geometries (i.e. profile plane strike and axial plane strike directions, and profile plane dip angles) may have been affected by such a ‘channel’ reflecting a flow of material towards its centre.

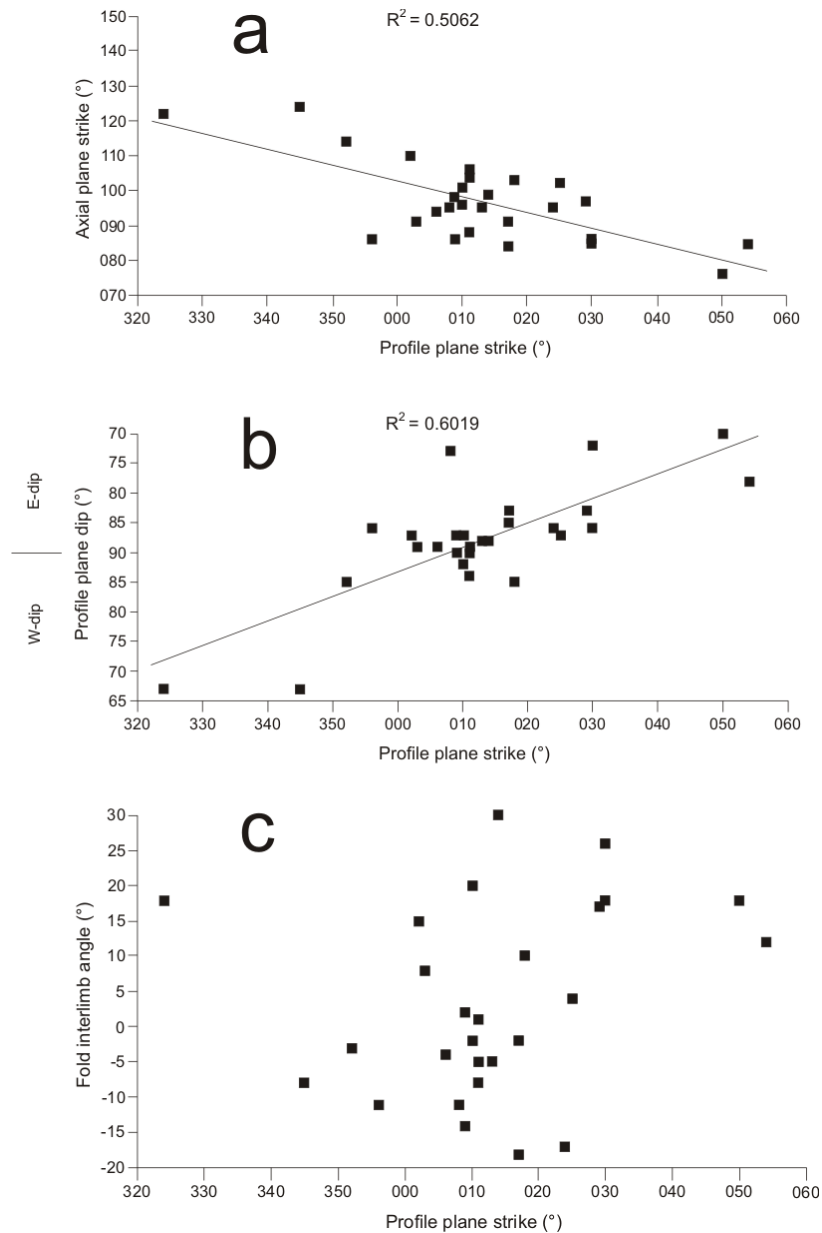


Fig. 5.12: Fabric topology plots in the Black Rock Slump Bed at Black Rock to describe the variation in profile plane strike orientation for detached slump raft folds with: (a) axial plane strike orientation (slight negative correlation;  $R^2 = 0.5062$ ); (b) profile plane dip (possible positive correlation;  $R^2 = 0.6019$ ); and (c) fold tightness or interlimb angle (no correlation)

In order to assess the relationships between the various slump fold geometries, fabric topology plots are constructed for the Black Rock Slump Bed at Black Rock. These plots are the same as with the “Lynstone Slump Bed”. When the restored profile plane strike direction is compared to the restored axial plane strike direction, there is a small reverse relationship between the features ( $R^2 = 0.5062$ ) (Fig. 5.12a). When the restored profile plane strike direction is compared to the restored profile plane dip angle, there is a possible direct (i.e. positive) relationship between the features ( $R^2 = 0.6069$ ) (Fig. 5.12b). In both cases, further data would be required to demonstrate that any clear relationships exists between the directions of the slump raft fold profile plane strike and axial plane strike, as well as the profile plane dip angles.

Consequently, the statistical analysis does not support the hypothesis that the raft folds were preferentially orientated within a 'channel' cut into the underlying shale bed.

### **Development of detached slump raft isoclinal-'elastica' interlimb angles**

In the Black Rock Slump Bed, the slump raft folds have isoclinal to 'elastica' interlimb angles (i.e.  $20^\circ$  to  $-20^\circ$ ). According to Strachan and Alsop (2006), slump raft folds tighten when their orientations are increasingly sub-parallel to the main down-slope direction. In order to test if this relationship holds for these slump raft folds, a third fabric topology plot is constructed in order to compare the profile plane strike direction (aligned with palaeo-slope direction; Table 5.2) and the fold tightness (i.e. interlimb angles) for each slump raft fold (Fig. 5.12c). The results of the topology plot show that no regression line could be fitted through the data ( $R^2 \approx 0$ ) and suggests strongly that there is no relationship between the palaeo-slope direction and the raft fold interlimb angles in the Black Rock Slump Bed. This result is surprising because it suggests that gravitationally-induced shear strain during slump transportation has not caused the detached slump rafts in the Black Rock Slump Bed to become tighter, as would have been expected from the results of Strachan and Alsop (2006).

### **Evidence for variable subsidence above the Black Rock Slump Bed**

Following deposition of the Black Rock Slump Bed at Black Rock (SS197017), black shale deposition recommenced (Fig. 5.7). Over-lying the shale, there is a succession of thinly-bedded siltstones and very fine-grained sandstones topped by a thick, laterally-continuous, very fine-grained sandstone bed. In order to describe the strata, 6 sedimentary logs were taken along the Black Rock foreshore. From the results of the correlated logs (Fig. 5.7), the Black Rock Slump Bed is much thicker in the centre and to the east of the foreshore (10-12 m in logs 1-4), but thinner (8 m) towards the west (logs 5-6). Similarly, the overlying black shale is thicker in the foreshore centre ( $> 1$  m in logs 2-4) but thinner (0.5 m) both towards the east (log 1) and west (logs 5-6). Between the black shale bed and the 2 m thick laterally-continuous sandstone bed at the top of the succession, there is a stack of beds up to 5 m thick towards the east (log 1) and west (logs 5-6). In the foreshore centre (logs 2-4), the stack of beds is between 3-4 m thick and the laterally-continuous sandstone bed at the top of the succession is 1 m thick (Fig. 5.7).

Reversal of the thickness trends between the slump bed, overlying shale and overlying clastic beds suggests that after slump bed and black shale deposition either: (1) there was reactivation and movement of the slump bed from the east (log 1) and west (logs 5-6) towards the centre of the foreshore (logs 2-4), causing the slump bed to thicken; or (2) the deposition of the over-lying strata onto the still liquefied slump bed caused the bed to dewater and compact. The second possibility may have been easier to achieve towards the west (log 1) and east (logs 5-6) where the overlying black shale bed is thinnest (Fig. 5.6) and is consistent with increased accommodation space created for deposition of the overlying beds at those positions.

## 5.4 Analyses of high-angle, strata-bound normal faults

Local, high-angle, strata-bound normal faults occur in Bude Formation outcrops in the study area between Northcott Mouth and Black Rock (SS202087-SS195015) and affect only one or a few beds at any particular location. With the strata-bound faults, beds above the faults may either drape or infill the hanging walls, causing onlap onto the faults. The faults may be folded around the hinges of chevron folds or on their limbs, with variably thick beds infilling the accommodation space generated, which Mapeo and Andrews (1991) suggested was “syn-sedimentary”. A test has been undertaken to see whether the faults described here accord with the ‘early’ normal faults of Enfield et al (1985) and the ‘pre-folding’ extensional faults of Mapeo and Andrews (1991), and as such may be described as ‘early’ structures as in Chapter 4.

In order to undertake this test, structural data have been collected from 29 local, high-angle, strata-bound normal faults from across the study area. Restoration of the fault data has been undertaken using stereonet where local faults are present on tilted beds in order to restore them to sub-horizontal. Examples of local high-angle, strata-bound normal faults are given here.

### 5.4.1 ‘Fanning’ array of high-angle normal faults

At Upton-Phillip’s Point (SS200045), a well-exposed, decimetre-thick sandstone bedding surface has been cut by high-angle normal faults (Fig. 5.13). The faults cease at the top of the sandstone bed and cut down into the underlying shale bed. The fault planes also display veins, which could not be scratched by a pen-knife. From acid tests on the veins, there was slight effervescence. This may still suggest that these are quartz veins but with carbonate impurities or washed-up calcareous micro-fossils.

To test if these are ‘early’ normal faults, observations have been made of ‘undeformed’ beds overlying and underlying these structures (see Section 5.2), with surrounding beds dipping approximately 25°S. As a result of the 3D exposure surface, onlap pinch-outs of variably thick infilling beds onto the faults have not been observed. This suggests that the normal faults are consistent with the ‘undeformed’ beds criterion and are described as ‘early’ high-angle normal faults (*sensu lato*) (Fig. 5.13) from the Zoetemeijer et al (1992), Nigro and Renda (2004) and Corredor et al (2005) convention (Fig. 5.3).

From restorations using stereonet analysis on the ‘early’ normal fault data at Upton-Phillips Point (SS200044) (Fig. 5.13), seven faults have been identified as dipping NNW (i.e. synthetic), whilst two dip SE and one dips SSE (i.e. antithetic). Of the seven synthetic faults, their strike orientations range between 047° and 076°, whilst of the three antithetic faults, their strike orientations are 044-045° and 078°. The mean fault profile through the poles to fault planes is oriented: 151/85SW. Striations observed on the fault planes are in a strongly down-dip direction (Fig. 5.13) and are sub-parallel to the profile plane to the faults. This suggests that the profile plane lies along the movement axis of the synthetic ‘early’ faults (oriented 148°-328°). As the striations tend down the fault slip surface, the main movement direction is towards 328°.

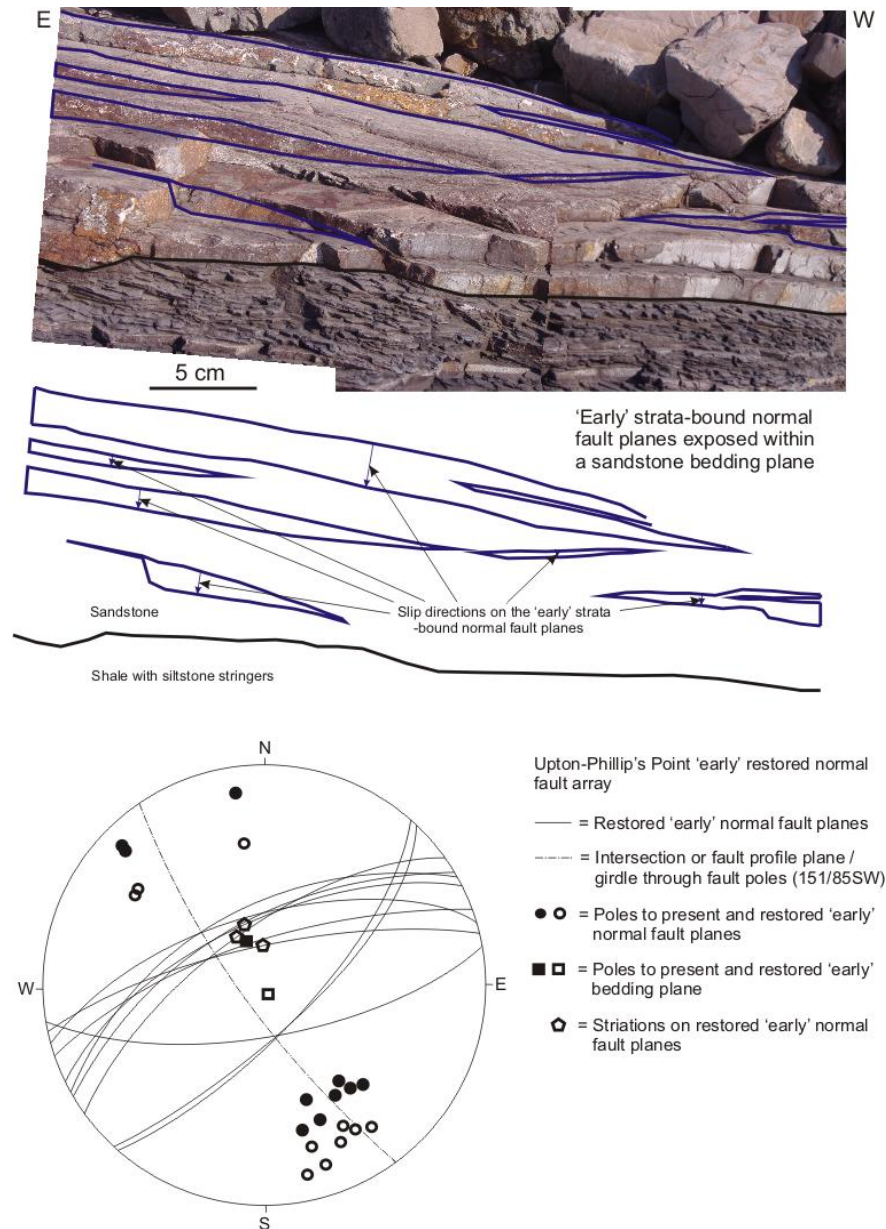


Fig. 5.13: Annotated photo-montage (top) and sketch of an 'early' normal fault array (centre) in a sandstone bed (rock sample 64378) at Upton-Phillip's Point (SS200044). A stereonet with a southern hemisphere projection shows the orientations of restored 'early' normal faults (bottom)

If the 'early' normal faults occurred at or near the palaeo-surface, then they may be influenced by gravity. In the Debacker et al (2009) model, slump fault orientations relate to palaeo-slopes in the basin during deposition. Although these 'early' faults occurred during deposition, they are not slump-generated and so the link to a palaeo-slope origin has not been demonstrated. Still, they may be the up-dip extensional fault scars of subaqueous but coherent landslides, which would suggest a palaeo-slope origin (Schack Pedersen, 1987). As tectonic extension is not being invoked during Variscan deformation, this would require further investigation to assess whether a palaeoslope origin is valid for the normal fault array.

Palaeo-flow indicators from sole marks on turbidite bed bases from Higgs (1991) and Burne (1995) suggest that the general palaeo-flow direction is southwards, but are perpendicular

to the eastwards orientations of trough cross-stratification structures from this work (see Chapter 3). As demonstrated with the opposing directions of the massive slump beds in Section 5.3.3, there may have been times when palaeo-slope directions changed. However, this does not demonstrate a palaeo-slope origin for the high-angle, strata-bound normal fault array at Upton-Phillip's Point.

#### 5.4.2 Reversed high-angle normal faults due to emergence on the palaeo-surface

At Upton (SS200046), stacked beds contain a set of high-angle, reversed normal faults that presently dip at approximately 9°SE. Each fault cuts 2 or 3 beds and have southwards movement directions (Fig. 5.14). The sandstone bed that drapes the reversed normal faults thickens considerably into the down-thrown fault block. Above the draping bed, the overlying beds are 'undeformed', whilst below the draping bed, underlying beds do not appear to correlate across the faults but instead pinch into the fault zone (Fig. 5.14). This suggests that the reverse faults are consistent with all three criteria and are considered as 'early' structures (*sensu stricto*) that occurred during deposition at or near the palaeo-surface, following the Zoetemeijer et al (1992), Nigro and Renda (2004) and Corredor et al (2005) convention (Fig. 5.3).

To study the affect of 'early' high-angle reverse faulting on deposition, two correlated sedimentary logs were taken either side of the faults (Fig. 5.14). The logs show that there are thickness changes in a sandstone bed that drapes the reversed fault, suggesting that the sandstone bed was deposited after fault movement. In the underlying beds, bed thickness and facies stacking pattern variations occur on either side of the faults. Commonly, the thicker beds are deposited on the upthrown side and may suggest that the downthrown side of the 'early' reversed normal faults emerged at the palaeo-surface and caused localised bathymetry changes. This is analogous to the reversed normal faults observed in the Gulf of Corinth region, Greece (photograph provided in Fig. 5.15 by S. Loveless, University of East Anglia).

Restorations using a stereonet on the reverse fault data (Fig. 5.16) show that the poles to fault planes fit a profile plane that is oriented: 159/71W. The restored reversed faults include occasional striations on the fault surfaces (measurements indicated by [ ]), which are oriented: 082/64N [64/351], 070/70N [70/348], 072/66N, 085/61N [60/352] and 081/71N. The striations are strongly dip-parallel and show that the 'early' reversed faults moved to the south or SSE.

The south-to-SSE fault movement direction is opposite to that of the 'early' normal fault array 100 m further south. The movement directions of these 'early' reverse faults are also sub-parallel to the palaeo-flow indicators of Higgs (1991), Burne (1995) and from this work (see Chapter 3). As with the 'early' fault array, the mean reversed fault profile plane strike direction is sub-parallel to the 'early' fault movement direction from the striations. Although these 'early' faults were not generated by slump movement processes, they may be the up-dip extensional fault scars of subaqueous but coherent landslides, which would suggest a palaeo-slope origin (Schack Pedersen, 1987), but which has not been proven.

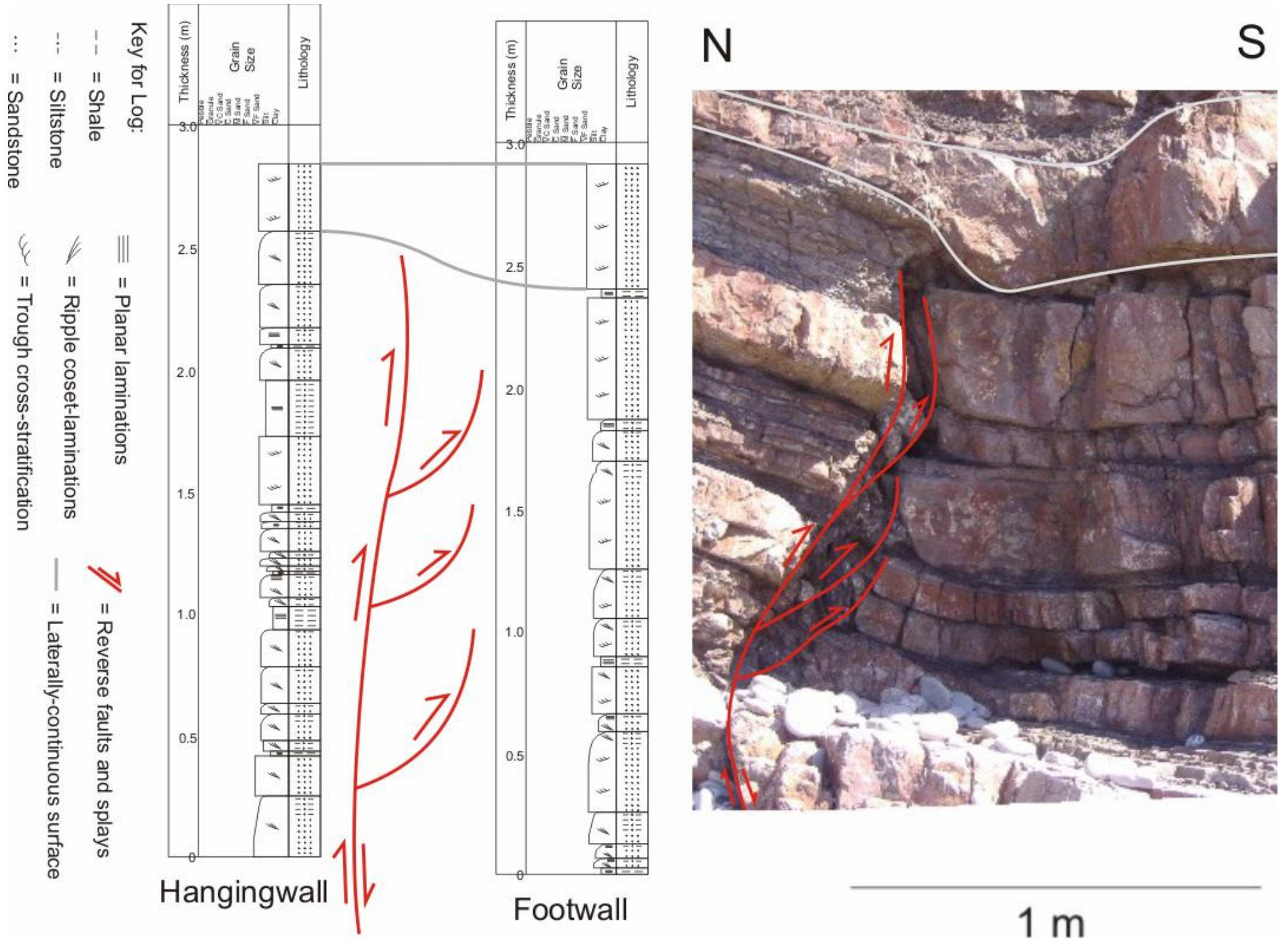


Fig. 5.14: Photo-montage and annotation of 'early' syn-depositional, high-angle reversed normal faults (right) at Upton (SS200045). Also, there are two correlated sedimentary logs to show thickness changes across the fault 'zone' (left). Rock sample 64379 taken in the fault 'zone' (see Chapter 3)



Fig. 5.15: Annotated photograph of a road cutting in the Gulf of Corinth, Greece. Photograph show high-angle reverse normal faults in uplifted sediments in the Gulf of Corinth (photograph provided by S. Loveless, University of East Anglia, 2010 – orientation not known)

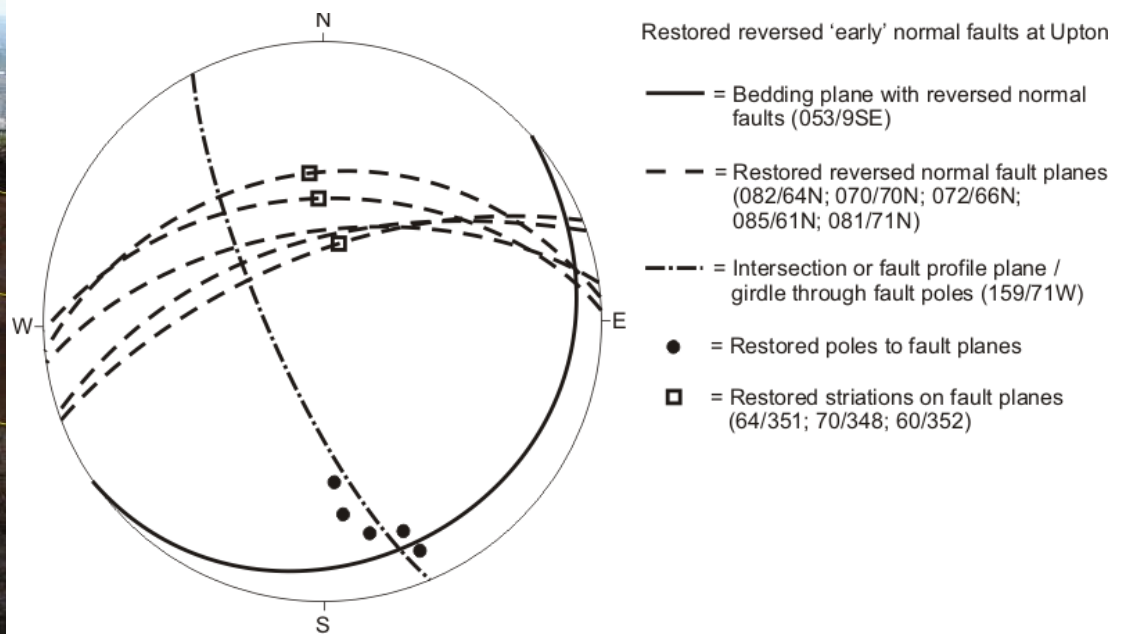


Fig. 5.16: Stereonet with a southern hemisphere projection for the restored data of high-angle, reversed normal faults at Upton (SS200045)

### 5.4.3 Regional variations in ‘early’ high-angle normal fault orientations

Along the Bude Formation outcrops from Northcott Mouth to Black Rock (SS202087-SS197015), 29 ‘early’ high-angle strata-bound, normal faults have been measured. Restorations of the ‘early’ fault data have been undertaken using stereonet in order to assess the original fault movement directions (Fig. 5.17) and where possible this was linked with striation measurements. The results from the stereonet suggest that there is a variation in ‘early’ high-angle normal fault slip direction vertically in the strata, as is seen in the beds between Northcott Mouth and Maer Cliff (SS202087-SS200075) (Fig. 5.17). The vertical movement direction change occurs across the Saturday’s Pit black shale bed with movement southward before black shale deposition and northward in later deposits (Fig. 5.17).

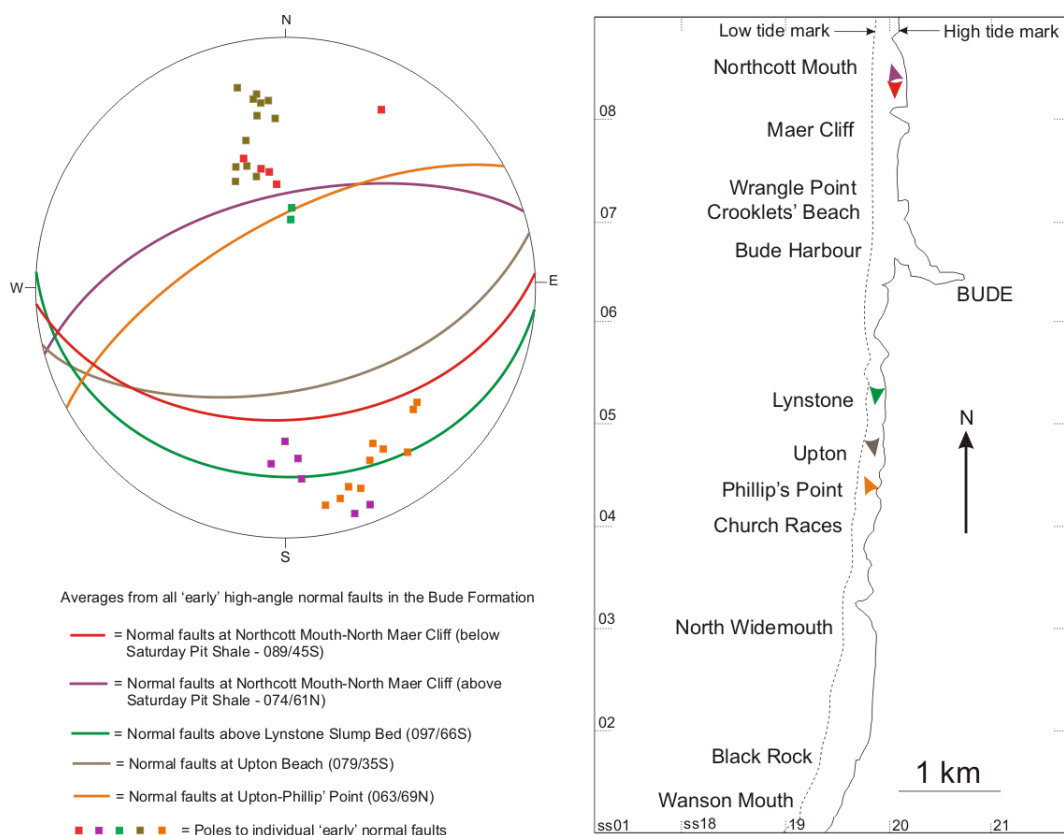


Fig. 5.17: Stereonet with a southern hemisphere projection (left) and a map describing mean restored ‘early’ high-angle strata-bound normal fault orientations (right) between Northcott Mouth and Phillip’s Point (SS202087-SS200044)

There is also a lateral variation in ‘early’ high-angle normal faulting directions across the coastal outcrops (Fig. 5.17). Above the Saturday’s Pit black shale, fault movement is generally to the north between Northcott Mouth and North Maer Cliff (SS202087-SS200075) and also Upton and Phillip’s Point (SS200045-SS200043). In contrast, the faults moved generally to the south between Lynstone and Upton (SS200055-SS200045). A key location is at Upton (SS200045) where ‘early’ normal fault movement directions face each other (i.e. faults to the south slipped northwards and vice versa) as shown in this section (see Figs. 5.13 & 5.14).

The variation in faulting directions across the coastal outcrops is displayed on a map (Fig. 5.17). However, no link has been demonstrated between fault movement direction from striations and the palaeo-slope directions derived from sole marks on turbidite bed bases as reported by Higgs (1991) and Burne (1995) between the Tom's Cove and Saturday's Pit shales (see Chapter 3).

Although a Variscan tectonic origin to the faulting during deposition is suggested (Mapeo & Andrews, 1991; see Chapter 4), further data collection would be required to link 'early' fault movement with the positions of mapped major folds from Freshney et al (1972; 1979). In addition to 'early' high-angle normal faults, there are bedding-parallel faults and low-angle thrusts with associated hanging wall folds that are described below.

## 5.5 Analyses of low-angle faults and associated folds

Bedding-parallel and low-angle faults occur in the Bude Formation outcrops across the study area between Northcott Mouth and Black Rock (SS202087-SS195015). Where faults are bedding parallel, they are difficult to observe but have occasionally 'ramped' through and cut overlying beds. Folds are associated with the low-angle faults either where they cut the beds. The fold geometries assist the geological interpretation not only by highlighting the faults but also in determining the local fault movement direction from the fold facing direction (Suppe, 1985) and in correlation of beds across the fault. Although quartz veins striations occur on low-angle fault planes, multiple generations of striations are observed, which prevents the determination of the original, local fault movement directions.

The low-angle faults are either folded around chevron fold hinges (i.e. 'pre-folding' thrusts of Mapeo and Andrews (1991) and 'early' bedding-parallel thrusts of Enfield et al (1985)) or tilted on their limbs (see Chapter 4), and affect only a few beds at any particular location above a basal shale bed. Beds below this shale bed are 'undeformed', whilst beds above the folds may either truncate the structure or infill the accommodation space on the limbs (see Mapeo and Andrews, 1991). The 'pre-chevron' thrusts of Lloyd and Chinnery (2002) are similar but are much larger (kilometric-scale) structures. A test has been undertaken to see whether the faults described here accord with the 'early' structures as in Chapter 4.

In order to undertake this test, structural data have been collected from 35 bedding-parallel faults and low-angle thrusts. Where the contractional structures are present in tilted beds, restoration of the fault and fold data has been undertaken using a stereonet. The restoration removes the chevron folds, so the beds and contractional structures return to sub-horizontal. Examples of bedding-parallel and low-angle faults, with their associated folds, are given from Northcott Mouth (SS202082) and Upton (SS200045).

### 5.5.1 Recognition of 'early' contractional structures

At Northcott Mouth (SS202082), on the limb of a larger-scale 'upright' chevron syncline, there is a fold pair above a basal bedding-parallel fault with a low-angle fault that cuts

the deformed strata (Fig. 5.18a-b; see Chapter 2). The beds in the fold pair are top-lap truncated by the overlying 'undeformed' beds, whilst the long limb of the local anticline is cut by another low-angle fault, which truncates against this overlying stack of 'undeformed' beds. Beds are repeated across both low-angle faults, which suggest that the faults are thrusts that moved to the north (Fig. 5.18a-b). Presently, the 'undeformed' beds dip at 35° S and variably thick beds are not observed overlying the local structures (Fig. 5.18). This suggests that the local structures are consistent with the 'undeformed' beds and truncated beds criteria and are considered as 'early' bedding-parallel faults, low-angle thrusts and folds (*sensu lato*) (Fig. 5.13) from the Zoetemeijer et al (1992), Nigro and Renda (2004) and Corredor et al (2005) convention (Fig. 5.3).

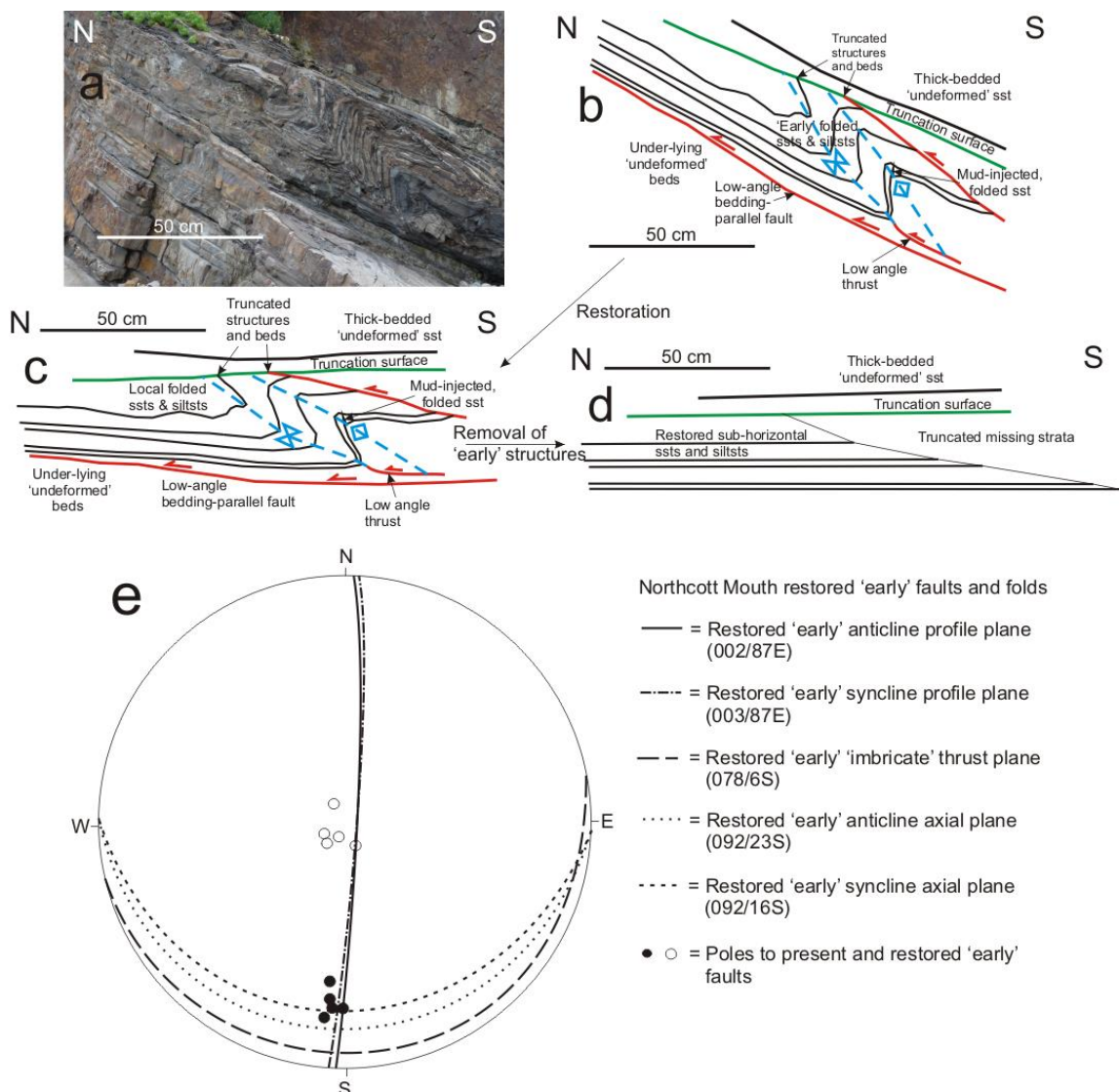


Fig. 5.18: Annotated photograph (a) and sketch (b) of a local fold pair above a bedding-parallel fault and low-angle thrusts at Northcott Mouth (SS202082). Restoring the local deformation (c) returns the faults and surrounding 'undeformed' beds to sub-horizontal. Removal of the local deformation (d) shows missing strata, which is truncated and overlain by 'undeformed' beds. A stereonet of restored data with southern hemisphere projection (e) shows the orientations of the restored local fault and fold structures (includes rock samples 64698-64703; see Chapter 3)

The beds and local ‘early’ structures have been restored to sub-horizontal by removing the affect of the ‘upright’ chevron folding (i.e. tilt on the limb). This shows that the beds on the fold limb between the local ‘early’ fold hinges are overturned, downwards facing and youngs to the north (Fig. 5.18c). Although the underlying bedding-parallel fault may have had a slight dip, this is too small to be estimated when restored. Removal of the ‘early’ structures places the beds into sub-horizontal orientations and shows that there is a large amount of missing strata towards the south that was uplifted during ‘early’ deformation (Fig. 5.18d). The missing strata were either cut by the local low-angle fault on the long limb of the local anticline or truncated above the local structures. The restoration using a stereonet on the ‘early’ structural data shows that the fold axial planes were ‘recumbent’ (synclinal axial plane reoriented to: 092/16S; anticlinal axial plane: 092/23S), whilst the low-angle thrust is reoriented to 078/06S (Fig. 5.18e).

The low-angle fault planes have veins that cannot be scratched by a steel pen-knife and suggests that they are quartz veins. Acid tests on the veins show that there was slight effervescence. This suggests that these are quartz veins (Mapeo & Andrews (1991) as the effervescence possibly resulting from reactions with carbonate impurities and washed-up calcareous micro-fossils. These veins show no visible striations to provide a fault movement direction, which is towards the north from the fold facing direction and bed repetition. However, the base of the overlying ‘undeformed’ bed has a quartz vein with multiple layers of striations on this truncation surface. The striations resulted from movement along this bedding plane, but this plane may have been exploited by flexural-slip movement during Variscan fold deformation (Tanner, 1989), and thus, it cannot be demonstrated to be a bedding-parallel fault.

The ‘early’ structures at Northcott Mouth sit on the limb of an ‘upright’ chevron syncline (Fig. 5.18). Although the deformation is described as ‘early’ (i.e. formed prior to ‘upright’ chevron folding at or near the palaeo-surface in sediment), it may be argued that the folds formed as a z-fold pair due to flexural slip during chevron folding (Tanner, 1989). However, this link to flexural slip folding has not been confirmed because:

1. No comparative s-folds occur on the other ‘upright’ chevron syncline limb;
2. No ‘z-folds’ developed in the ‘undeformed’ beds above and below the ‘early’ structures;
3. Other similar ‘pre-folding’ duplex structures observed by Mapeo and Andrews (1991) “display the wrong sense of transport for generation by the flexural slip mechanism and are in unfavourable orientations for post- or syn-chevron progressive fold generation”.

If the ‘early’ structures occurred at or near the palaeo-surface, it may also be argued that they are influenced by gravity. In the Debacker et al (2009) model, slump fault orientations relate to palaeo-slopes in the basin during deposition. Although these ‘early’ contractional structures occurred during deposition, they are not slump-generated. Still, they may be the down-dip toe thrusts of subaqueous but coherent landslides, which would suggest a palaeo-slope origin (Schack Pedersen, 1987), but which has not been proven. Also, palaeo-flow indicators

from sole marks on turbidite bed bases from this work are to the ENE, whilst Freshney et al (1979) suggested that there are numerous different palaeo-flow directions around Northcott Mouth and so, the palaeo-slope direction is variable (see Chapter 3). Thus, it has not been demonstrated that the northward movement directions of the ‘early’ structures at Northcott Mouth are related to the palaeo-slope direction.

### 5.5.2 Deformed strata below a normal-faulted sandstone bed

At Upton (SS200045), contractional and extensional structures overlie ‘undeformed’ beds. The beds include a mudstone bed that is cut by a near bedding-parallel basal fault to these structures (Fig. 5.19). There are no striations exposed on the vein surfaces that covered the low-angle fault planes in order to provide movement directions. Instead, the local structures affected the thin-bedded package above this basal fault and include an ‘inclined’ anticline that has an overturned, steep downwards facing limb that young to the SW (Fig. 5.20). Structural restoration using a stereonet shows that the anticlinal profile plane is reoriented to 010/75W and the axial plane used to be ‘inclined-to-recumbent’ (reoriented to 149/28NE) (Fig. 5.20).

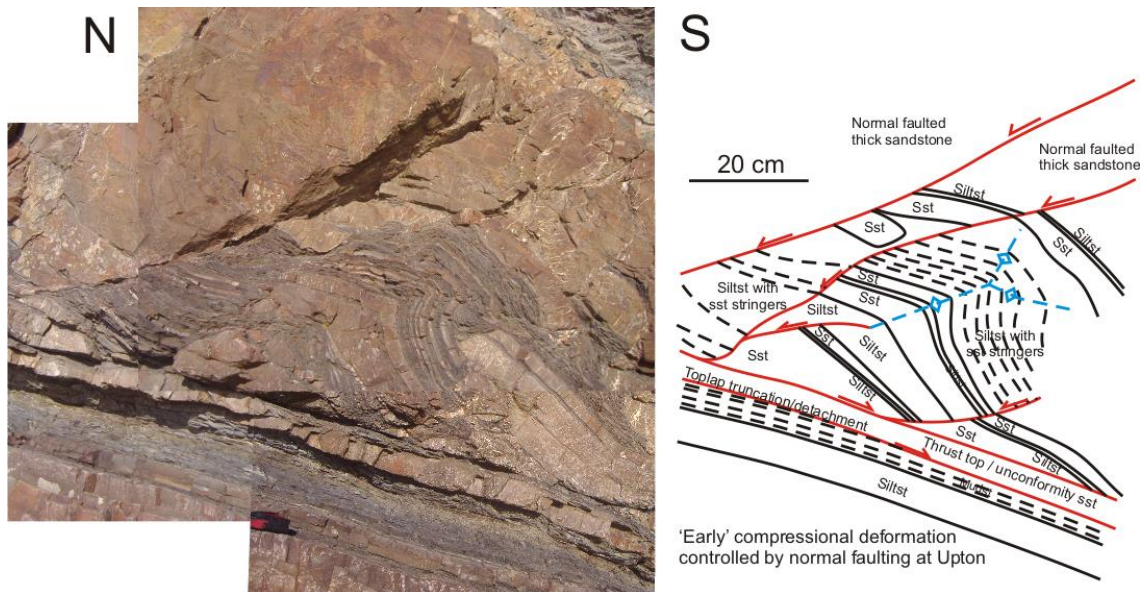


Fig. 5.19: Annotated photo-montage (left) and sketch (right) of deformed thin-bedded strata below thick-bedded sandstone at Upton (SS200045)

There is a set of normal faults that cuts the variably-thick sandstone bed and the thin stack of beds deformed by the local anticline down to the basal low-angle fault (Figs. 5.19-5.20). The variably thick sandstone is overlain by ‘undeformed’ beds that have not been cut by the normal faults and stratigraphically-above these ‘undeformed’ beds, there is the Upton Slump Bed (see Fig. 5.5). Therefore, the faults and folds are consistent with all three criteria to describe them as ‘early’ structures (Fig. 5.13) from the Zoetemeijer et al (1992), Nigro and Renda (2004) and Corredor et al (2005) convention (Fig. 5.3).

A model for the structural development is that after ‘early’ contraction, the folded beds were cut by a later but still ‘early’ set of conjugate normal faults (Figs. 5.19-5.20). The sandstone bed is structurally-above the normal faults and thickened into their hanging walls and thus, was deposited during ‘early’ deformation.

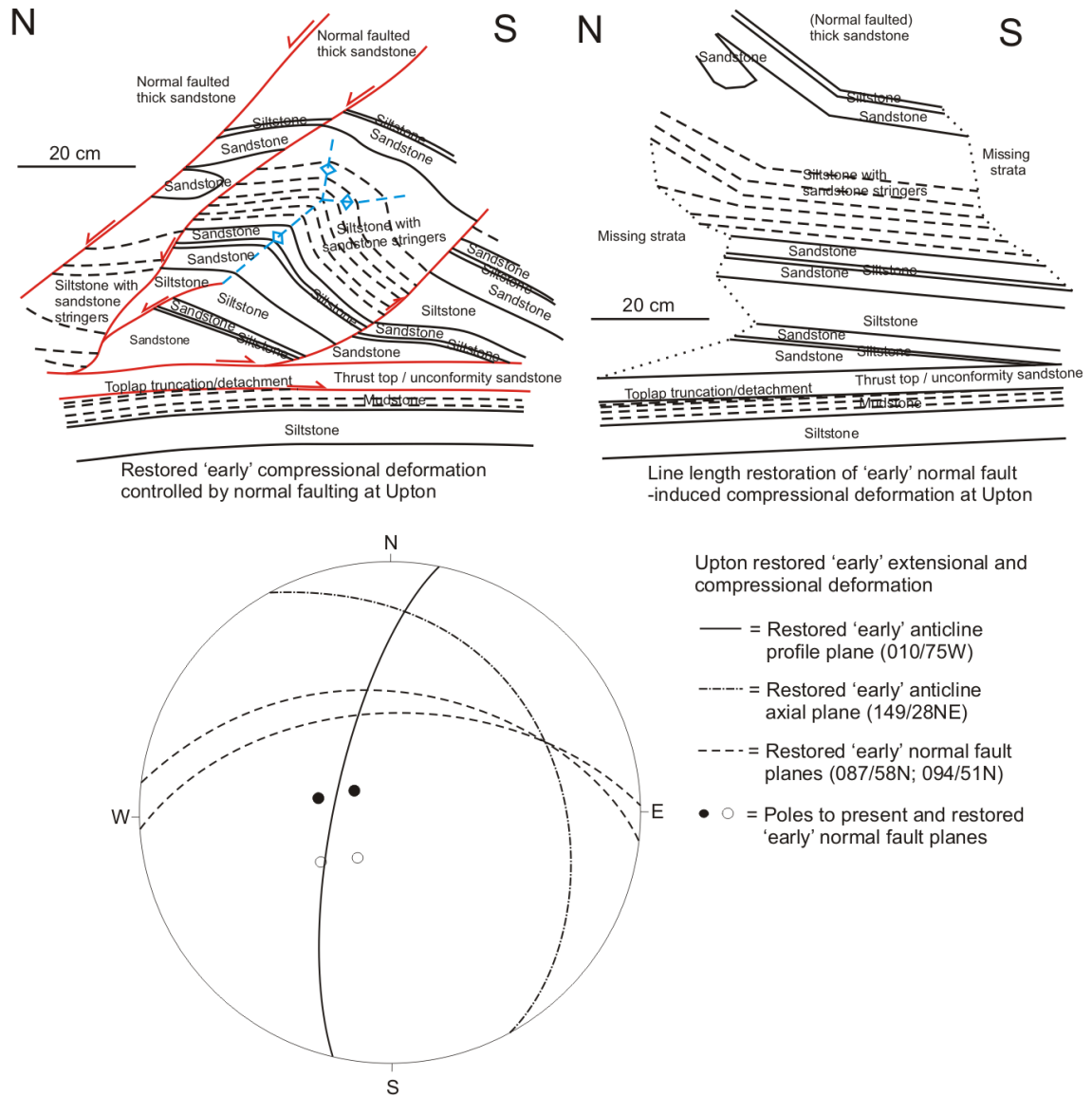


Fig. 5.20: Progressively restored sketches (top) from a photograph and sketch at Upton (SS200045) in Fig. 5.19. This involved restoring for the present dip of the deformed beds (top left) and line-lengths (top right). Also, a stereonet with a southern hemisphere projection is shown of the restored ‘early’ extensional and compressional deformation (bottom) at Upton

### 5.5.3 Regional variations in ‘early’ low-angle thrust orientations

In addition to the two examples given above, 35 ‘early’ bedding-parallel faults and low-angle thrusts have been measured in the Bude Formation outcrops between Northcott Mouth and Black Rock (SS202087-SS197015). From restorations using stereonets on the ‘early’ fault data (Fig. 5.21), assuming that the beds prior to chevron folding were sub-horizontal, the mean



features and formed due to deformation prior to folding at or near the palaeo-surface (Mapeo & Andrews, 1991; Zoetemeijer et al, 1992; Nigro & Renda, 2004; Corredor et al, 2005).

In this work, it was shown that some of the ‘early’ extensional structures (e.g. at Upton; Figs. 5.13 & 5.14) were emergent onto the palaeo-surface and affected deposition. This is consistent with the interpretations of Mapeo and Andrews (1991) of “syn-sedimentary” deformation but contradicts the deeper burial (i.e. > 50 m) theory of Whalley and Lloyd (1986).

An alternative explanation for the ‘early’ faults is that they are layer-bound compaction (polygonal) faults, as imaged in seismic sections from Early Eocene-Late Oligocene North Sea deposits (Cartwright & Dewhurst, 1998). Although the seismically-interpreted faults are on kilometric-scales, it is the range of non-preferred strike orientations that is relevant (see Fig. 3 of Cartwright and Dewhurst, 1998). The ‘early’ high-angle, strata-bound normal faults have a preferred range of strike orientations, contradicting the Cartwright and Dewhurst (1998) model.

The presence of palaeo-slopes during Bude Formation deposition has been described previously using palaeo-flow indicators from sole marks on turbidite bed bases (Freshney et al, 1979; Higgs, 1991; Burne, 1995; see Chapter 3). North of Bude, variable palaeo-slope directions have been inferred by Freshney et al (1979), but south of Bude, a general southward palaeo-slope direction is inferred (Higgs, 1991; Burne, 1995). In contrast, at least two palaeo-slopes are evidenced from the opposing palaeo-flow directions of the Lynstone and Black Rock Slump Beds (Figs. 5.8 & 5.13). North of Northcott Mouth (SS202087), the occurrence of slump beds, and hence, the generation of palaeo-slopes appear to increase higher in the Bude Formation (Enfield et al, 1985). The slumps may have been generated by the variable palaeo-slope directions inferred by Freshney et al (1979) and are described further in Chapter 9.

Although ‘early’ deformation modified the palaeo-surface during Bude Formation deposition (also see Chapter 4) a link between the ‘early’ structures and regional palaeo-slopes in the Culm Basin at that time has not been demonstrated. Instead, the ‘early’ structures could have developed locally as part of the Variscan deformation (Enfield et al, 1985; Whalley & Lloyd, 1986; Lloyd & Chinnery, 2002) and possibly during deposition (“syn-sedimentary” pre-folding structures of Mapeo & Andrews, 1991; see Figs. 4.11a, 4.13, 5.14 & 5.19).

However, Mapeo and Andrews (1991) suggest that their ‘pre-folding’ structures occurred in lithified rock due to the presence of quartz veins on ‘early’ (i.e. ‘pre-folding’) fault planes. This can be challenged on two grounds:

1. Hot (150-300°C) quartz-rich fluid fluxes are recognised in the Culm Basin during Variscan deformation (De Wall & Warr, 2004; see Chapter 3) and may have precipitated on ‘early’ fault planes, creating quartz veins with striations without need for deep burial.
2. On ‘early’ bedding-parallel faults, flexural-slip movement (Tanner, 1989) is likely to have been accommodated during progressive Variscan fold deformation, producing multiple quartz vein generations with striations on these planes and so, the presence of quartz veins may not reflect the lithological state at time of first deformation.

Whalley and Lloyd (1986) observed bedding-parallel north-directed thrusts that exploited slump beds. This thrust orientation may suggest that following slump bed deposition, this bed retained sufficiently elevated fluid pressures that it remained ‘weak’ (i.e. sediment). If this is the case, the thrust movement may have been assisted by such ‘weak’ beds.

| <b>Slump folds (from Strachan &amp; Alsop, 2006)</b>                                                   | <b>Faults in slumps (from Debacker et al, 2009)</b>                                                 |
|--------------------------------------------------------------------------------------------------------|-----------------------------------------------------------------------------------------------------|
| Little length change in direction parallel to strike of controlling palaeo-slope                       | Little displacement in direction parallel to strike of controlling palaeo-slope                     |
| Folds have axes parallel to palaeo-slope strike and hence have undergone no hinge rotation             | Fault plane strike is parallel to palaeo-slope strike and hence have undergone no rotation          |
| Vergence or facing direction is deemed as slip direction and is in a down-slope direction              | Fault movement direction is deemed as slip direction and is in a down-slope direction               |
| Folds generated by heterogeneous simple shear about the slip direction                                 | Faults generated by heterogeneous compression / extension about slip direction                      |
| In slumps, fold asymmetry senses oppose each other about down-slope average axis                       | <i>Antithetic / synthetic fault slip directions oppose each other about down-slope average axis</i> |
| Maximum fold elongation direction is aligned down-slope                                                | <i>Maximum fault displacement direction is aligned down-slope</i>                                   |
| <b>Fold profile plane is aligned with maximum fold elongation direction (down-slope direction)</b>     | Fault profile plane is aligned with maximum displacement direction (down-slope direction)           |
| Fold hinges will verge and face in a statistical arc about transport direction                         | Faults become listric (curve down) and face in a statistical arc about transport direction          |
| With applied shear stress, folds tighten and hinges rotate into a transport-parallel direction         | With applied shear stress, fault angle decreases and rotates into a transport-parallel direction    |
| In slumps, transport direction is parallel to mean axial-planar intersection of opposed vergence folds | Transport direction is parallel to mean fault plane intersection of opposed trending faults         |
| Hinges rotate at either end to form curvi-linear fold geometries                                       | Fault arrays form a curvi-linear break in affected strata                                           |

Table 5.3: Summary table of structural methods for studying palaeo-slope directions from slump analysis from both Strachan and Alsop (2006) and Debacker et al (2009). The method in **bold** is a new method designed and tested in this chapter. The potential methods in *italics* remain untested but may be recognised in faulted slump beds to enhance palaeo-slope methodology

### 5.6.1 Discussion on the palaeo-slope direction assessment methodologies

In this chapter, a series of methods drawn from Strachan and Alsop (2006) were employed to assess the palaeo-slope directions from the structural orientations of slump raft folds within both the Lynstone and Black Rock slump beds. The structural and statistical analyses indicated that there is a statistically-significant alignment between the slump raft fold profile plane direction ( $\pi$ -girdle) and the maximum fold elongation direction, and hence, the palaeo-slope direction (Table 5.3). This relationship is analogous to the fault profile plane ( $\pi$ -

girdle) alignment with the maximum displacement direction, and hence, the palaeo-slope directions from the methods for slump fault orientations of Debacker et al (2009).

Demonstrating that the slump fold methods of Strachan and Alsop (2006) and slump fault methods of Debacker et al (2009) are analogous implies that there could be other statistical relationships between the methods and therefore a comparison has been undertaken (Table 5.3). From the comparison, in addition to the slump fold method determined in this chapter (**bold** in Table 5.3), it appears that there are two slump fold relationships without existing analogous slump fault relationships. The potential slump fault relationships (in *italics* in Table 5.3) are: (1) antithetic / synthetic fault slip directions that oppose each other about a down-slope average axis; and (2) fault maximum displacement is aligned down-slope.

Therefore, the validity of the potential slump fault relationships needs to be tested on faults within a demonstrably faulted slump bed. Unfortunately, this was not possible in the Bude Formation and would require further study.

## 5.7 Summary of slumping and ‘early’ deformation in the Bude Formation

The Bude Formation contains a number of ‘early’ structures that lie between ‘undeformed’ beds. The structures include slumps that occurred in unlithified sediments at or near the palaeo-surface, which moved down palaeo-slopes in the Culm Basin during deposition. Other structures include ‘early’ high-angle, strata-bound normal faults, and both bedding-parallel fault and low-angle thrusts, with their associated folds, that occurred in unconsolidated sediments at or near the palaeo-surface (see Chapter 4). This is of importance to the general aim of the thesis, namely to establish criteria for distinguishing between folds in rock and sediment.

A palaeo-slope origin for the ‘early’ bedding-parallel faults and low angle thrusts, with their associated folds, is possible where their direction of movement is parallel to palaeoflow indicators and slump fold elongation directions, but has not been proven fully. In the case of the high-angle, strata-bound normal faults, as tectonic extension is not being invoked during Variscan compressional deformation, this may suggest that a palaeoslope origin could cause their generation. This requires further investigation to assess whether this is the case.

As the slump and ‘early’ deformation structures occurred in unlithified sediment, other soft-sediment and/or tectonically-deformed sediment features should be present in the Bude Formation outcrops as well. The purpose of Chapter 6 is to consider these additional sediment deformation structures as well, including what they suggest about the mechanical state of the Bude Formation beds during Variscan deformation, which is of importance to the general aim of the thesis.

## Chapter 6: Field evidence for deformation in sediment from the Bude Formation

### 6.1 Introduction

In Chapters 4 and 5, it was recognised that many Bude Formation folds formed in sediment at or near the palaeo-surface. In this chapter, further evidence is provided that is relevant to part of the general aim of the study, namely of the Bude Formation lithification state during folding, using observations and measurements between Northcott Mouth and Black Rock (SS202087-SS195015) of: (1) deformed bedding-parallel ankerite veins (see Chapter 3); (2) bulbous-hinged beds in folds; and (3) mud injections (see Chapter 2) cutting fold hinge zones.

Important Bude Formation structures described in the literature include: bulbous-hinged sandstone and siltstone beds in ‘upright’ chevron folds with inter-limb angles less than  $70^\circ$  (see Chapter 2; Sanderson, 1974); the ‘early’ structures and slumps deformed by ‘upright’ chevron folds (Enfield et al, 1985; Mapeo & Andrews, 1991; Hecht, 1992; see chapter 4 & 5); and sand volcanoes on the tops of contorted beds (Burne, 1970; see Chapter 2). However, the significance of the bedding-parallel ankerite veins (see Chapter 3) and mud injections (see Chapter 2) cutting chevron fold hinge zones have not been described previously for the Bude Formation beds.

The Bude Formation is a type area for chevron folds (Freshney et al, 1972; 1979; Ramsay, 1974; Sanderson, 1974; 1979; Lloyd & Whalley, 1986; Davison et al, 2004), with both ‘upright’ and ‘inclined-to-recumbent’ types observed. North-directed thrusts cut the chevron folded beds and have also been deformed by the chevron folds (Enfield et al, 1985; Whalley & Lloyd, 1986). Increasingly towards the south of the Culm Basin, the chevron folds have been modified by south-directed shear deformation, which generated increasingly south-directed ‘inclined-to-recumbent’ chevron folds (Sanderson, 1979; Lloyd & Whalley, 1986; see Chapter 4). North-directed chevron folds may have formed where thrusts and associated hanging wall folds have been emplaced prior to chevron folding and then refolded (Lloyd & Chinnery, 2002; see Chapter 2). In order to provide insights into the progressive Variscan deformation that affected the Bude Formation beds, data was collected from all the different structures in the Bude Formation outcrops. Its analysis has involved stereonet projections of structural features and restoration of some of the thrust faults also using stereonets (NB. each estimated angular data mean is accompanied by an estimated circular variance).

### 6.2 Bedding-parallel ankerite veins

Bedding-parallel ankerite veins are observed in many of the Bude Formation shale beds (see Chapter 3). As an example, the thin section 64375 from a shale sample gathered at Upton (SS200045) has an ankerite vein that was precipitated into a fracture as it opened. The fibres grew from a median line in the centre to the fracture edges (i.e. antitaxial; see Chapter 2). The

mineralogy of the vein differs from the present surrounding shale bed, which is predominately composed of kaolinite (Fig. 6.1), suggesting that ankerite-rich fluids migrated through Bude Formation deposits (see Chapter 3). The formation of bedding-parallel veins requires:

1. Bedding-parallel stresses ( $\sigma_{BP}$ ) greater than the bedding-normal stress ( $\sigma_{BN}$ );
2. A sub-vertical minimum principal stress direction ( $\sigma_{min}$ ) in extension;
3. All stresses reduced by high pore-fluid pressures (see Chapter 2).

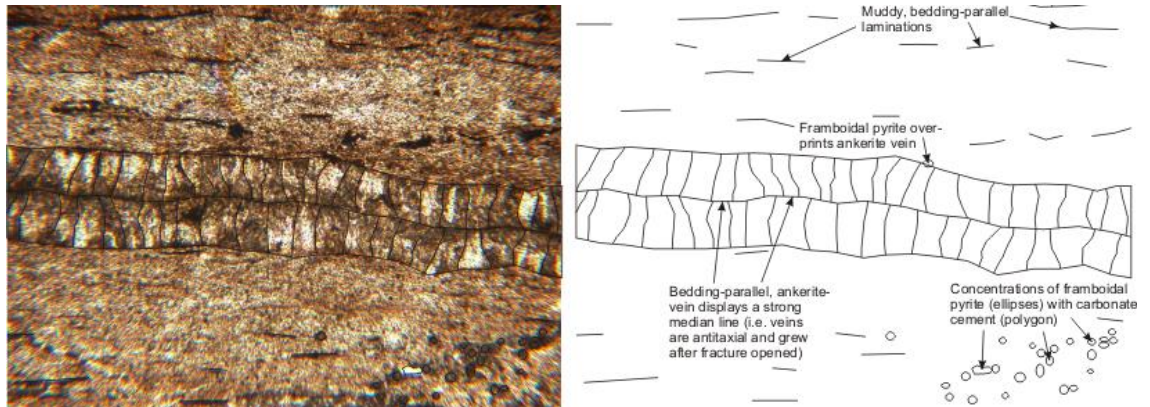


Fig. 6.1: Photomicrograph (plane-polarised light; view = 1 cm) and sketch of thin section 64375 with dilational, bedding-parallel ankerite veins. Vein growth is from the centre to the edges

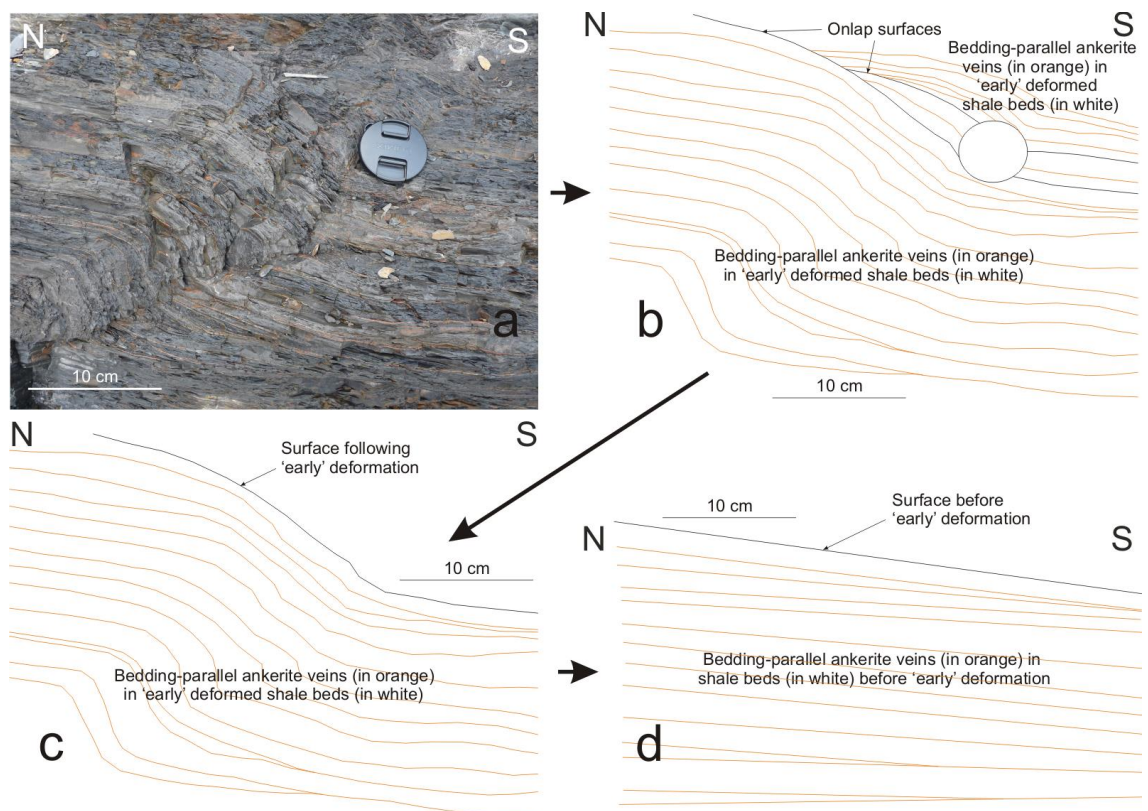


Fig. 6.2: (a) Photograph and (b) sketch of syn-depositional deformation of ankerite veins within a shale bed at North Upton (SS200048). Restoration (c and d) of the syn-depositional deformation has been undertaken (bottom) to show schematically how the stacked ankerite veins and inter-bedded shale may have looked before minor local deformation

In order to study the timing of the vein development, an assessment was made as to whether local structures had deformed the veins (see Chapter 3). In an example shale bed from North Upton (SS200047; Fig. 6.2a), a sequential set of diagrams shows the restoration of the deformation back to the original sub-horizontal mud bed with precipitated bedding-parallel ankerite veins (Figs. 6.2a-d). Initially, the bedding-parallel ankerite veins precipitated in the shale bed (Fig. 6.2d) prior to deformation of the bed into a local structure (Fig. 6.2c). After deformation, mud was deposited, with the variably thick deposits onlapping and then, draping the local structure (see chapters 4 & 5 for these criteria). In the later mud deposit, more bedding-parallel ankerite veins were precipitated up to the onlapping stratigraphic relationship onto the local structure (Fig. 6.2b; see chapters 2, 4 & 5).

The structural restoration (Fig. 6.2) shows ankerite veins precipitating near the palaeo-surface, penecontemporaneously with deposition. If this is the case, the overburden thickness ( $h$ ) would have been relatively small when the ankerite veins formed, so that the lateral bedding extent was relatively large in comparison. This caused the confining sub-horizontal bedding-normal stress ( $\sigma_{BN}$ ) to be large elevated pore-fluid pressures ( $P_f$ ) (Davis & Reynolds, 1996), possibly resulting from contemporaneous Variscan deformation (Enfield et al, 1985; Whalley & Lloyd, 1986; Leveridge & Hartley, 2006). This is consistent with Beach (1977) and Jackson (1991), who suggested that some of the Bude Formation veins are deformed by the ‘upright’ chevron folds. Alternatively, the ankerite veins may have exploited the laminations after the minor structure formed, due to migrating diagenetic fluids through the Culm Basin, although the veins have been described as siderite by De Wall and Warr (2004) (see Chapter 3).

### 6.3 Bulbous hinges in Bude Formation folded beds

Bulbous-hinged folds have thicker hinges than their limbs (i.e. dip isogon fold classes 1C to 3) (Ramsay, 1967). Ramsay (1974) maintained that bulbous-hinged folds are expected as a consequence of folding in variably-thick multi-layered rock. However, other explanations are possible because bulbous-hinged folds have developed in similar-thickness multi-layer plasticine models (Price & Cosgrove, 1990), folds demonstrably in sediment (i.e. slumps; see Chapter 2; Waldron & Gagnon, 2011) and folds that are assumed to have occurred in rock without fracturing in its outer arc (i.e. ‘upright’ and ‘inclined-to-recumbent’ chevron folds; Ramsay, 1974). In all cases, a degree of dilation is required in the hinge zone (Ramsay, 1974; Price & Cosgrove, 1990). Davis and Reynolds (1996) and Zoback (2008) showed that for dilation to occur: (1) the minimum principal stress direction ( $\sigma_{min}$ ) is in extension; (2) formation depths are in the top 5 km of the upper crust (i.e. temperatures below 150°C), where dilation is more likely; and (3) pore fluid pressures are elevated towards lithostatic pressure.

In the case of folded multi-layer slumps, the presence of bulbous hinges may reflect hinge zone dilation during sediment folding, where over-pressured water was unable to escape (see Chapter 2). However, in the case of Variscan chevron folding, Ramsay (1974) assumed that

the beds were lithified when the deformation took place. Examples in the Bude Formation outcrops of bulbous-hinged folds originally in sediment (i.e. slump folds) and folds assumed to have developed in rock (i.e. chevron folds) were used to assess the validity of this assumption.

### 6.3.1 Bulbous hinges in slump folded beds

Where multi-layered sandstones, siltstones and shales underwent slumping in the Bude Formation outcrops, bulbous-hinged beds are common. In an example at Upton (SS200046), the folded beds have irregular layer thicknesses along their limbs as well as bulbous hinges (Fig. 6.3). Similar observations in slump folded beds have been made by other authors (Woodcock, 1976; Patterson & Tobisch, 1993; Waldron & Gagnon, 2011). As all the lithologies in the folds have bulbous hinges (i.e. classes 1C to 3 dip isogons; Fig. 6.3), it suggests that all the beds had low coherence during slump deformation (Ramsay & Huber, 1987). This is to be expected given that slump beds were liquefied sediment when they were deformed (Owen, 1987).

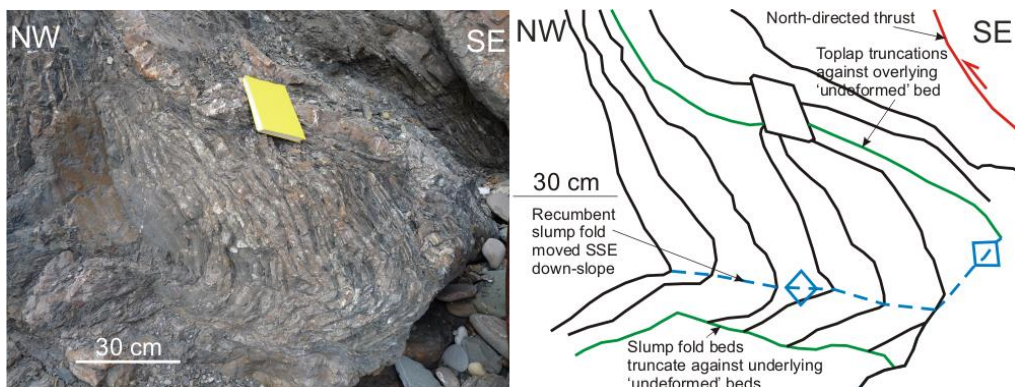


Fig. 6.3: Annotated photograph and sketch of the SSE-verging Upton attached slump fold (SS200045; looking 060°) with bulbous hinged beds, and 'undeformed' beds above the slump

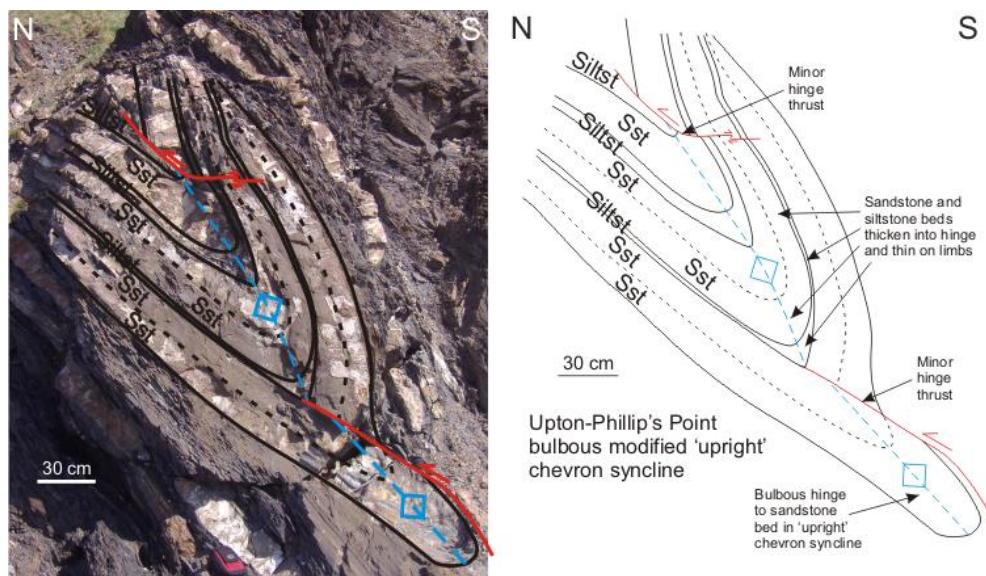


Fig. 6.4: Annotated photograph and sketch of an 'upright' chevron syncline at Upton-Phillip's Point (SS200045; looking 090°), with two bulbous-hinged siltstone and sandstone beds

### 6.3.2 Bulbous hinges in ‘upright’ chevron folded beds

Sanderson (1974) observed bulbous-hinged sandstone and siltstone beds in ‘upright’ chevron folds where their interlimb angles are less than  $70^\circ$ . An example is in a multi-layered stack of similar thickness beds at Upton-Phillip’s Point (SS200044; Fig. 6.4). In this example, all the lithologies in the folds show bulbous hinged beds and have similar bed geometries to the slump fold at Upton (SS200046; Fig. 6.3; see Chapter 5) that formed in sediment.

Many ‘upright’ chevron folded beds in the Bude Formation outcrops have bulbous hinges with dip isogon patterns that are indicative of low coherence (i.e. classes 1C to 3; Ramsay & Huber, 1987) (Fig. 6.4). However, Ramsay (1974) assumed that the beds were lithified during Variscan chevron folding. It would be expected that if this was the case, although the absolute rheology of the beds may not be important, the sandstone beds would have a higher coherence than the siltstone and shale beds, due to the lower clay content in the sandstone beds. This would result in more bulbous-hinged siltstone and shale beds (i.e. classes 1C to 3 dip isogons) than in the sandstone beds, with little bed thickness changes around the hinge (i.e. class 1B dip isogons; Ramsay & Huber, 1987). This is not the case in many Bude Formation folds.

### 6.3.3 Bulbous hinges in ‘inclined-to-recumbent’ chevron folded beds

In ‘inclined-to-recumbent’ chevron folded beds at Church Races (SS200042), there is an example of a south-directed ‘inclined-to-recumbent’ chevron anticline where only the shale beds have bulbous hinges (Fig. 6.5). This suggests that the shale beds were less coherent than the sandstone and siltstone beds during deformation. This is consistent with the description of folded rocks in Ramsay and Huber (1987) in which the more coherent sandstone beds have class 1 dip isogons and the less coherent shale beds have class 2 to 3 dip isogons.

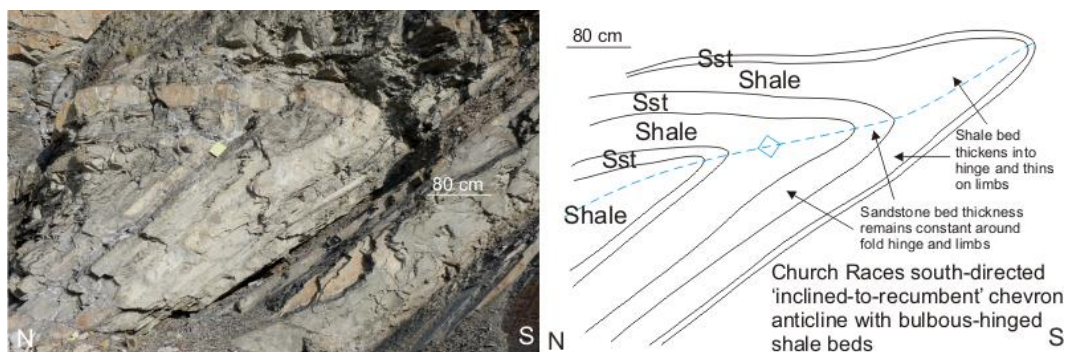


Fig. 6.5: Annotated photograph and sketch of a south-directed, ‘inclined-to-recumbent’ chevron anticline at Church Races (SS200042; looking  $090^\circ$ ) with bulbous-hinged shales

In contrast, bulbous-hinged multi-layer sandstone, siltstone and shale beds occur in other ‘inclined-to-recumbent’ chevron folds; an example being an ‘inclined-to-recumbent’ chevron anticline at Phillip’s Point (SS200043; Fig. 6.6). The bed geometries are similar to those observed in the Upton slump fold (SS200046; Fig. 6.3) and Upton-Phillip’s Point

‘upright’ chevron fold (SS200045; Fig. 6.4) but differ from those in an apparently similar fold nearby at Church Races (SS200042; Fig. 6.5). This apparent contradiction will be explored further in Chapters 7 and 8 using the dip isogon methods of Ramsay (1967).

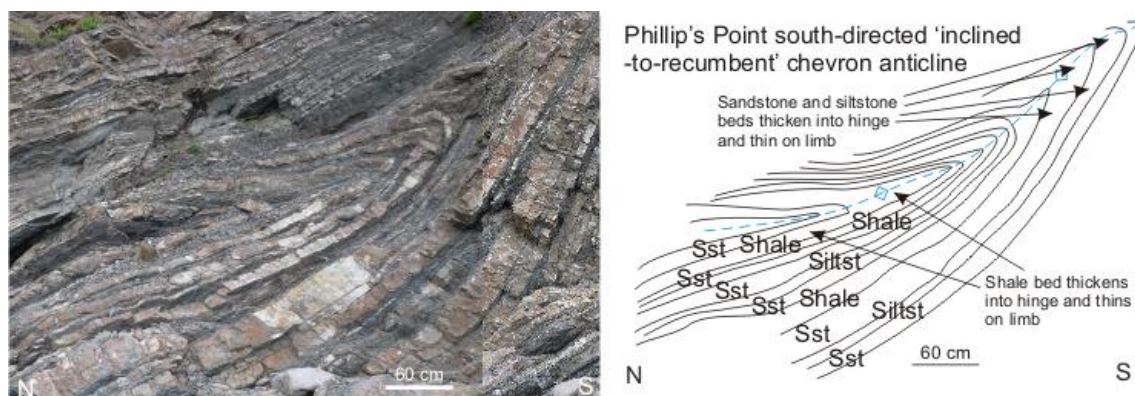


Fig. 6.6: Annotated photograph and sketch of south-directed ‘inclined-to-recumbent’ chevron anticline at Phillip’s Point (SS200043; looking 090°) with bulbous-hinged beds

## 6.4 Structural geometries of progressive Variscan deformation structures

To provide an overview of the Variscan deformation, structural data were collected between Northcott Mouth and Black Rock (SS202087-SS196015) from the ‘upright’ and ‘inclined-to-recumbent’ chevron folds (Figs. 6.4, 6.7 & 6.9) and the cross-cutting faults (Figs. 6.7-6.8). The chevron folds deform ‘early’ extensional and contractional structures (Mapeo & Andrews, 1991) and some of the north-directed thrusts (Enfield et al, 1985; Whalley & Lloyd, 1986). Although the ‘inclined-to-recumbent’ chevron folds are generally south-directed, north-directed chevron folds are also observed. In this section, descriptions are provided of the north-directed thrusts, followed by the two types of chevron folds observed in the Bude Formation.

### 6.4.1 Structural geometry of north-directed thrusts

A number of north-directed thrusts cut the chevron folded beds, whilst other thrusts have been deformed by chevron folds (Enfield et al, 1985; Whalley & Lloyd, 1986). Examples of folded thrusts are at Lynstone (SS200051; Enfield et al, 1985; see Chapter 5) and South Lynstone (SS200053; Fig. 6.7). In order to establish the original thrust orientations, restorations were undertaken using stereonet (Fig. 6.8) of 19 north-directed thrusts in the Bude Formation.

Restoration of the thrust data using a stereonet (Figs. 6.7 & 6.8) shows that the mean thrust orientation may have been 077/29S (strike circular variance  $\pm 6^\circ$ ; dip  $\pm 9^\circ$ ;  $n = 19$ ). However, it was not possible to collect striation measurements from the quartz veins on the thrust planes due to erosion of the veins and / or lack of surface exposure where veins were observed. If dip-slip movement occurred on the thrusts, this would be perpendicular to the strike direction and towards  $347^\circ$  (i.e. northwards), consistent with Whalley and Lloyd (1986).

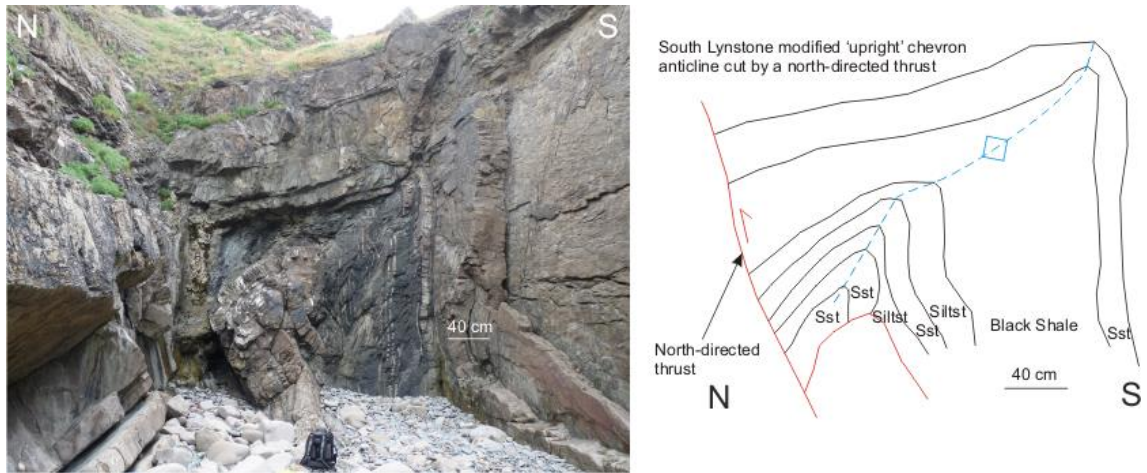


Fig. 6.7: Annotated photograph and sketch of a modified 'upright' chevron anticline hinge zone cut by a north-directed thrust at Lynstone (SS200050)

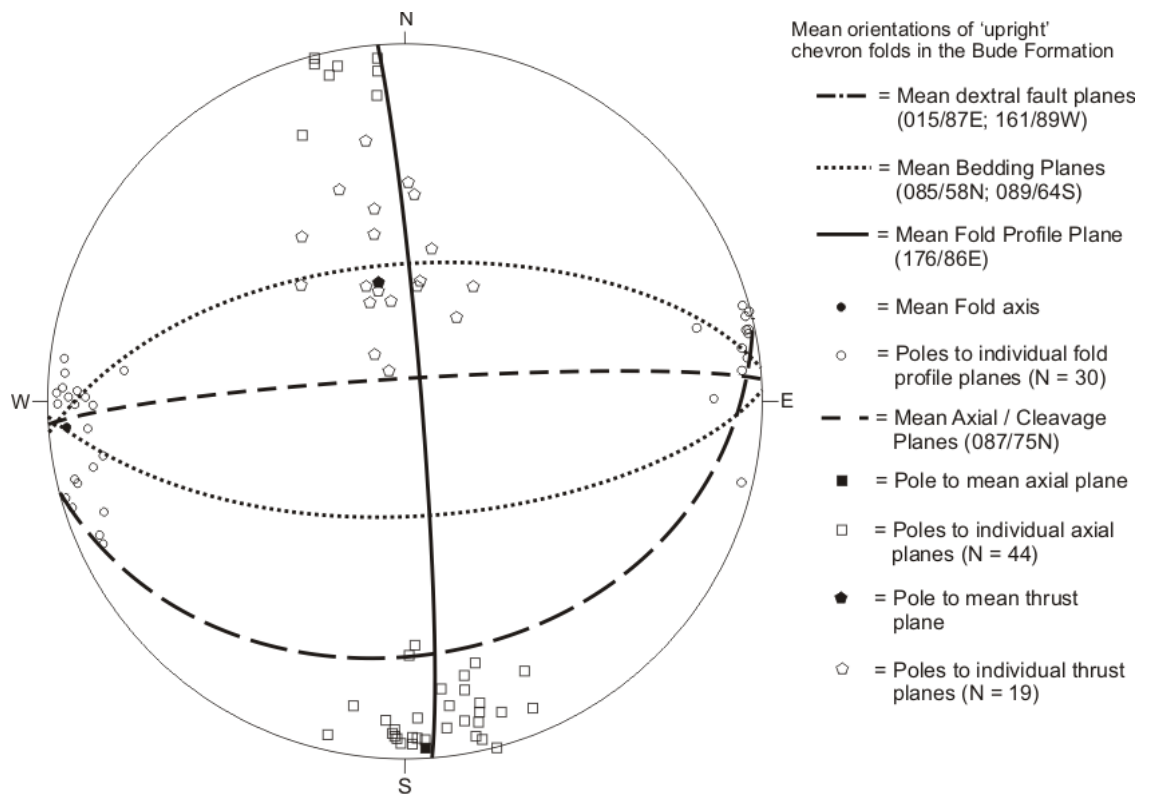


Fig. 6.8: Stereonet with a southern hemisphere projection showing the mean orientations of structures related to 'upright' chevron fold deformation in the Bude Formation. This includes restored north-directed thrusts that either cut the folds or have been deformed by the folds

#### 6.4.2 Structural geometry of 'upright' chevron folds

A structural analysis using a stereonet for 30 'upright' chevron folds in the Bude Formation (Fig. 6.8) gave the mean axial plane orientation as 087/84°N (strike  $\pm 2^\circ$ ; dip  $\pm 2^\circ$ ; n = 30; i.e. 'upright') and a mean interlimb angle of 67° ( $\pm 6^\circ$ ; n = 30). These match the results of Davison et al (2004) (see Chapter 2).

### 6.4.3 Structural geometry of south-directed, ‘inclined-to-recumbent’ chevron folds

Structural analysis using a stereonet for 30 south-directed ‘inclined-to-recumbent’ chevron folds in the Bude Formation (Fig. 6.9) gave the mean axial plane as 099/40N (strike  $\pm$  2°;  $n = 30$ ; Fig. 6.9; i.e. ‘inclined-to-recumbent’) and the mean interlimb angle as 54° ( $\pm$  5°;  $n = 30$ ). This is slightly more than the Davison et al (2004) estimate for same chevron fold type (see Chapter 2). Using the axial plane dip angle ( $\omega$ ), the formula estimating the dimensionless shear strain value ( $\gamma \geq 0$ ) accommodated by the chevron folded beds is (Davis & Reynolds, 1996):

$$\gamma = \tan (90^\circ - \omega) \quad (6.1)$$

The mean amount of south-directed shear strain accommodated in the Bude Formation to the south of Bude is:  $1.28 \pm$  st. dev. 0.50 ( $n = 30$ ). Across these outcrops, south-directed shear strain accommodation generally increases to the south (Sanderson, 1979), but the amount of strain accommodated varies laterally at any one point (Lloyd & Whalley, 1986; 1997). A further discussion of the accommodation of south-directed shear strain is provided in Chapter 8.

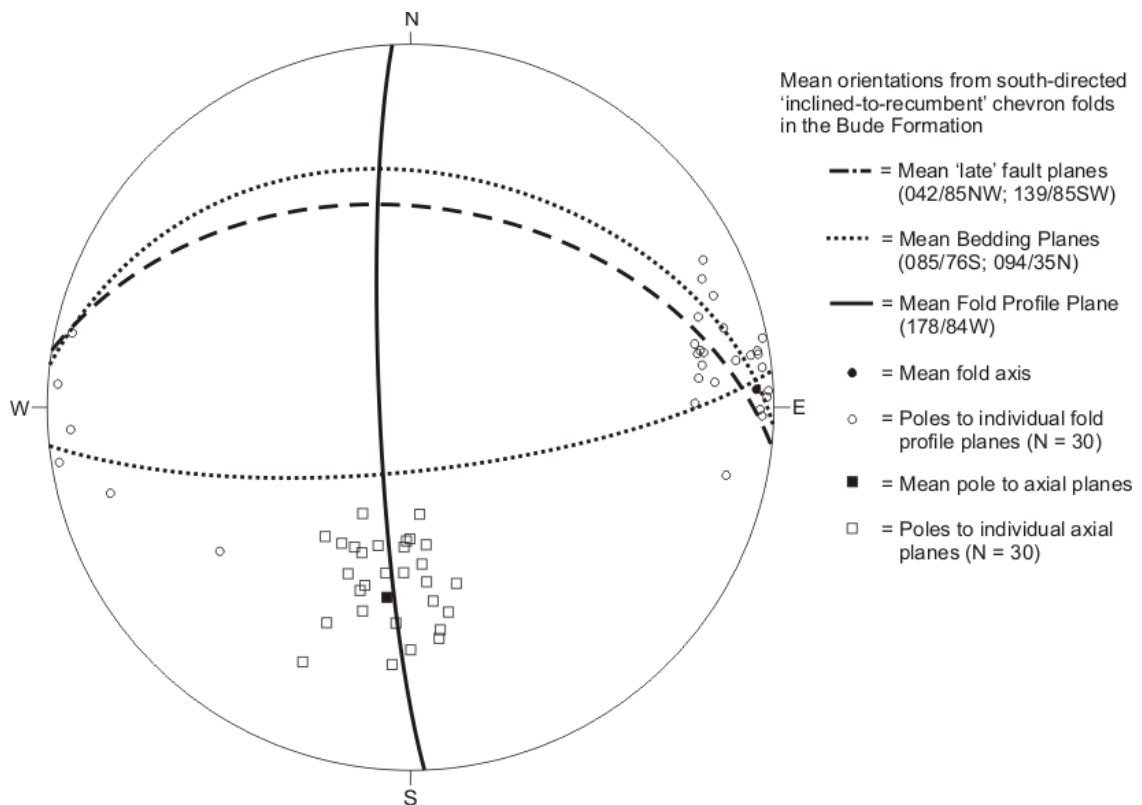


Fig. 6.9: Stereonet with a southern hemisphere projection showing the mean orientations of structures related to ‘inclined-to-recumbent’ chevron fold deformation in the Bude Formation

### 6.5 Mud injections cutting fold hinges

Mud injections occur in sedimentary successions where burial and / or deformation has caused mud to liquefy in order to overcome the overburden confining pressure ( $P_C$ ), by allowing fluids to escape during fluidisation (Owen, 1996; see Chapter 2). In the Bude Formation, mud

injections cut some of the ‘upright’ chevron folds hinges (e.g. Upton-Phillip’s Point; SS200044; Fig. 6.10) and possibly, a south-directed ‘inclined-to-recumbent’ chevron fold hinge at North Widemouth (SS200032; Fig. 6.12). Although the presence of mud injections suggests that the source bed was sediment, the surrounding beds may have been either sediment or rock.

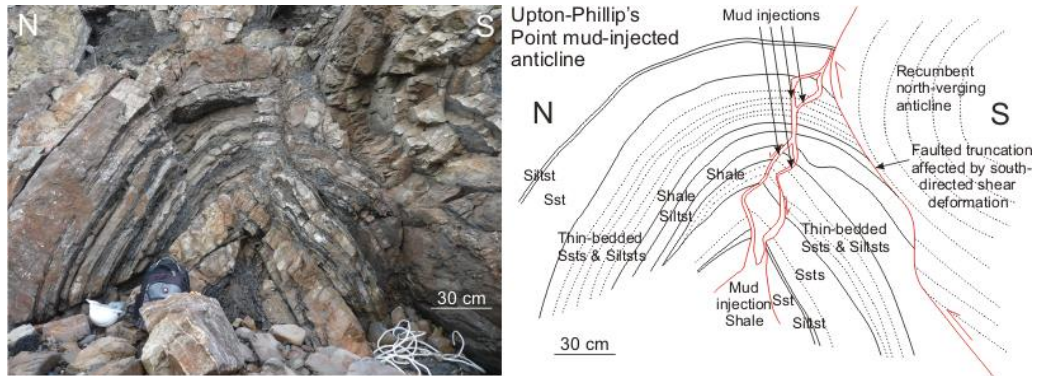


Fig. 6.10: Photograph and sketch of a mud-injected, ‘upright’ chevron anticline at Upton-Phillip’s Point (SS200045). Notice the ‘zigzag mud injections path and north-directed thrust cutting the folded beds. The thrust is deformed by the ‘inclined-to-recumbent’ chevron folding

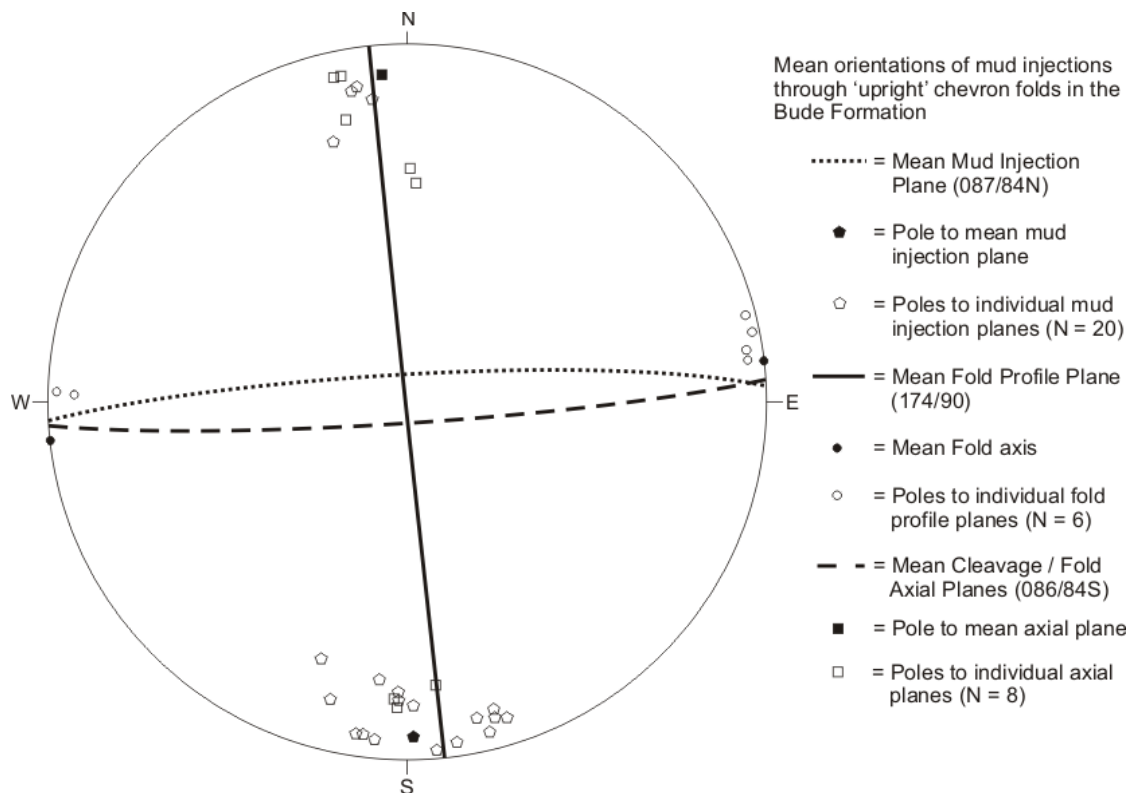


Fig. 6.11: Stereonet with a southern hemisphere projection showing the mean orientations for mud injections cutting their ‘upright’ chevron folds in the Bude Formation

### 6.5.1 Mud injections cutting ‘upright’ chevron fold hinge zones

Twenty mud injections were observed to cut stacked beds in ‘upright’ chevron fold hinges between Northcott Mouth and Black Rock (SS202087-SS195015). In all cases, minor

extensional offsets were accommodated along the mud injection planes that result either from volume reduction as mud-rich fluid escaped or from extensional reactivation. Most of the mud injection plane trajectories are complicated. For example, at Upton-Phillip's Point (SS200044) the mud injection has a bifurcating 'zigzag' pattern through the folded beds until it reaches an overlying folded thrust (Fig. 6.10). The mud injections have either exploited fractures associated with outer-arc extension or pre-existing weaknesses in the beds before chevron folding.

A structural analysis using a stereonet for the 20 mud injections (Fig. 6.11) gave the mean injection plane orientation as 087/84N (strike  $\pm 2^\circ$ ; dip  $\pm 3^\circ$ ;  $n = 20$ ), which is sub-parallel to the mean axial plane orientation, 086/84S (strike  $\pm 1^\circ$ ; dip  $\pm 8^\circ$ ;  $n = 20$ ; Fig. 6.11), of the mud-injected 'upright' chevron folds. Thus, it is possible that the injections exploited axial-parallel fractures formed by outer-arc extension. For the mud to inject through folded beds, the fluid pressures must exceed the lithostatic pressure and force the horizontal stress direction ( $\sigma_H$ ) into extension (Davis & Reynolds, 1996; Zoback, 2008; see Chapter 2).

### 6.5.2 Mud injections cutting a south-directed chevron fold hinge zone

In an example at North Widemouth (SS198029), mud lines a steeply north-dipping normal fault plane that cuts a south-directed 'inclined' anticlinal hinge (Fig. 6.12). The normal fault plane is oriented at 102/74N, which is oblique to the axial plane orientation (093/38N). The mud-lined normal fault becomes bedding-parallel, with a mud sediment bed on the overturned steep north-dipping limb of this 'inclined' chevron anticline (Fig. 6.12).

There are currently two possible explanations for the development of the fault plane. The first is that it is a normal fault plane that cuts the 'inclined' chevron anticline. The fault plane was smeared during its movement with mud from a thick mudstone bed that may have sat above the cliff line but has since been eroded away. Mud smears are continuous on normal fault planes only where the shale-to-gouge ratio (SGR), or the ratio of the total shale bed throw to the shale bed thickness, satisfies  $SGR \leq 3$ , but due to a lack of mud, a shale smear is only developed intermittently on fault planes with an  $SGR > 3$  (Couples, pers. comm., 2007). Fossen (2010) terms this the SGR, the 'shale smear factor' (SSF), which on fault throws  $\geq 10$  m, has a  $SSF \leq 4$ . Thus, the Couples (pers. comm., 2007) and Fossen (2010) models are consistent.

However, the source of the mud smear has not been established, although candidates include the Tom's Cove (TCS) and Saturday's Pit (SPS) shale beds. The TCS Bed is found in the nearby cliffs, but it may lie below the folded beds; whilst the SPS Bed is likely to have been above the cliff section and so has been eroded away (King, 1967; Freshney et al, 1972).

The second possible explanation is that this is a mud injection plane that exploited axial-parallel fractures formed by outer-arc extension. This suggests that mud sediment was folded during south-directed Variscan deformation. The source of the mud may have been a thin shale bed, marked in Fig. 6.12, within the folded bedding stack in the North Widemouth outcrop. In this case, this would require that some of the beds remained as mud sediment during

Variscan deformation. However, the volume of mud required to generate such an injection may be large because the mud lines this fault plane to the top of the cliff, and so, this potential source bed may have been too thin to have generated the required mud-fluid volumes. Also, as there are no structures that cross-cut the injection plane, the timing of the extensional movement during progressive Variscan deformation is not known.

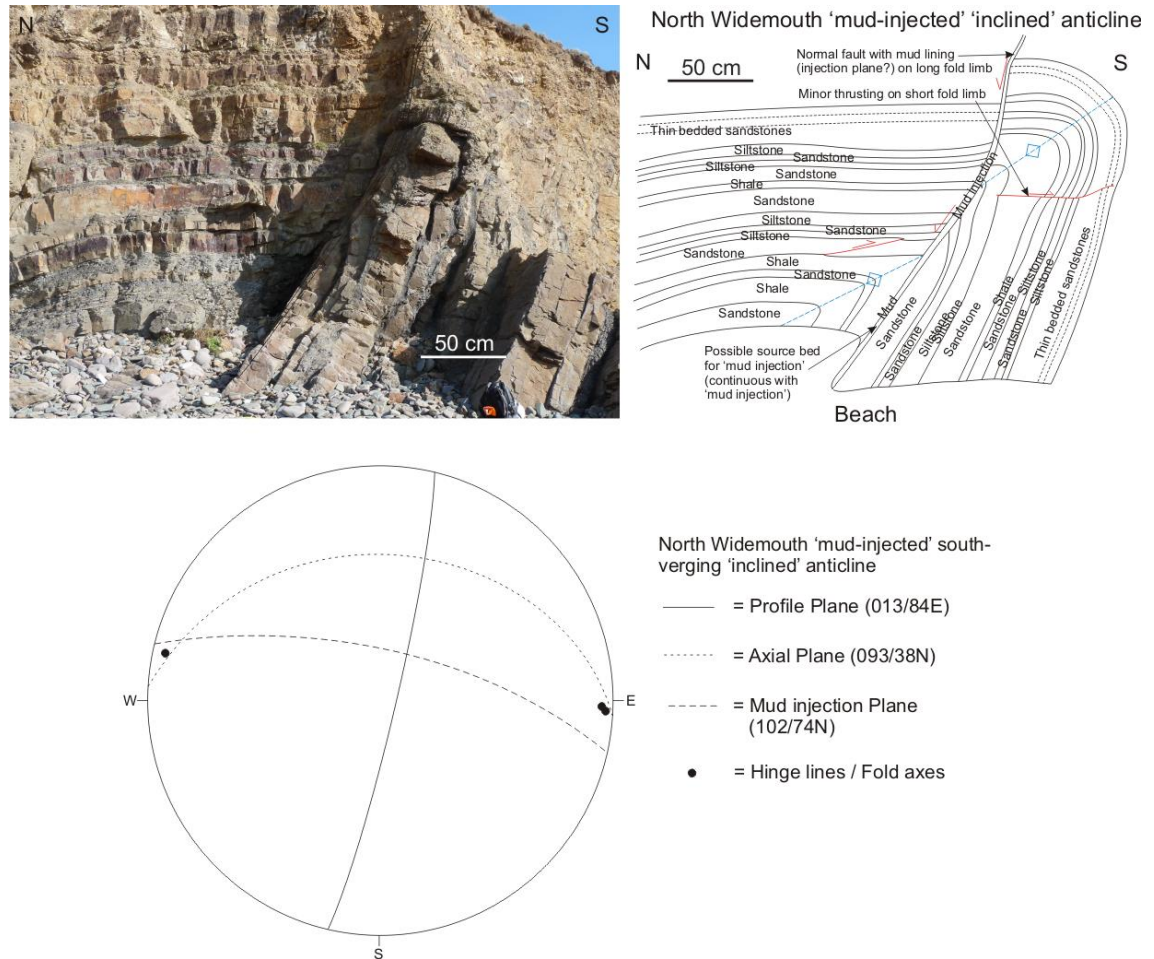


Fig. 6.12: Annotated photograph (top left), sketch (top right) and stereonet with a southern hemisphere projection (bottom) of the North Widemouth south-directed 'mud-injected' 'inclined' anticline, where a possible mud injection cuts the fold hinge and long limb (SS198029). Notice that extension accommodated on the injection plane reduces to zero where it cuts the fold hinge, whilst a minor thrust accommodates deformation on the short limb

## 6.6 Discussion

The evidence provided in this chapter and previously in Chapters 3, 4 and 5, suggests that the 'early' Variscan deformation in the Bude Formation occurred in sediment, near the palaeo-surface. Further analyses in this chapter includes evidence of:

1. Mud injections that cut the chevron folds, suggesting that some of the shale beds were still mud sediment during Variscan fold deformation;
2. Bedding-parallel ankerite veins affected by local folding at or near the palaeo-surface;

3. Bulbous-hinged multi-layer folded beds that form usually in all the lithologies in the slump, 'upright' and some 'inclined-to-recumbent' chevron folded beds.

Together, these observations and results raise questions and difficulties regarding the assumption that progressive development of Variscan folding occurred entirely in lithified rock (Ramsay, 1974). Clearly, a better understanding is needed of the mechanical state of the Bude Formation beds during Variscan deformation. Accordingly, Chapter 7 investigates the effect of the changes in the mechanical state of folded layers within multi-layered successions and materials. This idea has precedence. Waldron and Gagnon (2011) assessed the mechanical or lithification states of folded multi-layers from various formations, in order to demonstrate the differences in lithological coherence. They employed the dip isogon class methods of Ramsay (1967) and from their results on slump folds, developed geometric criteria:

1. Slump folded sand beds have class 3 dip isogons;
2. Slump folded mud beds have class 1 dip isogons.

In Waldron and Gagnon (2011), slump folded sand beds have a lower coherence than the slump folded mud beds, which is the reverse of the situation for folded sandstone and shale beds (Ramsay & Huber, 1987). However, from the observations in this chapter, these conclusions appear to be too simplistic. Therefore, in Chapter 7, a series of tests are described that employ both the dip isogon and quantitative layer thickness methods of Ramsay (1967).

## 6.7 Summary

The Bude Formation outcrops provide examples of structures that were formed in sediment during deformation or challenge the assumption that all folding occurred in rock (see also Chapters 4 & 5), which are of relevance to the general aim of the thesis and include:

1. Bedding-parallel ankerite veins that have been affected by local structures;
2. 'Early' folds and faults and also, slumped beds (see chapters 2, 4 & 5);
3. Mud injections (see Chapter 2) that cut chevron fold hinges;
4. Bulbous-hinged multi-layer folded beds, where the bulbous hinges form in all lithologies in the slump folds, 'upright' chevron folds and some 'inclined-to-recumbent' chevron folds.

Although all of the structures considered suggest that fold deformation occurred in part in sediment, it is the geometries of the bulbous-hinged folds that are most intriguing. As mentioned previously, there is an assumption that the chevron folding in the Bude Formation occurred in rock (Ramsay, 1974), but the four structures mentioned above provide some counter evidence. Consequently, a set of geometric criteria would be useful to distinguish between folds developed in rock and folds developed in sediment. These criteria are the general aim of the thesis, and are developed in Chapter 7 and applied to the Bude Formation folds in Chapter 8.

## Chapter 7: Distinguishing fold structures in sediment and rock

### 7.1 Introduction

Folds form in both sediment and rock, with sediment consisting of loose grains in a water-saturated bed that can move or 'flow' independently (Craig, 1997), whilst the grains in rock are bound together (e.g. by a cement) and move as unified system of beds (see chapters 1 & 2). The primary aim of this chapter and general thesis aim are to identify the distinguishing characteristics of fold deformation in sediment and rock. This is an important distinction as folds occur in sediments as described in chapters 2-6 in: (1) gravity-tectonic, delta toe and passive margin fold-thrust belts; and (2) tectonic foreland basins and accretionary wedges.

Folds developed in compressional setting display a variety of geometries, including different wavelengths, amplitudes, inter-limb angles, etc. Of particular note and interest is the variation in layer thicknesses around the fold. The well-established dip isogon and quantitative layer thickness methods of Ramsay (1967) are used to describe these variations and place geometric constraints on folded beds or layers. Using dip isogon and quantitative layer thickness analyses on folded layers, 'classes' are identified to describe the relative coherence of each layer involved in that fold deformation.

In order to test whether the dip isogon and layer thickness methods are applicable, a suite of examples have been measured from the literature covering demonstrably folded rocks and sediments. These examples include sediment folds in slumps and glacial till, and rock folds in different metamorphic facies. In addition, the dip isogon and quantitative layer thickness methods have been tested on examples of folded model materials (wax, plasticine and gelatine) and latterly, by way of a final test, migmatites. The model material layers are not comprised of grains, whilst the migmatites were partially-melted rock with weak 'grain binding' during folding. The results from the dip isogon and quantitative layer thickness analyses were used to define diagnostic criteria that identify the differences and similarities between the fold geometries developed in folded sediment and rock. These criteria are described in this chapter, with the term 'layer' being used to encompass both geological beds and model material 'layers'.

### 7.2 Methods

Dip isogon and quantitative layer thickness methods have been employed in order to test whether folds (in profile) developed in sediments and rocks can be distinguished using their geometric characteristics. Dip isogons are 'contour' lines connecting points of equal dip on the folded bedding planes or layers. Dip isogon analysis involved a scaled sketch of example folded layers drawn in profile from photographs either in the literature or in field outcrops, typically using a 10° dip interval. The points where the layer dips at 10°, 20°, etc., are marked around each folded layer and connected from layer-to-layer, producing a distinct dip isogon pattern for

the folded layers. From the pattern of dip isogons, different fold classes are distinguished (Figs. 7.1-7.2; Table 7.1), which are themselves related to their relative competence or coherence during fold deformation (Ramsay & Huber, 1987).

| Fold class | Adjacent isogons  | Relation between dip isogons and axial trace angles                |
|------------|-------------------|--------------------------------------------------------------------|
| 1A         | Converge strongly | Dip isogon angle with axial trace > angle of bed dip ( $\alpha$ )  |
| 1B         | Converge          | Dip isogon angle with axial trace = angle of bed dip ( $\alpha$ )  |
| 1C         | Converge slightly | Dip isogon angle with axial trace < angle of bed dip ( $\alpha$ )  |
| 2          | Parallel          | Dip isogon angle with axial trace < angle of bed dip ( $\alpha$ )  |
| 3          | Diverge           | Dip isogon angle with axial trace << angle of bed dip ( $\alpha$ ) |

Table 7.1: Comparison of fold classes to the pattern of dip isogons and the isogon relationship to the fold axial trace (modified from Ramsay, 1967), with all folds in profile

For the quantitative layer thickness analysis (Ramsay, 1967), the true layer thicknesses ( $t_a$ ) and axial-parallel thicknesses ( $T_a$ ) (both in metres) are measured at  $10^\circ$  intervals (Fig. 7.1a-b). The layer thicknesses are related to each other via the dip angle ( $\alpha$ ) by:

$$t_a = T_a \cos(\alpha) \quad (7.1)$$

Following this, the layer thickness ratios are calculated. For true layer thickness ratio, the true layer thickness ( $t_a$ ) is divided by the hinge thickness ( $t_0$ ) and then, this dimensionless ratio is plotted on its corresponding diagram at  $10^\circ$  intervals (Fig. 7.1c):

$$t'_a = t_a/t_0 \quad (7.2)$$

For the axial-parallel layer thickness dimensionless ratio, the same procedure is used but with the axial-parallel layer thickness ( $T_a$ ) instead of the true layer thickness ( $t_a$ ) (Fig. 7.1d):

$$T'_a = T_a/t_0 \quad (7.3)$$

These dimensionless ratios are related to each other via the dip angle ( $\alpha$ ) by:

$$t'_a = T'_a \cos(\alpha) \quad (7.4)$$

Quantitative layer thickness analysis was undertaken to provide a means of quantifying the dip isogon fold classes. The analysis produces plots of curves within dimensionless fields that correspond to each dip isogon class (Fig. 7.2). The idealised folded layer in profile (Fig. 7.1) represents the special case of a dip isogon class 2 fold where the isogons are drawn parallel to each other and the axial-parallel layer thicknesses are equal to each other at each  $10^\circ$  interval.

A modification to the Ramsay (1967) methods has been undertaken in order to show how the dip isogon classes vary from bed-to-bed. This is achieved by using an isogon log, which is presented with each sketch (e.g. Fig. 7.3). Each bar on the log includes information on

the layer properties in the fold hinge zone. These are: (1) thickness at the hinge (vertical axis); (2) dip isogon class (horizontal axis); and (3) lithology (bar colour).

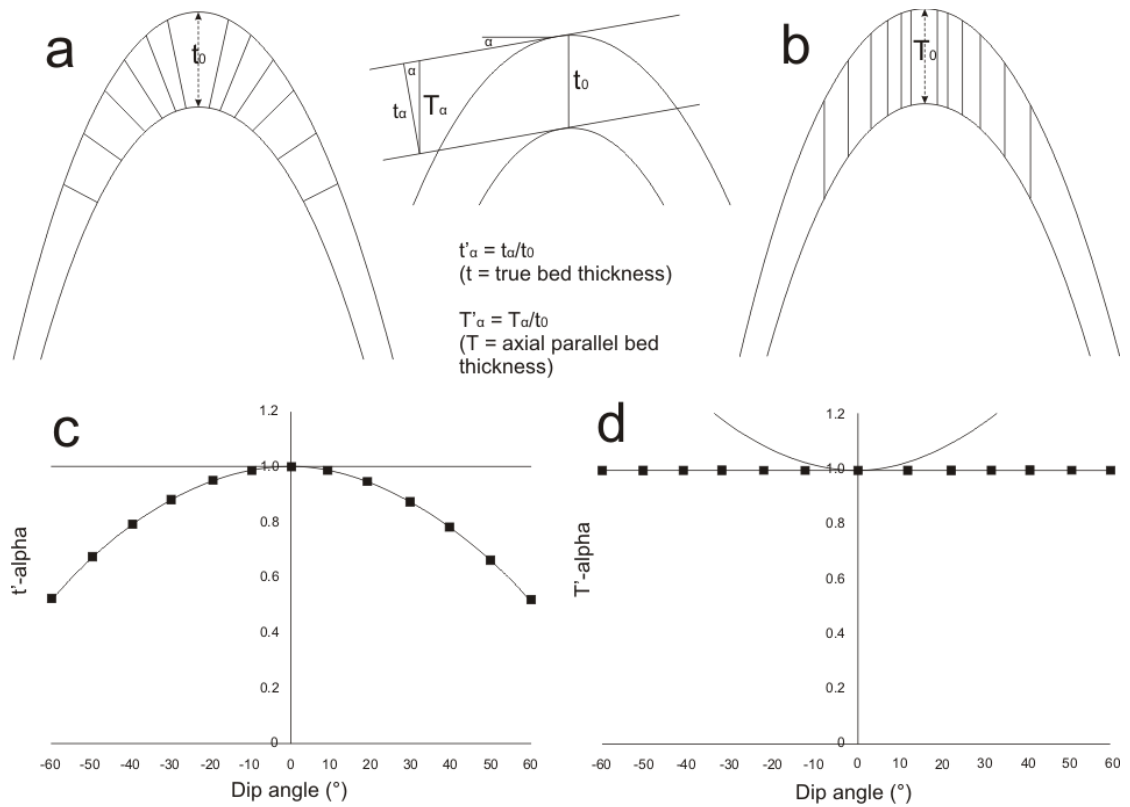


Fig. 7.1: Idealised folds in profile to calculate the layer thickness dimensionless ratios (modified from Ramsay, 1967). All intervals are taken at 10°

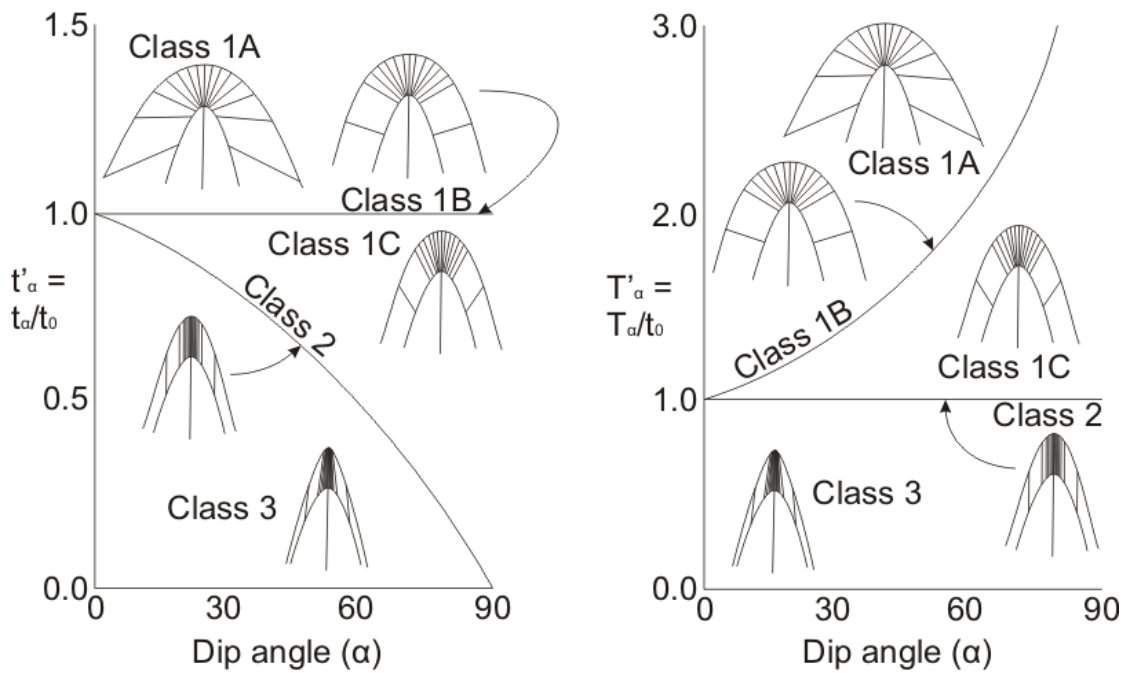


Fig. 7.2: Diagram plots for quantitative layer thickness analysis (see Fig. 7.1). Each fold class is shown in profile with its corresponding dip isogon pattern drawn on sketched idealised folded layers at 10° intervals (modified from Ramsay, 1967)

The use of dip isogons to distinguish the mechanical state of different folded sediment and rock layers in profile has a degree of precedence. In rocks, commonly shale or pelite is less coherent (i.e. less competent, 'softer', more viscous) than sandstone or psammite. When these layers are folded, the sandstone or psammite has class 1 dip isogons, whilst the shales and pelites have class 3 (i.e. less coherent) dip isogons. The class 1 dip isogons occur when there is little or no thickness changes around the folded layer (i.e. more coherent), whilst the class 3 dip isogons occur when the layer 'flows' into the fold hinge zone (i.e. less coherent), creating a thick, bulbous hinge compared to the fold limbs (Ramsay & Huber, 1987).

A recent paper by Waldron and Gagnon (2011) that is independent of this research project, has been published, which has attempted to distinguish between folded rocks and slumps. In the paper, the authors describe the geometries of folded structures by using the Ramsay (1967) dip isogon method. In the Waldron and Gagnon model, in contrast to rocks (Ramsay & Huber, 1987), slump folds contain less coherent sand (class 3 dip isogons) and more coherent mud beds (class 1 dip isogons). This hypothesis has been tested using a suite of folds, including the slump fold examples employed by Waldron and Gagnon (2011).

The dip isogon methods have been applied also to slump folds in the Pigeon Point Formation, California, USA, by Patterson and Tobisch (1993). The dip isogon patterns that they recorded were irregular. They ranged between dip isogon class 1B to class 3 and "did not readily lend themselves to the Ramsay (1967) classification scheme". Layer thicknesses varied across the slump folds, but Patterson and Tobisch (1993) were unsure as to whether this resulted from variation in original layer thickness or slump-induced deformation. Also, they suggested that grain size was not a factor, but that water and/or phyllosilicate contents of layers may be factors in the irregular dip isogon patterns.

### 7.3 Dip isogon analyses of rock, sediment, material and migmatites folds

In order to test whether the fold geometries can be related to the mechanical state of the material at the time of folding, a range of folds developed in different material states have been selected for dip isogon and quantitative layer thickness analyses, which are as follows:

1. Folded rocks:
  - a. 5 meta-sedimentary folds (2 from N Norway (Fossen, 2010); 1 from Mull, W Scotland (Ramsay & Huber, 1987); and 2 from Roscolyn, NW Wales (Price & Cosgrove, 1990); Fig. 7.3);
  - b. 2 banded gneiss folds (1 from Gjerdoya Island, Norway (Lisle, 1992); and 1 from the Lepontine Alps (Ramsay & Huber, 1987); Fig. 7.3);
2. Folded sediments:
  - c. 2 slump folds in the Manly Slump Bed, New Zealand (Strachan, 2008; Fig. 7.3);
  - d. 5 siltstone slump fold rafts from Powys, Central Wales (Woodcock, 1976; Fig. 7.4);
  - e. 3 calcarenite slump folds from SW Turkey (Waldron & Gagnon, 2011; Fig. 7.4);

- f. 3 'glacio-tectonic' folds in till from NW Jylland, Denmark (Fossen, 2010; Fig. 7.4);
- 3. Folded materials:
  - g. 3 folds in buckled model materials (1 each from gelatine (Blay et al, 1977), wax and plasticine (Price & Cosgrove, 1990); Fig. 7.5);
- 4. Folded migmatites:
  - h. 4 folds from Ladakh, NW India (Weinburg & Mark, 2008; Fig. 7.5).

### 7.3.1 Descriptions of folded rocks, sediments, model materials and migmatites

In order to describe the folds in rocks, sediments, model materials and migmatites, dip isogon and quantitative layer thickness analyses have been undertaken on each folded layer (Figs. 7.3-7.5). Examples have been chosen from the folds in order to display the results (Figs. 7.6-7.9). The examples are all in profile except for the New Zealand slumps and are as follows:

1. 2 folded metamorphic rock examples from (a) Roscolyn, NW Wales (Price & Cosgrove, 1990; Fig. 7.6); (b) Gjerdoya Island, Norway (Lisle, 1992; Fig. 7.6);
2. 4 folded sediment examples from: (c) New Zealand slumps in plan view (Strachan, 2008; Fig. 7.7); (d) Central Wales slumps (Woodcock, 1976; Fig. 7.7); (e) SW Turkey slumps (Waldron & Gagnon, 2011; Fig. 7.8); and (f) Denmark tills (Fossen, 2010; Fig. 7.8);
3. 1 buckle experiment in: (g) wax bilaminate (Price & Cosgrove, 1990; Fig. 7.9);
4. 1 fold in: (h) migmatites from Ladakh, NW India (Weinburg & Mark, 2008; Fig. 7.9).

#### a. Meta-sedimentary folds

The folded rocks at Roscolyn, NW Wales, are in a Precambrian meta-sedimentary succession (Price & Cosgrove, 1990; Figs. 7.3 & 7.6). The layers are deformed as harmonic fold structures with 'inclined-to-recumbent' axial planes and closed-to-tight ( $90^{\circ}$ - $40^{\circ}$ ) interlimb angles.

#### b. Banded gneiss folds

The folded rocks in the banded granitic and tonalitic gneiss occur in very high-grade metamorphic rocks and are from the Proterozoic part of the Fennoscandian Shield in the Svatisen Window, Gjerdoya Island, Norway (Lisle, 1992; Skar, 2002; Figs. 7.3 & 7.6). The gneiss contains lighter-grey felsic and darker-grey mafic bands that have been deformed as harmonic fold structures with closed-to-tight ( $90^{\circ}$ - $40^{\circ}$ ) interlimb angles (Lisle, 2004).

#### c. Manly Slump Bed folds

The slump folds in the Manly Slump Bed, North Island, New Zealand, are from the Early Miocene Waitemata Basin (Strachan, 2008; Figs. 7.3 & 7.6). The layers are deformed as disharmonic fold structures, with 'recumbent-to-reclined' axial planes and isoclinal-to-'elastica' ( $20^{\circ}$  to  $-20^{\circ}$ ) interlimb angles (also see Chapter 2).

#### d. Clastic slump folds

The slump folds in the Montgomery Trough, Central Wales, are from the Late Silurian Ludlow Series (Woodcock, 1976; Figs. 7.4 & 7.7). The layers are deformed as disharmonic fold

structures, with ‘recumbent-to-reclined’ axial planes and isoclinal-to-‘elastica’ ( $20^\circ$  to  $-20^\circ$ ) interlimb angles (also see Chapter 2).

#### **e. Calcarenite slump folds**

The calcarenite slump folds are from the Jurassic Antalya Complex, SW Turkey (Waldron & Gagnon, 2011; Figs. 7.4 & 7.8). The layers are deformed as disharmonic fold structures, with ‘recumbent’ axial planes and isoclinal-to-‘elastica’ ( $20^\circ$  to  $-20^\circ$ ) interlimb angles.

#### **f. Glacial till folds**

The Pleistocene glacial till folds in NW Jylland, Denmark (Fossen, 2010; Figs. 7.4 & 7.8) were deformed in a hydro-plastic state (Denis et al, 2009; see Chapter 2) by glacial movement under fluid over-pressure conditions (Phillips et al, 2008). The layers are deformed as disharmonic fold structures with ‘upright’ axial planes and closed-to-tight ( $90^\circ$ - $40^\circ$ ) interlimb angles.

#### **g. Folds in wax, plasticine and gelatine**

The model materials used in the buckle experiments include gelatine (Blay et al, 1977), plasticine and wax (Price & Cosgrove, 1990; Figs. 7.5 & 7.9). The model materials were originally horizontal-bedded, 1 cm-thick, alternating lighter and darker coloured multi-layers. All the folds have strongly ‘upright’ axial planes and closed-to-tight ( $90^\circ$ - $40^\circ$ ) interlimb angles.

#### **h. Migmatite folds**

The migmatite folds in the Karakoram Shear Zone, Ladakh, NW India (Figs. 7.5 & 7.9), occurred in extremely high-grade, partially-melted metamorphic rock near to granitic magma (Weinburg & Mark, 2008). The layers are deformed as disharmonic fold structures with tight-to-isoclinal ( $60^\circ$ - $10^\circ$ ) interlimb angles.

## 7.4 Dip isogon and quantitative layer thickness analyses

### 7.4.1 Folded rocks in profile

#### **Results**

Analysis of the dip isogon logs for folded rocks (Figs. 7.3, 7.6-7.7) show that the felsic and pelite layers in the meta-sedimentary and gneissose folds, respectively, have higher dip isogon classes (i.e. classes 2 to 3) than the psammite / quartzite and mafic layers (i.e. classes 1A to 2). The analysis of the folded rock examples (Figs. 7.3 & 7.6-7.7) show symmetric, non-repeating and harmonic dip isogon patterns on each limb. The quantitative layer thickness analysis plots of the folded rock examples (Fig. 7.6) have symmetric curves about the hinge position (i.e.  $\alpha = 0^\circ$ ) on each limb. The curves remain within a single field that represents a single ‘Ramsay’ dip isogon class, as is found from dip isogon analysis.

## Meta-sedimentary, gneissose and slump folds

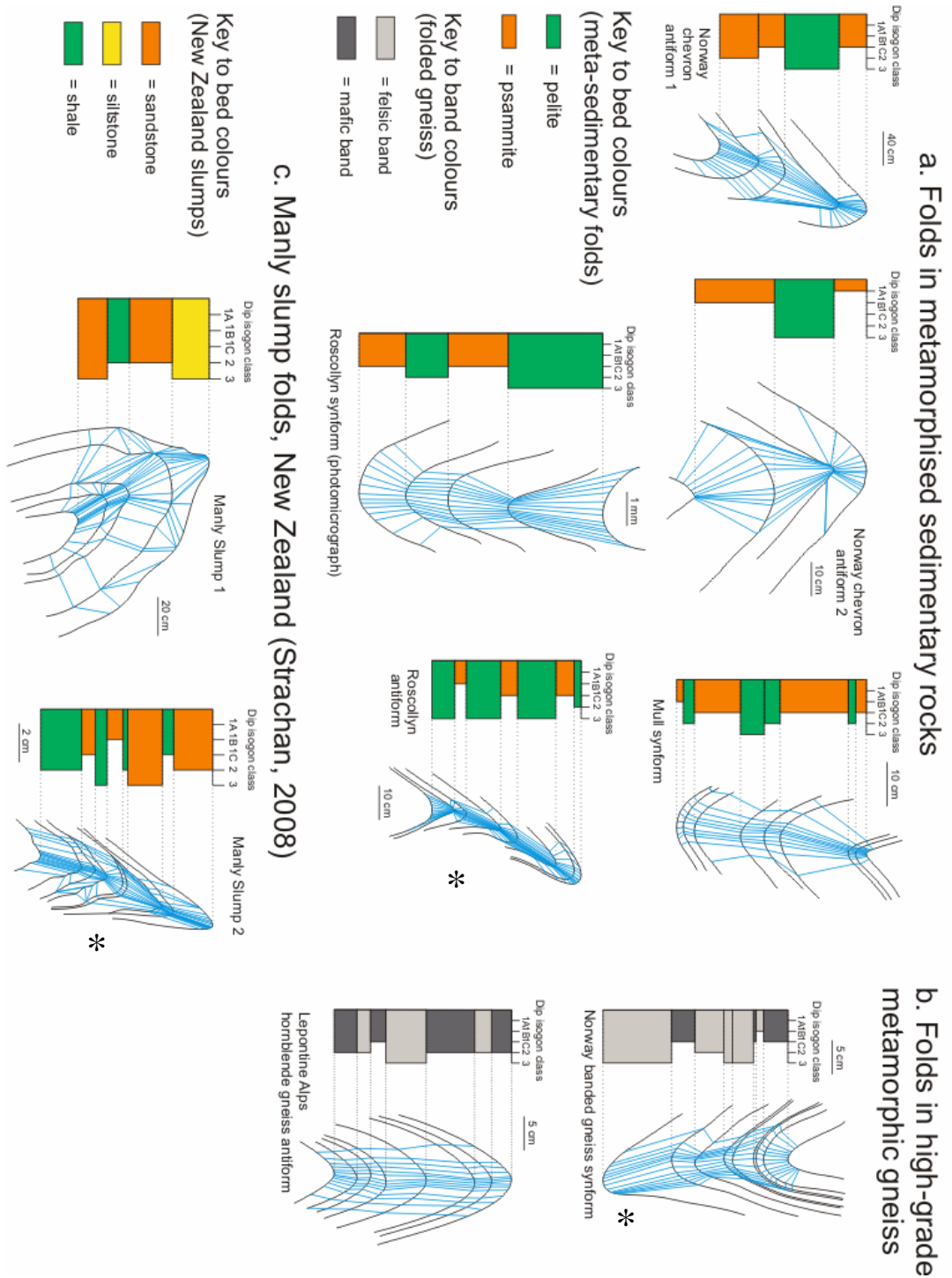
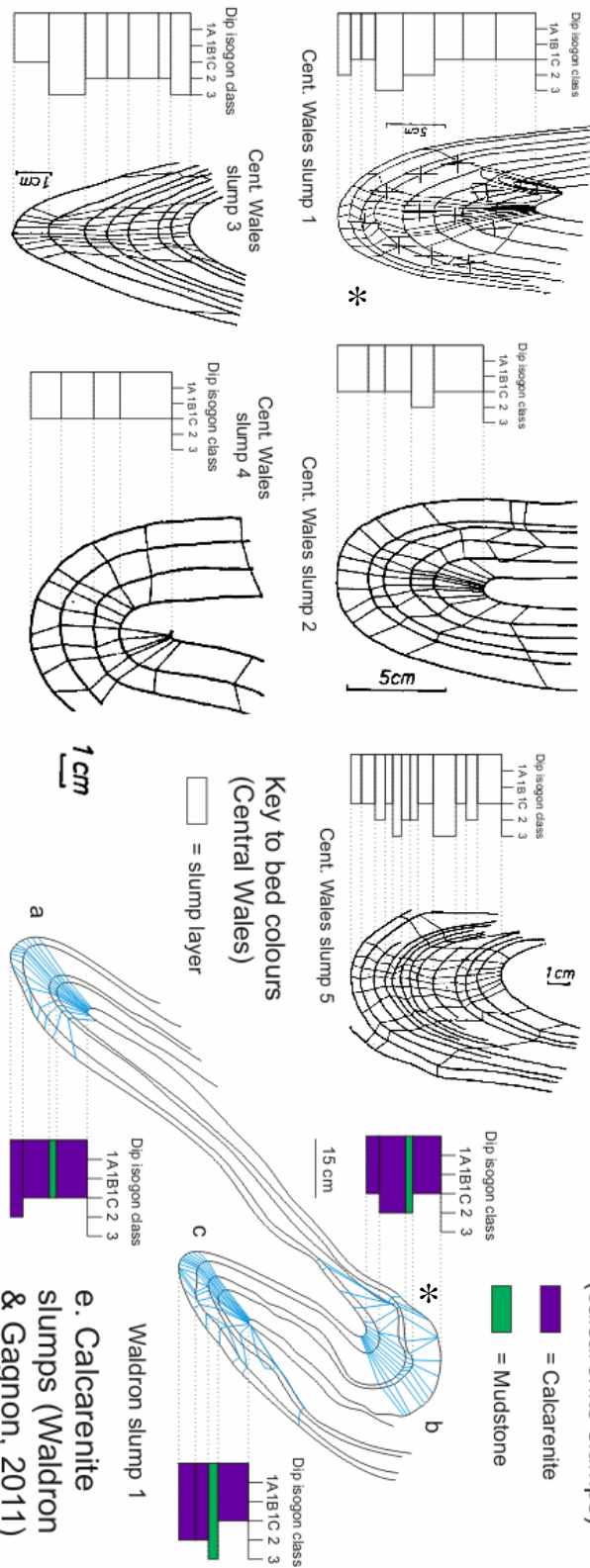


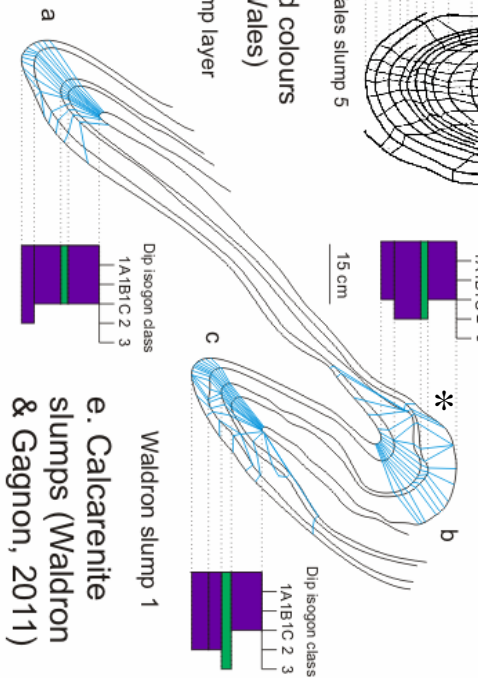
Fig. 7.3: Dip isogon sketches: (a) 5 meta-sedimentary rock folds in profile (modified from Ramsay & Huber, 1987; Price & Cosgrove, 1990; Fossen, 2010); (b) 2 high-grade gneiss folds in profile (modified from Ramsay & Huber, 1987; Lisle, 1992); and (c) 2 slump folds, Manly Slump Bed, New Zealand (modified from Strachan, 2008). Dip isogon logs show how the dip isogon class varies from layer-to-layer, giving an indication of how the relative coherences of the stacked layers change. The examples used in Figs. 7.6-7.7 for the dip isogon and quantitative layer thickness analyses have an asterisk next to them

Folds developed in Central Wales and SW Turkey slumps, and Denmark glacial till

d. Central Wales slump folds (Woodcock, 1976)



e. Calcarenite slumps (Waldron & Gagnon, 2011)



f. Denmark (glacio-tectonic) 'upright' chevron folds (Fossen, 2010)

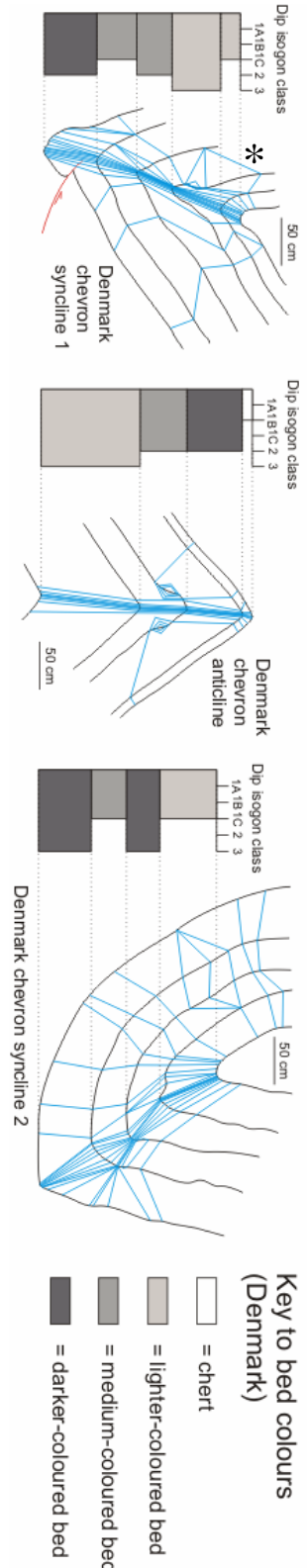
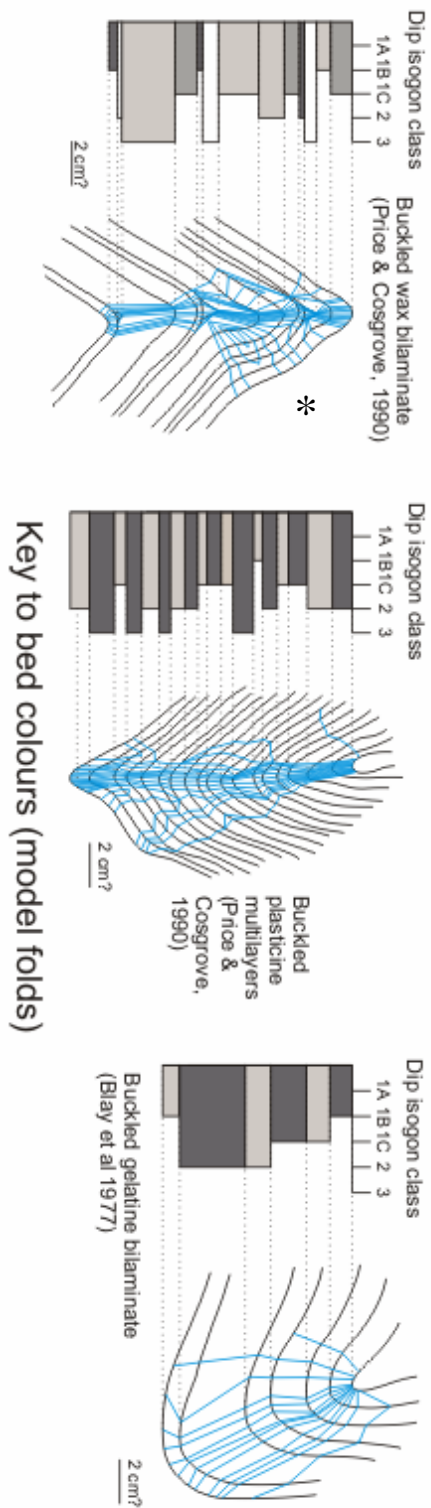


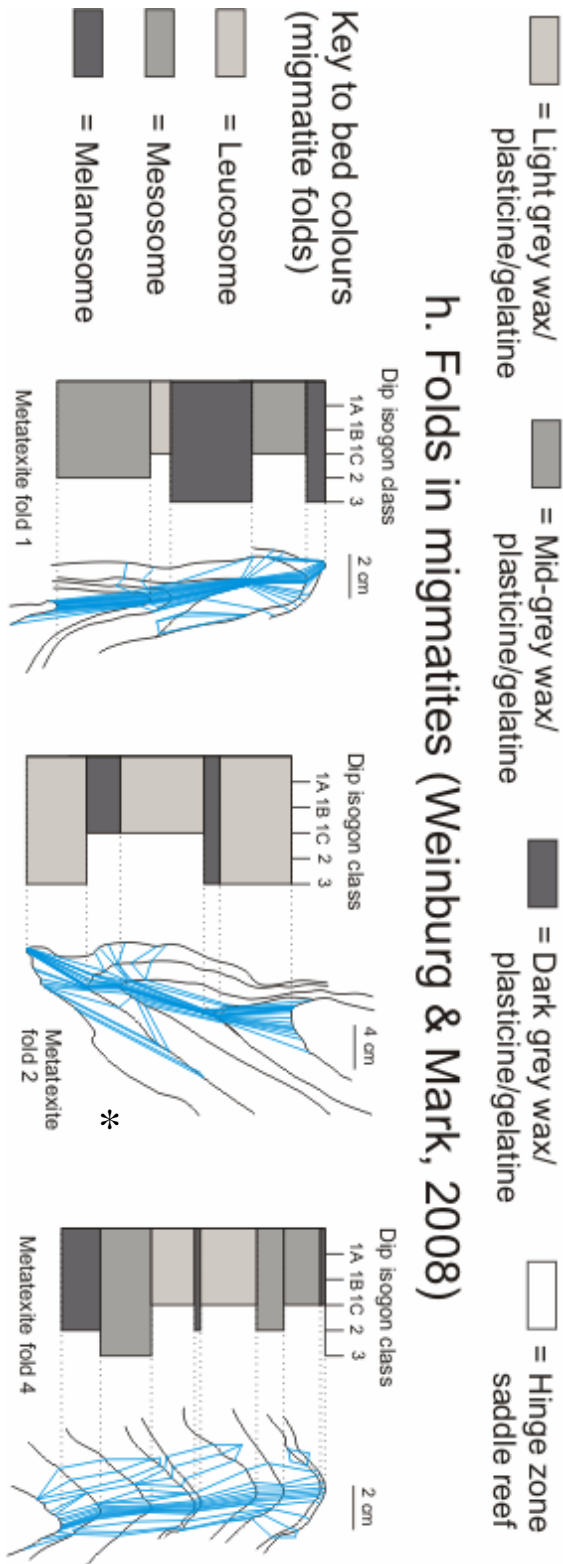
Fig. 7.4: Dip isogon sketches in profile: (d) 5 Central Wales slump folds (from Woodcock, 1976); (e) 3 SW Turkey calcarenite slump folds (modified from Waldron & Gagnon, 2011); and (f) 3 glacial till folds, Denmark (modified from Fossen, 2010). Dip isogon logs show how the dip isogon class varies from layer-to-layer, giving an indication of how the relative coherences of the stacked layers change. The examples used in Figs. 7.6-7.8 for the dip isogon and quantitative layer thickness analyses have an asterisk next to them

## Folds in model materials and migmatites

### g. Folds developed in buckle experiments from model materials



### h. Folds in migmatites (Weinburg & Mark, 2008)



[Light grey box] = Light grey wax/  
 plasticine/gelatine

[Mid-grey box] = Mid-grey wax/  
 plasticine/gelatine

[Dark grey box] = Dark grey wax/  
 plasticine/gelatine

[White box] = Hinge zone  
 saddle reef

#### Key to bed colours (migmatite folds)

[Light grey box] = Leucosome  
 [Mid-grey box] = Mesosome  
 [Dark grey box] = Melanosome

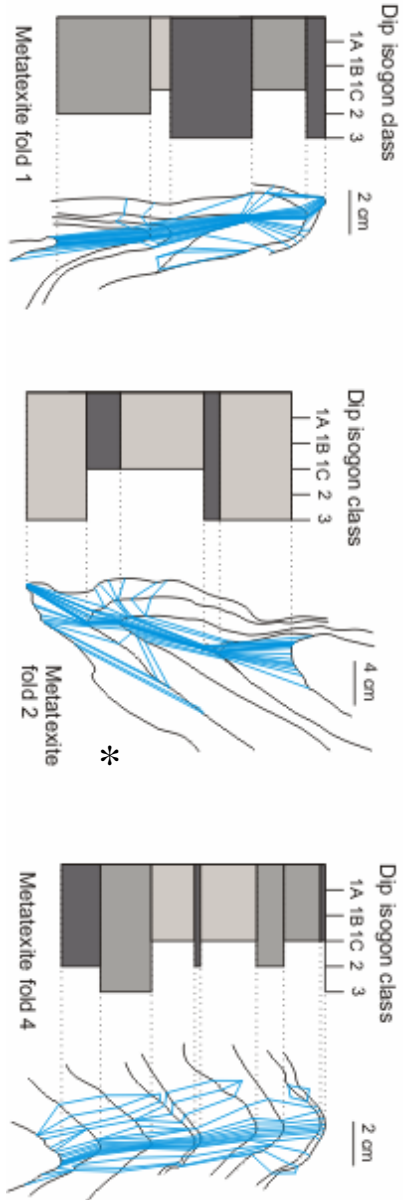


Fig. 7.5: Dip isogon sketches in profile: (g) 1 fold each in gelatine (modified from Blay et al, 1977), wax and plasticine (modified from Price & Cosgrove, 1990); and (h) 3 folds in migmatites from Ladakh, NW India (modified from Weinburg & Mark, 2008). Dip isogon logs show how the dip isogon class varies from layer-to-layer, giving an indication of how the relative coherences of the stacked layers change. The examples used in Fig. 7.9 for the dip isogon and quantitative layer thickness analyses have an asterisk next to them

### Interpretations

The combined results from the isogon log, dip isogon and quantitative layer thickness analyses for folded rocks show that:

1. The pelite and felsic layers in the meta-sedimentary and gneissose folds, respectively, are less coherence than the psammite / quartzite and mafic layers, respectively;
2. Each layer reacted to the fold deformation as a single unified system;
3. Each layer conforms to its own 'Ramsay' dip isogon class on both fold limbs with the layer retaining the same coherence throughout.

This conforms to the idealised dip isogon class patterns (Fig. 7.2), indicating that the criteria can be used to describe the mechanical state of folded rocks with:

1. Symmetric dip isogons and layer thickness ratio plots about the hinge;
2. Ordered, non-repeating dip isogons;
3. Conformity to a 'Ramsay' dip isogon class across the folded layer.

### 7.4.2 Folded sediments

#### Results

Analysis of the dip isogon logs for folded sediment (Figs. 7.4-7.8) shows that all layers have bulbous hinges and have high dip isogon classes (i.e. classes 1C to 3). Dip isogon analysis of the folded sediment examples (Figs. 7.4-7.8) produces asymmetric, scattered, repeating and disharmonic dip isogon patterns on each limb because the bed thickness varies across the slump and glacial till layers (after Patterson & Tobisch, 1993), causing the dip isogon pattern to show:

1. A range of 'Ramsay' classes within a layer;
2. Non-matching multiple 'Ramsay' classes in the layers across the limbs;
3. Repeated and looping dip isogons resulting from undulations and minor buckles.

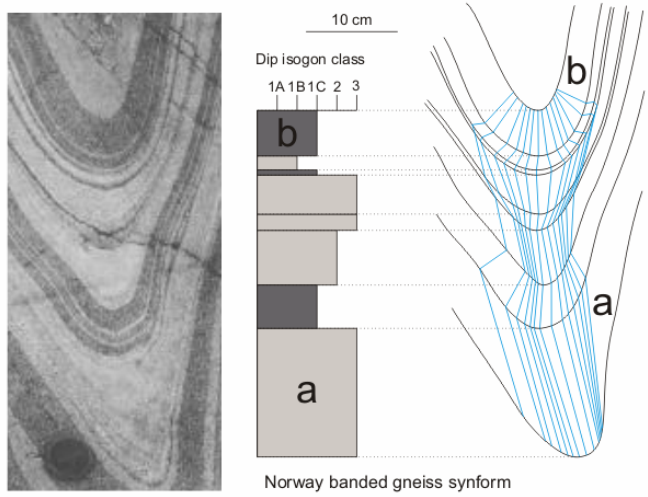
The quantitative layer thickness analysis plots of the folded sediment examples (Fig. 7.6) have a strong shape asymmetry and scatter in the curves about the hinge position (i.e.  $\alpha = 0^\circ$ ) on each limb. These results are similar to those from dip isogon analysis.

#### Interpretations

The combined results from the isogon log, dip isogon and quantitative layer thickness analyses of the slump sediment and glacial till folds show that:

1. The dip isogon patterns are indicative of deformed, low coherence layers;
2. Each layer reacted to the fold deformation independently;
3. Each layer does not conform to its own 'Ramsay' dip isogon class;
4. The layer does not retain the same coherence throughout.

## Norway metamorphic gneiss synform



## Roscollyn meta-sedimentary antiform

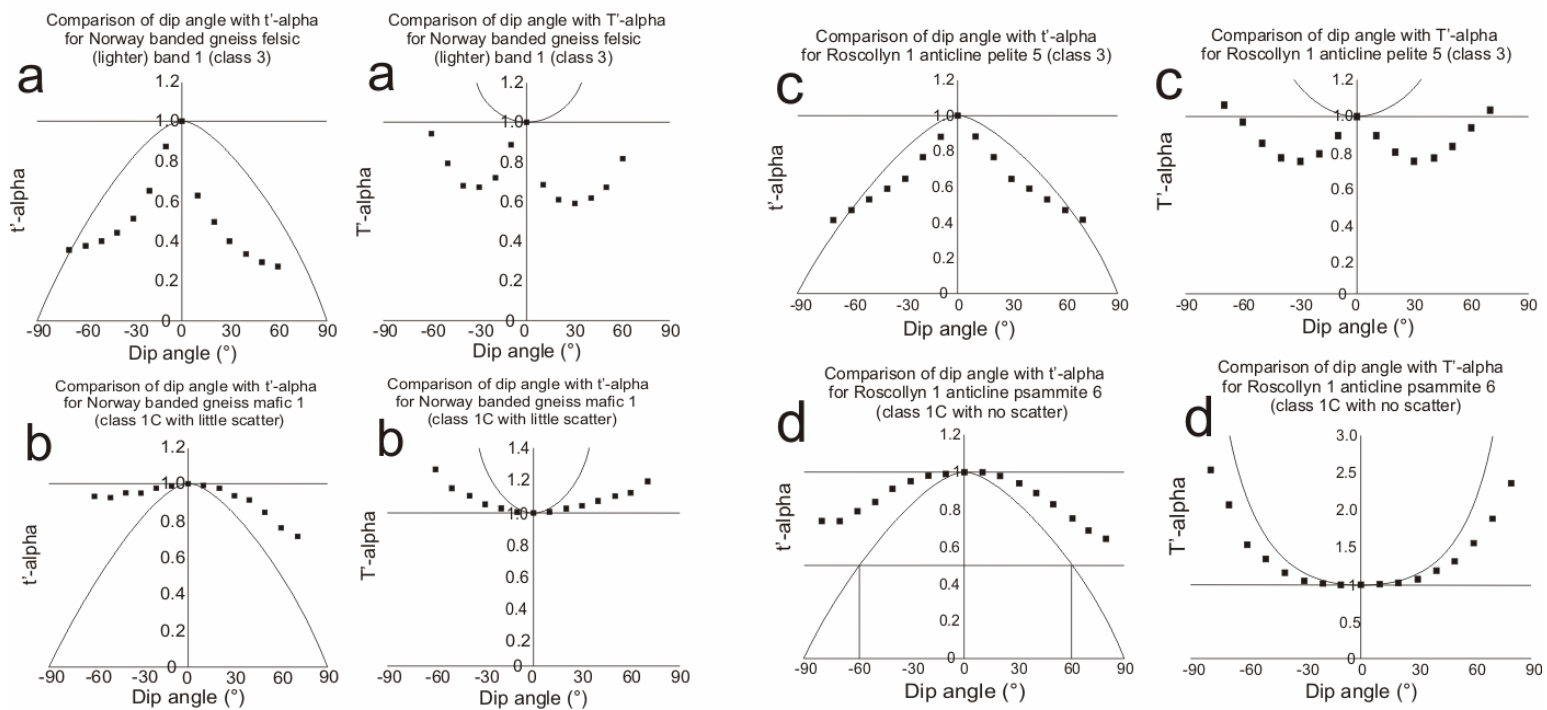
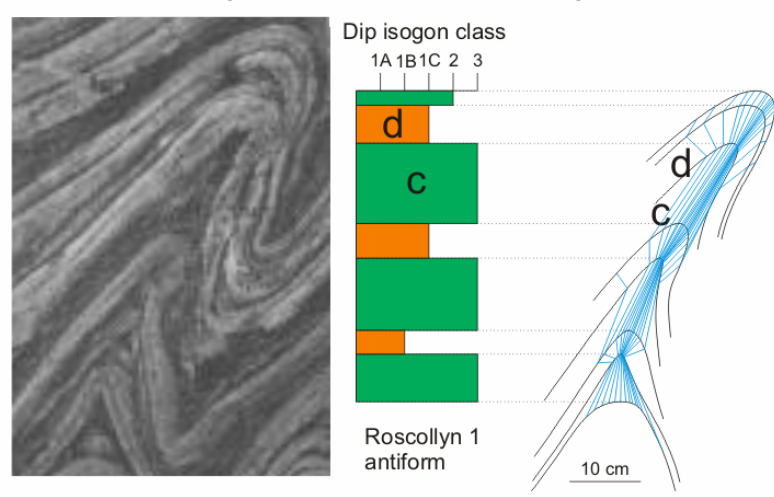
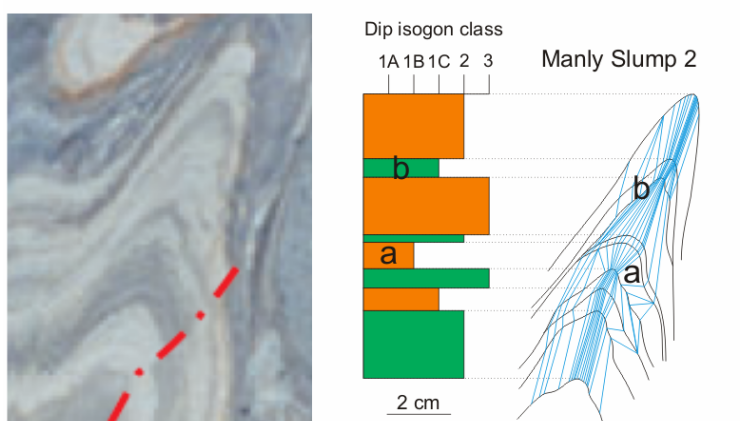


Fig. 7.6: Comparative dip isogon and layer thickness analyses of Norway metamorphic gneiss synform (modified from Lisle, 1992; see Fig. 7.3) with dip isogon logs (light grey = felsic; dark grey = mafic), and Roscollyn meta-sedimentary rock antiform (modified from Price & Cosgrove, 1990; see Fig. 7.3) with dip isogon logs (orange = sand; green = mud). All folds are in profile. Letters next to graphs relate to the layer being analysed

## Manly Slump Bed, New Zealand



## Central Wales slump fold 1

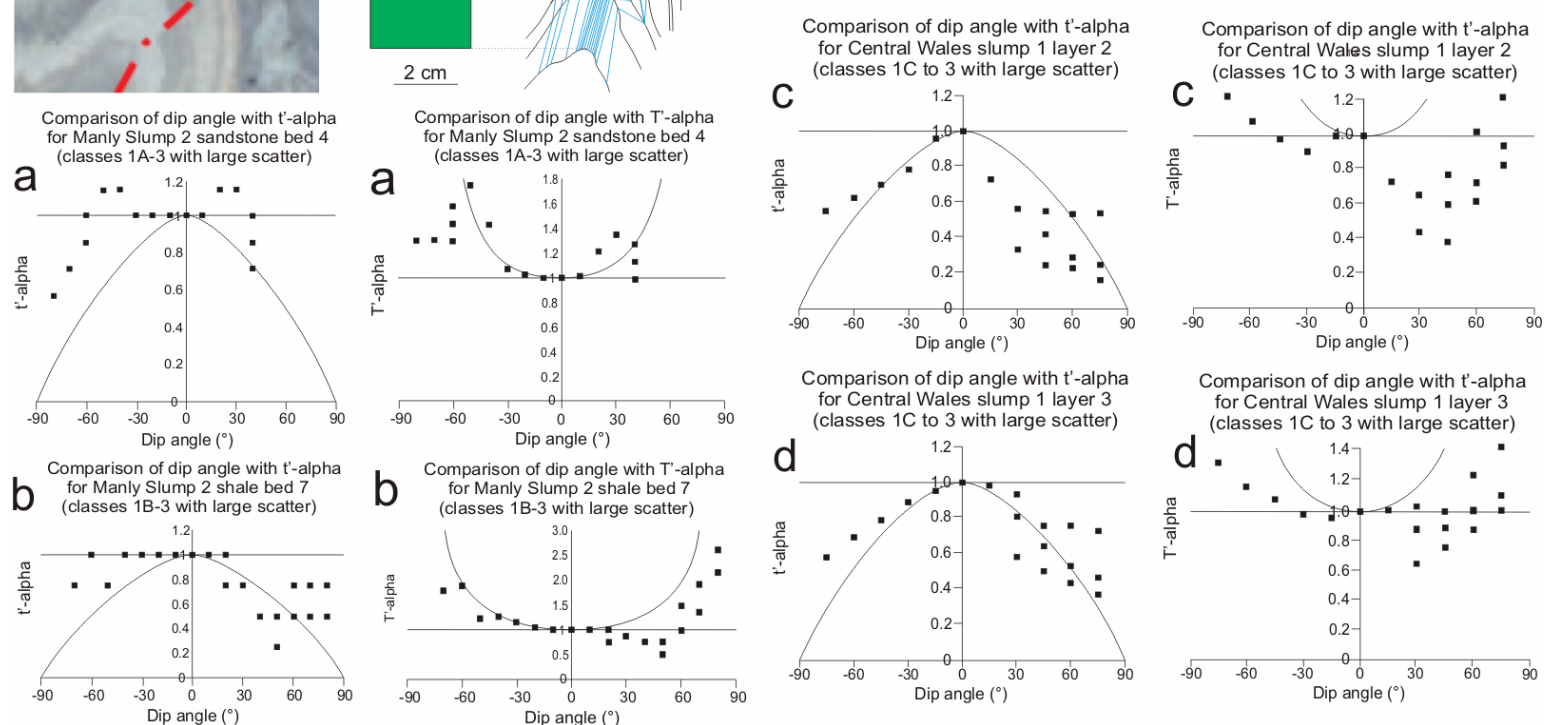
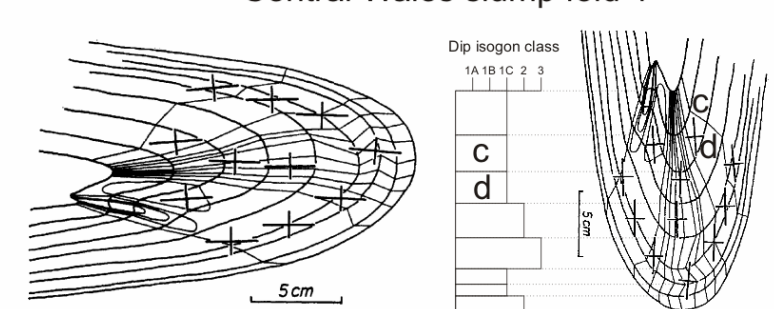


Fig. 7.7: Comparative dip isogon and layer thickness analyses of a slump fold from Manly Slump Bed, New Zealand in plan view (modified from Strachan, 2008; see Fig. 7.3) with dip isogon logs (orange = sand; green = mud) and Central Wales slump fold 1 in profile (from Woodcock, 1976; see Fig. 7.4) with dip isogon logs (no colour used as all layers are the same lithology). Letters next to graphs relate to the layer being analysed

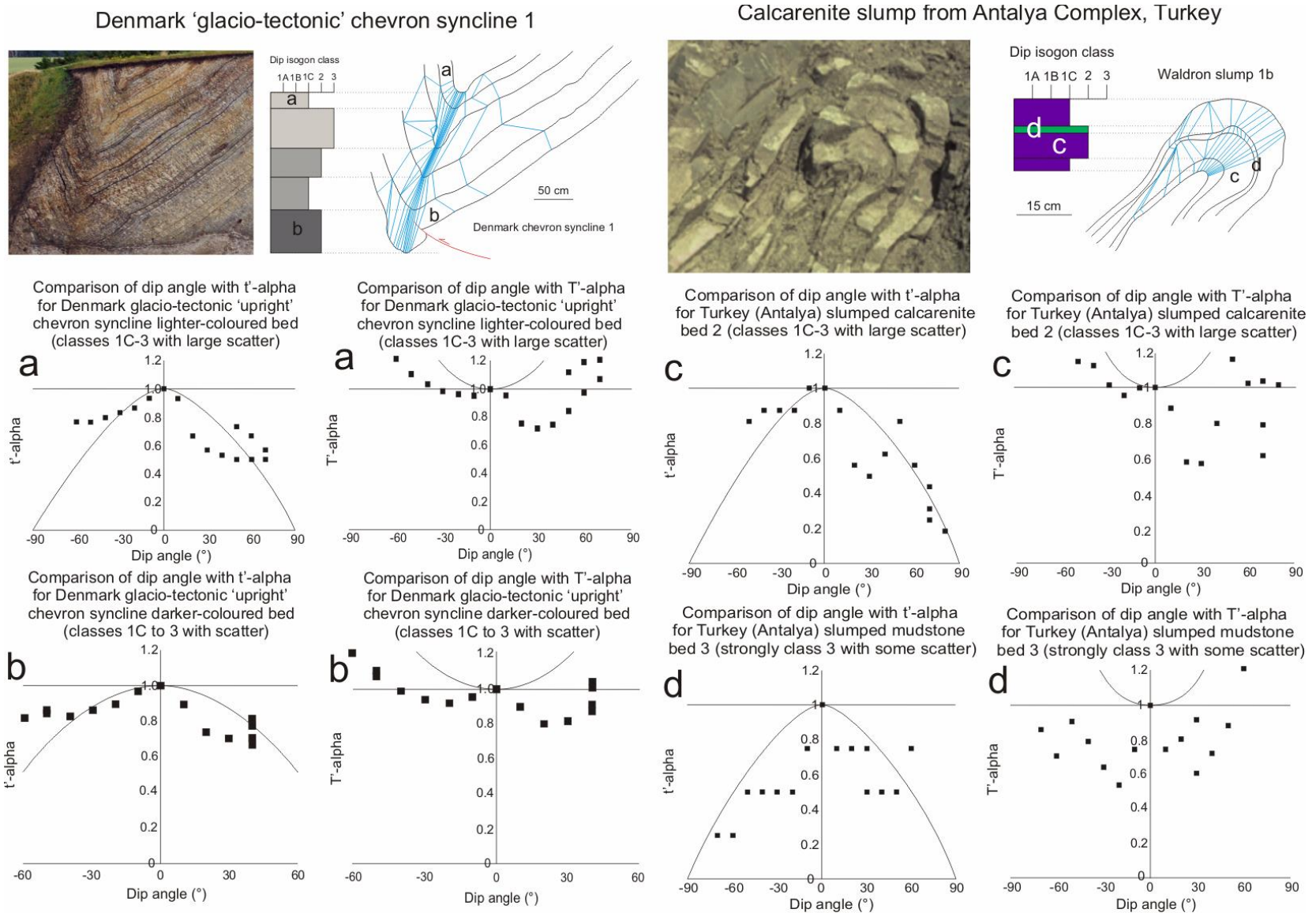


Fig. 7.8: Comparative dip isogon and layer thickness analyses for Denmark ‘glacio-tectonic’ chevron syncline 2 (modified from Fossen, 2010; see Fig. 7.4) with dip isogon logs (colours relate to the relative colours of the layers) and Calcarenite slump 1b (modified from Waldron & Gagnon, 2011; see Fig. 7.4) with dip isogon logs (purple = calcarenite; green = mudstone). All folds are in profile. Letters next to graphs relate to the layer being analysed

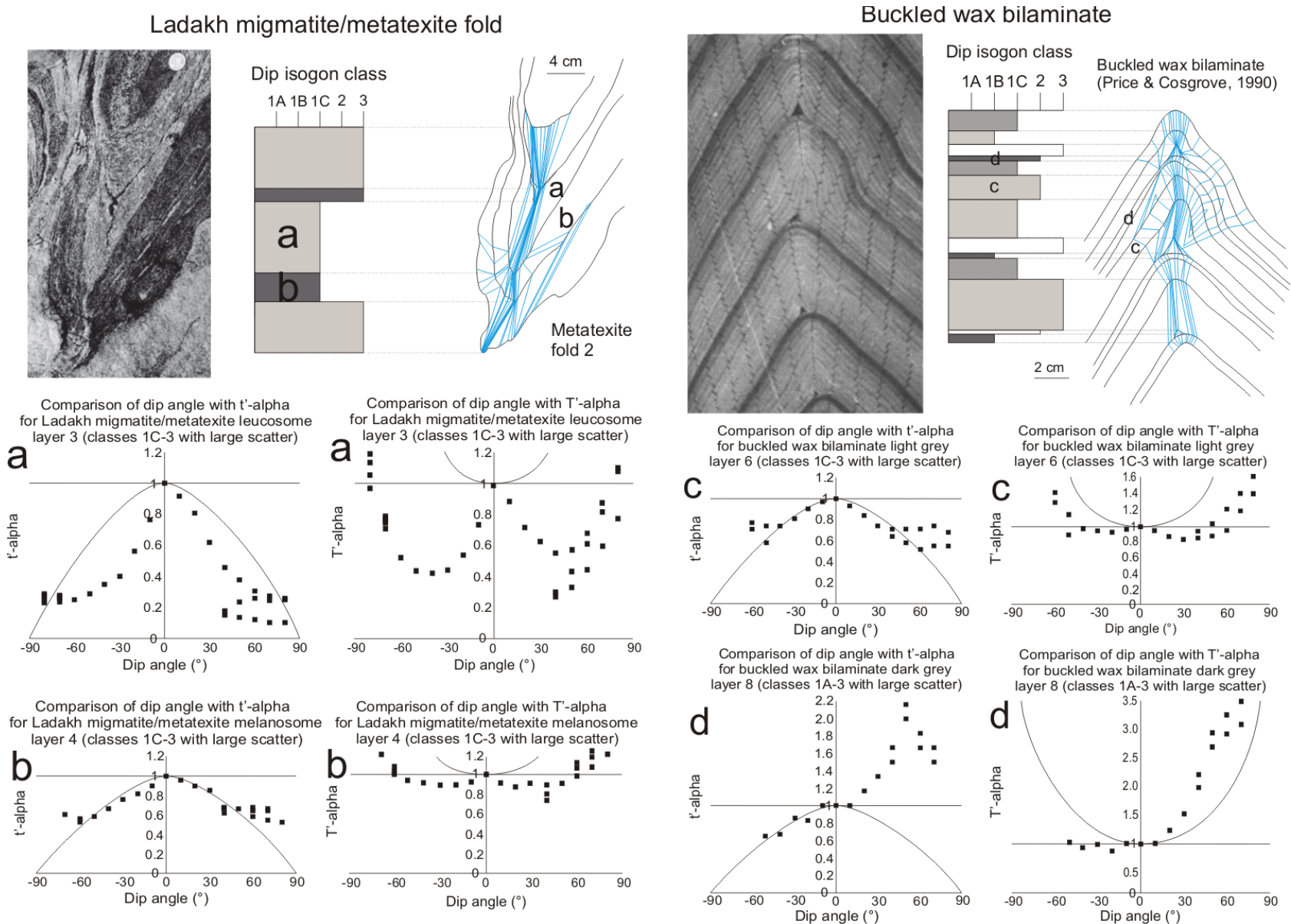


Fig. 7.9: Comparative dip isogon and layer thickness analyses for Ladakh migmatite fold 2 (modified from Weinburg & Mark, 2008; see Fig. 7.5) with dip isogon logs (light grey = leucosome; dark grey = melanosome) and buckled wax multi-layer (modified from Price & Cosgrove, 1990; see Fig. 7.5) with dip isogon logs (colours relate to colours of the wax; white = hinge zone saddle reef). All folds are in profile. Letters next to graphs relate to the layer being analysed

This does not conform to the idealised dip isogon class patterns used for folded rocks (after Patterson & Tobisch, 1993; Fig. 7.2) and instead, suggests that the following criteria can be used to describe the mechanical state of folded sediments:

1. Asymmetric dip isogons and layer thickness ratio plots about the hinge;
2. Scattered, repeating dip isogon curves;
3. Lack of conformity to a single 'Ramsay' dip isogon class within and across the folded layer.

### **Evaluation**

There appears to be no lithological control on the dip isogon pattern with all layers producing high dip isogon classes (i.e. classes 1C to 3). This is in contrast to the Waldron and Gagnon (2011) results of but similar to those of Paterson and Tobisch (1993). In the Waldron-Gagnon model, the slump folded sands should be less coherent (i.e. class 3 dip isogons) than the muds (i.e. class 1 dip isogons), but no such dip isogon pattern exists and suggests that their hypothesis is incorrect (see Methods). Also, the folded glacial till was modelled as a hydro-plastic fluid (Denis et al, 2009). In this state, the grains can 'flow' independently whilst the layer maintains cohesion (Craig, 1997; see Chapter 2). Modelling sediment as a hydro-plastic fluid gives a useful analogy to describe the mechanical states of the example slump folds during deformation (Woodcock, 1976; Strachan, 2008; Waldron & Gagnon, 2011; Figs. 7.6-7.8).

### **7.4.3 Folded model materials in profile**

#### **Results**

Analysis of the dip isogon logs for folded model materials (Figs. 7.5 & 7.9) shows that all layers have bulbous hinges and have high isogon classes (i.e. classes 1C to 3). Dip isogon analysis of the folded model materials (Figs. 7.5 & 7.9) produces asymmetric, scattered and repeating dip isogon patterns on each fold limb. This is the same dip isogon geometry as for both slump and glacial till folds with the dip isogon pattern showing:

1. A range of 'Ramsay' classes within a layer;
2. Non-matching multiple 'Ramsay' classes in the layers across the limbs;
3. Repeated and looping dip isogons resulting from undulations and minor buckles.

Likewise, quantitative layer thickness analysis plots of the folded model materials have a strong asymmetry, scatter and repetition in the curves about the hinge position ( $\alpha = 0^\circ$ ) for each limb. The curves display similar results on each limb as is found from dip isogon analysis.

#### **Interpretations**

The combined results from the isogon log, dip isogon and quantitative layer thickness analyses on folded model materials show that:

1. The dip isogon patterns are indicative of deformed, low coherence layers;
2. The dip isogon patterns are independent of lithology;
3. *The results and observations meet the criteria of folds developed in a plastic material analogous to sediment.*

It can be seen that the model materials do not behave like lithified rock. However, there is a potential dip isogon fold class dependence on the type of model material layer with lighter coloured wax layers having generally higher dip isogon classes (i.e. classes 1C to 3) than the darker coloured wax layers (classes 1B to 2), and vice versa for plasticine and gelatine layers.

#### **7.4.4 Folded migmatites in profile**

##### **Results**

Analysis of the dip isogon logs for folded migmatites (Figs. 7.5 & 7.9) shows that all layers have bulbous hinges and have high dip isogon classes (i.e. classes 1C to 3). Dip isogon analysis of the folded migmatites (Figs. 7.3 & 7.9) produces asymmetric, scattered and repeating dip isogon patterns on each fold limb because the thickness varies across the layers. This is the same dip isogon geometry as for slump, glacial till and model material folds:

1. A range of ‘Ramsay’ classes within a layer;
2. Non-matching multiple ‘Ramsay’ classes in the layers across the limbs;
3. Repeated and looping dip isogons resulting from undulations and minor buckles.

Likewise, quantitative layer thickness plots of the folded migmatites have a strong asymmetry, scatter and repetition in the curves about the hinge position ( $\alpha = 0^\circ$ ) for each limb. The curves display similar results on each limb as is found from dip isogon analysis.

##### **Interpretations**

The combined results from the isogon log, dip isogon and quantitative layer thickness analyses on the folded migmatites show that:

1. The dip isogon patterns are indicative of deformed, low coherence layers;
2. *The results and observations meet the criteria of folds that developed in a plastic material analogous to sediment;*
3. The ‘grain binding’ in partially-melted migmatites is strongly reduced and the grains ‘flow’ independently as in sediment (after Craig, 1997; see Chapter 2).

#### **7.5 Discussion**

The outcrops of the Bude Formation, SW England, provide a well-exposed and accessible example of chevron folds in profile (Freshney et al, 1972; 1979; Ramsay, 1974;

Sanderson, 1974; 1979; Lloyd & Whalley, 1986; Davison et al, 2004). As described in Chapter 5, the cliff outcrops at Lynstone (SS200053) are a potential microcosm of this progressive fold deformation (Enfield et al, 1985). Using the criteria established previously, dip isogon and quantitative layer thickness analyses have been undertaken in order to distinguish whether the folds in this outcrop developed in lithified rock or unlithified sediment.

In addition to this test of the criteria, there is a need to clarify where it is appropriate to use the Ramsay (1967) methods and what other methods can be employed to provide insights into the deformation accommodated by folded rock and sediment. A discussion is provided of:

1. The application of the dip isogon and quantitative layer thickness methods to slump folded layers in both plan-view and oblique sections;
2. The limits to the dip isogon and quantitative layer thickness methods;
3. Potential future work to distinguish the mechanical state of the folded material using the inverse thickness method (Lisle, 1992).
4. Whether the geometric criteria to distinguish folded rock and sediment result from:
  - a. Shear strain accommodation on the base slump fold limb caused by the down-slope flow (Patterson & Tobisch, 1993; Woodcock, pers. comm., 2011);
  - b. High strain rates in sediments and low rates in rocks (Gibbs, pers. comm., 2011);
  - c. Water and/or phyllosilicate content of slump layers (Paterson & Tobisch, 1993).

### **7.5.1 Initial application of methods to the Bude Formation**

In order to provide an initial test of the criteria, the methods have been applied to a contiguous set of folds in profile in the Lynstone cliff section (SS200053) of the Bude Formation, SW England. For the purposes of these analyses, the folds are described as (Fig. 7.10): (1) ‘early’; (2) ‘upright’; and (3) ‘late’; using terms defined by Enfield et al (1985).

#### **‘Early’ and ‘upright’ folds in profile**

The analysis of the dip isogon logs for the ‘early’ folds (marked **1** in Fig. 7.10) shows that the layers have a range of dip isogon classes (i.e. classes 1A to 3), with many bulbous hinges in the folded layers. However, with the ‘upright’ folds (marked **2** in Fig. 7.10), all lithologies display bulbous hinges with generally high dip isogon classes (i.e. classes 1C to 3). The dip isogon analysis shows that both the ‘early’ and ‘upright’ folds have asymmetric, scattered and disharmonic dip isogon patterns on adjacent limbs because the thicknesses vary across the layers. The dip isogon pattern on each limb display:

1. A range of ‘Ramsay’ classes within a layer;
2. Non-matching ‘Ramsay’ classes in the layers across the limbs;
3. Repeated and looping dip isogons resulting from undulations and minor buckles.

Quantitative layer thickness analysis plots of the ‘early’ and ‘upright’ fold examples (Fig. 7.10) have a strong asymmetry, scatter and repetition in their curves about the hinge position ( $\alpha = 0^\circ$ ) for each limb. *The characteristics meet the criteria of folds formed in sediment.*

### **‘Late’ folds in profile**

Analysis of the dip isogon logs (Fig. 7.10) show that some of the shale layers have higher dip isogon classes (i.e. classes 2 to 3) than the sandstone and siltstone layers (i.e. classes 1B to 2). However, in other layers, all lithologies show bulbous hinges with generally high dip isogon class values (i.e. classes 1C to 3).

The dip isogon analysis of the ‘late’ folds (**3 & 4**, respectively, in Fig. 7.10) have symmetric, ordered, non-repeating and harmonic dip isogon patterns on adjacent limbs and conform to the idealised dip isogon class patterns (Fig. 7.2). However, some inter-bedded folded layers have more asymmetric, scattered, repeating and disharmonic dip isogons, suggesting that:

1. Each layer conforms to its own ‘Ramsay’ dip isogon class on both fold limbs with the same coherence retained throughout the layer;
2. There is a lithological difference in layer coherence as found in rocks between the relatively high coherence (classes 1A to 1C) sandstones and low coherence (classes 2 to 3) shales.

Quantitative layer thickness analysis plots of some of the layers from the ‘late’ folds (Fig. 7.10) have a near symmetry to their curves about the hinge position ( $\alpha = 0^\circ$ ) on each limb. *This meets the criteria of folds that developed in rock.* However, there are scattered, repeating and disharmonic dip isogons in some layers on the ‘late’ fold limbs. *Such patterns indicate that folds developed in sediment.*

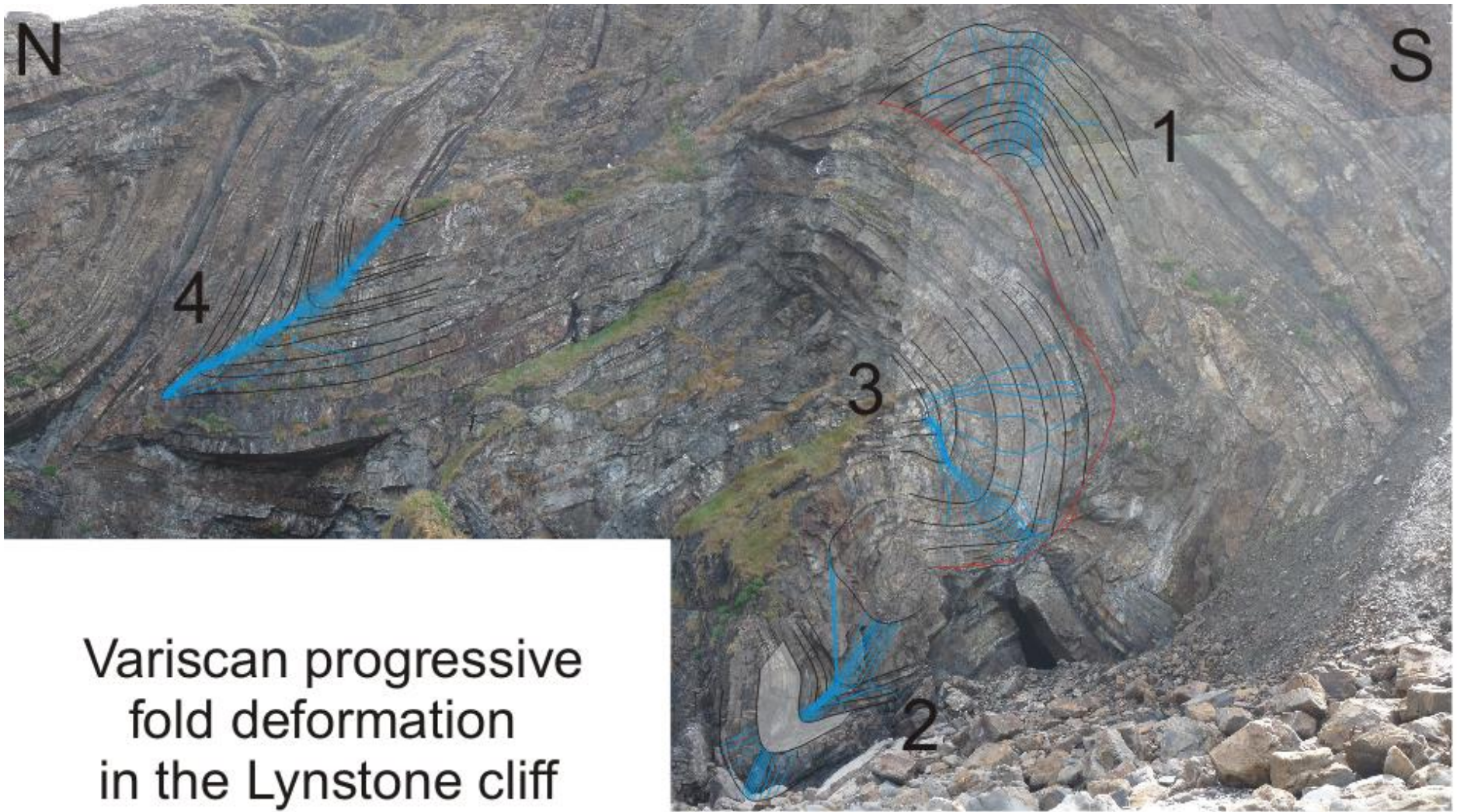
This apparent contradiction can be explained if the ‘late’ fold deformation affected the Bude Formation whilst the beds were lithifying (i.e. inter-bedded sediment and rock). If this was indeed the case, it is likely that the less coherent, water-saturated sediment layers folded passively in step with the more coherent rock layers.

### **Evaluation of the results**

From an evaluation of the results, it is possible to identify the steps in the lithification with fold deformation in the Lynstone cliff section (SS200055; Fig. 7.10):

1. ‘Early’ and ‘upright’ folds developed in sediment;
2. ‘Late’ fold deformation took place as some of the Bude Formation beds began to lithify.

Assuming that the Lynstone cliff section (SS200055; Fig. 7.10) is a potential microcosm of the progressive Variscan fold deformation in the Bude Formation (see Chapter 5), the results from these folds could also apply to the Bude and Crackington formations as a whole. This hypothesis will be tested for folds across the both formations in Chapter 8.



### Variscan progressive fold deformation in the Lynstone cliff section, Bude Fm

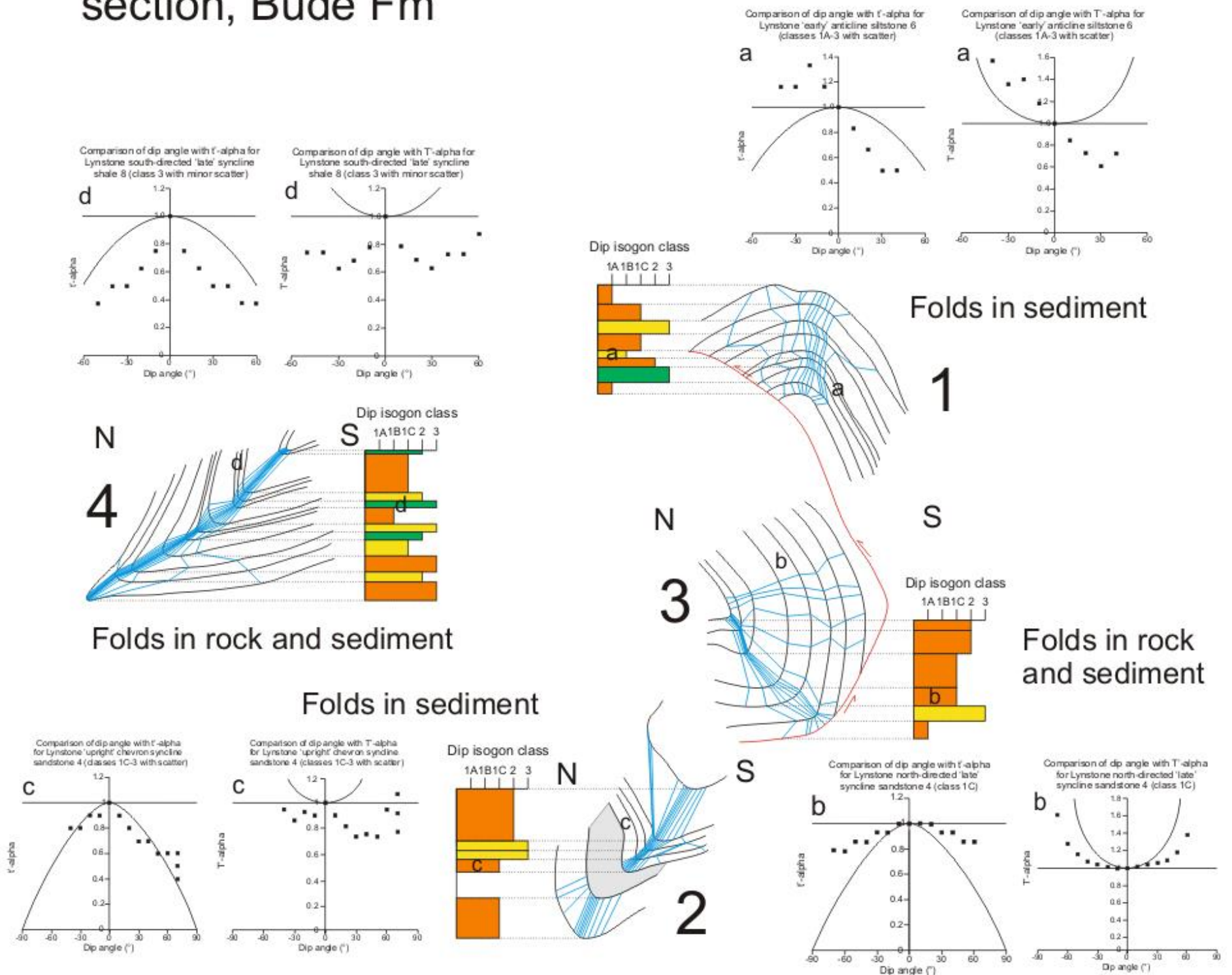


Fig. 7.10: Photo-montage and sketches of 4 folds from different Variscan progressive deformation 'events' in the Lynstone cliff section, Bude Formation, SW England (SS200053). Dip isogon and quantitative bed thickness analyses have been undertaken on all the fold types, with a dip isogon log next to each sketched fold (orange = sandstone; yellow = siltstone; green = shale). All folds are in profile. Letters next to graphs relate to the bed being analysed

### 7.5.2 Dip isogon methods for oblique and plan-view sections through folded layers

In this chapter, the dip isogon and quantitative layer thickness analyses have been applied to folds in profile sections where it is possible to determine the fold orientation. This is one of the constraints imposed on the methods by Ramsay (1967). However, in the case of the slump folds from the Manly Slump Bed (Strachan, 2008), the methods were applied to one fold oblique to the profile plane, and to another in plan-view section, sub-perpendicular to the profile plane (Figs. 7.3 & 7.7). The fold in plan-view from the Manly Slump Bed (Fig. 7.7) provides a test of whether the geometric criteria can be applied to folds in any plan-view section.

#### Results from the Manly Slump Bed example

The dip isogon logs of the Manly Slump Bed fold examples (Figs. 7.3 & 7.7) show that all layers have bulbous hinges and have high dip isogon classes (i.e. classes 1C to 3). The dip isogon analysis of the folded sediment examples (Figs. 7.3 & 7.7) produces asymmetric, scattered, repeating and disharmonic dip isogon patterns on each limb because of the varying bed thickness across the slump fold layers. These are the same dip isogon patterns as for the other sediment, model material and migmatite examples. Quantitative layer thickness analysis plots of the folded sediment examples (Fig. 7.7) show a strong asymmetry and scatter in the curves about the hinge position (i.e.  $\alpha = 0^\circ$ ) on each limb. Thus, the combined results of isogon log, dip isogon and quantitative layer thickness analyses in oblique and plan-view sections on the Manly Slump Bed example sections are exactly the same as for folds in profile section.

#### Evaluation

Evaluation of the results from the Manly Slump Bed examples suggest that *the geometric criteria for distinguishing folds in profile section from slumped sediment appear to hold also for folds from slumped sediment in both oblique and plan-view sections.*

Interestingly, similar dip isogon and quantitative layer thickness analyses have been undertaken by I. Alsop on metamorphic sheath folds from N Scotland (TSG Conf. comm., Durham, 2011), which presented similar results. Together, the use of the dip isogon methods by I. Alsop and in this work provide new research avenues into understanding of the mechanical state of the layers during fold deformation.

### 7.5.3 Limits to the dip isogon and quantitative layer thickness methods

There are four preconditions needed in order to undertake valid dip isogon and quantitative layer thickness analyses, otherwise the results may be misleading or incorrect. The four preconditions are that none of the following apply:

1. Liquefied layers were present, such as in massive, disaggregated slump beds, since the lack of friction (i.e. fluid-supported grains) in the layers would prevent folding;

2. Stratigraphic cut-offs (i.e. onlapping pinch-outs and toplapping truncations), as this produces irregular dip isogon patterns and layer thickness ratio plots;
3. Strongly-developed sedimentary structures that can be mistaken for bedding planes, resulting in unrealistic dip angles being measured;
4. Later deformation events by fracturing, faulting or refolding in the fold hinge zone, otherwise the results from the dip isogon analyses would reflect the later folding event (i.e. later folding must be on the limb of the original fold away from the hinge zone).

#### **7.5.4 Proposed future work using the inverse thickness method**

The dip isogon and quantitative layer thickness methods were also applied to a banded gneiss synform in profile from Gjerdoya Island, Norway (Figs. 7.3 & 7.6). However, Lisle (1992) proposed the inverse thickness method to analyse the fold, which is described below. This method has been employed on two example layers, one each from folded sediment and folded rock, in order to test whether the method distinguishes between them.

#### **Methods**

In the inverse thickness method, true layer thickness ( $t_0$ ) is measured at  $10^\circ$  intervals around the fold. The thickness measurements are inverted (i.e.  $n/t_0$ ) with the  $n$ -value dependant on the relative inverse thickness size calculated. The points are plotted in a polar co-ordinates graph at  $10^\circ$  intervals where “inverse thickness ( $n/t_0$ ) is plotted as a function of the orientation of the layer tangent”, so a strain ellipse can be fitted through the points (Lisle, 1992; Fig. 7.11).

#### **Data**

Two example layers are selected to test whether the inverse thickness method can be used to distinguish folded sediment and rock in addition to the dip isogon and quantitative layer thickness methods. The rock example is a mafic layer from a banded gneiss synform, Gjerdoya Island, Norway (Figs. 7.3, 7.6 & 7.11; Lisle, 1992). The sediment example is a sand layer from a calcarenite slump fold, Antalya, Turkey (Figs. 7.4, 7.8 & 7.11; Waldron & Gagnon, 2011).

#### **Results**

From inverse thickness analysis of the mafic layer in the banded gneiss synform, one strain ellipse is fitted through the inverse thickness points (Fig. 7.11a). The ellipse has its major axes oriented sub-parallel ( $005^\circ$ - $185^\circ$ ) (i.e. maximum extensional direction) and minor axes oriented sub-perpendicular ( $095^\circ$ - $275^\circ$ ) (i.e. maximum compressional direction) to the orientation of the fold axial trace. The strain ratio for the mafic layer is 1.97, which almost matches the Lisle (1992) estimate of 1.95 for the strain accommodated by this layer.

From inverse thickness analysis of the sand layer in the calcarenite slump fold, two strain ellipses are fitted through the inverse thickness points (Fig. 7.11b). The orientations of the

strain ellipses on the limbs have the major axes sub-parallel (left-hand limb: 120°-300°; right-hand limb: 170°-350°) and minor axes sub-perpendicular (left-hand limb: 030°-210°; right-hand limb: 080°-260°) to the bedding orientations. The strain ratio in the slump sand layer varies with each strain ellipse: (1) left-hand limb is 5.77; and (2) right-hand limb is 4.67.

### **Interpretations**

The inverse thickness analysis for the mafic layer (Fig. 7.11a) produces only *one definitive strain ellipse*. This suggests that:

1. The strain accommodated is the same across the layer;
2. The layer acted as a single unified system.
3. These interpretations compliment the criteria established for folded rock from dip isogon and quantitative layer thickness analyses.

Inverse thickness analysis for the slump sand layer (Fig. 7.11b) produces *two definitive strain ellipses, one each for the left-hand and right-hand limbs*. The major axes of the strain ellipses for both limbs indicate that maximum extensional directions are bedding-parallel and bedding-normal for maximum compressional directions (e.g. minor axes). This suggests that:

1. The limbs acted independently of each other;
2. The strain ellipses are recording a ‘flow’ of material that travelled towards the hinge zone during slump fold deformation.
3. These interpretations also compliment the criteria established for folded sediment from dip isogon and quantitative layer thickness analyses.

### **Evaluation**

The results of inverse thickness analysis (Lisle, 1992) suggest that this method can be used to distinguish folds developed in rock and sediment, in addition to the dip isogon and quantitative layer thickness analyses (Ramsay, 1967). The associated geometric criteria for strain accommodation in folded rocks are as follows:

1. One strain ellipse can be fitted to the points from inverse thickness analysis;
2. The ellipse describes the strain accommodation across the entire folded layer.

The geometric criteria for strain accommodation in folded sediment are:

1. Multiple strain ellipses can be fitted to the points from inverse thickness analysis;
2. Each ellipse describes the strain accommodation in part of a folded layer (e.g. a limb).

The potential geometric criteria may provide an extension of the inverse thickness methods to assess the mechanical or lithification state of layers during folding and compliment the geometric criteria developed from the dip isogon and quantitative layer thickness analysis.

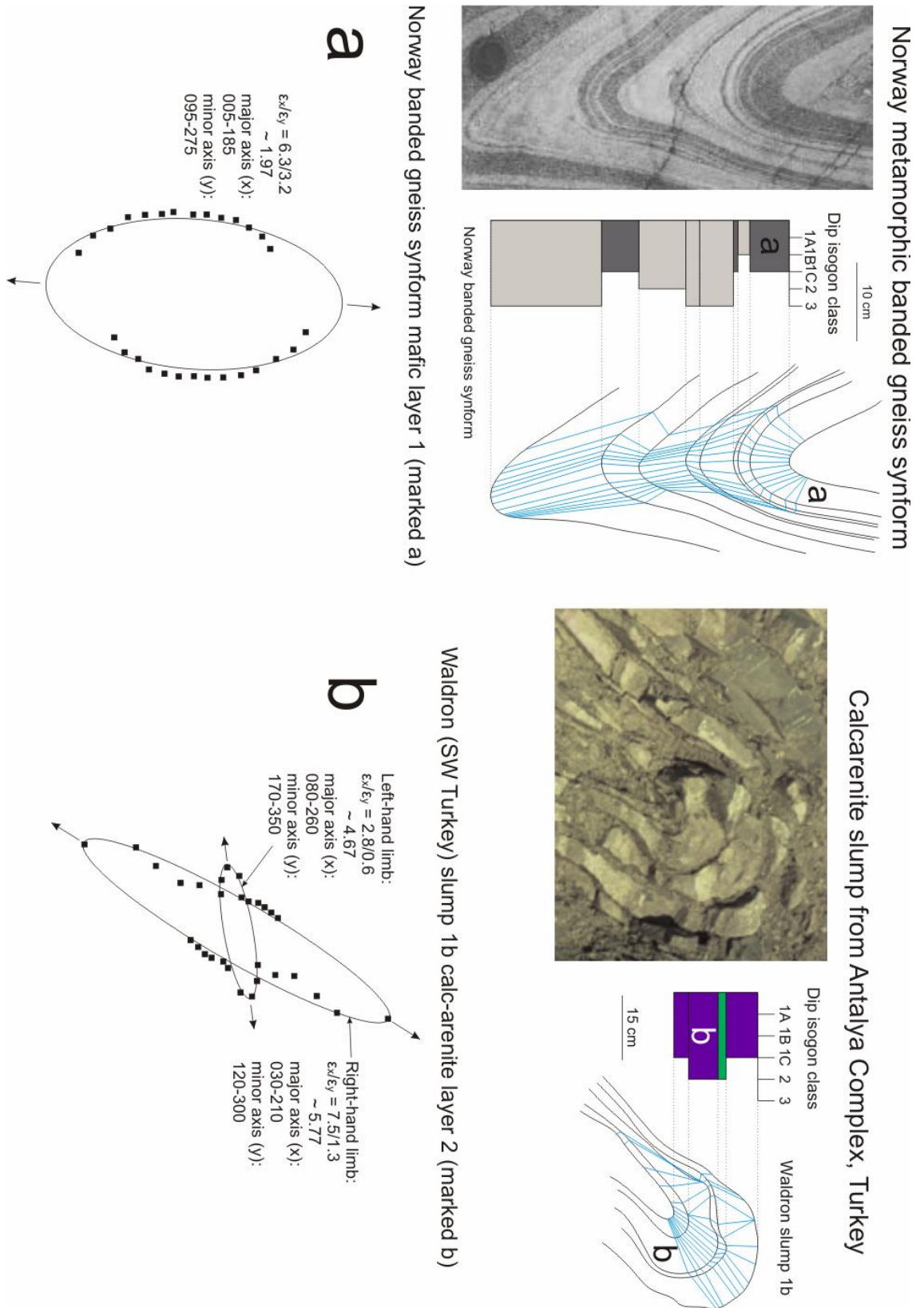


Fig. 7.11: Application of the inverse thickness method using a mafic layer in Norway banded gneiss synform (Figs. 7.3 & 7.6; modified from Lisle, 1992) and a calc-arenite layer in the Turkey slump fold (Figs. 7.4 & 7.8; modified from Waldron & Gagnon, 2011). In both cases for inverse thickness points, the left hand limbs have open squares and the right hand limbs have closed squares. All folds are in profile. Letters next to ellipses relate to the layer being analysed

### 7.5.5 Potential other relationships to the fold geometric criteria

#### a. Shear strain

It has been suggested (Paterson & Tobisch, 1993; Woodcock, pers. comm., 2011) that in slump folded layers there is a variation in the limb layer thickness between thinner base and thicker top layers. The thinning of the base slump fold limb may occur because it has accommodated more shear strain during down-slope movement. However, from analysis of slump fold limb thicknesses, such thickness variations are not observed in the slump folds from SW Turkey and New Zealand (Figs. 7.3-7.4 & 7.7-7.8), the Denmark glacial till folds (Fig. 7.4 & 7.8) and the 'early' fold at Lynstone (Fig. 7.10). In the case of the Central Wales slump folds (Woodcock, 1976; Figs. 7.4 & 7.7) only one fold example displays layers with a thinner base slump fold limb. Indeed, within the stack of layers involved in these slump folds from Central Wales, one of the layers on the base limb is thicker than on the top limb. Consequently, the thickness variations between limbs may reflect the original thickness of the pre-folded sediment layers (Paterson & Tobisch, 1993), rather than being a consequence of it being a slump fold.

#### b. Strain rate

It has been suggested (Gibbs, pers. comm., 2011) that relative strain rate may generate the geometric criteria observed. Thus, the symmetric geometric criteria for folded rocks may relate to the accommodation of strain at relatively low rates, whilst the asymmetric geometric criteria for folded sediments may relate to the accommodation of strain at relatively high rates. However, dip isogon and quantitative layer thickness analyses of the north- and south-verging, 'late' folds at Lynstone (Fig. 7.10) show that the folded inter-bedded layers with symmetric and asymmetric geometric criteria are found together. These layers presumably accommodated strain at the same rate during the same fold deformation event. Hence, the relative strain ratio cannot be responsible for the geometric criteria observed.

#### c. Water and/or phyllosilicate content

Paterson and Tobisch (1993) suggest that the water and/or phyllosilicate content of slump folded layers may have a relationship to the variation in dip isogon patterns observed. From petrographic analysis of thin sections, the phyllosilicate content in the matrix of slump folded layer samples has similar ranges to that of non-slump folded layers (i.e. 25 %  $\pm$  6 %; see Chapter 3). In terms of water content, it is not possible to determine the amount of water or the water pressure exerted in the sediment during deformation, as the slump folds have since lithified and have become exposed. However, pore-fluid pressure ( $P_f$ ) must have been sufficiently high that the thixotropic sediment 'fluid' (after Harris, 1977; Doe & Dott, 1980; after Vigneresse, 2004) or hydro-plastic (Denis et al, 2009) sediment 'fluid' could fold without fracturing (Craig, 1997; see Chapter 2).

## 7.6 Summary of geometric criteria to distinguish folded rock and sediment

The primary aim of the chapter and the general aim of this thesis have been to identify a set of geometric methods to distinguish between folded rock and folded sediment viewed in profile. To this end, it has been demonstrated that the dip isogon and quantitative layer thickness methods are applicable to distinguishing the mechanical state of the folded layers based on their geometries alone. The geometric criteria for distinguishing such folds in profile are as follows.

Folded rocks, with the exception of rocks at high temperatures, are characterised by:

1. Symmetric dip isogon patterns and layer thickness ratios about the fold hinge zones;
2. Ordered, non-repeating dip isogon patterns and layer thickness ratios on the fold limbs;
3. Conformity to a specific 'Ramsay' dip isogon fold class throughout the folded layer.

In contrast, folded sediments behave in a different manner and are characterised by:

1. Asymmetric dip isogon patterns and layer thickness ratios about the fold hinge zones;
2. Scattered, repeating dip isogon patterns and layer thickness ratios on the fold limbs;
3. Lack of conformity to any specific 'Ramsay' dip isogon fold class across the folded layer.

These criteria can be expressed in these terms:

1. Low-grade meta-sedimentary rocks are likely to have a marked rheological contrast between strong lithified layers (e.g. sandstones) and weaker less cemented layers (e.g. shales). Folds in such rocks therefore show a consistent contrast between class 1 folds in stiff layers and class 3 folds in weak layers, as described by Ramsay and Huber (1987).
2. Unlithified sediments and very high-grade metamorphic rocks show a smaller rheological contrast between different lithologies, which commonly display weak layers. Folds in such sediments or very high grade rocks therefore show less consistent geometry, both along layers and between layers.

Further to the criteria developed from using dip isogon and quantitative layer thickness methods to distinguish folded rock and sediment, potential complimentary geometric criteria are proposed from using inverse thickness analysis of the same folded layers and are as follows:

Folded rocks, with the exception of rocks at high temperatures, are characterised by:

1. One strain ellipse that can be fitted to the points from inverse thickness analysis;
2. An ellipse that describes the strain accommodation across the entire folded layer.

In contrast, folded sediments behave in a different manner and are characterised by:

1. Multiple strain ellipses that can be fitted to the points from inverse thickness analysis;
2. An ellipse that describes the strain accommodation in part of a folded layer (i.e. a limb).

## Chapter 8: Bude Formation lithification state during folding

### 8.1 Introduction

The Bude Formation coastal outcrops, SW England, have been studied by numerous authors (see references in Chapters 4-6). Particular attention has been given to the chevron folds that have low-curvature limbs and narrow high-curvature hinge zones (Ramsay, 1974) and which have been modified increasingly towards the south by south-directed shearing during progressive Variscan deformation (Sanderson, 1979; Lloyd & Whalley, 1986; 1997). This chapter considers the Bude Formation lithification state during folding via application of methods derived in Chapter 7, thus allowing its structural evolution to be reconsidered, which is relevant to both objectives of this thesis. Also, some of the folds described in Chapters 4-6 show evidence that some or all of their beds were folded whilst still unconsolidated sediment.

The Bude Formation has been used in the present study to measure and analyse the folded beds from which five fold types are recognised. Four of the fold types have been mapped in detail within the Black Rock-Wanson Mouth foreshore (SS196017-SS195013; see chapters 4 & 5) and all of them are observed elsewhere along the coastal outcrops. The fold types are: (a) 'reclined', 'elastica', detached slump raft folds within massive slump beds; (b) recumbent, tight-isoclinal, attached slump folds; (c) inclined, closed-tight, 'early' folds; (d) upright, closed-tight, chevron folds; and (e) inclined-to-recumbent, tight, chevron folds.

The two types of slump folds (types: a & b) have been measured and analysed to determine the variation in palaeo-slope directions during Bude Formation deposition (see Chapter 5). The 'early' folds have also been studied to understand their relationship with other Variscan deformation structures (see Chapter 4). All three types of slump and 'early' folds (types: a, b & c) are recognised as a result of criteria described in chapter 4 and 5 and that these fold types were generated at or near the palaeo-surface in unconsolidated sediment (see chapters 4 & 5), particularly the slump folds (Hartley, 1991). In contrast, the 'upright' and 'inclined-to-recumbent' chevron folds (types: d & e) have been assumed previously to have developed in rock (Ramsay, 1974).

Geometric criteria have been developed to distinguish folded sediment and rock in profile using dip isogon and quantitative bed thickness methods (see Chapter 7). In chapter 7, the term 'layer' was used to cover both a geological 'bed' and a model material 'layer'.

The Bude Formation contains examples of folded sediment and folded rock in profile, which provide suitable examples for field tests of the new methods. This is important because distinguishing between folds that developed in sediment or rock provides an additional means of establishing, for example, the timing of lithification during Variscan deformation. The results of these analyses are described in this chapter.

| <b>Fold</b> | <b>Fold type</b>                         | <b>Example name</b>                                   | <b>Figure</b> |
|-------------|------------------------------------------|-------------------------------------------------------|---------------|
| 1           | a. Detached slump raft fold              | Lynstone slump raft                                   | 8.3           |
| 2           | a. Detached slump raft fold              | Black Rock slump raft 3                               | 8.3           |
| 3           | a. Detached slump raft fold              | Black Rock slump raft 15                              | 8.3           |
| 4           | b. Attached slump fold                   | Upton attached slump                                  | 8.3           |
| 5           | b. Attached slump fold                   | Phillip's Point slump 1                               | 8.3           |
| 6           | b. Attached slump fold                   | Phillip's Point slump 3                               | 8.3           |
| 7           | c. 'Early' folds                         | Northcott Mouth 'early' anticline                     | 8.2b & 8.3    |
| 8           | c. 'Early' folds                         | Upton 'early' anticline                               | 8.2c & 8.3    |
| 9           | c. 'Early' folds                         | Upton 'early' fold pair                               | 8.3           |
| 10          | d. 'Upright' chevron folds               | Damehole Point chevron anticline                      | 8.4           |
| 11          | d. 'Upright' chevron folds               | Dyer's Outlook chevron anticline                      | 8.4           |
| 12          | d. 'Upright' chevron folds               | Hartland Quay chevron anticline 1                     | 8.4           |
| 13          | d. 'Upright' chevron folds               | Hartland Quay chevron anticline 2                     | 8.4           |
| 14          | d. 'Upright' chevron folds               | North Mear Cliff bulbous syncline                     | 8.4           |
| 15          | d. 'Upright' chevron folds               | South Mear Cliff large chevron syncline               | 8.4           |
| 16          | d. 'Upright' chevron folds               | Bude Harbour bulbous chevron anticline                | 8.4           |
| 17          | d. 'Upright' chevron folds               | North Upton large chevron anticline                   | 8.4           |
| 18          | d. 'Upright' chevron folds               | Upton-Phillip's Point bulbous chevron syncline        | 8.2d & 8.4    |
| 19          | e. 'Inclined-to-recumbent' chevron folds | Upton-Phillip's Point north-directed anticline        | 8.2e & 8.5    |
| 20          | e. 'Inclined-to-recumbent' chevron folds | Phillip's Point north-directed syncline               | 8.5           |
| 21          | e. 'Inclined-to-recumbent' chevron folds | Phillip's Point south-directed anticline              | 8.5           |
| 22          | e. 'Inclined-to-recumbent' chevron folds | Church Races south-directed anticline                 | 8.5           |
| 23          | e. 'Inclined-to-recumbent' chevron folds | North Widemouth south-directed (box) anticline        | 8.5           |
| 24          | e. 'Inclined-to-recumbent' chevron folds | North Widemouth mud-injected south-directed anticline | 8.5           |
| 25          | e. 'Inclined-to-recumbent' chevron folds | Millook recumbent fold 1                              | 8.5           |
| 26          | e. 'Inclined-to-recumbent' chevron folds | Mullion recumbent fold                                | 8.5           |

Table 8.1: Folds in the Bude and Crackington formations that were chosen for dip isogon and bed thickness analyses. Fold locations are given in Fig. 8.1

## 8.2 Methodology

Dip isogon and quantitative bed thickness methods (see Chapter 7) have been employed in order to establish the Bude Formation lithification state during folding. The methods, which use a set of diagnostic geometric criteria in order to distinguish between folded sediment and

rock beds, have been applied to 26 example folds, in profile, from across 28 km of north Cornwall and north Devon coastal outcrops (Table 8.1). The folds include 24 examples from the Bude Formation and 2 examples from the Crackington Formation (Fig. 8.1). These example folds form five recognised fold types that are described below.

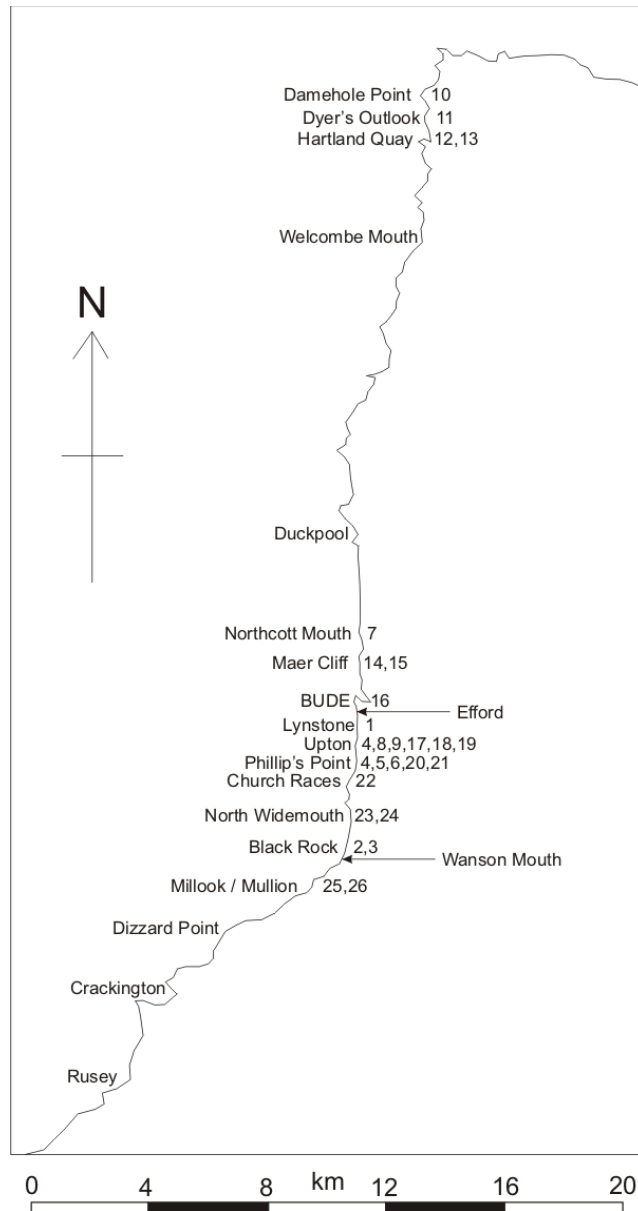


Fig. 8.1: Map of the SW England (Bude) coastline between Hartland (north) and Millook (south) showing the positions of the numbered fold examples displayed in Figs. 8.2-8.4

### 8.2.1 Description of the fold types recognised in the Bude Formation

The five recognised fold types in the Bude Formation include an ‘early’ fold type and two types of slump folded sediment (see chapters 3, 4, 5, 6 & 7), which have been folded or tilted by either an ‘upright’ chevron fold type or an ‘inclined-to-recumbent’ chevron fold type (Mapeo & Andrews, 1991). Further details of these five distinct types of fold are as follows:

**a. Detached slump raft folds:** The massive slump beds in the Bude Formation contain detached slump rafts whose bed thicknesses vary greatly (Fig. 8.2a) and were generated by movement of liquefied sediment during deposition (Strachan & Alsop, 2006; Debacker et al, 2009). The folds are sheath-like with ‘recumbent-to-reclined’ axial planes, isoclinal-to-‘elastica’ (20° to -20°) interlimb angles, and doubly-plunging, highly curvi-linear, elongated hinge lines developed in the palaeo-slope direction (see Chapter 5). Examples of the folds are found at locations 1, 2 and 3 (Fig. 8.1).

**b. Attached slump folds:** The attached slump folds (Fig. 8.2c) represent fold noses from thin (< 5 cm), liquefied, sand-silt-mud inter-beds that moved down a basin slope during deposition. The folds have ‘recumbent’ fold axial planes, tight-isoclinal (60°-10°) interlimb angles and doubly-plunging, elongated, curvi-linear hinge lines developed in the palaeo-slope direction (see Chapter 5). Examples of the folds are found at locations 4, 5 and 6 (Fig. 8.1).

**c. ‘Early’ folds:** The ‘early’ folds (Figs. 8.2b-c) resulted from decametric-scale, local folding above a basal fault that occurred during Variscan deformation. The folds are commonly observed on chevron fold limbs (Fig. 8.2b-c), are strata-bound and have beds overlying and underlying them that appear not to have been affected by the deformation. The folds have ‘inclined’ fold axial planes and tight (90°-40°) interlimb angles. Examples of the folds are found at locations 7, 8 and 9 (Fig. 8.1). Criteria to define them are provided in Chapters 4 and 5.

**d. ‘Upright’ chevron folds:** The ‘upright’ chevron folds (Figs. 8.2b & d) developed during Variscan deformation via flexural slip along bedding planes (Tanner, 1989), have ‘upright’ axial planes, closed-to-tight (90°-40°) interlimb angles and minor doubly-plunging, curvi-linear hinge lines (see Chapter 6). Examples of the folds are found at locations 10 to 18 inclusive (Fig. 8.1).

**e. ‘Inclined-to-recumbent’ chevron folds:** The ‘inclined-to-recumbent’ chevron folds (Figs. 8.2e-f) formed on overturned limbs of modified ‘upright’ chevron folds from shear strain accommodation during Variscan deformation (Lloyd & Whalley, 1986). The folds have ‘inclined-to-recumbent’ axial planes and tight-to-isoclinal (60°-10°) interlimb angles (see chapters 4 & 6). Examples in the Bude Formation are at locations 19 to 24 inclusive and Crackington Formation at locations 25 and 26 (Fig. 8.1).

### 8.3 Dip isogon and quantitative bed thickness analyses

To describe the folded rocks and sediments, dip isogon and quantitative bed thickness analyses have been undertaken on each of the folded beds in profile in Figs. 8.3-8.5. From the fold types, examples have been chosen to display the results (Figs. 8.6-8.8) and are as follows: Type a: Black Rock detached slump raft fold 3 (SS196017; location 2 in Fig. 8.1; Fig. 8.6); Type b: Phillip’s Point attached slump fold 3 (SS200043; location 6 in Fig. 8.1; Fig. 8.6); Type c: Upton ‘early’ fold pair (SS200045; location 9 in Fig. 8.1; Fig. 8.8); Type d: Bude Harbour bulbous chevron anticline (SS202065; location 16 in Fig. 8.1; Fig. 8.7); Type e: Church Races south-directed chevron fold (SS200042; location 22 in Fig. 8.1; Fig. 8.7).

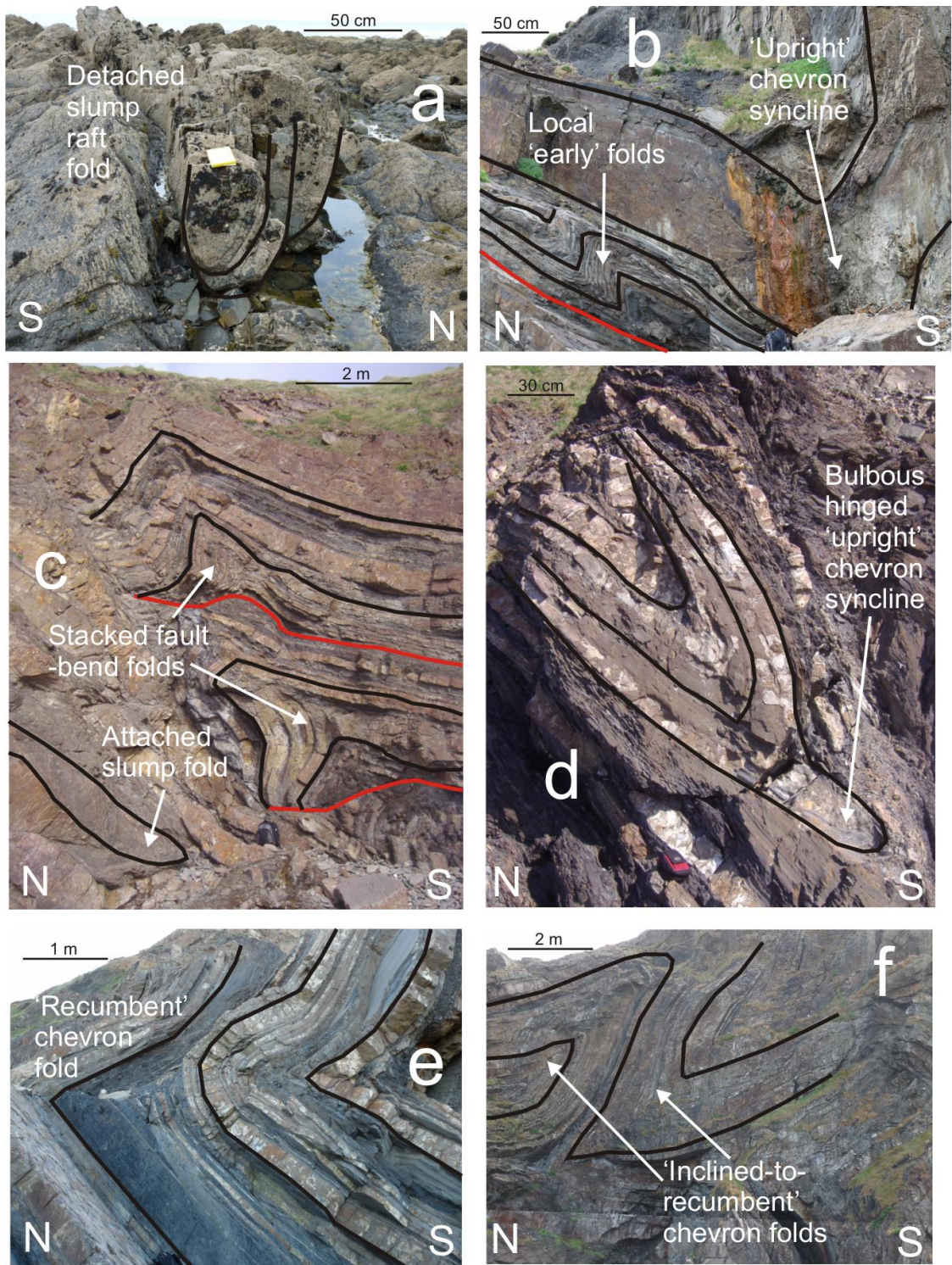


Fig. 8.2: Photographs of the five Bude Formation fold types in profile: (a) detached slump raft fold (type: a), Black Rock Slump Bed (SS196017; see Chapter 3); (b) 'early' fold pair (type: c) on a limb of an 'upright' chevron syncline (type: d), Northcott Mouth-Maer Cliff (SS202083; see Chapter 5); (c) 'early' stacked fault bend folds (type: c) above an attached slump fold (type: b), Upton (SS200045; see Chapter 5); (d) bulbous 'upright' chevron syncline (type: d), Upton-Phillip's Point (SS200044; see Chapter 6); (e) 'recumbent' chevron anticline (type: e), Upton-Phillip's Point (SS200044); and (f) 'inclined-to-recumbent' chevron fold pair (type: e), Lynstone (SS200053; see Chapter 7)

### 8.3.1 Slump and ‘early’ folds in profile (Fold types: a, b & c)

#### Results

Analysis of the dip isogon logs (Figs. 8.3, 8.6 & 8.8) shows that all beds have bulbous hinges with generally high dip isogon classes (i.e. classes 1C to 3). Dip isogon analysis of both slump folds (types: a & b) and ‘early’ folds (type: c) produces asymmetric, scattered, repeating and disharmonic dip isogon patterns on each limb (Figs. 8.3, 8.6 & 8.8). As with slump examples in Chapter 7, the dip isogon pattern has: (a) a range of ‘Ramsay’ classes within a bed; (b) non-matching multiple ‘Ramsay’ classes in the beds across both limbs; and (c) repeated and looping dip isogons resulting from undulations and minor buckles.

Quantitative bed thickness analysis plots of all three fold types (Figs. 8.6 & 8.8) have a strong asymmetry, scatter and repetition in the curves about the hinge position ( $\alpha = 0^\circ$ ) for each limb. The curves display similar results on each limb as is found from dip isogon analysis.

#### Interpretations

The combined isogon log, dip isogon and quantitative bed thickness analyses on the slump and ‘early’ fold types (i.e. types a, b & c) indicate that: (1) dip isogon patterns are independent of lithology and are indicative of low coherence layers; (2) results and observations meet the criteria of *folds formed in water-saturated, plastic sediment* (Craig, 1997; Denis *et al*, 2009); and (3) this is consistent with some of the Bude Formation folding occurring in sediment (i.e. slump folds; Enfield *et al*, 1985; Hartley, 1991; Hecht, 1992; Leveridge & Hartley, 2006).

### 8.3.2 ‘Upright’ chevron folds in profile (Fold type: d)

#### Results

Analysis of the dip isogon logs from the ‘upright’ chevron folds (type: d) (Figs. 8.4 & 8.7) shows that all beds have bulbous hinges with generally high dip isogon classes (i.e. classes 1C to 3). Dip isogon analysis produces asymmetric, scattered and repeating dip isogon patterns on each limb (Figs. 8.4 & 8.7). This is the same as is recognised for the slump and ‘early’ folds (types: a, b & c). The dip isogon pattern has: (1) a range of ‘Ramsay’ classes within a bed; (2) non-matching multiple ‘Ramsay’ classes in beds across both limbs; and (3) repeated and looping dip isogons resulting from undulations and minor buckles.

Quantitative layer thickness analysis plots of the ‘upright’ chevron folds (Fig. 8.7) have a strong asymmetry, scatter and repetition in the curves about the hinge position ( $\alpha = 0^\circ$ ) for each limb. The curves display similar results on each limb as is found from dip isogon analysis.

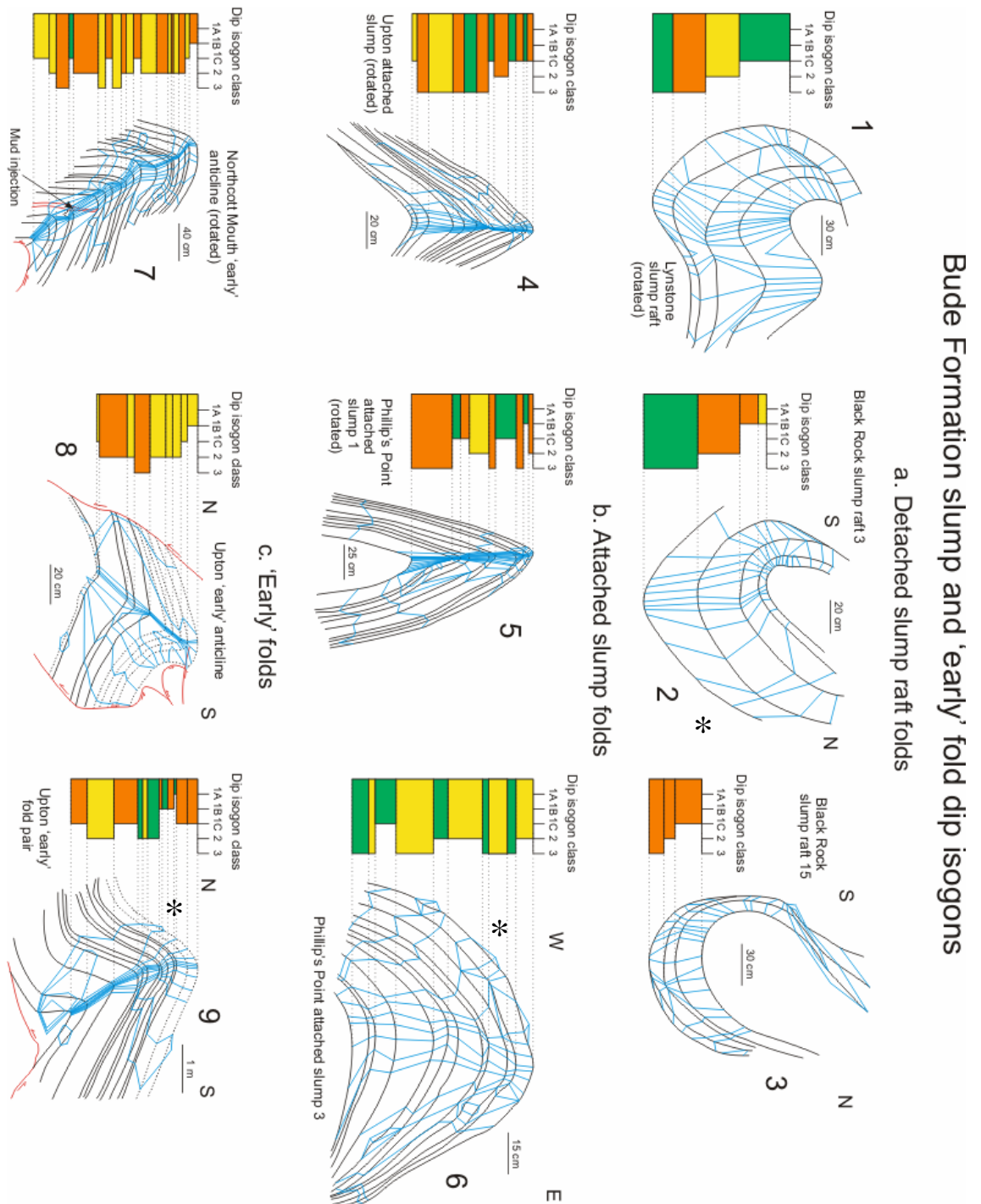


Fig. 8.3: The 3 dip isogon sketches each from the detached slump raft (type: a), attached slump (type: b) and 'early' (type: c) folds. Notice the repeated dip isogons on the limbs similar to those observed in the slump and glacial till (sediment) folds in Chapter 7. Dip isogon logs (orange = sandstone; yellow = siltstone; green = shale) show how the dip isogon class varies from bed-to-bed, giving an indication of how the relative coherences of the stacked beds change. The examples used in Fig. 8.6 (nos. 2 & 6) and Fig. 8.8 (no. 9) for the dip isogon and quantitative bed thickness analyses have an asterisk next to them. All folds are in profile

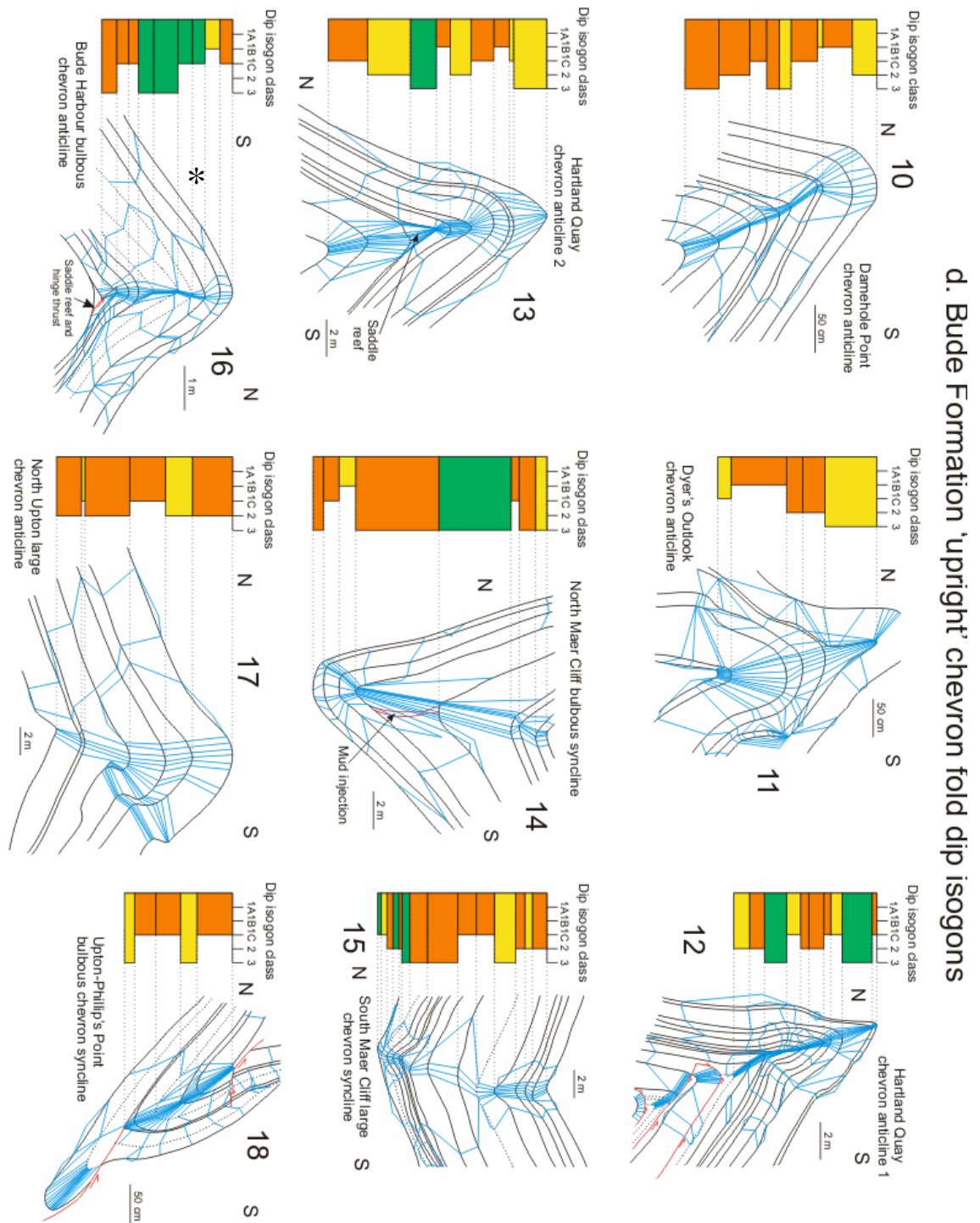


Fig. 8.4: The 9 'upright' chevron fold (type: d) dip isogon sketches (from this work & Ramsay, 1974). Notice the repeated dip isogons on the limbs similar to those observed in detached slump raft, attached slump and 'early' folds (see Fig. 8.3). Dip isogon logs (orange = sandstone; yellow = siltstone; green = shale) show how the dip isogon class varies from bed-to-bed, giving an indication of how the relative coherences of the stacked beds change. The example used in Fig. 8.7 (no. 16) for the dip isogon and quantitative bed thickness analyses have an asterisk next to it. All folds are in profile

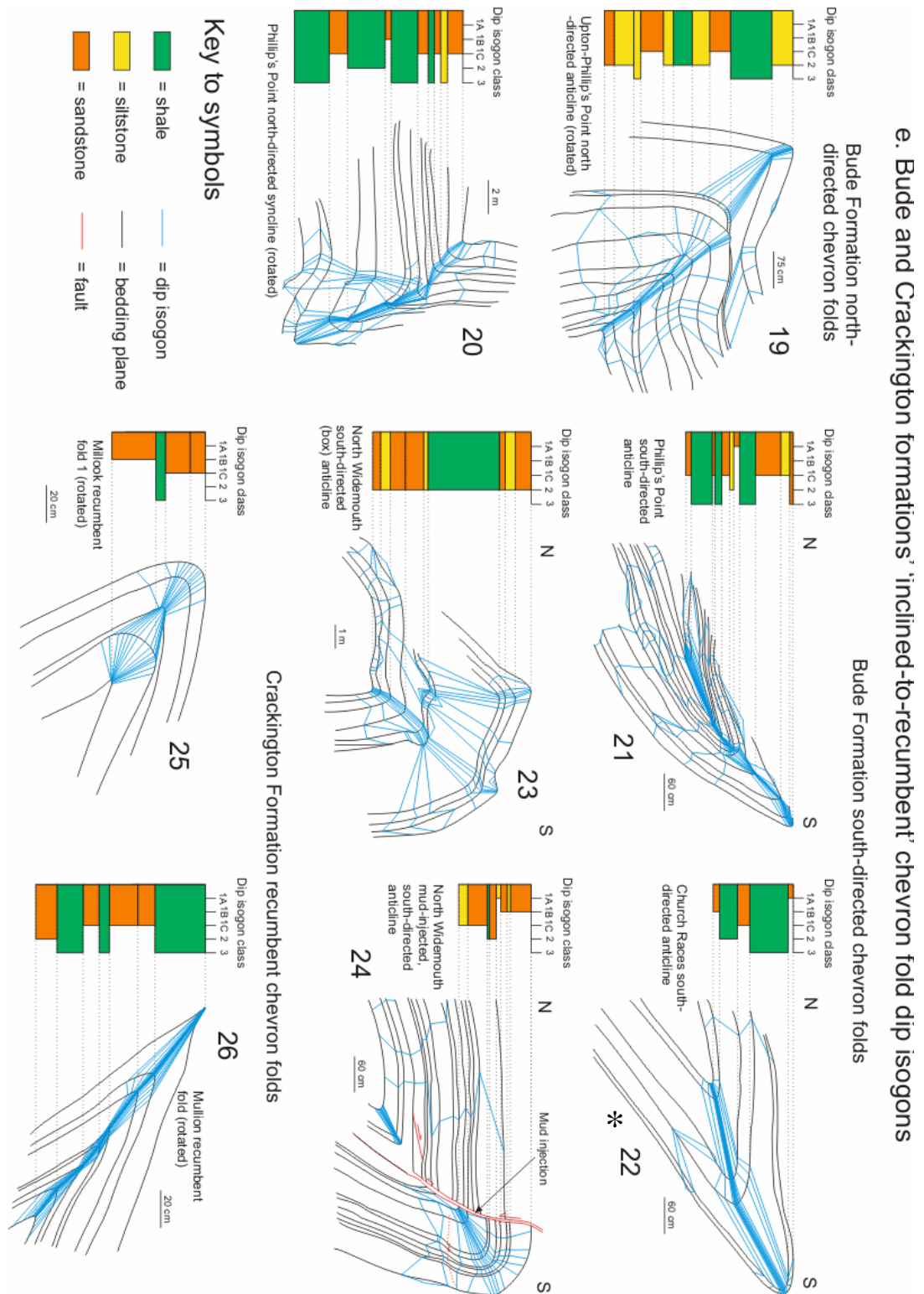


Fig. 8.5: The 6 Bude Formation north and south-directed, 'inclined-to-recumbent' chevron fold and 2 Crackington Formation 'recumbent' chevron fold (type: e) dip isogon sketches.

Commonly, the bulbous hinges (i.e. classes 2 to 3 dip isogons) are restricted to the shale beds and are rarely developed intermittently in different lithologies as observed in Figs. 8.3-8.4. Dip isogon logs (orange = sandstone; yellow = siltstone; green = shale) show how the dip isogon class varies from bed-to-bed, giving an indication of how the relative coherences of the stacked beds change. The example used in Fig. 8.7 (no. 22) for the dip isogon and quantitative bed thickness analyses have an asterisk next to it. All folds are in profile

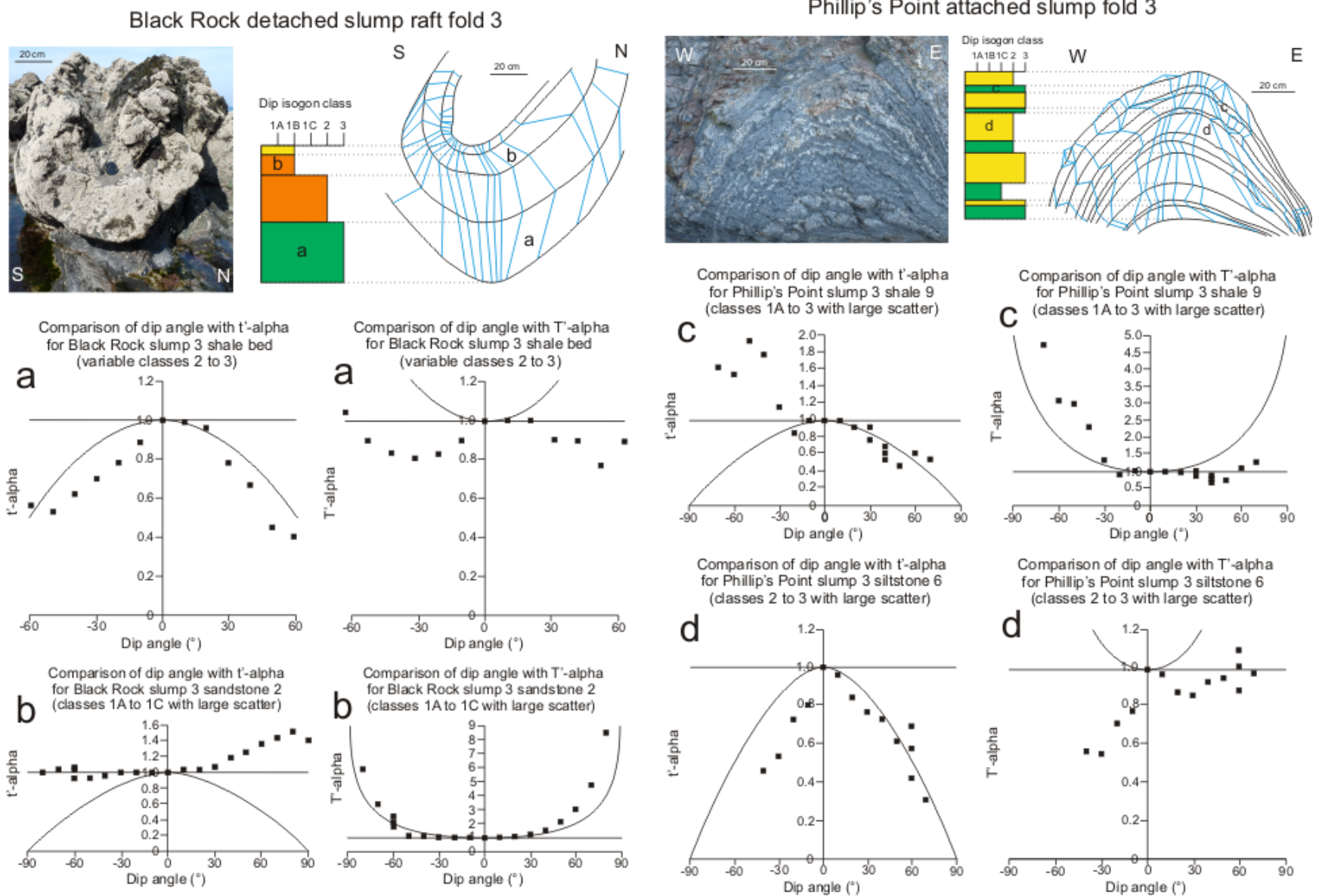


Fig. 8.6: Comparative dip isogon and bed thickness analyses for Black Rock detached slump raft 3 and Phillip's Point attached slump fold 3 (locations 2 & 6 in Fig. 8.1; nos. 2 & 6 in Fig. 8.3), with dip isogon logs (orange = sandstone; yellow = siltstone; green = shale). All folds are in profile. Letters next to graphs relate to the marked bed being analysed

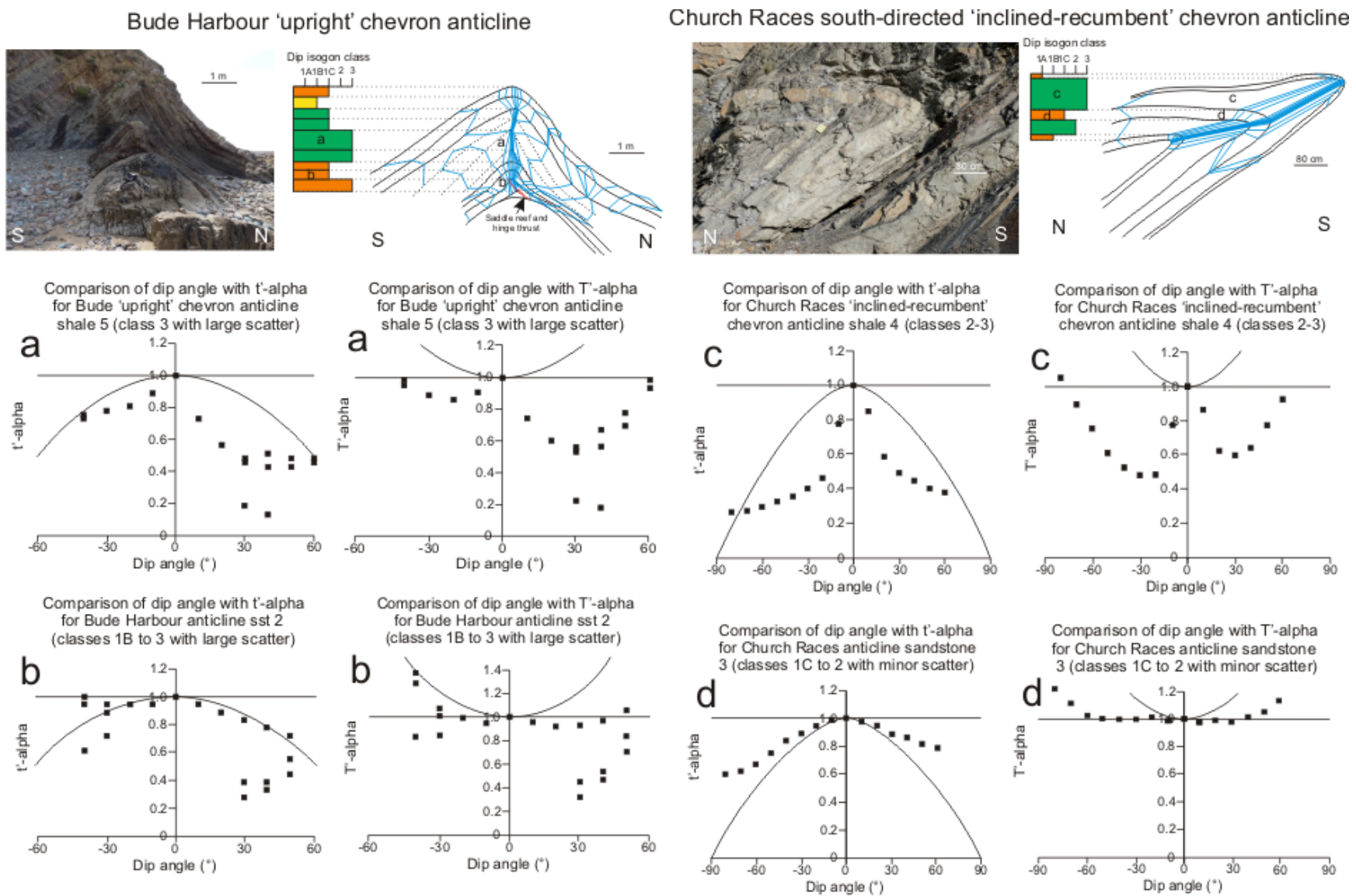


Fig. 8.7: Comparative dip isogon and bed thickness analyses for Bude Harbour 'upright' chevron anticline (location 16 in Fig. 8.1; no. 16 in Fig. 8.4) and Church Races south-directed, 'inclined-to-recumbent' chevron anticline (location 22 in Fig. 8.1; no. 22 in Fig. 8.5) with dip isogon logs (orange = sandstone; yellow = siltstone; green = shale). All folds are in profile. Letters next to graphs relate to the marked bed being analysed

## Interpretations

The combined results of isogon log, dip isogon and quantitative bed thickness analyses on the ‘upright’ chevron folds (type: d) indicate that: (1) dip isogon patterns are independent of lithology and are indicative of low coherence layers; and (2) results and observations meet the criteria of *folds developed in water-saturated, plastic sediment* (Craig, 1997; Denis et al, 2009).

### 8.3.3 ‘Inclined-to-recumbent’ chevron folds in profile

#### Results

Analysis of the dip isogon logs (Figs. 8.5 & 8.7) show that the shale beds in the Church Races fold and Crackington Formation fold examples have higher isogon classes (i.e. classes 2 to 3) than the sandstone and siltstone layers (i.e. classes 1B to 2). In beds from the other Bude Formation ‘inclined-to-recumbent’ chevron fold examples, any of the lithologies can have bulbous hinges with generally high isogon classes (i.e. classes 1C to 3).

Dip isogon analysis of ‘inclined-to-recumbent’ chevron folds (type: e) produces symmetric, ordered, non-repeating and harmonic dip isogon patterns in many of the beds on the fold limbs (Figs. 8.5 & 8.7). This is the same as is recognised in Chapter 7 for folded rocks. However, some of the beds display asymmetric, scattered and repeating dip isogon patterns on each limb. This is the same as is recognised in previous sections for both slump fold types, and both ‘early’ fold and ‘upright’ chevron fold types, and in Chapter 7 for folded sediment.

Quantitative layer thickness analysis plots of the ‘inclined-to-recumbent’ chevron folds (Fig. 8.7) show that many layers have nearly symmetric curves about the hinge position ( $\alpha = 0^\circ$ ) on each limb. However, in some beds, the plots have a strong asymmetry, scatter and repetition in the curves for each limb about the hinge position. The curves display similar results on each limb as is found from dip isogon analysis.

#### Interpretations

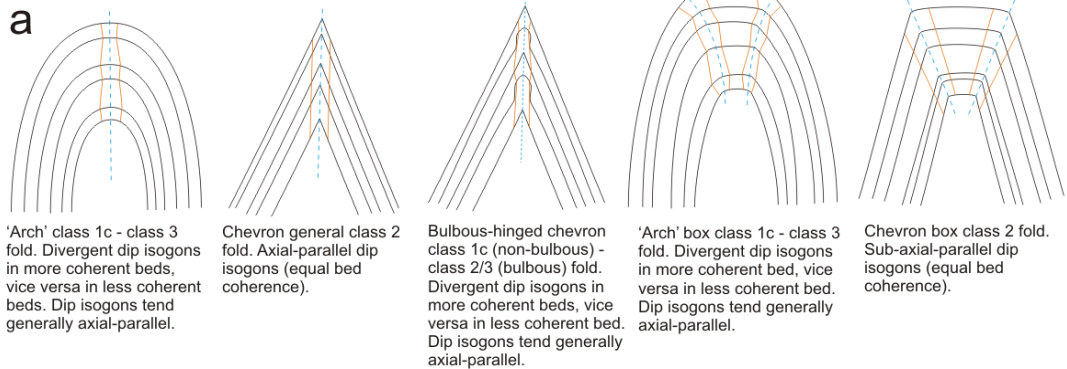
The combined results of isogon log, dip isogon and quantitative bed thickness analyses on the ‘inclined-to-recumbent’ folds (type: e), the results and observations meet the criteria of *folds developed in mixed layers of sediment and rock*. This suggests that during ‘inclined-to-recumbent’ chevron fold deformation, the Bude Formation beds were lithifying. However, it is possible that as the ‘inclined-to-recumbent’ chevron folds incorporated the effects of ‘upright’ chevron folding (i.e. sediment) into its bed thicknesses, and this may have caused the ‘inclined-to-recumbent’ chevron folded beds to appear to be sediment when in fact they were lithified.

## 8.4 Model for Bude Formation folds during deposition

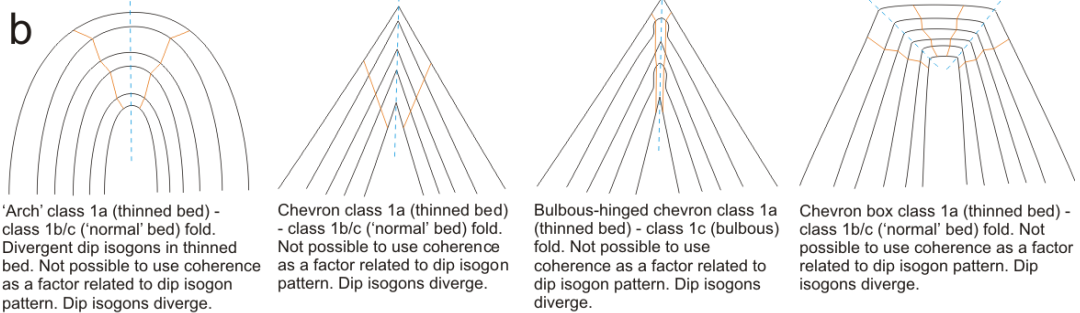
The dip isogon and quantitative bed thickness methods (see Chapter 7) can be used to distinguish ‘early’ folds viewed in profile. To aid its application, a model is developed of the

idealised dip isogon patterns in early' post-depositional folds and also, in the subsiding synclines and uplifting anticlines of 'early' syn-depositional folds (Fig. 8.8). The model is demonstrated (Fig. 8.9) on the 'early' syn-depositional fold pair at Upton (SS200045) (Fold type: c; location 9 in Fig. 8.1) and applied, together with the results of the dip isogon and quantitative bed thickness analyses of Bude Formation folds (Figs. 8.3-8.7 & 8.9), to determine the relative timing of lithification and fold deformation (Table 8.2).

Beds deformed post-depositionally (both anticlines and synclines)



Beds deformed syn-depositionally (anticlines only)



Beds deformed syn-depositionally (synclines only)

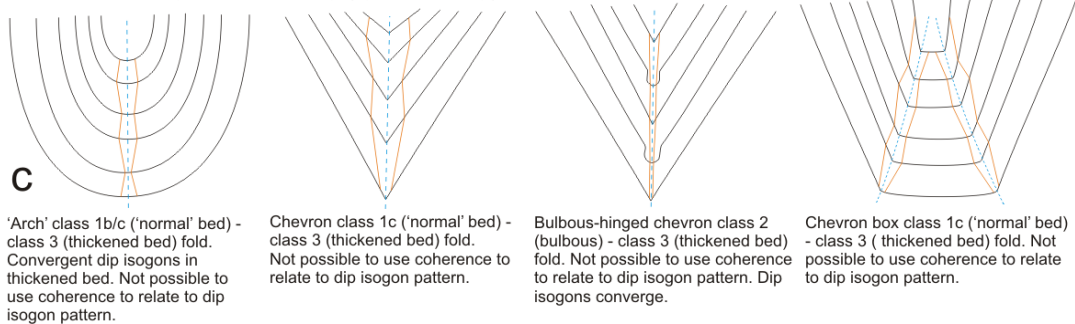


Fig. 8.8: Idealised folds in profile to demonstrate the difference in dip isogon patterns between those generated post- and syn-depositionally. Both patterns are best observed in the Upton 'early' fold pair (SS200045; location 9 in Fig. 8.1; Figs. 8.2c, 8.3 & 8.9)

#### 8.4.1 'Early' syn-depositional versus 'early' post-depositional dip isogon patterns

Fold deformation of sedimentary beds following their deposition can occur in either rock or sediment. However, where fold deformation occurs in a basin setting during deposition, the structures can affect the basin bathymetry and therefore, the thickness of subsequent beds.

## Upton 'early' fold pair

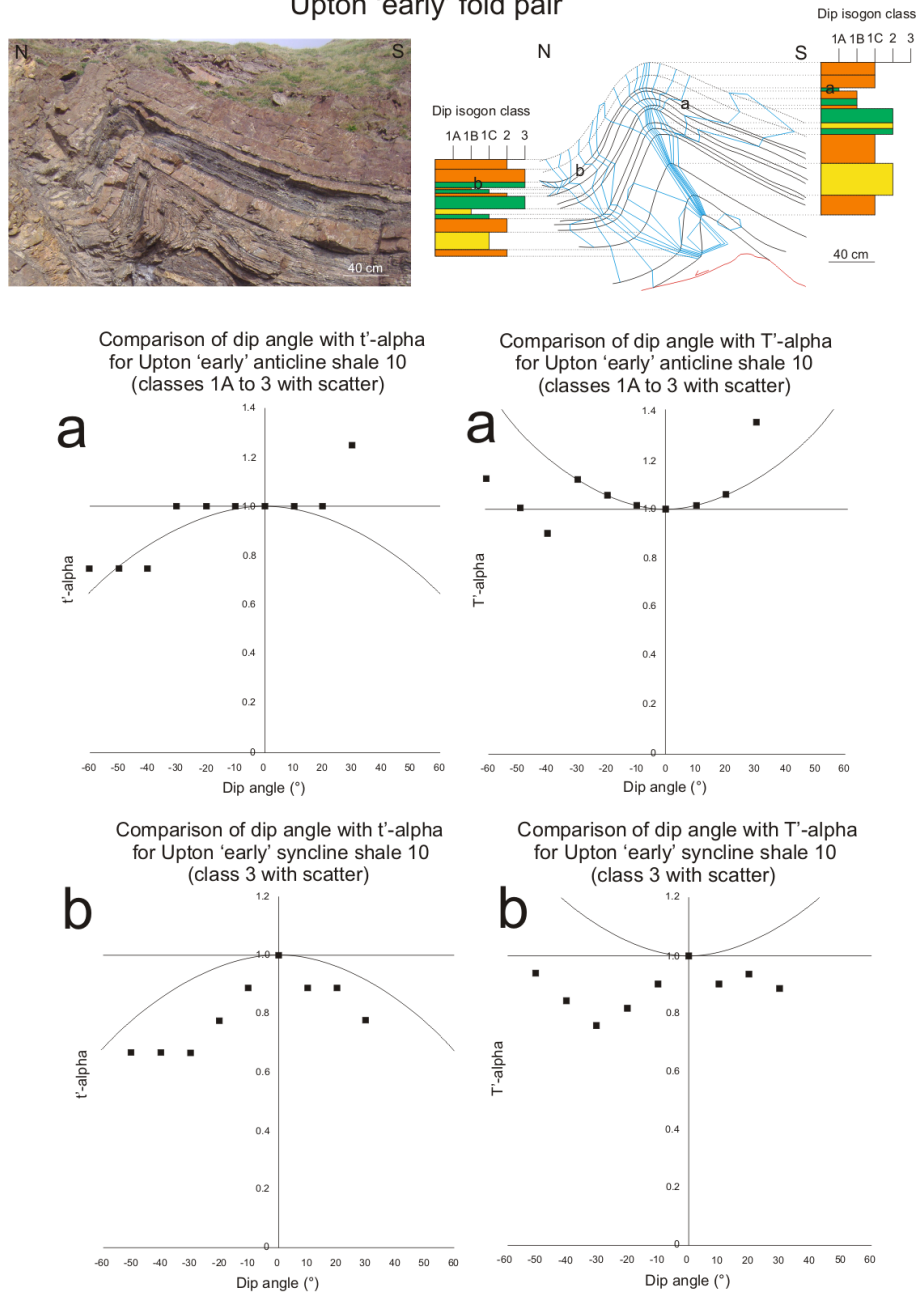


Fig. 8.9: Dip isogon and quantitative bed thickness analyses of Upton 'early' fold pair (SS200045; location 9 in Fig. 8.1; Figs. 8.2c & 8.3) with dip isogon logs (orange = sandstone; yellow = siltstone; green = shale). All folds are in profile. Letters next to graphs relate to the marked bed being analysed

### Dip isogon pattern in a post-depositional folded layer in profile

The dip isogon patterns for the folded rock and folded sediment were described in Chapter 7 for the beds deposited prior to folding. In this chapter, the model was applied to all the Bude Formation slump folds (types: a & b) and chevron folds (types: d & e). The geometries of the example folds described in this chapter (Figs. 8.6-8.7) have dip isogon patterns in each bed that depend upon their relative coherence and their mechanical or lithification state (i.e. sediment or rock) during folding. In rocks, the dip isogon patterns are regular and symmetrical

about the hinge, with the folded layer showing classes 1A to 1C dip isogons for more coherent layers and classes 2 to 3 dip isogons for less coherent layers (Ramsay, 1967). In contrast, the dip isogon fold patterns in folded sediment are irregular and asymmetrical about the hinge, with the folded layer showing a dip isogon pattern between classes 1A to 3 across the hinge ‘zone’.

#### **Dip isogon pattern in an ‘early’ syn-depositional folded layer in profile**

In the Bude Formation, there are examples of ‘early’ folds (type: c) that are recognised where the folded layers have ‘undeformed’ beds surrounding them, are truncated by over-lying beds and/or have growth strata deposited around them following the convention of Zoetemeijer et al (1992), Nigro and Renda (2004) and Corredor et al (2005) (see chapters 4 & 5). The example analysed here is the Upton ‘early’ fold pair (SS200045; location 9 in Fig. 8.1; Figs. 8.2c & 8.9), where there is a large thickness difference in one shale bed across the fold pair (*growth strata criterion*; see chapters 4 & 5). The shale is thinner over the anticlinal crest (i.e. class 1A dip isogon pattern; Fig. 8.9a) than in the synclinal trough (i.e. class 3 dip isogon pattern; Fig. 8.9b). This results from depositional thickness variations rather than ductile shale flow, which can occur in fault-propagation folding (Suppe, 1985). The dip isogon patterns around both fold hinges are irregular and asymmetric, matching the criteria for folded sediment.

#### **Interpretations from the dip isogon pattern in an ‘early’ syn-depositional folded layer**

The bed thickness variations over the fold hinges suggest that the anticlinal crest formed a positive, albeit small, bathymetric feature on the palaeo-surface during ‘early’ folding, causing thinner strata to be deposited above the ‘high’ compared to the fold limbs, whilst the synclinal trough received more sediment. If the coherence of the mud bed had remained the same across the fold pair, the differing dip isogon patterns between the two folds would have resulted from bed thickness changes only. To demonstrate this, a model was developed that displays idealised ‘early’ syn- and post-depositional fold examples (Fig. 8.8).

#### **8.4.2 Model for ‘early’ syn- and post-depositional fold dip isogon patterns**

In the post-depositional fold dip isogon model, the ‘layer-cake’ beds are assumed to be deposited on a palaeo-surface without any topography, so that the dip isogon fold patterns are dependent upon the mechanical or lithification state of the beds (i.e. sediment or rock beds). The geometric criteria to distinguish folded sediment and folded rock as described in Chapter 7.

Generalised descriptions of the anticipated dip isogon patterns are made using the sketches for both types of slump fold (types: a & b), both types of chevron fold (types: d & e) (Figs. 8.3-8.5) and the simplified sketch chevron fold examples (Fig. 8.8a). In general, the folds deformed post-depositionally and lacking bulbous-hinged beds, tend towards class 2 (axial parallel) dip isogon patterns. However, the folds with bulbous-hinged beds tend to have class 2 to 3 dip isogon patterns, with the surrounding folded beds having class 1C dip isogon patterns.

These same dip isogon descriptions may be applicable to ‘arch’, ‘arch’ box and chevron box folds as well (Fig. 8.8a).

In the ‘early’ syn-depositional anticline dip isogon model, the folded bed is assumed to be sediment and the original bed thickness decreases over the anticlinal crest because the depositing bed partially onlaps the uplifting high. The variation in original bed thickness affects the resulting dip isogon pattern, with the folding bed having a low dip isogon class (i.e. class 1A). Consequently, the resulting dip isogon pattern for the folded bed does not reflect the coherence of the bed during ‘early’ syn-depositional folding (Fig. 8.8b).

In the ‘early’ syn-depositional syncline dip isogon model, the folded bed is assumed to be sediment and the original layer thickness increases over the synclinal trough due to the depositing bed infilling the subsiding topographic low. The variation in original bed thickness affects the dip isogon pattern, with the folded bed having a high dip isogon class (i.e. class 3). Consequently, its resulting dip isogon pattern does not reflect the coherence of the bed during ‘early’ syn-depositional folding (Fig. 8.8c).

## 8.5 Geometries and lateral variation of structures in the Bude Formation

In this section, the geometries of the Bude Formation chevron folds and faults are described in terms of their lithification state during deformation and also, how the structural geometries vary laterally along the coastal outcrops. After this, a series of comparisons will be undertaken between the Sanderson (1979) results (see Chapter 2) and the results obtained using data from the unpublished M.Sc. thesis of Williams (2005). In the case of the Williams work, some results will be drawn directly from Williams (2005) and some gained through re-analysis of the data. The comparisons concern: (1) the interlimb angle and shear strain from the chevron folds between Duckpool and Dizzard Point in the Bude and Crackington formations; and (2) the lateral variation in shear strain accommodation in the study area between Northcott Mouth and Wanson Mouth (see Fig. 8.1). A review and comparison is then made between the Sanderson (1979) and Lloyd and Whalley (1986; 1997) models for south-directed ‘inclined-to-recumbent’ chevron folding that follows on from Chapter 4, which leads into a critical review of the Lloyd-Whalley model with respect to the chronology of the progressive Variscan deformation.

After the discussion of the structural geometries, the inverse thickness method (Lisle, 1992; see Chapter 7) is reviewed using two example Bude Formation folded beds: an ‘upright’ chevron fold (type: d); and an ‘inclined-to-recumbent’ chevron fold (type: e). Following this, two restoration models for the Black Rock and Wanson Mouth foreshores are used to interpret similar structures elsewhere in the Bude Formation outcrops.

### 8.5.1 Review of the Sanderson (1979) and Lloyd and Whalley (1986; 1997) models

In Chapter 4, a review was undertaken of the Sanderson (1979) and Lloyd and Whalley (1986; 1997) models. Both recognised that towards the south, the coastal outcrops of folded

beds in the Bude and Crackington formations show a generally increasing level of south-directed shear strain accommodation. A review of these models by Anderson and Morris (2004) suggested that a localised south-directed shear deformation can be invoked “as the cause of modification of an initial upright chevron geometry”. The difference between the models noted by Anderson and Morris (2004) is that they refer to different parts of the fold geometry:

1. Sanderson (1979) modelled the evolution of the initial ‘upright’ fold axial planes and interlimb angles with increasing shear strain in the fold hinge zones;
2. Lloyd and Whalley (1986; 1997) modelled only the limbs of initial ‘upright’ chevron folds as movement planes that produced the different ‘inclined-to-recumbent’ chevron fold types.

Lloyd and Whalley (1986; 1997) provided a mechanism by which the south-directed shearing deformation generated south-directed ‘inclined-to-recumbent’ folds during progressive deformation on south-dipping limbs of originally ‘upright’ chevron folds. This is a mechanism supported by the Ghosh (1966) experiments (see Chapter 4). Their model considered outcrop sections north of Bude (SS200065) where little or no south-directed shear deformation has been accommodated. Lloyd and Whalley (1986) examined the folds between Hartland and Dizzard and demonstrated, with examples such as the ‘Welcombe Diamond’ structure at Welcombe Mouth, that their model can be applied across the Culm Basin (see Fig. 8.1).

Sanderson (1979) also considered all the sections between Hartland and Rusey, which include folds where little or no south-directed shear strain has been accommodated by ‘upright’ chevron folding during Variscan deformation. As already noted, these sections include the field study area between Northcott Mouth and Wanson Mouth (SS202087-SS195013). ‘Upright’ chevron folds dominate the outcrops to the north of Efford (SS200062; see Fig. 8.1); whilst south of Efford, many of the fold axial planes have become increasingly ‘inclined-to-recumbent’. Many ‘upright’ chevron folds between Bude and Hartland considered by Sanderson (1979) have accommodated compressional strain via fold tightening, beyond the ‘lock-up’ interlimb angle of 60°. This has caused either hinge thickening with corresponding limb thinning, or alternatively, minor hinge thrusts (Ramsay, 1974; Davison et al, 2004), with cleavage development in some cases (Lloyd & Chinnery, 2002; see Chapter 4). This is consistent with the Sanderson (1979) model, of increased accommodation of south-directed shear strain by the chevron folds towards the south.

It can be noted that north-directed ‘inclined-to-recumbent’ chevron folds (see Figs. 8.2e & 8.5) are observed at Phillip’s Point (SS200044; Figs. 8.1 & 8.2e) but are neither described by Sanderson (1979) nor appear in Fig. 7 of Lloyd and Whalley (1986) (see section in Fig. 2.29 of Chapter 2). Lloyd and Whalley (1986) suggested that the north-directed ‘inclined-to-recumbent’ chevron folds formed where locally-emplaced thrusts and hanging wall folds were deformed during south-directed shear deformation (see Chapter 2). This suggests that north-directed thrusts propagated into the Bude Formation deposits whilst they were still sediment (Leveridge

& Hartley, 2006) and that the thrusts were later deformed by progressive Variscan folding as the Bude Formation became increasingly lithified, as demonstrated in this chapter (see Table 8.2).

Thus, the Sanderson (1979) model described the regional transition from ‘upright’ to ‘inclined-to-recumbent’ chevron folds in the Culm Basin by focussing on the fold hinge zones. In contrast, the Lloyd and Whalley (1986; 1997) model described the types of folds that can be generated where south-directed shear strain has been accommodated by the folded beds during Variscan deformation. This is presented as three sub-models focussing on the fold limbs, as described in chapters 2 and 4. Thus, the differences in focus relate to different but equally-important aspects of the fold geometries and so the models are not inconsistent with each other.

### **8.5.2 Chronology of the progressive Variscan deformation**

The Variscan deformation observed in the Culm Basin is widely described as regional and progressive (Ramsay, 1974; Freshney, 1972; 1979; Sanderson, 1974; 1979; Coward & Smallwood, 1984; see chapters 2, 4 & 6). Lloyd and Whalley (1986; 1997) modelled the ‘inclined-to-recumbent’ chevron folds as being the modification structures of original ‘upright’ chevron folds that developed during Variscan deformation by accommodating south-directed shear strain. They noted that: “in order to be available for modification, such [‘upright’] folds must have been initiated during the earliest, north-directed thrust movements and may represent geometrically necessary folds associated with ramps in the thrust planes”. This suggests that an original set of semi-isolated, hundreds of metres scale ‘upright’ chevron folds developed locally in the Culm Basin, in the vicinity of north-directed thrusts, early in the Variscan deformation. This could be interpreted as suggesting that the Variscan deformation in the Culm Basin was punctuated and involved changes in the deformation style, with periods of thrusting and folding.

However, to demonstrate that Variscan deformation is progressive, Whalley and Lloyd (1986) state: “It is possible to recognise folds which deform northerly directed thrust planes. There is evidence, therefore, of a continuous process of chevron fold initiation and development associated with the continuing thrusting deformation, and one should not envisage a discrete ordering of thrusting and folding events. This is in accord with the nature of the progressive, shearing deformation which must have occurred in this area throughout the period in question”.

The statements of Whalley and Lloyd (1986) could possibly lead to confusion regarding the progressive nature of the Variscan deformation. To reduce the potential for confusion, an analysis may be needed that takes account the Ramsay (1974) chevron fold model, using further structural data from the ‘upright’ chevron folds between Hartland and Bude. Also, a comparison of the Ramsay, Sanderson and Lloyd-Whalley models in the Culm Basin, together with models for fold development in other deformed basins, may provide further insights into progressive fold deformation. Furthermore, it would be useful to test whether the geometric criteria developed in Chapter 7 and this chapter, are applicable in other compressionally deformed basins to contribute to establishing the relative timing of folding and lithification elsewhere.

### 8.5.3 Lithification states of the chevron folds during progressive deformation

The results of the dip isogon and quantitative bed thickness analyses for the Culm Basin folds suggest that the ‘upright’ chevron folded beds meet the criteria for folding in sediment whilst the ‘inclined-to-recumbent’ chevron folded beds meet the criteria for folding in inter-bedded rock and sediment. This suggests that the ‘inclined-to-recumbent’ chevron folds developed after the ‘upright’ chevron folds, once the Bude Formation had begun to lithify. The different lithification states found from the results of the dip isogon and bed thickness analyses on the five fold types (Figs. 8.3-8.8) are summarised in Table 8.2.

| Fold No. | Fold type                             | Bed lithification state during fold deformation |                 |                |
|----------|---------------------------------------|-------------------------------------------------|-----------------|----------------|
|          |                                       | Water-saturated sediment                        | Sediment & Rock | Lithified rock |
| 1        | Detached slump raft folds             |                                                 |                 |                |
| 2        |                                       |                                                 |                 |                |
| 3        |                                       |                                                 |                 |                |
| 4        | Attached slump folds                  |                                                 |                 |                |
| 5        |                                       |                                                 |                 |                |
| 6        |                                       |                                                 |                 |                |
| 7        | 'Early' folds                         |                                                 |                 |                |
| 8        |                                       |                                                 |                 |                |
| 9        |                                       |                                                 |                 |                |
| 10       | 'Upright' chevron folds               |                                                 |                 |                |
| 11       |                                       |                                                 |                 |                |
| 12       |                                       |                                                 |                 |                |
| 13       |                                       |                                                 |                 |                |
| 14       |                                       |                                                 |                 |                |
| 15       |                                       |                                                 |                 |                |
| 16       |                                       |                                                 |                 |                |
| 17       |                                       |                                                 |                 |                |
| 18       |                                       |                                                 |                 |                |
| 19       | 'Inclined-to-recumbent' chevron folds |                                                 |                 |                |
| 20       |                                       |                                                 |                 |                |
| 21       |                                       |                                                 |                 |                |
| 22       |                                       |                                                 |                 |                |
| 23       |                                       |                                                 |                 |                |
| 24       |                                       |                                                 |                 |                |
| 25       |                                       |                                                 |                 |                |
| 26       |                                       |                                                 |                 |                |

Table 8.2: Table showing how the Bude Formation folded beds became more lithified during Variscan deformation

In the study area, ‘upright’ chevron folds were found between Northcott Mouth and Efford (SS202087-SS200056), Upton and Phillip’s Point (SS200052-SS200046) and at Black Rock (SS200020-SS196014) and ‘inclined-to-recumbent’ chevron folds were found between Efford and Lynstone (SS200060-SS200052), Phillip’s Point and North Widemouth (SS200046-SS200027) and at Wanson Mouth (SS195015-SS193015) (see Fig. 8.1). This shows that from north-to-south across the Bude Formation outcrops, there is an alternating sequence of areas with ‘upright’ and ‘inclined-to-recumbent’ chevron folds (types: d & e).

Contemporaneously with the chevron folding was the north-directed thrusting, both of which were affected by the accommodation of south-directed shear strain (Enfield et al, 1985; Whalley & Lloyd, 1986). The thrusts have a shallow northwards dip on the right-way up north-dipping limb of ‘inclined-to-recumbent’ chevron folds; but in contrast, have a steep northwards

dip on the overturned steep north-dipping limbs of the chevron folds. A model explaining these geometries was provided in Chapter 4 and is also restated later in order to explain this.

To the north of Bude (SS200065), the ‘upright’ chevron folds show little modification towards becoming ‘inclined-to-recumbent’, whilst to the south, the chevron folds show an ever increasing modification to this form. This is consistent with a regional southward increase in south-directed shear strain accommodation during Variscan deformation (Sanderson, 1979; see Chapter 4). According to the Ghosh (1966) and Lloyd and Whalley (1986; 1997) models, the ‘inclined-to recumbent’ chevron folds occurred on the south-dipping limbs of modified ‘upright’ chevron folds that were experiencing south-directed shear deformation (see chapter 2 & 4). This is consistent with ‘inclined’ fold development on tilted layers dipping in the shearing direction from the Ghosh (1966) experiments (see Fig. 4.4 in Chapter 4). The criteria based on dip isogon and bed thickness analyses that distinguish between folded rock and folded sediment (see sections 8.2 & 8.3) suggest that progressive Variscan deformation occurred in the chevron folded beds whilst the Bude Formation became increasingly lithified.

This contrasts with Warr (2002), who suggested that the under-thrusting of the Rusey Fault in the southern Culm Basin, caused ‘upright’ chevron folds to develop at the same time, or just after, the south-directed ‘inclined-to-recumbent’ chevron folds (see Chapter 2). These contrasting models for the Variscan deformation in the Culm Basin are discussed in Chapter 9 together with the regional Variscan deformation in SW England.

#### **8.5.4 Comparison of interlimb angle and shear strain (from Williams, 2005)**

The analyses described in this section use unpublished data from a set of folds from Williams (2005) to compare the interlimb angle with the axial plane angle and the shear strain (Figs. 8.10-8.11). Williams (2005) had calculated the accommodated shear strain and interlimb angles from data on 177 folds obtained in University of Leeds B.Sc. undergraduate fieldwork projects conducted between Duckpool and Dizzard Point (SS200115-SX154994; Fig. 8.1). These results are compared with those obtained from the same area, by Sanderson (1979) (see Fig. 2.23 in Chapter 2). The analysis of these interlimb and axial plane angles in this work (Fig. 8.10) and their comparison with the Sanderson (1979) results shows that:

1. There is a much larger number and range of the data values in the University of Leeds data for the study area (Sanderson’s data being from a much larger stretch of coastal outcrops);
2. Most folds in both data sets are ‘upright’ chevron folds, especially to the north of Bude;
3. The University of Leeds data shows a greater geographical overlap in the fold type clusters than is apparent from Sanderson’s data (see Fig. 2.23 in Chapter 2).

Comparing the data in Fig. 8.10 with that of Sanderson (1979) was statistically unsatisfactory due to the difference in the samples. The University of Leeds projects generated detailed data, but for just a small section of the coast between Hartland and Rusey (see Fig. 8.1)

considered by Sanderson (1979). Thus, the relative mix of fold types differs greatly between the two data sets, with the area north of Bude being dominated by ‘upright’ chevron folds. Unfortunately, Sanderson (1979) did not publish the precise locations of the folds measured, so it was neither possible to extract the small sub-set of data that was strictly comparable to the project data, nor possible to correct for the complications caused by the differences in the ‘mix’ of folds. Thus, from a statistical standpoint, the datasets are not strictly comparable despite being concerned with the same structural measurements.

The analysis of the interlimb angle and absolute shear strain accommodated by the chevron folds from this work (Fig. 8.11) shows that there is:

1. Increasing numbers of folds accommodating large shear strains towards the south (i.e. deeper structural and stratigraphic levels), which fits with the results of Sanderson (1979);
2. A general decrease in interlimb angle with increasing shear strain, which fits with the results from Sanderson and Dearman (1973) and Sanderson (1979);
3. A large spread in ‘upright’ chevron fold inter-limb angles with no change in shear strain.

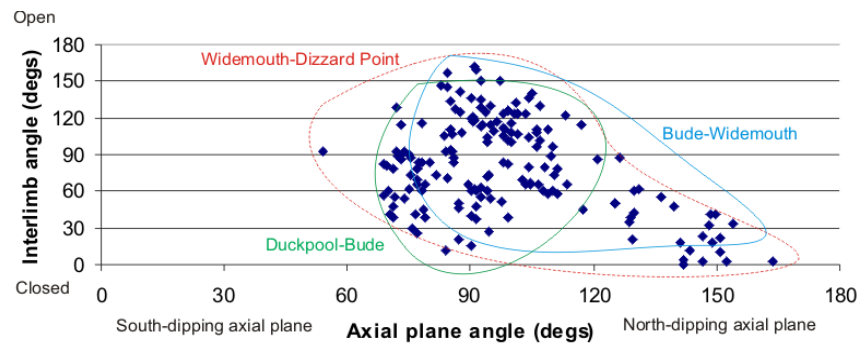


Fig. 8.10: Comparison of the interlimb and axial plane angles for each geographical area (data from Williams, 2005). The spread of the data points for each area is marked.

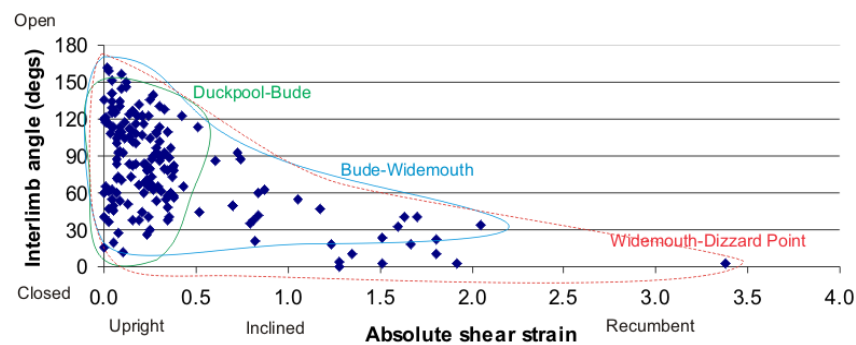


Fig. 8.11: Comparison of the variable interlimb angle and shear strain for each geographical area (data from Williams, 2005). The spread of the data points for each area is marked.

The interlimb angle and absolute shear strain accommodated by the chevron folds (Fig. 8.11) has a large range of interlimb angles between  $180^\circ$  and  $0^\circ$  for ‘upright’ chevron folds (fold type: d). Many of the ‘upright’ chevron folds between Duckpool and Dizzard Point (see Fig.

8.1) have interlimb angles below  $60^\circ$ ; which is the angle at which fold ‘lock-up’ occurs (Price & Cosgrove, 1990). This results in the bulbous-hinged folds of Ramsay (1974). In contrast, some of the ‘inclined-to-recumbent’ chevron folds (fold type: e) show decreasing inter-limb angles ( $< 90^\circ$ ) with increasing shear strain accommodation ( $> 0.5$ ). This suggests that there is a regional inverse relationship between the structural parameters, with an increasing level of south-directed shear strain accommodated towards the south of the Culm Basin (Sanderson, 1979).

### 8.5.5 Variable shear strain model for Bude Formation folds (from Williams, 2005)

Williams (2005) studied how the shear strain varied in the ‘upright’ and ‘inclined-to-recumbent’ chevron folds between Duckpool and Dizzard Point (SS202115-SX165988; Fig. 8.1), which includes the study area between Northcott Mouth and Wanson Mouth (SS202087-SS195013; Fig. 8.1). The dataset and the results of Williams study were used when generating a model to explain the variation in shear strain accommodation across the Bude and Crackington formations (Fig. 8.12). From Williams (2005), the shear strain accommodated by the Bude Formation folds in the study area has two ‘peaks’ of high shear strain that correspond to two discrete coastal sections with south-directed ‘inclined-to-recumbent’ chevron folds (Fig. 8.12):

1. Efford and Lynstone (UK national grid northings 061-048), shear strain range = 1.0 - 3.5;
2. Phillip’s Point and Widemouth (grid northings 044-020) shear strain range = 2.5 - 4.0.

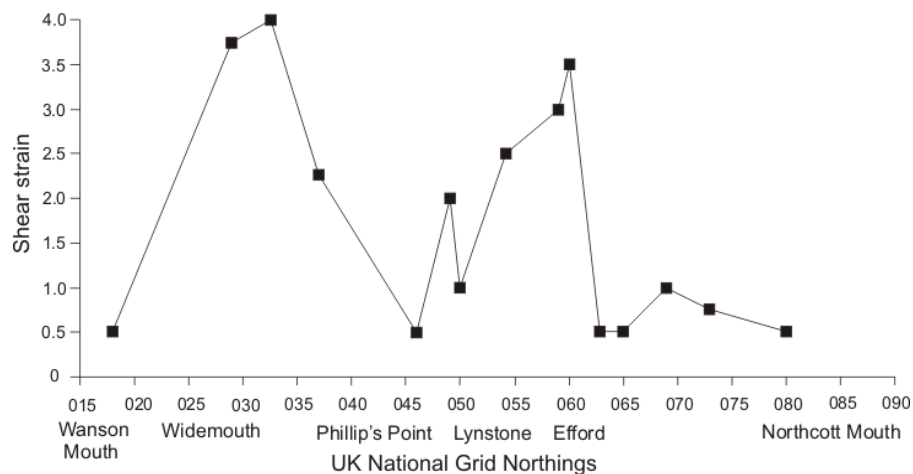


Fig. 8.12: Diagram of mean south-directed shear strain accommodation in the Bude Formation folds between Northcott Mouth and Wanson Mouth (Grid northings SS 015-090). Notice two peaks in the data corresponding to coastal sections exhibiting south-directed ‘inclined-to-recumbent’ chevron folds (modified from Williams, 2005). South is to the left

Williams (2005) data showed that there is increasing shear strain accommodated by the chevron folds towards the south of the study area (Fig. 8.12), which is consistent with the Sanderson’s model of a regional increase in shear strain accommodated towards the south of the Culm Basin. However, the amount of shear strain accommodated varies around the trend, as had been noticed also by Sanderson (1979) between Widemouth and Saltstone (see chapters 2 & 4).

In particular, around Phillip's Point (SS 045) (Fig. 8.12), an area of 'upright' and north-directed 'inclined-to-recumbent' chevron folds where south-directed shear strain accommodation is low.

## 8.6 Inverse thickness method

Two example Bude Formation folded beds in profile are analysed using the inverse thickness analysis (see Chapter 7). The examples are a sandstone bed from the Church Races 'inclined-to-recumbent' chevron anticline (SS200042; fold type: e) (location 22 in Fig. 8.1; no. 22 in Fig. 8.5; Fig. 8.7) and a shale bed from the Bude Harbour 'upright' chevron anticline (SS202065; fold type: d) (location 16 in Fig. 8.1; no. 16 in Fig. 8.4; Fig. 8.7).

### 8.6.1 Results

One strain ellipse is required for the plotted points of the sandstone bed in the Church Races 'inclined-to-recumbent' anticline (Fig. 8.13a). A slight dumb-bell shape is produced, which could result from minor variations in original bed thickness rather than from variations in the shortening accommodated on each limb. The maximum extensional direction (major axis) is  $005^{\circ}$ - $185^{\circ}$ ; and the maximum compressional direction (minor axis) is  $095^{\circ}$ - $275^{\circ}$ ; which are sub-parallel and sub-perpendicular to the axial trace, respectively, and have a strain ratio of 2.21.

In contrast, three strain ellipses are fitted to the points for the shale bed in the Bude Harbour 'upright' chevron anticline (Fig. 8.13b). The orientations on the far right limb and the right limb-to-hinge zone both have major and minor axes are  $135^{\circ}$ - $315^{\circ}$  and  $045^{\circ}$ - $225^{\circ}$ , respectively. These orientations are oblique to those for the left limb-to-hinge zone, which are  $020^{\circ}$ - $200^{\circ}$  and  $110^{\circ}$ - $290^{\circ}$ , respectively. In both cases, the major axes of the ellipses are sub-parallel to the bedding planes. The strain ratio in the shale bed vary considerably: (1) far right limb: 6.05; (2) right limb-to-hinge zone: 2.28; and (3) left limb-to-hinge zone: 1.94.

### 8.6.2 Distinguishing folded rock and folded sediment (from Chapter 7)

From the results of inverse thickness analysis in Chapter 7, folded rocks are characterised by one strain ellipse that can be fitted through the inverse thickness points, which describes the strain accommodation across the entire folded layer. In contrast, folded sediments are characterised by multiple strain ellipses that can be fitted through the inverse thickness points, which describe the strain accommodation in part of a folded layer (a limb or hinge zone).

The results from inverse thickness analysis suggest that the sandstone bed in the Church Races 'inclined-to-recumbent' chevron anticline meet the criteria for folds developed in rock, whilst the shale bed in the Bude Harbour 'upright' chevron anticline meet the criteria for folds developed in sediment (Fig. 8.13). These results of the mechanical or lithification state for the folded beds are consistent with those from dip isogon and quantitative bed thickness analysis in Fig. 8.7. Thus, the geometric criteria from inverse thickness analysis developed to distinguish folded rock and folded sediment in profile can be applied to the Bude Formation folds.

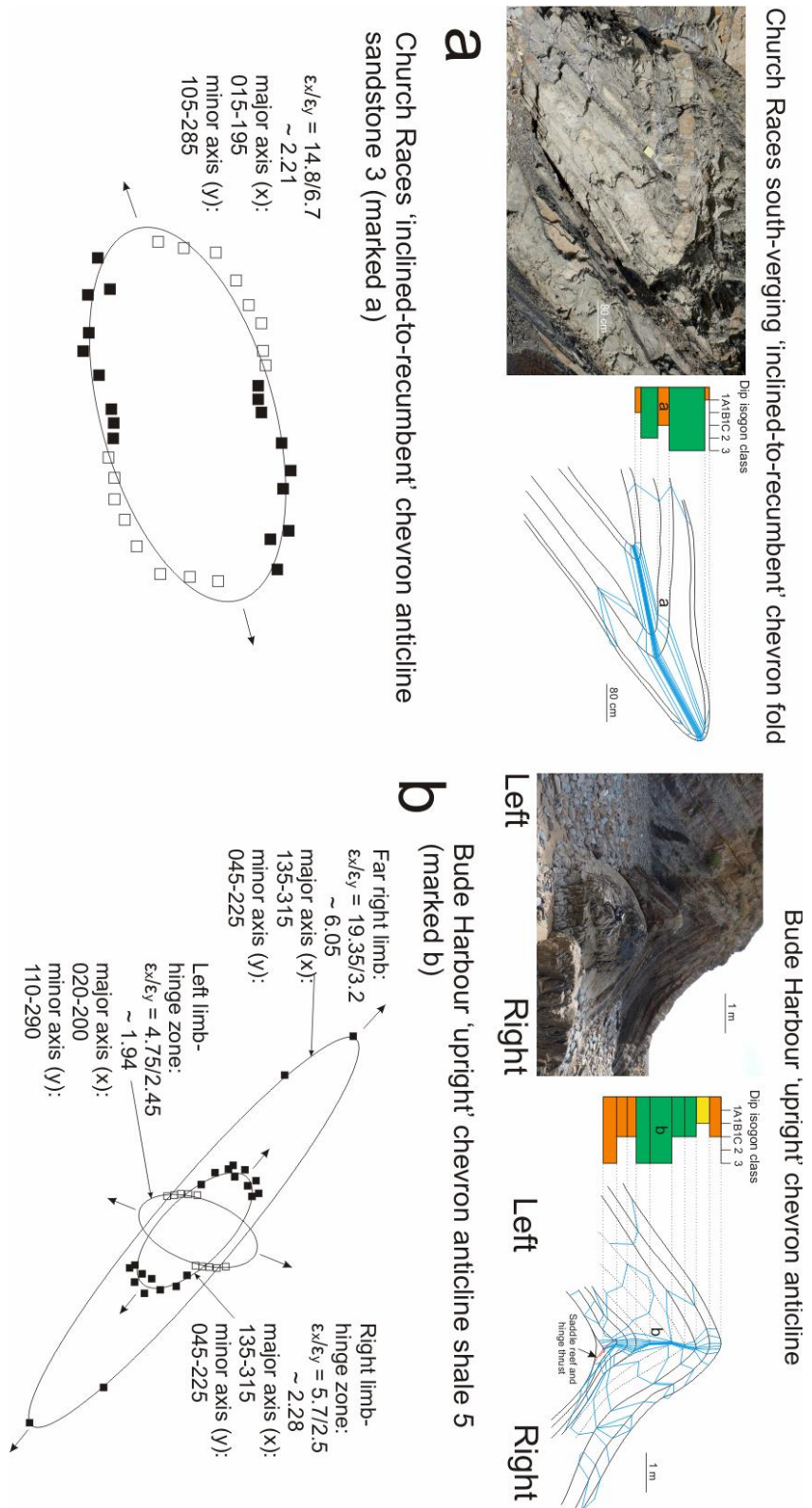


Fig. 8.13: Application of the inverse thickness method using a sandstone bed in the Church Races 'inclined-to-recumbent' chevron anticline (Figs. 8.5 & 8.7) and a shale bed in the Bude Harbour 'upright' chevron anticline (Figs. 8.4 & 8.7). For inverse thickness points in the Church Races anticline, the top-most limb has open squares and the bottom-most limb has closed squares. In the Bude Harbour anticline, the left-hand limb has open squares and the right-hand limb has closed squares. All folds are in profile. Letters next to ellipse relate to the marked bed being analysed

## 8.7 Application of results from the Widemouth South Fault (WSF)

In Chapter 4, the deformation structures observed in the Black Rock and Wanson Mouth foreshores were described as having been juxtaposed by the Widemouth South Fault. One model developed in this study by the author for the WSF was of a north-directed thrust that became inverted during progressive Variscan deformation. Here, a brief review is provided of the author's model and the Freshney et al (1972) 'late' normal fault model, prior to a discussion on how the models can be used as a guide in restoring sections and how other methods can be applied to the faults that cross-cut the Bude Formation chevron folds. The restorations are undertaken in steps for practicality and to make the structural relationships clear.

### 8.7.1 Widemouth South 'late' normal fault model (Freshney et al, 1972)

The Freshney et al (1972) normal fault model (see Chapter 4), the WSF was viewed as a 'late' normal fault that juxtaposed the Black Rock and Wanson Mouth foreshore successions after Variscan deformation (Fig. 8.14a (i)). This model appears to be plausible because the WSF truncates all previous structures, implying that the last displacement on the fault must have been greater than the wavelength of any fold structure formed previously.

The first restoration removes the normal faults and 300 m of stratigraphic separation between the foreshores (Fig. 8.14a (ii); see Chapter 4). This leaves the Black Rock foreshore with an 'upright' chevron fold train on the shallow north-dipping limb of a larger-scale chevron anticline, whilst the Wanson Mouth foreshore has a 'cascade' of 'inclined-to-recumbent' chevron folds on the overturned north-dipping limb of a different larger-scale chevron anticline.

The second restoration (Fig. 8.14a (iii)) removes the 'inclined-to-recumbent' chevron fold deformation, so that the beds retain their present overturned steep northwards dip and cut across the entire Wanson Mouth foreshore (Fig. 8.14a (iii)). In the now separate Black Rock foreshore succession, there continues to be an 'upright' chevron fold train. The deformed beds in both foreshores have become more laterally-continuous and lie on the limbs of separate larger scale folds that have a stratigraphic separation of 300 m (Fig. 8.14a (iii); see Chapter 4).

The third restoration (Fig. 8.14a (iv)) removes the overturned steep northwards dip of the beds and returns them to a right way-up, sub-horizontal orientation. The Black Rock and Wanson Mouth beds are shown as two layer-cake laterally continuous successions separated by a stratigraphic distance of 300 m (see Chapter 4).

### 8.7.2 Inverted Widemouth South Fault model

In the inverted Widemouth South Fault model, the faults in the Wanson Mouth foreshore are viewed as 'late' normal faults (Fig. 8.14b (i)) that cause only tens of metres of displacement (Freshney et al, 1972). To explain the 300 m stratigraphic separation across the WSF (Freshney et al, 1979; see Chapter 4), the 'late' normal fault movement along the WSF is viewed as a reactivation of a previous thrust (i.e. earlier form of the WSF; Enfield et al, 1985).

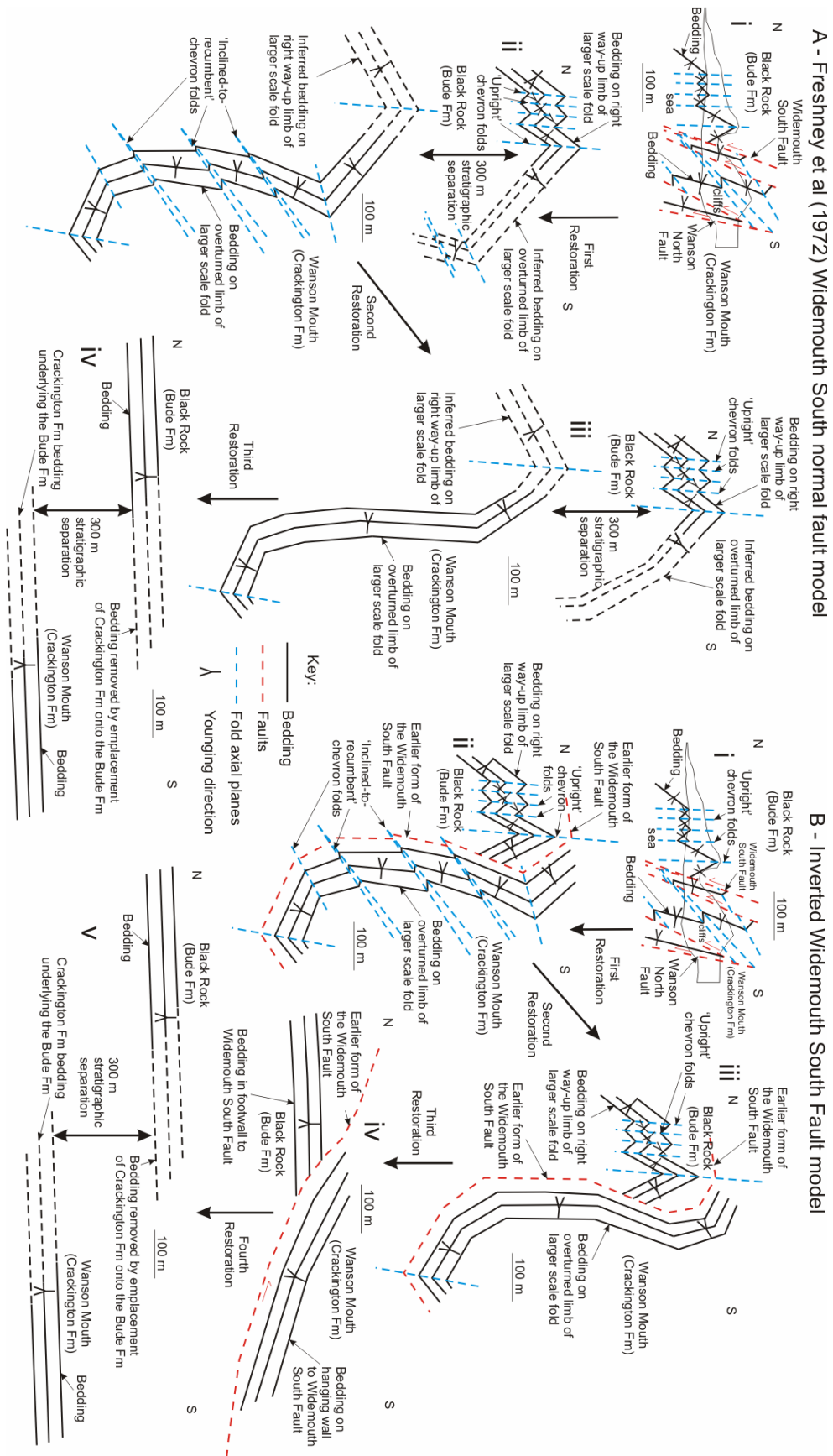


Fig. 8.14: Two schematic structural restoration models to explain the geological evolution of the Black Rock and Wansong Mouth foreshores. The models are: (a) the Freshney et al (1972) ‘late’ normal fault model; and (b) the inverted Widemouth South Fault model, which has been reactivated as a ‘late’ normal fault

The first restoration removes the hundreds of metres long ‘late’ faults, except for the WSF, and restores the beds to their pre-‘late’ normal fault positions (Fig. 8.14b (ii)). The Black Rock foreshore succession has an ‘upright’ chevron fold train on the shallow north-dipping limb of a larger-scale chevron anticline, whilst the Wanson Mouth foreshore has a ‘cascade’ of ‘inclined-to-recumbent’ chevron folds on the overturned north-dipping limb of this larger-scale chevron anticline. Also, the earlier form of the WSF is deformed by the ‘inclined-to-recumbent’ chevron folds (see gusset; see Section 4.6).

The second restoration (Fig. 8.14c (iii)) removes the ‘inclined-to-recumbent’ chevron fold pair. The Wanson Mouth beds retain their present overturned steep northwards dip and cut across the entire foreshore, whilst the ‘upright’ chevron fold train in the Black Rock foreshore, is interpreted to be on the north-dipping limb of the same larger scale chevron anticline. The earlier form of the WSF is present and cuts the overturned limb of the larger-scale chevron fold.

The third restoration (Fig. 8.14b (iv)) removes the overturned steep northwards dip of the beds in the Wanson Mouth foreshore, whilst the Black Rock beds are restored to a right way-up, sub-horizontal orientation. The Black Rock beds are on the footwall and the Wanson Mouth beds are on the hanging wall to the earlier form of the WSF. This fault has emplaced the older Crackington Formation onto the younger Bude Formation, as described by Enfield et al (1985) (Fig. 4.7). Thus, the earlier form of the WSF is interpreted as a thrust accommodating a vertical displacement of 300 m (i.e. the stratigraphic separation between the foreshores).

The fourth restoration (Fig. 8.14b (v)) removes the thrust emplacement along the earlier form of the WSF returns all the beds to a right way-up, sub-horizontal orientation but separated by a stratigraphic distance of 300 m. With the removal of the WSF, the beds in both foreshores are more laterally-continuous.

### **8.7.3 Application of the models to the Bude Formation coastal outcrops**

The deformation in the Bude Formation between Bude and North Widemouth (SS200065-SS200032) includes trains of both ‘upright’ (type: d) and ‘inclined-to-recumbent’ (type: e) chevron folds that have been cut by steeply dipping faults and chevron folds that deform the faults (Freshney et al, 1972; Sanderson, 1979; Enfield et al, 1985; Whalley & Lloyd, 1986). Some of the steeply dipping faults in these outcrops appear to be similar to the WSF that juxtaposes structures in the Black Rock and Wanson Mouth foreshores (see Chapter 4). From the Anisotropy of Magnetic Susceptibility (AMS) analysis by Anderson and Morris (2004), the last movement accommodated by the WSF was extensional. This suggests that the WSF movement post-dates development of the ‘upright’ (type: d) and ‘inclined-to-recumbent’ (type: e) chevron folds although the amount of movement accommodated by the fault differs greatly between the models.

In order to assess the movement directions of the steeply-dipping faults that cross-cut the Bude Formation chevron folds between Bude to North Widemouth, it is proposed that future

work includes collecting structural data on the folds and faults, followed by AMS analysis of the faults. Understanding the movement on these faults would allow for an improved assessment of the strain accommodation in these deformed deposits and how this varied on a kilometric-scale.

## 8.8 Summary of the structural evolution for the Bude Formation

Geometric criteria derived from the results of dip isogon and quantitative bed thickness analyses (see Chapter 7) have been applied to the Bude Formation folded beds to establish their lithification state during Variscan fold deformation as set out in the general aim of this thesis.

During deposition, two types of slump fold formed in sediment: detached slump raft folds in massive slump beds (fold type: a) and attached slump folds (fold type: b) (see Chapter 5). During and just following deposition, 'early' folds (fold type: c) were also formed in sediment (see chapters 4 & 5). As Bude Formation deposition continued and burial occurred throughout Variscan deformation, the chevron folds formed. The first type were 'upright' chevron folds (fold type: d), which developed due to compressional deformation in sediment; an explanation that contradicts the previously held assumption that the folds developed in rock (Ramsay, 1974). This fold type is observed in many of the Bude Formation cliff sections, especially to the north of Bude. As Variscan deformation continued, the Bude Formation beds became increasingly lithified and 'inclined-to-recumbent' chevron folds (fold type: e) developed in the folded beds. The dip isogon criteria indicate that these folds have the characteristics of inter-bedded folded sediment and folded rock. The 'inclined-to-recumbent' chevron folds are found generally to the south of Bude and developed due to the accommodation of increasing south-directed shear strain to the south.

In conclusion, this is the first occasion that tectonic deformation structures have been described in terms of their timing with respect to their lithification state. A microcosm for all this folding to affect the Bude Formation beds is in the Lynstone cliff section (SS200055; see Chapter 7). The importance of the dip isogon methods in developing this explanation demonstrates that these methods provide a powerful set of geometric tools to describe the mechanical or lithification state of folded beds during fold deformation and are the general aim of this thesis.

In Chapter 9, the deformation described in the Culm Basin will be related to the Variscan deformation across SW England (see Chapter 2), which is important to the specific aim of this thesis.

## Chapter 9: Discussion

### 9.1 Introduction

This thesis considered the geological evolution of the Bude Formation (see chapters 2, 4, 5 & 6) and the mechanical conditions under which fold deformation occurred to differentiate clearly between folds in unconsolidated sediment and lithified rock (see chapters 7 & 8).

The geological evolution of the Bude Formation was part of the regional geological evolution of SW England during the Late Carboniferous, with its deposition and deformation in the Culm Basin affected by Variscan tectonics (Leveridge & Hartley, 2006; Shail & Leveridge, 2009). In this chapter, the deformation history of the Culm Basin is placed within a larger-scale context by considering three models of the progressive Variscan deformation in SW England. Following this, the basin (Culm) and regional (SW England) scale interactions between tectonics and deposition are considered in terms of the Bude Formation, using schematic cross-sections and basin-scale sedimentary logs.

### 9.2 Models for the Variscan orogenesis in SW Britain

The Variscan orogeny in SW England has been studied by numerous authors (see references herein). However, in the Geological Society Special Publication 14 (1984), there was debate as to the regional setting and, in particular, whether a décollement underlies the 'orogenic belt'. Three distinct models were proposed:

1. Shortening accommodated throughout the sedimentary cover and also in the continental basement at depth (Sanderson, 1984; Fig. 9.1);
2. 'Thin-skinned' tectonics, with a shallow south-dipping décollement that deformed only the sedimentary cover under the Culm Basin (Brooks et al, 1983; Shackleton, 1984);
3. 'Thick-skinned' tectonics, with a shallow south-dipping regional mid-crustal décollement that deformed the overlying basement and sedimentary cover (Brooks et al, 1984; Leveridge et al, 1984) and described recently by Shail and Leveridge (2009) (see Chapter 2).

#### 9.2.1 The basement and sedimentary cover shortening model

In the Sanderson (1984) model, the continental crust in SW England has been described as a Palaeozoic passive margin with a simple stretching factor ( $\beta$ ) of 2. This stretching caused the approximately 30 km thick pre-extensional continental crust to be thinned to approximately 15 km and generated passive margin basins into which approximately 5 km of sediments were deposited (Fig. 9.1a). The 20 km thick continental crust was then shortened by the Variscan deformation, by approximately 40%, thereby thickening it to approximately 33 km. In order to account for the shortening, Sanderson (1984) suggested that the Gramscatho Basin of SW Cornwall had experienced significant under-plating and under-thrusting of thinned continental

crust and obducted oceanic crust from the Lizard ophiolite (Fig. 9.1b). This north-directed thrusting propagated into and deformed the Trevone Basin in central Cornwall and South Devon (Fig. 9.1c). In this model, reactivation of the passive margin normal faults has not been envisaged to have occurred, except in the Culm Basin. The reactivation of these faults formed the Culm Synclinorium and outward-facing chevron folds during late-stage Variscan deformation at the end of the Carboniferous (Fig. 9.1d) (Warr, 2002; Shail & Leveridge, 2009; see Chapter 2). Thus, Sanderson (1984) did not envisage a ‘master’ décollement, but modelled shortening of the continental crust and the overlying sedimentary cover.

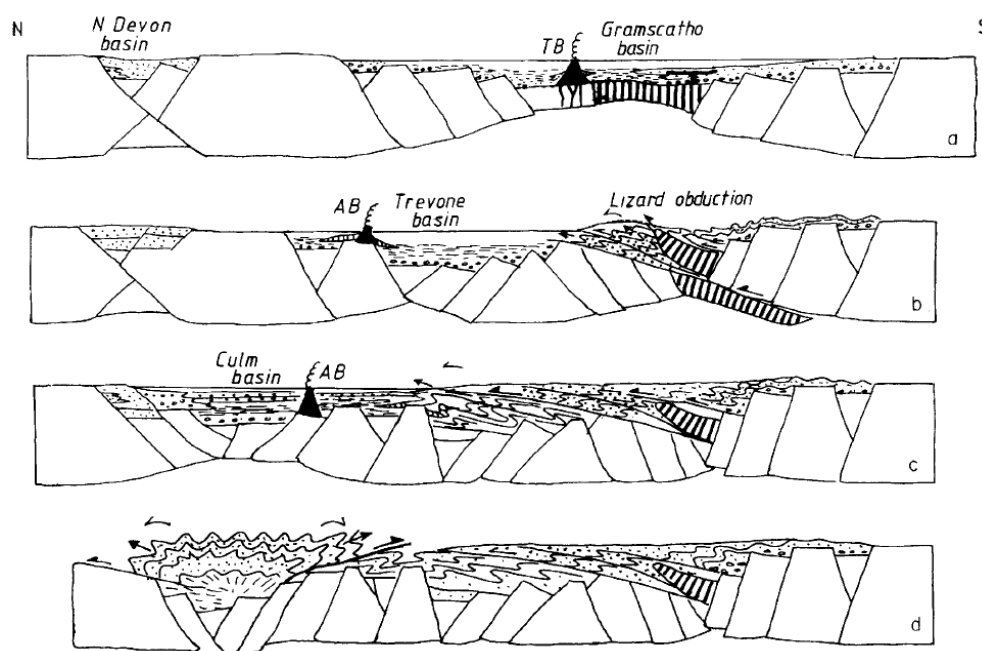


Fig. 9.1: Sketch sections from Sanderson (1984) showing the evolution of SW England prior to and during the Variscan orogeny: (a) Early Devonian passive margin in the Gramscatho Basin; (b) Late Devonian under-plating and Lizard ophiolite obduction; (c) Carboniferous thrusting and deformation of the Trevone Basin; and (d) end-Carboniferous thrusting and deformation of the Culm Basin (**AB** = alkali basalts; **TB** = tholeiites; vertical stripping = oceanic crust)

### 9.2.2 ‘Thin-skinned’ tectonics model

In the Shackleton (1984) ‘thin-skinned’ tectonics model, a gently south-dipping décollement is proposed to underlie the Variscan structures across SW England. This décollement cuts upwards from the Precambrian continental basement where it is modelled to have been affected by the basement ‘grain’, except where it cuts through to the pre-Variscan sedimentary cover. Shackleton (1984) suggested that basement influence on the décollement ceased in south Cornwall at a line “where the trend of the Variscan changes from E-W to ENE-WSW” (Sanderson & Dearman, 1973). From the seismic survey of Brooks et al (1983), a significant reflector has been interpreted under the SW Wales and the Bristol Channel area from depths of 7.5 km to the present surface. This reflector was interpreted by Brooks et al (1983) as

a regional thrust that cut through the sedimentary cover and so, may fit with the ‘thin-skinned’ décollement of Shackleton (1984).

A ‘thin-skinned’ tectonics model was proposed for the Variscan deformation in Pembrokeshire, SW Wales, by Coward and Smallwood (1984) and Smallwood (1985) and is shown in cross-sections along its eastern coast (Tenby-Saundersfoot) (Fig. 9.2a) and its western coast (St Ann’s Head-Settling Nose) (Fig. 9.2b). In the Tenby-Saundersfoot section (Fig. 9.2a), the shallow décollement emerges from the over-thrusting Retic Thrust at Tenby and cuts the surface at Saundersfoot. In the St Ann’s Head-Settling Nose section (Fig. 9.2b), the shallow décollement emerges from the Benton-Johnson thrust duplex near Little Haven and cuts the surface at Settling Nose. In both sections, north-directed ‘inclined’ folds occur in the hanging walls to the ‘imbricate’ thrusts that cut up from the shallow décollement (Fig. 9.2).

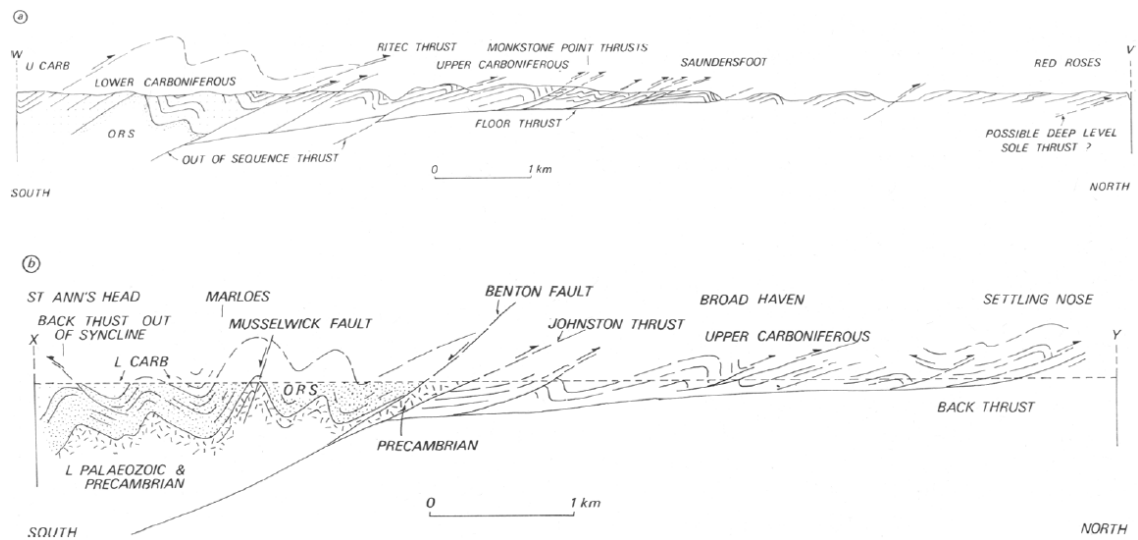


Fig. 9.2: (a) Simplified balanced cross-section along the east Pembrokeshire coast (ORS = Old Red Sandstone; Devonian); and (b) Simplified synoptic section along the west Pembrokeshire coast. In both cases, horizontal scale = vertical scale (from Coward & Smallwood, 1984)

### 9.2.3 ‘Thick-skinned’ tectonics model

Although Shackleton (1984) modelled a décollement cutting the sedimentary cover, it was also suggested that this structure had cut upwards from the Precambrian basement (Fig. 9.3). In Brooks et al (1984), a further seismic survey was undertaken across SW England and a major mid-crustal regional reflector was interpreted at a depth of 15-12 km in Cornwall and south Devon and at 13-10 km in north Devon. Brooks et al (1984) suggested that the reflector dips to the south at less than  $5^\circ$  and that it equated to a surface at the base of the batholith. This surface is most likely to be a thrust that may post-date the granite intrusion. Alternatively, the thrust may have exploited an “originally tabular-shaped intrusion” (Brooks et al, 1984). In Shail and Leveridge (2009), it is suggested that the granite batholith, which had a lower crustal source with a mantle component from beneath the mid-crustal reflector has a tabular form up to 9 km

thick and was emplaced during extensional reactivation of the Variscan thrusts. This batholith may have exploited the mid-crustal décollement during post-Variscan extension.

Regional Variscan thrusting is supported by evidence from other seismic surveys across Europe. Leveridge et al (1984) interpreted thrusts in the Rheinisch massif, Germany, climbing northwards to depths of 6-4 km, in Devizes, SW Britain; climbing north-westwards to depths of 6.6-3.8 km, and beneath the English Channel, climbing steeply northwards (Brooks et al, 1984) from a sole thrust at depths of 15-13.5 km. The latter thrust may connect with the Carrick nappe that cuts Devonian strata at depths of 12-10.5 km in south Cornwall (Leveridge et al, 1984).

In the Shail and Leveridge (2009) 'thick-skinned' tectonics model (Fig. 9.3; see Chapter 2), it has been suggested that the mid-crustal décollement propagated northwards during the Variscan orogenesis. This movement would have caused the original south-dipping passive margin normal faults to be inverted progressively during this orogenesis and resulted in a sequence of foreland basins being developed progressively to the north (see Chapter 2). The last and structurally-highest Variscan basin to develop was the Culm Basin during the Late Carboniferous (Namurian to Westphalian stages; Freshney et al, 1972; 1979). During the Westphalian, the northward slip along the mid-crustal décollement ceased and southwards back-thrusting began (Coward & Smallwood, 1984; see Chapter 2). In the Shail and Leveridge (2009) model, north-dipping passive margin normal faults were also inverted, with thrusting along the Rusey Fault causing the south-directed deformation observed in the south of the Culm Basin (Sanderson, 1979; Lloyd & Whalley, 1986; see chapters 2, 4 & 8). This is the preferred model as it explains the seismic interpretations better than the other models.

### 9.3 Regional and basin-scale deposition and tectonics

The Bude Formation outcrops along the north Cornwall-Devon coastline have been deformed by chevron folding. The deposits have been described on a basin scale in BGS Memoirs 307/308 and 322 (Freshney et al, 1972; 1979) and these data have been used to generate basin-scale correlated sedimentary logs (Fig. 9.4), some of which were used in Chapter 3 (see Figs. 3.1a & b & 3.14). Using the work by Freshney et al (1979), correlations were established between the laterally-continuous black shale beds using biostratigraphy for the Warren Gutter (WGS) and Sandy Mouth (SMS) shales and lithostratigraphy for the Saturday's Pit (SPS) and Tom's Cove (TCS) shales (see chapters 3 & 4; see Figs. 3.4 & 3.5). The logs show a number of important features (Fig. 9.4):

1. The youngest and thickest Bude Formation deposits are near Duckpool (SS198114) in the core of the Culm Synclinorium (Freshney et al, 1979);
2. Large thickness variations between the correlated black shale horizons (also see Chapter 4);
3. It is argued in this thesis that it is invalid to correlate the Black Rock Slump Bed (BRSB) at South Widemouth with a similar slump bed at Lynstone (see Chapter 5; see Figs. 3.1a & b);
4. Increased slumping is recorded towards the top of the Bude Formation (Enfield et al, 1985).

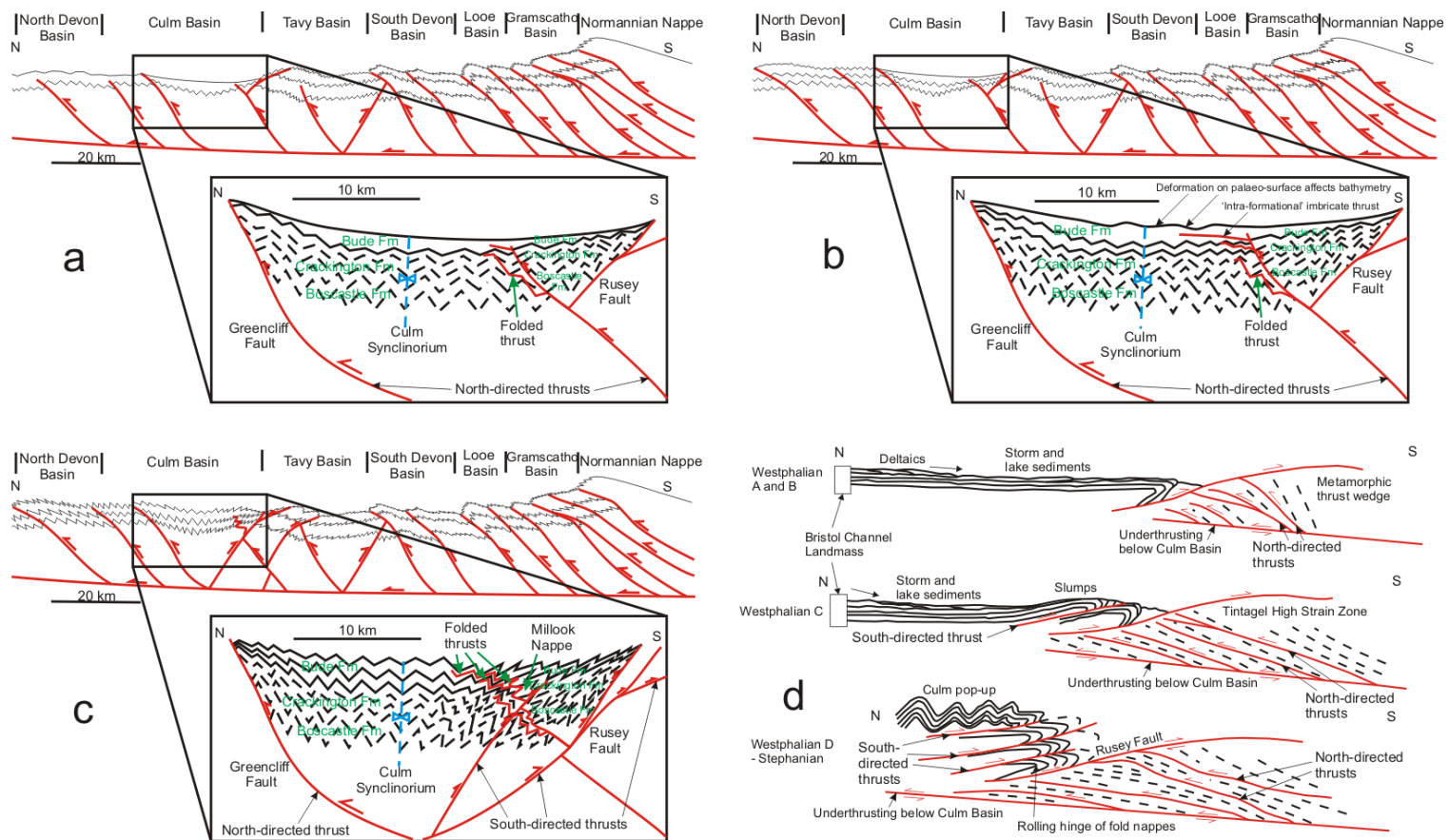


Fig. 9.3: Schematic cross-sections of the progressive Variscan deformation in SW England with inset Culm Basin cross-section (modified from Shail & Leveridge, 2009) during: (a) Westphalian B (Crackington Formation folding and Bude Formation deposition); (b) late Westphalian B to early Westphalian C (folding in both formations and Bude Formation deposition); and (c) Westphalian D (increasing south-directed shear deformation to the south and exhumation). The cross-sections modified from Warr (2002) in (d) show contemporaneous progressive Variscan deformation within the Culm Basin but with ‘upright’ chevron folding as a late event (Westphalian D to Stephanian) and south-directed ‘inclined-to-recumbent’ chevron folding at the same time or slightly earlier than the ‘upright’ chevron folds

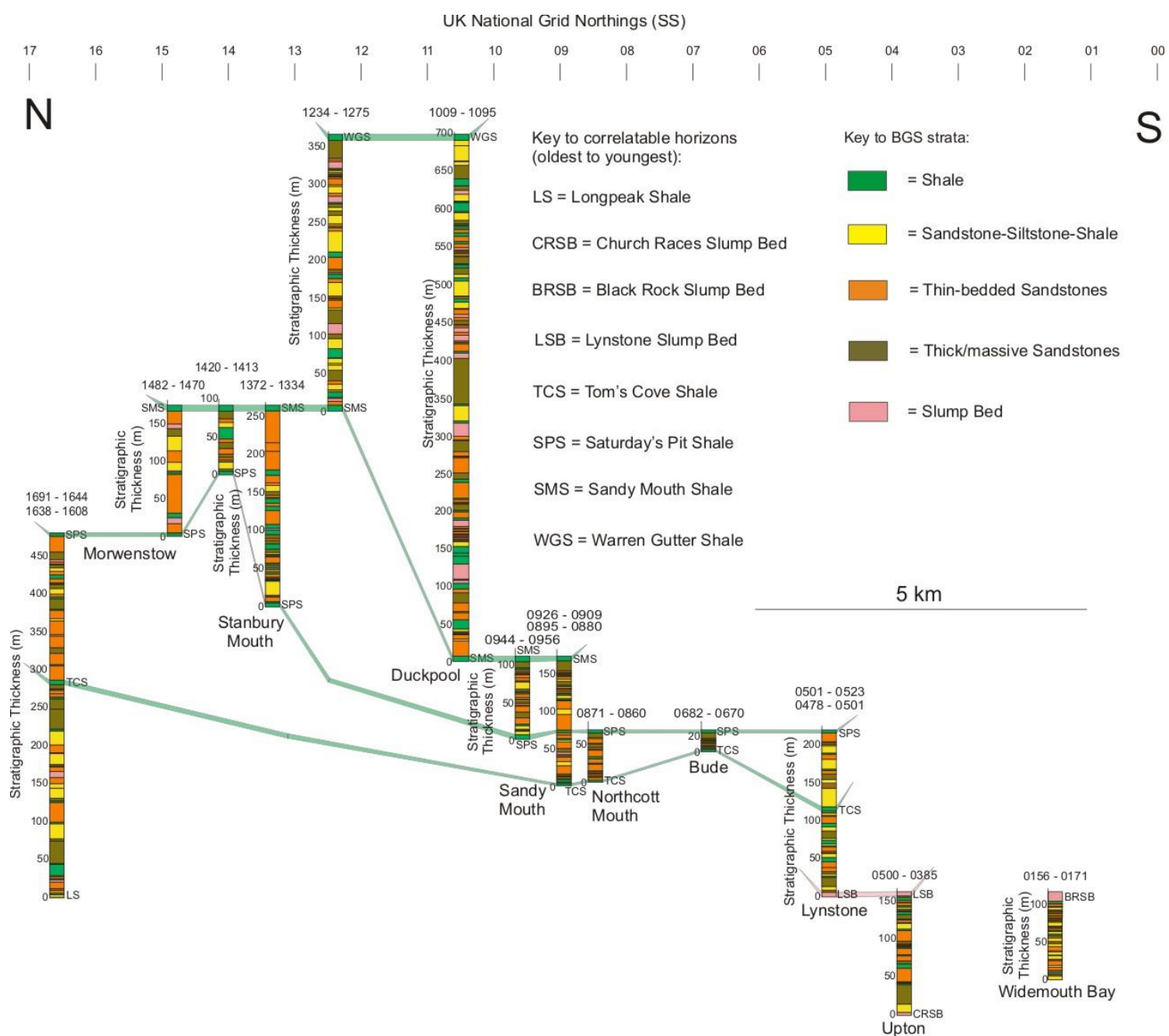


Fig. 9.4: Correlated Bude Formation sedimentary logs from the descriptions of Freshney et al (1972; 1979). Correlation is biostratigraphically-calibrated between the Warren Gutter (WGS) and Sandy Mouth (SMS) shales but lithostratigraphically-correlated between the Saturday’s Pit (SPS) and Tom’s Cove (TCS) shales, as well as the Black Rock Slump Bed (BRSB) equivalents (correlation between Northcott Mouth and Widemouth Bay is provided in Chapter 3; see Figs. 3.1a & b). The Freshney et al (1972; 1979) sedimentary descriptions assume that there is no thrust repetition of the Bude Formation, as described by Lloyd and Chinnery (2002)

These features suggest that the Culm Basin had variable accommodation space during Bude Formation deposition (see Chapter 3), especially during the Westphalian B-C when the top of the formation was deposited (Rippon, 1996). This is indicated in the sedimentary logs by increased thicknesses between the biostratigraphically-calibrated Warren Gutter Shale (WGS), and Sandy Mouth Shale (SMS) at Stanbury Mouth (thinner) and Duckpool (thicker) (Fig. 9.4). Thus, the Culm Synclinorium probably experienced increased subsidence with a higher deposition rate compared to surrounding areas. It is also possible that this increased subsidence in the Culm Synclinorium and the Variscan uplift during the Westphalian generated palaeoslopes in the basin (Shail & Leveridge, 2009; see chapters 2 & 3). This is consistent with the dominantly westward palaeo-flow indicators in the turbidites between the WGS and SMS (Freshney et al, 1979) and the increased numbers of slump beds (Enfield et al, 1985; Fig. 9.4).

Furthermore, these deposits were deformed by 'upright' chevron folding, as described in chapters 6 and 8. From the geometric criteria for distinguishing folded sediment and folded rock described in chapters 7 and 8, these chevron folded beds show geometries that are consistent with folding in sediment and indicates that this deformation occurred relatively soon after deposition. This is consistent with the descriptions of Leveridge and Hartley (2006). Such high level folding could have generated associated surface deformation (see Fig. 3.14).

The Freshney et al (1972; 1979) sedimentary descriptions used for the logs in Fig. 9.4 assume that there has been no thrust repetition of the Bude Formation beds (see Chapter 2). In contrast, Lloyd and Chinnery (2002) suggested that north-directed, usually bedding-parallel, 'intra-formational' imbricate thrusts (see Chapter 5) are responsible for repetition of the strata between Duckpool and Bude (SS202115-SS200067). Bedding-parallel thrusts often have been missed, as in the Black Rock foreshore (SS196016; see Chapter 4) and elsewhere in the Bude Formation (Mapeo & Andrews, 1991; see Chapter 5). Lloyd and Chinnery (2002) suggested that the thrust repetition reduces the 1300 m Bude Formation stratigraphic thickness proposed by Freshney et al (1979) (see Chapter 2). The lack of correlatable sedimentary packages between the correlated black shales (green in Fig. 9.4) provides some evidence for such thrust repetition of the beds. This is clearest in the Lloyd-Chinnery study area between the TCS and SPS shale beds from Northcott Mouth to Lynstone (SS202087-SS200053; see Chapter 5) and between the SPS and SMS shale beds from Sandy Mouth to Northcott Mouth (SS201100-SS202087).

Across SW England, Variscan deformation moved northwards at a slow time-averaged displacement rate of 0.25 to 0.4 cm/yr (Coward & Smallwood, 1984; see Chapter 2). The northward propagation is consistent with striations and fibre growths on faults in north Devon, that show a dominant N-S trend, perpendicular to the chevron fold axes (Coward & Smallwood, 1984). In both the Warr (2002) and Shail and Leveridge (2009) models, the Culm Basin evolved from a rift basin into a thrust-top basin. In order to understand how progressive Variscan deformation may have affected the Culm Basin, three regional and basin-scale sketch cross-sections were drawn (Figs. 9.3a-c). The sections show the Bude Formation thickness variations,

with the thicker deposits being towards the Culm Synclinorium around Duckpool, together with the growth of Variscan structures across SW England and in the Culm Basin (see Chapter 3).

### 9.3.1 Restoration of the progressive Variscan structures

The first section (Fig. 9.3a) shows the northward-moving Variscan 'Front' affecting the southern Culm Basin during Westphalian B (312 Ma; Gradstein et al, 2004). Both the thrusts and chevron folds are modelled as deforming the Crackington Formation, which led to basin-scale subsidence and thicker Bude Formation deposits in the Culm Synclinorium around Duckpool (Freshney et al, 1979; Shail & Leveridge, 2009; Fig. 9.4). Tectonic movements in the Bude Formation may have caused some massive slumps and 'early' structures to develop (Enfield et al, 1985; see chapters 4 & 5). Contemporaneously, inversion began in the northern Culm Basin and up to the Bristol Channel (Fig. 9.3a), perhaps with thrusting along the Greencliff Fault (Shail & Leveridge, 2009). The uplift may have also created a sill, separating the Bude and Bideford formations (Higgs, 1991; Burne, 1995; see Chapter 3), but which is not shown in the more localised cross-section modified from Warr (2002) (Fig. 9.3d).

The second section (Fig. 9.3b) shows the northward-moving Variscan 'Front' affecting the whole Culm Basin during late Westphalian B to early Westphalian C (311 Ma; Gradstein et al, 2004), but with the northward slip rate slowing (Coward & Smallwood, 1984; Enfield et al, 1985; see Chapter 2). The Bude Formation began to accommodate compressional deformation, which also continued to affect the Crackington Formation (Warr, 2002, Fig. 9.3d). The Bude Formation was affected by north-directed thrusts, which were either cut by the 'upright' chevron folds or deformed by these folds (Whalley & Lloyd, 1986; Lloyd & Chinnery, 2002; Leveridge & Hartley, 2006; see Chapter 6). Bude Formation deposition continued, with the thickest and youngest sediments still being towards the Culm Synclinorium around Duckpool (Fig. 9.3b & 9.4; Freshney et al, 1979). This is consistent with the 'upright' chevron folds meeting the criteria for folding in sediment (see Chapter 8). However, this modifies the Warr (2002) model in which south-directed thrusts and 'inclined-to-recumbent' folds developed in the southern Culm Basin but without 'upright' chevron folds to the north (Fig. 9.3d; see Chapter 2).

The third section (Fig. 9.3c) is a snapshot of the deformation that had developed by Westphalian D times (309-308 Ma; Gradstein et al, 2004) after Bude Formation deposition above the WGS had ceased and the deposits had been exhumed. This led to erosion (Cornford et al, 1987; Warr, 2002; Shail & Leveridge, 2009) and formation of the Variscan Unconformity in the topmost Westphalian C (Rippon, 1996; see chapters 2 & 3), as observed in the Culm Synclinorium around Duckpool. Also, the tectonic slip direction may have changed in the southern Culm Basin as the deposits emerged, causing south-directed shear deformation (see chapters 2, 4 & 6; Sanderson, 1979; Coward & Smallwood, 1984; Lloyd & Whalley, 1986; Shail & Leveridge, 2009). Alternatively, Warr (2002) suggested that the deformation of the Culm Basin deposits is a progressive process, with increasing amounts of south-directed shear

deformation of the southern Culm Basin towards the Rusey Fault (Sanderson, 1979; see chapters 2 & 4) throughout the Westphalian and into the Stephanian (Fig. 9.3d). Alternatively, Shail and Leveridge (2009) suggested that the south-directed shear deformation occurred during uplift and emergence in the latest Westphalian (see Fig. 2.20). South directed thrusting is shown along the Rusey Fault by Shail and Leveridge (2009) and described under the Millook Nappe by Rattay and Sanderson (1982) (Fig. 9.3c; see Chapter 2).

During progressive Variscan deformation, the Bude Formation may have begun to lithify and the Crackington Formation may have become fully lithified (see Chapter 8). This is suggested by the ‘inclined-to-recumbent’ chevron folds in both formations meeting the criteria for folding in either rock or inter-bedded sediment and rock (see Chapter 8). However, this contradicts the Warr (2002) model in which the ‘upright’ chevron folds began to develop during Culm Basin uplift and emergence in the Westphalian D to Stephanian (Fig. 9.3d; see Chapter 2).

The comparable models proposed above provide an overview of the Variscan deformation observed both regionally (SW England) and in the Culm Basin, during and just after the Bude Formation was deposited. However, it is important to consider how the different models relate to the deformation observed on the Rusey Fault at the southern end of the Culm Basin (see Chapter 4) and how the preferred ‘thick-skinned’ tectonic model of Shail and Leveridge (2006) (see Section 9.2.3) impacts on the Bude Formation depositional environment.

### **9.3.2 Discussion of the Rusey Fault**

In Chapter 4, Thompson and Cosgrove (1996) suggested that the Rusey Fault was a thrust with top-to-NW movement. This is consistent with Zwart (1964), who suggested an originally north-directed thrust emplacing Early Carboniferous metamorphosed ‘infra-structure’ (Tavy Basin) over the Late Carboniferous non-metamorphosed ‘supra-structure’ (Culm Basin). In contrast, Warr (2002) suggested that the Boscastle Formation under-thrusted the Crackington Formation along the Rusey Fault (Fig. 9.3d). Also, Shail and Leveridge (2009) showed the Rusey Fault as a south-directed thrust (Fig. 9.3c), but did not describe its geometry. This is surprising as the southern Culm Basin has accommodated large amounts of south-directed shear deformation (Sanderson, 1979). It would require further investigation that is beyond this study, to understand the deformation around the Rusey Fault and the southern Culm Basin.

### **9.3.3 Models for regional tectonics and Bude Formation deposition**

There are two models that are considered to be consistent with the preferred ‘thick-skinned’ tectonics model of Section 9.2.3 (Shail & Leveridge, 2009), particularly as they may account for the different Bude Formation depositional environments proposed in Chapter 3.

The first model proposes that the Bude Formation beds were deposited in a generally shallow water environment (see Chapter 3), so that localised uplift during Variscan deformation may have caused the formation to shallow upwards locally and thus, become exposed above the

developing anticlines (see Section 9.3). Only local unconformities were observed in the Bude Formation outcrops and these, alternatively, may have resulted from sediment avulsion and erosional bypass (e.g. channels; see chapters 3 & 4) rather than by exposure because palaeo-soils did not develop as in the Bideford Formation (de Raaf et al, 1965; Li, 1990). Also, it is unlikely that 1300 m of Bude Formation strata (Freshney et al, 1979) would have been laid down in only 1.5 Myrs (after Rippon, 1996) if large basin-wide unconformities had occurred.

In the second model, the Bude Formation deposits were laid down initially in a generally deeper water environment (see Chapter 3), so that localised uplift during Variscan deformation is likely to have caused bathymetry to develop (i.e. accommodation to decrease) without exposing the Bude Formation during its deposition. As few unconformities have been observed in the Bude Formation outcrops that may have resulted from sediment avulsion and erosional bypass (e.g. channels; see chapters 3 & 4), deposition is considered to have been generally continuous, as suggested by Freshney et al (1979) (Fig. 9.4). However, from the 'intra-formational' imbricate thrust model of Lloyd and Chinnery (2002), there is some uncertainty about the 1300 m of Bude Formation deposits in the Freshney et al (1979) model, because of significant repetition of the strata by thrusting (also see chapters 4, 5 & 6; see Section 9.3; Enfield et al, 1985; Whalley & Lloyd, 1986; Leveridge & Hartley, 2006). This thrusting may have added to the apparent substantial thickness of the Bude Formation (Fig. 9.4).

The latter model is preferred as it agrees better with the observations of the facies in the Bude Formation and the proposed depositional environment for the formation in Chapter 3.

## 9.4 Summary

In this discussion, three models are presented in order to explain the regional Variscan deformation observed in SW England. In the Sanderson (1984) model, no regional décollement was envisaged either in the basement or in the overlying sedimentary cover. However, from seismic surveys by Brooks et al (1983; 1984) and field descriptions by Leveridge et al (1984), a regional mid-crustal décollement (15-12 km in Cornwall-south Devon and at 13-10 km in north Devon) has been interpreted across SW England (Brooks et al, 1984). Of these, the preferred 'thick-skinned' tectonics model of Shail and Leveridge (2009) in which the décollement became shallower to the north and cut the sedimentary cover in north Devon and south Wales, is preferred because it fits best with the existence of the mid-crustal décollement, although this is also envisaged in the 'thin-skinned' tectonics model of Shackleton (1984).

In order to demonstrate how the Culm basin deformation fits into the regional context, three schematic cross-sections were drawn for the Westphalian of the Variscan deformation in SW England, each with an inset of the Culm basin. These show the development of 'upright' chevron folds in sediment (see Chapter 8), followed by the development of south-directed 'inclined-to-recumbent' chevron folds in rock or inter-bedded rock and sediment as the Bude Formation lithified (see Chapter 8) and then, the slip direction changed from being north-

directed to south-directed (Coward & Smallwood, 1984; see Chapter 2). This conflicts with the Warr (2002) model in which 'upright' chevron folds only began to develop during uplift and emergence of the Culm Basin in the Westphalian D to Stephanian (also see Chapter 2).

In order that the 'thick-skinned' tectonics model (Shail & Leveridge, 2009) continues to hold, a deep water sedimentation model for the Culm basin during Bude Formation deposition is preferred. This agrees with the depositional environment model for the Bude Formation proposed in Chapter 3.

## Chapter 10: Conclusions

The specific aim of the thesis was to investigate the sedimentary and structural evolution of the Culm Basin, looking at the Bude Formation depositional environment; the geometric variation in progressive Variscan deformation structures; the identification of ‘early’ structures; and deformation within sediment. The general aim of this thesis was to investigate fold deformation in sediment and rock, the premise which was achieved, being that fold geometries could be used to distinguish between folds in sediment and folds in lithified rock. Using structural data from the folds in the publicly-available literature, interpretation of the results from dip isogon and quantitative layer thickness analyses on the folded layers provided the geometric criteria required for distinguishing folded sediment from folded rock. These methods and geometric criteria were then applied to the well-exposed and accessible folds in the coastal outcrops of the Late Carboniferous (Westphalian A-C) Bude Formation, Culm Basin, SW England, and allowed a reappraisal to be undertaken of the timing of Variscan deformation with respect to the lithification of the Bude Formation. All these areas are summarised below.

### 10.1 Re-interpretation of the Bude Formation depositional environment

The Bude Formation contains a number of key sedimentary and geochemical features that have been studied by the author and include:

1. Previously unidentified centimetric-scale mud-draped ripple laminations (facies 1b) that could have been generated by uni-directional meteorological “tidal” currents or short duration muddy sandy turbidity flows;
2. Centimetric-scale non mud-draped ripple (facies 1a) and millimetric scale planar laminated beds (facies 5a) as well as metric scale massive structureless beds (facies 6 and 7) with both sharp tops and sharp bases, and basal sole marks, which may be turbidites;
3. Previously unidentified decimetric-scale mud-draped troughs (facies 2b) that may be interpreted as meteorological “tidal” bedforms;
4. Metric-scale tabular cross-stratification (facies 4) and reactivation surfaces that may relate to storm activity in the lower shoreface;
5. Rare metric-scale symmetrical undulations from oscillatory flows that could have been driven by storm waves, generating hummocky cross-stratification (facies 3b);
6. Common metric to decametric scale slumps and contorted beds (facies 9) that resulted from earthquakes, sediment loading or storm wave activity;
7. Occasional low diversity and density *Skolithos* ichnofabrics, with a slightly more diverse suite of ichnofabrics found in some clastic beds within black shale beds (facies 8);
8. Absence of stenohaline ichnospecies, suggesting non-marine environments;
9. Results from carbon-sulphur (C/S) analysis that suggest that in all but two of the Bude Formation continuous black shale beds (Sandy Mouth and Warren Gutter shales), fresh to brackish water proxy salinities occurred during deposition.

Taking the features together, this suggests that the Bude Formation was deposited in fresh to brackish water, possibly in a lacustrine or marginal marine environment situated behind a sill. The salinity changes could have resulted from variations in either river discharge, or lake base levels, or influxes of saline waters. Thus, the Bude Formation depositional environment is complex, variable and mixed and also, that simple models are probably inadequate. The Bude Formation beds may represent stacked turbidites and meteorological “tidal” bedforms generated by variations in wind direction and fluvial discharge in a lake that experienced significant changes in base level.

## 10.2 Structural deformation in the Black Rock-Wanson Mouth foreshores

From the map work undertaken in the Black Rock and Wanson Mouth foreshores, an improved understanding was gained of the geometries of the progressive Variscan deformation structures in both foreshores and also, the timing of movement along the Widemouth South Fault (WSF) that juxtaposes the two successions. Previously unrecognised ‘early’ structures occur in the Black Rock foreshore, some of which were refolded by ‘upright’ chevron folding.

The juxtaposition of the very different structures across the WSF and the 300 m stratigraphic gap between the successions are important and only partially explained features of the geology. Three models were considered for explaining the structural evolution of the WSF and the deformation accommodated in the two foreshores and includes: the ‘late’ extensional WSF model (Freshney et al, 1972); the inverted thrust duplex model (Enfield et al, 1985); and the inverted WSF model of the author. Although no model can be demonstrated to hold fully, it is concluded that the ‘late’ extensional WSF model (Freshney et al, 1972) is the most plausible.

## 10.3 Bude Formation deformation structures that occurred in sediment

Across the Bude Formation outcrops, there are a number of slump beds sitting between underlying and overlying ‘undeformed’ beds that formed in unconsolidated sediments at or near the palaeo-surface and that moved down palaeo-slopes during Bude Formation deposition. The massive disaggregated Black Rock Slump Bed at both Black Rock and Lynstone is up to 12 m thick, contains slump ‘raft’ folds within its ‘matrix’ and was strongly folded. From the results of restorations using stereonet on the slump raft fold data, it was established that the slumped material moved down two different palaeo-slopes and thus, it was concluded that the Black Rock Slump Bed is in fact two, completely separate massive slump beds.

Thus, the Bude Formation outcrops provide examples of structures that either were formed in sediment during deformation or challenge the assumption that all folding occurred in rock. The features that challenge the assumption of fold deformation in rock are:

1. Bedding-parallel ankerite veins that have been affected by local structures;
2. ‘Early’ folds and faults and also, slumped beds;
3. Mud injections that cut chevron fold hinges;

4. Bulbous hinged beds in all lithologies from slump, 'upright' chevron and some 'inclined-to-recumbent' chevron folds.

#### 10.4 Distinguishing folds developed in rock and sediment

In order to demonstrate that folds within the Bude Formation occurred in sediment, a set of geometric criteria were developed in order to distinguish folds that developed in sediment as opposed to lithified rock using the Ramsay (1967) dip isogon and quantitative layer thickness methods. The methods were applied to a suite of folded rocks, sediments, model materials and migmatites. From analyses undertaken using the methods, it was concluded that folded rocks, with the exception of rocks at high temperatures, are characterised by:

1. Symmetric dip isogon patterns and layer thickness ratios about fold hinge zones;
2. Ordered, non-repeating dip isogon patterns and layer thickness ratios on fold limbs;
3. Conformity to a specific 'Ramsay' dip isogon fold class throughout the folded layer.

In contrast, folded sediments behave in an essentially opposite manner and are characterised by:

1. Asymmetric dip isogon patterns and layer thickness ratios about fold hinge zones;
2. Scattered, repeating dip isogon patterns and layer thickness ratios on fold limbs;
3. Lack of conformity to any specific 'Ramsay' dip isogon fold class across the folded layer.

Use of these geometric criteria provides a powerful method for distinguishing the mechanical state of folded layers during fold deformation. In order to illustrate this, the criteria were applied to the five recognised Bude Formation fold types that were generated during Variscan deformation, using example folded layers from each fold type. This established which fold types developed in sediment and which in lithified rock. From Ramsay (1974), it had been assumed previously that both 'upright' and 'inclined-to-recumbent' chevron folds developed in rock. The results of dip isogon and quantitative bed thickness analyses on the Bude Formation fold examples show that:

1. Only one studied 'inclined-to-recumbent' fold met the criteria for folding in lithified rock;
2. The other Bude Formation 'inclined-to-recumbent' chevron folded beds were consistent with being composed of inter-bedded folded rock and sediment;
3. The other fold types, including all the 'upright' chevron folds, met the criteria consistent with that of folded sediment.

This is of geological importance because this is the first time that tectonic deformation structures have been described in terms of their timing with respect to their lithification state. Also, the conclusion that the 'upright' chevron folds (fold type: d) developed in sediment, contradicts the previously held assumption that the folds developed in rock by Ramsay (1974).

## 10.5 Recommendations for further work

In this thesis, a number of areas of potential future study were highlighted. From this, a set of recommendations for further work are provided here:

1. A combined geochemical and geothermal study of the Bude Formation, with an investigation into its diagenetic and temperature evolution related to Variscan and post-Variscan deformation (see Chapter 3);
2. A combined structural and palaeo-magnetic study in the Bude and Crackington formations, using outcrop studies and analyses of rock samples for Anisotropy of Magnetic Susceptibility (AMS) studies to understand the lateral variation in strain accommodation related to progressive fold and fault deformation between Bude and Rusey (see Chapter 4). This may also be linked with a study to gain an improved understanding of the structural evolution of the Rusey Fault and southern Culm Basin (see chapters 4 & 8);
3. A structural study of enhance slump folding and slump-related faulting methods related to palaeo-slope analysis (see Chapter 5). This could be further linked to a study of seismic surveys where slumped beds have been interpreted;
4. A development of the inverse thickness methods (Lisle, 1992) to distinguish folded rock from folded sediment and how they can be linked to the results and criteria developed from dip isogon methods of Ramsay (1967) (see Chapter 7);
5. A test of whether the geometric criteria from dip isogon analyses developed in Chapter 7, are applicable in other compressionally deformed basins to contribute to establishing the relative timing of folding and lithification elsewhere (see Chapter 8);
6. A seismic survey across the Culm Basin, including acquisition and interpretation linked to interpretation of previous and / or new acquisition of gravity and magnetic data, to provide more details on the kilometric-scale structures within the basin (see Chapter 8).

## References

- Ainsworth, R.B., Hasiotis, S.T., Amos, K.J., Krapf, C.B.E., Payenberg, T.H.D., Sandstrom, M.L., Vakarelov, B.K., Lang, S.C., 2012; Tidal signatures in an intracratonic playa lake. *Geol.*, Vol. **40** (7), pp. 607-10
- Alsop, G.I., Holdsworth, R.E., 2002; The geometry and kinematics of flow perturbation folds. *Tectono.*, Vol. **350**, pp. 99-125
- \_\_\_\_\_, \_\_\_\_\_, 2004; The geometry of topology of natural sheath folds: a new tool for structural analysis. *J. Struct. Geol.*, Vol. **26**, pp. 1561-89
- \_\_\_\_\_, Marco, S., 2011; Soft-sediment deformation within seismogenic slumps of the Dead Sea Basin, *J. Struct. Geol.*, Vol. **33**, pp. 433-57
- Anderson, M.W., Morris, A., 2004; The puzzle of axis-normal magnetic lineations in folded low-grade sediments (Bude Formation, SW England). *Geol. Soc. Sp. Pub.* **238**, pp. 175-90
- Andrews, J.R., 1992; Evidence for Variscan dextral transpression in the Pilton Shales, Croyde Bay, North Devon. *Proc. Ussher Soc.*, Vol. **8** (1), pp. 198-9
- \_\_\_\_\_, Barker, A.J., Pamplin, C.F., 1988; A reappraisal of the facing confrontation in North Cornwall: fold or thrust-dominated tectonics? *J. Geol. Soc.*, Vol. **145**, pp. 777-88
- Arch, J., Maltman, A.J., Knipe, R.J., 1988; Shear-zone geometries in experimentally deformed days: the influence of water content, strain rate and primary fabric. *J. Struct. Geol.*, Vol. **10** (1), pp. 91-9
- Arkai, P., Faryad, S.W., Vidal, O., Balogh, K., 2003; Very low-grade metamorphism of sedimentary rocks of the Meliata unit, Western Carpathians, Slovakia: implications of phyllosilicate characteristics. *Int. J. Earth Sci.*, Vol. **92**, pp. 68-85
- Baas, J.H., Best, J.L., Peakall, J., 2011; Depositional processes, bedform development and hybrid bed formation in rapidly decelerated cohesive (mud-sand) sediment flows. *Sediment.*, Vol. **58**, pp. 1953-87
- Bastida, F., Aller, J., Toimil, N.C., Lisle, R.J., Bobillo-Ares, N.C., 2007; Some considerations on the kinematics of chevron folds. *J. Struct. Geol.*, Vol. **29**, pp. 1185-200
- Bayly, B., Borradaile, G.J., Powell, C.McA., 1977; Atlas of Rock Cleavage. University of Tasmania, Hobart
- Bazalgette, L., Petit, J.-P., 2007; Fold amplification and style transition involving fractured dip-domain boundaries: buckling experiments in brittle paraffin wax multi-layers and comparison with natural examples. *Geol. Soc. Sp. Pub.* **270**, pp. 157-69
- Beach, A., 1977; Vein arrays, hydraulic fractures and pressure-solution structures in a deformed flysch sequence, S.W. England. *Tectono.*, Vol. **40**, pp. 201-225.
- Bense, V.F., Van der Berg, E.H., Von Balen, R.T., 2003; Deformation mechanisms and hydraulic properties of fault zones in unconsolidated sediments; the Roer Valley Rift System, The Netherlands. *Hydrogeo. J.*, Vol. **11**, pp. 319-32

- Berner, R.A., Raiswell, R., 1984; C/S method for distinguishing fresh-water from marine sedimentary rocks. *Geol.*, Vol. **12**, pp. 365-8
- Beutner, E.C., 1980; Slaty cleavage unrelated to tectonic dewatering: the Siamo and Michigamme slates revisited. *GSA Bull.*, Vol. **91**, pp. 171-8
- Bishop, P.M.E., 1990; Isotopic systematics and microstructures of slates and shales from south-west England and north Wales. Unpublished Ph.D. thesis, University of Leeds
- Bjerstedt, T.W., 1987; Trace fossils indicating estuarine depo-systems of the Devonian-Mississippian Cloyd Conglomerate Member, Price Formation, Central Appalachians. *Palaios*, Vol. **2**, pp. 339-49
- Blay, P., Cosgrove, J.W., Summers, J.M., 1977; Experimental investigation of the development of structures in multilayers under the influence of gravity. *J. Geol. Soc.*, Vol. **133**, pp. 329-42
- Blenkinsop, T.G. 2012; Visualizing structural geology: From Excel to Google Earth. *Computers & Geosciences*, Vol. **45**, pp. 52-6
- Bond, D., Wignall, P.B., Racki, G., 2004; Extent and duration of marine anoxia during the Frasnian-Famennian (Late Devonian) mass extinction in Poland, Germany, Austria and France. *Geol. Mag.*, Vol. **141** (2), pp. 173-93
- Borradaile, G.J., 1981; Particulate flow of rock and the formation of cleavage. *Tectono.*, Vol. **72**, pp. 305-21
- \_\_\_\_\_, Bayly, M.B., Powell, C.McA., 1982; Atlas of Deformational and Metamorphic Rock Fabrics. Springer, New York
- Brooks, M., Mechie, J., Llewellyn, D.J., 1983; Geophysical investigations in the Variscides of Southwest Britain. *The Variscan Fold Belt in the British Isles*, pp. 186-97
- \_\_\_\_\_, Doody, J.J., Al-Rawi, F.R.J., 1984; Major crustal reflectors beneath SW England. *J. Geol. Soc.*, Vol. **141**, pp. 97-103
- Brothers, R.J., Kemp, A.E.S., Maltman, A.J., 1996; Mechanical development of vein structures due to the passage of earthquake waves through poorly-consolidated sediments. *Tectono.*, Vol. **260**, pp. 227-44
- Burbank, D.W., Anderson, R.S., 2001; Tectonic Geomorphology. Blackwell Science
- Burne, R.V., 1970; Origin and significance of sand volcanoes in the Bude Formation (Cornwall). *Sediment.*, Vol. **15**, pp. 211-88
- \_\_\_\_\_, 1995; The return of 'The Fan That Never Was': Westphalian turbidite systems in the Variscan Culm Basin: Bude Formation (SW England). *Sp. Pub. int. Ass. Sed.* **22**, pp. 101-35
- Caine, J.S., Minor, S.A., 2009; Structural and geochemical characteristics of faulted sediments and inferences on the role of water in deformation, Rio Grande Rift, New Mexico. *GSA Bull.*, Vol. **121**, pp. 1325-40
- Cartwright, J.A., Dewhurst, D.N., 1998; Layer-bound compaction faults in fine-grained sediments. *GSA Bull.*, Vol. **110**, pp. 1242-57

- Collinson, J.D., Thompson, D.B., Mountney, N., 2006; *Sedimentary Structures*. 3<sup>rd</sup> edition, Terra Publishing
- Conners, C.D., Shaw, J.H., 1999; Use of compressive growth strata to infer folding mechanism. *AAPG An. Meet. Exp. Abs.*, pp. A25-6
- Cornford, C., Yarnell, L., Murchiston, D.G., 1987; Initial vitrinite results from the Carboniferous of North Devon and North Cornwall. *Proc. Ussher Soc.*, Vol. **6**, pp. 461-7
- Corredor, F., Shaw, J.H., Bilotti, F., 2005; Structural styles in the deep-water fold and thrust belts of the Niger Delta. *AAPG Bull.*, Vol. **89** (6), pp. 753-80
- Cosgrove, J.W., 2001; Hydraulic fracturing during the formation and deformation of a basin: A factor in the dewatering of low-permeability sediments. *AAPG Bull.*, Vol. **85** (4), pp. 737-48
- Coward, M.P., McClay, K.R., 1983; Thrust tectonics of S Devon. *J. Geol. Soc.*, Vol. **140**, pp. 215-28
- \_\_\_\_\_, Smallwood, S., 1984; An interpretation of the Variscan tectonics of SW Britain. *Geol. Soc. Sp. Pub.* **14**, pp. 89-102
- Craig, R.F., 1997; *Soil Mechanics*. E. & F.N. Spon, 6<sup>th</sup> edition
- Crans, W., Mandl, G., Haremboure, J., 1980; On the theory of growth faulting; a geomechanical delta model based on gravity sliding. *J. Petrol. Geol.*, Vol. **2** (3), pp. 265-307
- Dahlstrom, C.D.A., 1969; Balanced cross-sections. *Can. J. Earth Sci.*, Vol. **6**, pp. 743-57
- Darbyshire, D.P.F., Shepherd, T.J., 1985; Chronology of granite magmatism and associated mineralization – SW England. *J. Geol. Soc.*, Vol. **142**, pp. 1159-77
- Davis, G.A., Wang, C., Zheng, Y., Zhang, J., Zhang, C., Gehrels, G.E., 1998; The enigmatic Yinshan fold-and-thrust belt of northern China; new views on its intraplate contractional styles. *Geol.*, Vol. **26** (1), pp. 43-6
- Davis, G.H., Reynolds, S.J., 1996; *Structural Geology of Rocks and Regions*. Wiley Press
- Davison, I., Jeffcoate, A., Qing, H., 2004; Geometry of chevron folding and shortening estimates at Hartland Quay, North Cornwall, UK, and some regional implications for Culm Basin development. *Proc. Ussher Soc.*, Vol. **11** (1), pp. 42-50
- De Boer, P.L., Oost, A.P. & Visser, M.J., 1989; The diurnal inequality of the tide as a parameter for recognizing tidal influences. *J. Sed. Pet.*, Vol. **59**, pp. 912-21.
- De Raaf, J.F.M., Reading, H.G., Walker, R.G., 1965; Cyclic sedimentation in the lower Westphalian of north Devon, England. *Sediment.*, Vol. **4**, pp. 1-52
- De Vera, J., Granado, P., McClay, K., 2010; Structural evolution of the Orange Basin gravity-driven system, offshore Namibia. *Mar. Petrol. Geol.*, Vol. **27** (1), pp. 223-37
- De Wall, H., Warr, L.N., 2004; Oblique magnetic fabric in siderite-bearing pelitic rocks of the Upper Carboniferous Culm Basin, SW England: an indicator for palaeo-fluid migration? *Geol. Soc. Sp. Pub.* **238**, pp. 493-507
- Debacker, T.N., Sintubin, M., van Noorden, M., 2006; Distinguishing syn-cleavage folds from pre-cleavage folds to which cleavage is virtually axial planar: examples from the Cambrian core

- of the Lower Palaeozoic Anglo-Brabant Deformation Belt (Belgium). *J. Struct. Geol.*, Vol. **28**, pp. 1123-38
- \_\_\_\_, Dumon, M., Matthys, A., 2009; Interpreting fold and fault geometries from within the lateral to oblique parts of slumps: A case study from the Anglo-Brabant Deformation Belt (Belgium). *J. Struct. Geol.*, Vol. **31**, pp. 1525-39
- DeCelles, P.G., Giles, K.A., 1996; Foreland basin systems. *Basin Res.*, Vol. **8**, pp. 105-23
- Del Pino-Sanchez, A., 2006; Kinematic significance of small-scale remobilisation fabrics in deep-water sediments: implications for facies architecture in slope-adjacent settings. Unpublished Ph.D. thesis, University of Leeds
- Denis, M., Buoncristiani, J-F., Guiraud, M., 2009; Fluid-pressure controlled soft-bed deformation sequence beneath the surging Breiðamerkurjökull (Iceland, Little Ice Age). *Sed. Geol.*, Vol. **221**, pp. 71-86
- Deville, E., Guerlais, S.H., Griboulard, R., Battani, A., Herbin, J.P., Houzay, J.P., Muller, C., Prinzhofer, A., 2003; Mud volcanism origin and processes: new insights from Trinidad and Barbados prism. *Geol. Soc. Sp. Pub.* **216**, pp. 475-90
- \_\_\_\_, \_\_\_\_ , \_\_\_\_ , Callec, Y., Huyghe, P., Lallemand, S., Mascle, A., Noble, M., Schmitz, J., Caramba working group, 2006; Liquefied vs. stratified sediment mobilization processes: insight from South Barbados accretionary prism. *Tectono.*, Vol. **428**, pp. 33-47
- Diskin, S., 2008; Geochemistry of the Bude and Bideford Formations, Devon. *Proc. Ussher Soc.*, Vol. **12** (1), pp. 41-8
- Dodson, M.H., Rex, D.C., 1970; Potassium-Argon ages of the slates and phyllites from SW England. *Quat. J. Geol. Soc.*, Vol. **126**, pp. 469-99
- Doe, T.W., Dott, Jr., R.H., 1980; Genetic significance of deformed cross-bedding – with examples from the Navajo and Weber Sandstones of Utah. *J. Sed. Pet.*, Vol. **50** (3), pp. 793-812
- Durrance, E.M., 1985; A possible major Variscan thrust along the southern margin of the Bude Formation, South-West England. *Proc. Ussher Soc.*, Vol. **6** (2), pp. 173-9
- EDINA™; UK national academic data centre. University of Edinburgh (<http://edina.ac.uk/>)
- Elliott, T., Lapido, K.O., 1981; Syn-sedimentary gravity slides (growth faults) in the Coal Measures of South Wales. *Nature*, Vol. **291**, pp. 220-2
- Enfield, M.A., Gilchrist, J.R., Palmer, S.N., Whalley, J.S., 1985; Structural and sedimentary evidence for the early tectonic history of the Bude and Crackington Formations, north Cornwall and Devon. *Proc. Ussher Soc.*, Vol. **6**, pp. 165-72
- Engelder, T., Marshak, S., 1985; Disjunctive cleavage formed at shallow depths in sedimentary rocks. *J. Struct. Geol.*, Vol. **7**, pp. 327-43
- Farrell, S.G., 1984; A dislocation model applied to slump structures, Ainsa Basin, South Central Pyrenees. *J. Struct. Geol.*, Vol. **6**, pp. 727-36
- Forey, P.L., 1981; The coelacanth *Rhabdoderma* in the Carboniferous of the British Isles. *Palaeontol.*, Vol. **24**, pp. 203-29

- Fossen, H., 2010; *Structural Geology*. Cambridge University Press
- Freshney, E.C., McKeown, M.C., Williams, M., 1972; Geology of the coast between Tintagel and Bude. Memoir for part of the geological sheet **322**, British Geological Survey
- \_\_\_\_\_, Taylor, R.T., Edmonds, E.A., Williams, B.J., 1979; Geology of the country around Bude and Bradworthy. Memoir for 1:50,000 geological sheets 307 and 308, British Geological Survey
- Gayer, R.A., Cornford, C., 1992; The Portledge-Peppercombe Permian outlier. *Proc. Ussher Soc.*, Vol. **8** (1), pp. 15-8
- \_\_\_\_\_, Nemcok, M., 1994; Transpressionally driven rotation in the external Variscides of south-west Britain. *Proc. Ussher Soc.*, Vol. **8** (3), pp. 317-20
- Ghosh, S.K., 1966; Experimental tests of buckle folds in relation to strain ellipsoid in simple shear deformations. *Tectono.*, Vol. **3**, pp. 169-85
- Glen, J.W., Donner, J.J., West, R.G., 1957; On the mechanism by which stones in till become oriented. *Am. J. Sci.*, Vol. **255**, pp. 194-205
- Google Earth™ Version 5; [http://www.google.co.uk/intl/en\\_uk/earth/](http://www.google.co.uk/intl/en_uk/earth/)
- Gradstein, F.M., Ogg, J.G., Smith, A.G., 2004; *A Geologic Time Scale*. Cambridge University Press
- Grainger, P., Witte, G., 1981; Clay mineral assemblages of Namurian shales in Devon and Cornwall. *Proc. Ussher Soc.*, Vol. **5**, pp. 168-78
- Gringras, M.K., Bann, K.L., MacEachern, J.A., Waldron, J., Pemberton, S.G., 2009; A conceptual framework for the application of trace fossils. Society for Sedimentary Geology (SEPM), Applied Ichnology (SC52), pp. 1-26
- Hardy, S., Poblet, J., 1994; Geometric and numerical model of progressive limb rotation in detachment folds. *Geol.*, Vol. **22**, pp. 371-4
- Harris, J. 1977; *Rheology and non-Newtonian flow*. Longman, London and New York, 1<sup>st</sup> ed.
- Harris, N.B., Freeman, K.H., Pancost, R.D., White, T.S., Mitchell, G.D., 2004; The character and origin of lacustrine source rocks in the Lower Cretaceous synrift section, Congo, west Africa. *AAPG Bull.*, Vol. **88** (8), pp. 1163-84
- Hart, J.K., 1999; The inter-relationship between warm-based saturated deforming layers, cold-based frozen deforming layers, debris-rich basal ice and deformed massive ice. *GSA Abs.*, Vol. **31** (7), p. 204
- \_\_\_\_\_, Rose, K.C., Martinez, K., Ong, R., 2009; Subglacial clast behaviour and its implication for till fabric development: new results derived from wireless subglacial probe experiments. *Quat. Sci. Rev.*, Vol. **28**, pp. 597-607
- Hartley, A., 1991; Debris flow and slump deposits from the Upper Carboniferous Bude Formation of SW England: implications for Bude Formation facies models. *Proc. Ussher Soc.*, Vol. **7**, pp. 424-6
- \_\_\_\_\_, Warr, L.N., 1990; Upper Carboniferous foreland basin evolution in SW Britain. *Proc. Ussher Soc.*, Vol. **7** (3), pp. 212-6

- Haslam, H.W., Scrivener, R.C., 1991; A geochemical study of turbidites in the Bude and Crackington Formations north of Exeter. *Proc. Ussher Soc.*, Vol. **7**, pp. 421-3
- Hayslett, H.T., Murphy, P., 1971; *Statistics Made Simple*. 2<sup>nd</sup> ed., W.H. Allen & Co., Ltd.
- Hecht, C.A., 1992; The Variscan evolution of the Culm Basin, South-west England. *Proc. Ussher Soc.*, Vol. **8**, pp. 33-8
- Higgs, R., 1984; Possible wave-influenced sedimentary structures in the Bude Formation (Lower Westphalian, south-west England), and their environmental implications. *Proc. Ussher Soc.*, Vol. **6**, pp. 88-94
- \_\_\_\_\_, 1986; 'Lake Bude' (early Westphalian, SW England): storm-dominated siliciclastic shelf sedimentation in an equatorial lake. *Proc. Ussher Soc.*, Vol. **6** (3), pp. 417-8
- \_\_\_\_\_, 1991; The Bude Formation (Lower Westphalian), SW England: siliciclastic shelf sedimentation in a large equatorial lake. *Sediment.*, Vol. **38**, pp. 445-69
- \_\_\_\_\_, 2004. Ross and Bude Formations (Carboniferous, Ireland and England): Reinterpreted as lake-shelf turbidites. *J. Petrol. Geol.*, Vol. **27** (1), pp. 47-66.
- Holdsworth, R.E., 1989; Short paper: The Start-Parranporth line: a Devonian terrane boundary in the Variscan orogen of SW England? *J. Geol. Soc.*, Vol. **146**, pp 419-21
- Holloway, S., Chadwick, R.A., 1986; The Sticklepath–Lustleigh fault zone: Tertiary sinistral reactivation of a Variscan dextral strike-slip fault. *J. Geol. Soc.*, Vol. **143**, pp. 447-52.
- Hooyer, T.S., Iverson, N.R., 2000; Clast-fabric development in a shearing granular material: Implications for subglacial till and fault gouge. *GSA Bull.*, Vol. **112** (5), pp. 683-92
- Houston, J., Hart, D., Houston, A., 2008; Neogene sedimentary deformation in the Chilean forearc and implications for Andean basin development, seismicity and uplift. *J. Geol. Soc.*, Vol. **165**, pp. 291-306
- Hudleston, P.J., 1973; An analysis and interpretation of minor folds in the Moine rocks of Monar, Scotland. *Tectono.*, Vol. **16**, pp. 89-132
- Jackson, R.R., 1991; Vein arrays and their development to transpression during fold development in the Culm Basin, central SW England. *Proc. Ussher Soc.*, Vol. **7**, pp. 356-62
- Jansma, P.E., Speed, R.C., 1993; Deformation, dewatering and décollement development in the Antler foreland basin during the Antler orogeny. *Geol.*, Vol. **21**, pp. 1035-8
- Jeffery, G. B., 1922; The Motion of Ellipsoidal Particles Immersed in a Viscous Fluid. *Proc. Roy. Soc. A*, Vol. **102** (715), pp. 161-79
- Jolly, R.J.H., Lonergan, L., 2002; Mechanisms and controls on the formation of sand intrusions. *J. Geol. Soc.*, Vol. **159**, pp. 605-17
- Jones, P.B., 1982; Oil and gas beneath east-dipping underthrust faults in the Alberta foothills. In: *Geologic Studies of the Cordilleran Thrust Belt*. Rocky Mountain Association of Geologists, Denver, Colorado, pp. 61-74.
- Kelm, U., Robinson, D., 1989; Variscan regional metamorphism in north Devon and west Somerset. *Proc. Ussher Soc.*, Vol. **7**, pp. 146-51

- King, A.F., 1966; Structure and stratigraphy of the Upper Carboniferous Bude Sandstones, North Cornwall. *Proc. Ussher Soc.*, Vol. **1** (3), pp. 229-232
- \_\_\_\_\_, 1967; Stratigraphy and structure of the Upper Carboniferous Bude Formation, North Cornwall. Unpublished Ph.D. thesis, University of Reading
- \_\_\_\_\_, 1971; Correlation in the Upper Carboniferous Bude Formation, North Cornwall. *Proc. Ussher Soc.*, Vol. **2** (4), pp. 285-8
- Kneller, B., 1991; A foreland basin on the southern margin of Iapetus. *J. Geol. Soc.*, Vol. **148**, pp. 207-10
- \_\_\_\_\_, Branney, M.J., 1995; Sustained high-density turbidity currents and the deposition of thick massive sands. *Sediment.*, Vol. **42**, pp. 607-16
- Kübler, B., 1967; La cristallinité de l'illite et les zones tout à fait supérieures du métamorphisme. *In: Etages Tectoniques, Colloque de Neuchâtel*, pp. 105-22. A la Baconniere, Neuchâtel.
- Lambe, T.W., Whitman, R.V., 1969; Soil Mechanics. John Wiley & Sons, New York
- Lander, R.H., Larese, R.E., Bonnell, L.M., 2008; Toward more accurate quartz cement models: The importance of euhedral versus noneuhedral growth rates. *AAPG Bull.*, Vol. **92**, pp. 1537-63
- Leclair, S.F., Arnott, R.W.C., 2005; Parallel lamination formed by high-density turbidity currents. *J. Sed. Res.*, Vol. **75** (1), pp. 1-5
- Leeder, M., 1987; Sediment deformation structures and the palaeotectonic analysis of sedimentary basins, with a case study from the Carboniferous of northern England. *Geol. Soc. Sp. Pub.* **29**, pp. 137-46
- Leveridge, B.E., Holder, M.T., Day, G.A., 1984; Thrust nappe tectonics in the Devonian of south Cornwall and the western English Channel. *Geol. Soc. Sp. Pub.* **14**, pp. 103-12
- \_\_\_\_\_, Hartley, A.J., 2006; The Variscan Orogeny: the development and deformation of Devonian / Carboniferous basins in SW England and Wales. *In: Brenchley, P.J., Rawson, P.E. (eds.); The Geology of England and Wales*. The Geological Society, London, pp. 225-55
- Li, X., 1990; Changes in deltaic sedimentation in the Upper Carboniferous Westward Ho! Formation and Bideford Group of SW England. *Proc. Ussher Soc.*, Vol. **7**, pp. 232-6
- Lin, M.-L., Chung, C.-F., Jeng, F.-S., 2006; Deformation of overburden soil induced by thrust fault slip. *Engineer. Geol.*, Vol. **88**, pp. 70-89
- Lisle, R.J., 1992; Strain estimation from flattened buckle folds. *J. Struct. Geol.*, Vol. **14** (3), pp. 369-71
- \_\_\_\_\_, 2004; Geological Maps and Structures – A Practical Guide, 3<sup>rd</sup> ed., Elsevier
- Lloyd, G.E., Whalley, J.S., 1986; The modification of chevron folds by simple shear: examples from north Cornwall and Devon. *J. Geol. Soc.*, Vol. **143** (1), pp. 89-94
- \_\_\_\_\_, \_\_\_\_\_, 1997; Simple shear modification of chevron folds: implications for facing interpretations, strain analysis and deformation history. *In: Sengupta, S., (ed.); Evolution of Geologic Structures from Micro to Macro Scales*. Chapman and Hall, pp. 373-96

- \_\_\_\_, Chinnery, N., 2002; The Bude Formation, SW England – a three-dimensional, intra-formational Variscan imbricate stack? *J. Struct. Geol.*, Vol. **24**, pp. 1259-80
- Lohrmann, J., Kukowski, N., Adam, J., Oncken, O., 2003; The impact of analogue material properties on the geometry, kinematics and dynamics of convergent sand wedges. *J. Struct. Geol.*, Vol. **25**, pp. 1691-711
- Mackintosh, D.M., 1967; Quartz-carbonate veining and deformation in Namurian turbidite sandstones of the Crackington Measures, North Cornwall. *Geol. Mag.*, Vol. **104** (1), pp. 75-85
- Maltman, A.J., 1984; On the term 'soft-sediment deformation'. *J. Struct. Geol.*, Vol. **6** (5), pp. 589-92
- \_\_\_\_, 1987; Shear zones in argillaceous sediments – an experimental study. *Geol. Soc. Sp. Pub.* **29**, pp. 77-87
- \_\_\_\_, 1998; Deformation structures from toes of active accretionary prisms. *J. Geol. Soc.*, Vol. **155**, pp. 639-50
- \_\_\_\_, Bolton, A., 2003; How sediments become mobilised. *Geol. Soc. Sp. Pub.* **216**, pp. 9-20
- Mapeo, R.B.M., Andrews, J.R., 1991; Pre-folding tectonic contraction and extension of the Bude Formation, North Cornwall. *Proc. Ussher Soc.*, Vol. **7**, pp. 350-5
- Martin, K.D., 2004; A re-evaluation of the relationship between trace fossils and dysoxia. *Geol. Soc. Sp. Pub.* **228**, pp. 141-56
- McCaffrey, W.D., Gupta, S., Brunt, R., 2002; Repeated cycles of submarine channel incision, infill and transition to sheet sandstone development in the Alpine Foreland Basin, SE France. *Sediment.*, Vol. **49**, pp. 623-35
- McClay, K.R., 2004; *The Mapping of Geological Structures*. John Wiley & Sons
- McKay, J.L., Longstaffe, F.J., Plint, A.G., 1995; Early diagenesis and its relationship to depositional environment and relative sea-level fluctuations (Upper Cretaceous Marshybank Formation, Alberta and British Columbia). *Sediment.*, Vol. **42**, pp. 161-90
- McQuarrie, N., 2004; Crustal scale geometry of the Zagros fold-thrust belt, Iran. *J. Struct. Geol.*, Vol. **26**, pp. 519-35
- Melvin, J., 1986; Upper Carboniferous fine-grained turbiditic sandstones from southwest England: a model for growth in an ancient delta-fed sub-sea fan. *J. Sed. Pet.*, Vol. **56**, pp. 19-34
- Middleton, G.V., Hampton, M.A., 1973; Sediment gravity flows: mechanics of flow and deposition. *In: Middleton, G.V., Bouma, A.H. (eds.); Turbidites and deep water sedimentation. SEPM, Pacific Section*
- Molenaar, N., 1986; The inter-relation between clay infiltration, quartz cementation and compaction in Lower Givetian terrestrial sandstones, northern Ardennes, Belgium. *J. Sed. Pet.*, Vol. **56** (3), pp. 359-69
- Montenat, C., Barrier, P., d'Estevou, P.O., Hibsich, C., 2007; Seismites: An attempt at critical analysis and classification. *Sed. Geol.*, Vol. **196**, pp. 5-30

- Mosar, J., Kangarli, T., Bochud, M., Glasmacher, U.A., Rast, A., Brunet, M.-F., Sosson, M., 2010; Cenozoic-Recent tectonics and uplift in the Greater Caucasus; a perspective from Azerbaijan. *Geol. Soc. Sp. Pub.* **340**, pp. 261-80
- Mouthereau, F., Tensi, J., Bellahsen, N., Lacombe, O., De Boisgrollier, T., Kargar, S., 2007; Tertiary sequence of deformation in a thin-skinned/thick-skinned collision belt: The Zagros Folded Belt (Fars, Iran). *Tectonics*, Vol. **26** (5), **TC5006**, 28pp.
- Nemcok, M., Schamel, S., Gayer, R., 2005; Thrustbelts: Structural Architecture, Thermal Regimes and Petroleum Systems. Cambridge University Press
- Nichols, G., 1999; Sedimentology and stratigraphy. Blackwell publishing
- Nigro, F., Renda, P., 2004; Growth pattern of under-lithified strata during thrust-related folding. *J. Struct. Geol.*, Vol. **26**, pp. 1913-30
- Owen, G., 1987; Deformation processes in unconsolidated sands. *Geol. Soc. Sp. Pub.* **29**, pp. 11-24
- \_\_\_\_\_, 1996; Experimental soft-sediment deformation: structures formed by the liquefaction of unconsolidated sands and some ancient examples. *Sediment.*, Vol. **43**, pp. 279-93
- \_\_\_\_\_, 2003; Load structures: gravity-driven sediment mobilization in the shallow subsurface. *Geol. Soc. Sp. Pub.* **216**, pp.21-34
- \_\_\_\_\_, Moretti, M., 2008; Determining the origin of soft-sediment deformation structures: A case study from Upper Carboniferous delta deposits in south-west Wales, UK. *Terra Nova*, Vol. **20**, pp. 237-45
- Palmer, S.N., Barton, M.E., 1987; Porosity reduction, micro-fabric and resultant lithification in UK uncemented sands. *Geol. Soc. Sp. Pub.* **36**, pp. 29-40
- Paterson, S.R., Tobisch, O.T., 1993; Pre-lithification structures, deformation mechanisms, and fabric ellipsoids in slumped turbidites from the Pigeon Point Formation, California. *Tectono.*, Vol. **222**, pp. 135-49
- Peacock, D.C.P., Anderson, M.W., Morris, A., Randall, D.E., 1998; Evidence for the importance of 'small' faults on block rotation. *Tectono.*, Vol. **299**, pp. 1-13
- Phillips, E., Lee, J.R., Burke, H., 2009; Progressive proglacial to subglacial deformation and syntectonic sedimentation at the margins of the Mid-Pleistocene British Ice Sheet: evidence from north Norfolk, UK. *Quat. Sci. Rev.*, Vol. **27**, pp. 1848-71
- Piper, D.J.W., von Heune, R., Duncan, J.R., 1973; Late Quaternary sedimentation in the active eastern Aleutian Trench. *Geol.*, Vol. **1**, pp. 19-23
- Pitman, J.K., Steinshouer, D., Lewan, M.D., 2004. Petroleum generation and migration in the Mesopotamian Basin and Zagros Fold Belt of Iraq: results from a basin-modelling study. *GeoArabia*, Vol. **9** (4), pp. 41-72
- Poblet, J., Munoz, J.A., Trave, A., Serra-Kiel, J., 1998; Quantifying the kinematics of detachment folds using three-dimensional geometry: Application to the Mediano anticline (Pyrenees, Spain). *GSA Bull.*, Vol. **110**, pp. 111-25

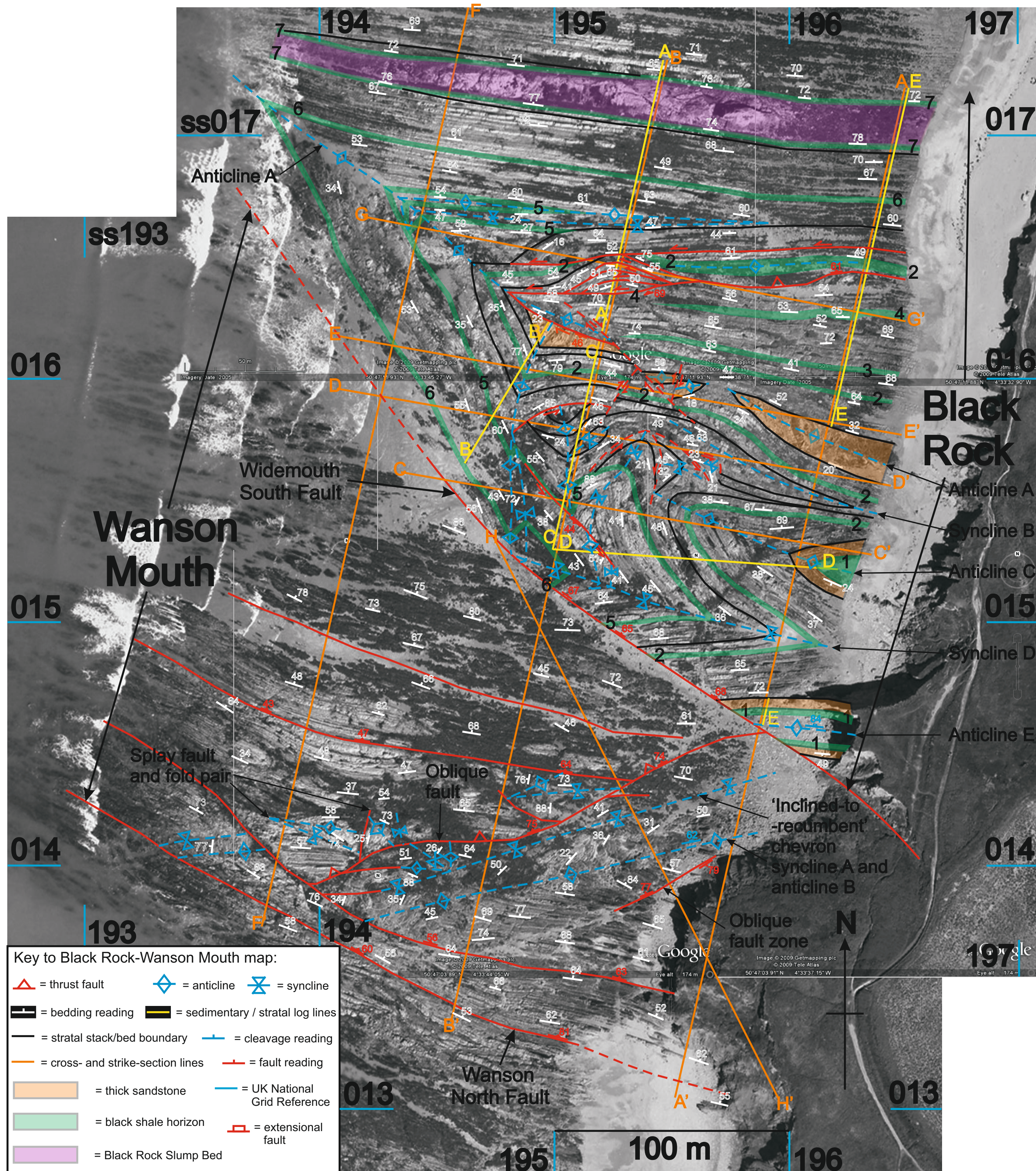
- \_\_\_\_, Lisle, R.J., 2011; Kinematic evolution and structural styles of fold-and-thrust belts. *Geol. Soc. Sp. Pub.* **349**, pp. 1-24
- Price, N.J., 1966; Development of asymmetric buckle folds in non-metamorphosed sediments. *Tectono.*, Vol. **4**, pp. 173-201
- \_\_\_\_, Cosgrove, J.W., 1990; Analysis of Geological Structures. Cambridge University Press
- Primer, T.J., 1985a; A transition from diagenesis to greenschist facies within a major Variscan fold/thrust complex in SW England. *Min. Mag.*, Vol. **49**, pp. 365-74
- \_\_\_\_, 1985b; Low grade Variscan regional metamorphism in SW England. Unpublished Ph.D. thesis, University of Bristol
- Prior, D.B., Coleman, J.M., 1978; Disintegrating retrogressive landslides on very-low-angle subaqueous slopes, Mississippi Delta. *Mar. Geotech.*, Vol. **3** (1), pp. 37-60
- Ramsay, J.G., 1967; Folding and fracturing of rocks. McGraw-Hill.
- \_\_\_\_, 1974; Development of Chevron Folds. *GSA Bull.*, Vol. **85**, pp. 1741-54
- \_\_\_\_, Huber, M.I., 1987; The Techniques of Modern Structural Geology. Vol. **2**: Folds and Fractures, pp. 308-700. Academic Press Ltd., London
- Rattee, P.R., Sanderson, D.J., 1982; Patterns of folding within nappes and thrust sheets: Examples from the Variscan of southwest England. *Tectono.*, Vol. **88**, pp. 247-67
- Reading, H.G., 1965; Recent finds in the Upper Carboniferous of south-west England and their significance. *Nature*, Vol. **208**, pp. 745-7
- \_\_\_\_, 1996; Sedimentary Environments: Processes, Facies and Stratigraphy. Blackwell Publishing, 3<sup>rd</sup> ed.
- Rippon, J.H., 1996; Sand body orientation, palaeoslope analysis and basin-fill implications in the Westphalian A-C of Great Britain. *J. Geol. Soc.* **153**, pp. 881-900
- Roberts, D.H., Hart, J.K., 2005; The deforming bed characteristics of a stratified till assemblage in north East Anglia, UK: investigating controls on sediment rheology and strain signatures. *Quat. Sci. Rev.*, Vol. **24**, pp. 123-40
- Rodrigues, N., Cobbold, P.R., Loseth, H., Ruffet, G., 2009; Widespread bedding-parallel veins of fibrous calcite (beef) in a mature source rock (Vaca Muerta Fm, Neuquén Basin, Argentina): evidence for overpressure and horizontal compression. *J. Geol. Soc.*, Vol. **166**, pp. 695-709
- Sanderson, D.J., 1974; Chevron folding in the Upper Carboniferous rocks of North Cornwall. *Proc. Ussher Soc.*, Vol. **3** (1), pp. 96-103
- \_\_\_\_, 1979; Transition from upright to recumbent folding in the Variscan foldbelt of southwest England: a model based on kinematics of simple shear. *J. Struct. Geol.*, Vol. **1**, pp. 171-80
- \_\_\_\_, 1984; Structural variation across the northern margin of the Variscides in NW Europe. *Geol. Soc. Sp. Pub.* **14**, pp. 149-65
- Schack Pedersen, S.A., 1987; Comparative studies of gravity tectonics in Quaternary sediments and sedimentary rocks related to fold belts. *Geol. Soc. Sp. Pub.* **29**, pp. 165-80
- Schofield, A., Wroth, P., 1978; Critical State Soil Mechanics. Cambridge University Press

- Schwab, F.L., 1986; Sedimentary 'signatures' foreland basin assemblages: real or counterfeit? *Spec. Pub. Int. Ass. Sediment.*, Vol. **8**, pp. 395-410
- Selwood, E.B., Stewart, H., Thomas, J.M., 1985; Upper Palaeozoic sediments and structure in north Cornwall – a reinterpretation. *Proc. Geol. Ass.*, Vol. **96**, pp. 129-41
- \_\_\_\_\_, Thomas, J.M., 1986a; Upper Palaeozoic successions and nappe structures in north Cornwall. *J. Geol. Soc.*, Vol. **143**, pp. 75-83
- \_\_\_\_\_, \_\_\_\_\_, 1986b; Variscan facies and structures in central SW England. *J. Geol. Soc.*, Vol. **143**, pp. 199-207
- Shackleton, R.M., 1984; Thin-skinned tectonics, basement control and the Variscan front. *Geol. Soc. Sp. Pub.* **14**, pp. 125-9
- \_\_\_\_\_, Ries, A.C., Coward, M.P., 1982; An interpretation of the Variscan structures in SW England. *J. Geol. Soc.*, Vol. **139**, pp. 533-41
- Shail, R.K., Leveridge, B.E., 2009; The Rhenohercynian passive margin of SW England: Development, inversion and extensional reactivation. *C.R. Geosci.*, Vol. **341**, pp. 140-55
- Shaw, J.H., Novoa, E., Connors, C., 2004; Structural controls on growth stratigraphy in contractional fault-related folds. *AAPG Mem.*, Vol. **82**, pp. 400-12
- Shin, H., Santamarina, J.C., Cartwright, J.A., 2008; Contraction-driven shear failure in compacting uncemented sediments. *Geol.*, Vol. **36** (12), pp. 931-4
- Sinclair, H.D., 1997; Tectonostratigraphic model for underfilled peripheral foreland basins: an Alpine perspective. *GSA Bull.*, Vol. **109**, pp. 324-46
- Skar, O., 2002; U–Pb geochronology and geochemistry of early Proterozoic rocks of the tectonic basement windows in central Nordland, Caledonides of north-central Norway. *Precamb. Res.*, Vol. **116**, pp. 265-83
- Smallwood, S., 1985; A thin-skinned thrust model for Variscan Pembrokeshire, Wales. *J. Struct. Geol.*, Vol. **7**, pp. 683-7
- Sorby, H.C., 1853; On the origin of slaty cleavage. *New Phil. J. Edinb.*, Vol. **55**, pp. 137-48
- Strachan, L.J., 2008; Flow transformations in slumps: a case study from the Waitemata Basin, New Zealand. *Sediment.*, Vol. **55**, pp. 1311-32
- \_\_\_\_\_, Alsop, G.I., 2006; Slump folds as estimators of palaeoslope: a case study from the Fisherstreet Slump of County Clare, Ireland. *Basin Res.*, Vol. **18**, pp. 451-70
- Suppe, J., 1983; Geometry and kinematics of fault-bend folding. *Am. J. Sci.*, Vol. **283**, pp. 684-721
- \_\_\_\_\_, 1985; Principles of Structural Geology. Prentice-Hall, New Jersey, 537 p.
- Tanner, P.W.G., 1989; The flexural-slip mechanism. *J. Struct. Geol.*, Vol. **11** (6), pp. 635-55
- Tavani, S., Storti, F., Salvini, F., 2006; Double-edge fault-propagation folding: geometry and kinematics. *J. Struct. Geol.*, Vol. **28**, pp. 19-35
- Tobisch, O., 1984; Development of foliation and fold interference patterns produced by sedimentary processes. *Geol.*, Vol. **12**, pp. 441-4

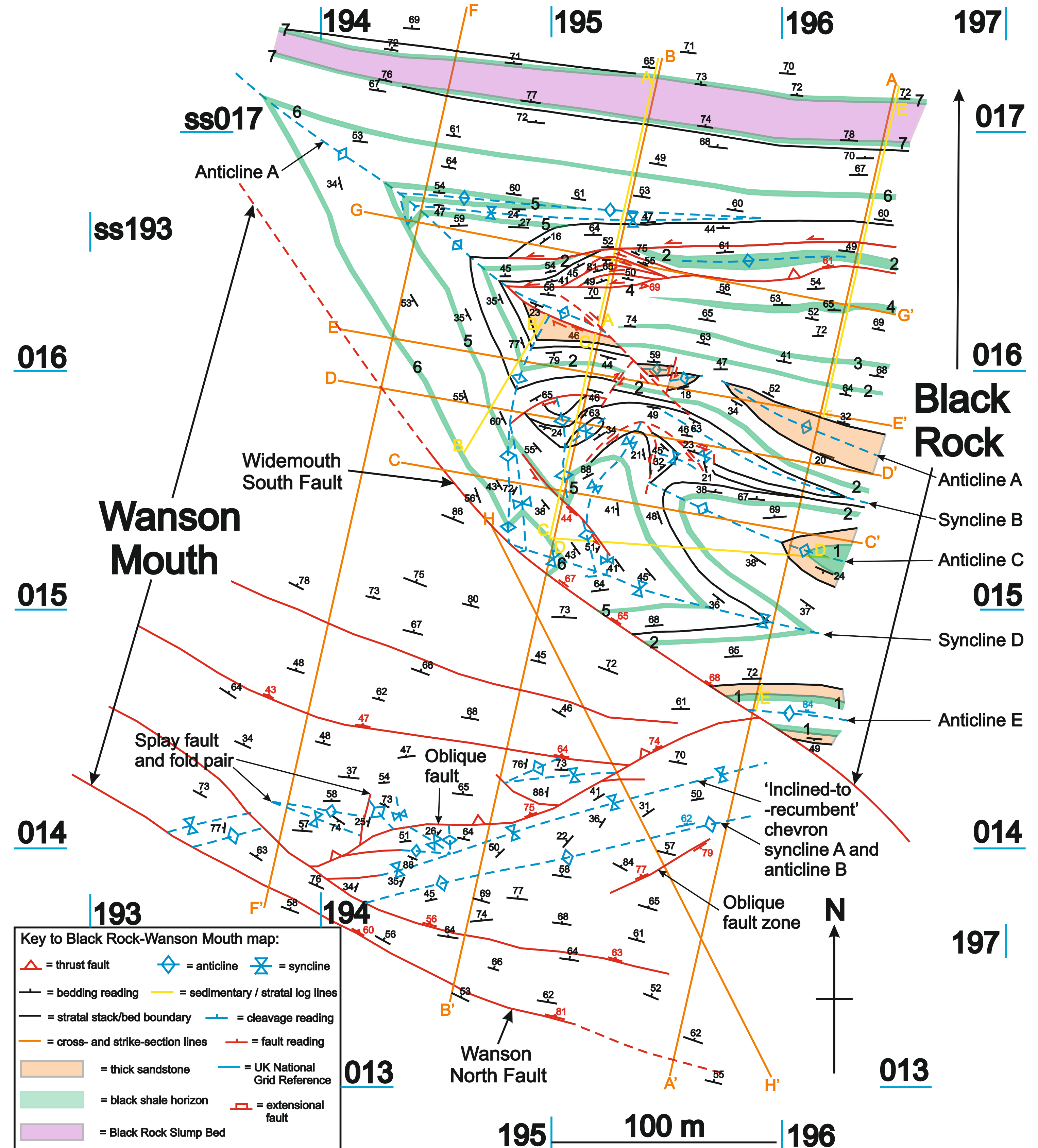
- Thompson, E., Cosgrove, J.W., 1996; The structural and regional setting of the rocks of the Rusey headland. *Proc. Ussher Soc.*, Vol. **9** (1), pp. 133-5
- Twiss, R.J., Moores, E.M., 1992; Structural Geology. W.H. Freeman & Co Ltd.
- Van Rensbergen, P., Hillis, R.R., Maltman, A.J., Morley, C.K., 2003; Subsurface sediment mobilization: introduction. *Geol. Soc. Sp. Pub.* **216**, pp. 1-8
- Vignerresse, J.L., 2004; Rheology of a two-phase material with applications to partially molten rocks, plastic deformation and saturated soils. *Geol. Soc. Sp. Pub.* **224**, pp. 79-94
- Visser, M.J., 1980. Neap-spring cycles reflected in Holocene subtidal large-scale bedform deposits: a preliminary note. *Geol.*, Vol. **8**, pp. 543-6.
- Walderhaug, O., 1994; Precipitation Rates for Quartz Cement in Sandstones Determined by Fluid-Inclusion Microthermometry and Temperature-History Modeling. *J. Sed. Res.*, Vol. **64A** (2), pp. 324-33
- Waldron, J.W.F., Gagnon, J.-F., 2011; Recognizing soft-sediment structures in deformed rock of orogens. *J. Struct. Geol.*, Vol. **33** (3), pp. 271-9
- Walker, J.D., Geissman, J.W., 2009; Geologic Time Scale: Geological Society of America
- Warr, L.N., 1989; The structural evolution of the Davidstow Anticline and its relationship to the Southern Culm Overfold, North Cornwall. *Proc. Ussher Soc.*, Vol. **7**, pp. 136-40
- \_\_\_\_\_, 2002; The Variscan Orogeny: the welding of Pangaea. *In*: Woodcock, N., Strachan, R., (eds.); Geological History of Britain and Ireland. Blackwell Publishing, 1<sup>st</sup> ed.
- \_\_\_\_\_, Primmer, T.J., Robinson, D., 1991; Variscan very low-grade metamorphism in southwest England: a diastathermal and thrust-related origin. *J. Meta. Geol.*, Vol. **9**, pp. 751-64
- \_\_\_\_\_, Hecht, C.A., 1993; A clay mineral crystallinity investigation of the Upper Carboniferous Culm Basin of south-west England. *Proc. Ussher Soc.*, Vol. **8**, pp. 94-8
- Weinberg, R. F., Mark, G., 2008; Magma migration, folding, and disaggregation of migmatites in the Karakoram Shear Zone, Ladakh, NW India *GSA Bull.*, Vol. **120** (7/8), pp. 994-1009
- Weller, J.M., 1959; Compaction of sediments. *AAPG Bull.*, Vol. **43** (2), pp. 273-310
- Whalley, J.S., Lloyd, G.E., 1986; Tectonics of the Bude Formation, north Cornwall – the recognition of northerly directed décollement. *J. Geol. Soc.*, Vol. **143** (1), pp. 83-8
- Wignall, P.B., Best, J.L., 2000; The Western Irish Namurian Basin reassessed. *Basin Res.*, Vol. **12**, pp. 59-78
- Wilhelm, O., Ewing, M., 1972; Geology and history of the Gulf of Mexico. *GSA Bull.*, Vol. **83**, pp. 575-600
- Williams, G., 2005; Chevron folding from Duckpool to Chipman Point, Cornwall. Large scale modeling of shear strain and initial inter-limb angle using the Lloyd and Whalley model (1986, 1997). Interpretations and implications for the area. Unpublished M.Sc. thesis, University of Leeds
- Williams, M., King, A.F., Freshney, E.C., 1970; Itinerary III: Salthouse, Widemouth Sand, to Millook Haven. *In*: Dearman, W.R., Freshney, E.C., King, A.F., Williams, M., McKeown,

- M.C.; The North Coast of Cornwall from Bude to Tintagel (Ed.: Capewell, J.G.) Geologists' Association Guide, No. **10**, pp. 18-22
- Woodcock, N.H., 1976; Structural style in slump sheets: Ludlow Series, Powys, Wales. *J. Geol. Soc.*, Vol. **132**, pp. 399-415
- \_\_\_\_\_, 1979; The use of slump structures as palaeoslope orientation estimators. *Sediment.*, Vol. **26**, pp. 83-99
- Yang, X., Gray, D.R., 1994; Strain, cleavage and microstructure variations in sandstone: implications for stiff layer behaviour in chevron folding. *J. Struct. Geol.*, Vol. **16**, pp. 1353-65
- Zoback, M., 2008; Reservoir Geomechanics. Cambridge University Press
- Zoetemeijer, R., Sassi, W., Roure, F. Cloetingh, S., 1992; Stratigraphic and kinematic modeling of thrust evolution, northern Apennines, Italy. *Geol.*, Vol. **20**, pp. 1035-8
- Zwart, H.J., 1964; The development of successive structures in the Devonian and Carboniferous of Devon and Cornwall. *Geologie en Mijnbouw*, Vol. **43**, pp. 516-26

Photograph in Chapter 5, Fig. 5.25, from Sian Loveless, University of East Anglia, 2010

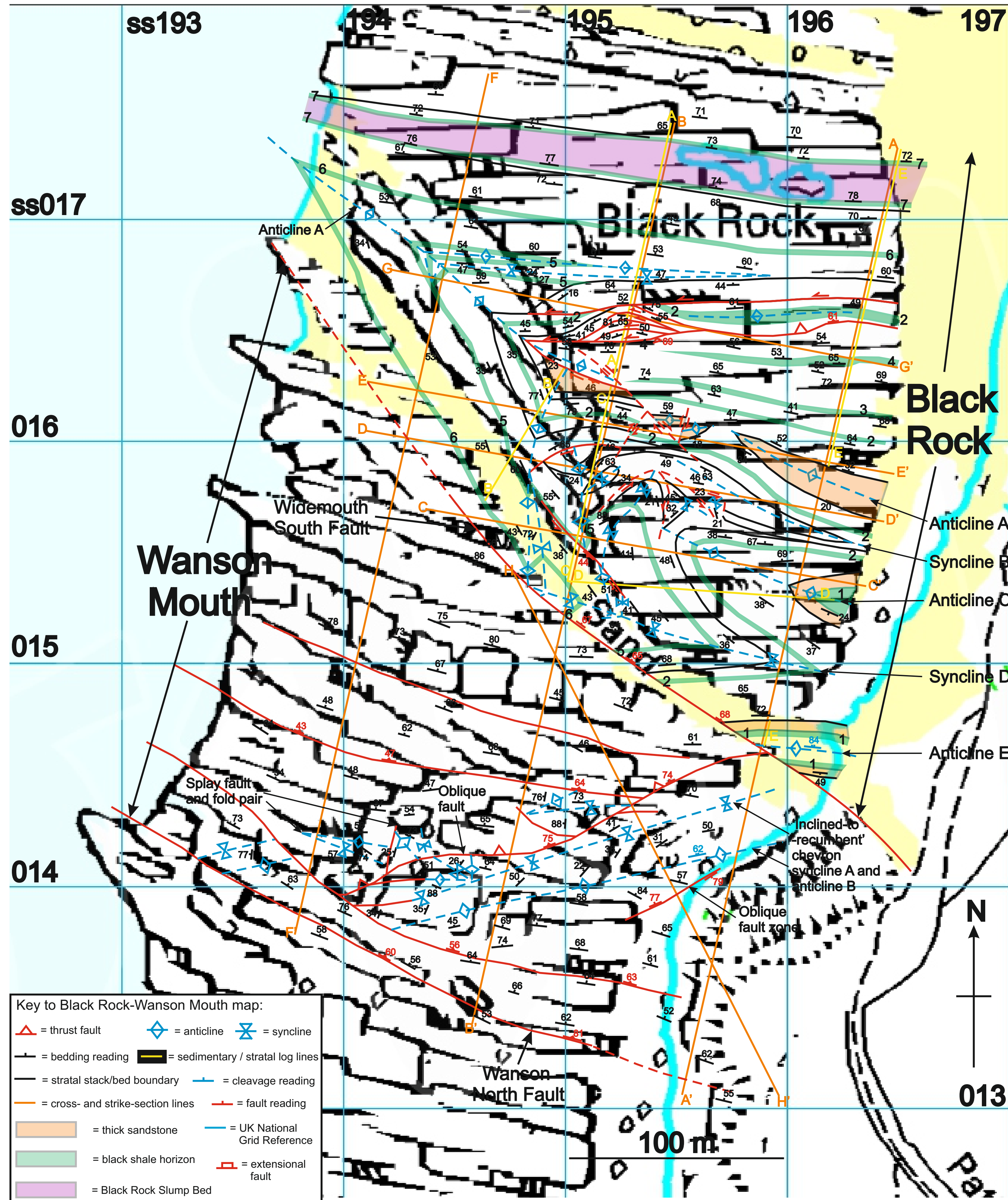


Mapping data plotted onto a Google Earth™ image montage



Mapping data plotted without any background

Mapping data plotted onto an Ordnance Survey/EDINA™ base slip



Dip-sections A-A', B-B' and F-F' across both foreshores

